

## Product Lifecycle Management

# Product Lifecycle Management

*Geometric Variations*

Edited by  
Max Giordano  
Luc Mathieu  
François Villeneuve

ISTE

 WILEY

First published 2010 in Great Britain and the United States by ISTE Ltd and John Wiley & Sons, Inc.

Apart from any fair dealing for the purposes of research or private study, or criticism or review, as permitted under the Copyright, Designs and Patents Act 1988, this publication may only be reproduced, stored or transmitted, in any form or by any means, with the prior permission in writing of the publishers, or in the case of reprographic reproduction in accordance with the terms and licenses issued by the CLA. Enquiries concerning reproduction outside these terms should be sent to the publishers at the undermentioned address:

ISTE Ltd  
27-37 St George's Road  
London SW19 4EU  
UK

[www.iste.co.uk](http://www.iste.co.uk)

John Wiley & Sons, Inc.  
111 River Street  
Hoboken, NJ 07030  
USA

[www.wiley.com](http://www.wiley.com)

© ISTE Ltd 2010

The rights of Max Giordano, Luc Mathieu, François Villeneuve to be identified as the authors of this work have been asserted by them in accordance with the Copyright, Designs and Patents Act 1988.

---

Library of Congress Cataloging-in-Publication Data

Giordano, Max.  
Product lifecycle management : geometric variations / Max Giordano, Luc Mathieu, François Villeneuve.  
p. cm.  
Includes bibliographical references and index.  
ISBN 978-1-84821-276-3  
1. Product life cycle--Congresses. 2. Tolerance (Engineering)--Congresses. 3. Geometry, Descriptive.--Congresses. I. Mathieu, Luc, 1954- II. Villeneuve, François, 1960- III. Title.  
TS172.G56 2010  
620'.0045--dc22

2010029307

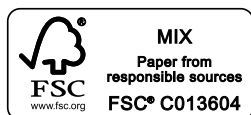
---

British Library Cataloguing-in-Publication Data

A CIP record for this book is available from the British Library  
ISBN 978-1-84821-276-3

---

Printed and bound in Great Britain by CPI Antony Rowe, Chippenham and Eastbourne.



## Table of Contents

<b>Preface</b> . . . . .	xix
<b>PART I. TOLERANCE ANALYSIS AND SYNTHESIS</b> . . . . .	1
<b>Chapter 1. A New Method of Expressing Functional Requirements and How to Allocate Tolerance to Parts</b> . . . . .	3
Pierre-Antoine ADRAGNA and Pascal HERNANDEZ	
1.1. Introduction. . . . .	3
1.2. Brief review . . . . .	4
1.2.1. How to compare. . . . .	4
1.2.2. Statistical tolerancing methods . . . . .	6
1.3. Proposed method . . . . .	10
1.3.1. Functional requirements . . . . .	11
1.3.2. The tolerancing strategy . . . . .	14
1.4. Discussion . . . . .	17
1.4.1. Efficiency of the proposed method . . . . .	17
1.4.2. Comparison to existing approaches . . . . .	17
1.5. Bibliography . . . . .	19
<b>Chapter 2. A Parametric Approach to Determine Minimum Clearance in Overconstrained Mechanisms</b> . . . . .	21
Philippe SERRÉ, Faïda M'HENNI and André CLÉMENT	
2.1. Introduction. . . . .	22
2.2. Compatibility relations between specification parameters . . . . .	24
2.2.1. Modeling the geometric constraints problem. . . . .	24
2.2.2. Compatibility relations for assemblability requirement . . . . .	25
2.2.3. Compatibility relations for mobility requirement . . . . .	27
2.3. Framework for minimum clearance determination. . . . .	29



2.3.1. Nominal and associated mechanism . . . . .	30
2.3.2. Actual and associated parts . . . . .	31
2.3.3. Synthetic scheme . . . . .	32
2.4. Application . . . . .	33
2.4.1. First case . . . . .	33
2.4.2. Second case . . . . .	35
2.5. Conclusion . . . . .	36
2.6. Bibliography . . . . .	37
<b>Chapter 3. Quick GPS: Tolerancing of an Isolated Part . . . . .</b>	<b>39</b>
Robin CHAVANNE and Bernard ANSELMETTI	
3.1. Introduction. . . . .	39
3.2. Mechanism definition. . . . .	40
3.2.1. The positioning plan . . . . .	40
3.2.2. Description with positioning tables . . . . .	41
3.3. Datum system specifications. . . . .	42
3.3.1. Positioning requirements . . . . .	42
3.3.2. Positioning specifications . . . . .	42
3.4. Relative position of reference frames . . . . .	47
3.4.1. Links between reference frames . . . . .	47
3.4.2. Specification corresponding to links. . . . .	49
3.5. VBA application. . . . .	52
3.5.1. General structure . . . . .	52
3.5.2. Data acquisition and verification. . . . .	53
3.5.3. Tolerancing process . . . . .	55
3.6. Conclusion . . . . .	57
3.7. Bibliography . . . . .	57
<b>Chapter 4. Synthesis and Statistical Analysis for 3D Tolerancing . . . . .</b>	<b>59</b>
Max GIORDANO, Pascal HERNANDEZ and Dimitri DENIMAL	
4.1. Introduction. . . . .	59
4.1.1. Literature review . . . . .	60
4.1.2. The domain model . . . . .	61
4.2. Stack-up tolerance synthesis. . . . .	61
4.2.1. Serial mechanisms . . . . .	61
4.2.2. Analysis for worst case stack-up tolerances . . . . .	63
4.2.3. Analysis with the statistical approach . . . . .	64
4.2.4. Synthesis for stack-up tolerances. . . . .	65
4.3. Serial mechanisms with non-perfect contacts. . . . .	66
4.3.1. Analysis in the worst case. . . . .	67
4.3.2. Analysis with the statistical approach . . . . .	67
4.3.3. Synthesis for a serial mechanical system . . . . .	68

4.4. “Reducible” structure . . . . .	68
4.4.1. Parallel mechanical structure . . . . .	68
4.4.2. Introduction to “reducible” structure . . . . .	70
4.4.3. Algorithm and computational method . . . . .	71
4.5. Example of the pin-hole assembly . . . . .	72
4.5.1. Main data. . . . .	72
4.5.2. Major results. . . . .	74
4.6. Conclusion and discussion . . . . .	75
4.6.1. Conclusion. . . . .	75
4.6.2. Discussion and future works . . . . .	75
4.7. Bibliography . . . . .	76
<b>Chapter 5. Reliability Analysis of the Functional Specification Applied to a Helicopter Gas Turbine . . . . .</b>	<b>77</b>
Yann LEDOUX, Denis TEISSANDIER and Samir SID-AHMED	
5.1. Introduction. . . . .	77
5.2. Studied case . . . . .	78
5.2.1. Tolerancing model . . . . .	79
5.3. Deterministic approach . . . . .	83
5.3.1. Sensitivity and elasticity analysis . . . . .	84
5.3.2. Discussion about the determinist results . . . . .	86
5.4. Probabilistic approach . . . . .	86
5.4.1. Definition of the state functions . . . . .	88
5.4.2. Determination of the statistical parameters from the tolerancing model . . . . .	89
5.4.3. Failure rate estimation . . . . .	90
5.4.4. Influence of the tolerancing parameters on the failure probability . . . . .	91
5.4.5. Sensibility analysis on the failure probability . . . . .	93
5.4.6. Parametric analysis of the $\gamma_8$ parameter . . . . .	94
5.5. Conclusion . . . . .	96
5.6. Acknowledgments. . . . .	96
5.7. Bibliography . . . . .	97
<b>Chapter 6. Inertial Tolerancing According to ISO GPS . . . . .</b>	<b>99</b>
Dimitri DENIMAL, Max GIORDANO, Maurice PILLET and Alain SERGENT	
6.1. Introduction. . . . .	99
6.2. Tolerance synthesis . . . . .	100
6.2.1. Definition of the functional requirement domain (FRD) applied to localization specification . . . . .	101
6.2.2. Tolerance synthesis of a stack of parts . . . . .	103
6.2.3. Example of tolerance synthesis. . . . .	105

6.2.4. Process capability indices applied to SDT . . . . .	109
6.2.5. Statistical tolerancing risk. . . . .	110
6.2.6. Inertial tolerancing: short reminder . . . . .	111
6.2.7. Inertial tolerancing with stack-up problem . . . . .	112
6.3. 3D inertia . . . . .	114
6.3.1. 3D inertia definitions and comparison. . . . .	114
6.3.2. 3D inertia definitions comparison . . . . .	117
6.3.3. 3D inertia in the industrial context. . . . .	119
6.3.4. 3D inertia - conclusions . . . . .	121
6.4. Conclusions. . . . .	121
6.5. Bibliography . . . . .	122
<b>Chapter 7. Tolerance Analysis based on Quantified Constraint Satisfaction Problems . . . . .</b>	<b>125</b>
Ahmed Jawad QURESHI, Jean-Yves DANTAN, Jérôme BRUYÈRE and Régis BIGOT	
7.1. Introduction. . . . .	125
7.2. Quantifier notion and mathematical formulation of tolerance synthesis . . . . .	127
7.2.1. Quantifier notion for geometrical product requirement. . . . .	127
7.2.2. Mathematical formulation of tolerance analysis for geometrical product requirement . . . . .	128
7.3. Worst case tolerance analysis based on quantified constraint satisfaction problems . . . . .	132
7.3.1. QCSP . . . . .	132
7.3.2. New mathematical formulation of tolerance analysis for QCSP solver . . . . .	133
7.4. Statistical tolerance analysis based on constraint satisfaction problems and Monte Carlo simulation . . . . .	134
7.4.1. Algorithm for statistical tolerance analysis by Monte Carlo simulation and CSP technique . . . . .	135
7.5. Applications . . . . .	139
7.6. Discussion . . . . .	141
7.7. Bibliography . . . . .	142
<b>Chapter 8. Tolerance Analysis in Manufacturing Using the MMP, Comparison and Evaluation of Three Different Approaches . . . . .</b>	<b>145</b>
Mojtaba KAMALI NEJAD, Frédéric VIGNAT and François VILLENEUVE	
8.1. Introduction. . . . .	146
8.2. MMP. . . . .	147
8.3. Tolerance analysis and virtual gauge . . . . .	149
8.4. Worst case searching . . . . .	150

8.4.1. Optimization technique . . . . .	150
8.5. Combined approach . . . . .	155
8.5.1. The combined approach functional elements. . . . .	155
8.6. Monte Carlo simulation. . . . .	158
8.7. Example and comparison. . . . .	160
8.7.1. First section . . . . .	160
8.7.2. Second section . . . . .	164
8.7.3. Discussion . . . . .	168
8.8. Conclusion . . . . .	169
8.9. Bibliography . . . . .	170
<b>PART II. SIMULATION OF ASSEMBLIES . . . . .</b>	<b>173</b>
<b>Chapter 9. A Chronological Framework for Virtual Sheet Metal Assembly Design . . . . .</b>	<b>175</b>
Johan SEGEBORN, Anders CARLSSON, Johan S. CARLSON and Rikard SÖDERBERG	
9.1. Introduction. . . . .	175
9.1.1. A generic product development process . . . . .	176
9.1.2. Automotive sheet metal assembly . . . . .	177
9.2. Proposed framework . . . . .	179
9.2.1. Planning . . . . .	181
9.2.2. Concept development . . . . .	181
9.2.3. System-level design . . . . .	182
9.2.4. Detail design. . . . .	185
9.3. Summary and future work . . . . .	188
9.4. Acknowledgments. . . . .	189
9.5. Bibliography . . . . .	189
<b>Chapter 10. A Method to Optimize Geometric Quality and Motion Feasibility of Assembly Sequences . . . . .</b>	<b>191</b>
Domenico SPENSIERI, Johan S. CARLSON, Lars LINDKVIST, Robert BOHLIN and Rikard SÖDERBERG	
10.1. Introduction . . . . .	191
10.1.1. Problem motivation . . . . .	191
10.1.2. Related work . . . . .	192
10.2. Modeling and algorithms . . . . .	194
10.2.1. Modeling connections . . . . .	194
10.2.2. Stability and variation analysis . . . . .	199
10.2.3. Assembly sequences . . . . .	200
10.2.4. Path planning . . . . .	203
10.3. Assembly planning. . . . .	204

10.4. Industrial test case . . . . .	204
10.5. Conclusions and future work. . . . .	206
10.6. Acknowledgments . . . . .	207
10.7. Bibliography . . . . .	207
<b>Chapter 11. Modeling and Simulation of Assembly Constraints in Tolerance Analysis of Rigid Part Assemblies . . . . .</b>	<b>209</b>
Pasquale FRANCIOSA, Salvatore GERBINO and Stanislao PATALANO	
11.1. Introduction . . . . .	209
11.2. SVA-TOL methodology overview . . . . .	211
11.3. Assembly constraint modeling. . . . .	212
11.3.1. Fully-constrained assembly . . . . .	217
11.3.2. Over-constrained assembly . . . . .	221
11.4. Case study one: assembly of two-part assembly . . . . .	222
11.5. Case study two: industrial application . . . . .	225
11.6. Conclusions . . . . .	227
11.7. Bibliography . . . . .	228
<b>Chapter 12. Tolerance Analysis with detailed Part Modeling . . . . .</b>	<b>231</b>
Tobias STOLL, Stefan WITTMANN and Harald MEERKAMM	
12.1. Introduction . . . . .	231
12.2. Related work . . . . .	232
12.3. The proposed modeling and analysis of toleranced assemblies. . . . .	233
12.4. Simulation of non-ideal parts . . . . .	234
12.5. Relative positioning . . . . .	235
12.5.1. Defined objective functions . . . . .	236
12.5.2. Particle swarm optimization. . . . .	237
12.5.3. Independence of the positioning steps . . . . .	238
12.5.4. Parallelization . . . . .	238
12.6. Analysis of the positioned assemblies . . . . .	239
12.7. Example . . . . .	239
12.8. Summary . . . . .	241
12.9. Acknowledgements . . . . .	242
12.10. Bibliography. . . . .	242
<b>Chapter 13. Assembly Method Comparison Including Form Defect . . . . .</b>	<b>245</b>
Stéphane MORIÈRE, Jean MAILHÉ, Jean-Marc LINARES and Jean-Michel SPRAUEL	
13.1. Introduction . . . . .	245
13.1.1. Topic . . . . .	245
13.1.2. Actual lack of CAD. . . . .	246
13.1.3. State of the art and proposal. . . . .	246

13.2. Geometric model for simulation . . . . .	248
13.2.1. Part with form defects . . . . .	248
13.2.2. Assembly process . . . . .	250
13.2.3. Function for optimization . . . . .	250
13.2.4. Constraints . . . . .	252
13.3. Experimentation . . . . .	252
13.3.1. Case study . . . . .	252
13.3.2. Simulation setup . . . . .	253
13.4. Result discussion . . . . .	253
13.4.1. Case 1 . . . . .	253
13.4.2. Case 2 . . . . .	254
13.4.3. Case 3 . . . . .	255
13.4.4. Case 4 . . . . .	255
13.5. Summary . . . . .	256
13.6. Bibliography . . . . .	256
<b>Chapter 14. Influence of Geometric Defects on Service Life. . . . .</b>	<b>259</b>
Laurent ZAMPONI, Emmanuel MERMOZ, Jean-Marc LINARES and Jean-Michel SPRAUEL	
14.1. Introduction . . . . .	259
14.1.1. Topic . . . . .	259
14.1.2. Service life functional requirements . . . . .	260
14.1.3. State of the art . . . . .	261
14.2. Calculation methodology of contact pressure and orbital speed variation . . . . .	263
14.2.1. Schedule of the methodology . . . . .	265
14.2.2. Introduction of geometric defects in FEM . . . . .	265
14.2.3. Model of geometric defect . . . . .	266
14.3. Simulation . . . . .	268
14.3.1. Studied case . . . . .	268
14.3.2. Effect of the localization defect on orbital speed variation . . . . .	269
14.3.3. Effect of the orientation defect on the contact load and orbital speed variation . . . . .	269
14.3.4. Effect of the form defects and undulation on speed variation . . . . .	270
14.4. Summary . . . . .	271
14.5. Bibliography . . . . .	272
<b>Chapter 15. GapSpace Multi-dimensional Assembly Analysis . . . . .</b>	<b>273</b>
Edward MORSE and Xiaobin YOU	
15.1. Introduction . . . . .	273

15.2. Representing dimensions and tolerances . . . . .	275
15.3. Geometric tolerances . . . . .	276
15.4. Perfect form tolerance zones . . . . .	279
15.5. Assembly tolerance specification . . . . .	279
15.6. Floating assembly . . . . .	280
15.7. Kinematic assembly . . . . .	282
15.8. Manufacturing dimensioning schemes . . . . .	282
15.9. The revised 2D tolerance chart. . . . .	284
15.10. Parametric representation of the PF-tolerance zone of a CS-feature . . . . .	284
15.11. Surfaces of revolution . . . . .	288
15.12. Nominal dimensions of the CS . . . . .	288
15.13. 1D constraining simplices. . . . .	289
15.14. 2D constraining simplices. . . . .	290
15.15. Case study . . . . .	293
15.16. Conclusion. . . . .	297
15.17. Acknowledgements . . . . .	298
15.18. Bibliography. . . . .	298
<b>PART III. MEASUREMENT. . . . .</b>	<b>299</b>
<b>Chapter 16. Impact of the Sampling Strategy on Geometrical Checking Uncertainties. . . . .</b>	<b>301</b>
Jean MAILHÉ, Jean-Marc LINARES, Jean-Michel SPRAUEL and Jean-Paul RAYNAL	
16.1. Introduction . . . . .	301
16.2. Geometrical verification and virtual gauges . . . . .	302
16.2.1. Verification by virtual gauge without best fit. . . . .	302
16.2.2. Verification with associated feature . . . . .	303
16.2.3. Statistical point of view . . . . .	304
16.3. Field of probability of the presence of matter . . . . .	304
16.4. Virtual gauges . . . . .	306
16.5. Interference probability map . . . . .	308
16.5.1. Geometrical verification process . . . . .	308
16.6. Experiment . . . . .	309
16.6.1. Envelope zone specification. . . . .	309
16.6.2. Perpendicularity specification. . . . .	312
16.7. Conclusion . . . . .	314
16.8. Bibliography . . . . .	315

<b>Chapter 17. Predetermination of Measurement Uncertainty in the Application of Computed Tomography</b> . . . . .	317
Albert WECKENMANN and Philipp KRÄMER	
17.1. Introduction . . . . .	317
17.2. Prior investigations . . . . .	318
17.3. Measurements of user-controllable influences . . . . .	319
17.4. Estimation of influences . . . . .	323
17.5. Calculation of the task-specific measurement uncertainty according to GUM . . . . .	325
17.6. Summary . . . . .	329
17.7. Acknowledgments . . . . .	330
17.8. Bibliography . . . . .	330
 <b>Chapter 18. Application of Function Oriented Parameters for Areal Measurements in Surface Engineering.</b> . . . .	331
Albert WECKENMANN and Özgür TAN	
18.1. Introduction . . . . .	331
18.2. Surface measurements. . . . .	332
18.3. Functional parameters . . . . .	333
18.3.1. 2D functional parameters from ISO 13565-2 . . . . .	333
18.3.2. 3D functional parameters . . . . .	334
18.4. Characterization of the whole application . . . . .	335
18.5. Case study: spreading liquid on metal surfaces . . . . .	336
18.5.1. Step 1: gathering information . . . . .	336
18.5.2. Step 2: modeling the system. . . . .	336
18.5.3. Step 3: application of a functional test. . . . .	337
18.5.4. Step 4: surface requirements . . . . .	341
18.5.5. Step 5: measurement system . . . . .	341
18.5.6. Step 6: functional parameters . . . . .	342
18.6. Conclusions . . . . .	343
18.7. Acknowledgments . . . . .	343
18.8. Bibliography . . . . .	343
 <b>Chapter 19. Validation of a Reception or Production Control Process by the Inertial Indicator <math>I_G</math></b> . . . . .	345
Daniel DURET, Maurice PILLET, Alain SERGENT and Dimitri DENIMAL	
19.1. Introduction . . . . .	345
19.2. Comparison of the “production controls” and “reception controls” approaches . . . . .	346
19.3. Production bias and measure bias . . . . .	348
19.4. Inertial capability. . . . .	348



19.5. Inertia of the control process and inertia of the production process . .	349
19.5.1. Law of composition. . . . .	349
19.5.2. Disturbances due to bias . . . . .	350
19.5.3. Definition of the inertial “ndc” . . . . .	350
19.6. Inertia of the control process and total customer inertia (control of reception). . . . .	352
19.7. Conclusions . . . . .	353
19.8. Bibliography . . . . .	354
<b>Chapter 20. Detection of Areas with Critically Reduced Thickness of Formed Sheet Metal Parts Using Two Oppositely Positioned Fringe Projection Systems . . . . .</b>	<b>355</b>
Albert WECKENMANN and Natasa PETROVIC	
20.1. Introduction . . . . .	355
20.2. Methods . . . . .	356
20.2.1. Measuring system and data fusion . . . . .	356
20.2.2. Methods of data analysis. . . . .	360
20.2.3. Algorithm for the calculation of minimal wall thicknesses. . . . .	362
20.3. Visualization and discussion of results . . . . .	367
20.4. Summary . . . . .	369
20.5. Acknowledgments . . . . .	370
20.6. Bibliography . . . . .	370
<b>Chapter 21. Variability of the Manufacturing Process in the GPS Framework: A Case Study . . . . .</b>	<b>371</b>
Manuela DE MADDIS and Martina GANDINI	
21.1. Introduction . . . . .	371
21.2. Variability sources . . . . .	373
21.2.1. Measurement uncertainty . . . . .	374
21.2.2. Process variability. . . . .	378
21.3. Simulations . . . . .	378
21.3.1. Simulations with independent component analysis (ICA) . . . . .	379
21.4. Simulation with seasonal trend decomposition (STL) . . . . .	382
21.5. Summary . . . . .	383
21.6. Bibliography . . . . .	384
<b>Chapter 22. Virtual CMM-based Sampling Strategy Optimization . . . . .</b>	<b>385</b>
Giovanni MORONI and Stefano PETRÒ	
22.1. Introduction . . . . .	385
22.1.1. Conformance to geometric tolerances . . . . .	386
22.1.2. Evaluating geometric error . . . . .	387
22.1.3. Goals . . . . .	388

22.2. State of the art . . . . .	389
22.3. Proposed methodology . . . . .	390
22.3.1. Evaluation of $C_M$ . . . . .	390
22.3.2. Evaluation of $C_E$ . . . . .	391
22.3.3. Evaluating the uncertainty: the virtual CMM . . . . .	392
22.3.4. Cost function minimization . . . . .	395
22.4. Case study . . . . .	395
22.5. Conclusions . . . . .	399
22.6. Acknowledgments . . . . .	401
22.7. Bibliography . . . . .	401
 <b>Chapter 23. Impact of Workpiece Shape Deviations in Coordinate Metrology</b> . . . . .	 405
Gisela LANZA and Jochen PETERS	
23.1. Introduction . . . . .	405
23.2. Evaluation in coordinate metrology . . . . .	407
23.3. The Jackknife . . . . .	409
23.4. Application to CMM data . . . . .	410
23.4.1. Resampling point clouds . . . . .	410
23.4.2. Influence of single measurement points . . . . .	411
23.4.3. Evaluation uncertainty . . . . .	412
23.4.4. Example of use . . . . .	413
23.5. Simulation . . . . .	415
23.5.1. Simulation procedure . . . . .	415
23.5.2. Simulation results . . . . .	416
23.6. Summary and outlook . . . . .	417
23.7. Bibliography . . . . .	418
 <b>Chapter 24. Quality Assurance of Micro-gears via 3D Surface Characterization</b> . . . . .	 419
Gisela LANZA and Benjamin VIERING	
24.1. Introduction . . . . .	419
24.2. Test specimen and experimental equipment . . . . .	420
24.3. 3D characterization . . . . .	421
24.3.1. Benefits of a 3D characterization . . . . .	421
24.3.2. Approach . . . . .	423
24.4. Summary . . . . .	428
24.5. Acknowledgments . . . . .	428
24.6. Bibliography . . . . .	429

<b>PART IV. TOLERANCING IN THE PLM</b> . . . . .	431
<b>Chapter 25. Geometric Specification at the Beginning of the Product Lifecycle</b> . . . . .	433
Renaud COSTADOAT, Luc MATHIEU, Hugo FALGARONE and Benoît FRICERO	
25.1. Introduction . . . . .	433
25.2. Study of the skeleton . . . . .	436
25.2.1. Presentation of the models used . . . . .	436
25.2.2. Description of the mechanism and first simulations . . . . .	437
25.2.3. Conclusion of the first step . . . . .	441
25.3. Study of the functional surfaces . . . . .	442
25.3.1. Presentation of the models used . . . . .	442
25.3.2. Details of the mechanism and second step of simulation . . . . .	443
25.3.3. Conclusion of the second step . . . . .	450
25.4. Specification . . . . .	450
25.5. Conclusion . . . . .	451
25.6. Bibliography . . . . .	452
<b>Chapter 26. Ontological Model of Tolerances for Interoperability in Product Lifecycle</b> . . . . .	455
Gaurav AMETA and Patrick HOFFMANN	
26.1. Introduction . . . . .	455
26.2. Ontology . . . . .	456
26.2.1. Information modeling as an ontology . . . . .	457
26.2.2. Choice of ontology language . . . . .	457
26.3. Literature survey . . . . .	458
26.4. Ontology of tolerances . . . . .	459
26.5. Example of tolerance ontology instantiation . . . . .	464
26.6. Summary . . . . .	465
26.7. Bibliography . . . . .	466
<b>Chapter 27. A PLM-Based Multi-Sensor Integration Measurement System for Geometry Processing</b> . . . . .	469
Zhao HAIBIN, Nabil ANWER and Pierre BOURDET	
27.1. Introduction . . . . .	469
27.2. Sensor integration methodology . . . . .	471
27.2.1. System framework . . . . .	471
27.2.2. Physical integration of multiple sensors . . . . .	473
27.2.3. Laser guide metrology . . . . .	474
27.3. Ontology modeling in a PLM-context . . . . .	475
27.3.1. Description of ontology modeling . . . . .	476
27.3.2. Ontology modeling in Protégé . . . . .	476

27.4. Geometry processing . . . . .	478
27.4.1. Shape analysis based on the shape index and curvedness . . . . .	478
27.4.2. Quality evaluation. . . . .	479
27.5. Experiments validation . . . . .	480
27.6. Conclusion . . . . .	482
27.7. Acknowledgments . . . . .	483
27.8. Bibliography . . . . .	483
 <b>Chapter 28. Comparison of Gear Geometric Specification</b>	
<b>Models Regarding the Functional Aspect . . . . .</b>	<b>485</b>
Jean-Paul VINCENT, Jean-Yves DANTAN, Gerth GOCH and Régis BIGOT	
28.1. Introduction . . . . .	485
28.2. Specification models. . . . .	489
28.3. Comparison method . . . . .	490
28.3.1. Global approach . . . . .	490
28.3.2. Geometrical modeling . . . . .	492
28.3.3. Virtual meshing simulation . . . . .	493
28.3.4. Virtual metrology . . . . .	495
28.3.5. Evaluation of the kinematic characteristics . . . . .	496
28.4. Criteria comparison . . . . .	497
28.4.1. Objective . . . . .	497
28.4.2. Example. . . . .	497
28.4.3. Comparing the results . . . . .	498
28.5. Conclusion . . . . .	499
28.6. Bibliography . . . . .	502
 <b>Chapter 29. Effects of Geometric Variation</b>	
<b>on Perceived Quality . . . . .</b>	<b>503</b>
Karin FORSLUND and Rikard SÖDERBERG	
29.1. Introduction . . . . .	503
29.1.1. Types of robustness. . . . .	504
29.1.2. The product experience. . . . .	505
29.1.3. Perceived quality of non-nominal products . . . . .	505
29.1.4. Design as a process of communication . . . . .	506
29.2. A framework for describing visual robustness	
to geometric variation . . . . .	507
29.2.1. Visual reference level. . . . .	508
29.2.2. Optical level . . . . .	511
29.2.3. Perception level . . . . .	512
29.2.4. Response level . . . . .	513

29.3. Visual fit complexity assessment method . . . . .	511
29.4. Discussion and conclusions . . . . .	517
29.5. Bibliography . . . . .	518
<b>Chapter 30. Geometric Requirement Variations Throughout the Product Lifecycle</b> . . . . .	521
Guillaume MANDIL, Alain DESROCHERS and Alain RIVIÈRE	
30.1. Introduction . . . . .	521
30.2. Literature review . . . . .	522
30.2.1. Related standards . . . . .	522
30.2.2. Related research . . . . .	522
30.3. Definitions and concepts . . . . .	523
30.3.1. Dimensions . . . . .	523
30.3.2. Functional requirements . . . . .	524
30.4. Functional requirements throughout lifecycle stages . . . . .	525
30.4.1. General principles . . . . .	525
30.4.2. Computational rules . . . . .	527
30.5. Case study: a simple 1D crosshead guide . . . . .	531
30.5.1. Hypothesis . . . . .	531
30.5.2. Dimension driven calculation . . . . .	533
30.5.3. Functional requirement driven calculation . . . . .	535
30.5.4. Geometry driven calculation . . . . .	537
30.6. Conclusion and perspectives . . . . .	539
30.6.1. High level management of functional requirements . . . . .	539
30.6.2. Further work . . . . .	540
30.7. Acknowledgments . . . . .	540
30.8. Bibliography . . . . .	541
<b>List of Authors</b> . . . . .	543
<b>Index</b> . . . . .	549

## Preface

Computer-aided tolerancing (CAT) is an important topic in the field of mechanical design and production manufacturing.

Every two years, since 1981, the CIRP (International Institution for Production Engineering Research) has organized a seminar on “CAT”. In 2009, this CAT seminar became the CAT Conference. Control of the geometric quality is essential in the whole product lifecycle management (PLM), from the expression of functional requirements to recycling. The necessity of optimizing design and manufacturing processes, saving materials and energy, guaranteeing safety, always respecting more numerous functional constraints, imposes an increased rigor in the control process of the product geometric quality.

Previous research in the field of tolerancing is particularly focused on the modeling for the calculation assessment of 3D specifications, or on the processes of production and inspection. We should not forget that these various aspects are connected and impose a global vision of the “chain of the geometric quality” in the PLM.

The previous conferences made it possible to show the advances in these various domains and their applications for systems of CAT. This 2009 CAT conference tried to extend those preoccupations to the entire global product life cycle.

The subject of the present book *Product Lifecycle Management* focuses on the importance of geometric product quality interconnected in design, production manufacturing and inspection processes. In any design project development, the cost of design change increases with project time quasi-exponentially. To reduce costs, design parameters that influence the geometric quality must be defined and their influence must be known.

Increasingly realistic simulation software must be used with the best parameters and coherent data for all the process stages of design, manufacturing, assembly and inspection.

This book is an excellent resource for anyone interested in CAT, and it is intended for a wide audience, including:

- researchers in the fields of product design, computer-aided process planning, precision engineering, inspection, quality, inspection and dimensional and geometric tolerancing;
- teachers, instructors and students of design courses that are offered either for degrees by universities and technical schools, or for professional development through commercial short-courses;
- practitioners of design, design engineers, manufacturing engineers, staff in R&D and production departments at industries that make mechanical components and machines;
- software developers for CAD/CAM/CAX and CAT application packages;
- technicians and engineers of standardization, who are interested in the evolving ISO standards for tolerancing in mechanical design, manufacturing, and inspection;
- individuals interested in design, assembly, manufacturing, precision engineering, inspection, and CAD/CAM.

Following the editor's preface, the book is organized into 4 parts:

- tolerance analysis and synthesis;
- simulation of assemblies;
- measurement;
- tolerancing in the PLM.

Although some chapters cover far more than one topic, due to the general theme of the conference, we have chosen the most representative topics to include in this book. These have been classified according to the most representative themes.

Part I focuses on the more general problems of tolerance analysis and synthesis, for tolerancing in mechanical design and manufacturing processes, including statistical tolerancing approaches, for the management of the quality connected to manufacturing. A large number of papers were presented on this important topic, only the most representative have been selected for this book.

Part II specifically highlights the simulation of assemblies with defects, and the influence of tolerances on the quality of the assembly. Several cases are considered such as the case of non-rigid parts or assemblies of parts taking into account the form defects.

Part III deals with measurement aspects, which are, of course, crucial to quality control throughout the lifecycle. Different measurement technologies and methods for estimating uncertainty are considered.

In Part IV, different aspects of tolerancing and their interactions are explored, from the definition of functional requirement to measurement processes in a PLM approach.

As editors, we wish to express our sincere gratitude to the authors for their contributions; the members of the international program committee and the organizing committee; the additional reviewers and our colleagues from the French Research Group in Tolerancing (GRT) for their efforts in getting this book published.

Max GIORDANO  
University of Savoy

François VILLENEUVE  
Grenoble University

Luc MATHIEU  
ENS Cachan, University of Paris XI

August 2010



PART I

Tolerance Analysis and Synthesis

## Chapter 1

# A New Method of Expressing Functional Requirements and How to Allocate Tolerance to Parts

This chapter proposes a new approach for expressing the functional requirement, based on the non-quality cost that can be non-symmetrical if necessary. This is very realistic from the point-of-view of functional requirements. Then a link between mean and variance of the functional dimension is identified for a chosen loss cost. Specifications on parts are expressed in a system of inequalities that link the means and variances of the functional dimensions. It is then possible to allocate the functional requirements on parts. To illustrate the concept, the case of application with unidirectional tolerancing is presented. The results are compared to the usual tolerancing approaches.

### 1.1. Introduction

When dealing with assembly tolerance synthesis, several key points can be identified such as the expression of the functional requirements, the identification of the dimension chains and then the allocation of the component tolerances. In this chapter, it is assumed that the dimension chains are identified, hence two key points are focused upon: the expression of the assembly functional requirements and the allocation of the tolerances for the assembly components.

---

Chapter written by Pierre-Antoine ADRAGNA and Pascal HERNANDEZ.

The first part of this chapter is a short review of some existing statistical tolerancing methods. Two approaches are presented, traditional statistical tolerancing using tolerance interval, and inertial tolerancing. For each approach, their capability indices and several tolerancing methods are presented. In order to compare the different tolerancing methods, statistical tolerance zones and their composition are used. The case of application is also presented. It is based on a five component stack up, for which the functional requirement is a unidirectional combination of the component dimensions.

The second part of this chapter presents a new approach to the expression of the functional requirements and how to allocate component tolerances. The first key point concerning the functional requirement is presented. The functional requirements can either be symmetrical as usual or asymmetrical if necessary. Depending on the assumption of the assembly resultant distribution, the functional requirement can be transcribed into inequalities on the assembly resultant mean and variance. The second key point dealing with the allocation of the functional requirement on the assembly components is also presented in this first part. The only strategy presented here aims to maximize the variances of components.

The case of application illustrates all the presented tolerancing methods in the first and the second part, and performance indices are presented to compare the efficiency of the methods. The chapter then ends with a short discussion.

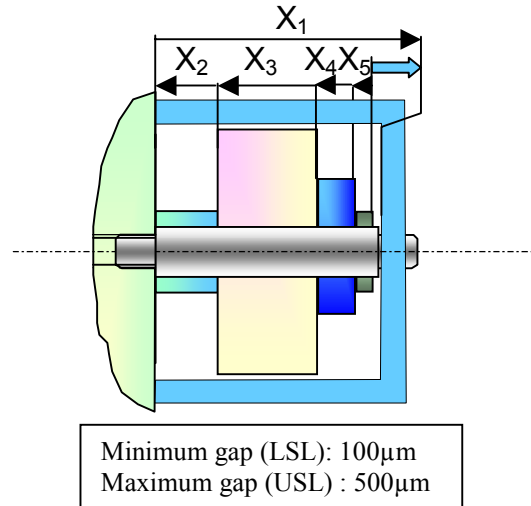
## **1.2. Brief review**

This section presents the case of application and the statistical tolerance zone that are used to compare the different tolerancing approaches. The section then deals with some existing methods of statistical tolerancing with tolerance intervals.

### **1.2.1. *How to compare***

The following presents the application to which the tolerancing methods are applied, and a technique for tolerance analysis that enables us to qualify the efficiency of the tolerancing method.

#### 1.2.1.1. The case of application



**Figure 1.1.** The case of application

To illustrate the proposed method, a five component stack up is chosen as an application case. This mechanical example also enables us to apply and compare the existing tolerancing approaches briefly presented in this part. The functional requirement of the assembly mechanism is composed of two limits:

- a minimum gap of 100 μm, to allow the free rotation of the inner parts, then the good working condition of the mechanism;
- a maximum gap of 500 μm, to minimize the free translation of the inner parts, thus to minimize the noise while shaking the mechanism.

#### 1.2.1.2. Statistical tolerance zones

In order to graphically compare the tolerance allocation results of the different tolerancing methods, the statistical tolerance zones (STZ) and their composition are used. This technique proposed by [SRI 97] allows us to describe each tolerance by a domain in the  $(\mu, \sigma)$  plane. Within the  $(\mu, \sigma^2)$  plane, it is possible to convolute the domain of the possible deviation of the assembly resultant given the tolerance domain of the components. The assembly resultant domain can then be compared to its functional requirement domain. This method is used in this chapter to compute the assembly resultant domain for each tolerancing method.

This technique allows us to graphically compare each tolerancing method result to the functional requirement, and it is more interesting to compare one to the other. Two indices are introduced to qualify the efficiency of the tolerancing methods:

- $R_{NC}$ , the ratio of the non-conforming area, that compares the area of the assembly resultant domain out of the functional requirement domain to the functional requirement domain area.
- $R_{exp}$ , the exploitation ratio that compares the area of the assembly resultant domain inside the functional requirement domain to the functional requirement domain.

If the  $R_{NC}$  index equals 0, this means that the tolerancing approach offers no non-conforming configuration, thus it is a no-risk tolerancing method. If the  $R_{exp}$  index equals 1, this means that the entire assembly functional requirement domain is exploited by the tolerancing method. If the index  $R_{NC}$  equals 0 and  $R_{exp}$  equals 1, the result of the tolerancing approach perfectly fits the functional requirement domain.

### 1.2.2. Statistical tolerancing methods

The statistical tolerancing methods presented in this second section are applied to the symmetrical functional requirement. The functional requirement is expressed to take into account a non-conformity rate on each functional limit. The chosen maximum rate is  $NCR_{Max} = 1,350$  ppm on each limit. Considering a normal distribution of the assembly resultant, this is the equivalent of taking into account a capability index  $Cpk_{FR} = 1$ .

#### 1.2.2.1. Traditional statistical tolerancing

This is the most common approach, where the statistical tolerances of components are expressed by tolerance intervals.

##### 1.2.2.1.1. Capability indices

In the case of traditional tolerancing, we can identify three main capability indices [KOT 93]:

- the  $Cp$  index that compares the variance of the batch to the tolerance interval:

$$Cp = \frac{USL - LSL}{6.\sigma} \quad [1.1]$$

– the  $Cpk$  index that indicates the rate of the batch that lies within the tolerance interval, but does not indicate the centering of the batch:

$$Cpk = \min\left(\frac{\mu - LSL}{3\sigma}; \frac{USL - \mu}{3\sigma}\right) \quad [1.2]$$

– the  $Cpm$  index, also called the Taguchi capability index, that indicates the centering of the batch within the tolerance interval:

$$Cpm = \frac{USL - LSL}{6\sqrt{\left(\mu - \frac{USL + LSL}{2}\right)^2 + \sigma^2}} \quad [1.3]$$

#### 1.2.2.1.2. Tolerancing methods

Let us consider the following notation:

–  $IT_{FR}$ , the tolerance interval of the functional requirement,

$$IT_{FR} = USL - LSL \quad [1.4]$$

–  $n$ , the number of component in the dimension chain.

The three main traditional statistical tolerancing approaches are:

– classic statistical tolerancing [EVA 75]:

$$IT_i = \frac{IT_{FR}}{\sqrt{n}} \quad [1.5]$$

– inflated statistical tolerancing, where  $f$  is a constant value around 1.5 to 1.6 [GRA 01] and [GIL 51]:

$$IT_i = \frac{IT_{FR}}{f\sqrt{n}} \quad [1.6]$$

– “semi-quadratic” tolerancing where the component characteristics  $(\mu, \sigma)$  are independently toleranced: 1/4 and 3/4 of a tolerance interval respectively [ANS 03]:

$$IT_i = \frac{IT_{FR}}{\sqrt{n}} \quad [1.7]$$

1.2.2.2. *Inertial tolerancing*

[PIL 04] proposes a single criterion  $I$  that combines the batch characteristics  $(\mu, \sigma)$  based on the Taguchi loss function and the batch inertia:

$$I = \sqrt{\left(\mu - \frac{USL + LSL}{2}\right)^2 + \sigma^2} \quad [1.8]$$

Thus, the inertial criterion qualifies the batch centering.

## 1.2.2.2.1. Capability indices

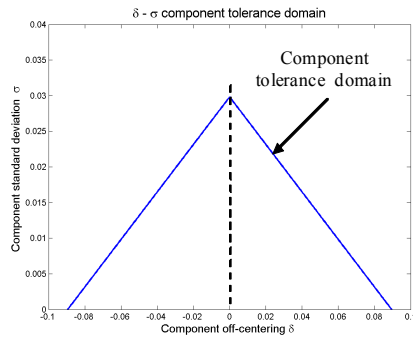
Two capability indices are defined:

– the  $C_p$  index that, similarly to the traditional  $C_p$  index, compares the batch standard deviation to the tolerance:

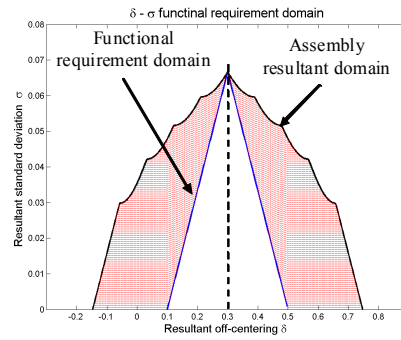
$$C_p = \frac{I}{\sigma} \quad [1.9]$$

– the  $C_{pi}$  index that compares the batch off-centering to the inertial tolerance:

$$C_{pi} = \frac{I}{\sqrt{\left(\mu - \frac{USL + LSL}{2}\right)^2 + \sigma^2}} \quad [1.10]$$

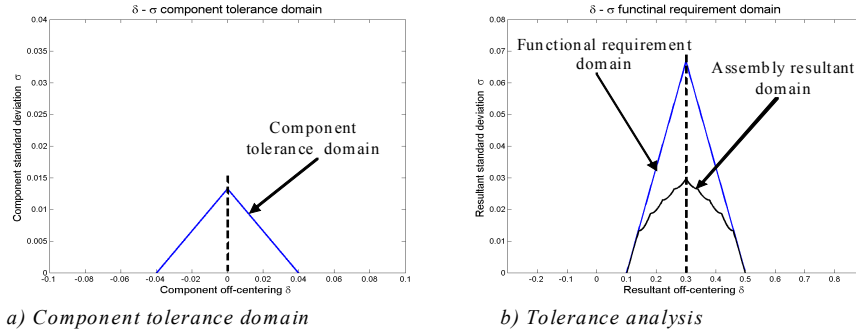


a) Component tolerance domain

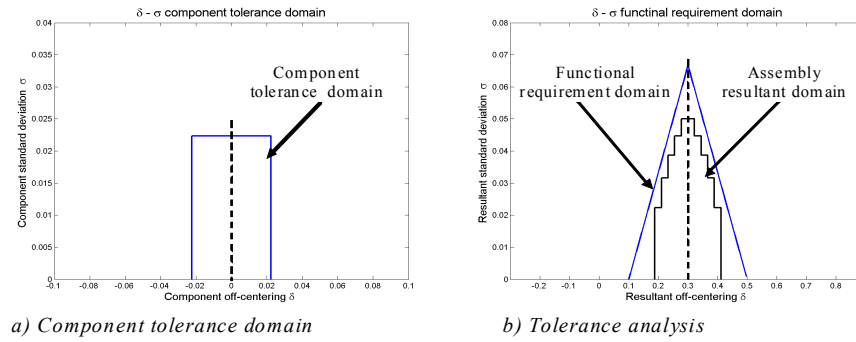


b) Tolerance analysis

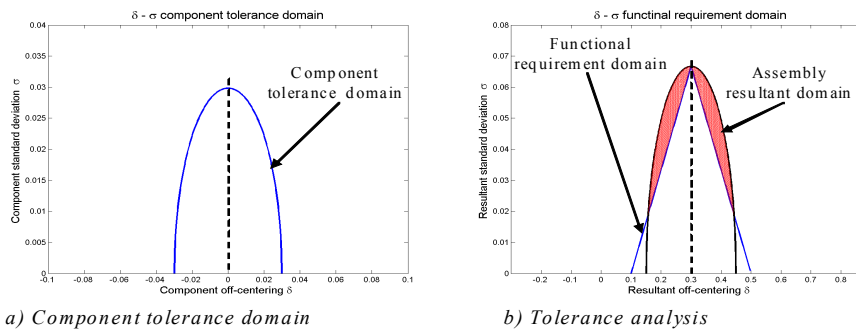
**Figure 1.2.** Tolerance analysis of the classic statistical tolerancing,  
 $R_{NC} = 1.83$  and  $R_{exp} = 1$



**Figure 1.3.** Tolerance analysis of the inflated statistical tolerancing,  
 $R_{NC} = 0$  and  $R_{exp} = 0.56$

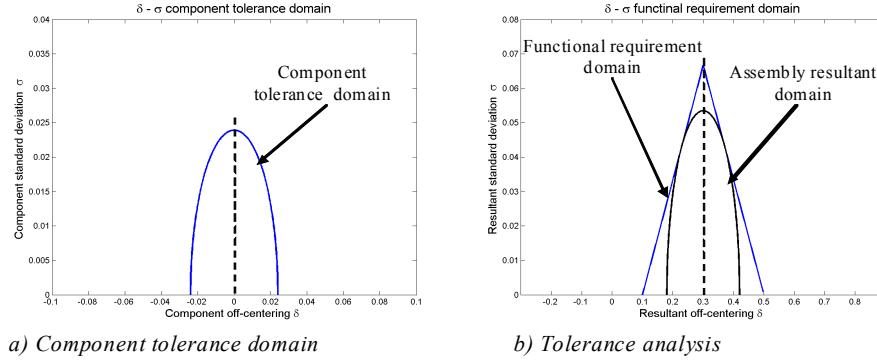


**Figure 1.4.** Tolerance analysis of the "semi-quadratic" tolerancing,  
 $R_{NC} = 0$  and  $R_{exp} = 0.57$



**Figure 1.5.** Tolerance analysis of the classic inertial tolerancing,  
 $R_{NC} = 0.24$  and  $R_{exp} = 0.92$





**Figure 1.6.** Tolerance analysis of the adjusted inertial tolerancing,  
 $R_{NC} = 0$  and  $R_{exp} = 0.75$

#### 1.2.2.2.2. Capability indices

Two main inertial tolerancing methods are proposed:

– classic inertial tolerancing:

$$I_i = \frac{IT_{FR}}{6 \cdot \sqrt{n}} \quad [1.11]$$

– adjusted inertial tolerancing, where  $I_C$  depends on the functional requirement expressed by a tolerance interval and a  $Cpk_{FR}$  index [ADR 06], or a non-conformity-rate  $NCR_{FR}$  [ADR 07]:

$$I_i = \frac{IT_{FR}}{6 \cdot I_C \cdot \sqrt{n}} \quad [1.12]$$

### 1.3. Proposed method

This section presents the new approach for the expression of the functional requirements and a strategy to allocate the functional requirements on the components of the assembly dimension chains.

### 1.3.1. Functional requirements

#### 1.3.1.1. Expression of the functional requirement

Generally, the functional requirement is specified by a bilateral tolerance. The quality of the assembly product is considered as acceptable if the assembly characteristic lies within the functional tolerance. In the common case, the bilateral tolerance is characterized by a target and a tolerance interval around this target. This implies that the target, corresponding to the middle of the bilateral tolerance, is the optimal value assembly resultant.

Here another point-of-view is presented. Instead of identifying the target value of the functional requirement, our approach consists of identifying the limits of the functional requirement. The limits of the functional requirement are given by the function of the assembly product, for instance: a minimum or a maximum limit on a gap. A non-conformity loss cost is associated with the functional limit. In the case of bilateral limits, loss costs can either be equal or not, depending on how critical the limit is. For instance, we can imagine three critical levels:

- the first level, with the lower loss cost, corresponds to a performance loss but the assembly mechanism still works;
- the second level, with a higher loss cost, corresponds to a non-working or non-assembling mechanism;
- the third and most critical level, with the highest loss cost, corresponds to a safety limit that guarantees the safety of the product user.

Of course, these levels are just examples and we can identify others. Once the levels have been identified, the designer has to set the financial loss corresponding to each level. An example is given with the case of application.

Let us define the cost associated with a single non-conforming product  $L_{NC}$  in the case of a symmetrical functional requirement. The cost of a single non-conforming product is  $L_{NC,LSL}$  if the  $LSL$  is not taken into account, otherwise  $L_{NC,USL}$ . The average loss of a functional limit is the cost of non-conforming product times the probability of making non-conforming product.

Figure 1.7 shows the two functional loss costs:

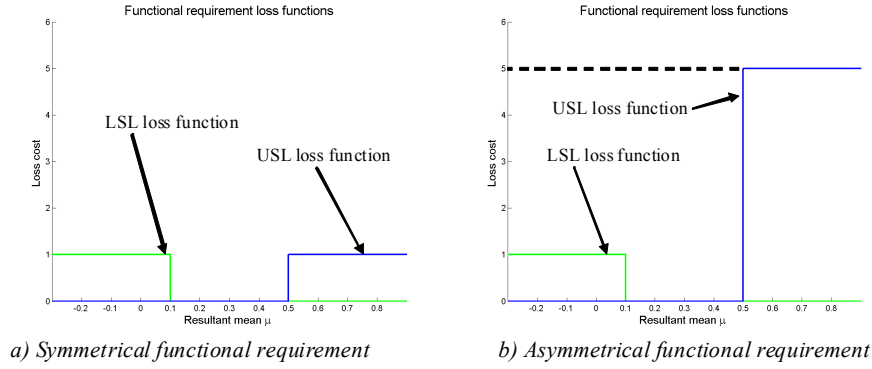
- a symmetrical loss cost of the less critical level, both  $L_{NC,i} = 1$ ;
- an asymmetrical loss cost,  $L_{NC,LSL} = 1$  is the lowest critical level, and  $L_{NC,USL} = 5$  corresponds to the second critical level.

In the general case of an asymmetrical functional requirement, the average losses are:

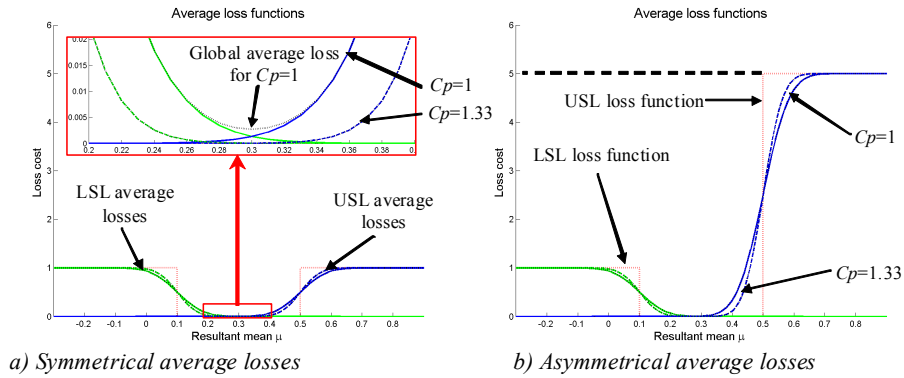
$$\overline{L}_{NC,LSL} = L_{NC,LSL} \cdot P(Y < LSL) \quad [1.13]$$

$$\overline{L}_{NC,USL} = L_{NC,USL} \cdot P(Y > USL) \quad [1.14]$$

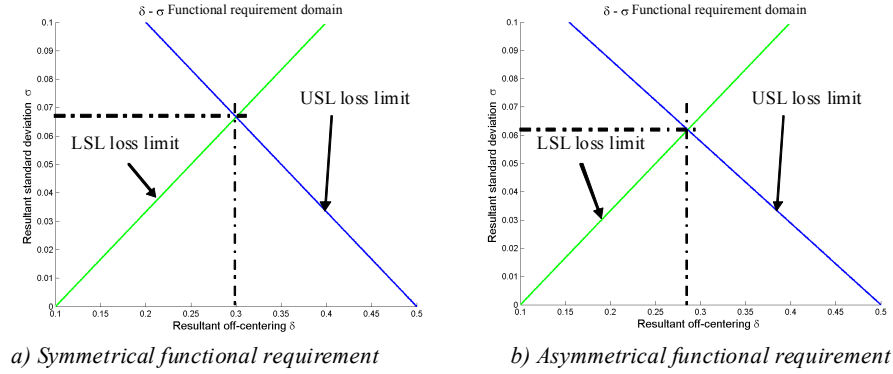
The main approach while dealing with loss costs is to evaluate the global average loss that is the combination of all average losses [DEN 06]. Our approach consists of considering each average loss independently in order to respect each functional requirement limit. Moreover, this approach enables us to avoid dependence between cost losses of the functional requirement.



**Figure 1.7.** a) Symmetrical loss function, b) asymmetrical loss function



**Figure 1.8.** The average and global losses for  $Cp=1$  and  $Cp=1.33$



**Figure 1.9.** Domain of the functional requirement characteristics for the given budget loss

### 1.3.1.2. Functional requirement and statistics

Dealing with statistical tolerancing, the distribution law of the assembly resultant has to be estimated. Let us make the assumption of a normal distribution on the assembly functional dimension. This assumption may not be far from reality:

- if the components of the assembly are normally distributed, then the assembly resultant is normally distributed;
- if the dimension chain contains several components of the same range of dispersion, and given the central limit theorem, the assembly resultant is normally distributed.

Hence, given the statistical characteristics of the assembly resultant, it is possible to evaluate the average loss cost on each functional requirement limit. Figure 1.8 [GRA 00] shows the variation of the averages loss costs for each functional limit depending on the assembly resultant variance,  $\sigma$  ( $Cp = 1$  and  $1.33$ ), and the position of the mean dimension,  $\mu$ . The objective is to identify the  $(\mu, \sigma)$  characteristics that keep each loss cost below the budget loss  $L_B$ . Here, the loss budget  $L_B$  is arbitrarily chosen such that the lowest critical level implies 1,350 ppm of  $NCR$ . Thus:

$$L_B = \frac{L_{NC,1}}{1350} = 7.41 \times 10^{-4} \quad [1.15]$$

where  $L_{NC,1} = 1$  is the loss cost of the first critical level. Therefore, the second level implies a  $NCR$  of 270 ppm, which is five times smaller.

### 1.3.1.3. *The functional requirement domain*

Given the objective loss budget, it is possible to evaluate the limit in the  $(\mu, \sigma)$  plane where the loss cost equals the budget. Figure 1.9 illustrates each functional requirement limit for the given budget. We can observe the linear relation between the functional requirement characteristics. In fact the functional requirement limits can be written as:

$$\mu + k_{USL} \cdot \sigma \leq USL \quad [1.16]$$

$$\mu - k_{LSL} \cdot \sigma \geq LSL \quad [1.17]$$

That can also be expressed similarly to the  $Cpk$  index as:

$$\text{Min} \left( \frac{\mu - LSL}{k_{LSL} \cdot \sigma}, \frac{USL - \mu}{k_{USL} \cdot \sigma} \right) \geq 1 \quad [1.18]$$

In the case of normal distribution, the  $k_i$  constants can be expressed as:

$$k_{USL} = P^{-1} \left( 1 - \frac{2 \cdot L_B}{L_{NC, USL}} \right) = 3.46 \quad [1.19]$$

$$k_{LSL} = P^{-1} \left( 1 - \frac{2 \cdot L_B}{L_{NC, LSL}} \right) = 3 \quad [1.20]$$

### 1.3.2. *The tolerancing strategy*

This part considers that the functional requirements are expressed and the associated domain is defined. One strategy is presented for the components tolerance allocation. The aim is to allocate the maximum variance on the component of the dimension chain; two steps can be identified:

- identification of the optimal target and allocation of the components variances;
- determination of the components tolerance domains.

### 1.3.2.1. Maximum variance allocation

The maximum variance of the functional requirement  $\sigma_{FR, Max}$  is found for the intersection of the functional requirement limits. This enables us to identify the target of the functional requirement.

– In the case of a symmetrical functional requirement, the target corresponds to the middle of the functional tolerance interval:

$$T = \frac{USL + LSL}{2} = 300\mu m \quad [1.21]$$

– In the case of an asymmetrical functional requirement, the optimal target is:

$$T = \frac{k_{USL} \cdot LSL + k_{LSL} \cdot USL}{k_{USL} + k_{LSL}} = 286\mu m \quad [1.22]$$

It is now possible to evaluate the maximum variance of the functional requirement  $\sigma_{FR;Max}$ . Considering the components in the dimension chain as independent, the uniform variance allocation is made as follows:

$$\sigma_{i,Max} = \frac{\sigma_{FR,Max}}{\sqrt{n}} \quad [1.23]$$

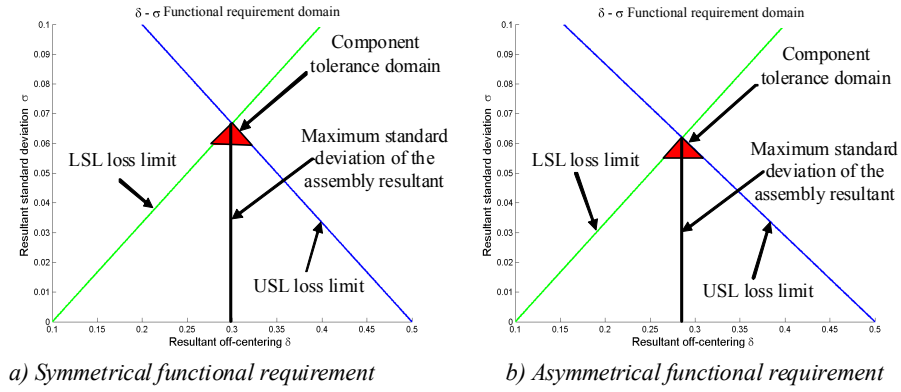
### 1.3.2.2. The component tolerance domain

The functional requirement target and maximum variance are identified and allocated to components. The big deal now is to identify the component tolerance domain. The identification of a component tolerance domain consists of:

- considering all other components of the dimension chain on their target and at their maximum variance;
- the component tolerance domain is the possible variation domain that respects the functional requirement.

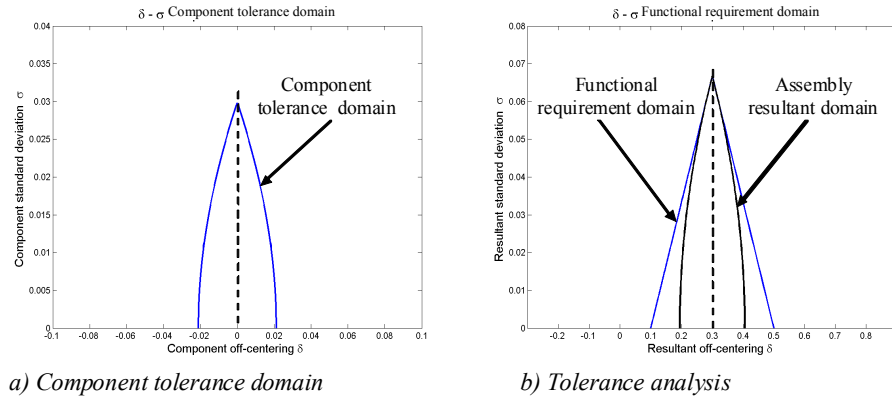
Figure 1.10 illustrates the component tolerance domain. The tolerance domain of the  $i^{th}$  component can then be expressed as:

$$\text{Min} \left( \frac{\mu_i - LSL}{k_{LSL} \cdot \sqrt{\sigma_i^2 + \sum_{j \neq i} \sigma_{j,Max}^2}}, \frac{USL - \mu_i}{k_{USL} \cdot \sqrt{\sigma_i^2 + \sum_{j \neq i} \sigma_{j,Max}^2}} \right) \geq 1 \quad [1.24]$$

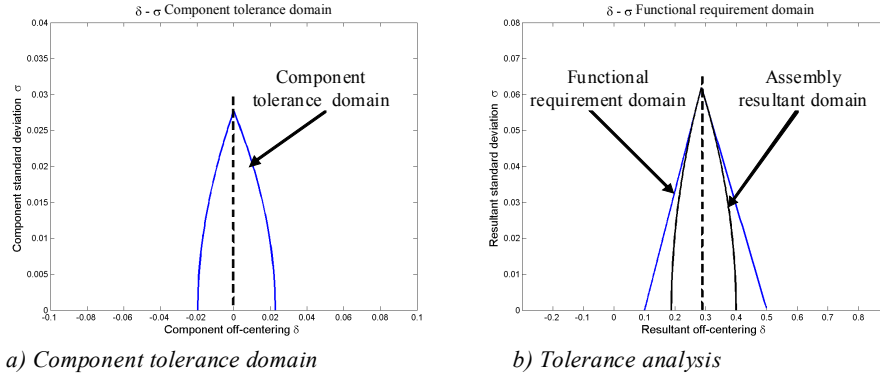


**Figure 1.10.** Maximum variance allocation and identification of the component tolerance domain

Figures 1.11 and 1.12 illustrate the analysis of this tolerancing approach for both functional requirements. In both cases, symmetrical or asymmetrical functional requirement, the  $R_{NC}$  indices are null. This shows that the proposed method absolutely takes into account the functional requirement.



**Figure 1.11.** Tolerance analysis of the proposed tolerancing method in case of symmetrical functional requirement,  $R_{NC} = 0$  and  $R_{exp} = 0.70$



**Figure 1.12.** Tolerance analysis of the proposed tolerancing method in case of asymmetrical functional requirement,  $R_{NC} = 0$  and  $R_{exp} = 0.70$

#### 1.4. Discussion

This section briefly discusses a demonstration of the efficiency of the proposed tolerancing approach, and its comparison to existing tolerancing methods.

##### 1.4.1. Efficiency of the proposed method

Here we do not give the demonstration of the efficiency of the method, we just give the idea.

The idea is that all components of the dimension chain take into account the tolerance domain, given by [1.24]. Then the assembly resultant of the dimension chain automatically accounts for the functional requirement expressed by [1.18]. Figures 1.11 and 1.12 illustrate that purpose for two particular cases.

##### 1.4.2. Comparison to existing approaches

Two key points will be discussed: the expression of the functional requirement, and the expression of the component tolerance domains. Then a general discussion about the efficiency will be proposed.

###### 1.4.2.1. The functional requirement

The solution proposed here to express the functional requirement by a loss cost can be seen as a globalization of the more common method using NCR. As the reader may have seen, the loss costs are linked to the NCR. Hence, it may seem



simpler to express the functional requirement by NCRs instead of loss cost level. It is just a matter of translation. Moreover, the most frequent expression of statistical functional requirement is based on NCR.

#### 1.4.2.2. *The tolerance domain*

The component tolerance domain of the proposed method is interesting because it links the component characteristics ( $\mu_i, \sigma_i$ ) to the assembly functional requirement ( $k_{LSL}, LSL, k_{USL}, USL$ ). The tolerancing approach is then logical with the statistical tolerance synthesis:

- the component standard deviations ( $\sigma_{i,Max}$ ) are allocated from the maximum standard deviation of the assembly resultant ( $\sigma_{FR,Max}$ );
- the component tolerance domain is also allocated from the assembly resultant functional requirement.

#### 1.4.2.3. *Efficiency comparison*

Illustrated by this case of application, we can note that the classic statistical tolerancing without precaution is not appropriate at all [GRA 00]. The classic inertial tolerancing offers some non-conforming configurations that can be avoided with the use of the *Cpi* capability index.

The other tolerancing methods seem to correctly allocate tolerances to components in this particular case. However, that is not the case for any dimension chain. For some tolerancing methods:

- with 6 components or more, the inflated statistical tolerancing using  $f = 1.5$  offers some non-conforming configurations;
- with 7 components or more, the inflated statistical tolerancing using  $f = 1.6$  offers some non-conforming configurations;
- with 9 components or more, the “semi-quadratic” tolerancing offers some non-conforming configurations.

On the contrary, the adjusted inertial tolerancing and the proposed tolerancing method absolutely takes into account the functional requirements for any number of components in the dimension chain.

Moreover, comparing the  $R_{exp}$  index that indicates how much of the functional requirement domain is exploited, we can note that the adjusted inertial tolerancing and the proposed method are better than the other method.

In order to differentiate these two efficient tolerancing methods, we can say that:

- the proposed approach perfectly fits the idea of tolerance allocation (allocation of component variance and tolerance domain);
- the adjusted inertial tolerancing modifies the existing components tolerance domain with the use of a homothetic transform for which the ratio is based on the functional requirement.

Although the results are similar (functional requirements are perfectly respected and highly exploited), the idea is different.

### 1.5. Bibliography

- [ADR 06] ADRAGNA P.-A., PILLET M., SAMPER S., FORMOSA F., “Inertial tolerancing guarantying a cpk index on the final characteristic in an assembly production”, *6<sup>th</sup> International Conference on Integrated Design and Manufacturing in Mechanical Engineering*, IDMME, Grenoble, France, 2006.
- [ADR 07] ADRAGNA P.-A., PILLET M., SAMPER S., FORMOSA F., “Guarantying a maximum of non-conformity rate on the assembly resultant with a statistical tolerancing approach”, *10<sup>th</sup> CIRP Conference on Computer Aided Tolerancing*, CAT, Erlangen, Germany, 2007.
- [ANS 03] ANSELMETTI B., RADOUANI R., “Calcul statistique des chaînes de cotes avec des distributions hétérogènes non indépendantes”, *Revue Internationale de CFAO et d’Infographie*, Vol. 18, No 3, pp. 303-319, 2003.
- [DEN 06] DENNISTON B., “Capability indices and conformance to specification: the motivation for using cpm”, *Quality Engineering*, Vol. 18, No. 1, pp. 78-88, 2006.
- [EVA 75] EVANS D. H., “Statistical tolerancing: the state of the art”, *Journal of Quality Technology*, Vol. 7, No. 1, pp.1-12, 1975.
- [GIL 51] GILSON J., *A New Approach to Engineering Tolerances*, The Machinery Publishing Co., LTD, London, pp. 42-48, 1951.
- [GRA 00] GRAVES S., BISGAARD S., “Five way statistical tolerancing can fail, and what to do about them”, *Quality Engineering*, Vol. 13, No. 1, pp. 73-82, 2000.
- [GRA 01] GRAVES S., “Tolerance analysis tailored to your organization”, *Journal of Quality Technology*, Vol. 33, No. 3, pp. 293-303, 2001.
- [KOT 93] KOTZ S., JOHNSON N. L., *Process Capability Indices*, Chapman and Hall, 1993.
- [PIL 04] PILLET M., “Inertial tolerancing”, *The Total Quality Management Magazine*, Vol. 6, No. 3, pp. 202-209, 2004.
- [SRI 97] SRINIVASAN V., O’CONNOR M.A., SCHOLZ F.W., “Techniques for composing a class of statistical tolerance zones”, *Advanced Tolerancing Techniques*, John Wiley & Sons, pp. 139-165, 1997.

## Chapter 2

# A Parametric Approach to Determine Minimum Clearance in Overconstrained Mechanisms

The need to introduce minimum clearances into an overconstrained mechanism in order to make it actually work, results from the observation of a physical effect. We will call it the clearance effect. The clearance effect transforms an overconstrained model that is perfectly accurate but impracticable, into a realistic, but limited accuracy, model.

We will first present vectorial modeling of a mechanism which enables us to generate a set of relations between the dimensional parameters of each part and the movement parameters of each joint; this equations system will represent the studied mechanism. Next, we will analyze this equations system, making a clear distinction between dimension and movement parameters, because we know that movement parameters may adjust naturally and instantaneously to slight variations in the dimension parameters of the machining parts.

We propose to explicitly determine the minimum clearance values that are absolutely necessary for assembly, or mobility in cases where the mechanism is mobile. The method will be illustrated for an instance of a given mechanism (all the actual dimensions of manufactured parts are known with a high degree of accuracy). For this purpose, two new concepts will be defined: firstly the ideal mechanism and secondly the associated mechanism. These two concepts come from metrology and

---

Chapter written by Philippe SERRÉ, Faïda M'HENNI, André CLÉMENT.

tolerancing languages. In fact, ideal mechanism defines the class of mechanism composed of ideal or machining parts and ideal joints (without clearance). The associated mechanism defines the closest ideal mechanism associated with the set of studied machining parts. It is a similar concept to “associated surfaces” used in the metrology field.

## 2.1. Introduction

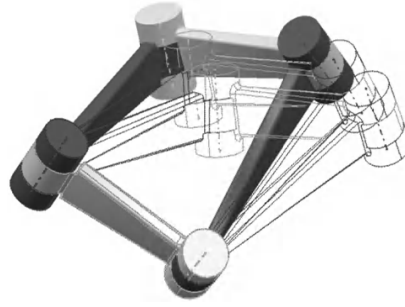
During the design stage, an engineer wishes to characterize a mechanism using a set  $s$  of functional parameters called “specification parameters”. These parameters  $s_i$  are distances or angles between geometric elements, mechanical resistance, speed, acceleration, mass or cost, etc. Unfortunately, for several reasons, these  $s_i$  specification parameters chosen by the designer do not univocally define the required mechanism. There are sometimes too few, in this case the mechanism is not fully defined, or too many, in this case the mechanism is functional only when parameter values are intercompatible. In other cases, specification parameters appear to be independent but are not, and the mechanism cannot, therefore, be constructed (throughout this chapter, the word mechanism means a mobile assembly, whereas an assembly is simply an association of parts).

The objective of this chapter is to present a method to assist engineers during the tolerancing parameter specification stage. Primarily, the provided assistance indicates whether specifications are complete and consistent. In particular, it gives the compatibility relations that must exist between one another in overconstrained problems. Finally, this method will enable the designer to determine the minimum clearance in the joints to ensure interchangeability of the production components.

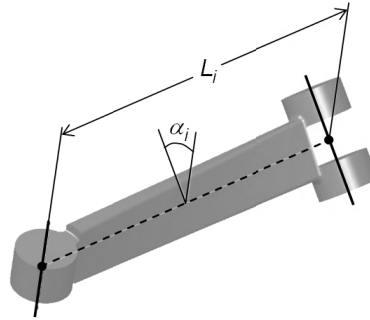
Presentation of the method is divided into two parts. The first one shows the vectorial modeling of the geometric problem. The second part presents techniques used to express compatibility relations between the variations of the specification parameters, to allow either the assemblability or the mobility of a studied mechanism. The article ends with section 2.3, dedicated to the definition of a framework. This is used to calculate the necessary minimum clearance in overconstrained and mobile mechanisms.

Throughout this chapter, the proposed method is illustrated by the Bennett linkage (). It is a spatial single degree of freedom mechanism consisting of four bars connected by revolute joints. This is an overconstrained mechanism. Although the mechanism has been used as a basic module to form large deployable structures for aerospace applications, interesting fundamental questions regarding its geometric variations still exist. Each of the bars is specified by two geometric parameters: the

common perpendicular length between the revolute joints axes and the angle between these axes. Representation of one bar is given in Figure 2.2.



**Figure 2.1.** *Bennett linkage*



**Figure 2.2.** *Specification parameters of i-th bar*

The nominal dimensions of the studied mechanism are set out in Table 2.1

Bar 1	$L_1 = 1 \text{ dm}$	$\alpha_1 = 30^\circ$
Bar 2	$L_2 = \sqrt{3} \text{ dm}$	$\alpha_2 = -60^\circ$
Bar 3	$L_3 = 1 \text{ dm}$	$\alpha_3 = 30^\circ$
Bar 4	$L_4 = \sqrt{3} \text{ dm}$	$\alpha_4 = -60^\circ$

**Table 2.1.** *Nominal values of Bennett linkage*

Note that lengths are positive and angles vary between  $-180^\circ$  and  $180^\circ$ . The positive sign (negative resp.) of  $\alpha_i$  means that the scalar triple product of the three direction vectors:

- the joint axis between bars  $i-1$  and  $i$ ,
- the joint axis between bars  $i$  and  $i+1$ ,
- the common perpendicular (the way is defined from bar  $i-1$  towards bar  $i+1$ ),

taken in this order, is positive (negative resp.).

## 2.2. Compatibility relations between specification parameters

### 2.2.1. Modeling the geometric constraints problem

This method is based on vectorial modeling of geometric elements and constraints using a set of modeling parameters  $q$  which, by definition, forms a complete, consistent, minimal system. By writing the equivalence of the two sets of parameters,  $s$  and  $q$ , we will deduce the completeness and consistency of the specification as well as the clearance required.

An equations system (1) of the following type are obtained:

$$\begin{cases} T(q) = K(s) \\ B(q) = 0 \end{cases} \Leftrightarrow F(q,s) = 0 \quad [2.1]$$

with  $q = (q_1, q_2, \dots, q_n)$  representing the modeling parameters and  $s = (s_1, s_2, \dots, s_l)$  the specification parameters.

This vectorial modeling based on the TTRS has already been presented in [CLE 97] and [LES 00]. Other models are possible; note, for example, those developed in [GIO 03], [BAL 03] and [CHA 97].

Analyzing the completeness of a mechanism specification amounts to solving the rank  $r$  system below, composed of  $m$  equations and  $n$  modeling parameters. We then find situations that mechanical engineers are quite familiar with: when, starting from a specified set  $s$ , we univocally determine the modeling parameters  $q_i$ , the system is said to be isoconstrained. When starting from  $s$ , we are unable to univocally determine all the parameters  $q_i$ . The system is said to be

underconstrained when it lacks specifications and overconstrained when certain specifications are overabundant or not independent. Certain specification systems may be simultaneously under- and overconstrained.

### 2.2.2. Compatibility relations for assemblability requirement

In this study, we are only looking for overconstrained systems and propose a method to establish the compatibility relations between specification parameters. These relations are often difficult to express in general terms; on the other hand, they are simple to determine for a specific position by differentiation and discussion of the linear system thus obtained. See [SER 03] and [MHE 07a] for more information.

The equations system [2.1] after differentiation is written:

$$J_q \cdot dq + J_s \cdot ds = 0 \quad [2.2]$$

where  $j_{q_{ij}} = \frac{\partial F_i}{\partial q_j}$  and  $j_{s_{ij}} = \frac{\partial F_i}{\partial s_j}$ .

System [2.2] becomes  $A \cdot dq = B \cdot ds$  with  $A = \begin{pmatrix} \frac{\partial T_i}{\partial q_j} & \frac{\partial B_i}{\partial q_j} \end{pmatrix}^T \in \mathbb{R}^{m \times n}$  and  $B = \begin{pmatrix} \frac{\partial K_i}{\partial s_j} & 0 \end{pmatrix}^T \in \mathbb{R}^{m \times l}$ .

Analyzing the geometric problem is equivalent to analyzing system [2.2]. The developed solution uses the singular value decomposition (SVD) of matrix  $A$ . The result gives:

$$(U_1 \ U_2) \times \begin{pmatrix} \Sigma_1 & 0 \\ 0 & 0 \end{pmatrix} \times (V_1 \ V_2)^t \times dq = B \times ds \quad [2.3]$$

With  $U = \begin{bmatrix} (U_1)_{m \times r} & (U_2)_{m \times (m-r)} \end{bmatrix} \in \mathbb{R}^{m \times m}$  and  $V = \begin{bmatrix} (V_1)_{n \times r} & (V_2)_{n \times (n-r)} \end{bmatrix} \in \mathbb{R}^{n \times n}$  two unit matrices, and  $\Sigma_1 = \text{diag}(\sigma_i)$ ,  $i = 1, \dots, r$  with  $\sigma_1 > \sigma_2 > \dots > \sigma_r > 0$ .

Passing the  $U$  matrix to the right-hand side of the equals sign, we obtain:

$$\begin{bmatrix} \Sigma_I \times V_I^t \\ \theta_{(m-r) \times n} \end{bmatrix} \times dq_{n \times 1} = \begin{bmatrix} U_1^t \\ U_2^t \end{bmatrix} \times B_{m \times l} \times ds_{l \times 1} \quad [2.4]$$

Compatibility relations for the assemblability requirement between specification parameters variations are written by noting that  $m-r$  relations only bring the specification parameters into play. These  $m-r$  relations (called  $CA$ ) are:

$$U_2^t \cdot B \cdot ds = 0 \quad [2.5]$$

In this section, we have presented a general method that enables the compatibility relations between the variation of specification parameters to be expressed, using minimum vectorial modeling.

The modeling of Bennett linkage is explained in [SER 02] and [MHE 07b]. Some results are given here. The geometric problem is represented by eight vectors, there are 22 modeling parameters ( $n=22$ ), nine specification parameters (four lengths and four angles of bars and one command angle, named  $\theta$ , defined between bars 1 and 2). The system to be resolved contains 25 equations ( $m=25$ ). Its rank is 22. Finally, there are three compatibility relations.

When the command angle value is 20 degrees, the three compatibility relations of the studied Bennett linkage are:

$$M_{CA_{(\theta=20^\circ)}} \cdot (dL_1 \ dL_2 \ dL_3 \ dL_4 \ d\alpha_1 \ d\alpha_2 \ d\alpha_3 \ d\alpha_4 \ d\theta)^T = \begin{pmatrix} 0 \\ 0 \\ 0 \end{pmatrix} \quad [2.6]$$

with

$$M_{CA_{(\theta=20^\circ)}} = \begin{pmatrix} -0.03381343 & 0.013852838 & -0.397698 \\ -0.01383742 & 0.08220959 & -0.39041114 \\ 0.016208213 & -0.10238861 & 0.38742942 \\ 0.024001801 & -0.03109344 & 0.396339703 \\ -0.25337716 & 0.143837734 & 0.026668012 \\ -0.2615418 & 0.087497073 & 0.056515932 \\ 0.283870296 & 0.009510719 & -0.00888232 \\ 0.271706175 & -0.03638092 & -0.05058737 \\ 0 & 0 & 0 \end{pmatrix}^T \quad [2.7]$$

This set of relations is called  $CA_{(\theta_0=20^\circ)}$ .



When these relations are taken into account, the mechanism may be assembled in the neighborhood of the initial position  $\theta = 20^\circ$ . Note that, in  $M_{CA_{(\theta_0=20^\circ)}}$  matrix, the coefficients of  $d\theta$  parameter vanish. This proves that the dimensional variations of the bars cannot be “corrected” by the variation of the command angle. It is the general case of mechanisms with degree of freedom.

### 2.2.3. Compatibility relations for mobility requirement

The aim of this section is to expose a solution allowing us to write the compatibility relations between the variations of the specification parameters to assure the mobility of a mechanism. These relations are called *CM*.

Before continuing, it is useful to clarify some notations. When angles or lengths specified by one or several designers concern parts, the parameters are called *sp*. When angles or lengths specified by one or several designers concern joints between parts, the parameters are called *sm*.

The previous relations *CA* are insufficient when the designer wishes to describe a mechanism with degrees of freedom. Recall that they only ensure the assemblability of a set of parts in a given position. To find the supplementary relations that permit the mechanism mobility, it is necessary to take into account that geometric dimensions of the parts do not change when the command parameter values change. To do that, we use a well-known principle in the kinematic domain [PER 03] or [MAV 94]. This consists of writing the compatibility relations for assemblability *CA* in several positions while imposing that variations of the *sp* parameters are identical for these different positions. The number of positions which it is necessary to study depends on the number of kinematic degrees of freedom of the mechanism. This solution is in theory applicable for kinematics with one or several loops.

This work being complete, the mathematical study of the new system enables us to determine the dependency relations (called *CM*) between the variations of the *sp* parameters and consequently of the minimal number of parameters which it is necessary to impose.

This principle is applied to the studied Bennet linkage, for which it is sufficient to write *CA* relations in two different positions. This was realized for the command angle values  $\theta = 20^\circ$  and  $\theta = 30^\circ$ . The compatibility relations ensuring the mobility of the mechanism are established by building the following system:

$$M_{CM} \cdot (dL_1 \ dL_2 \ dL_3 \ dL_4 \ d\alpha_1 \ d\alpha_2 \ d\alpha_3 \ d\alpha_4 \ d\theta)^T = \begin{pmatrix} 0 \\ 0 \\ 0 \end{pmatrix} \quad [2.8]$$

with

$$M_{CM} = \begin{pmatrix} M_{CA_{(\theta=20^\circ)}} \\ M_{CA_{(\theta=30^\circ)}} \end{pmatrix} \quad [2.9]$$

And the numeric application gives

$$M_{CM} = \begin{pmatrix} -0.03381343 & 0.013852838 & -0.397698 & 0.173788535 & -0.01914466 & -0.32744781 \\ -0.01383742 & 0.08220959 & -0.39041114 & 0.15423375 & -0.12379933 & -0.31236936 \\ 0.016208213 & -0.10238861 & 0.38742942 & -0.13263564 & 0.148212653 & 0.315807942 \\ 0.024001801 & -0.03109344 & 0.396339703 & -0.17799339 & 0.049281889 & 0.319089638 \\ -0.25337716 & 0.143837734 & 0.026668012 & -0.26432324 & -0.0662704 & -0.13564255 \\ -0.2615418 & 0.087497073 & 0.056515932 & -0.27413041 & 0.026140112 & -0.07536524 \\ 0.283870296 & 0.009510719 & -0.00888232 & 0.193044334 & -0.15728192 & 0.155803387 \\ 0.271706175 & -0.03638092 & -0.05058737 & 0.25037077 & -0.10065755 & 0.082085523 \\ 0 & 0 & 0 & 0 & 0 & 0 \end{pmatrix}^T \quad [2.10]$$

The rank of  $M_{CM}$  matrix is five. It is thus possible to calculate five parameters, suitably chosen, from four others. Here, the choice was to calculate the variations of the five parameters  $dL_3$ ,  $dL_4$ ,  $d\alpha_2$ ,  $d\alpha_3$  and  $d\alpha_4$ , with respect to variations of the four parameters  $dL_1$ ,  $dL_2$ ,  $d\alpha_1$  and  $d\theta$ . The result (obtained with Matlab) is as follows:

$$\begin{pmatrix} dL_3 \\ dL_4 \\ d\alpha_2 \\ d\alpha_3 \\ d\alpha_4 \end{pmatrix} = \begin{pmatrix} 1.000000000 & 0 & 0 & 0 \\ 0 & 1.000000000 & 0 & 0 \\ 1.732050807 & -1.000000000 & -3.000000000 & 0 \\ 0 & 0 & 1.000000000 & 0 \\ 1.732050807 & -1.000000000 & -3.000000000 & 0 \end{pmatrix} \cdot \begin{pmatrix} dL_1 \\ dL_2 \\ d\alpha_1 \\ d\theta \end{pmatrix} \quad [2.11]$$

As expected, variations of the  $sp$  parameters are independent of the variation of the command parameter  $\theta$  because the last column of the matrix vanishes. The second expected result is that the variation of length and angle of two opposite bars is identical. However, and to be completely sure that this result is correct, we

resumed the formal relations of compatibility ensuring the mobility of the Bennett linkage to validate it. These relations, already presented in [SER 02], are attributed to [BRI 27]. They are as follows:

$$\begin{cases} L_1 = L_3, L_2 = L_4, \alpha_1 = \alpha_3 \text{ and } \alpha_2 = \alpha_4 \\ \frac{L_1}{\sin \alpha_1} = -\frac{L_2}{\sin \alpha_2} \end{cases} \quad [2.12]$$

The first four relations are taken into account. The last relation is used to finalize the process of validation. For that purpose, it is enough to differentiate the last relation. So

$$d\left(\frac{L_1}{\sin \alpha_1}\right) = -d\left(\frac{L_2}{\sin \alpha_2}\right) \quad [2.13]$$

Rewriting the relation gives:

$$d\alpha_2 \approx \frac{-1}{L_1 \cdot \cos \alpha_2} (L_1 \cdot \sin \alpha_2 + L_2 \cdot \sin \alpha_1 + \sin \alpha_2 \cdot dL_1 + \sin \alpha_1 \cdot dL_2 + L_2 \cdot \cos \alpha_1 \cdot d\alpha_1)$$

and numeric application provides the expected result:

$$d\alpha \approx \sqrt{3} \cdot dL_1 - dL_2 - 3 \cdot d\alpha_1 \quad [2.14]$$

This validation enables us to prove that compatibility relations calculated with the proposed method are identical to those obtained by the formal compatibility relations provided by Bricard. The advantage of the proposed method is the generality and it is thus useful for various mechanisms. Naturally, it does not enable us to obtain the formal relations. It is also necessary to recall that the generated relations are valid only in the neighborhood of the nominal mechanism.

### 2.3. Framework for minimum clearance determination

Adding clearance in a mechanism's joints is useful to allow the interchangeability of the manufactured parts, sufficiently respecting the expected functional conditions. These two reasons are contradictory. The first incites us to define large clearances whereas the second incites us to define small clearances. So to assist the designer in his tolerancing task, it is essential to know the biggest value of acceptable clearance which ensures the correct functionality of the mechanism.

Indeed, this limit quantity imposes the maximal dimensional variations which are acceptable for the manufacturing parts. Control of these values is essential during the product industrialization phase because the manufacturing cost is strongly linked with the desired accuracy [PEZ 06].

The aim of this section is to define a “framework” of parametric tolerancing simulation for mechanisms with degrees of freedom and for assemblies. The objective of this tool is to assist designers during the phase of determining the acceptable variations of the manufacturing parts dimensions. This framework is built on the results of two functions. First, the vectorial modeling of the parts, assemblies and mechanisms; second the determination of the compatibility relations between the variations of the specification parameters (results presented in the previous section).

To calculate the minimum clearance, we use a solution inspired by the association methods employed in the metrology field. In this domain, to identify the characteristics of a real shape, it is necessary to proceed in two stages: firstly, to know the global shape (plane, cylinder, spherical, etc.) of the measured element. This element is called the “ideal element”. Secondly, to find geometric parameters of an ideal element which is closer to the shape built with the measured points on the actual surface according to a chosen algorithm. This object is called the “associated element”.

In the proposed approach, an “ideal mechanism” is defined: it is a mechanism composed of “ideal” or “associated” parts and “ideal” joints (this means that parts are in contact). It possesses the same properties as the nominal mechanism (assemblability or mobility).

Afterwards, only mechanisms with degrees of freedom are studied.

### 2.3.1. *Nominal and associated mechanism*

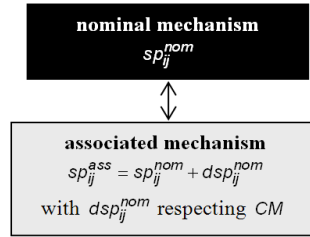
An associated mechanism is defined as a mechanism with degrees of freedom and without joint clearances. Its dimensions differ slightly from the nominal mechanism’s dimensions. Consequently, the variations of the specification parameter of an associated mechanism have to take into account the compatibility relations  $CM$ .

Before continuing, it is necessary to clarify some notations: the  $i$ -th specification parameter of the  $j$ -th part of the nominal mechanism is called  $sp_{ij}^{nom}$ ; the  $i$ -th specification parameter of the  $j$ -th part of the associated mechanism is called  $sp_{ij}^{ass}$ .

These two types of parameters take into account the following relations:

$$sp_{ij}^{ass} = sp_{ij}^{nom} + dsp_{ij}^{nom} \quad [2.15]$$

With  $dsp_{ij}^{nom}$  respecting the compatibility relations  $CM$ . This is illustrated in Figure 2.3.



**Figure 2.3.** Nominal and associated mechanism

### 2.3.2. Actual and associated parts

The actual part is a model of the manufacturing part. The form defects are not taken into account. The dimensions of this part are measured and the gaps with regard to the nominal dimensions are determined. This gap between a measured dimension and the corresponding nominal dimension is called  $\Delta$ . Also, the gap of the  $i$ -th specification parameter of the  $j$ -th actual part is called  $\Delta sp_{ij}^{nom}$ . In the same way, the  $i$ -th specification parameter of the  $j$ -th actual part is called  $sp_{ij}^{act}$ .

These two parameter types respect the following relations:

$$sp_{ij}^{act} = sp_{ij}^{nom} + \Delta sp_{ij}^{nom} \quad [2.16]$$

Note that gaps depend on the manufacturing process of parts. They can take different values. The possible dependency relations between these gaps result from the behavior of the machine-tool used and are not considered here.

The relative position of the actual parts with regard to the associated parts is calculated by one of the association techniques used in the metrology field. We can give as an example, the methods using the small displacement torsor [BOU 96] or the variations of the specification parameters [CHO 07]. In the proposed method, it is possible to choose various association criteria. This is illustrated in Figure 2.4

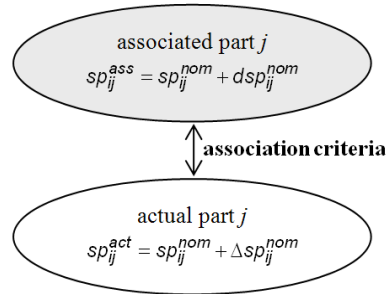


Figure 2.4. Actual and associated parts

### 2.3.3. Synthetic scheme

Remember that clearance exists in the joints of the actual mechanism while the parts of the associated mechanism are in contact.

When the relative position of each of the neighboring actual parts is known, the clearance between these parts is determined. To calculate the clearance between parts  $j$  and  $k$ , it is sufficient to calculate the relative position between the actual parts and the corresponding associated parts, then to take into account the relative position of associated parts in the associated mechanism. This aspect is illustrated in Figure 2.5.

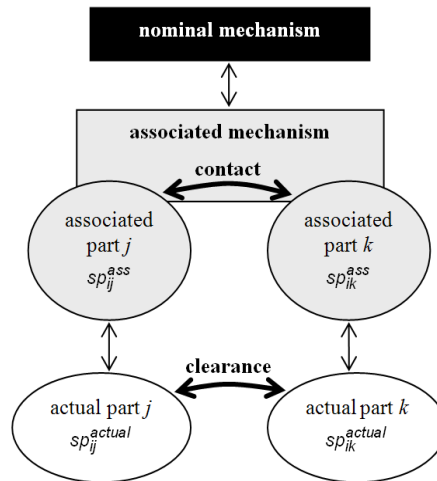


Figure 2.5. Synthesis diagram of the framework

## 2.4. Application

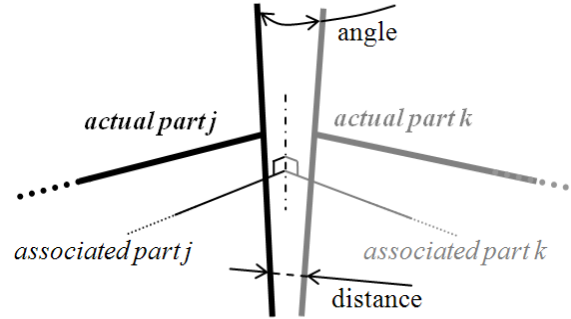
The studied mechanism is the Bennett linkage presented previously. The nominal dimensions are given in Table 2.1.

The gaps of actual part specification parameters are as follows.

Bar 1	$\Delta L_1 = 0.12 \text{ mm}$	$\Delta \alpha_1 = -0.5^\circ$
Bar 2	$\Delta L_2 = -0.18 \text{ mm}$	$\Delta \alpha_2 = 1.2^\circ$
Bar 3	$\Delta L_3 = 0.09 \text{ mm}$	$\Delta \alpha_3 = -0.8^\circ$
Bar 4	$\Delta L_4 = -0.1 \text{ mm}$	$\Delta \alpha_4 = 0.7^\circ$

**Table 2.2.** Gaps of actual parts

The clearance in a revolute joint is characterized by the parameters of distance and angle between the axis of both considered parts. The distance is measured according to the common perpendicular; see Figure 2.6.



**Figure 2.6.** Geometric parameters of revolute joint

### 2.4.1. First case

In this case, variations of the specification parameters for the associated parts are those presented in Table 2.3. These values were not optimized, they were chosen according to the gaps of the actual parts, to be mean values. Note, the results are already encouraging, but we can again hope to improve them by setting up a stage of optimization.

Bar 1	$dL_1 = 0.1 \text{ mm}$	$d\alpha_1 = -0.35^\circ$
Bar 2	$dL_2 = -0.15 \text{ mm}$	$d\alpha_2 = 1.23518287^\circ$
Bar 3	$dL_3 = 0.1 \text{ mm}$	$d\alpha_3 = -0.35^\circ$
Bar 4	$dL_4 = -0.15 \text{ mm}$	$d\alpha_4 = 1.23518287^\circ$

Table 2.3. Variations of associated parts

Note that these quantities respect the compatibility relations  $CM$ .

Evolution of distance and angle between the axes of the revolute joint according to the command angle is drawn on following both figures. For reasons of lightness, we have only represented results for the joint between bars 1 and 2 and the joint between bars 2 and 3.

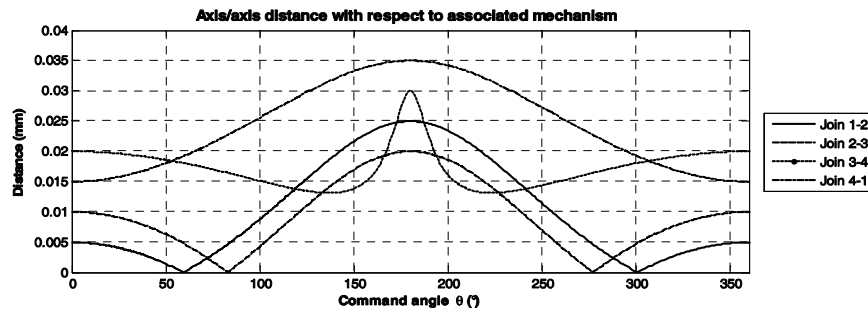


Figure 2.7. Evolution of axis/axis distance (first case)

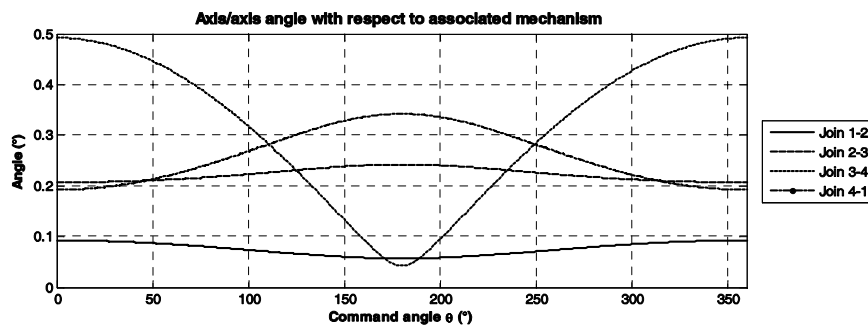


Figure 2.8. Evolution of axis/axis angle (first case)

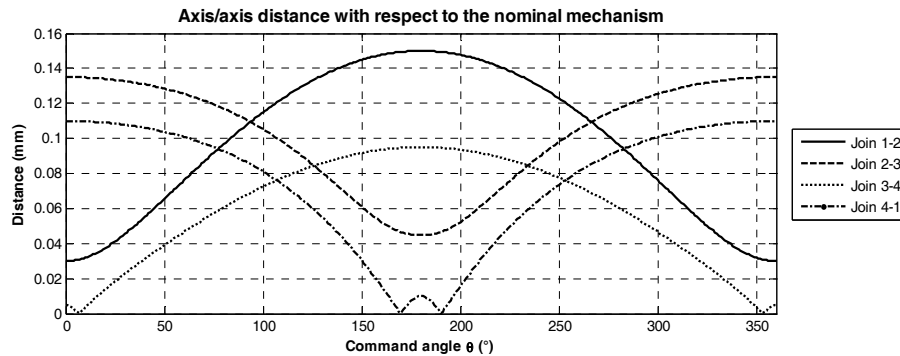


During one cycle, the distance belongs to interval  $[0; 0.025\text{mm}]$  for joint 1-2 and to interval  $[0; 0.02\text{mm}]$  for joint 2-3, whereas the angle belongs to interval  $[0.06^\circ; 0.09^\circ]$  for joint 1-2 and to interval  $[0.21^\circ; 0.24^\circ]$  for joint 2-3.

These various values give indications to the designer to build a technical solution which allows us to obtain the calculated clearance. For example, if the revolute joint is realized by two cylinders which fit together, then the diameters of these two surfaces should be determined according to these intervals. If this is the case, the movement of the actual mechanism is likened to the associated mechanism movement. A good approximation of the input-output law is given by the input-output law of the associated mechanism.

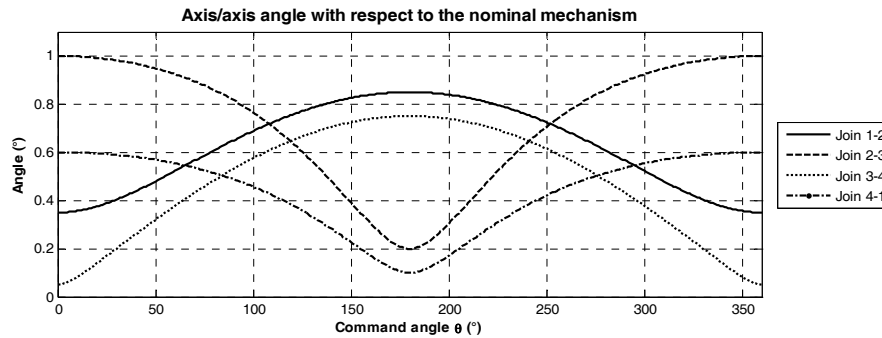
#### 2.4.2. Second case

What happens if the associated mechanism is the nominal mechanism? To give an answer to this question, the following simulation was realized. This simulation consists of imposing that the variations of the parts of the associated mechanism vanish. The following figures show the evolution of the previous four values when the mechanism makes one cycle.



**Figure 2.9.** Evolution of axis/axis distance (second case)

During one cycle, the distance belongs to interval  $[0.03\text{mm}; 0.15\text{mm}]$  for joint 1-2 and to interval  $[0.045\text{mm}; 0.135\text{mm}]$  for joint 2-3, whereas the angle belongs to interval  $[0.35^\circ; 0.85^\circ]$  for joint 1-2 and to interval  $[0.2^\circ; 1^\circ]$  for joint 2-3.



**Figure 2.10.** *Evolution of axis/axis angle (second case)*

Length intervals are approximately five times larger and angle intervals are approximately ten times larger than in the first case. This observation has strong consequences in practice because using these results would set up excessively large clearances in the joints and would unnecessarily degrade the mechanism's movement.

Keep in mind that the previous study was performed for one instance of a mechanism.

## 2.5. Conclusion

The first part of this chapter dealt with the presentation of a generic method to calculate the compatibility relations between the variations of the specification parameters for mechanisms and for assemblies. These relations are valid in the neighborhood of the studied mechanism or assembly.

The second part was dedicated to the presentation of an assistance framework for the determination of the minimal clearance in mechanisms with degree of freedom. A solution to calculate the minimum clearance was explained. This solution is based on the use of the new concept of associated mechanisms. It is inspired by those used in the manufactured parts metrology field.

It was shown that this technique gives variation intervals smaller than those obtained by using the usual method which consists of using the nominal mechanism. It also possesses the merit to provide to the designer or metrologist, a model of the behavior of the actual mechanism that is closer to reality. These conclusions are valid for a single mechanism and must be checked for a series of mechanisms.

This work must be continued in two ways. The first is rather conceptual, because it is a question of suggesting that the designer more precisely specifies the joint parameters that he wishes to control. It is also a question of optimizing some associated mechanism parameters to obtain a minimized cost function. The second is more experimental and consists of investigating the impact of various association criteria in the calculation of the studied values.

## 2.6. Bibliography

- [BAL 03] BALLOT E., BOURDET P., THIÉBAUT F., “Determination of relative situation of parts for tolerance computation”, *7th CIRP International Seminar on Computer Aided Tolerancing*, ENS de Cachan, Kluwer Academic Publishers, pp. 63-72, April 24-25, 2003.
- [BOU 96] BOURDET P., MATHIEU L., LARTIGUE C., BALLU A., “The concept of small displacement torsor in metrology”. In: *Advances in Mathematical Tools in Metrology II*, vol. 40. Edited by World Scientific Publishing Company, Series Advances in Mathematics for Applied Sciences- Vol. 40 pp. 110-122, 1996.
- [BRI 27] BRICARD R., *Leçons de cinématique*, Vol. 2, Gauthier-Villars, Paris, 1927.
- [CHA 97] CHASE K.W., GAO J., MAGLEBY S.P., “Tolerance Analysis of 2-D and 3-D Mechanical Assemblies with Small Kinematic Adjustments”, *Advanced Tolerancing Techniques*, John Wiley, pp. 103-137, 1997.
- [CHO 07] CHOLEY J.-Y., RIVIÈRE A., CLÉMENT A., BOURDET P., “A new variational association process for the verification of geometrical specifications”. *Journal of Computing and Information Science in Engineering*, Vol. 7, No. 1, pp. 66–71, 2007.
- [CLE 97] CLÉMENT A., RIVIÈRE A., SERRÉ P., VALADE C., “The TTRSS: 13 constraints for dimensioning and tolerancing”, *5th CIRP International Seminar on Computer-Aided Tolerancing*, Toronto (Canada), April 27-29, 1997.
- [GIO 03] GIORDANIO M., KATAYA B., PAIREL E., “Tolerance analysis and synthesis by means of clearance and deviation spaces”, *CIRP/JSPE/ASME Proceedings of the 4th CIRP Seminar on Computer Aided Tolerancing*, 2003.
- [LES 00] LESAGE D., LÉON J.C., SERRÉ P., “A declarative approach to a 2D variational modeler”, *3ème conférence internationale sur la conception et la fabrication intégrées en mécanique*, Montreal, Canada, May 16-19, 2000.
- [MAV 94] MAVROIDIS C., ROTH B., “Analysis and Synthesis of Overconstrained Mechanisms, in Mechanism Synthesis and Analysis”, *Proceedings of the 1994 ASME Design Technical Conferences*, Minneapolis, Vol. 125, No. 1, September, pp. 115-133, 1994.
- [MHE 07a] MHENNI F., MLIKA A., ROMDHANE L., SERRÉ P., RIVIÈRE A., “Geometric compatibility equations for overconstrained mechanisms”, *Conception et Modélisation des Systèmes Mécaniques CMSM 2007*, Monastir, Tunisia, 19-21 March, 2007.

- [MHE 07b] MHENNI F., SERRÉ P., MLIKA A., ROMDHANE L., RIVIÈRE A., “Dependency between dimensional deviations in overconstrained mechanisms”, *Conception et Production intégrées CPI 2007*, Rabat, Morocco, 22-24 October, 2007.
- [PER 03] PEREZ A., MCCARTHY J. M., “Dimensional Synthesis of Bennett Linkages”, *ASME Journal of Mechanical Design*, Vol. 125, No. 1, pp. 98-104, 2003.
- [PEZ 06] PEZZUTI E., STEFANELLI R., VALENTINI P.P., VITA L., “Computer-aided simulation and testing of spatial linkages with joint mechanical errors”, *International Journal for Numerical Methods in Engineering*, Vol. 65, No. 11, pp. 1735-1748, 2006.
- [SER 02] SERRÉ P., CLÉMENT A., RIVIÈRE A., “Vers une approche déclarative en CFAO. Application au mécanisme de Bennett”, *4th International Conference on Integrated Design and Manufacturing in Mechanical Design (IDMME2002)*, CDRom paper n°E6-2, 11 pages, Clermont-Ferrand, May 14-16, 2002.
- [SER 03] SERRÉ P., RIVIÈRE A., CLÉMENT A., “The clearance effect for assemblability of overconstrained mechanisms”, *8th CIRP International Seminar on Computer-Aided Tolerancing*, 12 pages, Charlotte, USA, April 28-29, 2003.

## Chapter 3

# Quick GPS: Tolerancing of an Isolated Part

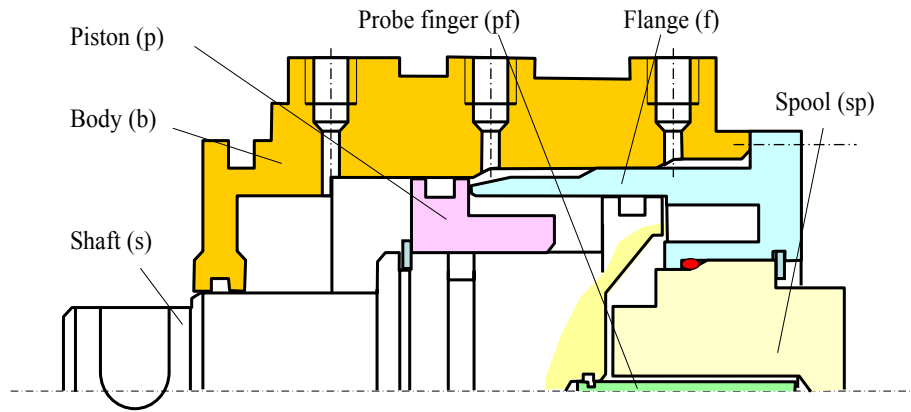
### 3.1. Introduction

In an academic approach to tolerancing, the designer is familiar with the mechanism drawing and determines the geometric functional requirements according to a functional analysis. For each requirement, the designer must identify the influential parts, as well as the dimensional and geometric specifications to be imposed on each of these parts; the designer's role includes establishing 3D tolerancing chains in order to analyze and synthesize tolerancing. This approach has already been developed by Anselmetti within the CLIC system [ANS 06].

In a great number of industries however, a designer is only responsible for a single isolated part. Therefore, the aim of this new approach, derived from the CLIC system and called Quick GPS, is to formalize a tolerancing method that corresponds to this industrial context. Such an approach is expected to guarantee coherent tolerancing of the complete mechanism, executed by a team of designers, each of whom assumes responsibility for a single part. This method does not enable us to generate tolerancing chains and thus cannot optimize tolerances; it merely provides a synthesis of specifications. The approach has been illustrated by application to the air control of a gearbox in three positions (left, center and right) (see Figure 3.1).

---

Chapter written by Robin CHAVANNE and Bernard ANSELMETTI.



**Figure 3.1.** *Right control configuration*

In the industrial context being studied, the designer is responsible for tolerancing the body and gains familiarity with the drawing and mechanism operations. To ensure coherent tolerancing of the entire mechanism, the team of designers must agree on the positioning plan for all mechanism parts.

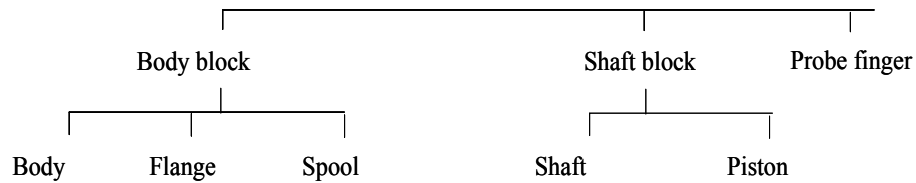
This chapter will focus on specification synthesis for a part, in accordance with the GPS standards used by industry; it will present a solution for achieving coherent tolerancing. Section 3.2 will provide a mechanism assembly description, while section 3.3 will develop the tolerancing rules for specifying all contact surfaces according to positioning requirements. Section 3.4 will then display a method that can be substituted for the classic approach of 3D chain transfers. Section 3.5 will demonstrate the application to automatically generate all these specifications using the QUICK GPS CAT system.

## 3.2. Mechanism definition

### 3.2.1. *The positioning plan*

The tolerancing of a functional mechanism depends on how parts are set. With the Quick GPS method, the team of designers determines the order in which parts are set: an initial part, called the “base”, is placed on the workbench. Each successive part is then positioned one by one onto the mechanism under construction. In principle, each part must be completely set with respect to the mechanism being built. It is also possible to assemble a subset, called a “block”, along with its proper base. This block is placed on the mechanism under construction. Figure 3.2 presents the positioning plan graph, which is similar for the

centered and right control configurations. The base lies on the left side of both the mechanism and each block. A partial or full block must be set on the surfaces of parts located to its left.



**Figure 3.2.** *Control positioning plan*

### 3.2.2. Description with positioning tables

The team of designers must proceed with a study of part set-up by taking into account the preponderance order of each positioning feature. The primary feature should impose the most feasible degree of freedom for the part. Then, the secondary and tertiary entities must offer each block at least one degree of freedom. Any elementary contact surfaces must be merged into a single composite positioning feature (e.g. set of parallel cylinders, coplanar planes). Moreover, the team needs to define the names of datum and types of interface between the features of both parts in contact. Classic interfaces consist of contact, clearance, blocked clearance or interference. During this step, designers are to take the functional context of parts into account and make key decisions regarding product quality and potential failure in the case of surface deviations. In addition, this approach serves to verify compliance of the positioning face dimensions with respect to the preponderance order.

This description of the mechanism differs from the classic approach, which uses a graph for each mechanism configuration. Graph nodes represent the parts, while arcs represent the links. A more detailed depiction of the component may be obtained by displaying component surfaces inside the graph nodes.

Linares [LIN 01] created functional groups of surfaces that include all contributing surfaces at a given joint. These groups are shown inside the nodes rather than inside the surfaces. In their work, Ballu and Mathieu [BAL 99] and Teissandier [TEI 97] indicated joint type on the arcs (e.g. plane joint, revolute joint). Samper [SAM 96] preferred noting the type of contact (e.g. fixed, sliding, floating and forbidden), whereas Marguet oriented arcs from the base to their end parts [MAR 01]. As for the Quick GPS and CLIC approaches, producing the positioning part table for both the studied part and its neighbor parts proves sufficient.

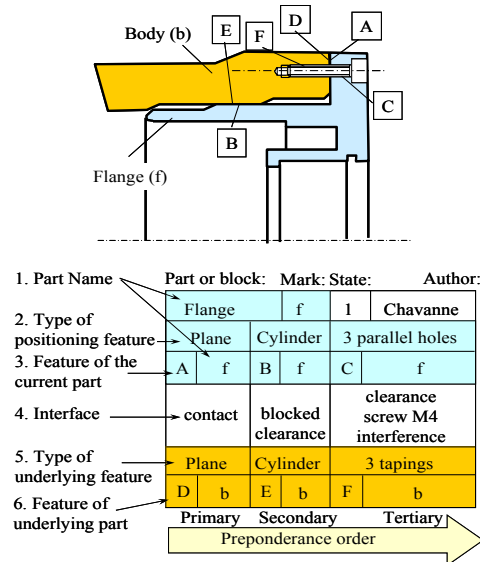


Figure 3.3. Positioning part table for the flange

3.3. Datum system specifications

3.3.1. Positioning requirements

In this step, the positioning tables are defined for each part and made available to each designer. The positioning tables now enable us to define the positioning requirements to ensure part assembly and contact quality (see Figure 3.4).

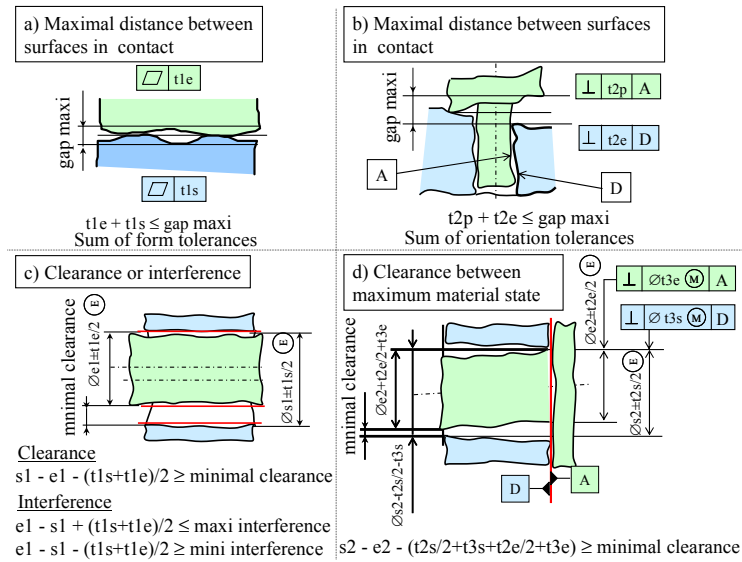
3.3.2. Positioning specifications

The joints that compose surface features in contact require the maximum gap between surfaces (the gap is considered to be the maximum distance between surfaces lying in contact with one another) to be controlled (see Figure 3.4). The gap between primary surfaces requires entities to specify the form of the surfaces in contact (see Figure 3.4a). The gap between secondary or tertiary surfaces imposes a specification orientation with respect to the primary reference (see Figure 3.4b).

In contrast, the joints composed of fitting features (i.e. hole and shaft) necessitate control of the minimum clearance or both the maximum and minimum interferences. The clearance or interference of a primary adjustment entity imposes part diameters along with the corresponding envelope requirement (see Figure 3.4c). The clearance



of a secondary or tertiary adjustment entity makes it necessary to specify diameters of the virtual maximum material (see Figure 3.4d).



**Figure 3.4.** Generation of positioning requirements

In choosing the positioning surface specification, Maeda [MAE 95] proposed a model to express the behavior of a tolerated feature by using the degree of freedom for this feature. TTRS (Technologically and Topologically-Related Surfaces) theory models surface associations and, based on these models, proposes standardized tolerancing [CLE 94]. Salomons used this same method with minor changes [SAL 96]. For assembly requirements however, it is possible to impose a specification to achieve optimal compliance.

Figure 3.5 contains patterns for each type of positioning feature and for the primary, secondary and tertiary cases as well. The corresponding pattern must be copied onto the definition drawing by adapting the datum names defined in the positioning table. The maximum material modifier should be introduced on either the tolerated surface or a datum surface should the interface be clearance.

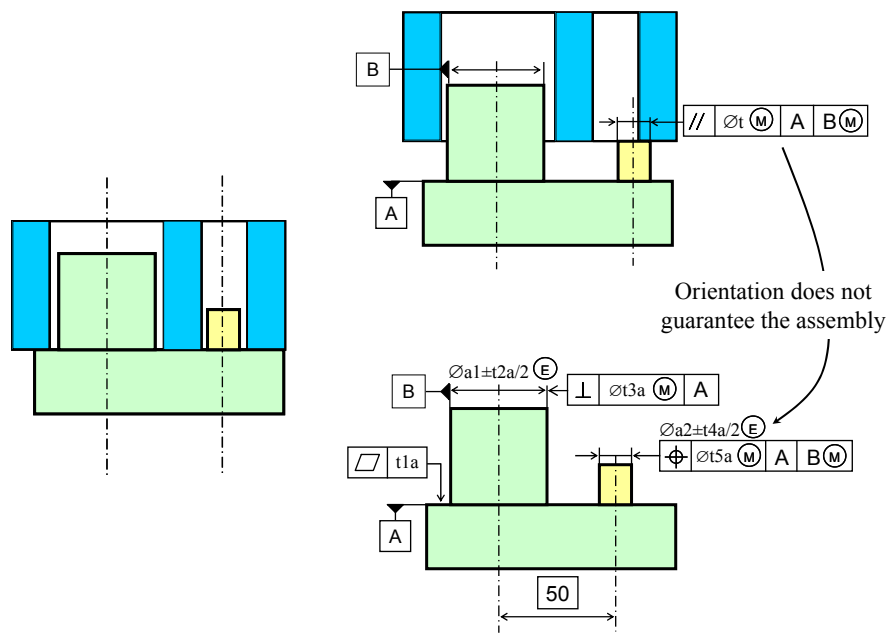
To simplify Figure 3.5, perpendicularity implies that the pattern corresponds to an orientation specification (perpendicularity or angularity), and localization corresponds to a position specification (localization or symmetry). The specification choice then depends on the relative position and orientation between tolerated surfaces and datum.

Primary feature	Secondary feature	Tertiary feature	Primary feature	Secondary feature	Tertiary feature
Plane			Symmetrical parallel planes		
Coplanar planes			Symmetrical planes extended		
Parallel planes			Cone		
Cylinder			Threading		
Coaxial cylinders			Sphere		
Set of cylinders			Continued surface		
Set of threads			Discontinued surface		

- (1) the location replaces the orientation if a dimension is possible between current feature and primary or secondary feature  
 (2) the datum reference frame must be defined with comment  
 (3) symbol (M) must be added on tolerated surface and on datum surface if this surface is a feature of size with clearance.

Figure 3.5. Patterns for the tolerancing of positioning features

Special tolerancing patterns have proposed two solutions: orientation or position for any features (plane, coplanar planes, cylinder, coaxial cylinders, symmetrical parallel planes, and threading). Most of these cases require orientation specification, yet position specification must be applied if a dimension can be defined between the tolerated surface and datum. In Figure 3.6, the secondary feature B demands simple perpendicularity with respect to the primary datum; and tertiary datum C needs to control a dimension between B and C in order to ensure potential assembly, given that parallelism is not sufficient.



**Figure 3.6.** Orientation or position specification

To formalize the specification for these features within the QUICK GPS system, TTRS theory is employed to identify all possible cases. The classic features belong to two TTRS classes: plane surfaces, which in accordance with TTRS encompass planes, coplanar planes and symmetrical parallel planes; and cylindrical surfaces, which account for cylinders, coaxial cylinders and threading. Table 3.1 sets out the specifications to be applied to these features, depending on the tolerated surface and datum. The tolerated surface is a secondary or tertiary feature, while datum is either primary or a data system composed of both primary and secondary data.

In Table 3.1, a star indicates that this case is impossible for positioning specifications. The reclassification result for both tolerated surface and datum should not be in the same class as the datum.

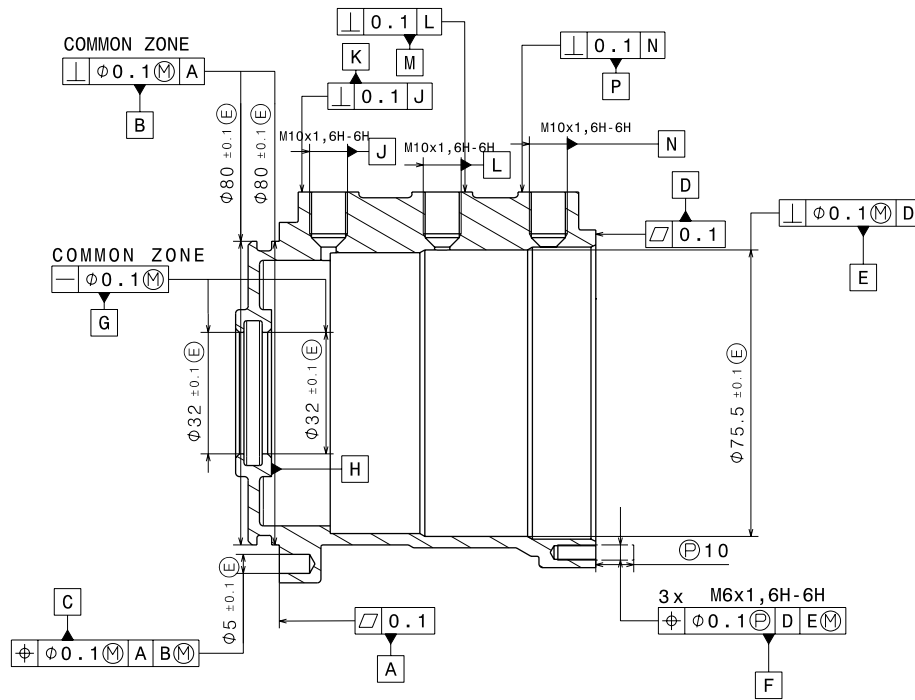
Datum	Planar surface	Cylindrical surface	Prismatic surface	Surface of revolution	Spherical surface	Any surface
Toleranced surface						
Planar surface 	$u \cdot v \neq 1$ $\oplus (*)$	$Dr \in Plt$ $\equiv$	$u \cdot v = 0$ $\oplus (*)$	$u \cdot v \neq 1$ $\oplus (*)$	$Cr \in Plt$ $\equiv$	$\oplus (*)$
	$u \cdot v = 0$ $\perp$	$u \cdot v = 0$ $\oplus$	$u \cdot v \neq 1$ $\perp$	$Dr \in Plt$ $\equiv$	$\equiv$	
	Else $\angle$	$u \cdot v \neq 1$ $\perp$	Else $\angle$	Else $\oplus$	Else $\oplus$	
		Else $\angle$				
Cylindrical surface 	$Dt \in Plr$ $\equiv$ without $\emptyset$	$Dt = Dr$ $\odot (*)$ with $\emptyset$	$u \cdot v \neq 1$ $\oplus (*)$	$Dt = Dr$ $\odot (*)$ with $\emptyset$	$Cr \in Dt$ $\equiv$	$\oplus (*)$
	$u \cdot v = 0$ $\oplus$ without $\emptyset$	$u \cdot v \neq 1$ $\oplus$ without $\emptyset$	with $\emptyset$	$u \cdot v \neq 1$ $\oplus$ without $\emptyset$	without $\emptyset$	
	$u \cdot v \neq 1$ $\perp$ with $\emptyset$	$Dt, Dr$ secant & $u \cdot v = 0$ without $\emptyset$ $\perp$	$u \cdot v = 0$ $\perp$ with $\emptyset$	$Dt, Dr$ secant & $u \cdot v = 0$ without $\emptyset$ $\perp$	without $\emptyset$	
	Else $\angle$ with $\emptyset$	$Dt$ & $Dr$ secant $\equiv$ without $\emptyset$ $\angle$	Else $\angle$ with $\emptyset$	$Dt$ & $Dr$ secant $\equiv$ without $\emptyset$ $\angle$	Else $\oplus$ without $\emptyset$	

Table 3.1. Specifications according to TTRS cases

Figure 3.7 presents results of the body specification for positioning requirements. Tolerance values are by default set at 0.1 and must be adjusted by the designer.

A, B and C represent the main reference frame (R1b) of the body to be located in the outside world. D, E and F constitute the auxiliary reference frame for the flange,

denoted A1f. G is a portion of the auxiliary primary datum of the shaft and, along with H, constitutes the datum reference frame named A1s. The pairs (J,K), (L,M) and (N,P) correspond to auxiliary reference frames (A1n, A2n, A3n).



**Figure 3.7.** Results for positioning requirement specifications

When the primary datum is partial, it becomes impossible to specify secondary datum with regard to the primary reference; hence in this case, surface H is not specified.

### 3.4. Relative position of reference frames

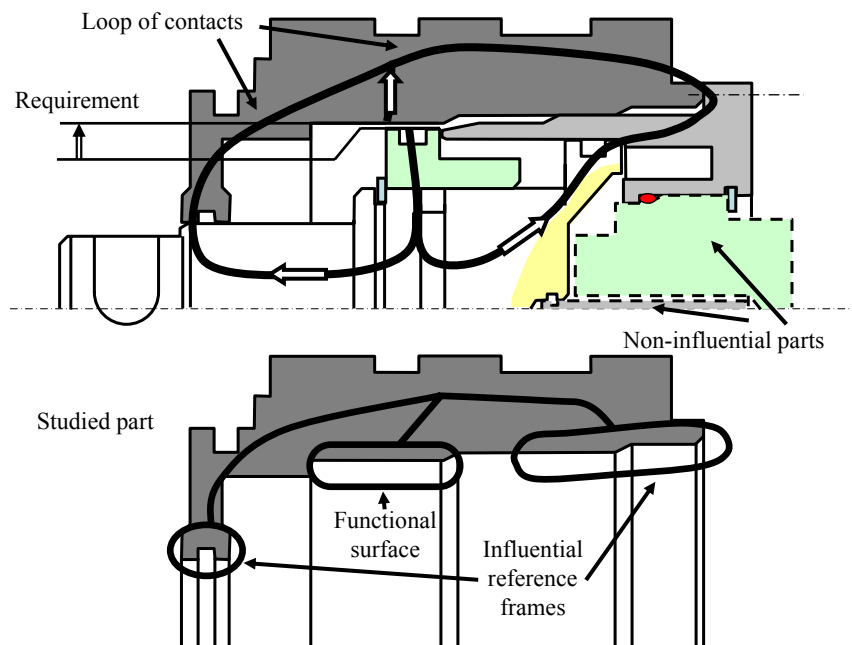
#### 3.4.1. Links between reference frames

To complete the body specification, it is necessary to take into account the other functional requirements. For each functional requirement, the CLIC method determines the loop of contacts linking functional surfaces, in addition to generating both functional specifications for influential surfaces and the relationship between

the tolerances for these specifications [ANS 06]. In this manner, the 3D tolerancing chain creates links between different datum reference frames of each part.

The designer assigned responsibility for a part must apply another method to complete the tolerancing step, meaning that the designer must know mechanism operations and determine the set of useful functional requirements.

The designer must systematically study whether a deviation in each surface of all auxiliary reference frames causes failure for the assembly or for product functioning. This failure would call for a functional requirement to be defined between the functional surfaces. One such surface sometimes lies directly on the studied part.



**Figure 3.8.** *Search for links*

In order to identify influential parts on this requirement, two methods will now be proposed:

- According to Figure 3.8, designers must find the loop of contacts that links functional surfaces. This loop actually links the influential reference frames of the studied part.

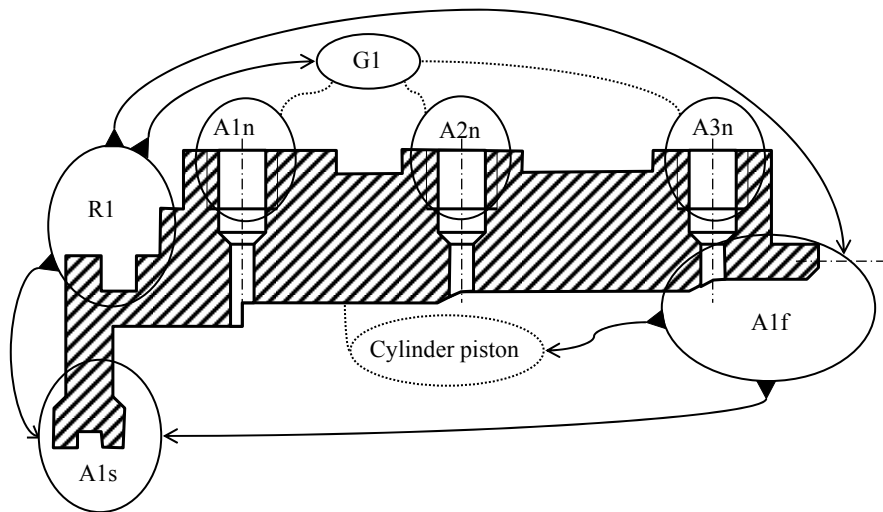
– The designer can virtually delete all parts that do not modify the relative position of functional surfaces. The reference frames of the studied part in contact with remaining parts are all influential.

Each surface of each influential auxiliary reference frame and each isolated functional surface must then be located with respect to one other influential reference frame (whether main or auxiliary). A set of similar systems can sometimes be combined. Figure 3.9 and Table 3.3 illustrate links on the body considered for all requirements of the studied control.

This search for links may proceed using the graphical approach [BAL 99, DAN 05].

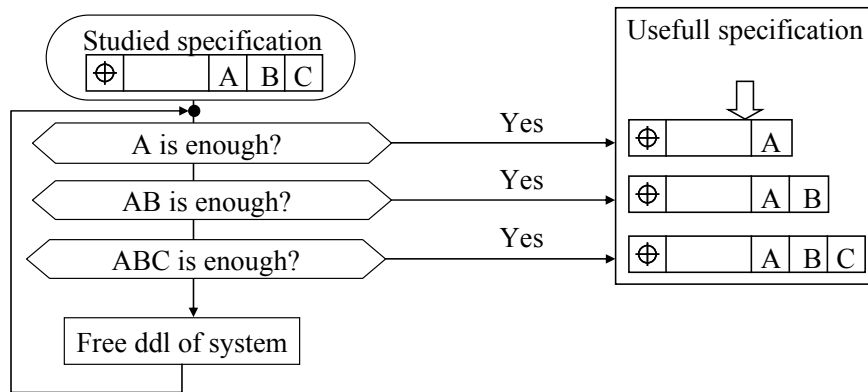
### 3.4.2. Specification corresponding to links

Figure 3.9 shows the links established between the datum reference frames created in Figure 3.7. The cylinder denoted “piston” is an isolated functional surface that ensures clearance and air tightness between the body and piston. A1f is chosen to close the loop presented in Figure 3.8. The link A1s/A1f completes the loop for this requirement. The links A1s/R1 and A1f/R1 are established to guarantee the position of the shaft relative to the shift fork. The group G1 is created and positioned relative to R1 to ensure the accessibility of the nipples for the outside world.



**Figure 3.9.** Links between datum reference frames

For each link presented in Figure 3.9, all surfaces of the specified frame must be located and/or oriented with respect to the reference frame. For each specification, the algorithm summarized in Figure 3.10 enables us to determine whether one, two or three references are needed.



**Figure 3.10.** *Test of datum frame combinations*

Table 3.2 describes in detail the condition employed to determine whether the reference frame is indeed sufficient. This frame is associated with a TTRS to be calculated by means of reclassification [CLE 94].

The choice of specification symbol has been presented in Table 3.1. The symbol used for features composed of many surfaces is the same as symbol shown in Figure 3.5. If the tolerated surface or datum is a fitting feature with clearance, it becomes necessary to add a minimum material modifier.

Figure 3.11 indicates the result of tolerancing obtained by the links defined in Figure 3.9. This specification may be excessive. For example, the localization (denoted with a star in Figure 3.11) of the group of three holes proves useless in our case. However, such a localization step would have been necessary if a hole in the flange had been positioned in front of a hole of the body in order to pass air through the flange.

The designer must therefore analyze the pertinence of the proposed specifications and eventually delete some of them. Experience demonstrates that this case is quite rare.



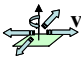

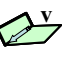
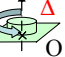
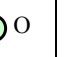
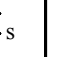

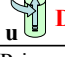

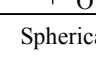
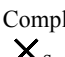

Datum $\rightarrow$	Planar	Cylindrical	Prismatic	Revolute	Spherical	Complex
Toleranced surface $\downarrow$						
Planar 	$u = \pm v$	no	$u \cdot v = 0$	$u = \pm v$	no	yes
Cylindrical 	no	$u = \pm v$ and $D = \Delta$	$u = \pm v$	$u = \pm v$ and $D = \Delta$	no	yes
Prismatic 	$u \cdot v = 0$	no	$u = \pm v$	no	no	yes
Revolute 	$u = \pm v$	no	no	$u = \pm v$ and $D = \Delta$	no	yes
Spherical 	no	no	no	$F \in \Delta$	$F = 0$	yes
Complex 	no	no	no	no	no	yes

Table 3.2. Datum system test for positioning

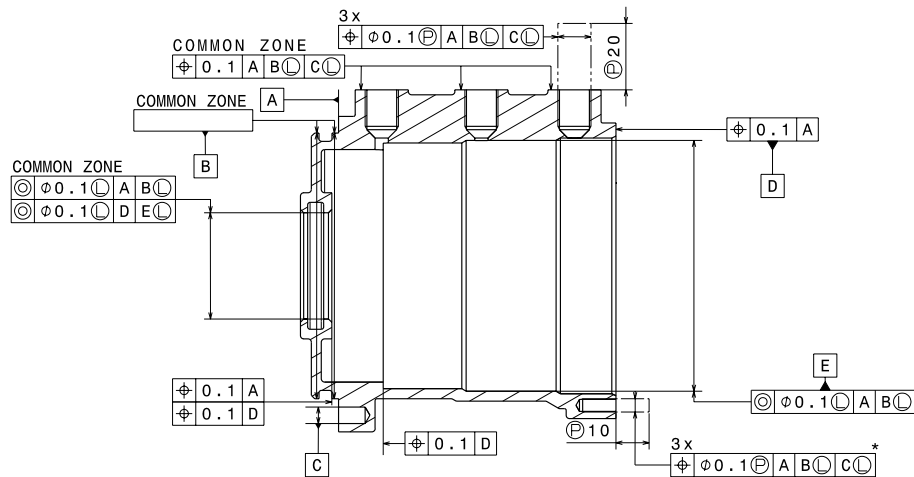


Figure 3.11. Positioning specification results for the body

### 3.5. VBA application

#### 3.5.1. General structure

The Quick GPS tolerancing method has been implemented within a CATIA VBA environment (Dassault Systèmes). Data are stored in a simple Excel spreadsheet. The application comprises 3 steps, the first of which enables an interactive dialog between the designer and the computer-aided tool. The designer selects the primary, secondary and tertiary features using the CATIA interface, with surface characteristics stored in the Excel spreadsheets. This step summarizes the concept of positioning part table. During the second step, the application generates data tolerancing, in accordance with the previous set of tolerancing rules. Finally in step 3, the application reproduces the tolerancing in 3D annotation with the FTA (Functional Tolerancing Annotations) interface (see Figure 3.12).

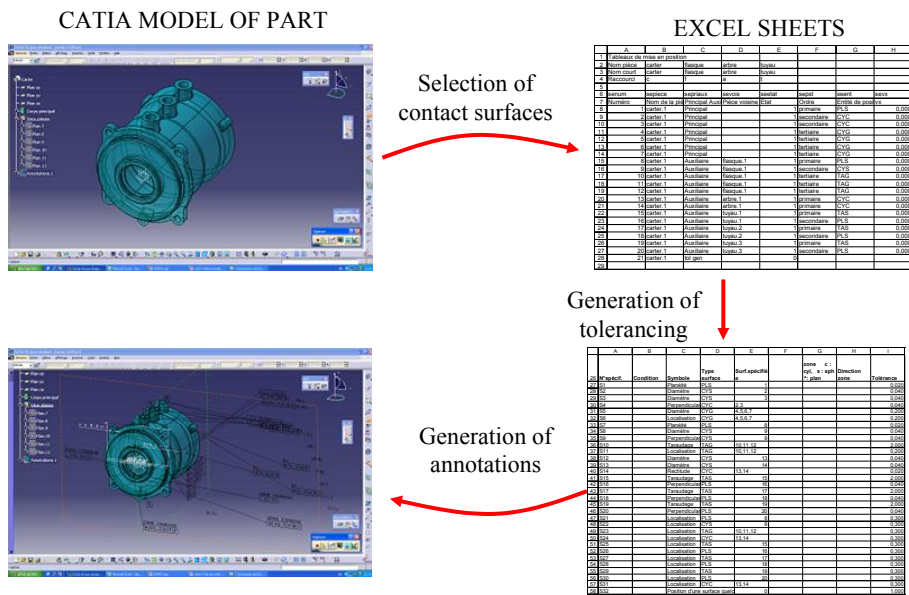
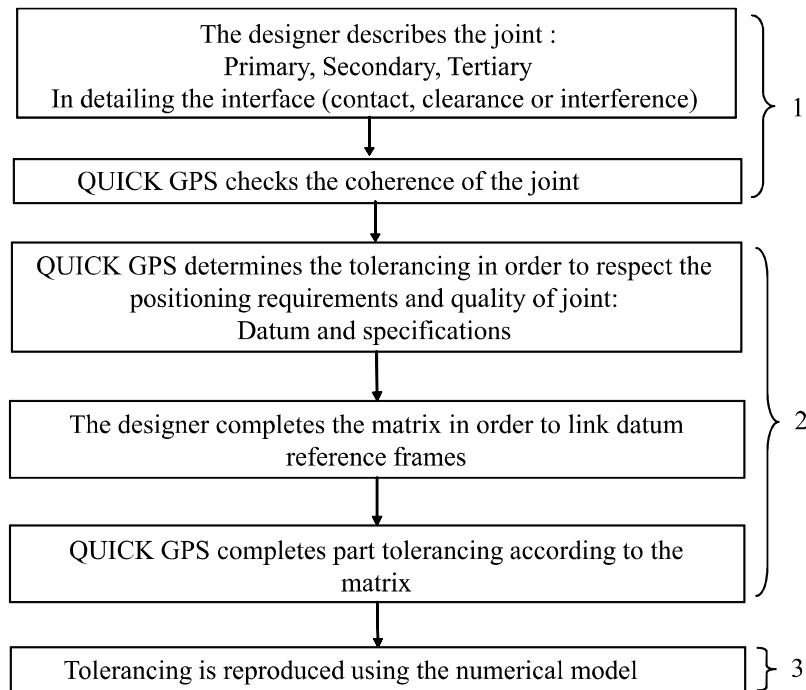


Figure 3.12. Interface with the CAD system

Figure 3.13 details these various application steps.



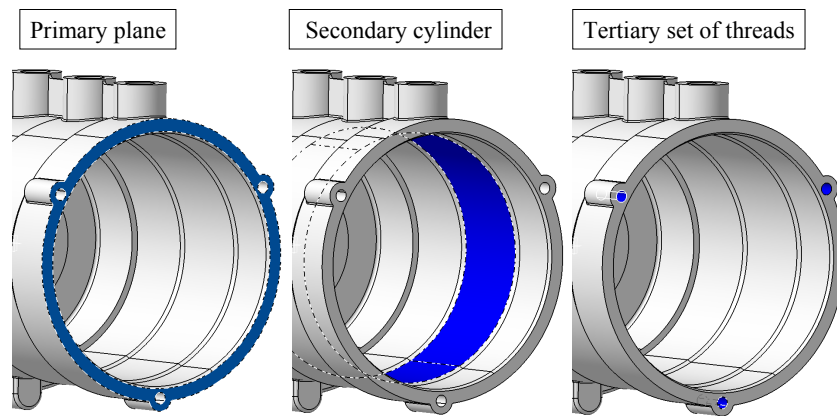
**Figure 3.13.** *Synopsis of the Quick GPS application*

### 3.5.2. Data acquisition and verification

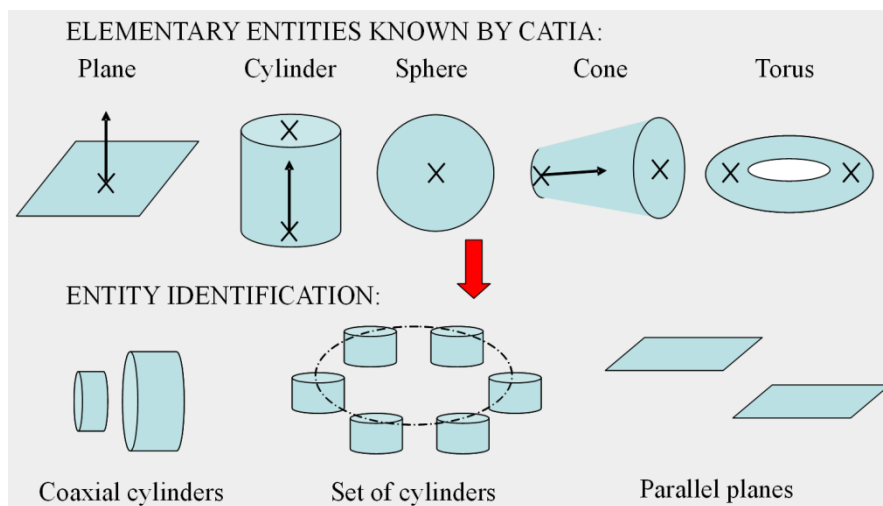
In the CAD system, the designer proceeds with a step-by-step selection of contact surfaces between each pair of parts. Figure 3.14 lays out the interactive selection showing flange positioning on the body. A dialog box enables the designer to detail the interface between the various contact surfaces (clearance, interference, etc.). Armillotta [ARM 07] proposed a method for automatically recognizing these contact surfaces on the CAD assembly model.

For each selection, VBA CATIA procedures recognize the elementary geometry (plane, cylinder, sphere, cone, torus). Geometrical characteristics can then be extracted from this specific geometry (point, vector, radius, etc.) (see Figure 3.15).

If the entity is composed of several elementary surfaces, the combinations between geometrical characteristics would enable us to determine the type of feature in order to differentiate coaxial cylinders from, for example, a set of parallel cylinders. Moreover, each positioning feature is associated with a TTRS class so as to apply the set of rules listed above.

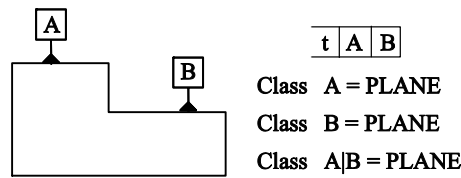


**Figure 3.14.** Selection of positioning surfaces



**Figure 3.15.** Entity identification

During each step, these rules serve to verify junction coherence. The first rule is based on TTRS theory to ensure that each datum reference frame created is indeed coherent. To illustrate this Figure 3.16 shows an incoherent system.



**Figure 3.16.** *Example of an incoherent reference frame*

The primary plane is a planar surface for TTRS theory, and the secondary plane is a planar surface as well. The reclassification of these parallel surfaces would thus also be a planar surface. The secondary datum does not, in fact, suppress any new degree of freedom.

The second rule performs a datum quality test. For example, if a primary cylinder is too short ( $\text{Length} < 0.5 \times \text{Diameter}$ ), a warning is displayed. The short cylinder is not correctly blocking two rotations, which need to be suppressed by a primary datum.

In addition, the designer selects one surface to be assigned a specification for general tolerancing of all part surfaces.

### 3.5.3. Tolerancing process

The tolerancing process is composed of four phases.

The first phase creates all datum reference frames and their corresponding specifications, as represented in Figure 3.7 with respect to the method presented in section 3.3.

During the second phase, a dialog box asks the designer to define a group of frames such that Group G1 is composed of A1n, A2n, A3n. This solution represents an alternative which is the most appropriate in some cases when the surfaces are similar, like coaxial cylinders or a set of cylinders. This avoids favoring one reference frame, like A1f for the requirement of clearance between the piston and the body.

The third phase displays the matrix (Table 3.3). The designer must now place the letter “P” to indicate a frame or a function with respect to a datum reference frame. However, if there are only two datum reference frames (a main and an auxiliary) in the part, the auxiliary references are automatically positioned relative to the main reference frame and the designer need not complete this table.

	References or functional surfaces to position							
	R1 (A,B,C)	A1f (D,E,F)	A1s (G,H)	A1n (J,K)	A2n (L,M)	A3n (N,P)	G1	Cylinder piston PLS 5
R1		P	P				P	
A1f			P					P
A1s								
A1n					G1	G1		
A2n				G1		G1		
A3n				G1	G1			

Table 3.3. Relative position between datum reference frames

The fourth phase generates the tolerancing corresponding to these links, in accordance with section 3.4.

Each specification listed in an Excel spreadsheet can be modified or suppressed and tolerances can be adjusted.

In this last phase of the application, all ISO functional specifications are transferred into the CAD model with VBA and CAA procedures, using the FTA semantic language. Figure 3.17 shows the exact, automatically-obtained captures and annotations.

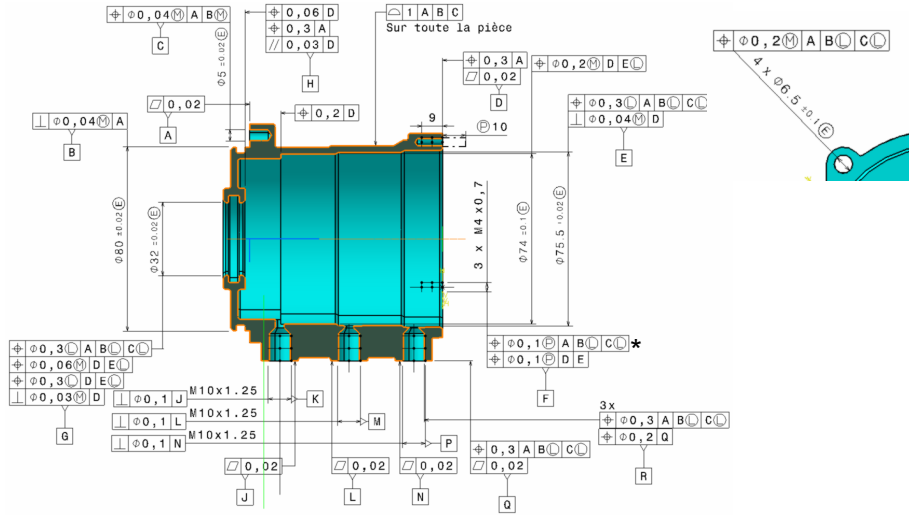


Figure 3.17. Tolerancing exported to CATIA

### 3.6. Conclusion

This chapter has shown that coherent tolerancing of a single part may be achieved with knowledge of the positioning tables and the matrix detailing the links between the various contact surfaces. This method provides an efficient solution for numerous industries, in cases where each designer is responsible for just a single part. The positioning part table offers a way to specify all joints in order to respect the positioning requirements. The table of the position between datum reference frames summarizes all links into the part and serves as an alternative to the classic 3D chain transfer approach for the contextual study of a single part.

This method has now been implemented within a VBA environment in interaction with the CATIA environment. This module has proven to be very effective: the selection of set-up surfaces takes just 5 min, and body tolerancing only needs 20 s.

This approach is not sufficient for tolerance optimization, a process that requires tolerance chains and a complex equation system. This result can still be studied with other commercial software, such as 3D CS and MECAMaster, to determine the effect of these tolerances on functional characteristics.

The automation of this work necessitates a complete view of the mechanism, as available in the CLIC system [ANS 06].

As opposed to Armillotta's findings [ARM 07], contact surfaces are not detected automatically, yet the subsequent goal of this application is to enhance the assembly method on a CAD model by integrating the positioning table concept. This new version is being created by CATIA CAA and will enable modifying tolerancing reproduction, which presents several shortcomings in the VBA language.

### 3.7. Bibliography

- [ANS 06] ANSELMETTI, B., "Generation of functional tolerancing based on positioning features", *Computer-Aided Design*, Vol. 38, pp. 902-919, 2006.
- [ARM 07] ARMILLOTTA, A., SEMERARO, Q., "A System for Modeling Geometric Tolerances for Mechanical Design", *10th CIRP Conference on Computer-Aided Tolerancing*, Erlangen, Germany, March 21-23, pp. 11-24, 2007.
- [BAL 99] BALLU, A., MATHIEU L., "Choice of functional specifications using graphs within the framework of education", *Proceedings of the 6th CIRP Seminar on Computer-Aided Tolerancing*, Enschede, The Netherlands, March 22-24, pp. 197-206, 1999.
- [CLE 94] CLEMENT, A., RIVIERE, A., TEMMERMAN, M., *Cotation tridimensionnelle des systèmes mécaniques: Théorie et pratique*, PYC Edition, France, 1994.

- [DAN 05] DANTAN, J-Y., LANDMANN, T., SIADAT, A., MARTIN, P., "A System for Modeling Geometric Tolerances for Mechanical Design", *Selected Conference Papers of the 9th CIRP International Seminar on Computer-Aided Tolerancing*, Tempe, Arizona, USA, April 10-12, pp. 55-64, 2005.
- [LIN 01] LINARES, J-M., MARTY, C., "Tolerancing by functional group", *Proceedings of the 3rd CIRP Seminar on Computer-Aided Tolerancing*, Cachan, France, April 27-28, pp. 267-277, 2001.
- [MAE 95] MAEDA, T., YONEKURA, D., TOKUEKA, N., "A toleranced feature modelling by constant of degree of freedom for assignment of tolerance", *Proceedings of the 4th CIRP Seminar on Computer-Aided Tolerancing*, Tokyo, Japan, April 5-6, pp. 121-128, 1995.
- [MAR 01] MARGUET, B., MATHIEU, L., "Method for Geometric Variation Management from Key Characteristics to Specification", *Selected Conference Papers of the 7th CIRP International Seminar on Computer-Aided Tolerancing*, Cachan, France, April 24-25, pp. 217-226, 2001.
- [SAL 96] SALOMONS, O.W., HAALBOOM, F.J., JONGE POERINK, H.J., VAN SLOOTEN, F., VAN HOUTEN, F.J.A.M., KALS, H.J.J., "A computer-aided tolerancing tool II: Tolerance analysis", *Computers in Industry*, Vol. 31, pp. 161-174, 1996.
- [SAM 96] SAMPER, S., GIORDANO, M., "Models for tolerancing process by considering mechanism flexibility", *Integrated Design and Manufacturing in Mechanical Engineering*, Kluwer Academic Publishers, pp. 349-356, 1996.
- [TEI 97] TEISSANDIER, D., COUETARD, Y., GERARD A., "Three-dimensional functional tolerancing with proportional assembly clearance volume (UPEL): Application to setup planning", *Proceedings of the 5th CIRP Seminar on Computer-Aided Tolerancing*, Toronto, April 27-29, pp. 113-123, 1997.



## Chapter 4

# Synthesis and Statistical Analysis for 3D Tolerancing

This chapter presents a general method for determining the dimensional and geometric tolerances of the various parts of a mechanism. The nominal geometry is known and the functional requirements are defined by tolerance zones. This method has three main stages: the first one is to decompose the functional tolerance into tolerance zones attached to each functional feature of the parts. The second stage draws from the ASME or ISO standards of possible specifications that correspond most closely to the outcome of the first stage. The third stage is an analysis in the worst case or has statistical assumptions to determine the numerical values that complement the determination of tolerances. In this presentation the statistical approach is developed and an example is presented.

### 4.1. Introduction

Nowadays, the optimization of geometrical tolerances is generally carried out empirically in most mechanical industries. Compromises are made between the functional requirements in the design process and the manufacturing step. A rational method and computer-aided tolerancing systems are particularly necessary for new products in the context of rigorous lifecycle management that takes into account the design and the manufacturing data simultaneously.

In this chapter, a method for allocating geometrical and dimensional tolerances is presented. This method is composed of three main stages. First a tolerance zone is

---

Chapter by Max GIORDANO, Pascal HERNANDEZ and Dimitri DENIMAL.

defined for each functional feature of the assembly. The second draws the tolerance specifications from the ASME or ISO standards. These two stages consist of a tolerance synthesis. Starting from a functional requirement, they give the tolerances in the qualitative form. The third stage is a quantitative analysis and it allows us to determine the optimum values for each specification that satisfied the functional requirement. Some manufacturing data are taken into account, in particular, process capability indices depending on the manufacturing process.

The outline of the chapter is as follows. The general problem is discussed, followed by a literature review with a presentation of the main mathematical tools in section 4.1. In section 4.2 the method is applied to stack-up tolerances. In section 4.3, the clearance is taken into account. In section 4.4, the method is applied to more complex mechanical structures: the parallel structure and what we call the “reducible” structure. In section 4.5 the statistical analysis method for general reducible structure is presented and a simulation example is given with more details to show the efficiency of the procedure.

#### **4.1.1. Literature review**

Different approaches for computer-aided tolerancing have been developed. The most common consists of considering a functional requirement “ $y$ ”, function of parameters  $x_i$  describing the geometry of parts:  $y=f(x_i)$ . From this function we can determine the variation of the characteristic  $y$  as a function of the variation of  $x_i$ . This problem can be solved in the worst case or more commonly by the statistical approach. For example, Nigam and Turner presented a review of the statistical approaches for the tolerance analysis starting from this parameterized form [NIG 95]. Huang and Ceglarek proposed a very efficient algorithm adapted for non-linear relations [HUA 04]. Unfortunately for the application to mechanical structures, this method is not compatible with geometrical tolerances defined in the ISO or ASME standards. On the other hand, the interfaces between the parts (clearance, gaps) have a different behavior compared to the deviation between the features of a part and are therefore difficult to be taken into account with this model.

The small displacement torsor, also called screw operator or screw, is widely used to represent the deviation between two faces of a part or the clearance in a joint between two parts. First used for metrology by Bourdet and Clément [BOU 88], it is also a very well suited tool for tolerance analysis and synthesis in a 3D context. For a stack-up of tolerances the calculation of the torsor associated to the requirement is a simple sum of the torsors associated to each functional deviation.

Desrochers uses the term of Jacobian-torsor because a transformation matrix is needed for the computation of the sum of the torsors [DES 03]. The torsors must be

projected in the same frame. In the general case, depending on the mechanical structure, it is possible to write the relation between the different small displacement torsors [BAL 95]. However, this is not sufficient for the tolerance analysis: one must translate each standardized specification into limits on the torsor components. Desrochers proposes to extend the Jacobian-torsor model to a tolerance zone model using an interval formulation [DES 03]. But in our opinion this model is not very close to the standard.

Davidson and Shah used a geometrical representation for the limits of the deviations with the concept of T-Map [DAV 02], this model presents some similarities compared to the model of domains we developed for example in [GIO 01] and will use hereafter.

#### **4.1.2. *The domain model***

In this chapter, the small displacement torsor model can represent either a deviation of one feature compared to another or compared to datum; in this case the torsor is noted with letter D. The displacement torsor model can also represent a deviation in a joint between two parts, in this case the torsor is represented by the letter J. A domain is a set of deviation torsors and is a model for any standardized specification, either a tolerance zone or a dimensional tolerance [GIO 01]. The concept of a joint domain is also used and will be defined in the following section.

The representation by graphs for mechanical structures or assemblies is useful to enable distinction of the different types of structures. In these graphs, each vertex is a Cartesian frame attached either to an elementary functional feature (generally simple face) or to a datum frame built from different features.

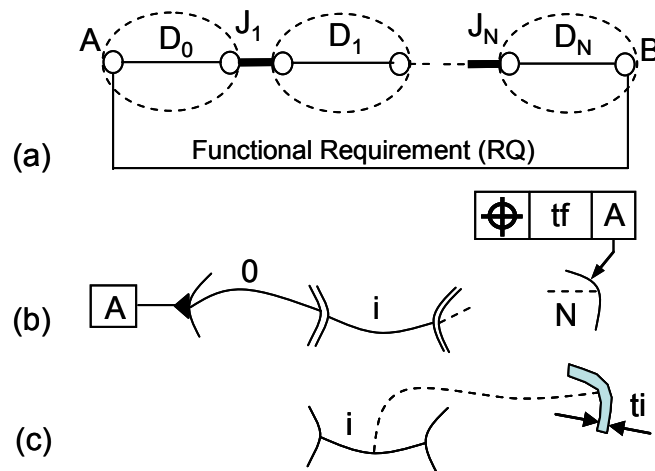
Each edge of the graph represents a small displacement between two frames compared to their relative nominal location. It may represent a functional requirement or a geometrical deviation, or a gap or a clearance between the faces. If the two vertices of the edge belong to the same part, then it is represented by a thin line, otherwise it is a thick line. The part is represented by an ellipse in a dotted line (see Figure 4.1a).

### **4.2. Stack-up tolerance synthesis**

#### **4.2.1. *Serial mechanisms***

The mechanical assembly is composed of parts arranged one after the other following the graphic and schematic representation of Figures 4.1a and 4.1b. Two

functional features belong to each part. We assume that each feature is a face such as a plane, cylinder, spherical, conical surface, etc. A geometrical or dimensional tolerance gives the limits of the deviations between the two surfaces in comparison with their theoretical relative position. The actual face is substituted by a theoretical surface called the surface of substitution. The least square criterion is usually used to determine this theoretical face from the actual one. In this model, it is assumed that each geometrical tolerance means that the substituted face must be inside the tolerance zone.



**Figure 4.1.** Serial mechanism: graphical (a) and schematical representation (b) and tolerance zone attached to each part (c)

The deviation of the tolerated face is characterized by a small displacement torsor. We call the set of inequalities between the components of the deviation torsor according to a tolerance the deviation domain. A domain can also be represented by a geometrical figure in the multidimensional space of the small displacement. The domain can be defined by a set of linear inequalities, the figure is then a polytope. When the domain is defined by non-linear inequalities, quadratic for example, the figure is a convex hull.

Figure 4.2 shows four cases of tolerances for rectangular planar faces and for cylinders. The components of the deviation torsor are given and the inequalities of the deviation domain correspond to the tolerance. We observe that the components depend on the tolerated face but also on the datum. The deviation torsor is denoted  $D$  while the deviation domain is denoted  $[D]$ .

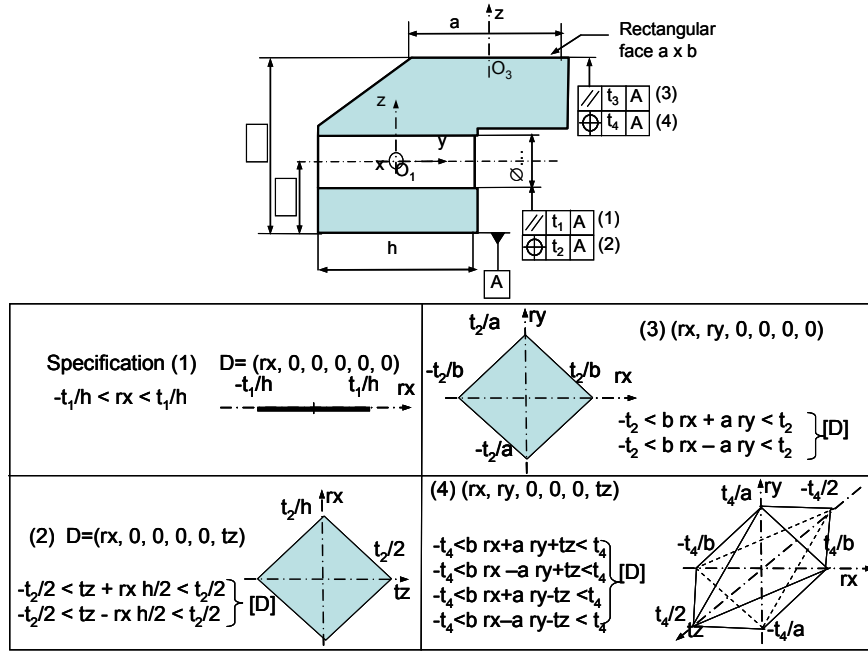


Figure 4.2. Four cases for the deviation torsor and deviation domain

#### 4.2.2. Analysis for worst case stack-up tolerances

For a serial mechanism (Figure 4.1a) with a perfect geometrical contact between the parts, the deviation between the faces A and B is given by the torsor:

$$D_{AB} = \sum D_i \quad (i=0 \text{ to } N) \quad [4.1]$$

Therefore, the torsors  $J_i$  are assumed to be equal to the null torsor. The components of the deviation torsors must be calculated in the same frame. Let  $O_i, x_i, y_i, z_i$  be the frame (i) attached to the face (i). It is the local frame where the deviation torsor is  $D_i^i = (rx_i, ry_i, rz_i, tx_i, ty_i, tz_i)$ : three components for the small angular deviation and three components for the small displacement of the point  $O_i$ .

We note  $D_i$  a torsor and  $D_i^j$  the six components of the torsor  $D_i$  in the frame  $(O_j, x_j, y_j, z_j)$ .

The new components of the same torsor but for the new frame (0) are given by:

$$D_i^0 = T_{0i} D_i^i \quad [4.2]$$

$T_{0i}$  is the transformation matrix (6x6). It depends on the relative position of the two frames. Stack-up tolerance analysis consists of determining the limits of the resulting deviation torsor  $D_{AB}$  when the limits of each deviation  $D_i$  are known. In other words, if the deviation domains  $[D_i]$  are known, the problem is to determine the resulting domain  $[D_{AB}]$ . A solution in the worst case is given by Minkowski sum of the domain  $[D_i]$ . The resulting domain is then:

$$[D_{AB}] = \Sigma [D_i] \quad [4.3]$$

In other words, starting from the inequalities corresponding to each tolerance, it is possible to calculate the set of inequalities that define the limits of the resulting torsor.

In the very simple particular case in which all the domains are homothetic, the sum of Minkowski is also homothetic to other domains. Two domains are homothetic if one is obtained from the other only by changing the scale.

#### 4.2.3. Analysis with the statistical approach

In the statistical approach, it is assumed that the components of the deviation torsor are random variables.

In the general case, it is also assumed that they are independent for the local frame (i). If the components must be calculated in another frame, the mean values and the covariance matrix are changed by the following relations:

$$Dm_i^0 = T_{0i} Dm_i^i \quad [4.4]$$

$$\Lambda_i^0 = T_{0i}^T \Lambda_i^i T_{0i} \quad [4.5]$$

$Dm$  is the torsor for which components are the mean value of the random components, and  $\Lambda$  is the covariance matrix (6x6) of the components.  $T_{0i}^T$  is the transposed matrix of the matrix  $T_{0i}$ .

For stack-up tolerances we then have:

$$Dm_{AB} = \Sigma Dm_i^0 \quad [4.6]$$

And assuming the deviation torsors are independent random variables:

$$\Lambda_{AB} = \Sigma \Lambda_i^0 \quad [4.7]$$

Then, when the statistical data of each deviation torsor are known (density of probability, mean values and standard deviations), we can calculate the statistical characteristics of the resulting functional requirement. Two methods can be used to achieve this: the analytical method requires complex computation; the Monte Carlo algorithm is the most commonly used but is very time-consuming to obtain good accuracy [NIG 95], [HUA 04], [SHA 99].

#### 4.2.4. Synthesis for stack-up tolerances

It is assumed that the functional requirement is given by a tolerance zone. The real value  $t_f$  is the size of this tolerance zone. The same tolerance zone is then put into effect for each functional face of the parts, as shown in Figure 4.1c. If  $t_i$  is the size of these zones, then in the worst case we must have  $t_f = \sum t_i$ , where the sum is extended to the number of tolerated faces. This relation is due to the property of homothetic deviation domains presented above. In this case, if the analysis is done, then all the deviation domains are homothetic and the Minkowski sum is also homothetic representing the functional requirement. The first stage of the method is then very simple. We call the corresponding domain the functional tolerance zone and the functional deviation domain.

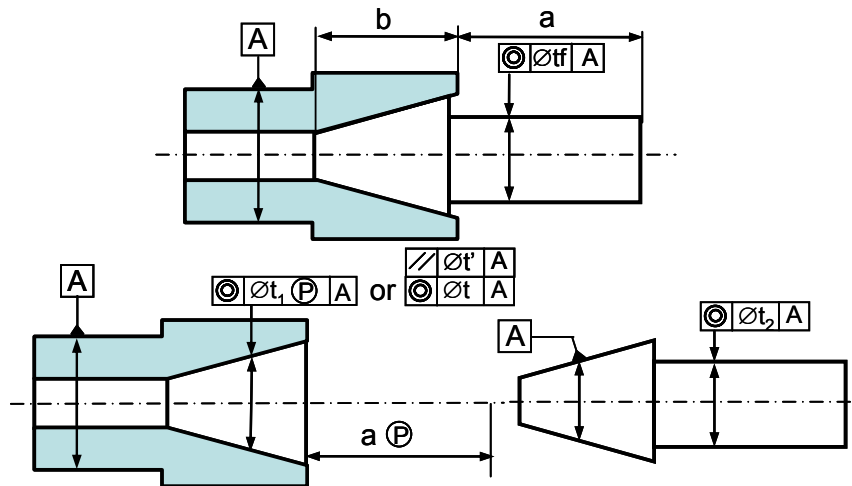


Figure 4.3. Example of a serial assembly

The second stage is more complex because it is not always possible to find the standardized specification corresponding to the given tolerance zone. Generally, the tolerance zone determined by this method is not located in the tolerated

geometrical feature. The projected tolerance allows us to build this type of tolerance zone, however the standard is only adapted for some particular cases and this type of specification is difficult to achieve in the manufacturing process. In this case a transfer of the tolerance is necessary. This consists of defining specifications so that the corresponding deviation domain can be inside the functional domain. The functional domain corresponds to the functional zone.

A very simple example in Figure 4.3 shows the method. Two shafts are linked by a conical fitting. The tolerance zone is first affected to the two parts (first stage) so that  $t_f = t_1 + t_2$ . Then the specifications are such that in the worst case, the associated domain is inside the functional domain (second stage):

$$t_1 = t + 2 \cdot t' \cdot a/b$$

#### 4.3. Serial mechanisms with non-perfect contacts

Assuming the non-interference of the solids, inequalities can be written between the bounded components of the joint torsor. These comprise the joint domain.

Figure 4.4 gives the joint torsor in the local frame, and the joint domain for a round planar face and a cylindrical surface. For a planar joint, if a clearance is possible between the two planar faces (floating contact) there are three bounded components ( $r_x$ ,  $r_y$ ,  $t_z$ ). For a round planar face, the non-interference is represented by the quadratic inequalities defining the joint domain.

The graph of the serial system is represented in Figure 4.1. The functional deviation torsor is:

$$E_{AB} = D_0 + J_1 + D_1 + J_2 + \dots + J_N + D_N \quad [4.8]$$

The sum of torsors is commutative and associative; this property allows us to write:

$$E_{AB} = D_{AB} + J_{AB} \quad [4.9]$$

with

$$D_{AB} = D_0 + \dots + D_N$$

and

$$J_{AB} = J_1 + \dots + J_N \quad [4.10]$$



The composition of displacement is not commutative, so the assumption of small displacements is necessary.

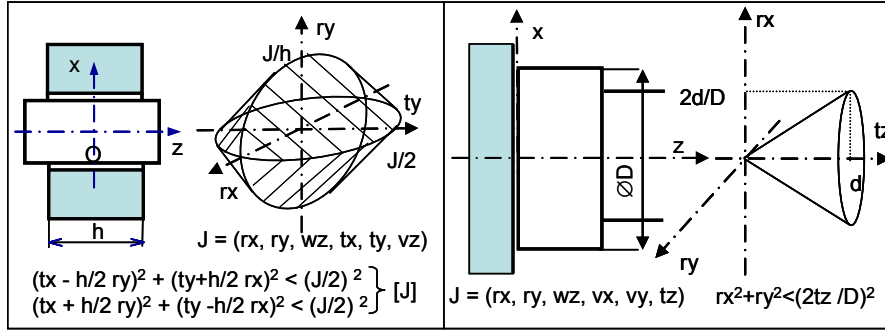


Figure 4.4. Joint torsor and joint domain

#### 4.3.1. Analysis in the worst case

In the worst case, Minkowski sums give two resulting domains: one  $[D_{AB}]$  represents the set of deviations between features A and B when all the joints are in their nominal configuration (contact for planar faces, coaxial axes for cylinders); and the other  $[J]$  represents the set of small displacements enabled thanks to the degrees of freedom and the clearance in the joints.

The functional requirement may be expressed on different forms depending on how these two domains are associated. For example, Minkowski sum gives the set of all the possible deviations for all the parts and all the configurations enabled by the clearances in the joints.

#### 4.3.2. Analysis with the statistical approach

For a given assembly, each part has deviations characterized by deviation torsors. We call “shifted joint domain” the set of displacements allowed by the degrees of freedom and the clearances in the joints.

$$[S] = [J] + D$$

$D$  is a torsor and it is assumed that the components are random variables.  $[J]$  is a domain the limits of which depend on the sizes of the joint features, the diameter for cylindrical faces for example. They are also random variables.

Then, for a sample of assemblies, statistical characteristics can be calculated both for the resulting deviation torsor, as we did for simple stack-up tolerances, and for the resulting joint domain bounded by random variables.

#### 4.3.3. *Synthesis for a serial mechanical system*

The functional requirement may be defined by two types of data, the resulting tolerance zone as it was done in the case of perfect joints, and some limits for the resulting joint domain. The previous synthesis method can be applied for the qualitative allocations of the tolerances by considering only the functional resulting deviation domain.

### 4.4. “Reducible” structure

#### 4.4.1. *Parallel mechanical structure*

The basic parallel structure consists of two parts linked by several contact faces. Figure 4.5 shows the graph of the general case. A frame is built from the different features. It is a datum reference frame for the tolerance of features A and B.

It is assumed that the functional requirement is defined by a tolerance zone between A and B. One of the two features can be the datum and the other the tolerated feature, or the two features can be in a common tolerance zone.

$$D_{AB} = D_A + D + D_B \quad [4.11]$$

$$D = D'_1 + J_1 + D''_1 = \dots = D'_i + J_i + D''_i = \dots = D'_N + J_N + D''_N \quad [4.12]$$

We set:  $D_i = D'_i + D''_i$

Then  $D = D_i + J_i \quad i=1 \text{ to } N$

For a given assembly, for each joint (i) a shifted joint domain can be built:  $[S_i] = D_i + [J_i]$ .

The feasible assembly check is the existence of the intersection of the N shifted joint domains.

In the worst case this intersection exists in the following case. For each joint the clearance between the faces of the two parts is a zone transformed into a tolerance zone allocated to the two faces. If the faces are perfectly connected without any clearance, the tolerance is zero and the face is a primary datum.

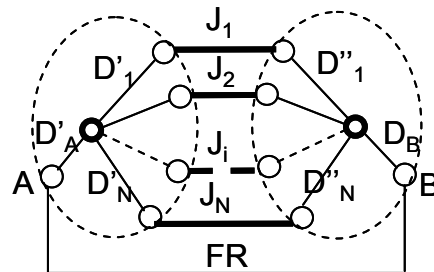


Figure 4.5. A parallel structure

The method for allocating geometrical tolerances to a qualitative view consists first of transforming the clearances of the joints into tolerance zones. The zones are ordered depending on technological data (relative dimensions, type of contact, clearance, etc.), some joints can be at the same level. In the second stage, the standardized specifications that correspond more closely to the tolerance zone and to the ordered faces are allocated. A simple example is presented in Figure 4.6.

Once the qualitative tolerance is defined, it is possible to analyze the functional requirement for given values of the tolerances. The statistical analysis for three dimensional tolerances has been done for a serial mechanism. Several works exist for parallel structures. Anselmetti proposes to decompose complex requirements into several minimum or maximum distance between two parts. This approach requires the determination of this kind of relation case by case [ANS 06].

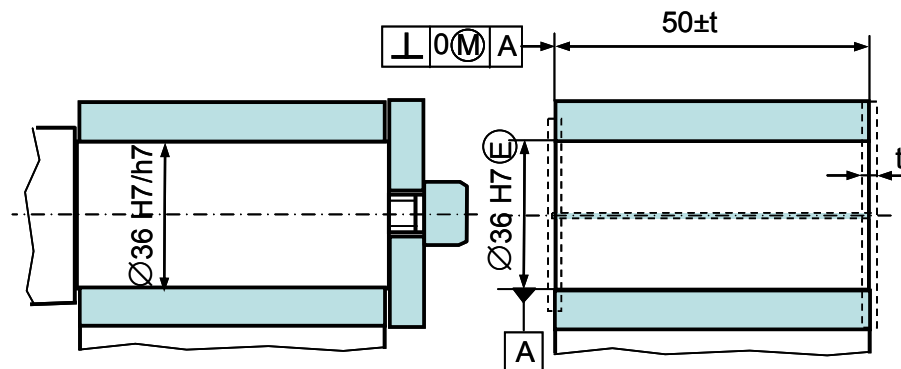


Figure 4.6. Example of a parallel structure

The particular case of an assembly made by two pins and holes is investigated by Shan, Roth and Wilson [SHA 99]. Any angular deviation of the holes is taken into account in their model and the inequalities that express the feasibility of the assembly are specific to the example.

#### 4.4.2. Introduction to “reducible” structure

We call a graph with two vertices linked by one or two edges an elementary graph. We call a reducible graph, a graph that can be transformed into an elementary graph by two types of simplifications:

- Serial simplification: (Figure 4.7a) A set of parts arranged one after the other is replaced by a single edge between two vertices. In the worst case analysis, the sum of Minkowski gives the resulting deviation domain and the resulting joint domain. In the case of the statistical analysis, the Monte Carlo algorithm needs to calculate the sum of random torsors using equations [4.1] and [4.2]. The analytical method can be achieved by equations [4.4], [4.5], [4.6] and [4.7].

- Parallel simplifications: (Figure 4.7b) A set of joints between two parts is replaced by a single joint represented on the graph by an edge. In the worst case analysis the condition for the assembly is checked. For a statistical analysis we only use the Monte Carlo method to check if the assembly is possible and to calculate the resulting deviation torsor and joint torsor, once the parts are linked together. The following section details the computation.

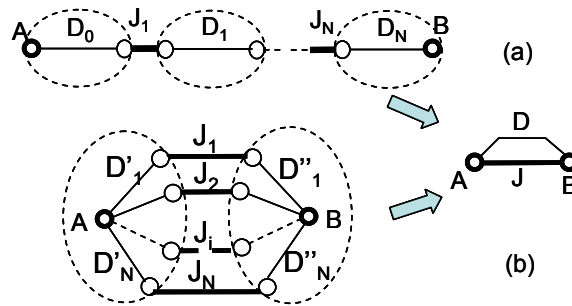
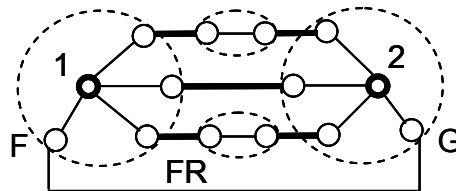
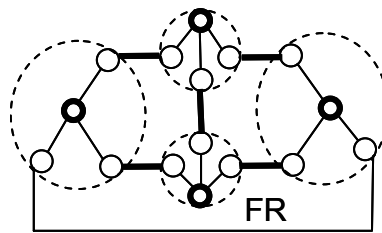


Figure 4.7. Serial and parallel simplification

By applying these two types of simplifications, it gradually transforms the complex structure into a simple system whose graph is elementary and corresponds to the functional condition. Figure 4.8 shows a reducible graph. The graph in Figure 4.9 is not reducible.



**Figure 4.8.** Reducible structure (two pins and two holes assembly)



**Figure 4.9.** Non-reducible graph

#### 4.4.3. Algorithm and computational method

The main originality of this work is the tolerance analysis for the parallel structures, so in the following is a description of the general algorithm for this computation. Three types of data are necessary:

- the nominal geometry: including the topological structure, the relative location of the functional faces and the bounds of these faces;
- technological data: type of joint, dimensional tolerance for cylinder or spherical surfaces;
- manufacturing data: such as capability indices, covariance, or probability density function or histogram.

The general algorithm for a parallel structure is the following:

For each joint ( $i=1$  to  $N$ )

Generate the random deviation torsors  $D_i^i$

Generate the random variables defining the joint domains  $[J_i]$

Starting from the nominal geometry, define the transformation matrices  $T_{i0}$

End For

For each assembly of the sample

Find a taylor S so that  $J_i = T_{i0} S - D_i^i$  ( $i=1$  to  $N$ ) is inside all the joint domain  $[J_i]$  ( $i=1$  to  $N$ ), (the inequalities must be checked)

if S exists the assembly is feasible

End For

For each feasible assembly compute a random configuration D so that all the torsors  $J_i$  are on the bounds of their domain.

Finally the resulting deviation taylor between the two datum frames is obtained, and the deviation taylor  $D_{AB}$  for the functional requirement is computed.

#### 4.5. Example of the pin-hole assembly

##### 4.5.1. Main data

The mechanical system is presented in Figure 4.10. Once the parts are assembled, screws that are not represented on the figure fix the parts together. The functional requirement is that the two cylinders F and G must be on the same axis with a limited deviation. The tolerances relative to the parts are given. Thus, the aim is to compute statistical characteristics of the deviations. First the tolerances must be allocated on a qualitative point of view. The graph is drawn in Figure 4.8.

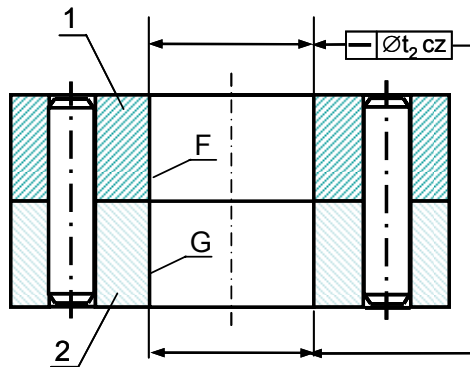


Figure 4.10. Two pins and two holes assembly

The planar contact is without clearance so this face is a primary datum. The two holes have a symmetrical technological function so they are at the same level and are toleranced together.

For each part (1) and (2) in Figure 4.10, the tolerance zones are attached to each functional face (see Figure 4.11). The geometrical tolerances in accordance with ISO standard are represented in Figure 4.11b. The two parts (1) and (2) have the same specifications. Since the parts must be fitted for the assembly, the maximal material condition is involved. For the functional requirement, the axes of each cylinder D and E belong to a cylindrical tolerance zone. So the tolerance for this cylinder is a location with the datum frame constituted by the planar face (primary datum A) and the two holes (secondary datum B). Since the deviation between the two frames (1) and (2) is due to the clearance at the pin and hole assembly, the minimum material may be involved for datum B.

The algorithm presented in the previous section is implemented in an oriented object program. The inequalities associated with joint domains are programmed on a generic form. The analytical method is applied for the serial composition of the deviation torsors.

The Monte Carlo simulation is implemented for the fitting condition. The mean hypotheses are the following: the sample consists of 105 assemblies; the capability indicator is equal to 1 for each component of the deviation torsor; the deviation torsors are independent and the components of a deviation torsor are independent in the local frame attached at the center of the toleranced face; the tolerances for diameters of the two pin holes and the geometrical tolerances are given in Table 4.1. The random variables have normal distribution, but others laws may be easily considered.

Diameters		Tolerances	
Pins 8h7	Holes 8H8	Location of the two holes	Location of the functional cyl.
7.9925±0.0075	8.011 ±0.011	t <sub>2</sub> =0.02	t=0.03

**Table 4.1.** *Tolerance data*

The assembly is possible if at least one configuration with the two pins in their holes exists without material deformation. The angular and linear deviations of the holes, the variation of their sizes and the size of the pins are randomly considered.

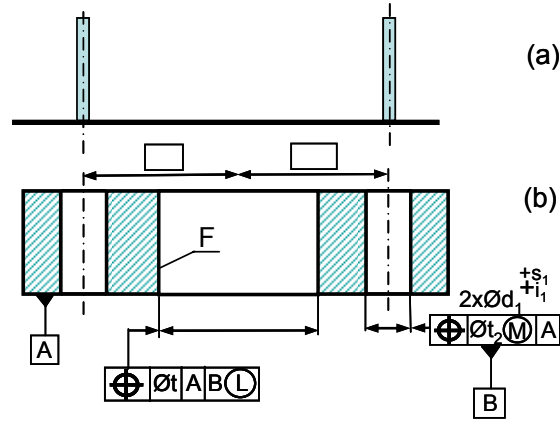


Figure 4.11. Qualitative tolerances for two pins and two holes assembly

#### 4.5.2. Major results

In the worst case the assembly is not possible, but for normal distribution of the independent variables only 210 assemblies are not feasible (and 99,790 are feasible). Figure 4.12 gives the histogram of the deviation between two frames (1) and (2) attached to each part for a simulation. If  $2a$  is the nominal distance between the two holes, this conventional deviation is calculated as follows:

$$d = \sqrt{(Tx^2 + (Ty + a Rz)^2)}$$

The torsor  $D_{12} = (0, 0, Rz, Tx, Ty, 0)$  describes the deviation between (1) and (2) once the assembly is complete.

It is assumed that when the screws are tightened the joint torsor reaches a random point of the bound of the joint domain. This is the reason why the histogram is not symmetrical and decentered to the high values.

Figure 4.12a gives the histogram of the resulting deviation between the two cylinders F and G. The resulting deviation torsor has the following form:

$$D_{FG} = (rx, ry, 0, tx, ty, 0)$$

The minimum diameter  $df$  of the common cylinder including the axes of the two cylinders F and G is calculated from this torsor. The histogram of the resulting random variable  $df$  is shown in Figure 4.12b.



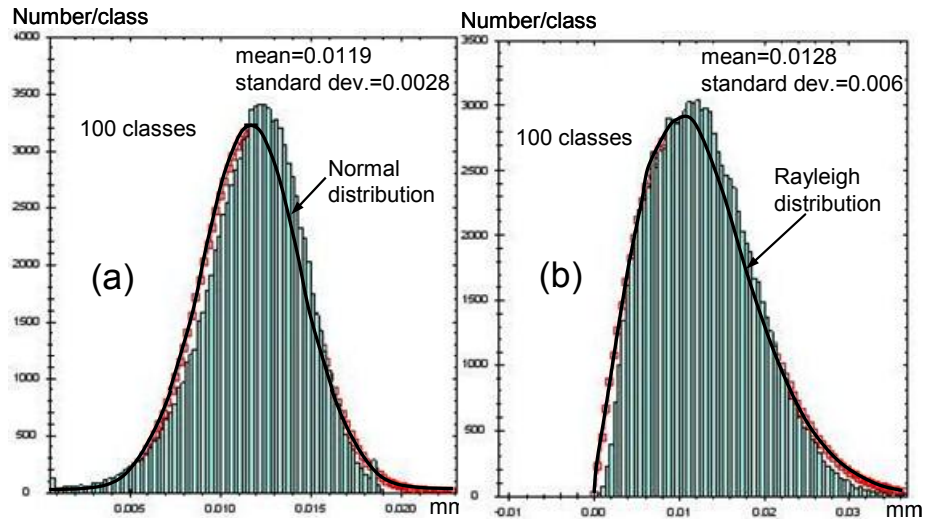


Figure 4.12. Histogram of the deviation assembly and resulting deviation

## 4.6. Conclusion and discussion

### 4.6.1. Conclusion

In this chapter the basis for a general method of allocating geometrical and dimensional tolerances in a qualitative aspect are presented. This step is essential for a coherent analysis. This method leads to consistent tolerances that enable a quantitative analysis. The statistical analysis of a toleranced assembly is carried out by a mixed method, analytic and Monte Carlo algorithm. The method can be generalized to any mechanical structure for which the graph is reducible. The deviations of the feature, including the angular deviations and the clearances at the joint are taken into account.

### 4.6.2. Discussion and future works

The method, however, needs to be improved. Generalization to any mechanism needs complementary studies, for non-reducible graphs for example. The generation of standardized tolerances starting from the tolerance zones is not automatic yet. The inequalities translating the behavior of the joints are difficult to generate in the general case. Nevertheless this method allows the designer to deal with a great number of current assemblies.

#### 4.7. Bibliography

- [ANS 06] ANSELMETTI B., "Generation of functional tolerancing based on positioning features", *Computer-Aided Design*, Vol. 38, pp. 902-919, 2006.
- [BAL 95] BALLOT E., BOURDET P., "Geometrical Behaviour Laws for Computer Aided Tolerancing", *Proceedings of the 4th CIRP Seminar on Computer Aided Tolerancing*, Tokyo, Japan, pp. 143-154, 1995.
- [BOU 88] BOURDET P., CLÉMENT A., "A study of optimal criteria identification based on the small displacement screw model", *Annal of CIRP*, Vol. 37, pp. 503-506, 1988.
- [DAV 02] DAVIDSON J.K., MUJEZINOVIC A., SHAH J.J., "A New Mathematical Model for Geometric Tolerances as Applied to Round Faces", *ASME Transactions, J. of Mechanical Design*, Vol. 124, pp.609-622, 2002.
- [DES 03] DESROCHERS A., GHIE W., LAPERRIÈRE L., "Application of a Unified Jacobian-Torsor Model for Tolerance Analysis", Special Issue on Computing Technologies to Support Geometric Dimensioning & Tolerancing, *Journal of Computing and Information Science in Engineering*, Vol. 3, No. 11, pp. 2425-2459, 2003.
- [GER 06] GERMAIN F., GIORDANO M., ADRAGNA P.A., "Taking manufacturing dispersions into account for assembly: modelling and simulation", *Journal of Machine Engineering*, Vol. 6, No. 1, pp. 83-94, 2006.
- [GER 07] GERMAIN F., GIORDANO M., "A new approach for three-dimensional statistical tolerancing", *10th CIRP Conference on Computer Aided Tolerancing*, Erlangen, Germany, 2007.
- [GIO 01] GIORDANO M., KATAYA B., PAIREL E., "Tolerance analysis and synthesis by means of clearance and deviation spaces", *Proceedings of 7th CIRP*, Cachan, France, 2001.
- [HUA 04] HUANG W., CEGLAREK D., "Tolerance Analysis for Design of Multistage Manufacturing Processes Using Number-Theoretical Net Method (NT-net)", *The international Journal of Flexible Manufacturing System*, Vol. 16, pp.65-90, 2004.
- [NIG 95] NIGAM S.D. and TURNER J.U., "Review of statistical approaches to tolerance analysis", *Computer-Aided Design*, Vol. 27, No.1, pp. 6-15, 1995.
- [SHA 99] SHAN A., ROTH R.N. and WILSON R.J., "A New Approach to Statistical Geometrical Tolerance Analysis", *Advanced Manufacturing Technology*, Vol. 15, pp. 222-230, 1999.

## Chapter 5

# Reliability Analysis of the Functional Specification Applied to a Helicopter Gas Turbine

### 5.1. Introduction

The objective of this chapter is to set up an analytical model which enables performance quantification of a high pressure turbine of a helicopter engine. The principle of these kinds of turboshaft engines is to transform the air flow coming from the input of the motor into mechanical energy to the rotor. This mechanical energy is produced by the air flow passing through the rotor blades. An important part of the fluid does not work due to the clearance between the tips of the blades and the stator. Thus, it is important to find a compromise between the maximal and the minimal values of clearance:

- a value of clearance that is too high decreases the performances of the engine;
- a value of clearance that is too low increases the risk of damage to the engine by contact between the rotor and the stator (this could lead to the destruction of the engine).

First, an analytical model of the clearance is made according to the architecture, the various parts and the connecting elements constituting the turbine. The turbine architecture is analyzed in order to obtain a tolerancing model of clearance. The worst case is applied and allows us to compute the extreme variations of clearance.

---

Chapter written by Yann LEDOUX, Denis TEISSANDIER and Samir SID-AHMED.

An influence analysis of every parameter of the tolerancing model is proposed and allows us to identify their contributions on the clearance.

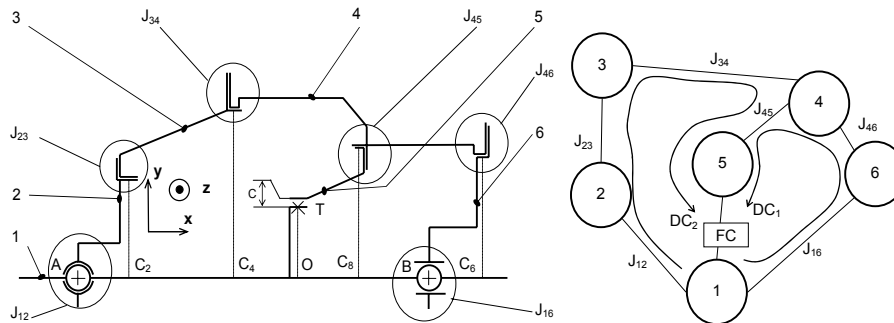
Second, a reliability analysis is performed. According to the two risk types presented previously (characterized by the maximal and minimal values of clearance), two limit state functions are defined respectively and correspond to both different failure zones. There is assumed to be a Gaussian distribution for each geometrical tolerance value where the average is the nominal value and the six times of the standard deviation correspond to the tolerance value. An estimation of the failure probability is then calculated directly by a stochastic simulation (Monte Carlo simulation).

The most probable point of failure for each limit state function is assessed by Form technique (first order method). The advantage of this approach is the sensitivity analysis. This calculation allows us to quantify the influence of the statistic modes (averages, standard deviations) on the failure probability. These different results are used to aid the designer in the attribution of nominal dimensions and geometrical tolerances in order to increase the performance of the high pressure turbine and to decrease the risk of interference between rotor and stator.

## 5.2. Studied case

A simplified architecture of the turbine studied is proposed in Figure 5.1. We assume the following hypotheses ([BOU 95], [CLO 01], [CLE 88] and [BAL 99]):

- no deformable part and non-local strains in contact surfaces;
- no form defaults in the real surface.



**Figure 5.1.** *Simplified representation of a turbine and the associated graph of joints with influent cycles on FC*

Let us consider the joints  $J_{23}$ ,  $J_{34}$ ,  $J_{46}$  and  $J_{45}$  (Figure 5.1). All these mechanical joints are constituted by a ball and cylinder pair along  $x$  and a planar pair along  $x$ . The mechanical joint  $J_{12}$  is considered as a spherical pair at point A and the mechanical joint  $J_{16}$  is considered as a ball and cylinder pair at point B along  $x$ .

### 5.2.1. Tolerancing model

Let us consider a general joint  $J_{ij}$  defined in point  $C_k$ , it is defined by two different displacement vectors:

- $\epsilon_{Ck,ij}$  corresponding to translation of part  $i$  with respect to part  $j$  in point;
- $\rho_{ij}$  corresponding to rotation of part  $i$  with respect to part  $j$ .

The 2D modeling of this turbine in the plane  $(O,x,y)$  allows us to write [5.1]:

$$\epsilon_{Ck,ij} = u_k \cdot \mathbf{x} + v_k \cdot \mathbf{y} \quad [5.1]$$

$$\rho_{ij} = \gamma_k \cdot \mathbf{z}$$

where:

- $u_k$  and  $v_k$  represent the geometrical deviations of translation at the point  $C_k$ , respectively along the  $x$ -axis and the  $y$ -axis between part  $i$  and  $j$ ;
- $\gamma_k$  represents the geometrical deviation of rotation along the  $z$ -axis between part  $i$  and  $j$ .

These geometrical deviations are due to manufacturing defects of the contact surfaces between part  $i$  and  $j$  and clearance of the mechanical joints. This model has been proposed by [BOU 95] and [CLO 01].

By using the small displacement theory (in fact by assuming an angular linearization), it is possible to write [CLE 88]:

$$\epsilon_{O,ij} = \epsilon_{Ck,ij} + OC_k \times \rho_{ij} \quad [5.2]$$

With  $OC_k = L_k \cdot \mathbf{x}$ , it is possible to write:

$$u_O = u_{Ck} - L_k \times \gamma_K \quad [5.3]$$

The different geometrical deviations of the joints  $J_{ij}$  are listed in Table 5.1 and illustrated in Figure 5.1.

Joint	Definition point	Small displacement parameters
$J_{12}$	$A, \mathbf{OA} = L_A \cdot \mathbf{x}$	$u_A, v_A, \Gamma_A$
$J_{23}$	$C_2, \mathbf{OC}_2 = L_2 \cdot \mathbf{x}$	$u_2, v_2, \gamma_2$
$J_{34}$	$C_4, \mathbf{OC}_4 = L_4 \cdot \mathbf{x}$	$u_4, v_4, \gamma_4$
$J_{46}$	$C_6, \mathbf{OC}_6 = L_6 \cdot \mathbf{x}$	$u_6, v_6, \gamma_6$
$J_{45}$	$C_8, \mathbf{OC}_8 = L_8 \cdot \mathbf{x}$	$u_8, v_8, \gamma_8$
$J_{16}$	$B, \mathbf{OB} = L_B \cdot \mathbf{x}$	$u_B, v_B, \Gamma_B$

**Table 5.1.** *Small displacement parameters of joints*

The parameters  $\Gamma_A$  and  $\Gamma_B$  represent the degrees of freedom respectively of  $J_{12}$  and  $J_{16}$  along the z-axis [BOU 95]. The functional condition FC on the clearance  $c$  can be defined as follows:

$$\text{FC: } c_{\min} \leq c \leq c_{\max} \quad [5.4]$$

Moreover, according to [5.3]:

$$c = \boldsymbol{\varepsilon}_{T,15} \cdot \mathbf{y}$$

and finally,

$$c = \boldsymbol{\varepsilon}_{O,15} \cdot \mathbf{y} \quad [5.5]$$

Taking into account the functional condition involves taking into account two different 3D dimension-chains  $DC_1$  and  $DC_2$  (also called influential cycles, [BAL 99]). This is shown in Figure 5.1. Then, both 3D dimension-chains are:

$$\begin{aligned} DC_1 : & \left\{ \begin{array}{l} \rho_{15} = \rho_{12} + \rho_{23} + \rho_{34} + \rho_{45} \\ \varepsilon_{0,15} = \varepsilon_{0,12} + \varepsilon_{0,23} + \varepsilon_{0,34} + \varepsilon_{0,45} \end{array} \right\} \\ DC_2 : & \left\{ \begin{array}{l} \rho_{15} = \rho_{16} + \rho_{64} + \rho_{45} \\ \varepsilon_{0,15} = \varepsilon_{0,16} + \varepsilon_{0,64} + \varepsilon_{0,45} \end{array} \right\} \end{aligned} \quad [5.6]$$

According to relation [5.6], it is possible to write relations [5.7] with [5.3] and [5.5]:

$$\begin{aligned} DC_1 : & \left\{ \begin{array}{l} \gamma_{15} = \Gamma_A + \gamma_2 + \gamma_4 + \gamma_8 \\ c = v_A - L_A \cdot \Gamma_A + v_2 - L_2 \cdot \gamma_2 + v_4 - L_4 \cdot \gamma_4 + v_8 - L_8 \cdot \gamma_8 \end{array} \right\} \\ DC_2 : & \left\{ \begin{array}{l} \gamma_{15} = \Gamma_B + \gamma_6 + \gamma_8 \\ c = v_B - L_B \cdot \Gamma_B + v_6 - L_6 \cdot \gamma_6 + v_8 - L_8 \cdot \gamma_8 \end{array} \right\} \end{aligned} \quad [5.7]$$

Finally, it is possible to deduce from equation [1.7] the following equations:

$$\begin{aligned} \Gamma_A &= \Gamma_B - \gamma_2 - \gamma_4 + \gamma_6 \\ \Gamma_B &= \frac{-v_A - v_B + (L_2 - L_A) \cdot \gamma_2 - v_4 + (L_4 - L_A) \cdot \gamma_4 - v_8 + v_6 + (-L_6 + L_A) \cdot \gamma_6}{L_B - L_A} \end{aligned} \quad [5.8]$$

Relations [1.8] are used to calculate the clearance c:

$$c = K_A \cdot v_A + K_B \cdot v_B + K_{21} \cdot v_2 + K_{22} \cdot \gamma_2 + K_{41} \cdot v_4 + K_{42} \cdot \gamma_4 + K_{61} \cdot v_6 + K_{62} \cdot \gamma_6 + K_{81} \cdot v_8 + K_{82} \cdot \gamma_8 \quad [5.9]$$

The 10 parameters  $K_A$ ,  $K_B$ ,  $K_{i1}$  and  $K_{i2}$  with  $i \in \{2,4,6,8\}$  are considered as coefficients of influence respectively of the parameters  $v_A$ ,  $v_B$ ,  $v_i$  and  $\gamma_i$  on the clearance c ([BOU 95], [CLO 01]). Table 5.2 indicates the value of the 10 coefficients of influence for every joint constituting the turbine.

	Coefficients of influence	Values
$J_{12}$	$K_A = \frac{L_B}{L_B - L_A}$	0.137
$J_{16}$	$K_B = \frac{-L_A}{L_B - L_A}$	0.863
$J_{23}$	$K_{21} = \frac{L_B}{L_B - L_A}$	0.137
	$K_{22} = \frac{L_A L_B - L_2 L_B}{L_B - L_A}$	15.605
$J_{34}$	$K_{41} = \frac{L_B}{L_B - L_A}$	0.137
	$K_{42} = \frac{L_A L_B - L_4 L_B}{L_B - L_A}$	37.098
$J_{46}$	$K_{61} = \frac{-L_A}{L_B - L_A}$	0.137
	$K_{62} = \frac{-L_A L_B - L_6 L_A}{L_B - L_A}$	44.882
$J_{45}$	$K_{81} = 1$	1
	$K_{82} = L_8$	48

**Table 5.2.** *Coefficients of influence and associated values*

Table 5.3 lists the different variations of every small displacement parameter of the c model.

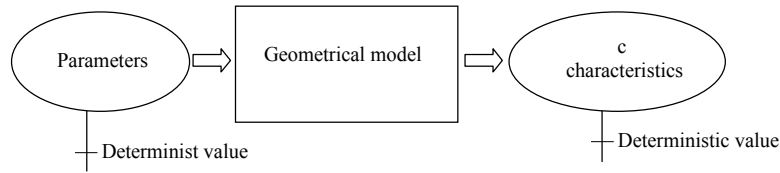
Small displacement parameters	Interval values: $v_i (mm)$ ; $\gamma_i (rad)$
$v_A$	[-0.00165;0.00165]
$v_B$	[-0.025;0.025]
$v_2$	[-0.012;0.012]
$v_4$	[-0.008;0.008]
$v_6$	[-0.01525;0.01525]
$v_8$	[-0.0065;0.0065]
$\gamma_2$	[-0.00005482;0.00005482]
$\gamma_4$	[-0.00010964;0.00010964]
$\gamma_6$	[-0.00008054;0.00008054]
$\gamma_8$	[-0.00327;0.00327]

**Table 5.3.** *List of the small displacement variations*



### 5.3. Deterministic approach

According to the design tolerancing allocation, reported in any part drawings, it is possible to estimate the final possible variation of the clearance  $c$  between the rotor and the stator of the turboshaft engine.



**Figure 5.2.** *Illustration of the deterministic approach*

The calculation made done according to the worst case calculation. As a function of the different value for every parameter (Table 5.2, 5.3 and equation [5.9]), it is possible to quantify the  $c$  value according to the worst case.

The variation of the  $c$  value is:

$$\Delta_c = 0.210 \text{ mm.}$$

With this value, the clearance between the blade and the stator of the turbine engine can vary as shown in equation [5.10].

$$c_{\text{nominal}} - \Delta_c \leq c \leq c_{\text{nominal}} + \Delta_c \quad [5.10]$$

We assumed that  $c_{\text{nominal}} = 0$ , consequently,

$$-0.21 \leq c \leq 0.21$$

The FC requirement imposes a variation of  $c$  in the following range:

$$[-0.16 \text{ mm}, 0.1 \text{ mm}], (\text{ie } c_{\text{min}} = -0.16 \text{ mm}, c_{\text{max}} = 0.1 \text{ mm})$$

With the value of  $c$  calculated, the value of the clearance can vary between -0.21 and 0.21 mm. The value of  $c_{\text{mini}}$  is too low compared to the risk of contact between the blade and the stator (mini value imposed -0.16 mm). Moreover, the maximum value of  $c$  is too significant 0.21 mm, whereas, according to the requirements on the efficiency of the turboshaft engine, the clearance  $c$  does not exceed 0.1 mm. The results show, with the specification on the different tolerancing parameter, that it is possible to have a no conform turbine to compare to the initial requirements. On the

other hand, with the worst case approach, it is impossible to quantify the risk of no conform turbine.

### 5.3.1. Sensitivity and elasticity analysis

According to the analytical model of  $c$  (equation [5.9]), it is possible to quantify the sensitivity  $s_{xi}$  of each small displacement parameter on the clearance value. Classically, a initial approach consists of estimating the calculation of the partial derivatives around the extreme geometrical values. This computation is done using equation [5.11].

$$s_x = \left. \frac{\partial c}{\partial x} \right|_{x_e} \quad [5.11]$$

where,  $x$  corresponds to the vector constituted of the different parameters listed in Table 5.3.  $x_e$  is the extreme value of every parameter.

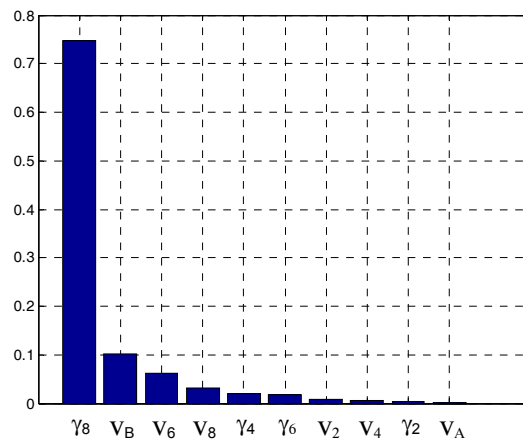
This computation is representative of the influence of every parameter on the  $c$  value. It is interesting “to normalize” all these contributions to compare the influence of one to each others on the  $c$  value. Thus, the calculation of elasticity is introduced (equation [5.12]), [SRI 99], [SKO 97]. All the different contributions are done in Table 5.4.

$$e_x = \frac{x_e}{\Delta c} s_x \quad [5.12]$$

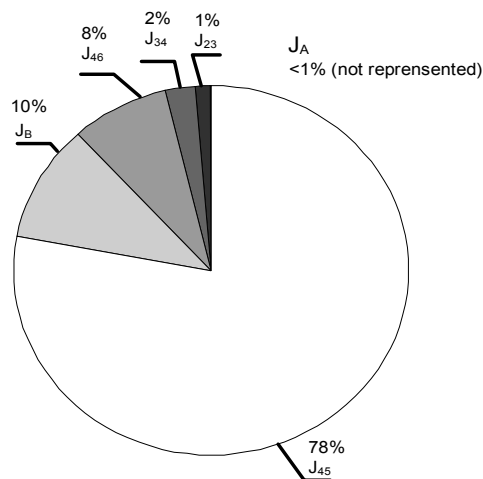
	Sensibility	Elasticity
$\gamma_8$	48	0.7485
$v_B$	0.863	0.1029
$v_6$	0.863	0.0628
$v_8$	1	0.031
$\gamma_4$	37.098	0.0194
$\gamma_6$	44.882	0.0172
$v_2$	0.137	7.83E-03
$v_4$	0.137	5.22E-03
$\gamma_2$	15.605	4.08E-03
$v_A$	0.137	1.08E-03

**Table 5.4.** Values of sensitivity and elasticity of the geometrical model (decreasing order)

The different elasticities are represented in Figure 5.3. The data are sorted according to their elasticity values in decreasing order. Note that the defect related to  $\gamma_8$  and  $v_8$  corresponding to the mechanical joint  $J_{45}$  represent more than 85% of the  $c$  value. The second most influential joint corresponds to the bearing in point B,  $J_B$  (close to the blade) with an effect of around 10%. These different contributions are represented in Figure 5.4. The other parameters of  $c$  clearance condition have a quasi-null effect according to the elasticity analysis.



**Figure 5.3.** Elasticity value of every geometrical parameter (sorted in decreasing order)



**Figure 5.4.** Influences of mechanical joints on  $c$  value

Thus, if we want to decrease the value of  $c$ , it is imperative to decrease the value of  $\gamma_8$ . It is possible to determine the contribution of each mechanical joint of the turbine on the  $c$  value. The link between the parameter  $\gamma_i$  and  $v_i$  and the different joints is realized with the use of equation [5.9] and Table 5.2. Figure 5.4 illustrates the different joint contributions.

### 5.3.2. Discussion about the determinist results

The deterministic approach allows us to calculate the extreme variation of the clearance  $c$  according to the worst case criterion. With this approach, if all parts are in conformity with the geometrical specifications of the detailed drawings, after the assembly process, it is impossible to obtain a  $c$  value outside of the functional requirements (defined in equation [5.4]). On the other hand, it is shown that the variation values of the  $c$  clearance are too significant compared to the requirements on the turboshaft engine. It was highlighted that there were two kind of risk:

- due to an insufficient  $c$  value, a contact between the blade and stator is possible;
- an excessive  $c$  value, induces a loss of mechanical efficiency.

According to the elasticity calculation, it is possible to identify the most influential parameters in the turbine and to deduce the leading actions in the aim to decrease the  $c$  range, or the action for redesigning the geometrical accuracy of the joint specified in all parts of the turbine. With the following deterministic approach, it is possible to see that some products could not be conformed to the customer requirement but, it is impossible to quantify the probability of non-conforming products. In section 5.4, a probabilistic approach is proposed making it possible to quantify the risk of blade-stator contact, or loss of efficiency, by realizing the assumption on the geometrical defect distribution.

### 5.4. Probabilistic approach

In the second part of this chapter, we propose a probabilistic approach to the  $c$  value. This calculation allows us to estimate:

- the  $c$  variation according to statistical criterion;
- the probability of taking into account the customer specification on  $c$ .

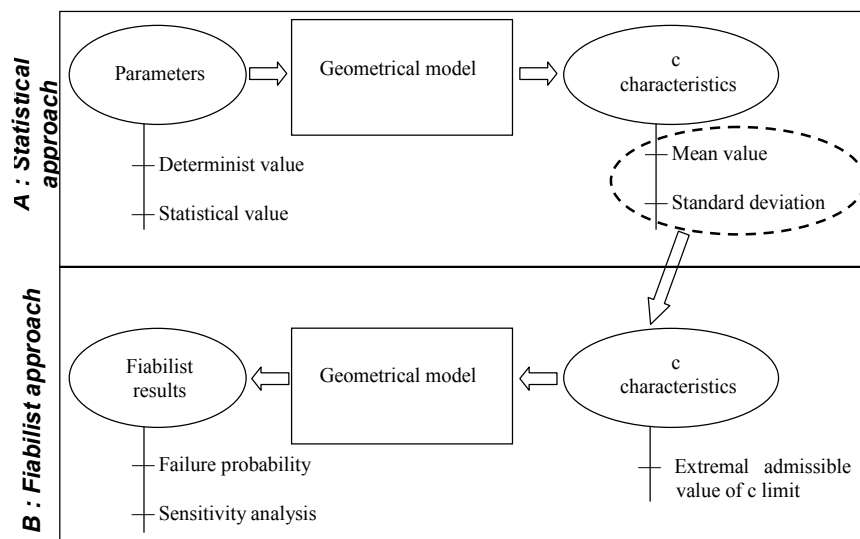
Different recent studies are proposed using a statistical approach coupling probabilistic aspects [GER 07], [BAL 08] and [DAN 08]. Initially, it is necessary to define in the  $c$  model the parameters which have:

- deterministic behavior, a constant value defines their level;
- statistical behavior, different statistical modes define their levels (mean, standard deviation, skewness, etc.).

For the second category of parameters, it is necessary to know precisely the statistical modes of the populations. This information is obtained in general by statements of measurements on manufactured part batches or according to the knowledge of experts on the production process. In the second time, scenarios of failure have to be defined. In our case, two different scenarios are possible:

- the clearance between the blade and stator is too small;
- the clearance between blade and stator is too great.

Estimation of the failure probability can be carried out according to various approaches. The most traditional approach is to make a Monte Carlo simulation. This approach consists of realizing random simulated turbines according to the statistical characteristics of every parameter. A ratio between a non-conforming turbine and an all-simulated turbine defines the probability of obtaining a non-conforming turbine, with these statistical parameter characteristics. This calculation is illustrated in Figure 5.5A with a statistical approach.



**Figure 5.5.** Illustration of the statistical (A) and fiabilist (B)

Other approaches exist to carry out this estimation. We can note the form or sorm method (first-order or second-order reliability methods). The estimation of the

failure probability is carried out by a local approximation of the most probable point in the iso-probabilistic space [BRE 88], [LEM 05] and [MAD 86]. With this approach, the probability of failure estimation is faster (less simulation is needed). Moreover, it is possible to quantify the effect of statistical characteristics of every parameter on the failure probability. Thus, a designer can identify most influent parameters in the failure probability value, and then, define the action to decrease it. Figure 5.5 represents the proposed approach for this fiabilistic analysis (Figure 5.5B).

#### 5.4.1. Definition of the state functions

The reliability calculation consists of defining a failure function. This approach has been developed by [LEM 05] and is implemented in the commercial software Phimeca® [PHI 03]. This method is commonly used in civil engineering and for mechanical structure analysis [LEM 05] and [NIA 07]. In the case of tolerancing analysis, the limit state corresponds to the  $c$  value limit. The considered limits are  $-0.16$  mm and  $0.1$  mm respectively for lower and upper bound. By definition, the failure zone is obtained if the limit state function (named  $G$ ) has null or negative value. This approach is illustrated in Figure 5.6 for the lower bound:

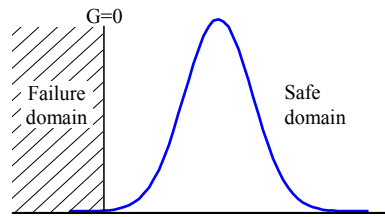


Figure 5.6. Definition of the limit state function  $G$

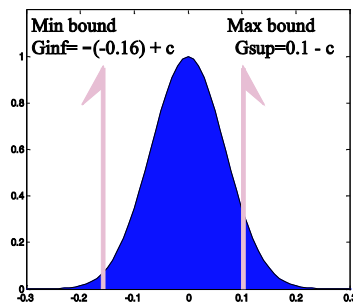


Figure 5.7. Definition of failure functions  $G_{inf}$  and  $G_{sup}$

According to the required specifications for  $c$ , it is possible to explain two different limit state functions for every bound as follows:

$$\text{For lower bound: } G_{\text{inf}} = -(-0.16 \text{ mm}) + c \quad [5.13]$$

$$\text{For upper bound: } G_{\text{sup}} = 0.1 \text{ mm} - c \quad [5.14]$$

Figure 5.7 illustrates the limit states around the distribution of  $c$  clearance.

In the following sections, all different statistical and fiabilistic calculations are realized using phimeca® software [PHI 03].

#### **5.4.2. Determination of the statistical parameters from the tolerancing model**

The  $c$  model is related to two types of parameters:

- the coefficients of influence linked to the architecture of the turbine (assumed to be deterministic values; values available in Table 5.2);
- the coefficients linked to the geometrical specifications of every part constituting the turbine.

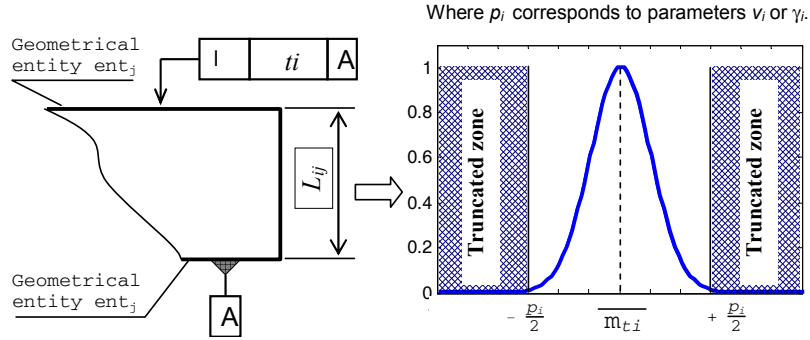
This last category is assumed to be statistical. It is assumed that there is no interaction between the different statistical parameters of the tolerancing model (no correlation).

For these parameters, a Gaussian distribution is used. In order to characterize this kind of statistical distribution, the first two statistical modes are necessary, i.e. the mean and the standard deviation. A truncated distribution is imposed with the aim of avoiding the extreme value outside of the geometrical specification. The statistical modes are defined as follows:

– Mean:  $\overline{m_{ti}} = 0$ , that is mean that the tolerance zone  $ti$  is centered around the nominal value of the dimension  $L_{ij}$  (between entity  $ent_i$  and  $ent_j$ ).

– Standard deviation:  $\sigma_{ti} = (ti/6)$ , with a Gaussian distribution, 99.73% of individuals are taken into account.

This correspondence between a drawing part and the statistical modes are illustrated in Figure 5.8, in the case of location specification.



**Figure 5.8.** Relation between geometrical specifications and statistical values

Calculation of the statistical modes of the  $c$  clearance is approximated according to stochastic simulation (called Monte Carlo simulation MCS). It is then possible to calculate these values:

$$\bar{c} = -1.37e - 005 \text{ mm}; \sigma_c = 0.0524 \text{ mm}.$$

The distributions of  $c$  as well as both functions of limit state ( $G_{\text{inf}}$  and  $G_{\text{sup}}$ ) are represented in Figure 5.7. Note that the  $c$  value has a Gaussian distribution. This observation is confirmed by the additive model of the  $c$  clearance.

#### 5.4.3. Failure rate estimation

Two probabilities of failure are calculated for both failure functions. The probability to obtain a clearance value inside the interval  $[-0.16 \text{ mm}, 0.1]$  corresponds to:  $P_{c \in [-0.16 \text{ mm}, 0.1]} = 1 - (P_{f_{c \leq -0.16 \text{ mm}}} + P_{f_{c \geq 0.1 \text{ mm}}})$

Different approaches are used to estimate the failure probability. The classic approach consists of realizing a Monte Carlo simulation. It is possible to calculate the confidence interval (CI) of the estimated failure probability according to equation [5.15], [SHO 68]:

$$CI(\%) = 200 \sqrt{\frac{1 - \tilde{P}f}{n \cdot \tilde{P}f}} \quad [5.15]$$

where  $\tilde{P}f$  corresponds to estimated probability and  $n$  the number of simulations.



This CI corresponds to a probability of 95% that the exact value of Pf is included in the interval:

$$Pf \in \tilde{Pf}.(CI) \quad [5.16]$$

The different probability and associated confidence intervals displayed in Table 5.5. The FORM line of Table 5.5 corresponds to the values found by an approximation method (first order method). This approximation allows us to estimate the probability of failure quickly by limiting the number of random individuals to trial and to have a quantitative analysis of the influence of the parameters on the analytical model and on the failure probability. As Form probability comes from approximation of the most probable failure point, it is important to compare its value to the one found with MCS technique. Here, both values are very closed and validate the approximate results.

	$Pf_{c \leq -0.16mm}$	$Pf_{c \geq 0.1mm}$	$P_{c \in [-0.16mm, 0.1mm]}$
Monte Carlo (MC)	$2.47 \times 10^{-2} \%$	2.84 %	97.14%
Error on the Pf estimation by MC simulation	$\pm 6.4\%$	$\pm 0.6\%$	$\pm 4.9 \times 10^{-2} \%$
FORM	$3.72 \times 10^{-2} \%$	2.86 %	97.10%

**Table 5.5.** Failure probability results by MCS and Form approximation, the number of individuals tested for MCS correspond to  $10^6$

#### 5.4.4. Influence of the tolerancing parameters on the failure probability

The probability analysis of the most probable failure point is called  $x_r$ .  $x_r$  is a vector for which its components correspond to the tolerancing parameters. This calculation is carried out thanks to a space transformation from natural variable into iso-probabilistic space [LEM 05]. In order to determine the influence of each parameter on the point  $x_r$ , it is necessary to calculate the coordinates of this point in this iso-probabilistic space. These values are given in Figures 5.10 and 5.11, respectively for the limit state functions  $G_{inf}$  and  $G_{sup}$ .

According to these calculations, it is possible to link parameters to the failure probability. Then, the most influential parameters are located in Figure 5.11.

In Figures 5.9 and 5.10, only the parameters which have an influence greater than 1% are represented. It is possible to see for both limit state functions that the most influential parameter on the failure probability corresponds to  $\gamma_8$ . The next most influential parameter is  $v_B$ , corresponding to the defect located in the bearing B. For the  $G_{inf}$  function, the same influential parameters are listed added to  $v_6$  which

corresponds to joint  $J_{46}$ . Consequently, if we want to decrease the probability of failure, it is necessary to modify the value of the  $\gamma_8$  parameter.

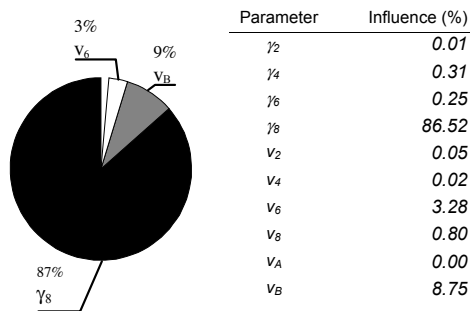


Figure 5.9. Contribution analysis of the tolerancing parameters of  $G_{inf}$

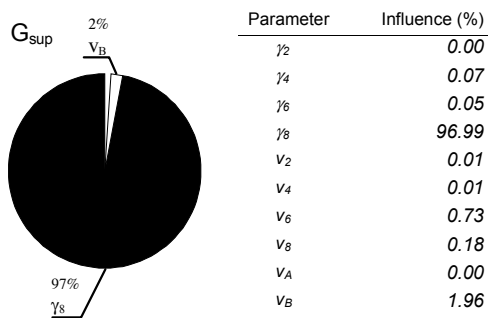


Figure 5.10. Contribution analysis of the tolerancing parameters of  $G_{sup}$

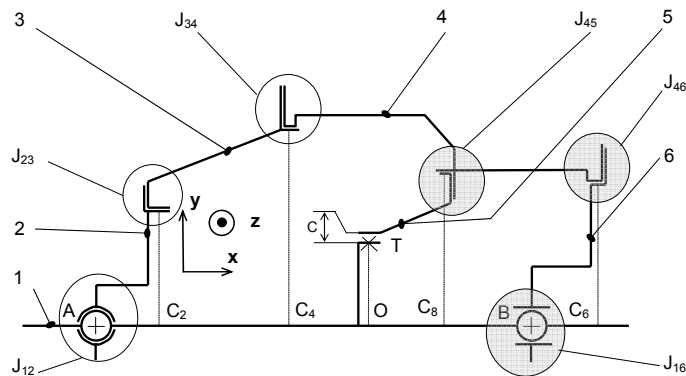


Figure 5.11. Localization of most influent joints (in gray color) on the failure probability

This predominance of  $\gamma_8$  in the contribution on the failure probability could be explained by a particular geometrical configuration: at the end of the dimension chains  $DC_1$  and  $DC_2$  (see Figure 5.1) and a significant value of the defect of the connection due to the difficulty of manufacturing this connecting surface.

#### 5.4.5. Sensibility analysis on the failure probability

The previous results allow us to make a hierarchy of the most influential parameters on the failure probability. But, we haven't any idea about the trends and the action to realize in the aim to improve the reliability of the turbine. We propose to calculate the sensitivity of the mean and standard deviation of every parameter on the failure probability (called the reliability sensitivity, equation [5.17], [LEM 05]).

$$s = \frac{\partial G(x)}{\partial x} \Big|_{x_r} \quad [5.17]$$

where  $x_r$  corresponds to the most probable failure point.

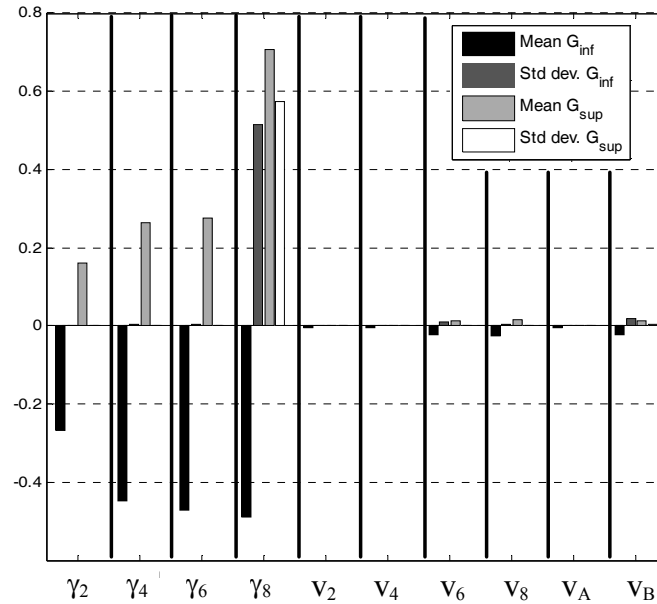
In Figure 5.12, the sensitivity values are normalized to compare to the norm of every contribution  $s$  (corresponding to vector of sensitivity). The normalized sensitivities are achieved according to equation [5.18].

$$s_{\text{normalized}} = \frac{1}{\|s\|} \cdot \frac{\partial G(x)}{\partial x} \Big|_{x_r} \quad [5.18]$$

The norm of  $s$  is respectively:

- for  $G_{\text{inf}}$ :  $s_{G_{\text{inf}}} = 2.09$ ;
- for  $G_{\text{sup}}$ :  $s_{G_{\text{sup}}} = 79.55$ .

All of the standard deviations of the parameters increase the failure probability of the two limit state functions  $G_{\text{inf}}$  and  $G_{\text{sup}}$ . This result confirms that an increase of the dimensions of tolerance zones and consequently, the values of standard deviations of parameters, increases the standard deviation of the clearance  $c$ ; and thus increase the failure rate. Concerning the effect of the mean values of every parameter, their effects are signed and have opposite effects on the limit state functions. For example, a rise of means decreases the failure probability of  $G_{\text{inf}}$  but increase  $G_{\text{sup}}$ . This phenomenon is explained by the definition of the failure function,  $c$  has an opposite sign in the two state functions.



**Figure 5.12.** Normalized sensitivity of every parameter on the failure probability

The most influential parameter in this reliability analysis is always parameter  $\gamma_8$ , for which the influence of the average and the standard deviation have the same effect on the failure probability. The standard deviations of the other parameters are negligible. That means that variation of the tolerance value have a second order effect to compare to the variation of the nominal position of the tolerated surface.

It is possible to observe that an increase of  $\gamma_2, \gamma_4, \gamma_6, \gamma_8$  mean values:

- decreases the failure probability for  $G_{inf}$ ;
- increases the failure probability for  $G_{sup}$ .

Thus, the nominal position effects of these parameters have an antagonist effect. It will be necessary, with this geometrical configuration, to find a compromise between the risk of contact between the rotor and the stator and the loss of engine efficiency.

#### 5.4.6. Parametric analysis of the $\gamma_8$ parameter

The objective is to quantify the effect of the mean and standard deviation variation of the  $\gamma_8$  parameter on the failure probability. It consists of a parametric

analysis. The variations of the statistical parameters of  $\gamma_8$  are made in equations [5.19] and [5.20]:

For standard deviation values:

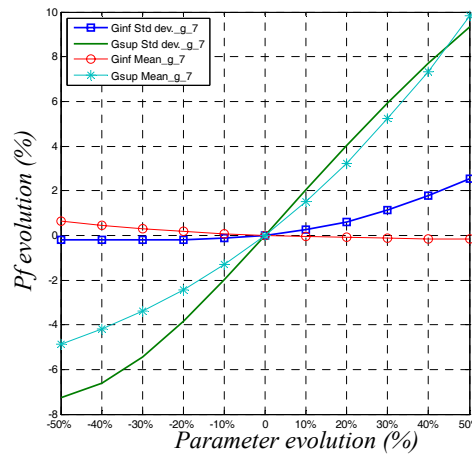
$$\Delta\sigma_{\gamma_8_{i\%}} = (s_{\gamma_8} \times (1 + i\%)) \text{ with } i \in [-50\%, 50\%] \quad [5.19]$$

For the mean value:

$$\Delta\bar{\gamma}_{8_{i\%}} = \bar{\gamma}_8 + (\sigma_{\gamma_8} \times (1 + i\%)) \text{ with } i \in [-50\%, 50\%] \quad [5.20]$$

Figure 5.13 represents the effect of the average and standard deviation variation of  $\gamma_8$  for the two functions  $G_{inf}$  and  $G_{sup}$ .

It is possible to see that the evolution of the failure probability is not linear according to the regular variation of the parameters. If we wish to decrease the risk of contact between the rotor and the stator ( $G_{inf}$ ), it is possible to increase the average of  $\gamma_8$  (in fact increases the nominal value) or to decrease the standard deviation by  $\gamma_8$  (i.e. the value of the dimensions of tolerance zones).



**Figure 5.13.** Parametric study of  $\gamma_8$  on failure probability (mean and standard deviation variation)

Concerning the  $G_{sup}$  probability (related to the engine efficiency), it is possible to decrease the average of  $\gamma_8$  or to decrease the value of the standard deviation of  $\gamma_8$ . Due to antagonist effect, the modification of the average seems to be a bad choice. It is more efficient to decrease the standard deviation of  $\gamma_8$ . For example, a decrease of

10% of the initial value of  $\sigma\gamma_8$  improves the reliability of the turboshaft engine by around 2% (from the initial value 92.54% to 94.5%).

### 5.5. Conclusion

This chapter proposes a reliable analysis of a high pressure turbine of a helicopter engine. First, a tolerancing model of the turbine is set up. A classic analysis, according to the worst case is undertaken. The extreme variation of the functional condition corresponding to the clearance between the rotor and the stator at the tip of the blades is calculated. The coefficient of influence is calculated by computing a local derivate of  $c$ . Thanks to these results, it is possible to identify most contributing parameters in the variation of the clearance value. On this kind of turbine, there are two kinds of requirements:

- a minimal value of the clearance with the aim of avoiding the contact between the blade and the stator;
- a maximal clearance value, with the aim of ensuring an acceptable turbine efficiency.

The determinist approach allows us to quantify the  $c$  value, and it is shown that the maximal allowed value is exceeded. However, with this kind of approach, it is impossible to quantify the risk and thus, the probability of an unacceptable turbine. Then, a statistical approach is proposed. This consists of making a correspondence between the geometrical specifications and an estimation of statistical modes of each parameter. It is then possible to quantify the rate of non-conforming turbines (clearance value over the requirements). The calculation of the reliability sensitivity informs on the influence of the mean and the standard deviation on the failure probability. A parametric analysis is carried out on the most influential parameter on the failure probability. In the studied case, the modification of the nominal value is not a good choice because it has an antagonistic effect on the failure probability. Thus, the best way consists of modifying the tolerance value of  $\gamma_8$ . Indeed, a reduction of 10% of the dimension of the tolerance zone leads an improvement in the reliability of the engine of around 2%. These parametric results allow us to guide the designer in the design decision with the aim of improving the reliability of the turbine.

### 5.6. Acknowledgments

This work was carried out within the framework of ERT 1070, joint research team of TREFLE-Turbomeca. Thanks to J.L. Breining, J G. Senger and R. Thomas of Turbomeca for their advice and technical assistance in carrying out this work.

## 5.7. Bibliography

- [BAL 08] BALLU, A., PLANTEC, J.-Y., MATHIEU L., “Geometrical reliability of over constrained mechanisms with gaps”, *CIRP Annals*, Vol. 57, pp. 45-49, January, 2008.
- [BAL 99] BALLU, A., MATHIEU, L., “Choice of functional specifications using graphs within the frame work of education”, *Proceedings of 6th CIRP Seminar on Computer Aided Tolerancing*, pp. 197-206, Kluwer Academic Publisher, 1999.
- [BOU 95] BOURDET, P., BALLOT, E. “Geometrical behavior laws for computer aided tolerancing”, *Proceedings of 4th CIRP Seminar on Computer Aided Tolerancing*, pp. 143-153, 1995.
- [BRE 88] BREITUNG, K., 1988, “Asymptotic approximations for the outcrossing rates of stationary vector processes”, *Stochast Process Appl*, Vol. 13, pp. 195–207.
- [CLE 88] CLÉMENT, A., BOURDET, P., “A study of optimal-criteria identification based on the small-displacement screw model”, *Annals of the CIRP*, Vol. 37, January, 1988.
- [CLO 01] CLOZEL, P., “3D tolerances analysis from preliminary study”, *Proceedings of the 7th CIRP Seminar on Computer Aided Tolerancing*, pp. 93-104, Kluwer Academic Publisher, 2001.
- [DAN 08] DANTAN, J.Y., QURESHI, Q., “Worse case and statistical tolerance analysis based on quantified constraint satisfaction problems and Monte Carlo simulation”, *Computer Aided Design*, doi: 10.1016/j.cad.2008.11.003, 2008.
- [GER 07] GERMAIN, F., Tolérancement statistique tridimensionnel, intégration en CFAO, PhD thesis, University of Savoy, 2007.
- [LEM 05] LEMAIRE, M., *Fiabilité des Structures – Couplage Mécano-Fiabiliste Statique*, Hermes Science, 2005.
- [MAD 86] MADSEN H.O, KRENK S, LIND N.C., *Methods of Structural Safety*, Prentice-Hall, Englewood Cliffs, 1986.
- [NIA 07] NIANDOU, H., BREYSSE, D., “Reliability analysis of a piled raft accounting for soil horizontal variability”, *Computers and Geotechnics*, Vol. 34, No. 2, pp. 71-80, 2007.
- [PHI 03] PHI-MECA Engineering S.A., User’s Manual, PHIMECA Software, 2003.
- [SHO 68] SHOOMAN, M.L., *Probabilistic Reliability: An Engineering Approach*, McGraw-Hill Book co., New York, 1968.
- [SKO 97] SKOWRONSKI, V.J., TURNER, J.U., “Using Monte Carlo variance reduction in statistical tolerance synthesis”, *Computer Aided Design*, Vol. 29, No. 1, pp. 63–69, 1997.
- [SRI 99] SRINIVASAN, V., “On interpreting key characteristics”, *Proceedings of the 1999 ASME Design Engineering Technical Conferences*, Las Vegas, Nevada, USA, 1999.

## Chapter 6

# Inertial Tolerancing According to ISO GPS

### 6.1. Introduction

In order to solve a dimensioning problem, two tolerancing approaches are applied by the designer:

- worst case tolerancing;
- statistical tolerancing [GIL 51], [EVA 74], [EVA 75].

The first has been characterized by a high cost, induced by the tight tolerances which are difficult to get during the run. The cost of inspection rejects and reworking increases as does the choice of a more sophisticated production method. However, the main advantage of this approach is the respect of the functional requirement (demand) at the final stage of the assembly. The second approach “statistical tolerancing” is developed by considering the low probability of having simultaneous components (elementary characteristics) within the tolerance limit. The basic assumption is the centering of all elementary characteristics on the target. This leads to a larger tolerance zone compared to the worst case tolerancing. However, this basic assumption is rarely respected by the run. Consequently, a batch of assembled parts cannot respect the functional characteristic in spite of the fact that every component is included within the tolerancing zone [GRA 00], [PIL 04].

---

Chapter written by Dimitri DENIMAL, Max GIORDANO, Maurice PILLET and Alain SERGENT.



A new tolerancing approach, called inertial tolerancing [PIL 04], is introduced. This method consists of tolerancing the mean square deviation in relation to the target in function of the standard deviation, contrary to the traditional formulation which presents the tolerancing in the form of a bi-limit. To our knowledge, this new tolerancing approach allows one to eliminate the ambiguities of the traditional tolerancing approach and the traditional process capability indices [ISO 06].

Until now, the designer has had three methods at his disposal to solve a dimensioning problem. But only the ASME standard [ASM 04] allows us to specify the name of the approach (worst case and statistical case) used by the designer. As we have seen, this information is important to the manufacturing process which must adapt the run monitoring and the process control depending of the tolerancing approach used.

Furthermore, lots of scientific approaches about the geometrical product specification tolerance (GPS) synthesis and analysis have been published but none are standardized [HON 02], [NGO 98].

Nevertheless, this chapter introduces the inertial tolerancing case as applied to the GPS Standard.

Indeed, the Geometrical Product Specification (GPS) Standard defines a useful specification when all measured points from a face are in the tolerance zone. Therefore, the decision accept is binary (“accept or do not accept”) resulting from the controlling operation.

However, with the inertial case applied to the GPS Standard, it is necessary to determine the geometrical variation compared to the “target geometry” according to the geometrical product specification standard.

## **6.2. Tolerance synthesis**

Tolerance synthesis is based on the small displacement torsors (SDT) introduced into a metrological context by Bourdet [BOU 87] and used by Giordano [GIO 93] and Germain [GER 07] using an approach based on 3D tolerance analysis, called the domain approach (DA).

Tolerance synthesis is introduced using the above approach. The principle consists of considering the positions and orientations of a frame (of an associated face). Consequently, the influence of the form defects of a face is not taken into account.

In this part, the definition of the functional requirement domain is presented then the quantitative synthesis approach is introduced.

### 6.2.1. Definition of the functional requirement domain (FRD) applied to localization specification

In this chapter, the functional requirement is expressed by a domain in the space of small displacements that represents all the variations permitted by the tolerance [GIO 93], [GER 07].

In Figure 6.1, a stack of parts ( $P_i$ ) is illustrated. The functional requirement (FR) is defined by the localization specification between two faces. The geometrical deviation between a face and a reference frame compared to their nominal position is represented by a deviation torsor. The components of this torsor are the small translations and small rotations which must be carried out in order for one of the faces to pass from its theoretical position to its real position. In the case of localization specification, the deviation torsor, called small displacement torsor  $SDT$ , is composed of one translation in  $z$  ( $t_z$ ) and two rotations in  $x$  and  $y$  ( $r_x$  and  $r_y$ ).

The literature about inertial tolerancing introduces three definitions for 3D inertial tolerancing according to the GPS Standard [PIL 05], [ADR 07], [NFX 09].

This chapter introduces a tolerance synthesis adapted to a stack of parts and based on the small displacement torsor [BOU 87]. The second part of this chapter, following section 6.2.5, presents the risks of using 3D statistical tolerancing and introduces the three definitions of 3D inertial tolerancing according to the GPS Standard. This chapter closes by opening out onto the conformity of a batch defined using 3D inertial definitions (section 6.3.1).

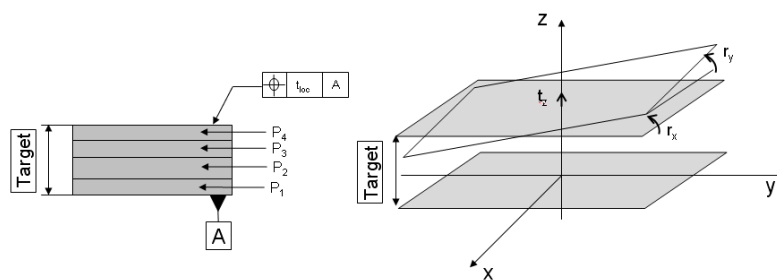
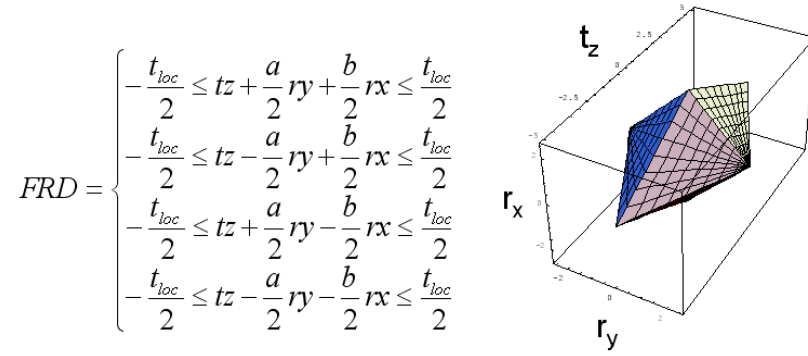


Figure 6.1. Small displacements

The part is defined by four extreme points. As the SDT of the face and the extreme points are known, a group of inequalities, which delimits an n-polytope (Figure 6.2) with n the dimension of the polytope, can be defined. The dimension n is defined by the number of components of the SDT which is necessary in order to go from the theoretical position to the real position. This n-polytope is called functional requirement domain (FRD) (Figure 6.2).



**Figure 6.2.** Inequalities and the representation of a 3D domain

The parameters  $a, b$  in Figure 6.2 correspond to the dimension of the face and the parameters  $t_{loc}$ , which is the value of the specification. The values allocated to  $t_{loc}$ ,  $a$ ,  $b$  are 0.1, 5, 5 respectively.

The notion of conformity is summarized by:

“The sum of the SDT components of every part ( $P_i$ ) must verify the inequalities of the FRD”.

$$\sum_{i=1}^k \{T_{P_{i,j}}\} \in FRD \quad [6.1]$$

with  $T_{P_{i,j}}$  being the SDT of face  $j$  of part  $P_i$ .

So, if the assembly is composed of three parts and there is only one face variation ( $j=0$ ) per part, we can deduce that:

$$\left\{ \begin{array}{l} -\frac{t_{loc}}{2} \leq \sum_{i=1}^3 tz_{P_i} + \frac{a}{2} \sum_{i=1}^3 ry_{P_i} + \frac{b}{2} \sum_{i=1}^3 rx_{P_i} \leq \frac{t_{loc}}{2} \\ -\frac{t_{loc}}{2} \leq \sum_{i=1}^3 tz_{P_i} - \frac{a}{2} \sum_{i=1}^3 ry_{P_i} + \frac{b}{2} \sum_{i=1}^3 rx_{P_i} \leq \frac{t_{loc}}{2} \\ -\frac{t_{loc}}{2} \leq \sum_{i=1}^3 tz_{P_i} + \frac{a}{2} \sum_{i=1}^3 ry_{P_i} - \frac{b}{2} \sum_{i=1}^3 rx_{P_i} \leq \frac{t_{loc}}{2} \\ -\frac{t_{loc}}{2} \leq \sum_{i=1}^3 tz_{P_i} - \frac{a}{2} \sum_{i=1}^3 ry_{P_i} - \frac{b}{2} \sum_{i=1}^3 rx_{P_i} \leq \frac{t_{loc}}{2} \end{array} \right. \quad [6.2]$$

### 6.2.2. Tolerance synthesis of a stack of parts

After the description of FRD, it is necessary to determine the tolerance for every part (face). Indeed, the FRD is defined by a domain and the result of the assembly of each part must be included.

Traditionally, designers authorize a quantity of assemblies outside the domain (the number of parts per million (ppm)) so as to reduce the requirements on the parts and the cost of the run.

In addition, the result of assembling the parts leads to a multivariate normal distribution, if two assumptions are verified (central limit theorem (CLT)) [KAL 97]:

- every SDT component is independent;
- every SDT component distribution has a similar range.

The purpose is to deduce, the parameters of the multivariate normal distribution (MND) which give the smallest requirement on each part from the FRD. The multivariate probability density is given by relation [6.3]:

$$f(X) = \frac{1}{(2\pi)^{N/2} (\det \Sigma)^{1/2}} \exp\left(-\frac{1}{2}(X - \mu_X)^t \Sigma^{-1} (X - \mu_X)\right) \quad [6.3]$$

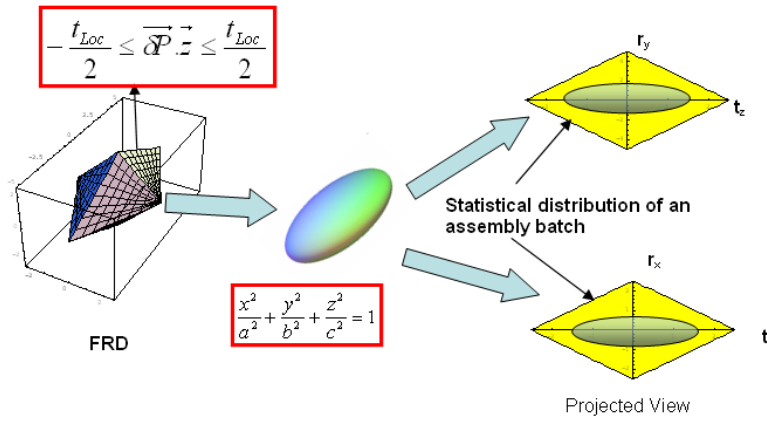
with X a random vector with N dimension equal to the FRD dimension, and  $\Sigma$  the covariance matrix of the SDT components.

In addition, the isodensity of an MND corresponds to a hyper ellipsoid (HE) using the following equation:

$$(X - \mu_X)^t \Sigma^{-1} (X - \mu_X) = M^2 \quad [6.4]$$

of which,  $M$  is the Mahanalobis distance [MAH 36],  $M \in \mathfrak{R}^+$ , whose value is generally equal to 1.

Consequently, the aim is to search for the largest hyper-volume of the HE included in the FRD (Figure 6.3).



**Figure 6.3.** Schematic representation of inertial tolerance synthesis

To determine the slopes of the HE, some considerations must be taken into account:

- the HE is centered on the FRD barycenter;
- the HE is tangent to the FRD plans.

The expression of the HE volume is given by [HOL 03]:

$$V_{HE} = g_N \sqrt{\text{Det}(\Sigma)} \quad \text{and} \quad g_N = \frac{\pi^{N/2}}{\Gamma(1 + N/2)} \quad [6.5]$$

With  $N$  the dimension of the FRD vector and  $\Gamma$  the gamma function  $\Gamma(N) = \int_0^{+\infty} t^{N-1} e^{-t} dt$  when  $N/2 \in \mathbb{Z}^+ \Rightarrow \Gamma(N) = (N-1)!$  with  $\mathbb{Z}^+$ , the set of positive integers.

For HE to be tangent to the FRD, it is necessary for the sum of the quadratic product of the plan and HE parameters to be equal to zero.

$$\{Plan\}_N^2 \cdot \{HE\}_N^2 - ConstPlan = 0 \quad [6.6]$$

with  $\{Plan\}_N^2$  and  $\{HE\}_N^2$  being the slopes of the N-dimension plan and the HE parameters of N-dimension HE respectively, the unknown values are the HE parameters. From [6.5] and [6.6], we deduce a function  $HV_{HE}$  with N-1 parameters. From this last function, the extrema (vector solution) are determined by solving the gradient of  $HV_{HE}$  [6.7]:

$$\nabla(HV_{HE}) = 0 \quad [6.7]$$

The relative maximum is given by the signature matrix of the quadratic derivative matrix.

$$\nabla^2(HV_{HE}(x_0)) < 0 \quad [6.8]$$

with  $x_0$  the solution vector of equation [6.7].

From these, the parameters of the HE with the largest hyper volume included in the FRD are obtained.

Once the parameters of the HE are known, those of the centered multivariate normal distribution must be established.

The solution proposed is as follows. The parameters of the  $HE_i$  are equal to 3\*standard deviation of the centered normal distribution and applied to the dimension  $i$  of the FRD.

In our case, we consider that  $I_i = HE_i/3$  with HE slopes  $i^{th}$  and the statistical interval  $i$  equal to  $2*HE_i$ .

### 6.2.3. Example of tolerance synthesis

The problem studied is presented in Figures 6.1 and 6.2.

The FRD dimensions are equal to 3 and the SDT components are composed of one translation ( $tz$ ) and two rotations ( $rx$ ,  $ry$ ).

From [6.4], the equation of the ellipsoid is:

$$\frac{tz^2}{a_{tz}^2} + \frac{rx^2}{b_{rx}^2} + \frac{ry^2}{c_{ry}^2} - 1 = 0 \quad [6.9]$$

The volume of the ellipsoid is deduced from relation [6.5]:

$$V_{ellipsoid} = \frac{4}{3} \cdot \pi \cdot a_{tz} \cdot b_{rx} \cdot c_{ry} \quad [6.10]$$

Equation [6.6] gives:

$$A^2 a_{tz}^2 + B^2 b_{rx}^2 + C^2 c_{ry}^2 - D^2 = 0 \quad [6.11]$$

with  $A, B, C$  being the slope of the plan and  $a_{tz}, b_{rx}, c_{ry}$  the slope of the ellipsoid.

The slopes of the plan are deduced from relation [6.12], quoted from [6.2]:

$$tz + \frac{a}{2}ry + \frac{b}{2}rx - \frac{t_{loc}}{2} = 0 \quad [6.12]$$

Thus,  $A=1, B=b/2, C=a/2$  and  $D=t_{loc}/2$ .  $a$  and  $b$  are the part dimensions.

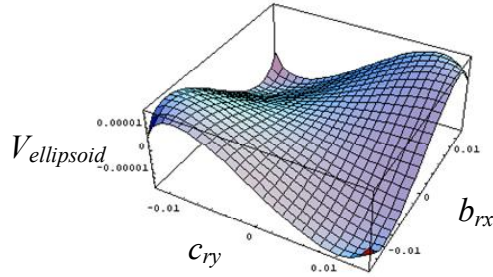
From [6.10], [6.11], we deduce:

$$a_{tz} = \sqrt{\left(\frac{t_{loc}}{2}\right)^2 - \left(\left(\frac{b}{2}\right)^2 b_{rx}^2 + \left(-\frac{a}{2}\right)^2 c_{ry}^2\right)} \quad [6.13]$$

and thus, the volume is defined by [6.13] and Figure 6.2.

$$V_{ellipsoid} = \frac{4}{3} \cdot \pi \sqrt{\left(\frac{t_{loc}}{2}\right)^2 - \left(\left(\frac{b}{2}\right)^2 b_{rx}^2 + \left(-\frac{a}{2}\right)^2 c_{ry}^2\right)} \cdot b_{rx} \cdot c_{ry} \quad [6.14]$$

Figure 6.4 represents the evolution of  $V_{ellipsoid}$  in function of the ellipsoid slopes ( $b_{rx}, c_{ry}$ ) (with  $t_{loc}=0.1, a=5, b=5$ ).

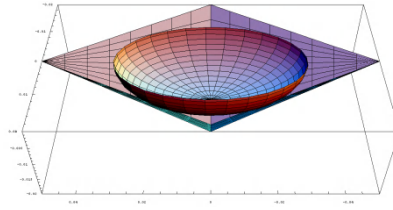


**Figure 6.4.** Representation of the function  $V_{ellipsoid}$

After solving equations [6.7] and [6.8], we obtain the following solution:

$$Sol = \begin{pmatrix} a_{tz} \\ b_{rx} \\ c_{ry} \end{pmatrix} = \begin{pmatrix} 0.0289 \\ 0.0115 \\ 0.0115 \end{pmatrix} \quad [6.15]$$

Figure 6.5 illustrates a transversal cross-section of the FRD and the ellipsoid.



**Figure 6.5.** 2D cross-section of the FRD and ellipsoid

Now the parameters of the HE are known, it is necessary to determine from [6.15] the SDT standard deviations of part  $i$ . Therefore, we define a quality level ( $Cp_{FRDj}$  [6.21]) for the SDT component  $i$  of the FRD. The tolerance interval of the component  $i$  ( $IT_{FRDi}$ ) is given by:

$$Sol = \begin{pmatrix} IT_{FRD_{tz}} \\ IT_{FRD_{rx}} \\ IT_{FRD_{ry}} \end{pmatrix} = \begin{pmatrix} 2.a_{tz} \\ 2.b_{rx} \\ 2.c_{ry} \end{pmatrix} = \begin{pmatrix} 0.0578 \\ 0.023 \\ 0.023 \end{pmatrix} \quad [6.16]$$



The coefficient  $a_{tz}$ ,  $b_{rx}$ ,  $c_{ry}$  from [6.9] correspond to half of the range of the HE (symmetry of the HE).

From [6.18] and [6.21], we can determine the standard deviation for a given  $Cp_{FRD}$ , and thus determine the standard deviation of every part  $i$  [6.17] of the assembly.

$$\sigma_i = \begin{cases} \sigma_{x_i} = \frac{0.0115}{3Cp_{FRD_{rx}}\sqrt{n}} \\ 0 \\ 0 \\ \sigma_{z_i} = \frac{0.0289}{3Cp_{FRD_{tz}}\sqrt{n}} \end{cases} \begin{cases} \sigma_{y_i} = \frac{0.0115}{3Cp_{FRD_{ry}}\sqrt{n}} \\ \sigma_{z_i} = \frac{0.0289}{3Cp_{FRD_{tz}}\sqrt{n}} \\ 0 \end{cases} \quad [6.17]$$

with  $i^{th}$  being the number of the part,  $n$  the number of parts in the assembly and  $Cp_{FRDi}$  we can specify a quality level on the FRD. In this chapter, these  $Cp_{FRDi}$  are equal to 1. From [6.19], we can determine the statistical tolerance [6.18].

$$IntS_i = \begin{cases} IntS_{rx_i} = \frac{2 * 0.0115}{Cp_{FRD_{rx}}\sqrt{n}} \\ 0 \\ 0 \\ IntS_{tz_i} = \frac{2 * 0.0289}{Cp_{FRD_{tz}}\sqrt{n}} \end{cases} \begin{cases} IntS_{ry_i} = \frac{2 * 0.0115}{Cp_{FRD_{ry}}\sqrt{n}} \\ IntS_{ry_i} = \frac{2 * 0.0115}{Cp_{FRD_{ry}}\sqrt{n}} \\ 0 \end{cases} \quad [6.18]$$

with  $i^{th}$  as the number of the part and  $IntS$  corresponding to the statistical interval,  $Cp_{FRDi}$  allows us to specify a quality level on the FRD.

Usually the quality level of a batch of assembled parts is specified by a number of ppm. The analytic calculation of this index consists of determining the number of assemblies outside the FRD [6.2] and in considering the resulting probability distribution of the assembly.

$$P((tx, \dots, tz, rx, \dots, rz) \in FRD) = 1 - \int_D f_X(tx, \dots, rz) dtx \dots drz \quad [6.19]$$

In order to reduce the calculation time, the number of ppm [6.19] is calculated using the Monte Carlo approach. The dimension of each simulation is equal to  $10^6$ . The confidence interval using the Monte Carlo approach to predict an assembly parameter may be estimated by means of the binomial distribution [SHA 81]. For example, the reject rate is expressed in ppm. The standard deviation predicted in ppm rejects may be calculated from [6.20].

$$\sigma_{ppm} = \sqrt{\frac{ppm(10^6 - ppm)}{n-1}} \quad [6.20]$$

with ppm as the estimated number of ppm rejected,  $\sigma_{ppm}$  (one-sigma) expresses the degree of uncertainty in calculating the number of predicted rejects.

The next section introduces process capability indices as applied to SDT.

#### 6.2.4. Process capability indices applied to SDT

The  $C_p$  and  $C_{pk}$  indices [ISO 06] are often contractual values between the customer and the supplier. Nevertheless, the first assumption in order to use these indices is that the geometrical specifications have a normal distribution. This assumption is not really verified when we consider a distance between two points. Nevertheless, in the case presented, only the components of the SDT are calculated from the reference face A so the distribution of these components is normal.

In the present case, the traditional process capability indices are fitted to the SDT approach.

The  $C_p$  indices are calculated for every component of the SDT:

$$Cp_{ij} = \frac{It_{ij}}{6\sigma_{ij}} \quad [6.21]$$

with  $i$  a component of the SDT, and  $\sigma$  the standard deviation of the component  $i$  of the SDT and  $j$  the part.

The  $C_{pk}$  indices are calculated using the relation:

$$Cpk_{ij} = \frac{\min\left(\frac{It_{ij}}{2} - \mu_{ij}; \mu_{ij} - \frac{It_{ij}}{2}\right)}{3\sigma_{ij}} \quad [6.22]$$

with  $i$  a component of the SDT,  $\sigma_{ij}$  the standard deviation and  $\mu_{ij}$  the mean of the component  $i$  of the SDT and  $j$  the part.

In this chapter, indices [6.21] and [6.22] are used to determine the off-centering [6.22] and the standard deviation [6.21] of every SDT component.

Other capability indices are introduced in scientific literature [KAR 94, CHA 91, WAN 00] which, until now, were unknown to industry. In this chapter, some adaptations of these indices are also proposed.

In the next section, the statistical tolerancing risk is presented using the SDT approach.

### 6.2.5. Statistical tolerancing risk

In this section, two cases are considered. The first case is an assembly of 4 parts of which the  $C_p=2.5$  and the  $C_{pk}=2$  on every SDT component of part j.

$$Cp_j = \begin{Bmatrix} Cp_{rx} = 2.5 & 0 \\ Cp_{ry} = 2.5 & 0 \\ 0 & Cp_{tz} = 2.5 \end{Bmatrix}_j \quad [6.23]$$

If the worst case is taken into account, the decentering of every SDT component is in the same direction, and the result on the HE functional domain is equal to 16,039 ppm ( $\sigma_{ppm}=125.6$ ) and if we consider the FRD Domain the number of ppm is equal to 10,150 ppm ( $\sigma_{ppm}=100.2$ ).

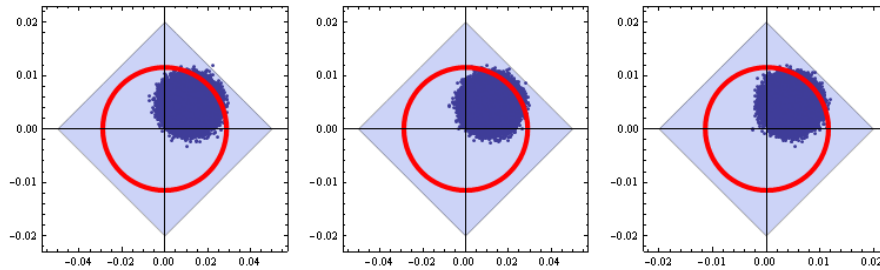


Figure 6.6.  $C_p=2.5$  and  $C_{pk}=2$  on every SDT component (projected view)

The second case is an assembly of 4 parts of which the  $C_p=2.5$  and the  $C_{pk}=1.5$  on every SDT components of the part j. If the worst case is taken into account, the decentering of every SDT component is in the same direction, and the result on the HE functional domain is equal to 998,732 ppm ( $\sigma_{ppm}=35.6$ ) and if we consider the FRD domain, the number of ppm is equal to 998,074 ppm ( $\sigma_{ppm}=43.8$ ).

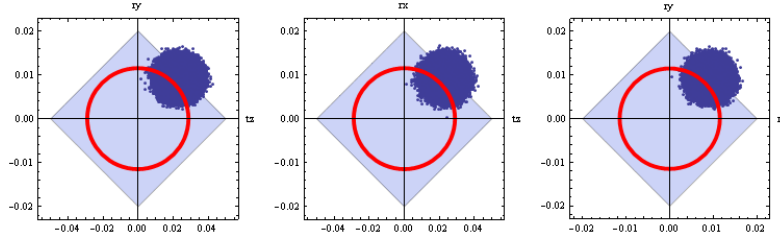


Figure 6.7.  $C_p=2.5$  and  $C_{pk}=1.5$  on every SDT component (projected view)

To conclude, 3D statistical tolerancing does not eliminate the customer risk which corresponds to the risk of accepting a batch of conform components and yet producing a non-conform assembly. In the one-dimensional case, the inertial tolerancing approach resolves this problem. In the next section, we propose to give a reminder of inertial tolerancing and then to take these configurations and to see the impact on the functional requirement domain.

#### 6.2.6. Inertial tolerancing: short reminder

In the case of the robust design, if all elementary characteristics are on the target, the quality of the assembled product is optimal. Nevertheless, the performance of the assembled product decreases proportionally to the increase of the off-center of every characteristic. This effect of off-centering every characteristic on the assembled product is characterized using the function of financial loss by Taguchi [TAG 87]. In this function, the financial loss on the batch ( $\bar{L}$ ) is related to the standard deviation  $\sigma$  and the distance between the mean and the target (nominal) of the batch,  $\delta$ .

$$\bar{L} = K(\sigma^2 + \delta^2) \quad [6.24]$$

According to a proportional value of Taguchi's lost function, the inertia is formulated on every elementary characteristic. This inertia is defined by:

$$I_{Batch} = \sqrt{\delta^2 + \sigma^2} \quad [6.25]$$

in which,  $I_{Batch}$  represents the inertia batch,  $\sigma$  is the standard deviation and  $\delta$  is the mean deviation compared to the target of the batch.

$$\delta = X_0 - \bar{X} \quad [6.26]$$

in which  $\bar{X}$  is the mean of the batch and  $X_0$  is the target.

The quantification of the batch quality is specified by two process capability indices  $C_p$ ,  $C_{pi}$ . The first corresponds to the process capability indices considering a center process:

$$C_p = \frac{I_{Max}}{\sigma_{ST}} \quad [6.27]$$

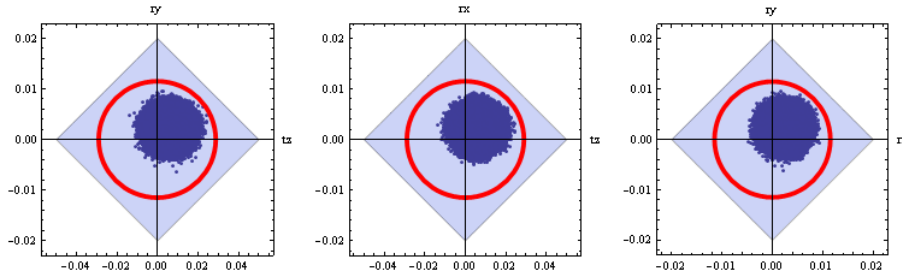
in which,  $I_{Max}$  is the inertia customer which corresponds to the maximum accepted inertia and  $\sigma_{ST}$  is the short term standard deviation. The second ( $C_{pi}$ ) corresponds to the short term capability process indice for an off-center process

$$C_{pi} = \frac{I_{Max}}{I_{Batch}}, \quad [6.28]$$

We can notice that  $C_p$  and  $C_{pi}$  can be assimilated to  $C_p$  and  $C_{pk}$  [ISO 06]. In this chapter, indices [6.27] and [6.28] are used to determine the off-centering [6.28] and the standard deviation [6.27] of every SDT component.

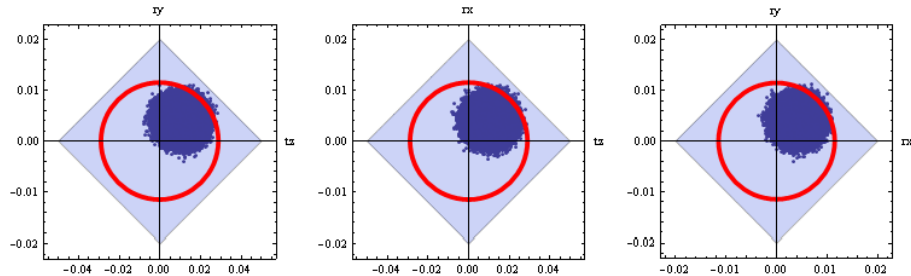
#### 6.2.7. Inertial tolerancing with stack-up problem

In the same way as in part 6.2.5, the inertia on every SDT component is specified. Thus, in the first example ( $C_p=2.5$  and  $C_{pi}=2$ ), and if the unfavorable case is taken into account, then the off-centering of every SDT component is in the same direction, and the result on the HE functional domain is equal to 0 ppm ( $\sigma_{ppm}=0$ ). If we consider the FRD domain, the number of ppm is equal to 0 ppm ( $\sigma_{ppm}=0$ ).



**Figure 6.8.**  $C_p=2.5$  and  $C_{pi}=2$  on every SDT component (projected view)

In the second example ( $C_p=2.5$  and  $C_{pi}=1.5$ ), the result on the HE functional domain (Figure 6.8) is equal to 3,284 ppm ( $\sigma_{ppm}=57.2$ ) and if we consider the FRD domain the number of ppm is equal to 1,841 ppm ( $\sigma_{ppm}=42.8$ ).



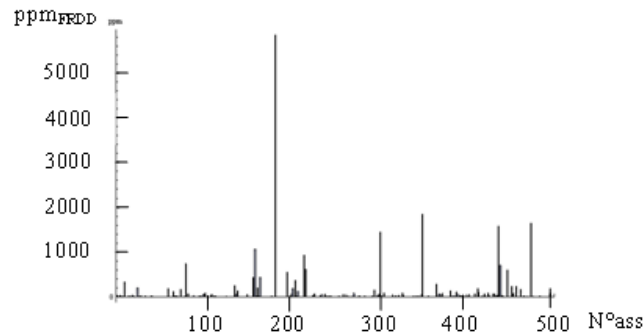
**Figure 6.9.**  $C_p=2.5$  and  $C_{pi}=1.5$  on every SDT component (projected view)

Table 6.1 presents the result of assembly simulation in the unfavorable case considering every SDT component as having a  $C_p$  equal to 2 and a  $C_{pi}$  which is variable. In this case, the off-centering,  $\delta$ , is simulated by a law of uniform distribution.

	$\text{ppm}_{\text{FRD}}$	$\sigma_{\text{ppm}}$
$C_{pi} = 2$	0	0
$C_{pi} = 1.75$	27	5
$C_{pi} = 1.5$	1841	42.
$C_{pi} = 1.25$	64	8
$C_{pi} = 1$	333	245.3
$C_{pi} = 0.75$	662	
	752	472.7

**Table 6.1.** Results of simulation for different  $C_{pi}$  imposed on every SDT component of the assembly ( $C_p=2$ )

From Table 6.1, we can observe the ppm evolution as a function of the  $C_{pi}$  index. The values, which are given in Table 6.1, correspond to an extreme position (unfavorable case) where all SDT components are off-centre in the same direction. If we consider a real situation, then the  $\text{ppm}_{\text{FRD}}$  is less than  $\text{ppm}_{\text{FRD}}$  in the unfavorable case. Figure 6.10 illustrates the  $\text{ppm}_{\text{FRD}}$  of a simulation of 500 assemblies of which every SDT component of the parts respects a  $C_{pi}$  of 1 and a  $C_p$  of 2. We can observe that mean  $\text{ppm}_{\text{FRD}}$  on 500 simulations is equal to 53.26.



**Figure 6.10.**  $C_p=2$  and  $C_{pi}=1$  on every SDT components

From Figure 6.10, the most important  $\text{ppm}_{\text{FRD}}$  concerns the simulation 182 ( $\text{ppm}_{\text{FRD}}=5,837$  and  $\sigma_{\text{ppm}}=76.77$ ). Nevertheless, most of the simulations (98.8%) are less than 1,000 ppm and 93% are less than 100 ppm.

A proposition of 3D inertia using SDT components has been introduced.

Previous scientific works have introduced some different ways of defining 3D inertial tolerancing.

In the next part, a reminder of the different 3D inertia definitions is given and the definitions are compared.

### 6.3. 3D inertia

The scientific literature differentiates between three expressions of 3D inertial tolerancing.

#### 6.3.1. 3D inertia definitions and comparison

##### 6.3.1.1. 3D inertia the first definition

The first definition was introduced by Pillet [PIL 05] and the purpose of which is to define the overall level of quality of a surface including all defaults related to shape and positioning. It is defined by measuring a number of predefined points  $X_{ij}$  on the face (Figure 6.11).

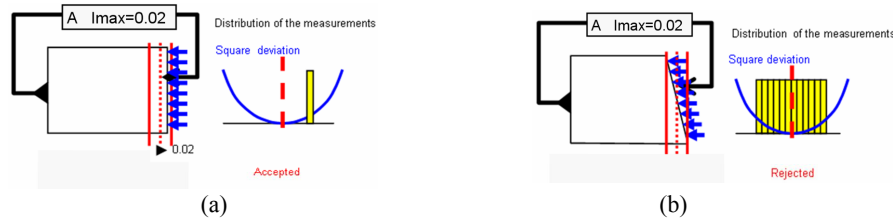


Figure 6.11. Example of the inertia using the first approach

Concerning the face  $i$ , the inertia is calculated using this relation:

$$I_i = \sqrt{\frac{1}{n} \sum_{j=1}^n (X_{ij} - T)^2} = \sqrt{\sigma_i^2 + (\bar{X}_i - T)^2} \quad [6.29]$$

with:

- $X_{ij}$  :  $j$  measurement of the part  $i$
- $\sigma_i$  : standard deviation of the measurement on the part  $i$
- $T$  : specification target
- $k$  : number of parts
- $n$  : number of measurements per part
- $I_i$  : calculated inertia on the  $n$  points of the part  $i$
- $I$  : overall inertia on the set of points measured ( $kn$ )
- $I_{Max}$  : maximal admissible inertia

and proposes an expression of the inertia for a batch:

$$I^2 = \frac{1}{k} \sum_{i=1}^k I_i^2 \quad [6.30]$$

#### 6.3.1.2. 3D adjusted inertia – the second definition

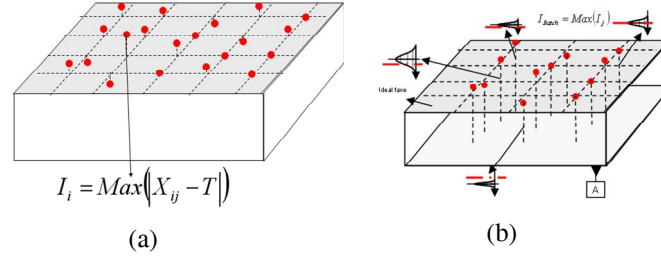
The second approach, 3D adjusted inertia, was introduced by Adragna [ADR 07]. It consists of defining one of the part's faces using the inertia of measure:

$$I_{Batch} = \text{Max}(I_j) \quad [6.31]$$

in which  $I$  is a scalar which presents 3D adjusted inertia, and  $I_j$  the  $j$  measurement.



Thus the inertia of a batch is defined by one measured point which has the maximum inertia. The definition of the inertia of a face is similar to the third definition of the approach [6.32].



**Figure 6.12.** Example of the inertia following the second approach (a) concerning a face of a part (b) concerning a batch

#### 6.3.1.3. 3D standard inertia – the third definition

The third approach is suggested using the standard [NFX 09] and proposed to define the inertia of a face by the maximum deviation:

$$I_i = \text{Max}(|X_{ij} - T|) = \text{Max}(|\delta_j|) \quad [6.32]$$

with  $\delta_j$  being the maximum deviation of measurement on the face  $i$  of the part.

And we deduce the inertia concerning a batch.

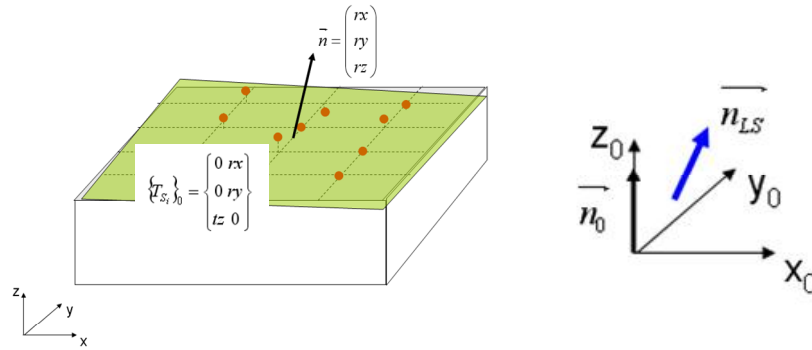
$$I_{Batch} = \sqrt{\frac{1}{k} \sum_{i=1}^k (I_i)^2} \quad [6.33]$$

The asset of the first approach is to include both form and orientation defects. This definition is therefore similar to the definition of positional tolerancing in the GPS standard [ISO 98].

#### 6.3.1.4. 3D SDT inertia – the fourth definition

In addition to the inertia literature we propose a fourth approach. The latter is based on the small displacement theory introduced by P. Bourdet and A. Clément [BOU 76]. This approach consists of determining the inertia of the components of the Small Displacement Torsor (SDT) from the nominal surface and the least square

surface. In this case of a batch, every element of the SDT is expressed in terms of inertia.



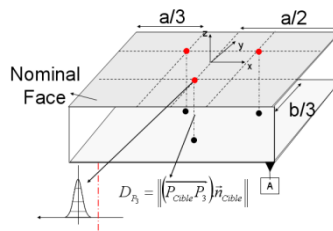
**Figure 6.13.** Example of the inertia using the fourth approach

In Figure 6.13, we can see that the plan's orientation is presented by the normal vector  $n$  and that the coefficient of the vector corresponds to the degree of freedom ( $rx$ ,  $ry$ ) of the plan. Regarding a batch, the coefficient  $rx$ ,  $ry$  and  $tz$  of the SDT are defined by a mean and a variance, and can thus be formulated by an inertia.

Four approaches have been presented; the purpose of the next part is a comparison between the approaches.

### 6.3.2. 3D inertia definitions comparison

The comparison is made using Figure 6.14. The aim is to simulate the geometric defects of a face, to calculate the inertia using the definitions presented and to see if there are similarities between these definitions.



**Figure 6.14.** Plan defined by 3 points

In this case, the geometric specification is the location of a plan compared to a reference plan (A). The reference plan is considered ideal (with no form or geometric defect). The localized plan is qualified by three points in which a normal distribution is allocated. This variation translates the geometric defect of the plan [GIL 88].

The size of the simulation is 40,000 batches of 25 parts. Each inertial definition has been calculated according to of the definition presented in the last part.

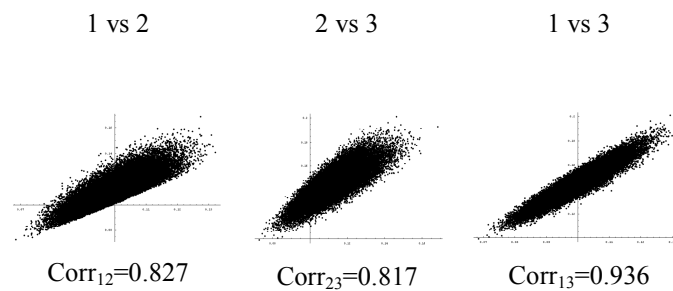
First, the parameters of the law of normal distribution of every point are independent but centered with a standard deviation equal to 0.3.

	Definitions	Mean	Standard deviation	Inertia
1	3D inertia	0.0997	0.008123	0.100
2	3D adjusted inertia	0.112	0.011056	0.1123
3	3D standard inertia	0.14502	0.0126	0.1455

**Table 6.2.** Results of the simulations

At first sight, the data (Table 6.2) have the same order of magnitude. We notice that the 3D inertia has the smallest value when we consider the mean and the standard deviation.

The observation of the correlation ( $\text{Corr}_{i,j}$ ) between the approaches allows us to verify the similarities between the definitions. The first line introduces the compared approaches (1 versus 2 -> 3D inertia versus 3D adjusted inertia (Table 6.2)).



**Figure 6.15.** Correlation between the approaches

Figure 6.15 underlines the correlation between the 3D inertia and 3D standard inertia (1 versus 3). Nevertheless, the definition of 3D adjusted inertia is correlated but the set of data is not homogeneous (caused by the difference in the distribution law). *A priori*, definitions 1 and 3 are related to a mathematical function.

### 6.3.3. 3D inertia in the industrial context

In the next part, the notions of tolerance synthesis and 3D inertia are introduced. Using the tolerance synthesis, we can determine the value of the 3D inertia in relation to the three 3D inertia definitions introduced.

From relation [6.17], the SDT is considered on every face for an assembly composed by 4 parts:

$$I_i = \begin{cases} 0 & I_{rx_i} = 0.0019 \\ 0 & I_{ry_i} = 0.0019 \\ I_{tz_i} = 0.0048 & 0 \end{cases} \quad [6.34]$$

If all the SDT components are centered and a  $C_{pi}=1$  is respected, then the  $ppm_{FRD}$  will be equal to 8,300.

From the example in Figure 6.14, the face is defined by three points  $P_{1j}$ ,  $P_{2j}$ ,  $P_{3j}$ , which have the following coordinates:

$$P_{1j} = \begin{pmatrix} \frac{a}{3} \\ \frac{b}{3} \\ Target + e \end{pmatrix}; P_{2j} = \begin{pmatrix} -\frac{a}{3} \\ \frac{b}{3} \\ Target + e \end{pmatrix}; P_{3j} = \begin{pmatrix} 0 \\ -\frac{b}{3} \\ Target + e \end{pmatrix}; \quad [6.35]$$

With  $a$  and  $b$  being the size of the part ( $a=b=5$ ); Target corresponds to the Target ( $Target=5$ ) and  $e$  corresponds to a variation generated using a law of normal distribution.

In the first case, the normal law distribution  $e$  is considered centered on the target with a standard deviation equal to 0.0048. The results of the FRD obtained by simulation (dimension=100,000 assemblies), are  $ppm=5,750$   $\sigma_{ppm}=75.14$ , the correlation coefficients between the dimensions are equal to zero (Figure 6.16).

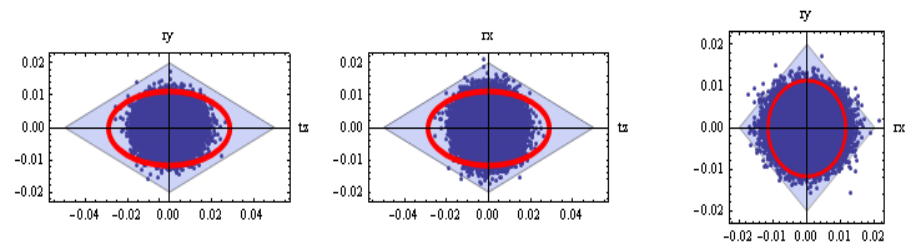


Figure 6.16. *Cpi=1 inertia on every SDT component (projected view) centered*

Table 6.3 sums up the different definitions of the 3D inertia and presents their values considering a batch of 400,000 parts. In this example, the value of 0.0048 was the maximal inertia for the measured points.

SDT inertia	3D inertia	3D adjusted inertia	3D standard inertia
Itz= 0.0027			
Irx= 0.0020	0.00479	0.00480	0.00696
Iry= 0.0017			

Table 6.3. *Calculation of the 3D inertia of a batch composed by 400,000 parts*

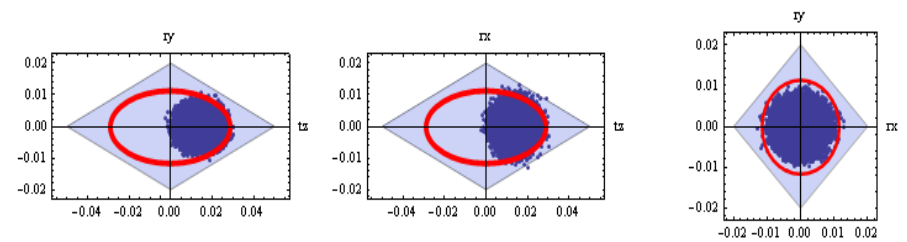


Figure 6.17. *Inertia on every SDT component (projected view) centered with off-centering of the measured points*

In the second case, the normal law distribution  $e$  is considered with an off-centering of 0.0034 and a standard deviation equal to 0.00336. The results of the FRD obtained by simulation (dimension=100,000 assemblies) are ppm=1,950  $\sigma_{ppm}$ =44, the correlation coefficients between the dimensions are null.

Table 6.4 sums up the different definitions of the 3D inertia and presents their values considering a batch of 400,000 parts. In this example, the value of 0.0048 was the maximal inertia of the measured points.

SDT inertial	3D inertia	3D adjusted inertia	3D standard inertia
Itz= 0.0039			
Irx= 0.0014	0.0048	0.00480	0.0067
Iry= 0.0012			

**Table 6.4.** Calculation of the 3D inertia of a batch composed by 400,000 parts (off-centering)

From Tables 6.3 and 6.4, we can observe that the value of the 3D inertia and 3D adjusted inertia is similar. The 3D standard inertia decreases the real level of quality of the batch compared to the others. However, with SDT inertia, it is possible to observe the difference between every batch. The impact on the translation and rotation is visible because off-centering was applied. Potentially, we observe that the inertia authorized by the SDT inertia is not attained. Thus it is necessary to find an optimal compromise between these definitions.

#### 6.3.4. 3D inertia - conclusions

In section 6.3.2, we have seen that definitions 1 (3D inertia) and 3 (3D inertia standard) were correlated and concluded that, potentially, a mathematical relation can be established in this case study.

Yet, in section 6.3.3, comparisons of inertial definitions were made from a geometric defect simulation obtained by the deviation of three points. In this part, a centered deviation and an off-centered deviation of these points were considered. As a function of this deviation, inertial definitions were calculated and it was underlined that the respect of the 3D inertia of a batch seemed to guarantee the  $\text{ppm}_{\text{FRD}}$  defined (here 8,300) regardless of the definition of 3D inertia chosen in the case study.

### 6.4. Conclusions

In this chapter, the notion of tolerance synthesis applied to a stack of parts and based on the SDT has been presented. In the first part, the 3D statistical tolerancing risk used with common process capability indices  $C_p$  and  $C_{pk}$ , was identified. The 3D statistical tolerancing risk does not eliminate the customer's risk which corresponds to the risk of accepting a batch of conform components and yet being

able to produce a non-conform assembly. Therefore, 3D inertia tolerancing in the SDT context has been presented and has shown that it limits the customer's risk.

In coming works, we will generalize this approach by including the notion of covariance matrix and propose a synthesis including a gap or a clearance in an assembly.

Other 3D inertia definitions have been introduced from previous works. The main purpose of this chapter is to make a comparison between the definitions and underline the first similarity. Thus, an important correlation has been presented between 3D inertia and 3D standard inertia. Furthermore, the definitions of 3D adjusted inertia and 3D standard inertia do not use all the potential that SDT inertia allows.

In coming works, an approach to determine the 3D inertia representative of the SDT inertia will propose mathematical relations between the definition of the 3D inertia and that of 3D standard inertia. We also propose a general approach to determine the maximal point inertia to be taken into account in order to guarantee the functional requirement.

## 6.5. Bibliography

- [ADR 07] ADRAGNA P.A., Tolérancement des systèmes assemblés, une approche par le tolérancement inertial, Thesis, University of Savoy, France, 2007.
- [ASM 04] ASME Y14.5M-1994, Dimensioning and tolerancing – ASME, 2004.
- [BOU 76] BOURDET P., CLÉMENT A., “Controlling a complex surface with a 3 axis measuring machine”, *Annals of the CRIP, Manufacturing Technology*, Vol. 25, pp. 359, 1976.
- [BOU 87] BOURDET P., Contribution A La Mesure Tridimensionnelle: Modèle d'Identification Des Surfaces, Métrologie Fonctionnelle Des Pièces Mécaniques, Correction Géométrique Des Machines A Mesurer Tridimensionnelles, Thesis, Nancy I - LURPA ENS CACHAN, France, 1987.
- [CHA 91] CHAN L.K., CHENG S.W., and SPIRING F. A., “A multivariate Measure of Process Capability”, *Journal of Modelling and Simulation*, Vol. 11, pp. 1-6, 1991.
- [CVE 98] CVETKO R., *et al*, “New metrics for evaluating Monte Carlo tolerance analysis of assemblies”, *Proceedings of the ASME International Mechanical Engineering Conference and Exposition*, 1998.
- [EVA 74] EVANS D.H., “Statistical tolerancing the state of art, Part I: background”, *Journal of Quality Technology*, Vol. 6, pp 188-195, 1974.
- [EVA 75] EVANS D.H., “Statistical tolerancing the state of art, Part II: methods for estimating moments”, *Journal of Quality Technology*, pp 1-12, Vol. 7, 1975.

- [GER 07] GERMAIN F., Tolérancement Statistique tridimensionnel, intégration en CFAO, Thesis, University of Savoy, France, 2007.
- [GIL 51] GILSON J., A.M.I.Mech.E., A.M.I.Prod.E., *A New Approach to Engineering Tolerances*, The Machinery Publishing CO. LTD, Chapter 3, pp. 42-48, 1951.
- [GIL 88] GILBERT O., Representation of geometric variations using matrix transforms for statistical tolerance analysis in assemblies, B.S. Industrial Engineering, Ecole Polytechnique de Montréal, 1988.
- [GIO 93] GIORDANO M., DURET D., "Clearance space and deviation space. Application to three dimensional chain of dimensions and position", *3rd CIRP Seminar on Computer Aided Tolerancing*, pp. 179-196, 1993.
- [GRA 00] GRAVES S., BISGAARD S., "Five ways statistical tolerancing can fail, and what to do about them", *Quality Engineering*, Vol. 13, No. 1, pp 73-82, January 2000.
- [HOL 03] HOLZER E.B., *Figure of Merit for Muon Cooling – An Algorithm for Particle Counting in Coupled Phase Planes*, 2003.
- [HON 02] HONG Y.S., "A comprehensive review of tolerancing research", *International Journal of Production Research*, Vol. 40, No. 11, pp. 2425 – 2459, 2002.
- [ISO 98] ISO 5458: 1998, ISO - Geometrical Product Specifications (GPS) - Geometrical tolerancing - Positional tolerancing, 1998.
- [ISO 06] ISO 3534-2, Statistics - Vocabulary and symbols - Part 2: Applied statistics, 2006.
- [KAL 97] KALLENBERG O., *Foundations of Modern Probability* Springer-Verlag, New York, 1997.
- [KAR 94] KARL D., MORISETTE P., TAAM W., "Some application of a multivariate capability index in Geometric Dimensioning and tolerancing", *Quality Engineering*, Vol. 6, pp. 649-655, 1994.
- [MAH 36] MAHALANOBIS P.C., "On the generalized distance in statistics", *Proceedings of the National Institute of Sciences of India*, Vol. 2, No. 1, pp. 49–55, 1936.
- [NFX 09] NF XP E 04-008, GPS – Méthode de tolérancement, expression et déclaration de la conformité, 2009.
- [NGO 98] NGOI B.K.A. and ONG C.T., "Product and process dimensioning and tolerancing techniques a state of the art review", *International Journal, Advanced Manufacturing Technology*, Vol. 14, No. 12, pp. 910-917, 1998.
- [PIL 04] PILLET M., "Inertial Tolerancing", *Total Quality Management*, Vol. 16, No. 3, pp. 202-209, 2004.
- [PIL 05] PILLET M., SAMPER S., FORMOSA F., *Geometrical Inertial Tolerancing*, 6th congress, Qualita, Bordeaux, France, pp. 757-764, 2005.
- [SHA 81] SHAPIRO S.S., GROSS A., *Statistical Modeling Techniques*, Marcel Dekker, 1981.



- [TAG 87] TAGUCHI G., "System of experimental design", *Engineering Methods to Optimize Quality and Minimize Costs*, Vol. 1 and 2, American Supplier Institute, Inc, Livonia, MI, 1987.
- [WAN 00] WANG F.K., *et al*, "Comparison of three multivariate Process Capability indices", *Journal of Quality Technology*, Vol. 32, No. 3, 2000.

## Chapter 7

# Tolerance Analysis Based on Quantified Constraint Satisfaction Problems

This chapter presents a mathematical formulation of tolerance analysis which simulates the influence of geometric deviations on the geometrical behavior of the mechanism and integrates the notion of quantifier (universal quantifier “ $\forall$ ” and existential quantifier “ $\exists$ ”). This model takes into account, the influence of geometrical deviations as well as the influence of type of contacts on the geometrical behavior modeled with the help of convex hulls defined in parametric space. With the help of these convex hulls, the quantifier notion is integrated into the model for admissible deviations of parts. To compute this mathematical formulation, an approach based on the quantified constraint satisfaction problem (QCSP) and the Monte Carlo simulation is proposed and tested.

### 7.1. Introduction

Mechanical product reliability is an important product quality factor and is dependent on different parameters among which tolerance design is an important activity. Proper tolerance design enables complex mechanical assemblies consisting of numerous parts to assemble and work together in a proper manner so that they fulfill their design objectives. As technology increases and performance requirements continually tighten, the cost and the required precision of assemblies increase as well. There is a strong need for increased attention to tolerance design in order to enable high-precision assemblies to be manufactured at lower costs. To do

---

Chapter written by Ahmed Jawad QURESHI, Jean-Yves DANTAN, Jérôme BRUYERE and Régis BIGOT.

so, a substantial amount of research has been devoted to the development of tolerance analysis. It can be either worst-case or statistical [CHA 91], [HON 02], [NIG 95], [ROY 99].

The tolerance analysis methods are divided into two distinct categories based on the type of accumulation input: displacement accumulation or tolerance accumulation.

The aim of displacement accumulation is to simulate the influences of deviations on the geometrical behavior of the mechanism. Usually, tolerance analysis uses a relationship of the form [NIG 95]:

$$y = f(x) \quad Y = f(x) \quad [7.1]$$

where  $Y$  is the response (characteristic such as gap or functional characteristics) of the assembly and  $x = \{x_1, x_2, \dots, x_n\}$  are the values of some characteristics (such as situation deviations or/and intrinsic deviations) of the individual parts or subassemblies making up the assembly. The part deviations could be represented by kinematic formulation, small displacement torsor (SDT), matrix representation, vectorial tolerancing, etc. The function  $f$  is the assembly response function which represents the deviation accumulation. The relationship can exist in any form for which it is possible to compute a value for  $y$  given values of  $x = \{x_1, x_2, \dots, x_n\}$ . It could be an explicit analytic expression or an implicit analytic expression. In a particular relative configuration of parts of an assembly consisting of gaps without interference between parts, the composition relations of displacements in some topological loops of the assembly enable us to determine the function  $f$ . For hyperstatic assembly, determination of function  $f$  is very complex, whereas this determination is easy for an open kinematic chain.

For statistical tolerance analysis, the input variables  $x = \{x_1, x_2, \dots, x_n\}$  are continuous random variables which enable us to represent tolerances. In general, they could be mutually dependent. A variety of methods and techniques (linear propagation (root sum of squares), non-linear propagation (extended Taylor series), numerical integration (quadrature technique), Monte Carlo simulation, etc.) are available for estimation of the probability distribution of  $y$  and the probability  $P(T)$  with respect to the geometrical requirement [NIG 95].

The aim of tolerance accumulation is to simulate the composition of tolerances, i.e. linear tolerance accumulation, 3D tolerance accumulation. Based on the displacement models, several vector space models map all possible manufacturing variations (geometrical displacements between manufacturing surfaces or between manufacturing surface and nominal surface) into a region of hypothetical parametric

space. The geometrical tolerances or the dimensioning tolerances are represented by deviation [GIO 93], [GIO 05], T-Map® [DAV 03] or specification hull [DAN 02], [DAN 05]. These three concepts are a hypothetical Euclidean volume which represents all possible deviations in size, orientation and position of features.

For tolerance analysis, this mathematical representation of tolerances allows calculation of the accumulation of tolerances using the Minkowsky sum of deviation and clearance domains [GIO 93], [TEI 99]; to calculate the intersection of domains for parallel kinematic chain; and to verify the inclusion of a domain inside another domain. The methods based on this mathematical representation of tolerances are very efficient for the tolerance analysis.

However, these two approaches do not take into account the quantifier notion. This notion translates the concept that a functional requirement must be respected in at least one acceptable configuration of gaps (existential quantifier “there exists”), or that a functional requirement must be respected in all acceptable configurations of gaps (universal quantifier “for all”) [DAN 05], [DAN 03]. A configuration is a particular relative position of parts of an assembly consisting of gaps without interference between parts.

The quantifier notion impacts the result of the tolerance analysis [DAN 03], [DAN 05]. Therefore, we propose a mathematical formulation of tolerance analysis which simulates the influences of geometrical deviations on the geometrical behavior of the mechanism, and integrates the quantifier notion.

## **7.2. Quantifier notion and mathematical formulation of tolerance synthesis**

In this section, the quantifier notion is illustrated with geometrical requirement and assembly requirement.

### **7.2.1. *Quantifier notion for geometrical product requirement***

A mechanism is a set of parts with joints. Most joints have a functional gap. These gaps induce displacements between parts. Each relative position defines a configuration of the joint. A configuration is a particular relative position of parts of an assembly consisting of gaps without interference between parts. The product geometrical requirement limits the variation between two surfaces of the mechanism, which are in functional relation. This requirement is a condition on the functional characteristic between these surfaces. For any given mechanism with gaps [DAN 02], [DAN 05], the relative orientation or position of these surfaces depends on the configuration, which is not single. Therefore, the value of the

functional characteristic depends on the configuration of the mechanism. There is an ambiguity in the expression of the requirement because the considered configuration is not described. In order to address this problem, it is necessary to specify in which configuration, the condition of the geometrical requirement must be checked. The expression of the geometrical product requirement is not univocal [DAN 03].

So, to define a univocal expression of the condition corresponding to a geometrical product requirement, this expression is completed by a quantifier ( $\exists$  or  $\forall$ ). The quantifier translates the concept that the condition must be respected in at least one configuration of the mechanism ( $\exists$ ), or that the condition must be respected in all configurations of the mechanism ( $\forall$ ):

- In the case of the quantifier ( $\exists$ ), if there exists one configuration of the mechanism such as the value of the functional characteristic is less than or equal to the tolerance, then the geometrical product requirement is respected.
- In the case of the quantifier ( $\forall$ ), if for all configurations of the mechanism, the value of the functional characteristic is less than or equal to the tolerance, then the geometrical product requirement is respected.

### ***7.2.2. Mathematical formulation of tolerance analysis for geometrical product requirement***

The approach used in this chapter is a parameterization of deviations from theoretical geometry; the real geometry of parts is apprehended by a variation of the nominal geometry. The substitute surfaces model these real surfaces. This parameterization of variations is detailed in the following section, and it enables us to define a variations parametric space, in which each coordinate system axis represents a parametric variable.

The mathematical formulation of tolerance synthesis takes into account not only the influence of geometrical deviations on the geometrical behavior of the mechanism and on the geometrical product requirements, but also the influence of the types of contacts on the geometrical behavior; all these physical phenomena are modeled by convex hulls (compatibility hull, interface hull and functional hull); these convex hulls are detailed in the following sections which are defined in the variations parametric space. A *convex hull* or a *convex polytope* [BIS 94], [ZIE 94] may be defined as a finite set of points, as the intersection of a set of *half-spaces*, or as a region of n-dimensional space enclosed by *hyperplanes*.

With this description by convex hulls, a mathematical expression of the admissible deviations of parts is detailed in the section relations between convex hulls (section 7.2.2.3).

#### 7.2.2.1. Geometrical description by variations parametric space

The geometrical behavior model needs to be aware of the surface deviations of each part (situation deviations and intrinsic deviations) and relative displacements between parts according to the gap (gaps and functional characteristics). Compared with the nominal model, each substitute surface has position variations, orientation variations and intrinsic variations:

- *Situation deviations* define the orientation and position variations between a substitute surface and the nominal surface.
- *Intrinsic deviations* of substitute surface are specific to their type. They define the surface variations. For instance, the intrinsic variation of a substitute cylinder is radius variation between the substitute cylinder and the nominal cylinder, also two types of relative displacements between parts.
- *Gaps* define the orientation and position variations between two substitute surfaces in contact.
- *Functional characteristics* define the orientation and position variations between two substitute surfaces in a functional relation.

The deviation of part surfaces, the gaps between parts and the functional characteristics between parts are described by parameters. Thereafter, the geometrical behavior of parts will be defined in space such that each coordinate axis corresponds to a parameter that is the variations parametric space. Four types of subspace corresponding to the four types of parameters are displayed in Table 7.1 [DAN 02].

Subspace name	Column vector	Designation
Situation	$s$	space of all situation deviations of parts
Intrinsic	$i$	space of all intrinsic deviations of parts
Gap	$g$	space of all gaps between parts
Functional characteristic	$fc$	space of all functional characteristics between parts

**Table 7.1.** Subspace description

#### 7.2.2.2. Geometrical behavior description using convex hulls

The tolerance synthesis model is based on the expression of the geometrical behavior of the mechanism; various hulls modeling the geometrical behavior of the mechanism are defined for 1D and 3D applications.

Relationships between small displacements of surfaces of parts lead to the compatibility hull ( $D_{\text{compatibility}}$ )

Composition relations of displacements in the various topological loops express the geometrical behavior of the mechanism [DAN 02], [DAN 05], [ZIE 94]. The composition relations define compatibility equations between the situation deviations and the gaps. The set of compatibility equations, obtained by the application of composition relation to the various cycles, makes a system of linear equations. So that the system of linear equations admits a solution, it is a requirement that compatibility equations be checked. These compatibility equations characterize some hyperplanes in the Situation  $\times$  Gap  $\times$  Functional characteristic space.

Constraints of contacts between parts surfaces nominally in contact lead to the interface hull ( $D_{\text{interface}}$ )

Interface constraints limit the geometrical behavior of the mechanism and characterize non-interference or association between substitute surfaces, which are nominally in contact [DAN 02], [GIO 93], [ROY 99]. These interface constraints limit the gaps between substitute surfaces. These constraints define the interface hull in Gap  $\times$  Intrinsic space. In the case of floating contact, the relative positions of substitute surfaces are constrained technologically by the non-interference, the interface constraints result in in-equations defined in Gap  $\times$  Intrinsic space. In the case of slipping and fixed contact, the relative positions of substitute surfaces are constrained technologically in a given configuration by a mechanical action. An association models this type of contact; the interface constraints result in equations defined in Gap  $\times$  Intrinsic space.

Functional constraints between part surfaces in functional relation lead to the functional hull ( $D_{\text{functional}}$ )

The functional requirement limits the orientation and the location between surfaces, which are in functional relation. This requirement is a condition on the relative displacements between these surfaces. This condition could be expressed by constraints, which are in-equations. These constraints define the functional hull in Functional characteristic  $\times$  Intrinsic space.

#### 7.2.2.3. Relations between convex hulls

The objective of this mathematical formulation is to define the necessary and optimal constraints on deviations of each part, i.e. the vectors  $\mathbf{s}$  and  $\mathbf{i}$ . The previous geometrical behavior description and the quantifier expression enable us to define the admissible deviations of parts such that the functional requirement is respected. These admissible deviations form a hull in this situation and intrinsic spaces called a

specification hull. To define it, we formalize a textual relation and a mathematical relation between various hulls [DAN 02], [DAN 05].

In the case of the quantifier  $\exists$ , the specification hull is defined as:

“The deviations are admissible” is equivalent to “there exists an admissible gap configuration of the mechanism and a functional characteristic such as the geometrical behavior and the functional requirement are respected”.

The mathematical expression of this equivalence is:

$$\begin{aligned}
 & (s, i) \in D_{\text{specification}} \\
 & \Leftrightarrow \exists g \{g \in \text{Gap} : (s, g, i) \in D_{\text{compatibility}} \cap D_{\text{interface}}\}, \\
 & \exists fc \in \text{Functional characteristic}, \\
 & : (s, g, i, fc) \in D_{\text{compatibility}} \cap D_{\text{interface}} \cap D_{\text{functional}} \\
 & (s, i) \in D_{\text{specification}} \\
 & \Leftrightarrow \exists g \in \{g \in \text{Gap} : (s, g, i) \in D_{\text{compatibility}} \cap D_{\text{interface}}\}, \\
 & (fc \text{ (Functional characteristic,} \\
 & : (s, g, i, fc) (D_{\downarrow \text{compatibility}} \cap D_{\downarrow \text{interface}} \cap D_{\downarrow \text{functional}})
 \end{aligned} \tag{7.2}$$

In the case of the quantifier  $\forall$ , the specification hull is defined as:

“The deviations are admissible” is equivalent to “for all admissible gap configurations of the mechanism, there exists a functional characteristic such as the geometrical behavior and the functional requirements are respected”.

The mathematical expression of this equivalence is:

$$\begin{aligned}
 & (s, i) \in D_{\text{specification}} \\
 & \Leftrightarrow \forall g \in \{g \in \text{Gap} : (s, g, i) \in D_{\text{compatibility}} \cap D_{\text{interface}}\}, \\
 & \exists fc \in \text{Functional characteristic}, \\
 & : (s, g, i, fc) \in D_{\text{compatibility}} \cap D_{\text{interface}} \cap D_{\text{functional}}
 \end{aligned} \tag{7.3}$$

For assembly requirement, the quantifier is  $\exists$ . The specification hull is defined as:

“The deviations are admissible” is equivalent to “there exists an admissible gap configuration of the mechanism such as the geometrical behavior and the assembly requirement (interface constraints) are respected”.



$$\begin{aligned}
& (s, i) \in D_{\text{specification}} \\
& \Leftrightarrow \exists g \in \text{Gap} : (s, g, i) \in D_{\text{compatibility}} \cap D_{\text{interface}} \\
& (s, i) \in D_{\text{specification}} \\
& \Leftrightarrow \exists g \left( \text{Gap} : (s, g, i) \left( D_{\downarrow \text{compatibility}} \right) \left( D_{\downarrow \text{interface}} \right) \right)
\end{aligned} \tag{7.4}$$

This quantifier notion enables us to formalize the relationship between hulls (compatibility hull, interface hull and functional hull) and specification hull. These relations are a theoretical formulation of tolerance synthesis.

### 7.3. Worst case tolerance analysis based on quantified constraint satisfaction problems

In this section, we consider the more general framework of quantified constraint satisfaction problems, which are defined as follows, and we illustrate its application for worse case tolerance analysis.

#### 7.3.1. QCSP

The QCSP is an extension of the constraint satisfaction problem (CSP) in which variables are totally ordered and quantified either existentially or universally [BOR 02]. QCSP provides a better expressiveness for modeling problems. The goal in a QCSP can be either to determine satisfiability or to find a consistent instantiation of the existential variables for all instantiations of the universal ones. The QCSP can be used to model PSPACE-complete decision problems from areas such as planning under uncertainty, adversary game playing, and model checking. For tolerancing application, the QCSP is used to check the model.

In standard CSPs all variables are existentially quantified whereas QCSPs are more expressive than CSPs in the sense that they allow universally quantified variables. They enable the formulation of problems where all contingencies must be allowed for.

A quantified constraint satisfaction problem (QCSP) is a formula of the form  $QC$  where  $Q$  is a sequence of quantifiers  $Q_1x_1 \dots Q_nx_n$  where each  $Q_i$  quantifies ( $\exists$  or  $\forall$ ) a variable  $x_i$  and each variable occurs exactly once in the sequence.  $C$  is a conjunction of constraints ( $c_1 \dots c_m$ ) where each  $c_i$  involves some variables among  $x_1, \dots, x_n$ .

Example:

$$\{ \forall x_i, \exists x_j ; D(x_i)=[0,1], D(x_j)=[0,1] ; c_i: x_i = x_j \} \tag{7.4}$$

Bordeaux and Monfroy extend the definition of arc consistency to QCSPs [BOR 02]. When applying AC on a constraint  $c_{ij}$ , the filtering achieved depends on the type of quantification for variables  $x_i, x_j$  and on the order in which the variables appear in the quantification formula. For a binary constraint there are four possible orders. AC for a constraint  $c_{ij}$  uses the following general rules; one for each order of quantification:

–  $\exists x_i \exists x_j$  : this is the case for standard CSPs. Constraint  $c_{ij}$  is AC if each value  $a \in D(x_i)$  is supported by at least one value  $b \in D(x_j)$ . If a value  $a \in D(x_i)$  has no support in  $D(x_j)$  then AC will remove  $a$  from  $D(x_i)$ . If  $D(x_i)$  becomes empty then the problem is unsatisfiable.

–  $\forall x_i \forall x_j$  : constraint  $c_{ij}$  is AC if each value  $a \in D(x_i)$  is supported by all values in  $D(x_j)$ . If a value  $a \in D(x_i)$  is not supported by all values in  $D(x_j)$  then the problem is unsatisfiable.

–  $\forall x_i \exists x_j$  : constraint  $c_{ij}$  is AC if each value  $a \in D(x_i)$  is supported by at least one value in  $D(x_j)$ . If a value  $a \in D(x_i)$  has no support in  $D(x_j)$  then the problem is unsatisfiable.

–  $\exists x_i \forall x_j$  : constraint  $c_{ij}$  is AC if each value  $a \in D(x_i)$  is supported by all values in  $D(x_j)$ . If a value  $a \in D(x_i)$  is not supported by all values in  $D(x_j)$  then AC will remove  $a$  from  $D(x_i)$ . If  $D(x_i)$  becomes empty then the problem is unsatisfiable.

The algorithm takes a QCSP with a set  $X$  of existentially or universally quantified variables in a given order, and computes the arc consistent sub-domains in case the problem is arc consistent or returns FALSE in case the problem is not arc consistent.

### 7.3.2. New mathematical formulation of tolerance analysis for QCSP solver

In this section we propose a new method which enables us to solve a tolerancing problem while utilizing and integrating the notion of QCSP. To do so, we need to transform the mathematical expression of tolerance analysis for assembly requirement:

$$\begin{aligned} & \forall x_1, \forall x_2, \forall x_3, \dots, \forall x_n, \exists x_{n+1}, \dots, \exists x_m; \\ & D(x_1), D(x_2), D(x_3), \dots, D(x_n), D(x_{n+1}), \dots, D(x_m); \\ & c_1, \dots, c_p \end{aligned} \quad [7.5]$$

- $x_1, x_2, \dots, x_n$  are the variables which represent each part deviation ( $s, i$ ),
- $x_{n+1}, \dots, x_m$  are the variables which represent each gap between parts ( $g$ ),
- the mathematical representation of geometrical specifications is a set of intervals which limit each part deviation like vectorial tolerancing:  $x_i \in D(x_i)$  with  $x_i$  a part deviation and  $D(x_i)$  its tolerance interval,  $D(x_1) \times \dots \times D(x_n) = D_{\text{specification}}$ ,
- the mathematical representation of interface constraints is a set of inequations which limit each gap:  $x_j \in D(x_j)$  with  $x_j$  a gap and  $D(x_j): x_j \geq 0$ ,  $D(x_{n+1}) \times \dots \times D(x_m) = D_{\text{interface}}$ ,
- the mathematical representation of the compatibility equations is a set of constraints:  $cl, \dots, cp$ .

Therefore, the mathematical expression of tolerance analysis for assembly requirement is: “for all acceptable deviations (deviations which are inside tolerances), there exists a gap configuration such as the assembly requirement (interface constraints) and the compatibility equations are verified”.

The expressive power of QCSP integrates the notion of quantifier in the expression of the mathematical expression for tolerance and allows us to model the mathematical formulation of tolerance analysis for assembly requirement with a vectorial tolerancing model.

However, there remains limitations in the QCSP expression power that need to be addressed in terms of implicit universal quantification of the variables which do not have the direct property of projectability. The lack of ability of universal quantification of variables which do not possess the property of projectability means that other means need to be adopted to circumvent this limitation. An instance of this problem occurs during the universal quantification of the gaps depending upon  $s$  and  $i$ .

#### 7.4. Statistical tolerance analysis based on constraint satisfaction problems and Monte Carlo simulation

In order to ensure the robustness of design, it is necessary to simulate and study the affect of variations on assembly due to variation in manufacturing. Variations may take place in any random pattern concurrently in the concerned dimension and may affect the assemblability and function of the assembly. In the following section, the approach discussed above will be modified and integrated with the Monte Carlo simulation tool to obtain an algorithm which performs the tolerance analysis of a

mechanical assembly from a sample population of components generated by Monte Carlo simulation.

The tolerance analysis method adopted in this report is based on using Monte Carlo simulation and quantifier notion to a solution of a CSP in order to calculate the probability of assembly and functioning of a given assembly. The application of this approach to 1D and 3D tolerance analysis will be discussed.

#### ***7.4.1. Algorithm for statistical tolerance analysis by Monte Carlo simulation and CSP technique***

A new algorithm has been developed which integrates the QCSP for tolerance analysis. This algorithm has been developed and tested in Mathematica® and validated for a number of different example assemblies. The algorithm is based on the statistical sampling power of the Monte Carlo simulation and the main calculation engine uses the quantifier notion built in the QCSP for tolerance analysis problem resolution.

The following section details the general description of the algorithm. In order to apply the notion, we need to transform the following into mathematical expressions:

- For assembly requirement, the mathematical expression is:

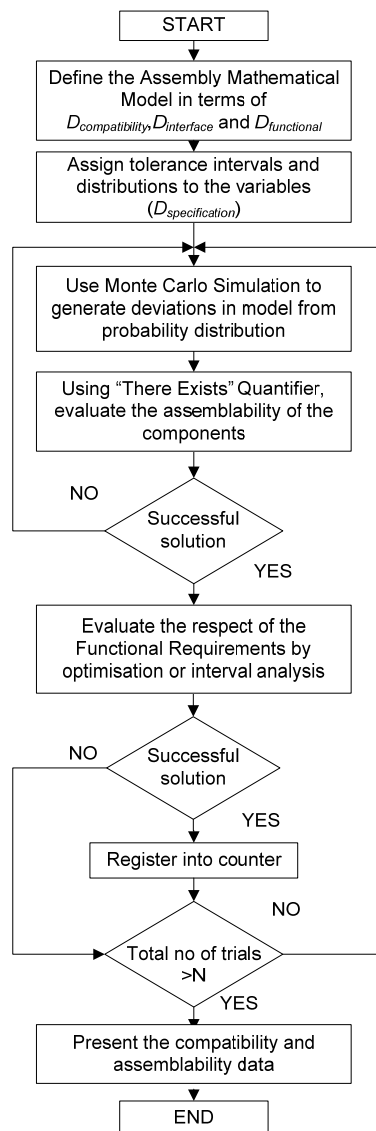
“For each sample (Monte Carlo simulation) of acceptable deviations (deviations which are inside tolerance limit), there exists a gap configuration such as the assembly requirement (interface constraints) and the compatibility equations are verified”.

- For functional requirement, the mathematical expression is:

“For each sample (Monte Carlo simulation) of acceptable deviations (deviations which are inside tolerances), the worst case of functional characteristics must be respected, the functional requirements such as the interface constraints and the compatibility equations are verified”.

A general flow chart describing the module for tolerance analysis is shown in Figure 7.1. The main principle behind the algorithm is to simulate and evaluate the influence of the manufacturing deviations on the nominal dimensions of an assembly.

In order to achieve this, the Monte Carlo simulation and quantifier notion are used to simulate the deviations and to quantify the variables in the CSP respectively. This process is repeated recursively for a large sample of deviations to establish a resultant distribution of assembly probability in order to perform the tolerance analysis of any given assembly consisting of sub components.



**Figure 7.1.** General scheme of Tolerance analysis with the Monte Carlo simulation

A mathematical model of the assembly is expressed in the form of the compatibility, interference and functional hulls, it is defined by a set of variables and a set of constraints on subsets of the variables:

Constraints describing the compatibility hull generally formulated as:

$$C_c(s, g, fc) = 0 \Leftrightarrow (s, g, fc) \in D_{compatibility} \quad [7.6]$$

Constraints describing the interface hull:

$$C_i(i, g) \leq 0 \text{ and } C_i(i, g) = 0 \Leftrightarrow (i, g) \in D_{interface} \quad [7.7]$$

Constraints describing the functional hull:

$$C_f(i, fc) \leq 0 \Leftrightarrow (i, fc) \in D_{functional} \quad [7.8]$$

The part deviations  $(s, i)$  are then evaluated recursively within the algorithm. Monte Carlo simulation is used to generate random variables simulating the part deviations with all the generated deviations within the  $D_{specification}$ . A sample of part deviations is noted:

$$\mathbf{s}' = \{s'_1, s'_2, \dots, s'_n\}, \mathbf{i}' = \{i'_1, i'_2, \dots, i'_o\}$$

For any given instance of iteration, the part deviations generated by the Monte Carlo simulation should satisfy the set of constraints:

$$(\mathbf{s}', \mathbf{i}') \in D_{specification}$$

To evaluate the assemblability of each sample (instance of part deviations), we verify if there exists an admissible gap configuration of the mechanism such as the assembly requirement (interface constraints) and the compatibility equations are verified:

$$(\mathbf{s}', \mathbf{i}', \mathbf{g}) \in D_{compatibility} \cap D_{interface}$$

This check is performed with help of translation of relation [7.4]. In the algorithm, for an instance of iteration, its mathematical form becomes

$$\exists \mathbf{g} : (\mathbf{s}', \mathbf{i}', \mathbf{g}) \in D_{compatibility} \cap D_{interface} \quad [7.9]$$

Depending on this decision process it may be desirable to determine whether a solution exists (verify the consistency of the constraint satisfaction problem), to find one solution, to compute the space of all solutions of the constraint satisfaction

problem, or to find an optimal solution relative to a given cost function which respects all constraints ( $C_c$  and  $C_i$ ).

In our case, the goal is not to find a particular solution. It is possible to check the existence of the solution using the inbuilt Mathematica® function “Exists”. The result of this step effectively establishes if the individual parts with the simulated deviations would be able to be assembled.

Moreover, the check of the solution existence could be made by a hull-consistency algorithm, the key idea is to generalize constraint-consistency [BOR 02] criterion to a higher level where the set of all constraints is seen as a single global constraint. Hence, it must guarantee arc-consistency at the bounds of the variable domains for this single global constraint.

To evaluate the respect of the functional requirements of each sample (instance of part deviations) that assembles, we verify whether for all admissible gap configuration of the mechanism there exists functional characteristics such as the functional requirements which are verified:

$$(s', i', g, fc) \in D_{compatibility} \cap D_{interface} \cap D_{functional} \quad [7.10]$$

This check is performed with help of translation of equation [7.3]. In the algorithm, for an instance of iteration, its mathematical form becomes:

$$\begin{aligned} & \forall g \in \{g \in \text{Gap} : (s, g, i) \in D_{compatibility} \cap D_{interface} \\ & \quad \exists fc \in D_{functional} \\ & : (s', i', g, fc) \in D_{compatibility} \cap D_{interface} \cap D_{functional} \\ & \forall g \left( \left\{ g(Gap : (s, g, i)) \left( D_{\downarrow compatibility} \left( D_{\downarrow interface} \right. \right. \right. \right. \\ & \quad \exists fc \left( D_{\downarrow functional} \right. \\ & : (s', i', g, fc) \left( D_{\downarrow compatibility} \cap D_{\downarrow interface} \cap D_{\downarrow functional} \right. \end{aligned} \quad [7.11]$$

Depending on this decision process it may be desirable to determine the space of all solutions of the constraint satisfaction problem, or to find an optimal solution relative to a given cost function which respects all constraints ( $C_c$ ,  $C_i$  and  $C_f$ ).

For examples pertaining to elementary levels, the check of the solution is made possible by using the inbuilt Mathematica® function “For All”. However, with an increase in complexity of the assembly usage of the built in Mathematica® function becomes time consuming.

Two alternative approaches to translating relation [7.3] have been formalized which are (a) optimization of worst-case values, (b) interval propagation with help of interval arithmetic to reduce the domain of the variables (functional characteristics).

We use the optimization approach to find the worst case values of the functional characteristics:

$$\begin{aligned}
 &fc_{\max} = \text{Max}(fc(g, s', i')) \\
 &\text{S.T.} \\
 &\quad C_c(s', g, fc) = 0 \\
 &\quad C_i(i', g) \leq 0 \text{ and } C_i(i', g) = 0 \\
 &\quad C_f(i', fc) \leq 0 \\
 &fc_{\min} = \text{Min}(fc(g, s', i')) \\
 &\text{S.T.} \\
 &\quad C_c(s', g, fc) = 0 \\
 &\quad C_i(i', g) \leq 0 \text{ and } C_i(i', g) = 0 \\
 &\quad C_f(i', fc) \leq 0 \\
 &fc_{\max} \in D_{\text{functional}} \text{ and } fc_{\min} \in D_{\text{functional}}
 \end{aligned} \tag{7.13}$$

The result of this step evaluates if the individual parts with the simulated deviations would be able to assemble as well as if the resultant assembly would respect the functional requirements.

## 7.5. Applications

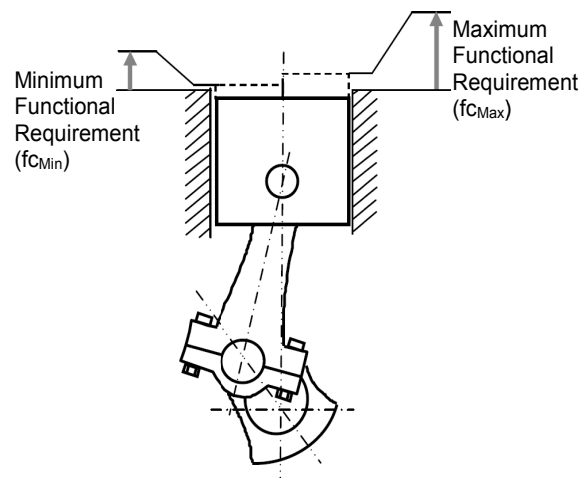
The approach developed for the tolerance analysis for 1D and 3D mechanical assemblies has been applied and validated over different models with and without GD & T specifications. For the sake of brevity and clarity of application, in this chapter, a simple mechanical assembly as shown in Figures 7.2 and 7.3 is taken as an example.

Figure 7.3 shows a simplified cross-section of an IC-engine. The simplified assembly consists of 5 individual components:

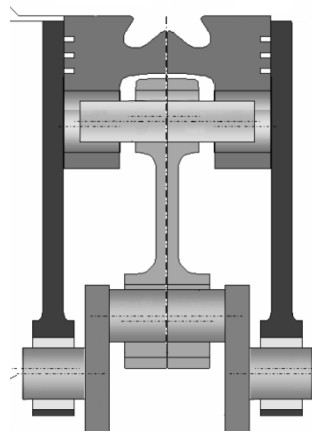
1. engine block;
2. piston;
3. connecting rod;
4. crank shaft;
5. gudgeon pin.



The functional requirement to be taken into account in this example is the minimum and maximum piston-head clearance (Figure 7.2). The tolerance analysis of the assembly shown in the figure was performed using normal distribution, for each component, with a mean at zero and dimension specific standard deviations derived from specified tolerance. The program also calculated the worst case values of the gaps “g” for which the assembly conditions and functional requirements were respected.



**Figure 7.2.** *IC engine assembly functional requirements*



**Figure 7.3.** *IC engine assembly*

The results were validated against the tolerance values based on a worst case analysis provided with the drawings. The results obtained were in accordance with the tolerancing specified on the drawings. In addition to this, the program was tested for tolerance values varying away from the worst case values and the results were noted. The results displayed the varying assembly assemblability probability values confirming the functionality of the program.

## 7.6. Discussion

In this chapter, we introduce a discussion about tolerance analysis, and we compare this tolerance analysis approach with the mathematical approaches developed by Davidson and Shah [DAV 03], Giordano [GIO 05], Teissandier [TEI 99]. In these approaches, the geometrical tolerances, the dimensioning tolerances or the contact constraints are represented by deviation domain/clearance domain or T-Map ®. These three concepts are a hypothetical Euclidean volume which represents all possible deviations in size, orientation and position of features. For tolerance analysis, this mathematical representation of tolerances allows us to calculate the composition of tolerances: using the Minkowsky sum of deviation and clearance domains to calculate the intersection of domains for parallel kinematic chain, and to verify the inclusion of a domain inside other one. The methods are very efficient for the tolerance analysis, but the computational cost depends on the number of Minkowsky sums.

In the proposed approach, we use the same mathematical representation, and we add the compatibility domain which represents the composition relations of displacements in the various topological loops, and the mathematical formulation based on the quantifier notion. Therefore, we do not use the Minkowsky sum for the resolution, we use the QCSP technique. This QCSP technique coupled with the Monte Carlo simulation allows resolution for worst case analysis or statistical analysis.

Mathematical formulation of tolerance analysis with integration of the Quantifier notion is a new technique that uses the notion of the universal quantifiers, and which provides a univocal expression of the condition corresponding to a geometrical product requirement. The application of tolerance analysis developed in this work relies upon QCSP and uses the integrated concept of quantifiers to quantify, control and verify the respect of the required functional requirement (quantifier) as well as the geometrical product requirement (quantifier). This addition adds a qualitative and quantitative nature to the tolerance analysis process allowing the user to specify the control elements in a model as well providing the necessary tools for validation via worst case scenario application or probability based statistical analysis.

The algorithm developed in this chapter addresses 1D and 3D application of tolerance analysis. The fundamental steps of the algorithm however remains the same for all the applications, i.e.:

- the definition of the product parametric model with the help of variation parametric space in either 1D or 3D using convex hulls;
- using quantifiers in the case of worst case tolerance analysis to define the deviation tolerance interval;
- use of the Monte Carlo simulation in case of statistical tolerance analysis;
- application of “There Exists” quantifier to ascertain that the model with generated deviations conforms to different convex hulls, i.e. respect of compatibility hull, interface hull and functional hull;
- displaying results of calculation regarding the conformity of the assembly with respect to the individual hulls.

In the statistical tolerance analysis module, Monte Carlo simulation has been used in conjunction with the QCSP to calculate the probability of the functional operation of an assembly.

The geometrical modeling approach is based on modeling by the parameterization of the component. Instead of an explicit model, the model is based on a set of equations and inequations which provide for the necessary constraints for product functioning and part compatibility. The resulting model is dependent not only on the nominal dimensions of the assembly but also on taking into account the required functional characteristic as well as the gaps.

Another unique area of application for this algorithm has been in the field of tolerance synthesis where it has been successfully applied to the tolerance synthesis of a mechanical assembly in conjunction with a genetic algorithm. Currently the scope of QCSP has also been expanded to include the domain of robust design of mechanical systems.

## 7.7. Bibliography

- [BAL 97] BALLOT E., BOURDET P., “A computation method for the consequences of geometric errors in mechanisms”, *CIRP Seminar on Computer Aided Tolerancing*, Toronto, Canada, April 1997.
- [BIS 94] BISZTRICZKY T., MCMULLEN P., SCHNEIDER R., WEISS A. W., *Polytopes: Abstract, Convex, and Computational*, Netherlands, Kluwer Academic Publishers, 1994.

- [BOR 02] BORDEAUX L., MONFROY E., "Beyond NP: Arc-consistency for Quantified Constraints", *Proceedings of CP-2002 8<sup>th</sup> International Conference on Principles and Practice of Constraints Programming*, September 8-13, Cornell University, Ithaca, New York, 2002.
- [BOU 96] BOURDET P., MATHIEU L., LARTIGUE C., BALLU A., "The concept of small displacement torsor in metrology", Advanced mathematical tool in metrology, Advances in mathematics for applied sciences, *World Scientific*, Vol. 40, 1996.
- [CHA 91] CHASE K.W., PARKINSON A.R., "A survey of research in the application of tolerance analysis to the design of mechanical assemblies", *Research in Engineering Design*, Vol. 3, pp.23-37, 1991.
- [DAN 02] DANTAN J.Y., BALLU A., "Assembly specification by Gauge with Internal Mobilities (G.I.M.): a specification semantics deduced from tolerance synthesis"; *Journal of Manufacturing Systems*, Vol. 21, No. 3, pp 218-235, 2002.
- [DAN 05] DANTAN J.Y., MATHIEU L., BALLU A., MARTIN P., "Tolerance synthesis: quantifier notion and virtual boundary", *Computer Aided Design*, Vol.37, No.2, pp.231-240, 2005.
- [DAN 03] DANTAN J.Y., MATHIEU L., BALLU A., "Geometrical Product Requirement: Uncertainty and expression", *8rd CIRP International Seminar on Computer-Aided Tolerancing*, USA, pp199-208, 2003.
- [DAV 03] DAVIDSON J.K. and SHAH J.J., "Using Tolerance-Maps to represent material condition on both a feature and a datum", *8th International CIRP Seminar on Computer Aided Tolerancing*, Charlotte, North Carolina, USA, 28-29 April 2003, pp.92-101.
- [DES 99] DESROCHERS A., "Modeling three dimensional tolerance zones using screw parameters", *25th Design Automation Conference, ASME*, Las Vegas, USA, September 1999.
- [GIO 93] GIORDANO M., DURET D., "Clearance space and deviation space, application to three-dimensional chain of dimensions and positions", *CIRP Seminar on Computer Aided Tolerancing*, ENS Cachan, France, May 1993.
- [GIO 05] GIORDANO M., SAMPER S., PETIT J.P., "Tolerance analysis and synthesis by means of deviation domains, axi-symmetric cases", *9th CIRP International Seminar on Computer-Aided Tolerancing*, held at Arizona State University, Tempe, Arizona, USA, 10-12 April, 2005.
- [GUP 97] GUPTA S., TURNER J.U., "Variational solid modeling for tolerance analysis", *IEEE Computer Graphics & Application*, Vol.13, No. 3, pp.64-74, 1993.
- [HON 02] HONG, Y. S., CHANG, T-C., "A comprehensive review of tolerancing research", *International Journal of Production Research*, Vol. 40, No. 11, pp. 2425-2459, 2002.
- [NIG 95] NIGAM S.D., TURNER J.U., "Review of statistical approaches to tolerance analysis", *Computer Aided Design*, Vol.27, No. 1, pp.6-15, 1995.
- [ROY 99] ROY U., LI B., "Representation and interpretation of geometric tolerances for polyhedral objects", *Computer Aided Design*, Vol.31, No. 4, pp.273-285, 1999.

- [SAC 98] SACKS E., JOSKOWICZ L., "Parametric kinematic tolerance analysis of general planar systems", *Computer Aided Design*, Vol. 30, No. 9, pp. 707-714, 1998.
- [TEI 99] TEISSANDIER D., COUÉTARD Y., GERARD A., "A computer aided tolerancing model: proportioned assembly clearance volume", *Computer Aided Design*, Vol.31, No. 13, pp.805-817, 1999.
- [ZIE 94] ZIEGLER G.M., "Lectures on Polytopes", *Graduate Texts in Mathematics*, Vol 152, Springer Verlag, 1994.

## Chapter 8

# Tolerance Analysis in Manufacturing Using the MMP, Comparison and Evaluation of Three Different Approaches

In previous works, we have developed the model of manufactured part (MMP) [VIL 05], a method for modeling the different geometrical deviation impacts on the part produced (error stack-up) in a multi-stage machining process. They also proposed different solution techniques to identify the worst case for the purpose of tolerance analysis. The first proposed solution technique consists of optimization techniques such as sequential quadratic programming (SQP) or genetic algorithms (GA) [KAM 08a]. The second solution combines the MMP and the Jacobian-torsor model [GHI 03] [KAM 08b] that benefits from the interval arithmetic advantages to solve the worst case searching problem. The last technique uses the Monte Carlo simulation to generate a population of virtually manufactured parts representative of the real produced parts [VIG 08].

This chapter first reviews the MMP model and the different solution techniques. The different strategies to simulate the deviation parameters of the model are then discussed. For each of the three proposed solution techniques, its convenience and inconvenience is explored in detail. The solution technique performances are compared from different points of view (i.e. rapidity, convergence to the global minimum, analyzed case, etc.) and some perspectives are presented.

---

Chapter written by Mojtaba KAMALI NEJAD, Frédéric VIGNAT and François VILLENEUVE.

### 8.1. Introduction

Today, manufacturing engineers are faced with the problem of selecting the appropriate process plan (machining processes and production equipment) to ensure that design specifications are satisfied. Developing a suitable process plan for release to production is complicated and time-consuming. Currently, trial runs or very simple simulation models (1D tolerance charts for example [WHY 90]) are used to check the quality criterion. The trial runs are very costly and, on the other hand, the accuracy of simulation fails to meet today's requirements. These problems can be overstepped by developing accurate models and methodologies for simulating the manufacturing process and predicting geometrical variations in the parts produced. More accurate models will make it possible to evaluate the process plan, determine the tolerance values in terms of manufacturing capabilities during the design phase, and define the manufacturing tolerances to be checked for each setup. In the literature available on this subject, the evaluation of a process plan in terms of functional tolerances is called the tolerance analysis. In this chapter the model of manufactured part (MMP) is used for simulating the manufacturing process and then the worst case technique and statistical approach are used for the aim of tolerance analysis.

In this chapter we shall focus on tolerance analysis relating to error propagation in a multi-stage machining process. Huang *et al.* [HUA 03] propose a state space model to describe part error propagation in successive machining operations. Surface deviation is expressed in terms of deviation from nominal orientation, location and dimensions. The error sources in machining operations are classified as fixture errors, datum errors and machine tool errors. A part's deviation is expressed in terms of the deviation of its surfaces and is stored in a state vector  $x(k)$ . This vector is then modified by moving from operation  $k$  to  $k+1$ . Zhou *et al.* [ZOU 03] use the same state model but the surface deviation compared with the nominal state is expressed using a differential motion vector. However, these two models require specific fixture setups (e.g. an orthogonal 3-2-1 fixture layout). More recently, Loose *et al.* [LOO 07] used the same state space model with a differential motion vector but including general fixture layouts. Although a general fixture layout is considered, the error calculation of a fixture is based on its locator deviations (a locator is a punctual connection). Hence, positioning cases with plane/plane contact or cylinder/cylinder floating contact are not envisaged.

Huang *et al.* [HUA 04] propose a simulation-based tolerance stack-up analysis. Manufacturing errors are classified as follows: work holding errors (i.e. fixture errors, datum errors and raw part errors), machine tool errors and cutting tool errors. A surface is modeled using uniformly distributed sample points (point cloud), which is a basic technique applied in CMM type inspections. By putting the part through different machining setups, the coordinates of these points in the local part

coordinate system are changed due to manufacturing errors. The Monte Carlo method is used to perform the simulation. The different possible errors are considered in this simulation but part/fixture interaction is not studied and it is assumed that part/fixture contact is perfect.

This chapter firstly recalls the MMP [VIL 05], [GHI 03], [VIL 07]; a method for modeling the different geometrical deviation impacts on the part produced (error stack-up) in a multi-stage machining process. Previously, the same authors presented a generic formulation for tolerance analysis based on searching for the worst case using the MMP. This chapter discusses the different numerical solution technique for performing the worst case based tolerance analysis. Worst case technique then will be compared with statistical tolerance analysis. The statistical approach uses the Monte Carlo Simulation. The convenience and inconvenience of each technique will then be discussed.

## 8.2. MMP

[VIL 05], [VIG 07] and [VIL 07] propose a method for modeling successive machining processes that takes into account the geometrical and dimensional deviations produced with each machining setup and the influence of these deviations on further setups. In the MMP, the errors generated by a manufacturing process are considered to be the result of two independent phenomena: *positioning* and *machining*. These deviations are accumulated over the successive setups (see Figure 8.1). The result is expressed in terms of deviation of the actual surfaces compared with those of the nominal part. In order to capture the error stacks, an intermediate virtual part (MWP) is put through the different setups. In setup  $k$ , the machined surface deviation is the combination of positioning errors and machining errors. Positioning errors are caused by surface deviations from a previous setup (datum errors) and fixture surface deviations in setup  $k$ . Machining errors are machined surface deviations compared with the nominal position in the machine tool in setup  $k$ . These errors stem from multiple and various sources ranging from machine geometry and control to cutting deformations.

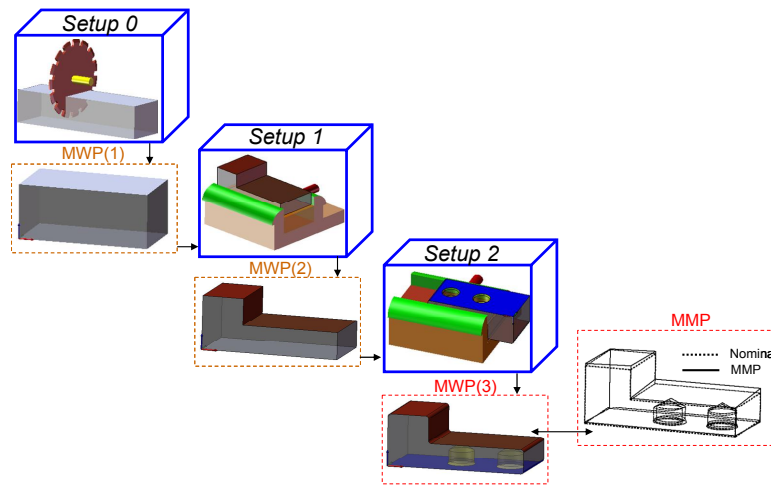
At the end of the modeling process, a virtual manufactured part (MMP) is created. This MMP stores data about the deviations generated (combination of parameters and range of variation) during the full machining process; see Figure 8.1.

The MMP not only represents a model of one manufactured part containing a description of the process in terms of geometrical deviations and accumulated defects. In fact, because it indicates the variation range of the generated defects it also represents the series of parts produced. The model describes the defects, classifies them and indicates their variation range.



Small Displacement Torsors (SDT) describe the MMP surface deviations, i.e. the MMP parameters, which can be classified according to four categories:

- machining deviations DM,  $(rx_i, ry_i, tz_i \dots)$ ;
- fixture surface deviations DH,  $(rx_{iSj}, tx_{iSj}, \dots)$ ;
- link parameters LHP,  $(lrx_{iSj}, ltx_{iGj} \dots)$ ;
- actual surface deviations relative to the nominal part  $(rx_{P, Pi}, ry_{P, Pi}, \dots)$ .



**Figure 8.1.** *Tolerance stack-up model*

The DM are limited by constraints (CM) representing machine and tool capabilities. The DH parameters are limited by constraints (CH) representing the fixture quality.

Due to the type of connection (floating or slipping), the LHP values are determined by a specific algorithm (CHP) including constraints and, in certain cases, a positioning function.

For each MWP surface made, the positioning and machining deviations are added. The deviation relative to the nominal part is determined and expressed as  $T_{P, Pi}$  for surface  $i$  of the MWP; see Figure 8.1. This Torsor will be kept in the MWP data for possible further use in another setup for an assembling procedure or for the purposes of tolerance analysis. In the example of Figure 8.1, surface deviations relative to the nominal part regarding surface 3 are expressed as equation [8.1].

$$T_{P,P3} = \begin{bmatrix} rx_{P,P3} & 0 \\ 0 & 0 \\ 0 & tz_{P,P3} \end{bmatrix}_{LCS3} \quad \text{Where : } \begin{cases} tz_{P,P3} = 7.07 \text{ } lrx_{1S2} + 0.7 ( -ltz_{1S2} + ltz_{2S2} ) - 7.07 \\ rx_1 + 7.07 rx_{1S2} + 0.7 ( -tz_1 - tz_{1S2} + tz_2 + tz_{2S2} ) + tz_3 \end{cases}$$

[8.1]

### 8.3. Tolerance analysis and virtual gauge

Two techniques have been used in tolerance analysis: worst case analyzing and statistical analyzing. In worst case tolerance analyzing (WC), it is assumed that all deviations could simultaneously occur at their worst limits. The extreme value of a functional tolerance under any possible variations caused by deviations is determined. In statistical tolerance analysis, it is assumed that individual deviations are independent and have some frequency distribution, which allows us to compute the probability that the product can be found at the end of machining and will function under given individual tolerances, often by Monte Carlo methods.

In this chapter, both of the above mentioned tolerance analysis techniques will be applied with the MMP. First of all, we introduce how we check the conformity of an individual part with the functional tolerances by means of a virtual gauge. Secondly the worst case search and statistical tolerance analysis will follow. Because of the different nature of WC tolerance analysis and statistical analysis, they will be presented in two separate sections.

In this chapter, functional tolerance compliance is checked using a virtual gauge. Each tolerance is modeled by a virtual gauge according to the standard concerned. A virtual gauge is a nominal part made up of positioning surfaces and tolerance zones (see Figure 8.1). This gauge is assembled with the MMP according to the chosen standard rules (usually ISO or ASME). The gauge and MMP assembling process is based on a set of hierarchically organized elementary connections. The gauge/MMP assembly link parameter values (LGP) are determined by a specific algorithm (CGP) similar to the CHP algorithm used to calculate the MWP/Fixture assembly link parameters. Once the gauge and MMP assembly is finished, functional tolerance compliance is verified by the  $\text{GapGP}_k$  signed distance measured between the virtual gauge modeling the tolerance and the MMP surfaces concerned. This distance is measured at the necessary points along the boundary of the toleranced surface. The distance with the positive sign represents a point inside the tolerance zone and a distance with a negative sign represents a point outside of tolerance zone.

#### 8.4. Worst case searching

If the worst part in a series of manufactured parts complies with the functional tolerance, it is logical to conclude that all of the parts manufactured will comply. This technique is a little far from reality. It means that even if the worst part in a series of manufactured parts does not comply with the functional tolerance, the majority of manufactured parts could be acceptable. However this technique is largely used in the manufacturing of high precision parts like for plane engines and the army. We developed two techniques for worst case searching associated with MMP: the optimization technique and the combined approach.

##### 8.4.1. Optimization technique

A generic formulation of the worst case searching problem, as proposed by Villeneuve *et al* [VIL 05], consists of solving the following objective functions:

$$\min_{CM, CH, CHP} \left( \max_{CGP} (GapGP_{\min}) \right) \quad [8.2]$$

These functions express the search for the worst case in terms of the functional tolerance under analysis. A process plan is considered able to satisfy the functional tolerance if the value determined in equation [8.2] remains positive or zero while the MMP parameters vary in their limited variation domain. As previously underlined, functional tolerance compliance is verified by the signed distance  $GapGP_k$ . For a given problem, the critical distance is the minimum distance denoted by  $GapGP_{\min}$  as developed in [8.3].

$$GapGP_{\min} = \min_{k=1,2,\dots} (GapGP_k) \quad [8.3]$$

The Gauge/MMP assembly is not always complete and some limited relative displacements remain possible due to the material condition modifiers, incomplete datum frames or the type of tolerance (i.e. orientation tolerance). These displacements may correspond to the degrees of freedom ( $LGP_{DOF}$ ) of the Gauge/MMP assembly or to the parameters of a floating contact ( $LGP_f$ ).

In the second case, the displacements are described by the link parameters and their limits by the positioning algorithm CGP (generally non-penetration condition) complying with the chosen tolerancing standard (ISO, ASME). Within the limits of these displacements, the most favorable position for the virtual gauge relative to the MMP can thus be found. In this position, the  $GapGP_{\min}$  has a maximum value. In other words, the virtual gauge will be displaced by an optimization algorithm that explores possible displacements until the best position with respect to the MMP is

found. In this position, all the  $\text{GapGP}_k$  will be measured for functional tolerance verification. This procedure is expressed by [8.4].

$$\max_{LGP}^{CGP} (...) \quad [8.4]$$

The  $\text{GapGP}^*$  solution provided by [8.4] is also interpreted as a virtual measurement of an individual part. As previously stated, the method presented in this study for analyzing functional tolerance consists of finding the worst case (minimum value of the  $\text{GapGP}^*$ ). The search for the worst case is an optimization task that can be expressed as shown below, [8.5]. The objective function in this optimization is the  $\text{GapGP}^*$ . The variables are the CM, CH, and LHP. The limits of these variables are expressed by constraints (CM and CH) and the positioning algorithm (CHP).

$$\min_{DM, DH, LHP}^{CM, CH, CHP} (...) \quad [8.5]$$

#### 8.4.1.1. Technique used in the solution

[8.2] is a multi-layer constrained optimization problem. It checks whether a process plan is able to satisfy functional tolerance requirements. In order to provide a clearer mathematical representation of [8.2], a new formulation for worst case identification shall be put forward in this section. Secondly, a technique for solving the worst case search issue shall be discussed.

To simplify the technique adopted, the problem is broken down into two sub problems, [8.6] and [8.7], and variable substitution is applied [KAM 08a].

$f$ : function expressing the  $\text{GapGP}$  equation

$g$  and  $h$ : positioning functions for MWP/fixture and gauge/MMP assemblies respectively

$m$ : number of elementary MWP/fixture connections

$n$ : number of elementary gauge/MMP connections

$$x = \{DM, DH, LHP_f, LHP_{DOF}\}, \quad y = LHP_s, \quad z = \{LGP_f, LGP_{DOF}\},$$

$$w = LGP_s$$

where  $LHP_{DOF}$ ,  $LHP_s$  and  $LHP_f$  are the DOF, slipping and floating LHP parameters respectively

and  $LGP_{DOF}$ ,  $LGP_s$  and  $LGP_f$  are the DOF, slipping and floating LGP parameters respectively

Sub I:

$$\begin{aligned}
 \text{Worst case value} &= \min_x F(x, y) \\
 \text{Subject to : } &c(x, y) \geq 0 \\
 \text{Where: } &y = \{y_1, y_2, \dots, y_i\} \\
 \text{With : } &\forall i \in [1, m], y_i = \text{Solution of: } \max_{y_i} g_i(y_i) \\
 &\text{Subject to : } c(x, y) \geq 0
 \end{aligned} \tag{8.6}$$

Sub II:

$$\begin{aligned}
 F(x, y) &= \max_z \min_{\{f_i\}} \{f_i(x, y, z, w)\} \\
 \text{Subject to : } &c(x, y, z, w) \geq 0 \\
 \text{Where: } &w = \{w_1, w_2, \dots, w_i\} \\
 \text{With : } &\forall i \in [1, n], w_i = \text{Solution of: } \max_{w_i} h_i(w_i) \\
 &\text{Subject to : } c(x, y, z, w) \geq 0
 \end{aligned} \tag{8.7}$$

The task in Sub I is to find the worst possible part produced in a multi-stage machining process in relation to the tolerance being analyzed. The task in Sub II is to perform a virtual measurement of one individual part. In Sub II, the value of  $F(x, y)$  is calculated and supplied to Sub I. To be able to solve the positioning algorithms (CHP and CGP), each sub problem is broken down into different layers. Readers should refer to [KAM 08a] for more information and details on Sub problems and the layers concerned.

#### 8.4.1.2. *Solution strategy*

Based on the constraints associated with DM and DH, the proper optimization algorithm should be applied. One iteration in the Sub I level follows with many iterations in Sub II and its layers. If the gradient optimization method is used for Sub I, the initial gauss plays a very important role. If the wrong gauss is chosen, there is a high risk of reaching a local minimum (instead of a global minimum).

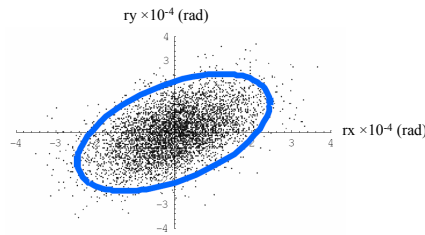
Stochastic methods such as genetic algorithms can be applied as well. The advantage of this kind of algorithm is that, by creating a big enough population, the probability of finding the global minimum point is higher. The drawback is the time needed to run such an algorithm.

#### 8.4.1.3. *Quality constraints*

The machined surface deviation torsor parameters, known as machining deviation parameters (DM), are limited by constraints (CM) stemming from the machine tool capabilities. The parameters of the fixture surface deviation torsor (DH) are also limited by constraints (CH) arising from the fixture quality. These constraints limit either one or a set of parameters. There are 3 main strategies for defining these constraints.

##### Using the measurement results

In this strategy, a sufficient number of parts have to be produced and measured. The manufacturing conditions (temperature, machine tool, etc.) should be the same as for the simulation. The machined surface or positioning surface deviation ranges are obtained from the measurement data. Readers can refer to [TIC 07] for more details about how the measurements are performed. In this strategy, the measurement results will be modeled, assuming that the deviation parameters are not independent. Based on the measurement results obtained, the co-relation between the parameters is then sought (see Figure 8.6). This strategy is very close to reality, but it is complicated to express the co-relation between the parameters.



**Figure 8.2.** Co-relation between deviations parameters ( $rx$ ,  $ry$ ) [GER 07]

With this strategy, the constraints obtained for the deviation parameters can be expressed as [8.8].

$$a \cdot rx^2 + b \cdot ry^2 + c \cdot rx \cdot ry \leq d \quad [8.8]$$

##### Using the measurement results (independent parameters)

As explained for the previous strategy, the parameter deviation ranges are obtained by measurements. As opposed to the previous strategy, the parameters here are assumed to be independent variables (for the purposes of simplification) with a normal distribution that varies in the interval defined by  $[-3\sigma \text{ } +3\sigma]$ . With this strategy, the constraints obtained will as shown in equation [8.9], the case of a plane

SDT. The deviation variation range obtained is close to reality but considering independent parameters imply that these they can simultaneously attain their extreme limits. This is highly improbable in reality.

$$\begin{aligned} \underline{rx} &\leq rx \leq \overline{rx} \\ \underline{ry} &\leq ry \leq \overline{ry} \\ \underline{tz} &\leq tz \leq \overline{tz} \end{aligned} \quad [8.9]$$

Considering a variation zone with dependent parameters

In this strategy, a standard variation zone is used to represent the deviation range of a surface or its feature (axis, center, etc.). Desrochers [DES 99] proposes a 3D representation of the variation zones. A variation zone can be used in its generic form to present the potential variations along and about all the three Cartesian axes. The proposed representation comprises all standard variation zones, along with their corresponding SDT representation and geometrical constraints. The SDT parameter variations must be bound by the limits of the 3D variation zones they represent. These boundary areas are hyper-surfaces of the space spanned by the six small displacement variables ( $rx$ ,  $ry$ ,  $rz$ ,  $tx$ ,  $ty$ ,  $tz$ ). Illustrated below is the case of a planar variation zone showing how such constraints can be handled. In Figure 8.3, the variation zone is defined as the volume ranging between two parallel planes with a distance  $e$  between them. The ideal associated plane (shaded in Figure 8.3) must therefore lie inside this zone. The boundary points will be used to ensure that the associated surface remains within the variation zone. If four boundary points (A, B, C and D) are used on the associated plane with reference point O at the barycenter, it is possible to express their projection on the limiting planes, yielding to the linear set of inequalities in equation [8.10], where  $a$ ,  $b$  and  $e$  are known.

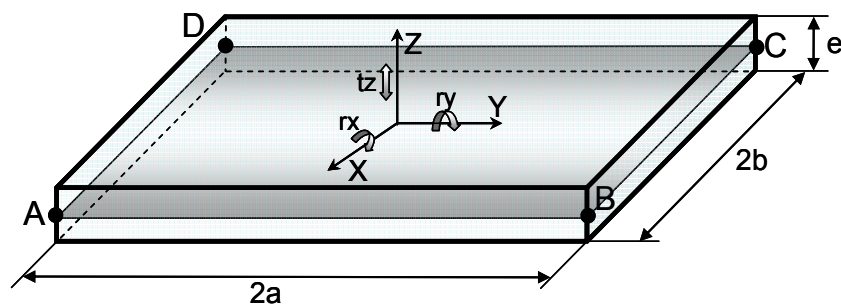


Figure 8.3. Planar variation zone

$$\begin{bmatrix} -\frac{e}{2} \\ \frac{e}{2} \\ -\frac{e}{2} \\ \frac{e}{2} \\ -\frac{e}{2} \\ \frac{e}{2} \end{bmatrix} \leq \begin{bmatrix} -a & b & 1 \\ -a & -b & 1 \\ a & -b & 1 \\ a & b & 1 \end{bmatrix} \bullet \begin{bmatrix} rx \\ ry \\ tz \end{bmatrix} \leq \begin{bmatrix} \frac{e}{2} \\ \frac{e}{2} \\ \frac{e}{2} \\ \frac{e}{2} \\ \frac{e}{2} \\ \frac{e}{2} \end{bmatrix} \quad [8.10]$$

### 8.5. Combined approach

The second approach for worst case searching is the combined approach. We built this combined approach on two existing models (the MMP and the Jacobian-Torsor model) for tolerance analysis in successive machining operations. It should be mentioned that the notation of the MMP and Jacobian-Torsor model has been homogenized in this chapter for better understanding. This approach combined the benefits of the Jacobian and torsor approaches developed for tolerancing. The proposed approach is formulated using interval-based arithmetic [KAM 08b].

This section presents the combined approach and a worst case based analysis of the functional tolerances. Firstly the functional elements will be introduced and then the formulation will be presented.

#### 8.5.1. The combined approach functional elements

Basically we consider three types of uncertainties as functional element (FE) deviations: machined surface deviation, fixture surface deviation and link. In other words every active surface which takes part in machining operation and the links are the functional elements. The possible deviations concerning the functional elements are expressed by small displacement torsors (SDT) with interval.

##### 8.5.1.1. Surface deviation representation by SDT with intervals

The SDT of a functional element reflects the deviation of the associated surface compared with its nominal position and is expressed in the local coordinate system of the FE concerned. This torsor will be used to express the machined surface deviations (machining errors) and the fixture surface deviations. The SDT can be represented by intervals where  $(\underline{rx}, \underline{ry}, \underline{rz}, \underline{tx}, \underline{ty}, \underline{tz})$  and  $(\overline{rx}, \overline{ry}, \overline{rz}, \overline{tx}, \overline{ty}, \overline{tz})$  signify the lower and upper limits of the small displacements  $rx$ ,  $ry$ ,  $rz$ ,  $tx$ ,  $ty$  and  $tz$  accordingly.



[8.11] shows the SDT with intervals for the  $i^{\text{th}}$  functional element:

$$[FE_i] = \{T\}_{FE} = \left\{ \begin{bmatrix} \underline{rx} & \overline{rx} \\ \underline{ry} & \overline{ry} \\ \underline{rz} & \overline{rz} \end{bmatrix} \begin{bmatrix} \underline{tx} & \overline{tx} \\ \underline{ty} & \overline{ty} \\ \underline{tz} & \overline{tz} \end{bmatrix} \right\}_{FEi} = \begin{bmatrix} \begin{bmatrix} \underline{rx} & \overline{rx} \\ \underline{ry} & \overline{ry} \\ \underline{rz} & \overline{rz} \end{bmatrix} \\ \begin{bmatrix} \underline{tx} & \overline{tx} \\ \underline{ty} & \overline{ty} \\ \underline{tz} & \overline{tz} \end{bmatrix} \end{bmatrix}_{FEi} \quad [8.11]$$

#### 8.5.1.2. Link representation by SDT with interval

The scope of variation of the link parameters can be expressed using intervals. To obtain the variation interval of the link parameters, it is necessary to identify the different possible contacts for a link. Here, we have used the method proposed by Villeneuve *et al.* [VIL 07]. This expresses the variation interval of the link parameters using an optimization problem. If the link parameters are considered as independent variables, their extreme bounds can be defined as shown in [8.12], [8.13].

Case of MWP/Fixture:

$$\overline{l^*} = \underset{DH,DM,LHP}{\text{Max}}^{CH,CM,CHP}(l^*), \quad \underline{l^*} = \underset{DH,DM,LHP}{\text{Min}}^{CH,CM,CHP}(l^*) \quad [8.12]$$

where  $l^*$  is the considered link parameter and

$$* \in \{rx_{kSj}, ry_{kSj}, rz_{kSj}, tx_{kSj}, ty_{kSj}, tz_{kSj}\}$$

Case of Gauge/MMP

$$\overline{l^*} = \underset{DM,LGP}{\text{Max}}^{CM,CGP}(l^*), \quad \underline{l^*} = \underset{DM,LGP}{\text{Min}}^{CM,CGP}(l^*) \quad [8.13]$$

where  $l^*$  is the considered link parameter and

$$* \in \{rx_{kGj}, ry_{kGj}, rz_{kGj}, tx_{kgj}, ty_{kgj}, tz_{kgj}\}$$

$k$  = surface number and  $j$  = setup number.

The link lower limit and upper limit values obtained will then be replaced in the link torsor as shown in [8.14].

As previously underlined, according to the type of connection (floating or slipping), the link parameter values (LHP) are determined by a specific algorithm (CHP) that takes into account the constraints and, in certain cases, a positioning function.

$$[FE_i] = \{T\}_{FE} = \left\{ \begin{bmatrix} \underline{lr_x} & \overline{lr_x} \\ \underline{lr_y} & \overline{lr_y} \\ \underline{lr_z} & \overline{lr_z} \end{bmatrix} \begin{bmatrix} \underline{lt_x} & \overline{lt_x} \\ \underline{lt_y} & \overline{lt_y} \\ \underline{lt_z} & \overline{lt_z} \end{bmatrix} \right\}_{FEi} = \begin{bmatrix} \begin{bmatrix} \underline{lr_x} & \overline{lr_x} \\ \underline{lr_y} & \overline{lr_y} \\ \underline{lr_z} & \overline{lr_z} \end{bmatrix} \\ \begin{bmatrix} \underline{lt_x} & \overline{lt_x} \\ \underline{lt_y} & \overline{lt_y} \\ \underline{lt_z} & \overline{lt_z} \end{bmatrix} \end{bmatrix}_{FEi} \quad [8.14]$$

#### 8.5.1.3. Tolerance analysis with the combined approach

By applying some modifications to the Jacobian-torsor model and combining it with the MMP a new method for tolerance analysis of manufactured parts has been developed. The defects are accumulated on the virtual manufactured part (MMP) and the compliance of the MMP and the functional tolerance can be checked by the  $GapGP_k$  that can be calculated by equation [8.15].

$$[GapGP] = [A] [FEs] \quad [8.15]$$

where:

[GapGP]: signed distance between virtual gauge and MMP, measured relative to the boundary of the tolerance zone;

[FEs]: functional elements SDT or link torsor;

[A]: coefficient matrix expressing the geometrical relation between [GapGP] and [FEs].

[8.15] is obtained from the virtual assembly of the MMP and the virtual gauge. Matrix A expresses the contribution of FE deviation into the GapGP distances. Concerning the column of FE in the right hand side of equation [8.15], the machined surfaces deviation (machining errors) and fixture surfaces deviation can be obtained for the specific machines and fixtures and should be kept in a database for use in the combined approach. The variation interval of link elements could be calculated by [8.12] and [8.13].

It is possible to check the compliance of the parts to the functional tolerances using the sign of the extreme values of the  $\text{GapGP}_k$  intervals. The process compliance condition for manufacturing good parts can be expressed as:

For  $i=1$  to number of verification point

$$\sup\{\text{GapGP}_i\} \geq 0 \text{ and } \inf\{\text{GapGP}_i\} \geq 0$$

More details and information concerning the combined approach is available in [KAM 08b].

## 8.6. Monte Carlo simulation

The method associated with Monte Carlo consists of producing a sufficient number of parts to check whether they all comply with the functional tolerance. The parts are virtually produced according to the defects generation procedure. The defects generation procedure should be compatible with the chosen quality constraints.

Actually in Sub I, the DM, DH and  $\text{LHP}_f$  parameters, which are represented by  $x$ , are generated randomly within the domain limited by the CM, CH and CHP. The random generation of the parameters is established in such a way that their distribution be uniform on the defined variation scope.

As we have seen in section 8.4.1.3, there are different possibilities for defining the constraints associated with DM and DH. Based on the chosen type of constraints, the DM and DH parameters should be generated for Monte Carlo simulation. For example if we consider the variation zone with dependent parameters, the DM and DH parameters cannot be generated directly using a random generator. Two different strategies are thus applied depending on the type of variation zone. For the cylindrical zone, a variable substitution is applied to be able

to generate the 4 variables with independent variances according to [8.16]. The 4 defect parameters describing the cylinder's "real" position are then calculated using [8.17], [VIG 08].

$$\begin{aligned}
 r_h &= \left\{ x \left| \begin{array}{l} 0 \leq x \leq r_{\text{variation zone}} \\ \text{probability density } F_r(x) = \left( \frac{x}{r_{\text{variation zone}}} \right)^2 \end{array} \right. \right\} \\
 r_l &= \left\{ x \left| \begin{array}{l} 0 \leq x \leq r_{\text{variation zone}} \\ \text{probability density } F_r(x) = \left( \frac{x}{r_{\text{variation zone}}} \right)^2 \end{array} \right. \right\} \\
 \theta_h &= \left\{ x \left| 0 \leq x \leq 2\pi \text{ with probability density } F_\theta(x) = \left( \frac{x}{2\pi} \right) \right. \right\} \\
 \theta_l &= \left\{ x \left| 0 \leq x \leq 2\pi \text{ with probability density } F_\theta(x) = \left( \frac{x}{2\pi} \right) \right. \right\}
 \end{aligned} \tag{8.16}$$

$$\begin{aligned}
 rx &= -r_h \sin(\theta_h) + r_l \sin(\theta_l) \\
 ry &= r_h \cos(\theta_h) - r_l \cos(\theta_l) \\
 tx &= \frac{r_h \cos(\theta_h) + r_l \cos(\theta_l)}{2} \\
 tz &= \frac{r_h \sin(\theta_h) + r_l \sin(\theta_l)}{2}
 \end{aligned} \tag{8.17}$$

For the planar variation zone as illustrated in Figure 8.3 each nominal vertex (A, B, C or D) of the nominal plane is randomly displaced to create a "real" vertex. The direction of the displacement is normal to the nominal plane and the value of the displacement is randomly generated between  $-e/2$  and  $e/2$  with a uniform density. Conversely, 4 random value between  $-e/2$  and  $e/2$  will be generated (called  $X_1$ ,  $X_2$ ,  $X_3$  and  $X_4$ ). A "real" plane is then positioned from the "real" vertices using a mean square root criteria. The 3 defect parameters  $rx$ ,  $ry$  and  $tz$  are then calculated from the "real" plane characteristics.

For determining the link parameters (LHP) in a same way it should be considered that they have to respect the positioning algorithm (CHP). The second requirement, for the determination of the link values, is that their density has to be uniform in the variation scope allowed by CHP.

More information regarding Monte Carlo associated with the MMP is available in [VIG 08].

## 8.7. Example and comparison

In this section, the three aforementioned techniques will be applied to a 3D example and their characteristics will be explored.

In the first section the quality constraints with independent parameters will be studied and in the second section the quality constraints with dependent parameters will be discussed. Actually, quality constraints with independent parameters can be treated by all the aforementioned techniques, but the quality constraints with dependent parameters can only be treated by the optimization technique and Monte Carlo. The part illustrated in Figure 8.4 will be used to perform a tolerance analysis of the double inclined machined plane with the aforementioned techniques.

Setup 1 of the process plan consists of preparing the raw blocks via a sawing operation. This results in the MWP that will go through setup 2. In setup 2, plane 4 is machined on a milling machine.

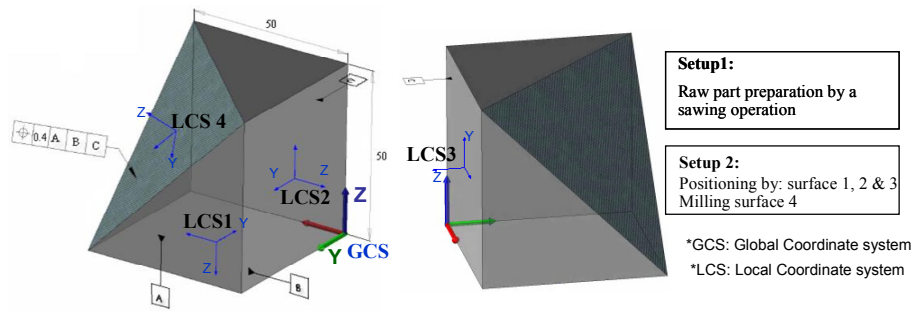


Figure 8.4. Definition of a 3D example

### 8.7.1. First section

#### 8.7.1.1. Combined approach

The approach is nonetheless limited by the fact that it considers the parameters independently. In other word, today we cannot consider the dependent DM and DH parameters with the combined approach.

So in this section the quality constraints “using the measurement results (independent parameters)” are considered and the MWP positioning surface deviation range, the machining errors and the fixture surface deviation range are obtained from a database created over the measurement results (the ranges are

available in Table 8.6). This section will not describe how to create the database (details about database creation can be found in [TIC 07]).

Results	Optimization		Combined Approach
	SQP	GA	
GapGP <sub>min</sub> (mm)	0.01	0.024	[0.01 0.30]

**Table 8.1.** Results for the first section

In the MWP/Fixture assembly in setup 2, the positioning surfaces of the MWP are plane 1, plane 2 and plane 3, and the positioning surfaces of the fixture are plane 1S2, plane 2S2 and plane 3S2. The assembling procedure for the MWP/Fixture assembly comprises three hierarchical slipping connections. The link parameters (LHP) and positioning algorithm (CHP) are given in Table 8.2 for each elementary connection. Then, the MMP is obtained by simulation of the manufacturing process.

A virtual gauge is then created based on the functional tolerance. The gauge and the MMP are assembled to check that the functional tolerance is satisfied. The links between the MMP and the Gauge are formed of three hierarchical slipping connections. The MMP positioning surfaces are plane 1, plane 2 and plane 3 and the related surfaces of the Gauge are plane 1G1, plane 2G1 and plane 3G1. The assembling process is similar to that of the MWP/fixture process so further details shall not be given here.

Machined plane 4 is measured by means of 3 verification points that lead to 6 GapGP distances. The final objective in this step is to find the coefficient matrices [A] (the obtained coefficient matrices are given in Table 8.6). In this step the extreme bounds of the link parameters related to the MWP/fixture and gauge/MMP assembly are calculated using [8.12], [8.13]. In the last step, the 6 GapGP<sub>k</sub> variation intervals are calculated using [8.15]. See Table 8.3.

#### 8.7.1.2. Optimization techniques

The quality constraints for defining the MWP positioning surface deviation range, the machining errors and the fixture surface deviation range in setup 2, have already been presented (Table 8.6) by “using the measurement results (independent parameters)” the assembling process of MWP/fixture and those of Gauge/MMP are explained just before.

To be able to validate the process plan for satisfying the localization tolerance of plane 4, the worst case is sought. In Sub II, there is no degree of freedom or floating link for the Gauge/MMP assembly.

The MATLAB software was used for programming with a Pentium®, 3.2 GHz. Both optimization algorithms (GA and SQP) were applied to minimize Sub I. Figure 8.6 represents the results obtained using the GA and Figure 8.5 represents those obtained using SQP.

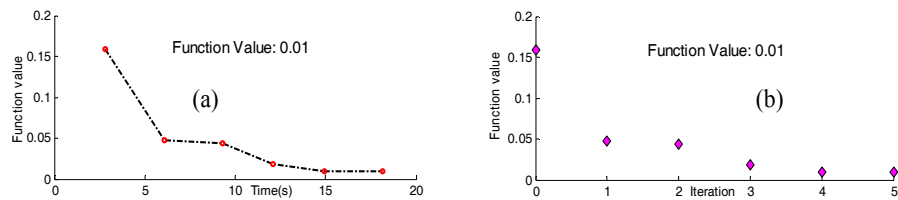


Figure 8.5. Optimization by SQP, first section

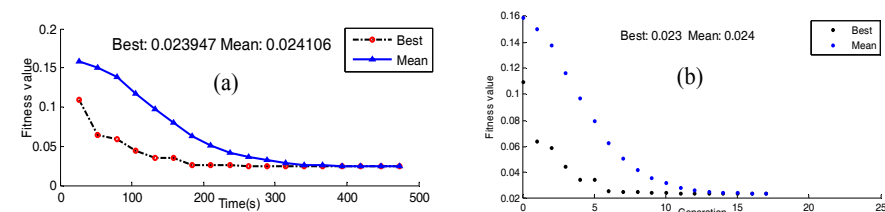


Figure 8.6. Optimization by GA, first section

### 8.7.1.3. Discussion

The GA is very sensitive to parameter settings such as crossover rate, mutation rate and population size (in this example, we used a population size of 200, a crossover rate of 0.8 and a Gaussian mutation rate). If these parameters are correctly adjusted, sufficient population is created and random phenomena are used, the point obtained is almost sure to be a global minimum.

SQP does not always converge towards a global minimum. The end result depends highly on the initial guess point. If the initial point is correctly defined, the SQP is able to reach the minimum quickly.

In the case of the “double inclined plane”, the results obtained confirm that the process plan is valid in terms of satisfying the functional tolerance. There is a small difference between the results obtained from these two different methods. So, in both approaches, there is no proof that the point obtained is the global minimum. The time required for the GA to find this point is nearly 30 times greater than the time required using SQP.

Setup2					
Fixture			Part (MWP)		
Surface	Surface deviation (DH)	Constraints (CH)	Surface	Surface deviation (DM)	Constraints (CM)
Plane 1S2	$rx_{1S2}, ry_{1S2}, tz_{1S2}$		Plane 1	$rx_1, ry_1, tz_1$	
Plane 2S2	$rx_{2S2}, ry_{2S2}, tz_{2S2}$		Plane 2	$rx_2, ry_2, tz_2$	
Plane 3S2	$rx_{3S2}, ry_{3S2}, tz_{3S2}$		Plane 3	$rx_3, ry_3, tz_3$	
Part/Fixture assembly					
Hierarchy	link parameters (LHP)	Type of link	Positioning algorithm (CHP)		
			Positioning function to	Non-penetration condition	
Primary	$lrx_{1S2}$ $lry_{1S2}$ $ltz_{1S2}$	Slipping	- $ltz_{1S2}$	$-25 lrx_{1S2} + 25 lry_{1S2} + ltz_{1S2} \geq 0$ $-25 lrx_{1S2} - 25 lry_{1S2} + ltz_{1S2} \geq 0$ $25 lrx_{1S2} - 25 lry_{1S2} + ltz_{1S2} \geq 0$ $25 lrx_{1S2} + 25 lry_{1S2} + ltz_{1S2} \geq 0$	
Secondary	$lry_{2S2}$ $ltz_{2S2}$	Slipping	- $ltz_{2S2}$	$25 lrx_{1S2} + 25 lry_{2S2} + ltz_{2S2} - 25 rx_1$ $+ 25 rx_{1S2} + 25 rx_2 - 25 rx_{2S2} \geq 0$ $25 lrx_{1S2} - 25 lry_{2S2} + ltz_{2S2} - 25 rx_1$ $+ 25 rx_{1S2} + 25 rx_2 - 25 rx_{2S2} \geq 0$ $-25 lrx_{1S2} - 25 lry_{2S2} + ltz_{2S2} + 25 rx_1$ $-25 rx_{1S2} - 25 rx_2 + 25 rx_{2S2} \geq 0$ $-25 lrx_{1S2} + 25 lry_{2S2} + ltz_{2S2} + 25 rx_1$ $-25 rx_{1S2} - 25 rx_2 + 25 rx_{2S2} \geq 0$	
Tertiary	$ltz_{3S2}$	Slipping	- $ltz_{3S2}$	$(-25 lry_{1S2} - 25 lry_{2S2} + ltz_{3S2} + 25 rx_3 + 25 rx_{3S2} - 25 ry_1 - 25 ry_{1S2} - 25 ry_2 - 25 ry_{2S2} - 25 ry_3 + 25 ry_{3S2}) \geq 0$ $(25 lry_{1S2} - 25 lry_{2S2} + ltz_{3S2} + 25 rx_3 + 25 rx_{3S2} + 25 ry_1 + 25 ry_{1S2} - 25 ry_2 - 25 ry_{2S2} + 25 ry_3 - 25 ry_{3S2}) \geq 0$ $(25 lry_{1S2} + 25 lry_{2S2} + ltz_{3S2} - 25 rx_3 - 25 rx_{3S2} + 25 ry_1 + 25 ry_{1S2} + 25 ry_2 + 25 ry_{2S2} + 25 ry_3 - 25 ry_{3S2}) \geq 0$ $(-25 lry_{1S2} + 25 lry_{2S2} + ltz_{3S2} - 25 rx_3 - 25 rx_{3S2} - 25 ry_1 - 25 ry_{1S2} + 25 ry_2 + 25 ry_{2S2} - 25 ry_3 + 25 ry_{3S2}) \geq 0$	

Table 8.2. Part/fixture assembly procedure



The combined approach converges to the global minimum if all the defect parameters (DM and DH) and the links (LHP and LGP) are assumed to be independent variables.

As can be found from Table 8.1, the obtained value from the combined approach and optimization techniques are the same in the case of such quality constraints. When using the quality constraints type “using the measurement results (independent parameters)” it is more meaningful to use the combined approach because it is faster compared with the optimization techniques (in the case of the current example the elapsed time is less than 1 second). It can quickly give the process planner an initial idea about the quality of manufactured parts with the chosen process plan.

Machined surface		Verification points	Results (mm)
Machined Plane 4	1	(50, 50, 0)	GapGP <sub>1</sub> = [0.11 0.38] GapGP <sub>2</sub> = [0.02 0.29]
	2	(0, 50, 50)	GapGP <sub>3</sub> = [0.03 0.28] GapGP <sub>4</sub> = [0.12 0.37]
	3	(50, 0, 50)	GapGP <sub>5</sub> = [0.01 0.30] GapGP <sub>6</sub> = [0.10 0.39]

**Table 8.3.** Results obtained by combined approach

### 8.7.2. Second section

In the first section the combined approach and optimization techniques are compared when dealing with independent quality constraints. In this section we will explain how we can treat the dependent quality constraints. In this section the same process plan will be treated but the variation range of DM and DH parameters are defined by the variation zones as indicated in Table 8.4.

The defect parameters variations, as mentioned in section 8.4.1.3, must be bound by the limits of the 3D variation zones they represent. The MATLAB software was used for programming with a Pentium®, 3.2 GHz.

Both optimization algorithms (GA and SQP) were applied to minimize Sub I. Figure 8.8 represents the results obtained using the GA and Figure 8.7 represents those obtained using SQP.

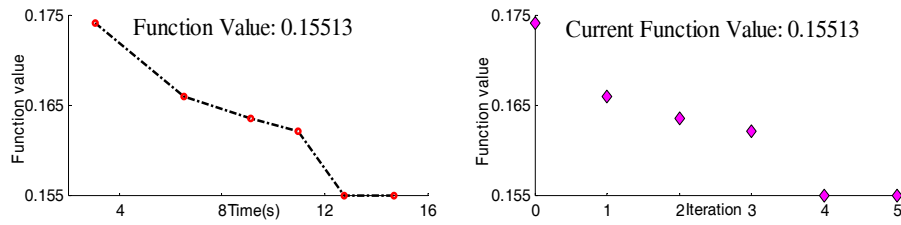


Figure 8.7. Optimization by SQP, second section

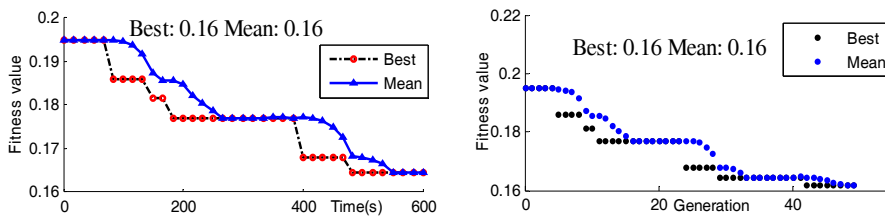


Figure 8.8. Optimization by GA, second section

For MC, one million parts are produced virtually according to the defect generation described in Table 8.4. The next step is to check the proportion of them that meet the functional tolerance. The GapGP are virtually measured between the part and the tolerance zone. The  $\text{GapGP}_{\min}$  is then selected and will be retained as a result of the control. The distribution of the  $\text{GapGP}_{\min}$  values obtained for the 100,000 parts is represented by the histogram Figure 8.9.

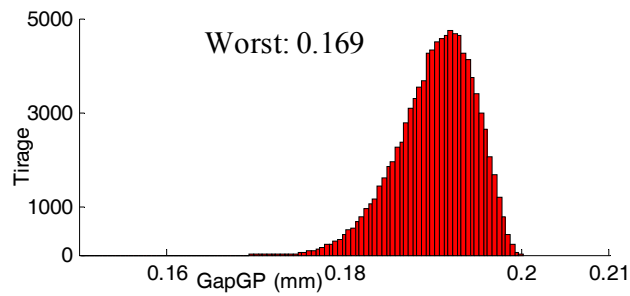


Figure 8.9. MC results

<u>Setup 1</u>	
Machining	
Plane 1	$rx_1, ry_1, tz_1$ Planar variation zone 0.01 (mm)
Plane 2	$rx_2, ry_2, tz_2$ Planar variation zone 0.01 (mm)
Plane 3	$rx_3, ry_3, tz_3$ Planar variation zone 0.01 (mm)
<u>Setup 2</u>	
Positioning	
Plane 1S2	$rx_{1S2}, ry_{1S2}, tz_{1S2}$ Planar variation zone 0.02 (mm)
Plane 2S2	$rx_{2S2}, ry_{2S2}, tz_{2S2}$ Planar variation zone 0.02 (mm)
Plane 3S2	$rx_{3S2}, ry_{3S2}, tz_{3S2}$ Planar variation zone 0.02 (mm)
Machining	
Plane 4	$rx_4, ry_4, tz_4$ Planar variation zone 0.006 (mm)

**Table 8.4.** Deviation range for a “double inclined plane” manufacturing process

Results	Optimization		MC simulation
	SQP	GA	
GapGP <sub>min</sub> (mm)	0.15	0.16	0.17

**Table 8.5.** Results for second section

Functional elements		Coefficient matrix [A]	Defects range
Prepared Surfaces by sawing	<b>Plane 1</b> $rx_1, ry_1, tz_1$	$[0]_{3 \times 6}$	$\begin{bmatrix} [-0.0005 \ 0.0005] \\ [-0.0003 \ 0.0003] \\ 0 \\ 0 \\ 0 \\ [-0.0051 \ 0.0051] \end{bmatrix}$
	<b>Plane 2</b> $rx_2, ry_2, tz_2$	$[0]_{3 \times 6}$	$\begin{bmatrix} [-0.0005 \ 0.0005] \\ [-0.0003 \ 0.0003] \\ 0 \\ 0 \\ 0 \\ [-0.0051 \ 0.0051] \end{bmatrix}$
	<b>Plane 3</b> $rx_3, ry_3, tz_3$	$[0]_{3 \times 6}$	$\begin{bmatrix} [-0.0005 \ 0.0005] \\ [-0.0003 \ 0.0003] \\ 0 \\ 0 \\ 0 \\ [-0.0051 \ 0.0051] \end{bmatrix}$
Fixture Surface Deviations	<b>Plane 1S2</b> $rx_{1S2}, ry_{1S2}, tz_{1S2}$	$\begin{bmatrix} -2887 & 2887 & 0 & 0 & 0 & -0.58 \\ 0 & -2887 & 0 & 0 & 0 & -0.58 \\ 2887 & 0 & 0 & 0 & 0 & -0.58 \end{bmatrix}$	$\begin{bmatrix} [-0.0013 \ 0.0013] \\ [-0.0007 \ 0.0007] \\ 0 \\ 0 \\ 0 \\ [-0.015 \ 0.015] \end{bmatrix}$
	<b>Plane 2S2</b> $rx_{2S2}, ry_{2S2}, tz_{2S2}$	$\begin{bmatrix} 0 & 0 & 0 & 0 & 0 & -0.58 \\ 0 & -28.87 & 0 & 0 & 0 & -0.58 \\ 0 & 28.87 & 0 & 0 & 0 & -0.58 \end{bmatrix}$	$\begin{bmatrix} [-0.0013 \ 0.0013] \\ [-0.0007 \ 0.0007] \\ 0 \\ 0 \\ 0 \\ [-0.015 \ 0.015] \end{bmatrix}$
	<b>Plane 3S2</b> $rx_{3S2}, ry_{3S2}, tz_{3S2}$	$\begin{bmatrix} 0 & 0 & 0 & 0 & 0 & -0.58 \\ 0 & 0 & 0 & 0 & 0 & -0.58 \\ 0 & 0 & 0 & 0 & 0 & -0.58 \end{bmatrix}$	$\begin{bmatrix} [-0.0013 \ 0.0013] \\ [-0.0007 \ 0.0007] \\ 0 \\ 0 \\ 0 \\ [-0.015 \ 0.015] \end{bmatrix}$
Machined Surface	<b>Plane 4</b> $rx_4, ry_4, tz_4$	$\begin{bmatrix} 40.82 & 0 & 0 & 0 & 0 & 1 \\ -20.41 & 35.36 & 0 & 0 & 0 & 1 \\ -20.41 & -35.36 & 0 & 0 & 0 & 1 \end{bmatrix}$	$\begin{bmatrix} [-0.0003 \ 0.0003] \\ [-0.0003 \ 0.0003] \\ 0 \\ 0 \\ 0 \\ [-0.0031 \ 0.0031] \end{bmatrix}$
MWP/Fixture Links	<b>Primary link</b> $lrx_{1S2}, lry_{1S2}, ltz_{1S2}$	$\begin{bmatrix} -28.87 & 28.87 & 0 & 0 & 0 & -0.58 \\ 0 & -28.87 & 0 & 0 & 0 & -0.58 \\ 28.87 & 0 & 0 & 0 & 0 & -0.58 \end{bmatrix}$	$\begin{bmatrix} [0 \ +0] \\ [0 \ +0] \\ 0 \\ 0 \\ 0 \\ [0 \ +0] \end{bmatrix}$

	<b>Secondary link</b> $lry_{2S2}, ltz_{2S2}$	$\begin{bmatrix} 0 & 0 & 0 & 0 & 0 & -0.58 \\ 0 & -28.87 & 0 & 0 & 0 & -0.58 \\ 0 & 28.87 & 0 & 0 & 0 & -0.58 \end{bmatrix}$	$\begin{bmatrix} 0 \\ 0 + 0 \\ 0 \\ 0 \\ 0 \\ 0.0901 \end{bmatrix}$
	<b>Tertiary link</b> $ltz_{3S2}$	$\begin{bmatrix} 0 & 0 & 0 & 0 & 0 & -0.58 \\ 0 & 0 & 0 & 0 & 0 & -0.58 \\ 0 & 0 & 0 & 0 & 0 & -0.58 \end{bmatrix}$	$\begin{bmatrix} 0 \\ 0 \\ 0 \\ 0 \\ 0 \\ 0.1201 \end{bmatrix}$
Gauge/MMP Links	<b>Primary link</b> $lrx_{1G1}, lry_{1G1}, ltz_{1G1}$	$\begin{bmatrix} 28.87 & -28.87 & 0 & 0 & 0 & 0.58 \\ 0 & 28.87 & 0 & 0 & 0 & 0.58 \\ -28.87 & -28.87 & 0 & 0 & 0 & 0.58 \end{bmatrix}$	$\begin{bmatrix} 0 + 0 \\ 0 + 0 \\ 0 \\ 0 \\ 0 \\ 0 + 0 \end{bmatrix}$
	<b>Secondary link</b> $lry_{2G1}, ltz_{2G1}$	$\begin{bmatrix} 0 & 0 & 0 & 0 & 0 & 0.58 \\ 0 & 28.87 & 0 & 0 & 0 & 0.58 \\ 0 & -28.87 & 0 & 0 & 0 & 0.58 \end{bmatrix}$	$\begin{bmatrix} 0 \\ 0 + 0 \\ 0 \\ 0 \\ 0 \\ 0.0251 \end{bmatrix}$
	<b>Tertiary link</b> $ltz_{3G1}$	$\begin{bmatrix} 0 & 0 & 0 & 0 & 0 & 0.58 \\ 0 & 0 & 0 & 0 & 0 & 0.58 \\ 0 & 0 & 0 & 0 & 0 & 0.58 \end{bmatrix}$	$\begin{bmatrix} 0 \\ 0 \\ 0 \\ 0 \\ 0 \\ 0.0351 \end{bmatrix}$

**Table 8.6.** Functional elements (FE) and their related coefficient matrices and Torsors with intervals

### 8.7.3. Discussion

The first point is that the values obtained in section 2 by means of optimization techniques are more than those obtained in section 1. This is because of the fact that in section 1 all the defect parameters of a plane could have their extreme value simultaneously but in the case of section 2 they are limited by the bounds of a 3D variation zone and thus cannot have their extreme value simultaneously. Actually the 3D bounded variation zone is closer to the tolerance standard. The value obtained by MC, accurately reflects the real production. From Figure 8.9 we see that the worst value obtained for  $GapGP_{min}$  is a little far from those obtained by optimization techniques. This stems from the fact that in real production the worst part might never be produced.

When using the optimization technique, the worst part is searched but with the Monte Carlo simulation the defects are generated randomly so the probability of finding the worst part is very low.

The difference between the Monte Carlo result and those of optimization (see Table 8.5) depends on the number of GapGP equation parameters. In fact this difference increases with the number of parameters.

### 8.8. Conclusion

This chapter presented three different solution techniques for searching the worst part within a process plan from a geometrical point of view for the aims of tolerance analysis in multi stage machining operations.

These techniques are compared using a 3D example and their characteristics are discussed.

Actually the optimization techniques and the Monte Carlo simulation can deal with all types of quality constraints. The combined approach can deal with quality constraints with independent parameters.

From the elapsed time point-of-view, the combined approach is very fast. The optimization techniques need much more time and based on the complexity of the problem the time could become long. The MC need much more time compared with optimization techniques. The defects are generated randomly, therefore for good coverage of the variation scope the number of virtual produced part should be sufficiently large (more than 100,000 parts, see [GER 07]). This leads to a long calculation time (30 minutes in the current example).

From a convergence point of view, when dealing with quality constraints with independent parameters, it is possible to check the results obtained by optimization techniques with those of the combined approach to make sure that the obtained point is the global minimum.

When dealing with quality constraints with dependent parameters, in both optimization approaches (GA and SQP), there is no proof that the point obtained is the global minimum. The time required for the GA to find the optimum point is much more than the time required using SQP. However, this time advantage for SQP is offset by the time needed to locate a suitable initial point.

As was previously highlighted, the value obtained by Monte Carlo simulation is a little far from optimization, this could be avoided by using a more efficient random generator for good coverage of the variation scope.

## 8.9. Bibliography

- [DES 99] DESROCHERS A., "Modeling three-dimensional tolerance zones using screw parameters", *CD-ROM Proceedings of 25th ASME Design Automation Conference*, Las Vegas, 1999.
- [GER 07] GERMAIN F., Statistical 3D Tolerancing, PhD Thesis, Savoy University, 2007.
- [GHI 03] GHIE W., LAPERRIERE L., DESROCHERS A., "A unified Jacobian-torsor model for analysis in computer aided tolerancing", In: Gogu, G., Coutellier, D., *et al.*, Eds, *Recent Advances in Integrated Design and Manufacturing in Mechanical Engineering, presented at: 4th International Conference on Integrated Design and Manufacturing in Mechanical Engineering*, Clermont Fernand, France. pp. 63-72, 2003.
- [HUA 03] HUANG Q., SHI J.J., "Part dimensional error and its propagation modeling in multi-operational machining processes", *Journal of Manufacturing Science and Engineering-Transactions of the ASME*, Vol. 125, pp. 255-262, 2003.
- [HUA 04] HUANG S.H., LIU Q., MUSA R., "Tolerance-based process plan evaluation using Monte Carlo simulation", *International Journal of Production Research*, Vol. 42, pp. 4871-4891, 2004.
- [KAM 08a] KAMALI NEJAD M., VIGNAT F., VILLENEUVE F., "Tolerance analysis in multi-operational machining process based on the model of manufactured part", In: *5th International Conference on Digital Enterprise Technology*, Nantes, France, 2008.
- [KAM 08b] KAMALI NEJAD M., DESROCHERS A., VIGNAT F., *et al.*, "Tolerance Analysis in Machining, An Approach Combining The Model of Manufactured Part and The Jacobian-torsor Model", presented at: *ASME 28th Computers and Information in Engineering Conference (CIE)*, New York City, US, 2008.
- [LOO 07] LOOSE J.P., ZHOU S. Y., CEGLAREK D., "Kinematic analysis of dimensional variation propagation for multistage machining processes with general fixture layouts", *IEEE Transactions on Automation Science and Engineering*, Vol. 4, pp. 141-152, 2007.
- [TIC 07] TICHADOU S., KAMALI NEJAD M., VIGNAT F., *et al.*, "3-D manufacturing dispersions: two experimental applications", *10th CIRP International Conference on Computer Aided Tolerancing*, Erlangen, Germany, 2007.
- [VIG 07] VIGNAT F., VILLENEUVE F., "Simulation of the Manufacturing Process, Generation of a Model of the Manufactured Parts", In: CUNHA P., MAROPOULOS, P., Eds, *Digital Enterprise Technology: Perspectives and Future Challenges presented at: 3rd International Conference on Digital Enterprise Technology*, Bath, pp. 545-552, 2007.
- [VIG 08] VIGNAT F., VILLENEUVE F., KAMALINEJAD M., "From the nominal model to a Model of Manufactured Parts in a CAD context", *CIRP Design Conference*, Netherlands, 2008.
- [VIL 05] VILLENEUVE F., VIGNAT F., "Manufacturing process simulation for tolerance analysis and synthesis", In: BRAMLEY, A., BRISSAUD, D., *et al.*, Eds, *Advances in Integrated Design and Manufacturing in Mechanical Engineering, presented at: 5th International Conference on Integrated Design and Manufacturing in Mechanical Engineering*, Bath, England. pp. 189-200, 2005.

- [VIL 07] VILLENEUVE F., VIGNAT F., "Simulation of the manufacturing process in a tolerancing point of view: Generic resolution of the positioning problem", In: DAVIDSON, J. K., Ed., *Models for Computer Aided Tolerancing in Design and Manufacturing*, Arizona, pp. 179-189, 2007.
- [WHY 90] WHYBREW K., BRITTON G., ROBINSON D., *et al.*, "A graph-theoretic approach to tolerance charting", *The International Journal of Advanced Manufacturing Technology*, Vol. 5, pp. 175-183, 1990
- [ZHO 03] ZHOU S.Y., HUANG Q., SHI J.J., "State space modeling of dimensional variation propagation in multistage machining process using differential motion vectors", *IEEE Transactions on Robotics and Automation*, Vol. 19, pp. 296-309, 2003.



## PART II

# Simulation of Assemblies

## Chapter 9

# A Chronological Framework for Virtual Sheet Metal Assembly Design

### 9.1. Introduction

The quality and sales price of a product are obviously decisive factors in attracting the customer. Geometric quality has a significant influence on the fulfillment of functional and aesthetic quality requirements. Equipment utilization is highly influential on plant investment and throughput, and thus also on break-even sales price. These two central characteristics can be significantly influenced in the product and process design.

In any product development project, the cost of design change increases exponentially with project time [BER 02]. Furthermore, the degree of design freedom decreases exponentially with project time.

Thus, to reduce cost and avoid suboptimal or even ad hoc design, design parameters that influence geometric quality and equipment utilization need to be analytically defined at the earliest project stage possible.

Furthermore, geometric quality and equipment utilization are coupled, as shown in [XIE 02] and [SEG 09]. Thus, to avoid suboptimal design, influential parameters need to be analytically treated together.

---

Chapter written by Johan SEGEBORN, Anders CARLSSON, Johan S. CARLSON and Rikard SÖDERBERG.

Automotive analysis and verification have gradually moved from a physical to a virtual engineering environment. Today, virtual models of products and processes are developed long before physical prototypes are built. Thus, analysis and verification, such as for instance assembly variation simulation and robotic assembly motion planning, can be initiated at earlier stages of a product development project. However, this relatively new opportunity is not yet fully utilized. Automotive sheet metal assembly design is still to a large extent based on experience. The challenge is to ensure that the gradual locking of design freedom is based on analytically or numerically obtained facts and not on assumptions, however well founded, or driven by time pressures or imperfect organizational structures.

Therefore, in this chapter, a chronological framework for virtual sheet metal assembly design parameter treatment is suggested. The framework conveys the order in which the parameters need to be introduced to ensure that each parameter is analytically determined. The introduction order is significant as design parameters are usually prerequisite to start the analysis of subsequent design parameters.

Moreover, project stages, at which product and process design will especially benefit from simultaneous design parameter and characteristics treatment, are identified.

A generic product development process is utilized as a chronological framework.

#### **9.1.1. A generic product development process**

Generic product development processes have been proposed by [ULR 04], [PAH 07], and [ULL 03]. The process suggested in [ULR 04] targets engineered products and is divided into six fundamental, within themselves, iterative phases, where the output of each phase is prerequisite to start the subsequent phase; see Figure 9.1. The fundamentals of each phase are briefly reproduced below:

1. *Planning*: The project mission statement is formulated. The planning phase, which actually precedes project approval, is the link to advanced research and technology development.

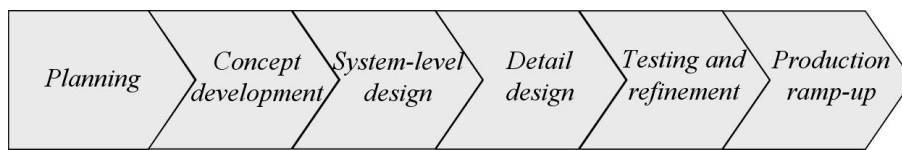
2. *Concept development*: Alternative concepts, in terms of functions, for example, features and styling are generated and evaluated against, for instance, competitor products, estimated manufacturing cost and production feasibility. One or more concepts are selected for further development along with an economical justification of the project.

3. *System-level design*: The product is decomposed into an architecture of subsystems, each entailed with its own set of functional requirements. Moreover, the logic factory flow is defined.

4. *Detail design*: Complete specifications of product and process geometries and materials are obtained, among other things in terms of CAD models. Detailed process plans for fabrication and assembly of the product are completed.

5. *Testing and refinement*: Various physical product prototypes are constructed for evaluation and requirement verification.

6. *Production ramp-up*: The product is built using the intended production system with a gradual transition to ongoing production.



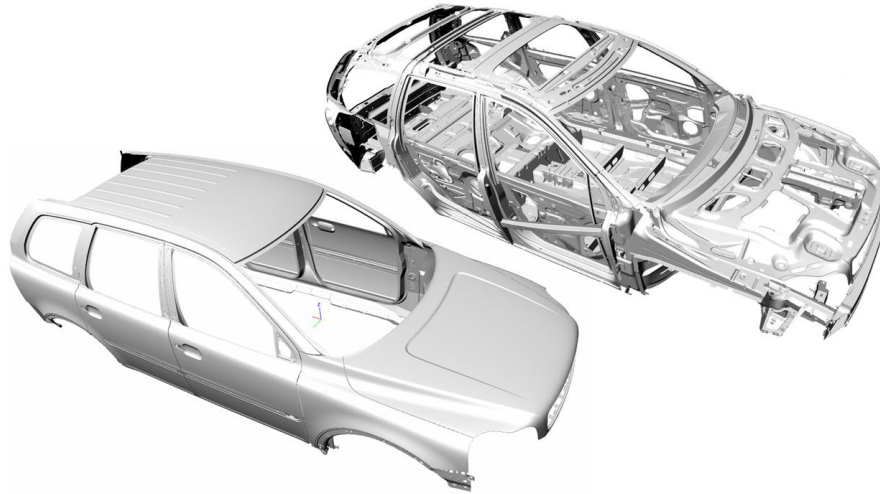
**Figure 9.1.** The six chronological phases of the generic product development process, suggested in [ULR 04]

### 9.1.2. Automotive sheet metal assembly

Typically, an automotive body-in-white (BiW) consists of about 300 steel sheet metal parts, joined by about 4,000 spot welds, which is the predominant and preferred type of joint. The workload is usually distributed to about 80 stations, which are mainly organized in production lines [DAH 03]. Other joining methods used in sheet metal assembly are for instance: arc welding, stud welding, gluing and riveting. Figure 9.2 depicts the styling sheet metal parts as well as the underlying body structure of a body-in-white.

The form of physical instances of sheet metal parts, which is usually obtained by stamping, differs from the nominal form, specified in the CAD models. The elastic spring-back that occurs when the part is released from the stamping tool leads to dimensional variation between the stamped instances of the part. As sheet metal parts are assembled, the variation of the various parts also propagates to the assembly.

Geometric quality can be defined as the level of dimensional requirement fulfillment and the robustness of design [SÖD 02]. Robust design suppresses the effect that the variation of individual parts has on the variation of the resulting assembly. Geometric quality has a significant influence on total product quality due to its influence on functional, aesthetic and assembly requirements. Many results have been reported regarding geometric quality. The parameters that influence the geometric quality of a sheet metal assembly have been identified in [DAH 03].



**Figure 9.2.** *Body-in-white*

The takt time of a factory is given by: customer demand, the number of working shifts and some overall factory reliability. If the entire production system is constituted by a single coupled production line, then all station cycle times would equal takt time. However, depending on, for instance, flow parallelization, allowed station cycle times, in order to meet takt time, can vary along the flow. When the flow is physically realized within required cycle times, the need for investment can be optimized with respect to equipment utilization and equipment reliability. Equipment utilization can be defined as executed workload per equipment invested. Equipment reliability can be defined as the fraction of time that the equipment is operational.

This work focuses on parameters that influence equipment utilization and geometrical quality in sheet metal assembly.

Project deliveries in automotive product development systems are secured by analysis and verification of geometrical quality and equipment utilization with respect to the following parameters:

- *Product parameters*: product architecture, number of parts, product part joints, locating scheme positioning, product part geometry, weld positions and number of welds.
- *Production process parameters*: logical process flow, concept factory layout, assembly sequence, support point positions, number of support points, fixture geometry, weld gun geometry and welding sequence.

These parameters are furthermore corroborated by earlier work, for instance in [DAH 03] and [SEG 09]. To secure equipment utilization, an additional number of station process layout parameters are analyzed and verified: number and sequence of station assembly steps, number of robots, robotic travel and station equipment (geometry, spatial positioning and reachability).

## 9.2. Proposed framework

The design parameters that influence geometric quality and equipment utilization were listed in section 9.1.2. In this section, the order in which these parameters need to be introduced to ensure that each parameter can be analytically determined is identified.

The generic product development phases suggested in [ULR 04] are used as a chronological framework; see Figure 9.1. However, in this chapter, the chronological level of detail is increased by further subdivision of the framework phases. The system-level and detail design phases are further subdivided using a discrete representation of the product and production process in increasing degrees of completion, such that each step is prerequisite to develop the subsequent step. The principle of subdivision is that the evolution of the product/factory concept as well as individual station concepts moves from the architecture of elements and functional couplings, via some detailed interface designs, to eventually end up with a detailed or complete design; see Figure 9.3.

An absolute deadline for all virtual product and process designs is when physical equipment manufacturing is initiated, which coincides with phase 5: testing and refinement. For instance, the stamping tools used to manufacture sheet metal parts are very expensive and manufacturing lead time is very long. Thus, only the first four phases suggested by [ULR 04] describe virtual design.

In the following sections, the proposed chronological framework, presented in Figure 9.3 and Table 9.1 will be argued for in detail. For each degree of product and process completion, possible parameter analysis and verification are listed in Table 9.1. Note that the result is presented up front and then argued for throughout the rest of the paper. Figure 9.3 and Table 9.1 will be continuously referred to.

To facilitate reading comprehension and cross references between figures and textual sections, in the rest of this chapter the degrees of product and process completion, presented in Figure 9.3, as well as the design parameters, presented in Table 9.1, and synonymous terms, will at all instances be denoted in *italics*.

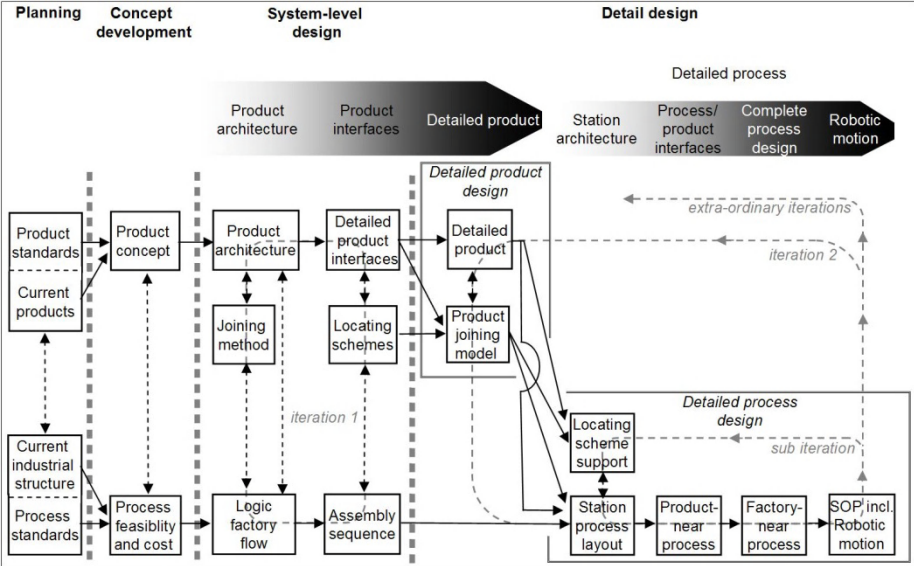


Figure 9.3. The proposed chronological framework for virtual sheet metal assembly design

Planning	Concept development	System-level design		Detail design			
Depending of prescriptiveness of standards and carry-over; before system-level design, all parameters range from undefined to fully defined.		Product architecture	Product interfaces	Detailed product	Detailed process		
					Station architecture	Process/ product interfaces	Complete process design
		Product architecture	Product part joints	Product part geometry	Support point positions	Fixture geometry	Station equipment geometry
		Number of parts	Locating scheme positioning	Weld positions	Number of support points	Weld gun geometry	Station equipment spatial positioning
		Logical process flow	Assembly sequence	Number of welds	Number of station assembly steps		Station equipment reachability
		Concept factory layout		Number of robots			Sequence of station assembly steps
							Robotic travel
							Welding sequence

Table 9.1. The design parameters that affect geometrical quality and equipment utilization, listed in section 1.1.2, are presented in the order that they can be initiated. The framework presented in Figure 9.3 is used as a chronological reference

### 9.2.1. Planning

In the planning phase, which precedes the project mission statement and approval, advanced research and technology development are accessed for project application. Quality and time assured *standard product and process solutions*, containing up to full representations of the parameters listed in section 1.1.2 are packaged in an ongoing work separate from the car development projects, and held ready for project application, since car development projects are pressed for time.

However, it is important to note that whereas various parameters may be known at this early stage, all chronological steps of parameter analysis, described in Figure 9.3 and Table 9.1, are needed to fully verify any specific parameter, since parameters as well as characteristics requirements are coupled.

In the automotive industry today, product platforms can span models from several brands. To utilize large-scale advantages, product and process development within the individual companies need to be coordinated. Therefore, a *standard product architecture* with a corresponding *standard assembly sequence* convey how the body-in-white by default should be broken down. Moreover, *process standards* prescribe for instance how joining concepts relate to various conceptual choices of *product architecture*.

The planning phase results in a project mission statement establishing the type of vehicle along with its technical content and corresponding manufacturing prerequisites.

### 9.2.2. Concept development

In the concept phase, alternative *product concepts*, in terms of function, features and styling, are generated and evaluated against *current products*, *current industrial structure*, *standard requirements*, competitor products, estimated manufacturing *cost* and production *process feasibility*.

Geometrically represented styling alternatives, i.e. the parts of the body-in-white visible to the customer, are presented. Split lines that divide the styling surfaces into individual sheet metal parts are however not introduced until the system-level design phase, as this needs to be done in parallel with the *product architecture* of the upper body structure on which the styling surfaces are attached; see Figure 9.2.

Conceptual body structure issues are for instance: choice of framing concept, type of under-body and body side structures. At this point, body structure geometries, if any, exist in a highly conceptual form. Whereas the *styling concept* geometries are designed independently of assembly concept, the *body structure concept* is highly dependent on assembly feasibility and efficiency.



A given *product concept* indicates a fundamental, very rough, non-geometrical *product architecture* and a corresponding process such as for instance the type of framing process or degree of possible flow parallelization.

In addition to prescriptive *standard requirements*, additional requirements on the *concept* are formulated. There are functional, aesthetic and legal requirements to consider. For instance, at Volvo Cars the rigorous safety requirements have far-reaching implications on body-in-white structural strength and structural deformation characteristics, and thus a significant influence on possible product concepts.

As a part of concept evaluation, decisions are made whether to carry over solutions from running production in the *current industrial structure* or to redesign; see Figure 9.3. For projects setting out from existing product platforms, product and process solutions will to a large extent be re-used or carried over. Within a certain product platform, it is for instance customary to carry over large parts of the under-body structure and its related production process investments. For instance, the three-piece under-body structures in Volvo S80, V70 and XC60 are shared within the product platform. Whereas the front and rear floor are basically identical, the models differ in the length of the central floor. Parts visible to the customer are on the other hand re-used less often in subsequent projects. Hence the upper body is usually redesigned. It is however significantly influenced by the styling language of the platform.

Furthermore, the factory, in which to build the car, is identified. With knowledge of customer demand previously acquired in the planning phase, the required takt time can then be determined.

Principle phase output consists of one or more *product* and *feasible production concepts* selected for further development along with an economical justification of the project, as illustrated in Figure 9.3.

### 9.2.3. System-level design

Principle input to the system-level design phase consists of one or more *product concepts* (BiWs) selected for further development along with corresponding *feasible production concepts* and *cost estimates*.

A conventional body-in-white can obviously not be manufactured in one piece. Thus, it needs to be broken down into a *product architecture* of parts to ensure manufacturability. The sheet metal stamping process limits the shapes and forms that technically can be stamped within feasible tolerances.

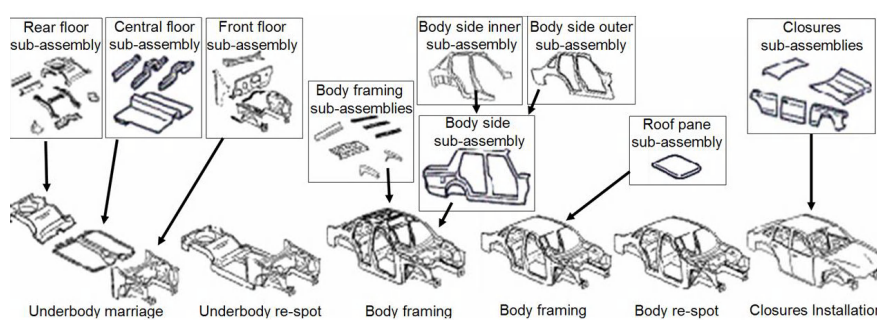
In parallel, all requirements on the overall *body-in-white concept* are broken down to part level such that each part contributes to the fulfillment of the overall requirements. The requirements are in turn broken down into functional specifications. In system-level design the *number of parts* can be estimated.

Whereas the division into sheet metal parts of the body structure are highly influenced by *logic factory flow* feasibility, the design and the split lines of the styling sheet metal parts, which are visible to the customer, are foremost determined on aesthetic grounds. The effect of styling sheet metal parts on *assembly sequence* as well as cycle time is limited due to hang-on assembly.

In dividing the *body-in-white concept* into individual sheet metal parts, *joining method* need to be taken into consideration, as for instance, spot welding needs access from both sides of the sheet metal assembly. *Joining methods* need furthermore to be known to determine a *logic factory flow*, within the *cost frame* previously specified in the concept development phase. This can for instance be addressed by flow simulation of material and equipment. The *logic factory flow* can be represented by two parameters: *concept factory layout* and *logical process flow*.

The *concept factory layout* describes the physical floor space required to realize the concept. For instance it includes material supply and transportation. The *logical process flow* is a rough flow simulation model on some higher assembly level, including degree of parallelization and major buffers.

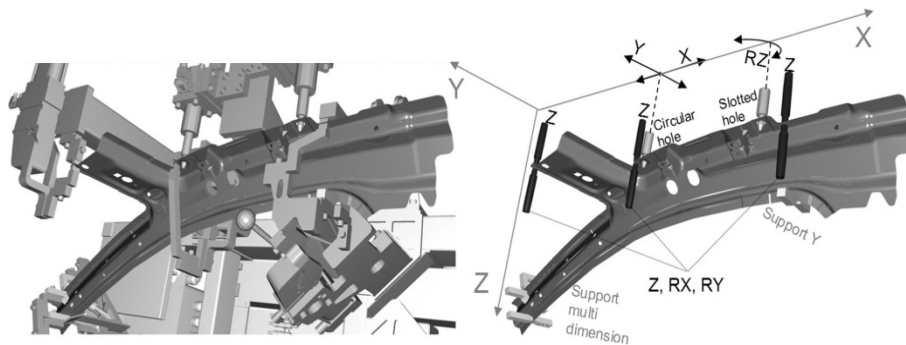
Later in the system-level design phase, when the *product part joints* are developed, this model can be extended or revised to address the part level, i.e. an *assembly sequence* with required buffers is obtained; see Figure 9.4. The *assembly sequence* is furthermore to some extent implicitly given by the *product architecture*, as parts that are built in into subassemblies, need to be assembled first.



**Figure 9.4.** Example of an assembly order at a coarse level of detail.  
Parallel sub assemblies supply the main line

However, some level of detail in the geometrical interfaces (*detailed product interfaces*) between the sheet metal parts is needed to fully verify the *assembly sequence*. *Product part joint* design addresses split line location as well as type of joint (butt, lap and butt-lap).

To ensure the robustness of each assembly and ultimately the geometric quality of the overall body-in-white, *locating schemes* for each *assembly step* need to be developed in parallel with the *product part joints*. A *locating scheme* is a set of 6 locating points, later in the project physically realized by the *fixture*, that deterministically locates a part at a defined position in space [SÖD 06]. In other words, it locks the six positional degrees of freedom of the part; see Figure 9.5. *Locating scheme positioning* influences required part tolerances, to ensure the fulfillment of functional, assembly and aesthetic requirements. A *locating scheme* that suppresses locating point variation propagation is said to be robust [SÖD 02]. Spreading the locating points increases robustness. *Locating scheme positioning* determines how part variation at the locating points propagates to the assembly.



**Figure 9.5.** The locating scheme of a body side sheet metal part including supporting points, along with its physical realization

We need to know in which area of a sheet metal part that the *locating scheme* needs to be robust, i.e. where to suppress propagated variation with respect to the requirements, and where not to. Thus, dimensional requirements on the overall body-in-white need to be broken down and cascaded to each assembly. The positioning of the locating points of a certain assembly might need to satisfy requirements originating from parts at numerous steps in the *assembly sequence*. Thus, if one *locating scheme* is changed, then it most likely will affect other *locating schemes*. Many results have been reported regarding *locating scheme positioning*. It is for instance treated in [SÖD 02], [CAI 97] and [SÖD 99].

Besides the interfaces between the sheet metal parts, the interfaces to all other parts that makes up the car, for instance the chassis and the interior parts like pedals and seats needs to be designed to ensure robust attachment to the body-in-white.

In conclusion, detailed product interfaces, locating schemes and assembly sequences need to be developed simultaneously.

#### 9.2.4. Detail design

Principle input into the detail design phase consists of *detailed product interfaces*, *locating schemes* and an *assembly sequence*. In the system-level design phase, the *product part joints* were designed in detail. Having secured the packing of the parts, detailed product design in general can proceed.

Obviously the *product part joints*, i.e. the surfaces or flanges that are joined, need to be designed before any actual *weld positions* can be determined. Moreover, to minimize spring-back, welds are positioned with respect to the *locating scheme*. Thus *product part joints* as well as *locating schemes* are needed to determine effective *weld positions*. Furthermore, virtual crash testing on FEM data, which requires *detailed product design* of some maturity, is needed to analytically determine the required *number of welds* and the *weld positions* of the *product joining model*.

Having obtained a *detailed product design* in terms of *detailed part geometries* along with related *product joining models*, *detailed process design* can then start. In the system-level design phase, six locating points that lock the six positional degrees of freedom of the part were determined for each assembly. In detail design the locating points are physically realized in the form of *fixtures and mating parts*. However, the large surfaces and thin geometry sections of compliant sheet metal parts usually require additional supporting points to withstand gravity, handling, and welding forces; see Figure 9.5. Many results have been reported regarding supporting points. *Supporting point positions* and *quantity* are for instance treated in [REA 93] and [CAI 96]. To define supporting points, *detailed product design* is needed to determine the stiffness of the sheet metal parts. Furthermore, the *product joining model* is needed to know where fixture supports need to compensate for robot welding forces. Moreover, *station process layout* is needed to know how the assembly is, for instance, spatially tilted to determine how to support for gravity.

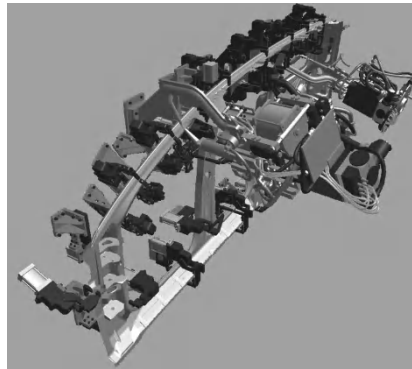
*Station process layout* design requires knowledge of the *assembly order* and the *product joining model*, to populate the station with consecutive parts and related workload. An initial *number of parts*, *robots* and *welds* are allocated to each station, based on non-geometrical estimates in the *logic factory flow* and standard time

allocations for different types of welds. Furthermore, *detailed product geometries* are needed for detailed descriptions of the *station assembly steps*.

To distribute parts and welds to stations, we need to be make sure that, in each station, the ingoing sheet metal parts can be joined with enough spot welds to give the outgoing assembly the sufficient structural integrity or strength to be transported to the subsequent stations without deformation, assuming that the fixture clamps need to be loosened in inter-station transport. The rest of the welds, whose purpose is to reinforce the assembly to meet operational use requirements, can be executed anywhere along the production line. The reinforcement type of welds, re-spot welds (see Figure 9.4) can be distributed along the product line to optimize equipment utilization.

With knowledge of *locating scheme support*, *station process layout* and the *detailed product design*, then detailed geometry design of the process equipment can proceed. Assuming that a considered part of the product is redesigned (as opposed to carried-over) and that there is limited process carry-over to relate to, then the product is the primary driver for process design. Thus, *product-near* detailed process geometry design should be initiated first.

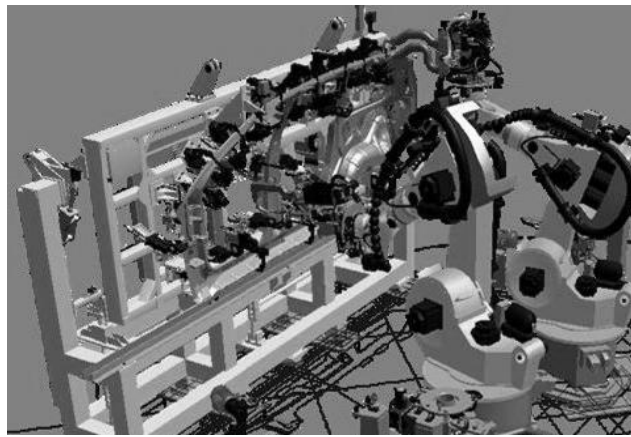
The *locating schemes* and *support points* are physically realized as *fixtures* and the *weld guns* are designed or chosen from standard tooling and consequentially statically packaged, against the *fixtures* and the *product geometries* at the various *welds*, i.e. collision-free access is ensured, as illustrated in Figure 9.6.



**Figure 9.6.** *Product-near process design*

One factor when distributing welds to stations is to be able to minimize the number of *weld gun* types. The reinforcement type of welds previously mentioned in this section can be distributed along the production lines. However, as previously

described, some welds need to be executed at specific stations in the flow to ensure dimensional integrity during inter-station transport. *Weld guns* that execute such welds are more likely to be specifically designed. When *weld gun* and *fixture design* exists, packaged against the product, then *factory-near detailed process design*, i.e. the *station equipment design*, can be initiated; see Figure 9.7. The remaining process geometries such as palettes and turntables for instance are designed or selected, and *spatially positioned*. Furthermore, robots are positioned to optimize *reachability* to the welds distributed to the station.



**Figure 9.7.** *Factory-near process design*

Upon completed *factory-near detailed process design*, complete geometrical representations of the stations are obtained. However, the parts, robots and welds allocated to each station are, as previously described, based on non-geometrical estimates in the *logic factory flow* and standard time allocations for different types of welds. Having complete geometrical representations of the stations, these initial allocations can now be optimized and revised using: robot path planning and optimization, station weld load balancing, robot coordination for simultaneous operation and ultimately line weld load balancing. *Robotic motion*, in terms of paths and *welding sequences* are planned such that *robotic travel* is minimized and geometrical quality is maximized. The station weld workload is balanced between the robots which furthermore are coordinated for simultaneous operation within each other's envelopes. Finally a *sequence of station assembly steps* is established.

The activities within each phase are, as illustrated in Figure 9.3, iterated. However emergency iterations which revisit design activities of previous phases are extraordinary. For instance, if changes in *product interfaces*, *locating schemes* and

*assembly sequence* are required in the detail design phase, it is difficult to overlook the required product and process re-optimization.

An absolute deadline for all product as well as process design changes is when physical equipment manufacturing is initiated.

### 9.3. Summary and future work

In this chapter a chronological framework for virtual sheet metal assembly design, described in Figure 9.3 and Table 9.1, has been proposed and argued for throughout section 9.2. The framework conveys the order, in which design parameters, which influence geometric quality and equipment utilization, need to be introduced to ensure that each design parameter is analytically determined. The order is significant, as design parameters are usually prerequisite to start analysis of subsequent design parameters.

Recent progress within product lifecycle management (PLM) and the advent of efficient analysis tools targeting most of the influential design parameters makes a holistic approach to sheet metal assembly design feasible. The chronological framework provides a roadmap in this effort.

The chronological framework applies to multi-station robotic sheet metal assembly in general. The terminology is however largely that of the automotive industry. In parts the framework may apply to assembly in general, including manual assembly and parts other than sheet metal parts. That is however not within the scope of this study.

We will conclude this chapter with an outline of future work. Whereas product and process design can run concurrently in the planning, concept development and system-level design phases, the information content to describe products and processes rapidly increases in the detail design phase. As a result, concurrent detailed product and process design is partially impeded. To ensure that all detailed process requirements can be fed back to detailed product design and station process layout design in time to be considered and preferably also iterated, then all four phases of detailed process design need to be rendered more efficient or even be automated. Today, there are efficient analysis methods and tools targeting most of the influential design parameters, and an effective corresponding PLM information infrastructure. One of the most qualifying prerequisites is recent scientific progress within the area of automatic path planning and optimization of industrial robots, which have conveyed a significant decrease in path planning and optimization times [LAV 99], [BOH 00]. In future work an automated process for detailed sheet metal assembly process design will be proposed.

#### 9.4. Acknowledgments

This work was supported by VINNOVA (the Swedish Governmental Agency for Innovation Systems) through the MERA program, and by the Volvo Car Corporation.

#### 9.5. Bibliography

- [BER 02] BERGMAN B., KLEFSJÖ B., *Quality from Customer Needs to Customer Satisfaction*, Studentlitteratur AB, Sweden, 2002.
- [BOH 00] BOHLIN R., KAVRAKI L. E., "Path planning using lazy PRM", in *Proceedings of the 2000 IEEE International Conference on Robotics & Automation*, San Francisco, 2000.
- [CAI 96] CAI W., HU J. S., YUAN J. X., "Deformable sheet metal fixturing: Principles, algorithms and simulations", *Journal of Manufacturing Science and Engineering*, Vol. 118, 1996, pp 318-324.
- [CAI 97] CAI W., HU J. S., YUAN J. X., "A variational method of robust fixture configuration design for 3-D workpieces", *Journal of Manufacturing Science and Engineering*, Vol. 119, 1997, pp 593-602.
- [DAH 03] DAHLSTRÖM S., Variation simulation of sheet metal assemblies for geometrical quality, PhD Thesis, Dept. of Product and Production Development, Chalmers University of Technology, Göteborg, 2003.
- [LAV 99] LAVALLE S. M., KUFFNER J. J., "Randomized kinodynamic planning", in *Proceedings of the IEEE International Conference on Robotics and Automation*, 1999.
- [PAH 07] PAHL G., BEITZ W., *Engineering Design: A Systematic Approach*, Springer, Berlin, Germany, 2007.
- [REA 93] REARICK M. R., HU J. S., WU S. M., "Optimal fixture design for deformable sheet metal workpieces", *Transactions of NARMI/SME*, Vol. 21, 1993, pp 407-412.
- [SEG 09] SEGEBOEN J., CARLSON J. S., CARLSSON A., SÖDERBERG R., "Parameters influencing geometrical quality and station cycle time in sheet metal assemblies", in *Proceedings of the 2<sup>nd</sup> Nordic Conference on PLM*, Göteborg, 2009.
- [SÖD 99] SÖDERBERG R., CARLSON J. S., "Locating scheme analysis for robust assembly and fixture design", in *Proceedings of the ASME DETC, DAC-8690 Conference*, Las Vegas, 1999.
- [SÖD 02] SÖDERBERG R., LINDKVIST L., "Stability and Seam Variation Analysis for Automobile Body Design", *Journal of Engineering Design*, Vol. 13, Issue 2, 2002.
- [SÖD 06] SÖDERBERG R., LINDKVIST L., "Managing physical dependencies through location system design", *Journal of Engineering Design*, Vol. 17, Issue 4, 2006.
- [ULL 03] ULLMAN D. G., *The Mechanical Design Process*, McGraw-Hill, New York USA, 2003.



- [ULR 04] ULRICH K. T., EPPINGER S. D., *Product Design and Development*, McGraw-Hill, Boston, USA, 2004.
- [XIE 02] XIE L. S., HSIEH C., “Clamping and welding sequence optimization for minimizing cycle time and assembly deformation”, *International Journal of Materials & Product Technology*, Vol. 17, 2002.

## Chapter 10

# A Method to Optimize Geometric Quality and Motion Feasibility of Assembly Sequences

### 10.1. Introduction

#### 10.1.1. *Problem motivation*

In today's market, diversifying a product in several product families and creating a new concept from zero requires very fast realization times and, above all, necessitates design and manufacturing processes of extremely high quality. Both time and quality are vital for a product in order to dominate, become successful, or in the worst case survive the worldwide competition.

Often, in the industry, designing a product and its realization belong to two distinct phases, separated not only because different people are responsible for each one, but even distinct in time. Of course a product is manufactured after its design, but there is the possibility to integrate these two phases in virtual environments, due to the fact that they may be strictly related. Indeed, one reason that makes them coupled is that the designer may have created a product that is impossible to realize due to manufacturing infeasibility. Another reason is that a product design may have different quality measures, depending on how it is manufactured.

---

Chapter written by Domenico SPENSIERI, Johan S. CARLSON, Lars LINDKVIST, Robert BOHLIN and Rikard SÖDERBERG.

Assembling a product consisting of several parts is a typical process at the borderline between design and manufacturing and is very crucial in the success of the product itself.

Planning how to assemble a product is often done manually by industrial engineers. Although they can be very experienced, their working procedure can result in being time consuming and error prone. Furthermore, small changes in design may require the entire re-thinking of the assembling procedure.

Quality is highly influenced by the assembly design. Managing variations, in fact, often depends on the order in which parts are assembled together and on the fixtures that are used. A bad design, from the geometrical quality point of view, can lead to tighten part tolerances, and probably to more expensive production processes.

On the other side, a design requiring certain assembling sequences may be completely impossible to produce. Discovering this very late, at the manufacturing stage, is also very expensive.

“Design For Assembly” (DFA) methodologies have been proposed over recent decades. They help in formalizing commonly used concepts and extend and improve important aspects. Introducing formalism in such areas also eases the creation of totally or partially automatic procedures, which can be transformed and implemented in very useful supporting tools for engineers.

These tools are often well separated among distinct phases of product realization. They often depend on each other, therefore, assembling needs a very frequent exchange of information between, for example, design and manufacturing simulations. Iterative working procedures, jumping from one simulation to the other, or integrated simulation environments would be very helpful in shortening setup times.

#### **10.1.2. *Related work***

A great attempt to formalize a theory for designing assemblies has been made by Whitney and Mantripragada, see [MAN 98] and [WHI 99]. In these works the “Datum Flow Chain” (DFC) is introduced as a way to model assemblies. In this model, the Key Characteristics of the assembly are highlighted and so are the kinematic constraints between the parts. At a more abstract level, the DFC can be represented as a graph where connections between parts (nodes in the graph) are represented by directed and undirected edges. Many of the ideas described in this

chapter come from that theory, which has mainly inspired the way assemblies are modeled here.

Other approaches use a contact-based representation of an assembly. Among the pioneers, there is the work of Bourjault, see [BOU 84]. Since then, several articles have been written about how to generate assembly sequences. In [DEF 87], a contact-based state space is described to generate feasible assembly sequences, partly based on the interaction with a user. In [HOM 90] the AND/OR graph is introduced for modeling subassemblies decomposition. The main advantage of this method is decreasing the number of states necessary to represent the assembling and disassembling process. However, path planning issues are not present here.

A lot of work has been done based on the assumption that assembling is the reverse of disassembling: AND/OR graphs, thus, become a great way of modeling and path planning techniques can be successfully applied to decide the order of assembling, because often planning from a cluttered start configuration is easier than the reverse operation. Big steps in this direction have been done by [WIL 92] and [HAL 00]: here, the motion space approach is elaborated and great results are shown, which exploit local directions of motion for assemblies consisting of a large number of parts. Here, geometric quality and assembly design are not considered.

In many of these works, the assembling operations are binary, see [WIL 92], meaning that two subassemblies at a time are brought together. This is made in order to manage the complexity in describing the possible assembling sequences. Recently, [WAN 05] and [WAN 07] have been striving towards a way to obtain k-ary operations and they also couple the assembling sequences to the quality of the final assembly, inspired by the DFC theory. The main investigation area is a multi-station assembly system with compliant parts. However, in contrast to this article, no path planning is performed there, to check for the feasibility of motion and an exhaustive search is done in order to choose the best assembling sequence.

Quality of the assembly, in terms of geometrical variations and sensitivity, is addressed in several papers. The one used in this chapter is described in [SÖD 99].

Strictly related to assembling theory is disassembly planning. They share many common aspects, mainly regarding the sequencing point of view and the geometric paths that bring one part in its final configuration in the assembly. However, some rules that help limit the search space are valid specifically in the assembly case. Also, variation analysis is a typical issue in the design of an assembly, not directly related to disassembling.

In this chapter we focus on assembling products.

## 10.2. Modeling and algorithms

### 10.2.1. Modeling connections

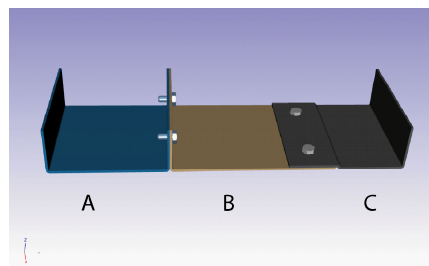
The modeling of assemblies requires first of all an analysis of the basic properties we want to capture. One way to start is to model only contacts among parts, and represent the assembly as an undirected graph, where, for example, nodes model single parts and edges model contacts between parts. Often, this static way of describing assemblies results in poor information for the designer. The kinematic connection between two parts is not modeled at all, the locating responsibility is not highlighted either. Without these elements, it is not possible to deduce if there are any under or over constrained parts, or to evaluate the assembly from a geometric quality point of view. Theories for modeling assemblies have been proposed in the past, which catch the kinematic constraints among components, and which define the key characteristics of the product; see [WHI 99].

Moreover, once the quality of the assembly has been evaluated, it would be good to state if assembling all the parts together will be feasible at the manufacturing stage.

Here, we present a method to generate an assembling plan for a product, considering both geometric quality and geometric feasibility.

The product to be assembled is represented by its CAD model and by the kinematics constraints between parts. One way to do this is to use the theory presented in [CAR 00].

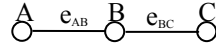
For example, in Figure 10.1, there is an assembly consisting of three parts, which we will name parts A, B and C, for simplicity. This example, with some modifications and at different levels of abstraction, is often used in the literature to illustrate the theory for designing assemblies (see [WHI 99]) and will be the pilot test case throughout this work.



**Figure 10.1.** Test assembly consisting of 3 parts: A, B, C

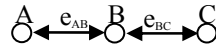
Parts A and B are mated together in such a way that one part locates the other in all the six degrees of freedom (dofs). Part A has two holes, while part B has one slot and one hole. The slot allows the assembly of the two parts to be feasible even in the presence of variations. The screws finalize the assembly AB.

Parts B and C are constrained by each other through a contact surface. They are also coupled through two holes on B, and two holes on C, these being smaller than the ones on B. These joints provide the parts with a way to be fastened together. From a kinematic point of view, this means that part B (resp. C) locates C (resp. B) by three dofs:  $T_Z$ ,  $R_X$ ,  $R_Y$ , respectively translation along Z-axis, rotation around the X-axis, and rotation around Y-axis. This situation may be represented through an undirected graph; see Figure 10.2.



**Figure 10.2.** Contact graph for assembly in Figure 10.1

In the theory concerning the Datum Flow Chain, see [MAN 98], undirected edges are used to represent *contacts* between parts, in contrast to *mates*, which instead perform locator function and transfer variation. In order to not create confusion, we may use a double directed edge instead of an undirected edge, i.e. one of the two possibilities has to be chosen; see Figure 10.3.

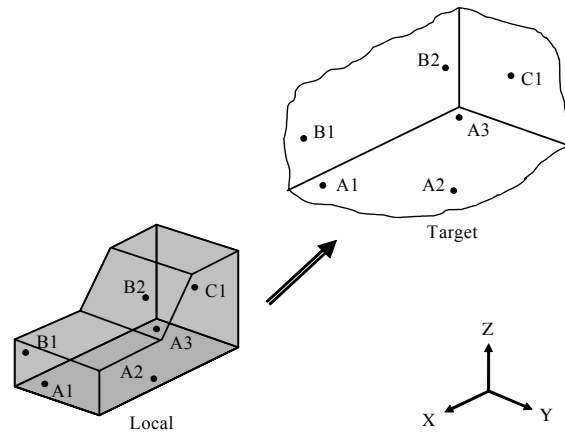


**Figure 10.3.** Directed graph representation of the assembly

In our model, actually, the graph is augmented with spatial information regarding the dofs involved in the features. This may be represented, see [CAR 00], by a locating scheme matrix  $J$ ,

$$J = \begin{bmatrix} (p_1 \times n_1)^T & n_1^T \\ \dots & \dots \\ (p_6 \times n_6)^T & n_6^T \end{bmatrix}$$

The contact points,  $p_i$ , and their relative constraint vectors,  $n_i$ , form a  $6 \times 6$  matrix. When the locating scheme is deterministic, the matrix  $J$  has maximum rank. A typical six-point locating scheme, often referred to as 3-2-1, is illustrated in Figure 10.4.



**Figure 10.4.** 3-2-1 locating scheme

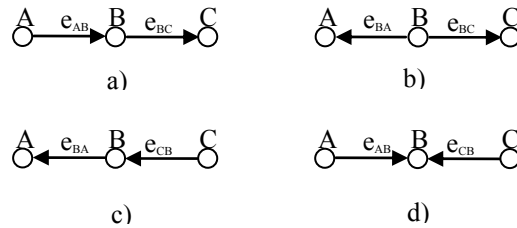
In reality, these points correspond to planes, holes and slots.

At this point it may seem that our assembly is completed. However, many choices remain, which have a great impact on the product quality, on manufacturing, and costs. In the graph above, it is not specified if part A should locate part B, or vice versa. No locating responsibility is established about the three dofs locked when joining together the surfaces between parts B and C. Common sense would suggest that a fixture would be positioned under the three parts. Thus, part B should partially locate part C, since the other way, i.e. assembling part B under C, would be quite impractical, after C has been positioned. Anyway, this does not emerge by just having a direct look at the graph above. The locating responsibility may be easily modeled by a directed edge in the graph, as in the DFC, see [MAN 98]. Thus, for the driving test case in Figure 10.1, four alternatives should be considered, illustrated in Figure 10.5.

Note that not all possibilities are consistent. A first analysis can be carried out by analyzing the sum of the number of dofs that each node has on its incoming edges. A sufficient condition stating that a part is over constrained is when this sum is greater than six.

Then, parts constraining themselves should also be avoided: this case is a cycle in the graph.

From Figure 10.5 it is possible to note how, in the locating scheme d, the above sufficiency condition is satisfied for part B, thus making the design of the assembly not acceptable in our framework. Indeed, part B is constrained by A with 6 dofs and by C with 3.



**Figure 10.5.** Four possible locating scheme graphs for assembly in Figure 10.3

It is important to highlight here that the number of all possible choices for such graphs can grow exponentially with the number of bi-directed edges. For small assemblies, however, and when many precedence relations are already locked, we can keep the computational burden at a reasonable level.

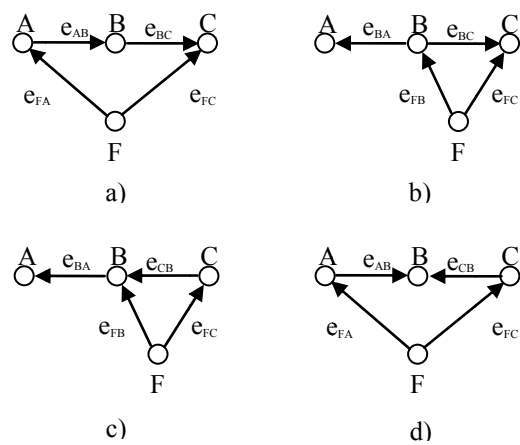
#### Fixtures

Under constrained parts can emerge, but in this case we assume that their missing dofs can be constrained by a fixture system. Once the part is located, the joints relative to the under constrained part are fastened. Another assumption in this work is that fastening parts is performed exactly after the parts involved are fully located and before placing other parts.

Applying these considerations to the assembly considered so far, we can fill up each locating scheme graph in Figure 10.5 with a node representing the fixture; see Figure 10.6.

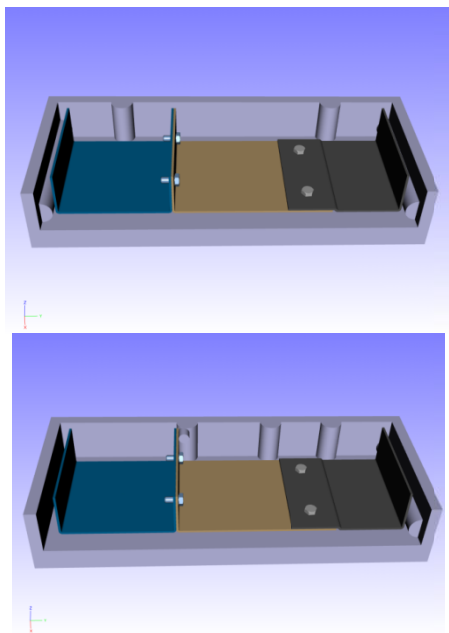
Note that no change is made to the information regarding the dofs constrained by the features between parts (excluding the fixture). In order to generate the resulting graphs in Figure 10.6, it is enough to consider the level of abstraction of the locating scheme graph. In any graph in Figure 10.5, just add a directed edge from the base fixture node to each node representing an under constrained part.





**Figure 10.6.** Locating scheme graphs with fixtures

We assume that a proper fixture system is available for any choice of a graph. Possible fixtures can look like those shown in Figure 10.7.



**Figure 10.7.** Two possible fixtures for the assembly in Figure 10.1, according to the locating scheme graphs in Figure 10.6

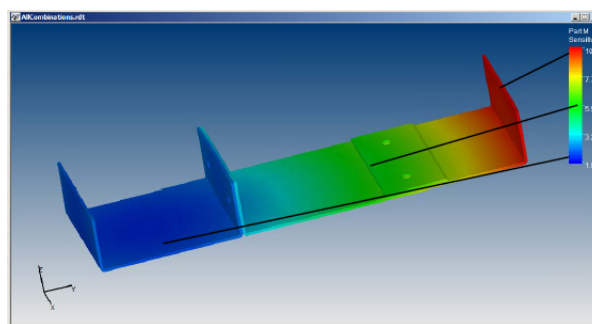
### 10.2.2. Stability and variation analysis

The stability analysis, see [LIN 03], evaluates the sensitivity of a concept to locators' variations. By varying each locating point with a small increment,  $\Delta input$ , one at a time,  $\Delta output / \Delta input$  may be determined in several directions separately for a number of output points representing the geometry. For each point of the geometry, a value can be determined and shown in color-coding: this value is coupled to the square sum of variations caused by displacements in the six locating points. Figure 10.8 shows a stability analysis for the three locating scheme graphs described in the previous section. The color-coding shows how variations will propagate from the locators (the inputs) to critical areas of the part or assembly. The bottom of the legend represents the stable area, with a sensitivity of 1.0, with almost no variations amplification at all, whilst the top area corresponds to a larger amplification of around 10.0.

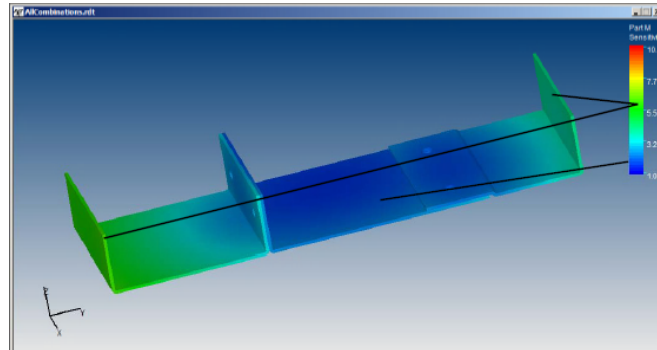
Note that the second locating scheme graph looks much better than the other two, having no area coded with a color close to the critical red zone.

However, if a particular critical dimension is more relevant than others, a variation analysis can be performed. The purpose of the variation analysis is to determine the expected variations in one or several critical output points, corresponding to a certain set of input variations, i.e. tolerances in locating points. In this example, Monte Carlo simulation is used to predict the output variation of the overall length of the assembly along the Y-axis. The result is that the first design has less variance than the other two on that dimension.

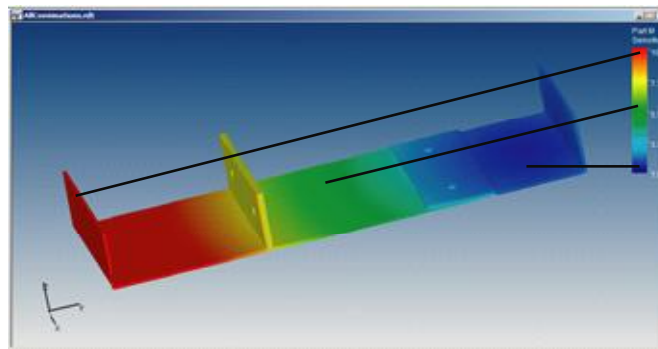
Based on these analyses, a trade-off naturally arises between global sensitivity (best in design 2) and variations of an important dimension of the assembly, the length along Y (best in design 1).



**Figure 10.8a.** Stability analysis for the assembly as modeled in Figure 10.6a



**Figure 10.8b.** *Stability analysis for the assembly as modeled in Figure 10.6b*



**Figure 10.8c.** *Stability analysis for the assembly as modeled in Figure 10.6c*

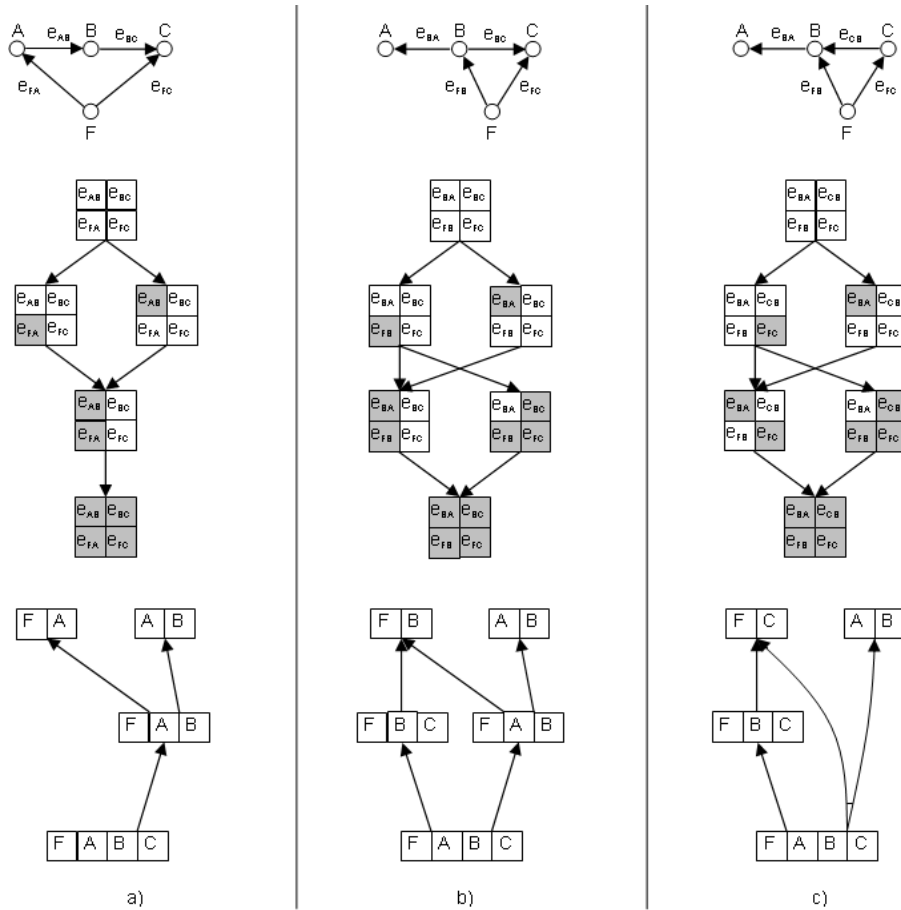
### 10.2.3. Assembly sequences

Let us analyze in more detail how it is possible to model different sequences, which are coherent with the locating scheme graphs given in Figure 10.6.

When generating assembling sequences, we consider only binary operations and generate subassemblies which correspond to connected sub-graphs in the undirected locating scheme graph. Moreover, we assume that a part is always fully located in all its six degrees of freedom before assembling other parts.

As in [MAN 98], subassemblies with under constrained parts are not allowed, except for one base node, thus subassemblies with multiple root nodes are not allowed.

One way to generate feasible sequences is to consider the state space given by the liaisons that are performed during the assembling process, and apply the rules as in [MAN 98]. See also [SPE 08] for a more detailed analysis of the Assembly Planner.



**Figure 10.9.** Possible locating scheme graphs and their related liaison-based and part-based assembly sequences

#### Case a

In this way, by considering the constraints imposed by the graph in Figure 10.9a, we can generate two different sequences for the pilot test case we are analyzing:

L1.  $e_{AB}, e_{FA}, e_{FC}, e_{BC}$

L2.  $e_{FA}, e_{AB}, e_{FC}, e_{BC}$

Note that the liaisons  $e_{FC}, e_{BC}$  are assumed to be done at the same time; thus it does not matter in this model which of the two connections happens first.

The sequences in the part-based state space, see [HOM 90], can be described by reversing the disassembling of the whole assembly  $\{FABC\}$ :

P1.  $\{F\}\{A\}\{B\}\{C\}, \{F\}\{AB\}\{C\}, \{FAB\}\{C\}, \{FABC\}$

P2.  $\{F\}\{A\}\{B\}\{C\}, \{FA\}\{B\}\{C\}, \{FAB\}\{C\}, \{FABC\}$

#### Case b

The second locating scheme alternative gives the sequences given in Figure 10.9b.

#### Case c

The third case is illustrated in Figure 10.9c. Here, we have three sequences modeled in the liaison-based case:

L1.  $e_{BA}, e_{FC}, e_{FB}, e_{CB}$

L2.  $e_{FC}, e_{BA}, e_{FB}, e_{CB}$

L3.  $e_{FC}, e_{FB}, e_{CB}, e_{BA}$

In the part-based space:

P1.  $\{F\}\{A\}\{B\}\{C\}, \{FC\}\{AB\}, \{FABC\}$

P2.  $\{F\}\{A\}\{B\}\{C\}, \{FC\}\{A\}\{B\}, \{FBC\}\{A\}, \{FABC\}$

Note that the cost of the connector joining  $\{FC\}$  and  $\{AB\}$  together does not differ if subassembly  $\{AB\}$  is done before  $\{FC\}$ , or vice versa. This implies that only two sequences can actually be modeled, in contrast to the three L1, L2, L3.

Has information been lost? It depends on what we look at:

- from the geometric quality point of view there is no difference between sequence L1 and L2, since they both lead to the same variations (and so does L3);

- from the path planning point of view, note that the two subassemblies are disconnected, thus they do not interfere with each other geometrically.

In other words, no collision is possible, independently of the order in which  $\{AB\}$  and  $\{FC\}$  are assembled together. We conclude that, for our purposes, modeling sequences in the part-based space is sufficient and allows us to save memory, due to fewer states being created; see [HOM 90].

### *Optimization*

The space of all possible assembly sequences can be searched for an optimal one through the AO\* algorithm, see [MAR 73] and [NIL 80]. When the graph is generated, each node expansion requires a feasibility check through the path planner. This well fits with the implicit search in AO\*. Furthermore, a node expansion requires the satisfaction of the necessary criteria that subassemblies should fulfill. Note that geometric feasibility, relative to the path planner, is much more computationally expensive than the verification of the logic constraints and dominates the total time and space complexity of the overall algorithm.

Several cost measures can be used. If we want to minimize rotations, we let the path planner module return the total rotation angle needed. Other possible measures may be the length of the disassembling path or the computing time. This last measure is indeed a useful motion complexity indicator. In fact, we can consider as a “complex” motion a disassembling motion where several translations and rotations are necessary, and where clearance is often small. The latter gives a finer sampling of the configuration space, and the former requires a large number of node expansions, thus both aspects increase running time.

#### **10.2.4. Path planning**

This module checks for the existence of a collision-free way of assembling parts together. No operator or tool is modeled. The advantages of producing a disassembling plan have been highlighted in previous literature. The path planner also benefits from this approach, since producing a collision free path from a more cluttered environment than the goal configuration is easier than trying to go in the converse direction.

A path for a rigid body may be defined as a continuous function:

$$\tau: [0, 1] \rightarrow SE(3)$$

where  $\tau(0)$  is the initial configuration,  $\tau(1)$  is the final one, and  $SE(3)$  is the special Euclidean group. For an overview of path planning algorithms, see [LAT 91] and [LAV 06].

Note that in our case the goal configuration is not determined uniquely, but is a configuration where the distance between the part and the rest of the environment is greater than a predefined value.

This module generates states in the configuration space  $SE(3)$ , by a sampling-based method. It tries to find a collision-free sequence of states from  $\tau(0)$  to a goal state, through an A\*-based search algorithm. Collision tests are performed in a lazy fashion (see [BOH 00]) through a hierarchical-based collision checker.

### 10.3. Assembly planning

Resuming what has been explained so far, the overall method may be described by the following steps:

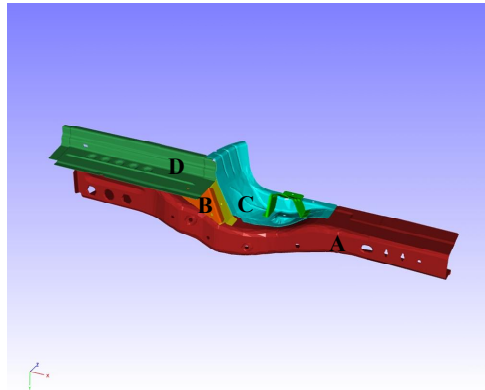
- Given a model of the assembly, create all possible locating scheme graphs, discarding unfeasible ones.
- For any graph computed at 1, generate models for feasible fixtures, providing the parts with the missing constraints.
- Evaluate each possible assembly design, generated so far, with respect to given quality measures.
- For each locating scheme graph, use the Assembly Planner to generate an optimal assembling sequence of operations.

### 10.4. Industrial test case

This case is adapted from an industrial environment. The assembly actually consists of compliant parts, but we treat them as rigid bodies, as a verification instance for the method presented. In any case, this could be used to analyze the level of approximation of the method with others, which refer to design strategies for compliant parts.

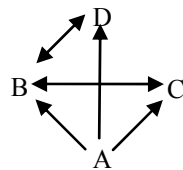
Four parts constitute the assembly, see Figure 10.10:

- longitudinal rear;
- reinforcement suspension;
- gusset;
- panel.



**Figure 10.10.** *Assembly*

The connections among them are illustrated in Figure 10.11.



**Figure 10.11.** *Directed graph representation of the assembly*

Note that some edges do not have double directions. This happens because the rear is considered a base part, with the possibilities of acting as fixture.

The four locating scheme graphs for the assembly are shown in Figure 10.12, with their relative stability analysis.

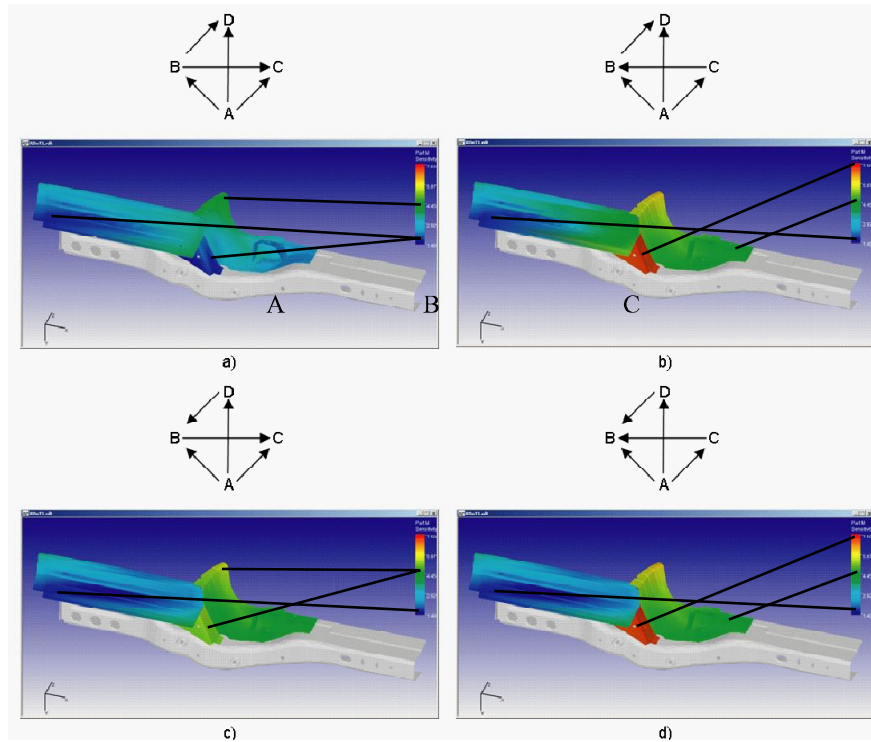
Looking at Figure 10.12, the smoothest design seems to be the one in a). Also we can see that assembling part B after part C (cases b) and d)), leads to poor quality for part B, with large high sensitivity areas (top of legend).

After running the Assembly Planner for the best design, we obtain a feasible collision-free assembling plan, which results in a linear assembly sequence:

$$\{A\} \{B\} \{C\} \{D\}, \{AB\} \{C\} \{D\}, \{ABD\} \{C\}, \{ABCD\}.$$



We have also run the Assembly Planner for the other three equivalence classes, and collision-free paths have been found for all, except the last one d). Indeed design constraints require us to assemble part B after parts C and D: this is not possible (just look at Figure 10.10).



**Figure 10.12.** Locating scheme graphs with relative stability analysis

### 10.5. Conclusions and future work

The new method presented in this work seems to catch the most important aspects of designing assemblies: modeling the assembly in an abstract way, geometric quality, variation and stability analysis, sequence optimization, and geometric feasibility. The pilot test case, a common thread throughout this chapter, shows computational results that mirror what we would expect theoretically. Most of the modeling theory is based on the articles [MAN 98] and [WHI 99].

Further work can be done. A deeper analysis can be carried out to improve the complexity of the generation of possible locating scheme graphs. It may be possible

to design a lazy algorithm implicitly detecting schemes with poor geometric quality. Another direction might be the relaxation of some of the hypotheses, as the binary operation assumption. This would require modeling time in the path planning algorithms.

## 10.6. Acknowledgments

The authors would like to thank the Swedish Governmental Agency for Innovation Systems, VINNOVA, for grants supporting this work, within the Wingquist VINN Excellence Centre.

## 10.7. Bibliography

- [BOH 00] BOHLIN R., KAVRAKI L., "Path planning using Lazy PRM", *Proceedings of the IEEE International Conference on Robotics and Automation*, Vol. 1, 521-528, 2000.
- [BOU 84] BOURJAULT A., Contribution à une approche méthodologique de l'assemblage automatisé: Elaboration automatique des séquences opératoires, PhD Thesis, University of Franche-Comté, 1984.
- [CAR 00] CARLSON J.S., How to reduce geometrical variation in assembled products, PhD Thesis, Chalmers University of Technology, 2000.
- [DEF 87] DE FAZIO T. L., WHITNEY D.E., "Simplified generation of all mechanical assembly sequences", *IEEE Journal of Robotics and Automation*, Vol. RA-3, No. 6, 1987.
- [HAL 00] HALPERIN D., LATOMBE J.-C., WILSON R.H., "A general framework for assembly planning: the motion space approach", *Algorithmica*, Springer-Verlag, 2000.
- [HOM 90] HOMEME DE MELLO L.S., SANDERSON A.C., "AND/OR graph representation of assembly plans", *IEEE Transactions on Robotics and Automation*, Vol. 6, No. 2, 1990.
- [LAT 91] LATOMBE J.C., *Robot Motion Planning*, Kluwer Academic Publishers, Boston, MA, 1991.
- [LAV 06] LAVALLE S.M., *Planning Algorithms*, Cambridge University Press, 2006.
- [LIN 03] LINDKVIST L., SÖDERBERG R., "Computer aided tolerance chain and stability analysis", *Journal of Engineering Design*, Vol. 14, No. 1, 17-39, 2003.
- [MAN 98] MANTRIPRAGADA R., WHITNEY D. E., "The Datum Flow Chain: a systematic approach to assembly design and modeling", *Research in Engineering Design*, Springer-Verlag, Vol. 10, No. 3, 150-165, 1998.
- [MAR 73] MARTELLI A., MONTANARI U., "Additive AND/OR graphs", *Proceedings of the 3<sup>rd</sup> International Joint Conference on Artificial Intelligence*, 1973.
- [NIL 80] NILSSON N.J., *Principles of Artificial Intelligence*, Tioga Publishing, 1980.

- [SPE 08] SPENSIERI D., CARLSON J.S., BOHLIN R., SÖDERBERG R., “Integrating assembly design, sequence optimization, and advanced path planning”, *Proceedings of the ASME International Design Engineering Technical Conferences & Computers and Information in Engineering Conference*, 2008.
- [SÖD 99] SÖDERBERG R., CARLSON J. S., “Locating scheme analysis for robust assembly and fixture design”, *Proceedings of the ASME Design Engineering Technical Conferences*, Las Vegas, 1999.
- [WAN 05] WANG H., CEGLAREK D.J., “Quality-driven sequence planning and line configuration selection for compliant structure assemblies”, *CIRP Annals – Manufacturing Technology*, Vol. 54, Issue 1, 31-35, 2005.
- [WAN 07] WANG H., CEGLAREK D.J., “Generation of assembly sequences with k-ary operations”, *IEEE International Symposium on Assembly and Manufacturing*, 2007.
- [WHI 99] WHITNEY D.E., MANTRIPRAGADA R., ADAMS J.D., RHEE S.J., “Designing assemblies”, *Research Engineering Design*, Vol. 11, 229-253, 1999.
- [WIL 92] WILSON R.H., On geometric assembly planning, PhD thesis, Department of Computer Science, Stanford University, 1992.

## Chapter 11

# Modeling and Simulation of Assembly Constraints in Tolerance Analysis of Rigid Part Assemblies

During recent years, variational models for tolerance analysis, both for rigid and compliant assemblies, have been implemented into CAT (Computer-Aided Tolerancing) systems to verify the fulfillment of functional requirements, performing virtual product validation from a dimensional and geometric point of view. In this chapter, starting from a numerical methodology, proposed by the same authors, that allows us to simulate variational features, assembly constraints among parts are modeled and simulated. During assembly operations, an “object” part has to be moved to satisfy constraints of “target” parts. To do this, an assembly transformation matrix is calculated. By using geometric entities such as point, line and plane and their combinations, kinematic joints are modeled; then, a numerical procedure is proposed to solve fully- and over-constrained assemblies. Therefore, the proposed model allows us to take into account different assembly sequences. The best fit alignment among mating features is performed using optimization algorithms. Finally, two case studies are described and analyzed.

### 11.1. Introduction

Assembly design and analysis are quite important in product development and in many application fields such as kinematic and dynamic analysis, assembly sequence generation and assembly-based design [WHI 04]. The assembly model is obtained

---

Chapter written by Pasquale FRANCIOSA, Salvatore GERBINO and Stanislao PATALANO.

by specifying assembly joints and then solving the specified assembly constraints to find out the relative positions of parts [KIM 04a], [KIM 04b], [KIM 05].

Several methods have been proposed to analyze assembly constraint problems. The modified Newton-Raphson method or the Levenberg-Marquardt method allows us to solve non-linear assembly equations in a simultaneous way by using an iterative algorithm. Other approaches are based on algebraic procedures, in which each assembly constraint is subdivided into a sequence of rotation and translation operations by using a reduction of Degrees of Freedom (DoFs) [TAN 92], [TUR 92].

Specific software, such as Working Model® and Adams®, provide a joint mating method that uses joint mating constraints to define relations between components and solve constraint equations [KRA 92]. Nowadays, modern CAD systems integrate “motion-based solvers” to perform assembly motion analyses, mainly based on an assembly constraint solver.

All the above methods are based on the main hypothesis of ideal-rigid parts. Part deformation and part-to-part contact may be accounted for in the FEM-based approaches. The mechanical contact problem of a deformable assembly is typically performed by means of the Lagrange multiplier method or the penalty method [WRI 02]. Generally speaking, non-linear contact problems are solved in an iterative way.

In the tolerance analysis field, evaluating geometric feature variations, for given assembly constraint sets, is of interest. Over recent years, several Computer-Aided Tolerancing tools (CAT) for 3D tolerance analysis have been developed, such as Vis-VSA® (by Siemens), eM-TolMate® (by Siemens), CETOL 6σ® (by Sigmetrix LLC.), 3DCS® (by Dimensional Systems Inc.), Mechanical Advantage® (by Cognition Co.) and Sigmund® (by Varatech Co.).

Many methodologies have been proposed to perform the analysis of 3D tolerance chains. Proposed methods may be separated into one-dimensional tolerance charts, parametric tolerance analysis, vector loop-based tolerance analysis and tolerance domain analysis [SHE 05]. A matrix approach is proposed in [WHI 04] by using 4x4 homogeneous matrices and multivariate joint probability density function. In [JIA 05] and [SHA 07] the Tolerance-Map (T-Map) model is presented. T-map is a domain, whose size and shape describe all variants for a variational feature. The domain approach is also used in [GIO 05] and [GER 07], where a numerical method to accomplish tolerance analysis, by using small displacement torsors and Minkowski sum operator, is presented.

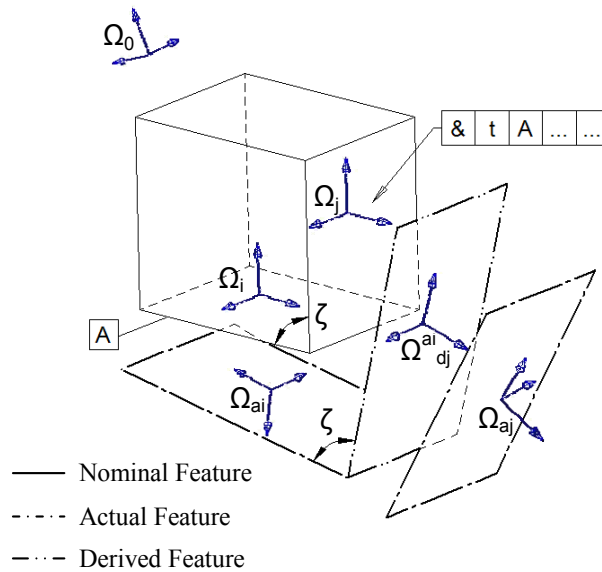
In this chapter, starting from the methodology, proposed by the same authors [FRA 08] and called SVA-TOL (Statistical Variation Analysis for Tolerancing),

assembly constraints among variational features of mating parts are modeled. The focus is on the analysis of alignment-based constraints. A numerical solution for the assembly constraint problem is provided, by using iterative algorithms, which give the best fit configuration among elementary geometric entities (such as points, lines and planes).

The chapter is arranged as follows: in section 11.2 SVA-TOL methodology for variational features is summarized; section 11.3 describes the proposed methodology to model assembly constraints among variational features; two case studies are described in sections 11.4 and 11.5; finally, section 11.6 draws conclusions.

## 11.2. SVA-TOL methodology overview

SVA-TOL methodology allows us to simulate variational features of mechanical rigid-part assemblies. Tolerance specifications are modeled for each part being assembled, according to ISO [ISO 04] or ANSI-ASME [ASM 94], [ASM 04] specifications.



**Figure 11.1.** Variational feature modeling [FRA 08]

This is done by using 4x4 transformation matrices. The general matrix variational model, stated in [11.1], expresses the transformation of any point belonging to the “j-th” variational feature into the assembly reference frame  $\Omega_0$

(Figure 11.1). This mathematical formulation takes into account the tolerance specification, related to the analyzed feature “j”, and datum reference frame constraints.

$$[M]_{\Omega_{aj} \rightarrow \Omega_0} = [M]_{\Omega_j \rightarrow \Omega_0} \cdot [M]_{\Omega_{aj} \rightarrow \Omega_j} \cdot [M_D]_{\Omega_j \rightarrow \Omega_i}^{-1} \cdot [M]_{\Omega_{ai} \rightarrow \Omega_i} \cdot [M_D]_{\Omega_j \rightarrow \Omega_i} \cdot [M]_{\Omega_j \rightarrow \Omega_0}^{-1} \quad [11.1]$$

Relationship [11.1] has to be calculated for any feature of any part being assembled. In this way, the assembly is modeled as a set of parameterized variational features.

Equation [11.2] includes the feature variational parameters;  $\{\Delta_F\} = \{\Delta_{xF}, \Delta_{yF}, \Delta_{zF}\}$  and  $\{\Theta_F\} = \{\alpha_F, \beta_F, \gamma_F\}$  are vectors of small displacements and small rotations, respectively.

$$[M]_{\Omega_j \rightarrow \Omega_{aj}} = \begin{bmatrix} 1 & -\gamma_F & \beta_F & \Delta_{xF} \\ \gamma_F & 1 & -\alpha_F & \Delta_{yF} \\ -\beta_F & \alpha_F & 1 & \Delta_{zF} \\ 0 & 0 & 0 & 1 \end{bmatrix} \quad [11.2]$$

Generally speaking, parameters  $\{\Delta_F\}$  and  $\{\Theta_F\}$  are dependent on each other [WHI 04]. Then, for each tolerance zone, variational parameter constraints are derived, and the  $R^n$  parametric space of all sources of variation – the so-called hyper-polyhedron – is introduced. Given this domain, variational features may be calculated in a closed form by using the general matrix relationship [11.1].

Once all features have been parameterized, the assembly can be made up by defining constraints among parts. In this contest, assembly modeling is accomplished in two main steps. In the first step, DoF analysis is performed. In the second step, assembly constraints among parts are introduced, accordingly.

The following sections give details of the proposed methodology to model and simulate assembly constraints among variational features.

### 11.3. Assembly constraint modeling

In the mechanical assembly field, three main types of assemblies may be introduced: under-, fully- and over-constrained. In the first case, the assembly is a mechanism with several degrees of freedom; fully-constrained are those assemblies

with the classic 3-2-1 location assembly scheme [MEA 97]; instead, in the third case, the location scheme is 3-2-(N<sub>OC</sub>+1), where “N<sub>OC</sub>” is the number of over-constraints.

Generally speaking, during assembly operations an Object Part (OP) has to be moved to satisfy constraints of Target Parts (TP).

The relative location of the object part, with respect to the target one, is represented by a 4x4 transformation matrix, as in equation [11.3], where  $[M]_{\Omega_{OP} \rightarrow \Omega_{TP}}$  is the assembly transformation matrix, and  $[R]$  and  $\{T\}$  are the rotational matrix and the translational vector, respectively.

$$[M]_{\Omega_{OP} \rightarrow \Omega_{TP}} = \left[ \begin{array}{ccc|c} R_{11} & R_{12} & R_{13} & T_{xa} \\ R_{21} & R_{22} & R_{23} & T_{ya} \\ R_{31} & R_{32} & R_{33} & T_{za} \\ \hline 0 & 0 & 0 & 1 \end{array} \right] = \begin{bmatrix} [R] & \{T\}^T \\ \{0\} & 1 \end{bmatrix} \quad [11.3]$$

This matrix is initially unknown and depends on the six rigid motion parameters (three rotations and three translations).

DoFs allowed for each joint are assumed to be invariants and, thus, they are not considered in the assembly simulation. This is made by DoF analysis allowing us to determine DoFs removed by assembly constraints. The “reduction constraint” method described in [TAN 92] or Screw Theory [WHI 04] could be adopted, but in our approach this is still a manual task.

In the small displacement hypothesis, equation [11.3] can be rearranged as in equation [11.4], where  $\{\Delta_A\} = \{\Delta_{xA}, \Delta_{yA}, \Delta_{zA}\}$  and  $\{\Theta_A\} = \{\alpha_A, \beta_A, \gamma_A\}$  are vectors of small translational and small rotational assembly parameters, respectively.

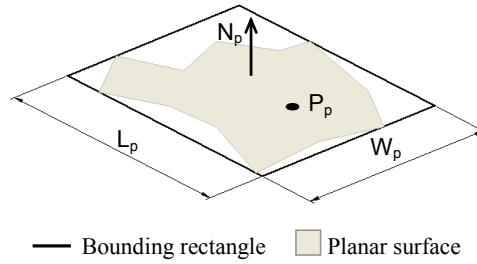
$$[M]_{\Omega_{OP} \rightarrow \Omega_{TP}} = \left[ \begin{array}{ccc|c} 1 & -\gamma_A & \beta_A & \Delta_{xA} \\ \gamma_A & 1 & -\alpha_A & \Delta_{yA} \\ -\beta_A & \alpha_A & 1 & \Delta_{zA} \\ \hline 0 & 0 & 0 & 1 \end{array} \right] = \begin{bmatrix} [R_A] & \{\Delta_A\}^T \\ \{0\} & 1 \end{bmatrix} \quad [11.4]$$

Each constraint may be considered to be a combination of elementary geometric entities (points, lines and planes) as proposed in TTRS theory [CLE 98]. The original TTRS theory proposed seven basic surfaces. In this chapter, two particular cases are considered: cylindrical and planar surfaces.

$$\text{Plane : } (P - P_p) \cdot N_p = 0 \quad [11.5]$$

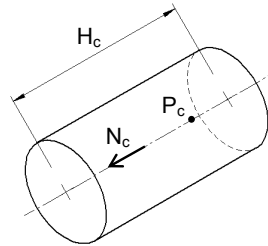


A planar surface is parameterized through the following data:  $N_p$  vector,  $P_p$  point,  $L_p$  length, and  $W_p$  width (see Figure 11.2.a). In this way the mathematical representation of a planar surface (“plane” entity) may be expressed as in [11.5], where  $P$  is any point belonging to the planar surface.



**Figure 11.2a.** *Planar surface parameterization*

Generally speaking, for planar surface with irregular boundaries the relative bounding rectangle is calculated. The bounding rectangle of a given planar geometry is the smallest rectangle which completely includes the geometry [LEN 03]. Principal Component Analysis (PCA) is used here to calculate this rectangle, by evaluating the eigenvectors of the statistical covariance matrix, related to the vertices of the planar geometry. In the following, each planar surface will be assumed to be a rectangular plane.



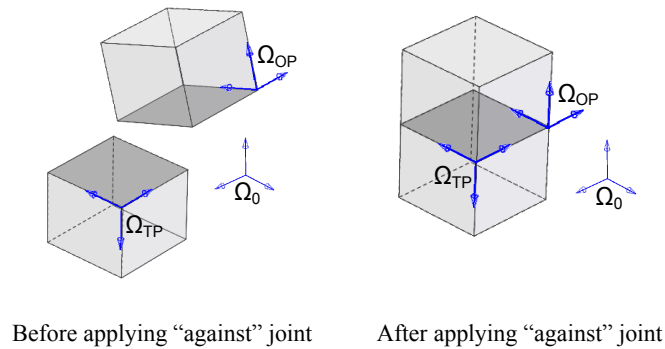
**Figure 11.2b.** *Cylindrical surface parameterization*

A cylindrical surface is defined by the following data:  $N_c$  vector,  $P_c$  point, and  $H_c$  height (see Figure 11.2.b).

$$\text{Line : } P(t) = P_c + t \cdot N_c \quad [11.6]$$

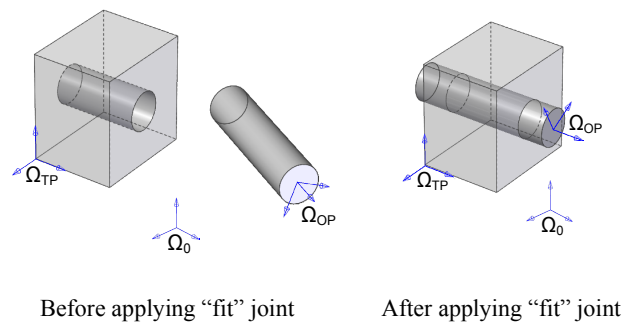
The cylindrical surface is associated with its axis (“line” entity). This means that the cylindrical surface diameter is not accounted for in this approach. The parametric representation of the cylindrical surface is defined in equation [11.6], where “ $t$ ” is the axis parameter.

“Against” and “fit” alignments are the two specific assembly joints [KIM 04a] considered in this work. The “against” condition holds between two planar surfaces and requires surfaces coming in contact. This condition is accomplished by constraining the two normal vectors to be opposite each other, and a point of the object plane to belonging to the target one (Figure 11.3).



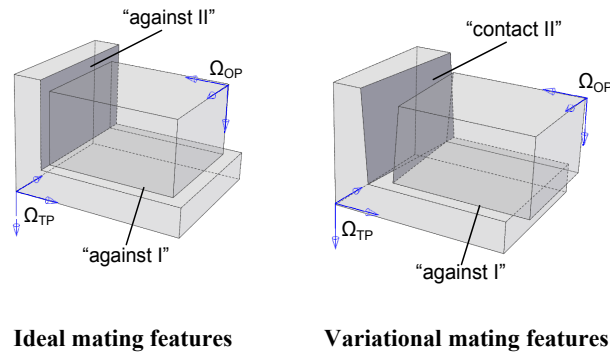
**Figure 11.3.** “Against” assembly joint

The “fit” condition, instead, holds between two cylindrical surfaces. This constraint is accomplished by imposing that target and object axes are parallel, and a point on the object axis belongs to the target one (see Figure 11.4).



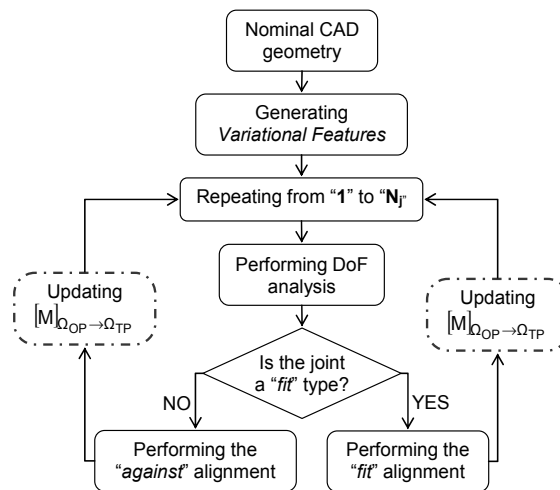
**Figure 11.4.** “Fit” assembly joint

All this is true for ideal mating features. If variational features are introduced, then a contact search algorithm has to be adopted. For example, in Figure 11.5, the mating joint “against II” (full plane-to-plane constraint) becomes the contact joint “contact II” (line-to-plane constraint) in the variational assembly.



**Figure 11.5.** *Ideal features vs variational features*

In this work, in order to automate the assembly constraint solution, a sequential constraint solver is adopted for fully-constrained assemblies.



**Figure 11.6.** *Workflow for fully-constrained assembly modeling*

Instead, for over-constrained assemblies, all constraint equations are simultaneously solved by using a least squares approach. For the latter assemblies, over-constraints may cause deformation on real parts during assembly phase. This is especially true for sheet-metal parts. However, the ideal-rigid hypothesis is accepted here.

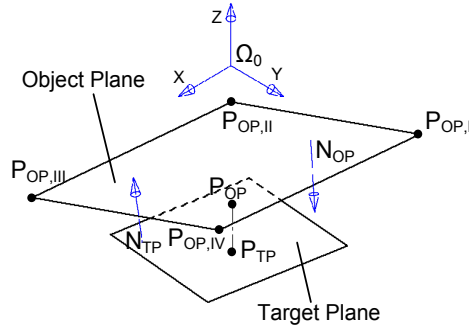
### 11.3.1. Fully-constrained assembly

Figure 11.6 depicts the general workflow adopted to perform the simulation of a fully-constrained assembly with alignment joints. DoF analysis is performed for each joint (“ $N_j$ ” is the total number of assembly joints) in order to reduce the DoFs of the object part with respect to the assembly reference frame,  $\Omega_0$ .

When solving an “against” joint, a contact search algorithm is used. A “best” fit solution, instead, is adopted to manage a “fit” joint condition.

#### 11.3.1.1. “Against” joint modeling

Looking at Figure 11.7, the aim is to best align the object plane (defined by means of the normal vector  $N_{OP}$  and the point  $P_{OP}$ ) with respect to the target one (defined by means of the normal vector  $N_{TP}$  and the point  $P_{TP}$ ).



**Figure 11.7.** “Against” joint condition

Initially, vector  $N_{OP}$  is transformed according to equation [11.7].

$$N_{OP} = \begin{bmatrix} 1 & -\gamma_A & \beta_A \\ \gamma_A & 1 & -\alpha_A \\ -\beta_A & \alpha_A & 1 \end{bmatrix} \cdot \begin{Bmatrix} N_{OPx} \\ N_{OPy} \\ N_{OPz} \end{Bmatrix} \quad [11.7]$$

Planes are best aligned if the relative angle is minimum. Then, the function to be minimized is:

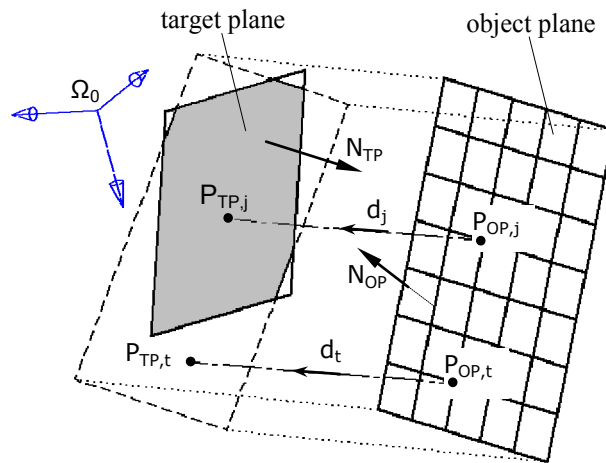
$$\min_{\alpha_A, \beta_A, \gamma_A} (J_{\text{against}}(\alpha_A, \beta_A, \gamma_A)) \quad [11.8]$$

$$J_{\text{against}}(\alpha_A, \beta_A, \gamma_A) = \|N_{TP} + N_{OP}\|$$

In the “against” joint, target and object vectors are opposite each other. Thus, equation [11.8] states that the relative angle is minimum when the resultant vector between  $N_{TP}$  and  $N_{OP}$  becomes minimum. The solution to equation [11.8] corresponds to find the minimum of a scalar function of the three variables,  $\alpha_A$ ,  $\beta_A$ ,  $\gamma_A$ . The MatLAB® “fminunc” routine is adopted here.

In the second phase, translational assembly parameters are calculated by evaluating on the object plane the point  $P_{OP,j}$ , which is the closest point to the target plane.

For this calculation, a mapped mesh is created on the object plane (see Figure 11.8).



**Figure 11.8.** Mapped mesh for the evaluation of assembly translational parameters in the “against” joint condition

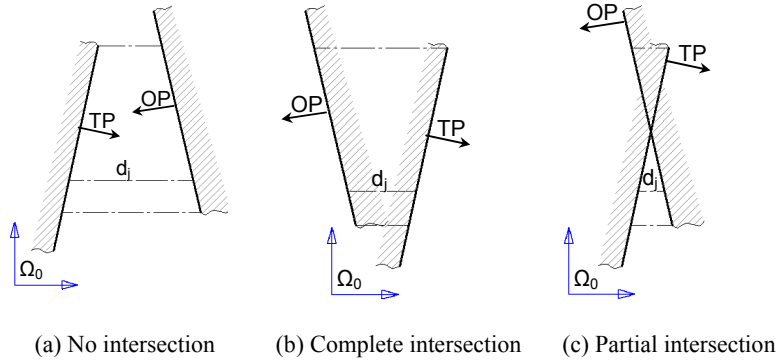
$$d_j = \frac{(P_{TP} - P_{OP,j}) \cdot N_{TP}}{i \cdot N_{TP}}$$

$$\Delta_{iA} = \begin{cases} i \cdot N_{TP} \geq 0 \rightarrow \max_j(d) \\ i \cdot N_{TP} < 0 \rightarrow \min_j(d) \end{cases} \quad [11.9]$$

$$\forall i = x, y, z, \forall j = 1, \dots, N$$

Each point of this mesh is projected on the target plane along the  $i$ -th assembly coordinate ( $i=x, y, z$ ). If the point  $P_{TP,j}$  belongs to the bounding rectangle of the target plane, then the  $i$ -th translation parameter is calculated as stated in relationship [11.9], where “ $N$ ” is the total number of points of the mapped mesh belonging to the target plane, and “ $d_j$ ” is the oriented distance from  $P_{OP,j}$  to  $P_{TP,j}$ .

It can be pointed out that this procedure assures no intersection between the two planes. In fact, if planes are initially not intersecting each other (Figure 11.9.a), then the oriented maximum distance is negative. Instead, for completely or partially intersecting planes (Figures 11.9.b and 11.9.c, respectively), the oriented maximum distance corresponds to a positive distance.



**Figure 11.9.** Target and object planes for different initial configurations

Once both rotational and translational assembly parameters have been calculated, the assembly transformation matrix is known.

#### 11.3.1.2. “Fit” joint modeling

Now, the aim is to align the object axis on the target one (Figure 11.10). As proposed for the “against” alignment, rotational assembly parameters can be calculated by applying relationship [11.10]. Similarly, we can write:

$$\min_{\alpha_A, \beta_A, \gamma_A} (J_{\text{fit}}(\alpha_A, \beta_A, \gamma_A)) \quad [11.10]$$

$$J_{\text{fit}}(\alpha_A, \beta_A, \gamma_A) = \|N_{\text{TP}} + N_{\text{OP}}\|$$

In this case, vectors  $N_{\text{OP}}$  and  $N_{\text{TP}}$  define the object and target axis directions, respectively.

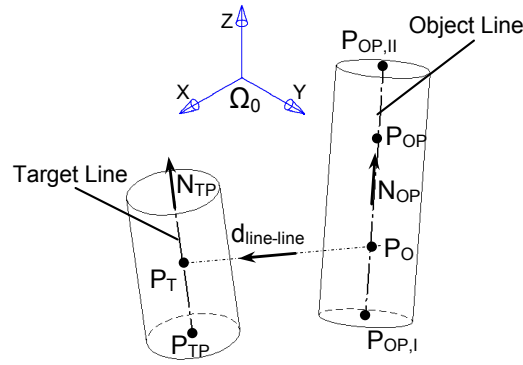


Figure 11.10. “Fit” joint condition

Translational assembly parameters are calculated by evaluating the minimum distance between two axes. Thus, by using the axis definition given in equation [11.6], we can write:

$$\begin{cases} P_O = P_{OP} + t_1 \cdot N_{OP} \\ P_T = P_{TP} + t_2 \cdot N_{TP} \end{cases} \quad [11.11]$$

and the distance becomes:

$$d_{\text{line-line}}(t_1, t_2) = \|P_O - P_T\| \quad [11.12]$$

The minimum value of function [11.12] can be found by calculating the partial derivatives with respect to  $t_1$  and  $t_2$ , as proposed in [LEN 03]. Once  $t_1$  and  $t_2$  are calculated, translational assembly parameters become:

$$\Delta_{iA} = [P_O(t_1) - P_T(t_2)] \cdot i, \quad \forall i = x, y, z \quad [11.13]$$

Equation [11.13] states that translational assembly parameters are the components, along the global coordinate frame, of the vector  $P_O(t_1) - P_T(t_2)$ .

### 11.3.2. Over-constrained assembly

Over-constrained assemblies may deform during the assembly phase. When deformation is neglected, all constraint equations can be solved simultaneously. In this chapter, a non-linear least squares solution is adopted.

The aim is to determine the best assembly configuration of the object part with respect to all assembly joint constraints. Therefore, an optimization algorithm is used. The objective function is built up by evaluating the distances of the object plane and object axis with respect to the target plane and target axis, respectively.

Looking at Figures 11.7 and 11.10, the distances from object and target planes are:

$$\text{dist}_{\text{against},i} = \left| (\mathbf{P}_{\text{TP}} - \mathbf{P}_{\text{OP},i}) \cdot \mathbf{N}_{\text{TP}} \right| \quad \forall i = \text{I, II, III, IV} \quad [11.14]$$

whereas, the distances between object and target axes are:

$$\text{dist}_{\text{fit},i} = \left\| (\mathbf{P}_{\text{TP}} - \mathbf{P}_{\text{OP},i}) \wedge \mathbf{N}_{\text{TP}} \right\| \quad \forall i = \text{I, II} \quad [11.15]$$

Point  $\mathbf{P}_{\text{OP},i}$  is iteratively updated by means of relationship [11.16].

$$\mathbf{P}_{\text{OP},i} = \begin{bmatrix} 1 & -\gamma_A & \beta_A & \Delta_{xA} \\ \gamma_A & 1 & -\alpha_A & \Delta_{yA} \\ -\beta_A & \alpha_A & 1 & \Delta_{zA} \\ 0 & 0 & 0 & 1 \end{bmatrix} \cdot \begin{Bmatrix} \mathbf{P}_{\text{OPx},i} \\ \mathbf{P}_{\text{OPy},i} \\ \mathbf{P}_{\text{OPz},i} \\ 1 \end{Bmatrix} \quad [11.16]$$

Thus, in the least squares sense, the assembly objective function may be written as in equation [11.17], where “ $N_{\text{fit}}$ ” and “ $N_{\text{against}}$ ” are the number of “fit” and “against” joint conditions, respectively.

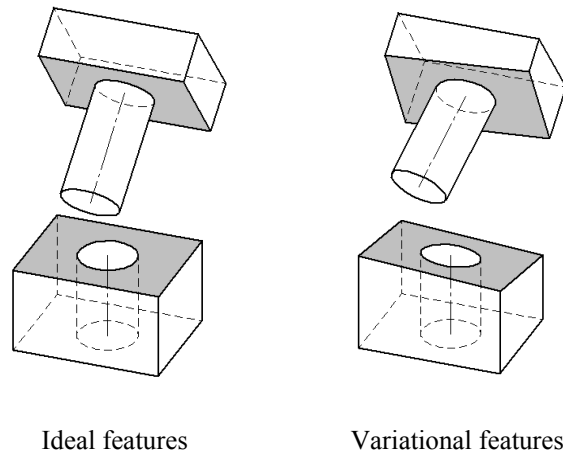
$$J_{\text{over}}(\alpha_A, \beta_A, \gamma_A, \Delta_{xA}, \Delta_{yA}, \Delta_{zA}) = \sum_{i=1}^{2 \cdot N_{\text{fit}}} d_{\text{fit},i}^2 + \sum_{j=1}^{4 \cdot N_{\text{against}}} d_{\text{against},j}^2 \quad [11.17]$$



It can be highlighted that equation [11.17] simultaneously considers all small motion parameters. Function “ $J_{\text{over}}$ ” can be minimized by using any non-linear least squares routine, such as the MatLAB® “lsqnonlin”.

#### 11.4. Case study one: assembly of two-part assembly

The proposed methodology, aimed both at detecting contact between planes and aligning axes, was tested on the two-part assembly, depicted in Figure 11.11.



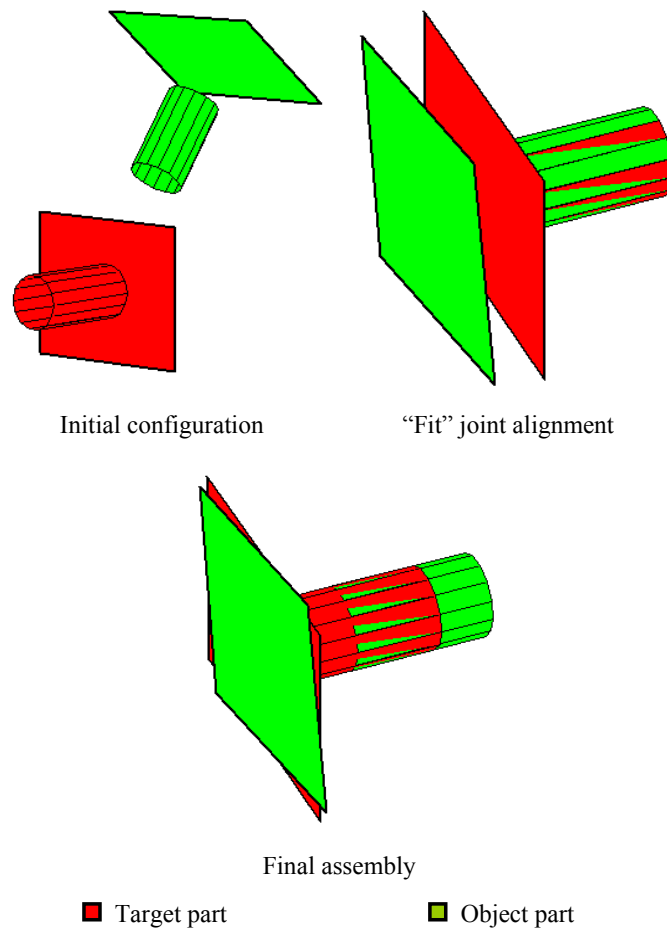
**Figure 11.11.** *Two parts being assembled*

Two assembly sequences, A and B, were analyzed. For the assembly sequence A, target and object planes are aligned after best fitting axes. Vice versa, in the second assembly sequence, B, target and object axes are aligned after best fitting planes.

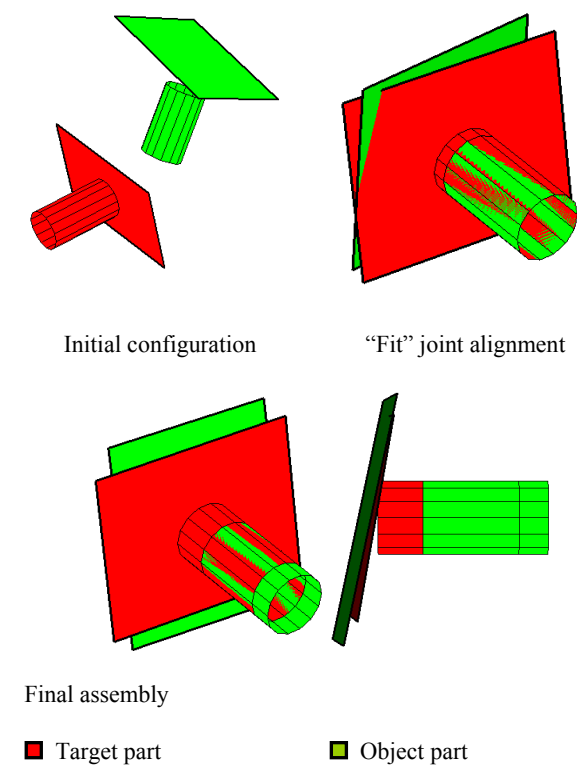
Figures 11.12 and 11.13 depict assembly configurations both for ideal and variational features, with respect to the assembly sequence A. Variational features were generated by applying the numerical procedure summarized in section 11.2 (all numerical simulations were performed in MatLAB®).

It can be highlighted that plane-to-plane contact becomes a three point contact (full contact) for ideal features, whereas it degenerates into a two point contact (partial contact) for variational features. Moreover, after the “fit” joint alignment, variational planes partially intersect (see Figure 11.13). Only by introducing the “against” joint is the right-contact between mating planes assured.

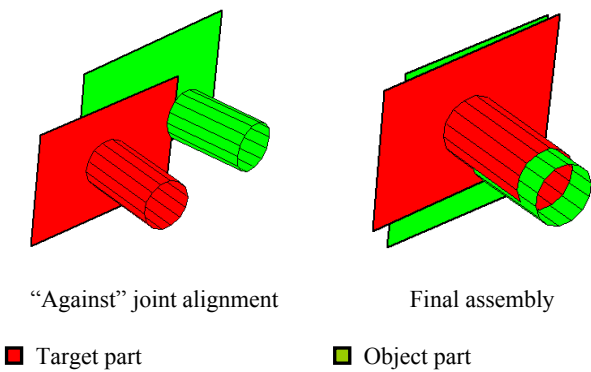
What happens for the assembly sequence B is depicted in Figure 11.14 (only variational features are depicted). In this case, the “against” joint assures a full contact between mating planes. Then, the “fit” joint tries to best align the two axes. However, cylindrical surfaces intersect each other. The proposed model does not take into account contact between cylindrical surfaces, but allows us to best fit the related axes. Therefore, for more realistic results, mating part flexibility should be introduced into the model.



**Figure 11.12.** *Assembly of ideal parts (sequence A)*



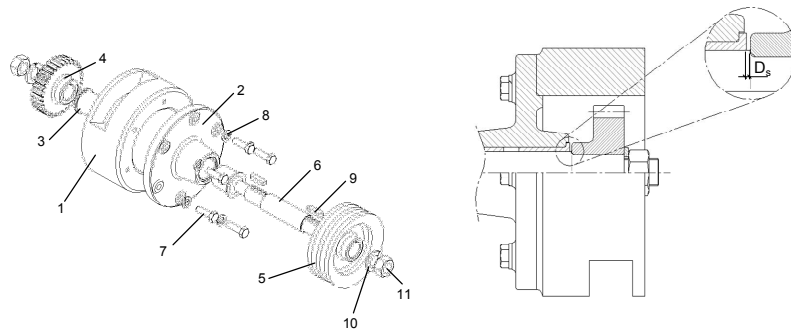
**Figure 11.13.** *Assembly of variational parts (sequence A)*



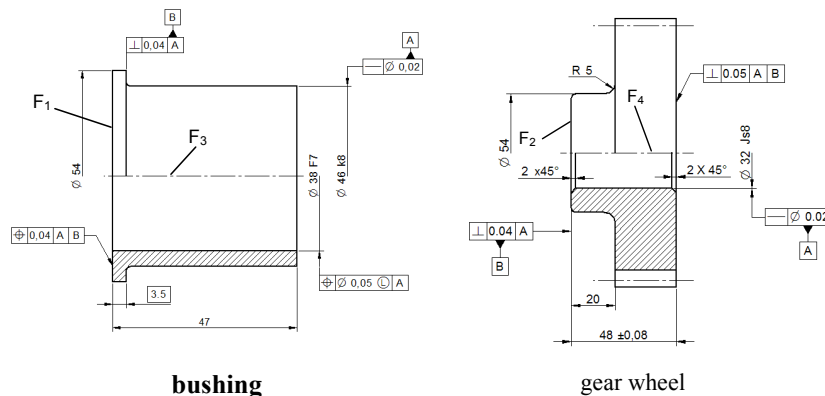
**Figure 11.14.** *Assembly of variational parts (sequence B)*

### 11.5. Case study two: industrial application

Figure 11.15 shows a transmission device. The aim is to analyze the functional distance,  $D_s$ , between features  $F_1$  and  $F_2$ , and the functional angle,  $A_n$ , between features  $F_3$  and  $F_4$  (see Figure 11.16).



**Figure 11.15.** Industrial application: 1-frame; 2-boss; 3-bushing; 4-gear wheel; 5-pulley; 6-shaft; 7-screw; 8-spring washer; 9-key; 10-washer; 11-screw nut



**Figure 11.16.** Tolerance specifications for the gear wheel

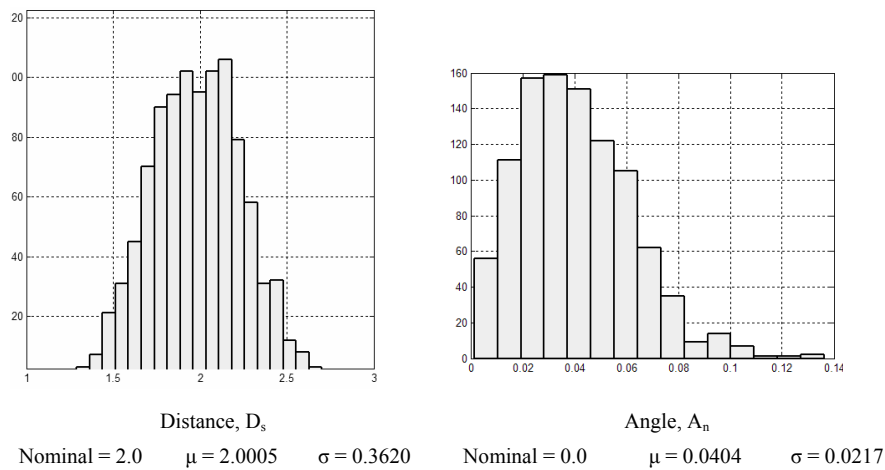
Functional requirements,  $D_s$  and  $A_n$ , depend on shaft rotation. In this chapter, the whole device was analyzed statically; thus, no shaft rotation was taken into account. Tolerances were assigned for each part. In particular, Figure 11.16 shows tolerance specifications for the bushing and the gear wheel. Each tolerance was modeled with a statistical normal distribution. The Monte Carlo method was used to generate random variational features, according to tolerance ranges. The following assembly

sequence was adopted: frame + boss + bushing + shaft + gear wheel. All parts that do not influence functional requirements,  $D_s$  and  $A_n$ , were not considered in the simulation. Table 11.1 shows the joint sequences used to constrain each part.

Parts	Joints
Frame + boss (I)	“against” + “fit”
Frame + bushing (II)	“fit” + “against”
Bushing + shaft (III)	“fit”
Shaft + gear wheel (IV)	“fit” + “against”

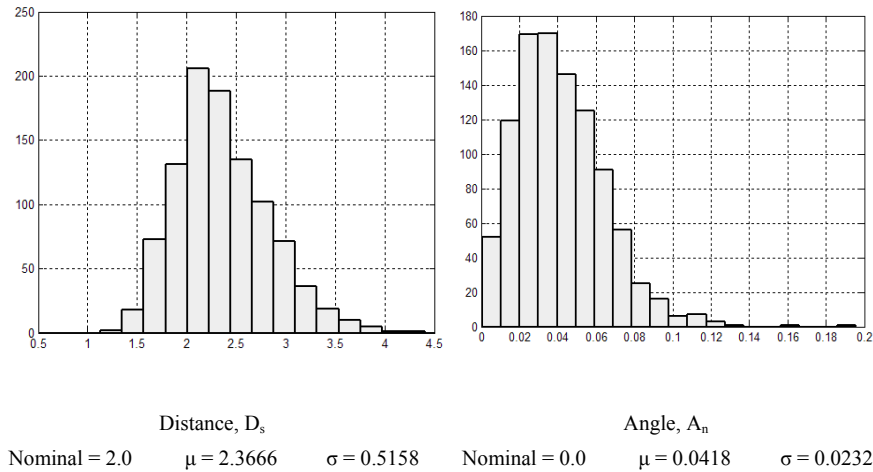
**Table 11.1.** Joint conditions adopted into analysis

Figure 11.17 shows the histogram of frequencies related to distance  $D_s$  and angle  $A_n$ .



**Figure 11.17.** Histogram of frequencies for functional requirements  $D_s$  and  $A_n$ .  
Number of Monte Carlo simulations = 1,000

It is of interest to verify assembly functional requirements when changing one of the joints in Table 11.1. In particular, joint (I) was inverted (now it is assumed as “fit”+“against”). Figure 11.18 shows the histogram of frequencies related to distance  $D_s$  and angle  $A_n$ , respectively, with respect to this new assembly constraint condition.



**Figure 11.18.** Histogram of frequencies for functional requirements  $D_s$  and  $A_n$ .  
Number of Monte Carlo simulations = 1,000; inverted joint (I)

## 11.6. Conclusions

In this chapter a numerical procedure was proposed to simulate assembly constraints among variational features. “Against” and “fit” joint conditions were modeled among planar and cylindrical surfaces.

For fully-constrained assemblies a sequential solver is proposed. Each assembly constraint is solved according to the DoFs of the object part. Best alignment among object and target parts is performed in two consecutive steps: in the first one, assembly rotational parameters are calculated by minimizing a scalar function; then, assembly translational parameters are evaluated by using a linear contact algorithm.

For over-constrained assemblies, all constraint equations are solved by using a non-linear least squares approach.

Two case studies were analyzed. The first one showed how the proposed constraint solver allows us to simulate different assembly sequences. More realistic results can be reached by combining contacts among cylindrical surfaces and FEM-based simulations into the assembly constraint model. In the second application, functional requirements among variational features were calculated by combining Monte Carlo simulation and the constraint solver. Numerical simulations highlighted that the assembly sequence and order of mating joints strongly influence final assembly deviations.

### 11.7. Bibliography

- [ASM 94] ASME, “Dimensioning and Tolerancing”, *ASME Y14.5M-1994*, American Society of Mech. Engineers, New York, 1994.
- [ASM 04] ASME, “Mathematical Definition of Dimensioning and Tolerancing Principles”, *ASME Y14.5.1M-1994*, American Society of Mech. Engineers, New York, reaffirmed 2004.
- [CLE 98] CLÉMENT A., RIVIÈRE A., SERRÉ P., VALADE C., “The TTRSs: 13 Constraints for Dimensioning and Tolerancing”, in *Geometric Design Tolerancing: Theories, Standard and Application*, Chapman and Hall, New York, 1998.
- [FRA 08] FRANCIOSA P., GERBINO S., LANZOTTI A., PATALANO S., “A Numerical Methodology for Worst-Case and Statistical Tolerance Analysis of Rigid Part Assemblies”, *Proc. of the CIRP-ICME*, Naples, 2008.
- [GER 07] GERMAIN F., GIORDANO M., “A New Approach for three-Dimensional Statistical Tolerancing”, *Proc. of the CIRP-CAT*, Erlangen, Germany, 2007.
- [GIO 05] GIORDANO M., SAMPER S., PETIT J. P., “Tolerance Analysis and Synthesis by means of Deviation Domains, Axi-Symmetric Cases”, *Proc. of the CIRP-CAT*, Tempe, Arizona, 2005.
- [KIM 04a] KIM J. S., KIM K. M., LEE J., JUNG H. B., “Solving 3D Geometric Constraints for Closed-Loop Assemblies”, *Int. Journal in Adv. Manuf. Technologies*, vol. 33, pp. 755–761, 2004.
- [KIM 04b] KIM J. S., KIM K. M., LEE J., JEONG J., “Generation of assembly models from kinematic constraints”, *Int. Journal in Adv. Manuf. Technologies*, vol. 16, pp. 131-137, 2004.
- [KIM 05] KIM J. S., KIM K. M., CHOI K., LEE J., “Solving 3D geometric constraints for assembly modeling”, *Int. Journal in Adv. Manuf. Technologies*, vol. 16, pp. 843–849, 2005.
- [KRA 92] KRAMER G. A., *Solving Geometric Constraint System: a Case Study in Kinematics*, MIT Press, 1992.
- [ISO 04] ISO 1101-2004, Geometrical Product Specifications Geometrical Tolerancing - Tolerances of Form, Orientation, Location and Run-out, 2004.
- [JIA 05] JIAN A. D., AMETA G., DAVIDSON J. K., SHAH J. J., “Tolerance Analysis and Allocation using Tolerance-Maps for a Power Saw Assembly”, *Prof. of the CIRP-CAT*, Tempe, Arizona, 2005.
- [LEN 03] LENGUEL E., *Mathematics for 3D Game Programming and Computer Graphics*, Charles River Media, 2<sup>nd</sup> Edition, 2003.
- [MEA 97] MEADOWS J. D., *Geometric Dimensioning and Tolerancing, Applications and Techniques for Use in Design, Manufacturing, and Inspection*, 1997.

- [SHA 07] SHAH J. J., AMETA G., SHEN Z., DAVIDSON J. K., “Navigating the Tolerance Analysis Maze”, *Computer-Aided Design & Applications*, vol. 4, pp. 705-718, 2007.
- [SHE 05] SHEN Z., AMETA G., SHAH J. J., DAVIDSON J. K., “A Comparative Study of Tolerance Analysis Methods”, *Int. Journal of Computing and Information Science in Engineering*, vol. 5, pp. 247-256, 2005.
- [TAN 92] TANAKA F., MURAI M., KISHINAMI T., TOKUNAGA H., “Constraint Reduction based on a Lie Algebra for Kinematic Analysis of Assembly”, *IEEE Transactions on Robotics and Automation*, pp. 741–750, 1992.
- [TUR 92] TURNER J. U., SUBRAMANIAM S., GUPTA S., “Constraint Representation and Reduction in Assembly Modeling and Analysis”, *IEEE Transactions on Robotics and Automation*, pp. 741–750, 1992.
- [WHI 04] WHITNEY D. E., *Mechanical Assemblies, Their Design, Manufacture, and Role in Product Development*, Oxford Univ. P, 2004.
- [WRI 02] WRIGGERS P., *Computational Contact Mechanics*, Wiley, New York, 2002.



## Chapter 12

# Tolerance Analysis with Detailed Part Modeling

### 12.1. Introduction

Currently most commercial tools for computer-aided tolerance analysis have to use simplified or abstracted models of part geometry and assembly to handle the required number of samples for meaningful statistical analysis. For example, planes remain flat surfaces, they are only tilted although shape deviations are defined. With these simplifications typically 10,000 to 30,000 samples with random deviation values are simulated, which allows a reasonable statistical analysis. The simplified model cannot be used in every case to represent and detect the arising deviations resulting from form tolerances. To include shape deviations in tolerance analysis, geometric models of higher detail are required, especially when all possible types of deviations should be taken into account. This leads to computationally expensive operations for the simulated assembly of parts. Therefore, detailed part models are not used for tolerance analysis in commercial CAT systems.

In this chapter a method which allows the analysis of a large number of part samples with high geometric detail in acceptable runtime is proposed. For the representation of the parts, triangle meshes of high resolution have been chosen. This allows the generation of arbitrary deviations within tolerance range by changing the position of the mesh vertices. In this chapter the simulated parts with deviations are referred to as non-ideal parts. The calculation of the relative position between these parts is much more complicated than the positioning of simplified

---

Chapter written by Tobias STOLL, Stefan WITTMANN and Harald MEERKAMM.

contact surfaces, but enables a reasonable integration of shape deviation impacts. To position the parts an optimization method is used, which consists of defined contact surfaces without collisions. Brute force collision detection (intersecting every  $n$  triangles of the non-ideal part with all  $m$  triangles of its environment) would take  $n$  times  $m$  intersection tests. By using hierarchical data structures, so-called kd-trees, this number is reduced drastically. To generate an assembly the parts are positioned successively in a given, defined assembly order. To generate  $x$  assemblies consisting of  $y$  parts, a large number of positioning steps ( $x \cdot (y-1)$ ) has to be made. However, often the positioning steps do not influence each other and therefore can be performed independently. To assure that one positioning step is independent of the other steps, a method has been developed to determine the maximum influence range of each non-ideal part. If the currently analyzed part is never in the range of the remaining assembly, the part can be independently placed on its contact surface. This reduces the necessary number of positioning steps significantly. To further accelerate the developed algorithm, it is parallelized to take advantage of multi-core processors.

## 12.2. Related work

When simulating the assembly of deviated parts, the non-ideal part has to be repositioned dependent on the surrounding parts. This process is called relative positioning. Several approaches to reposition planar parts can be found, e.g. in [LI 01] and [OST 05]. Here the parts are deformed by adding small displacement vectors on the edge vertices of the ideal part. Sodhi and Turner formulated relative positioning as an optimization problem [SOD 94], limited to planar parts. Based on [SOD 94], Inui, Miura and Kimura presented a method to calculate optimal intersection-free positions for non-ideal 2D parts [INU 95], represented by a fine polygonal representation of the parts' 2D-surface. Their method limits the search space to areas where the positioned part lies close to its counterparts. Still, only 2D problems are handled, which consists of two translational and one rotational degree of freedom for the positioned part.

In [STO 07] a framework for relative positioning with heuristic optimization is presented. The framework handles three-dimensional triangle meshes as part models and allows the modular definition of optimization criteria for the part positions (i.e. minimum distance, position tolerances).

The search space for three-dimensional rigid assemblies consists of six dimensions (three translational and three rotational degrees of freedom). The optimization process tries to find a six-dimensional position which is rated "positively" by the evaluation functions. These functions represent constraints like the prevention of part intersections or the minimization of defined distances. As a

source of non-ideal parts, mesh deformation methods described in [STO 06] are used; statistical tolerance simulations, manufacturing simulations or measurements of real parts could also be integrated.

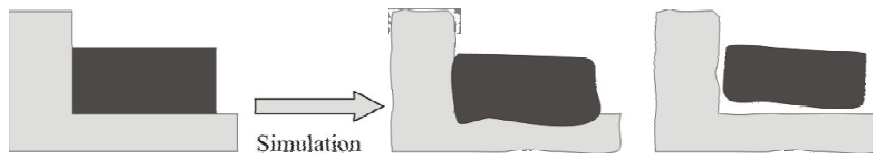
In [PIE 07], Pierce *et al.* describe a method where parts generated by end-milling operations are measured. The resulting NURBS-based solid models are positioned using a mathematical programming formulation. The algorithm takes into account two criteria:

- minimization of the distance between two adjacent faces;
- avoidance of collisions.

Distance and collisions are calculated by sampling one NURBS-face with a certain amount of points, and determining the distance of each point to the other face. If the distance is negative, the two faces collide, and the resulting distance is multiplied by a large constant. An optimization method is used to iteratively calculate the position of the non-ideal part.

### 12.3. The proposed modeling and analysis of toleranced assemblies

This section is an overview about the proposed part modeling and analysis method. The methods used for simulating part variance and relative positioning are explained in detail in the following two sections.



**Figure 12.1.** Positioning problems arising from shape deviations

To be able to include shape deviations appropriately into tolerance analysis the part geometry is simulated without simplification or abstraction. Therefore a fine triangular mesh with high accuracy is generated. The non-ideal parts are then generated by moving each vertex of the triangle mesh. The applied method assures that the resulting parts fulfill the tolerance definition of the product developer, like parallelism or roundness. Details about the method can be found in the next section. Thereafter the simulated parts have to be assembled according to the defined assembly order. For that reason a transformation matrix is calculated which positions the part appropriately. This is, compared to commonly used tolerance

analysis methods, much more difficult, since the non-ideal parts may have collisions or may float (see Figure 12.1).

To calculate the matrices, an optimizer is used which positions the part as close as possible to the contact surfaces without collisions. A particle swarm optimizer (PSO) is used to find an acceptable position. Therefore, objective functions have been defined to integrate collision detection and distance between two surfaces. When the position matrices are calculated, the results have to be presented to the user of the software in an appropriate way. With the proposed method it is possible to define different measurements after the analysis has run, presented as distribution curves like in other tolerance analysis methods. Additionally, the resulting assemblies can be visualized. If the positioning of some or all of the generated non-ideal parts is not possible this is determined without the need for measurements.

#### 12.4. Simulation of non-ideal parts

To simulate non-ideal variants of a part, a triangle mesh is generated out of the CAD-geometry and the vertices of the mesh are changed inside the defined tolerances. To apply this method it is important that the utilized mesh generator fulfills the following properties:

- **Low triangulation error:** triangle meshes can only approximate curved surfaces (see Figure 12.2). To assure that the simulation inaccuracy is low, the mesh should have a small error. The error can be reduced by generating more triangles. In practice a compromise between computational error and efficiency has to be made. If no additional accuracy is needed for visualization, good results have been achieved by setting the triangulation error to 1% of the smallest tolerance range.

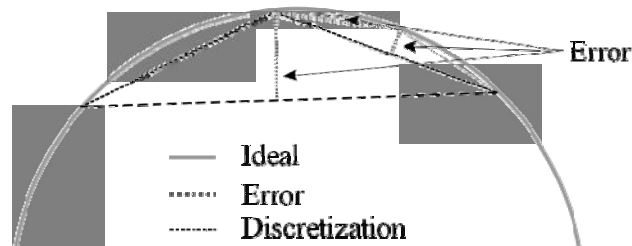


Figure 12.2. Discretization error of meshes approximating an arc

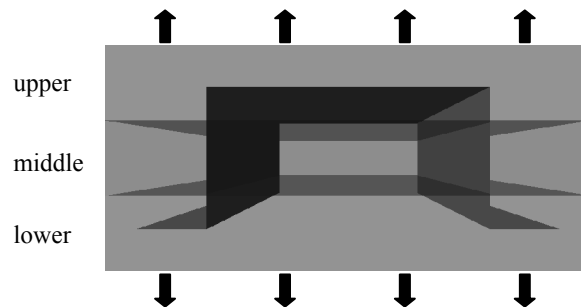
- **Fine mesh:** since the non-ideal parts are generated by moving each vertex of the mesh, and changes of the shape of the parts have to be made, it must be assured that the mesh is fine. One problem is that most available meshers only generate a

few triangles for planar surfaces. This problem can be avoided by specifying a maximum edge length for each triangle.

Sussner [SUS 08] describes different meshing technologies which allow a user to specify triangulation error and maximum edge length. Additional properties, which are important for high quality visualizations (e.g. edge neighborhood), are also discussed in his work.

To generate a part with deviations from the triangle mesh, it is not sufficient to simply scale a part. A scaled part would not exhaust the whole tolerance range for arbitrary geometry. Therefore, the following method is used (see [STO 06] for details):

- the ideal part is divided into different intervals. In each interval a function  $f(x, y, z) \rightarrow (x', y', z')$  is defined, which assigns a new coordinate for each vertex inside the interval. To increase the height of the part (as shown in Figure 12.3), in the upper interval a function adds a value in the  $z$  direction, while a function in the lower interval decreases the value in the  $z$  direction. To avoid big triangles at the border of the intervals, in the middle interval a function interpolates between the changes in the  $z$  direction between upper and lower interval.



**Figure 12.3.** *Changing the height of a part using the described interval method*

### 12.5. Relative positioning

The developed relative positioning algorithm is described in this section. As illustrated in [PIE 07] and [STO 05] the position is calculated by minimizing summed up objective functions with an optimizer (see Figure 12.4).

The objective function presented in section 1.5.1 represents constraints like the prevention of part intersections and the locating scheme. Section 1.5.2 describes the optimizer used followed by several approaches to speed up the computation.

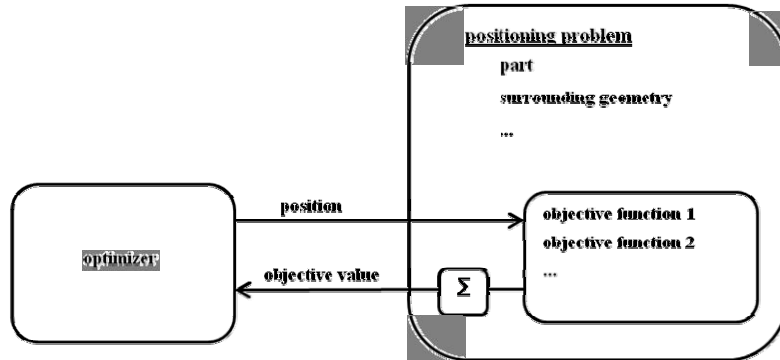


Figure 12.4. The relative positioning framework

### 12.5.1. Defined objective functions

The resulting objective function is a weighted sum of two different functions: the binary collision detection function and the distance function.

#### 12.5.1.1. Binary collision detection

Since collisions between the parts must be avoided, a collision detection algorithm is used to determine if a position which is evaluated by the optimizer causes an interference between parts. To detect the collisions, the PQP library is used, which is based on [GOT 96]. Brute force collision detection (testing each triangle of one mesh for collisions with each triangle of the environment) would be computationally expensive. Instead hierarchical data structures are used for both meshes to reduce the number of triangle-triangle intersection tests. The algorithm used is binary, which means that it only detects if collisions occur, but no quantitative value is returned on how deep the parts are interfering.

#### 12.5.1.2. Distance function

To define the position of a part clearly, a locating scheme is used. Söderberg *et al.* describe different locating schemes in [SÖD 06]. In the case of detailed part modeling the locating scheme is represented by the distance of each vertex of one non-ideal surface to a datum plane.

To calculate the distance between a triangle mesh and a datum plane, each point  $p$  of the triangle mesh is inserted into the plane equation ( $n$  is the normal vector of the plane,  $d_n$  is the distance of the plane to the origin):

$$d(p) = p \cdot n - d_n \quad [12.1]$$

If at least one point results in a negative value of  $d$ , a part of the mesh lies on the wrong side of the plane. A high constant value is returned as the result of the objective function in this case. Otherwise the sum of all distances of all points is returned. To reduce the error generated by the summation of a very large amount of floating point values which are in about the same range, the following recursive algorithm for summing a floating point array  $d$  (reaching from  $start$  to  $end$ ) is used:

```
sum(float[ ] d, int start, int end) {
    if (start==end) return d[start];
    mid = (start+end)/2;
    return sum(d, start, mid)
           + sum(d, mid+1, end);
}
```

If the sum can be calculated by simply adding all distances in one variable, the error resulting from floating point operations is significantly higher (see [MAL 71]).

To position the part it is often necessary to use more than one plane. In the example presented in section 12.7, three different datum planes were used to position each part. The result of this method is comparable to other existing locating schemes, like the 3-2-1 locating scheme and can handle shape deviations.

### 12.5.2. Particle swarm optimization

The approach of finding a good position for a non-ideal part by systematic sampling of the search space is computationally expensive: a relatively coarse sampling of 100 values per dimension would produce  $100^6$  position evaluations. Therefore, heuristic methods have been used to find solutions in acceptable time. Particle swarm optimization (PSO) is a relatively new heuristic optimization approach which was developed by Kennedy and Eberhart [KEN 95]. The algorithm imitates the behavior of individuals (called particles) in a swarm. Transferred to the relative positioning problem, each particle has a six-dimensional position, which represents the part's translation and rotation vector. Each particle moves through the 6D search space with a certain velocity and is attracted by the best found solution of particles in its neighborhood.

A neighborhood topology defines which particles can communicate directly, for example the whole swarm is connected or only adjacent swarm members are connected; see [MEN 03] for details. Additionally, each particle remembers the position of the best position it has reached so far. In each iteration step, the position and velocity of all particles is updated, taking into account the previous velocity, the position of the best neighbor and the own best found solution. For the studied positioning problem, the PSO showed the best and most robust performance,

compared to other tested heuristic approaches like evolutionary strategy, simulated annealing and problem-specific approaches.

### **12.5.3. Independence of the positioning steps**

To calculate one final part position the optimizer has to evaluate the objective function about 5,000 times or even more. This is, contrary to commonly used tolerance analysis methods, very time consuming. If an assembly with  $y$  parts is used for tolerance analysis, and  $x$  samples have to be generated  $x \cdot (y-1)$  positioning steps have to be made (assuming that the first part is not positioned).

In some cases the positioning of one part is only dependent on the contact surface on which it is positioned. It is not possible that it has collisions with other surrounding geometry (for example, chip 2 in Figure 12.5). The positioning is only dependent on the surface where it has to be placed. If the same non-ideal part has to be positioned on the same non-ideal surface in another of the samples it is possible to use the matrix that has already been calculated. In the Monte Carlo simulation a different non-ideal part is chosen for every assembly. The proposed acceleration cannot be used in this case. If instead a number of non-ideal parts are created at the beginning of the simulation, the desired amount of assemblies can be simulated by combining all non-ideal parts with each other. This method reduces the number of part variants drastically, but enables us to take advantage of the independence. If for example 10,000 samples of an assembly with five parts have to be calculated, and three parts are independent, the number of positioning steps is reduced from 40,000 to 300 (assuming, that 10 non-ideal part variants are generated). Because the number of generated parts is reduced, the method will not be as accurate as a Monte Carlo simulation, but the results can be generated much faster.

To determine automatically if a part is independent, a sphere which enclosing the part is generated. Afterwards an offset is added to the radius of the sphere, depending how big the search space for the relative positioning of the part is. Then an intersection test between the sphere and all other parts is made to determine which parts are inside the sphere. If more than one part is inside the sphere, the part is not independent.

### **12.5.4. Parallelization**

When parallelizing the relative positioning, there are several approaches of different granularity. The tasks distributed over the available processors can be:

- the complete positioning of one part;



- the evaluation of a single position of a part in search space;
- the evaluation of one component of the summed up objective function;
- the evaluation of a portion of an objective function.

To be able to speed up the process even if a single part is positioned, option 2 was chosen. The parallelization was implemented as an asynchronous master slave scheme that can be found in [VEN 05]: the master process distributes the evaluation of particle positions to free processors, until the complete swarm is evaluated and the next iteration can start. First results were encouraging: on a heterogeneous cluster of three PCs, the measured speedup factor was 2.1; on a Dual-Core PC, the speedup factor was 1.7. Therefore, the parallelization has significant effects on the relative positioning computation time; the benefit will even increase due to current processor developments (i.e. systems with two QuadCore CPUs).

### 12.6. Analysis of the positioned assemblies

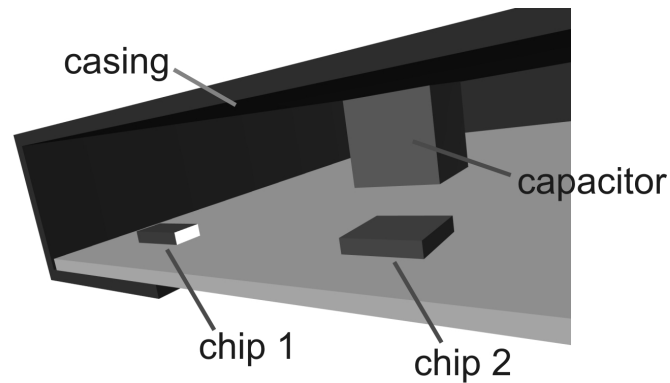
In commonly used CAT systems, results of the simulation are presented as distribution curves and statistical properties. Because the proposed method applies changes to triangle meshes of the parts it is possible to generate visualizations of the resulting assemblies (see Figure 12.6). The user can, e.g. visualize the assemblies with high deviations and will get an impression of the effect of the specified tolerances very fast. Aesthetic as well as functional properties of the assemblies can be revealed. By defining measurements between part features it is also possible to calculate distribution curves. Since the geometry of each non-ideal assembly is generated by the method, measurements can be calculated for each assembly and then summarized to obtain the distribution curve.

The results of the positioning can also be included in standard CAT-tools, which do not simulate the positioning effects of shape deviations (see Figure 12.7). The calculated transformation matrices of parts where shape deviations have a great impact can be used as input for the Monte Carlo simulation. This produces a compromise between standard CAT-simulation and the presented computationally expensive method.

### 12.7. Example

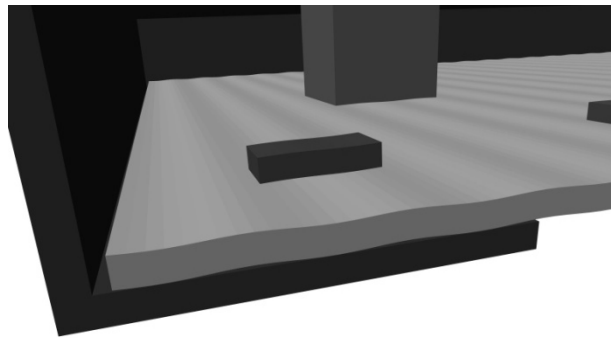
As an example, two chips and one capacitor are positioned on a circuit board, then the resulting assembly is put into a casing (see Figure 12.5). All surfaces of the circuit board are toleranced with a flatness of 1.0 mm, the surfaces of the chips and

the capacitor have a flatness of 0.5 mm. Exaggerated values have been used to generate visible defects.



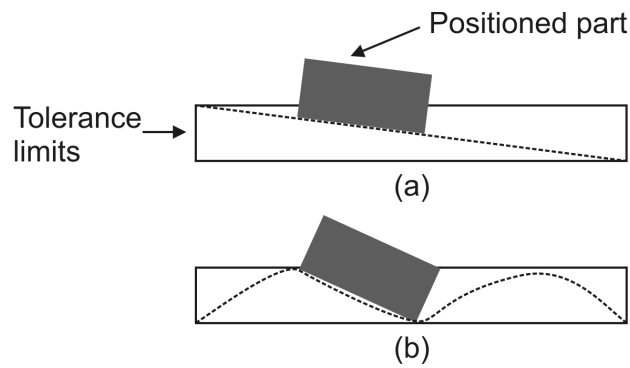
**Figure 12.5.** *Ideal circuit board and casing*

For the chips, the capacitor and the circuit board different non-ideal part variants with waviness have been generated within the tolerance limits. After this, the relative positioning algorithm has been applied. A visualization of a possible non-ideal assembly scenario with deviations is shown in Figure 12.6.



**Figure 12.6.** *Positioned non-ideal circuit board and electronic devices*

In commonly used tolerance analysis tools, the ideal plane of the circuit board would only be tilted. This would lead to a much smaller slope of the electronic devices compared to the above example; see Figure 12.7 for a comparison.



**Figure 12.7.** Comparison between different deviation types

Another advantage of the method is the integrated collision detection. If for example different capacitors or casings can be used, and this results in a collision between the capacitor and the upper surface of the casing, the algorithm presented detects the collision without the need of defining any measurements. This can prevent errors when design changes are made, and tolerance definitions are adopted from the previous design.

Regardless of the method used for positioning, a Monte Carlo analysis of an assembly has the run-time complexity  $m \cdot n \cdot c$ , where  $m$  is the number of generated assemblies,  $n$  the number of positioning steps and  $c$  is the computation time for one part positioning.

In the example presented the algorithm needs about 30 seconds for the positioning of one part ( $=c$ ), depending on size and mesh quality of the parts. Compared to the standard tolerance analysis method, where only some matrix multiplications are performed ( $c < 10\text{ms}$ ), this is extremely long. Nevertheless, the presented acceleration methods were able to significantly speed up the computation compared to [STO 07] and [PIE 07] where  $c \approx 10$  minutes.

## 12.8. Summary

This chapter presents a method which simulates different non-ideal parts with high geometric detail and positions them in an assembly. The approach can be used intuitively, because the inspected geometry is represented completely, and does not have to be simplified or abstracted. All collisions between parts are automatically detected and the generated assemblies can be analyzed with visualization techniques. After the positioning simulation the user can define arbitrary measurements. Corresponding distribution curves can be calculated afterwards. The detailed

geometric modeling increases the computational effort. For this reason different accelerations have been suggested. Hierarchical collision detection, parallelization and independence checks drastically reduce the computation time. Therefore, the presented method can already be used for practical tolerance analysis. It has also been illustrated how the results of the methods can be integrated into existing tolerance analysis tools.

## 12.9. Acknowledgements

The authors acknowledge support from the German Research Foundation DFG, grant PA 1576/1-1. We also like to thank Sabine Helwig for the particle swarm optimizer, Alexandr Gnezdilov for the parallel PSO and Dr. Gerd Sussner for his support in CAD tessellation.

## 12.10. Bibliography

- [GOT 96] GOTTSCHALK S., LIN M.C., MANOCHA D., 1996, "OBB-Tree: A Hierarchical Structure for Rapid Interference Detection", *Proceedings of ACM SIGGRAPH*, 1996, pp. 171-180.
- [INU 95] INUI M., MIURA M., KIMURA F., 1995, "Relative positioning of assembled parts with small geometric deviations by using hierarchically approximated configuration space", *Robotics and Automation*, Vol. 2, pp. 1605-1612.
- [KEN 95] KENNEDY J., EBERHART R.C., 1995, "Particle Swarm Optimization", *Proceedings of IEEE International Conference on Neural Networks*, pp. 1942-1948.
- [LI 01] LI B., ROY U., 2001, "Relative positioning of toleranced polyhedral parts in an assembly", *IEEE Transactions*, Vol. 33, pp. 323-336.
- [MAL 71] MALCOLM M. A., 1971, "On Accurate Floating Point Summation", *Communications of the ACM*, Vol. 14(11), pp. 731-736.
- [MEN 03] MENDES R., KENNEDY J., NEVES J., 2003, "Watch thy neighbor or how the swarm can learn from its environment", *Swarm Intelligence Symposium, 2003. SIS '03. Proceedings of the 2003 IEEE*, pp. 88- 94.
- [OST 05] OSTROSKY-BERMAN Y., JOSKOWICZ L., 2005, "Tolerance envelopes of planar mechanical parts with parametric tolerances", *Computer Aided Design*, Vol. 37 (5), pp. 531-544.
- [PIE 07] PIERCE R.S., ROSEN D., 2007, "Simulation of Mating Between Nonanalytic Surfaces Using a Mathematical Programing Formulation", *Journal of Computing and Information Science in Engineering*, Vol. 7, Nr. 4, pp. 314-321.
- [SÖD 06] SÖDERBERG R., LINDKVIST L., 2006, "Managing Physical Dependencies through Location System Design", *Journal of Engineering Design*, Vol 17(2), pp. 325-346.

- [SOD 94] SODHI R., TURNER J.U., 1994, "Relative positioning of variational part models for design analysis", *Computer Aided Design*, Vol. 26 (5), pp. 366-378.
- [STO 06] STOLL T., 2006, "Generieren von nichtidealer Geometrie", *Symposium Design for X*, Vol. 17, pp. 314-321.
- [STO 07] STOLL T., WITTMANN S., HELWIG S., PAETZOLD K., 2007, "Registration of measured and simulated non-ideal geometry using optimization methods", *Proceedings of the 10th CIRP International Seminar on Computer Aided Tolerancing*, Vol. 10.
- [SUS 08] SUSSNER G., 2008, Methoden zur Erzeugung und Darstellung von tessellierten Daten im Kontext der interaktiven virtuellen Qualitätskontrolle in der Fahrzeugentwicklung, Dissertation, Friedrich Alexander University, Erlangen-Nuremberg.
- [VEN 05] VENTER G., SOBIESZCZANSKI-SOBIESKI J., 2005, "A Parallel Particle Swarm Optimization Algorithm Accelerated by Asynchronous Evaluations", *6th World Congresses of Structural and Multidisciplinary Optimization*.

## Chapter 13

# Assembly Method Comparison Including Form Defect

### 13.1. Introduction

#### 13.1.1. *Topic*

The technological challenge that represents a relevant geometric specification of the mechanical system is, nowadays, a major issue for the control of a product's quality and cost. Mainly, for the past ten years, tolerance methodologies have not accounted for any form defect of the surfaces of the various parts of an assembly. Furthermore, assemblies generated on Computer-Aided Design (CAD) software are based on nominal geometry. With this kind of geometrical modeling, assemblies of parts are realized isostatically and surfaces in contact are modeled without form defects. The next step of geometric computer modeling for mechanical systems will be to generate a more realistic model. This advance will make it possible to simulate hyperstatic assemblies as well as the form defects of their components. To meet this challenge, new optimization and modeling methods must be developed. The aim of this chapter is to show the different modeling strategies of the contact between parts with form defects and multiple configurations of the assembly. This research work is part of a bigger picture trying to assess the relative positions of adjoining components, with defects, in a mechanical system. In this chapter, different aspects such as virtual contact sensor, criteria for optimization and parameterization for the complete assembly, will be detailed. Firstly, we will need to discuss and propose various solutions for the parameterization of the relative position between surfaces.

---

Chapter written by Stéphane MORIÈRE, Jean MAILHÉ, Jean-Marc LINARES and Jean-Michel SPRAUEL.

Secondly, different optimizing criteria or objective functions (minimax, least squares, algebraic norm, Chebyshev criteria, etc.) will be tested on typical assemblies. Thirdly, a number of ways for defining and building contact sensors will be shown (point to point distance, elementary volume collision). A comparative study of the various methods will be done. The evaluation criteria shown will be: the generic aspect of the method, implementation and computing times, accuracy and reliability of results obtained. These comparisons will rely on case studies.

### 13.1.2. Actual lack of CAD

Real surface form defects are, usually, described by four defect orders (ISO 1302:2002). The first order characterizes geometry and form defects. Other orders describe undulation and roughness. Actual CAD software is able to model parts without form defect. This nominal modeling made it possible to create complex systems and specified design characteristics [BAL 01a] (space required, kinematic), but the lack of information of the surface part defects limits the model representation level. In this chapter, we propose a method to describe first order defects in CAD software. This model allows us to model geometry and form defects of parts. To realize this improvement, we had to work on a new description of a part to include form defects and on a new way to assemble these parts.

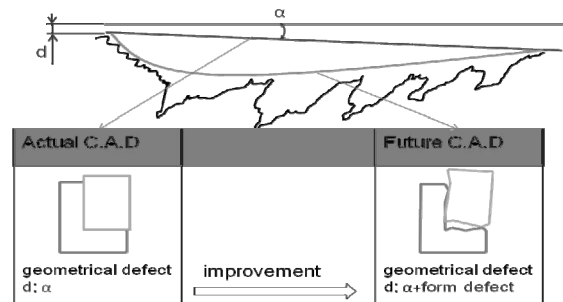


Figure 13.1. Improvement of the CAD

### 13.1.3. State of the art and proposal

Figure 13.2 describes the four principal points required to obtain an assembly with form defect: the part model, the form defect model, the geometric defect model and the assembly model. CAD software use their own native databases to store designed parts, but it can also save these design parts on exchange formats. A native database is usable only in the CAD software which designed the part. This major

disadvantage directed us to an exchange format to model each part of the assembly. STEP format is an exchange format based on the oriented object description of the part. This type of description is not well adapted to complex surface modeling. STL format has been developed for stereolithography and accurately describes the surface geometry of a 3D object. We therefore started with this type of part description, since it is sufficient to define our simple geometries and well adapted to model form defects. To work on a geometric defect model, the TTRS approach [CLE 97] makes it possible to describe the relative situation of surfaces.

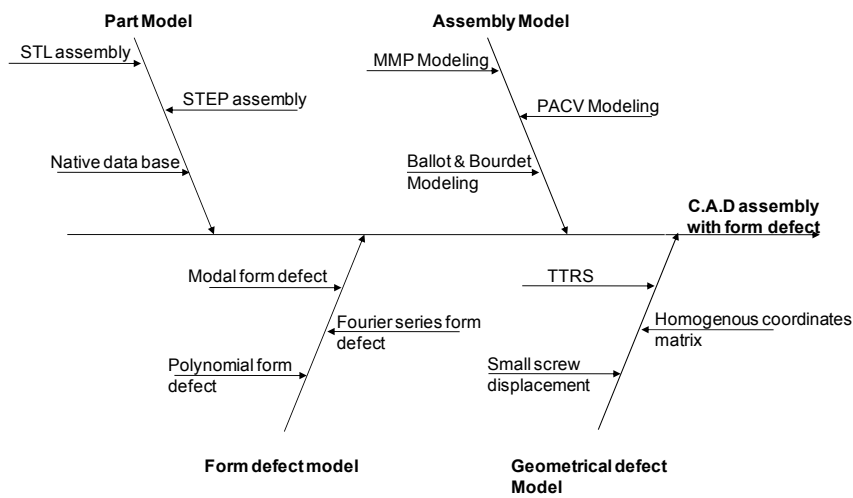


Figure 13.2. Ways to improve the CAD mode

Classical mathematical modeling of geometrical defects (small screw displacement [BOU 88] or homogeneous matrix transformation) can be used in our assembly model to describe the relative position of the surface part to simulate geometric defects. Form defects can be described by different mathematical models like the Fourier series, modal decomposition [FOR 05] or polynomial surface fitting. New part modeling involves a new assembly modeling. Several assembly methods based on clearance volume [TEI 99], manufactured model part [VIG 05] or small screw displacement [BAL 01b] have been developed. To realize CAD assembly with form defects, we work on two assembly models based firstly on distance minimization and secondly on volume minimization.

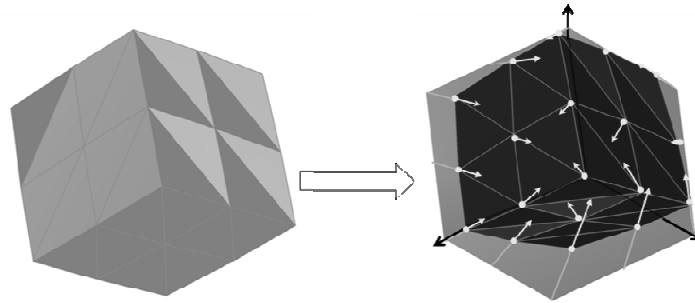


### 13.2. Geometric model for simulation

This section develops the geometric model used to realize an assembly with form defects. First, the creation of parts with form defects is explained. Then an assembly method is presented. Finally, the optimization functions and constraints are detailed.

#### 13.2.1. Part with form defects

STL format describes the geometry of a part through simplex surfaces. Working on CATIA™ CAD software to design nominal parts enabled us to get initial STL representations. The form and geometry defects are applied by simplex node displacement on the initial part.



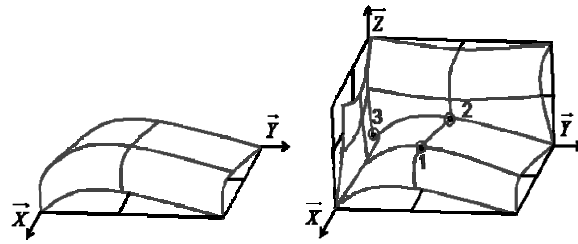
**Figure 13.3.** *Form defect implementation*

To keep part topology, node movement must not split surface contact. This constraint imposes that nodes belonging to multiple surfaces have displacement restrictions. All parts of the assembly studied in this chapter are half cubes; the form defects are applied on face mesh nodes. They have been designed with CATIA™. The STL nodes have been moved through a VB.net™ program.

Polynomial form defects have been fitted on each surface of the part with particular care on limit surface nodes. To simulate form defects, displacements have been applied on an initial node position defined by the initial STL CAD part. Each node is moved in the direction normal to its surface. In our case, the parts are specified with a local reference frame ( $X, Y, Z$ ). The initial position of a node is defined by its coordinates ( $X_0, Y_0, Z_0$ ).  $\Delta X, \Delta Y, \Delta Z$  are the displacements added to the initial coordinates. The values of these displacements are calculated by these equations:

$$\begin{aligned}
 \Delta X(y, z) &= a + b.y + c.y^2 + d + e.z + f.z^2 \\
 \Delta Y(x, z) &= g + h.x + i.x^2 + j + k.z + l.z^2 \\
 \Delta Z(x, y) &= m + n.x + p.x^2 + q + r.y + s.y^2
 \end{aligned}
 \tag{13.1}$$

Figure 13.4 represents a surface with form defect and a half cube with form defect. Node 1 belongs to plane X,Y with form defect, node 2 belongs to planes X,Y and Y,Z and node 3 fits in planes X,Y , Y,Z and X,Z.



**Figure 13.4.** Form defect modeled by a polynomial description

The coordinates of node 1 belonging face X, Y are:

$$\begin{aligned}
 &X0 \\
 &Y0 \\
 &Z0 + \Delta Z(X0, Y0)
 \end{aligned}
 \tag{13.2}$$

The coordinates of node 2 belonging to two faces X, Y and Y, Z are:

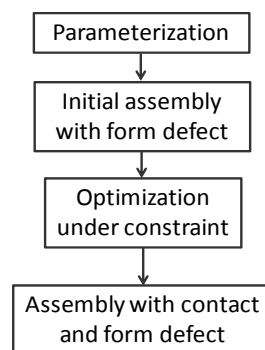
$$\begin{aligned}
 &X0 + \Delta X(Y0, Z0) \\
 &Y0 \\
 &Z0 + \Delta Z(X0, Y0)
 \end{aligned}
 \tag{13.3}$$

The coordinates of node 3 belonging to three faces X, Y; Y, Z and Z, X are:

$$\begin{aligned}
 &X0 + \Delta X(Y0, Z0) \\
 &Y0 + \Delta Y(X0, Z0) \\
 &Z0 + \Delta Z(X0, Y0)
 \end{aligned}
 \tag{13.4}$$

### 13.2.2. Assembly process

The assembly process of nominal parts is controlled nowadays. However, creating an assembly with form defects involves finding a new method connecting these parts. This method needs an initial parameterized assembly. This assembly is composed of parts with form defects localized via local reference frames positioned by three angles and three distances on a global reference frame. The assembly is actualized by the minimization under the constraint of an objective function that will be detailed in following section.

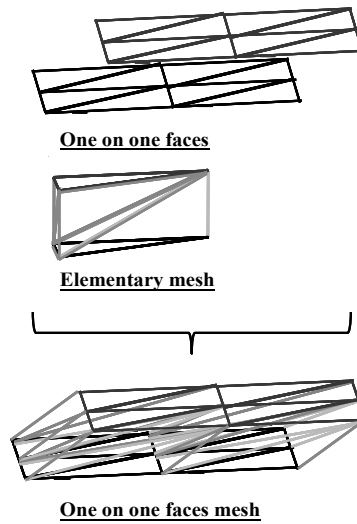


**Figure 13.5.** *Assembly process*

### 13.2.3. Function for optimization

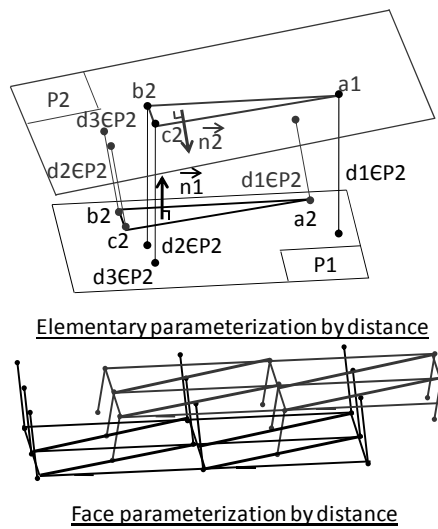
In this chapter two different optimization functions are developed: the first is based on the description of the volume between the two initial parts and the second relies on the calculus of one-on-one face distances. To define volumes, Gram determinants have been used. This mathematical tool enables us to obtain the signed volume of an elementary mesh. The elementary mesh is composed of 3 tetrahedrons. The creation of their geometric entities is made by fitting three tetrahedrons on a couple of one on one STL triangles. The result of the Gram determinant (three oriented vectors pointing on a vertex) is the signed volume of this 3D simplex. Determination of the sum of the three volumes of each elementary mesh gives the elementary mesh volume.

To characterize an assembly, the volume between the one-on-one face of every part of the assembly is decomposed into elementary mesh volumes. The optimization function is the sum of each elementary mesh signed volume.



**Figure 13.6.** *Volume sensor*

To build the optimization function based on one-on-one faces, six scalars have been calculated by pairs of STL triangles.



**Figure 13.7.** *Distance sensor*

The normalized normal vector of each triangle has been defined by the cross product of two vectors defined by the vertex of the STL. Once these unit vectors have been calculated, the scalar products of three vectors ( $a_1a_2$ ,  $b_1b_2$ ,  $c_1c_2$ ) are realized to get the distances between each STL triangle on the opposite face plane. Each couple of STL triangles is characterized by six scalars. The optimization function is the sum of all scalars calculated on the STL assembly.

#### **13.2.4. Constraints**

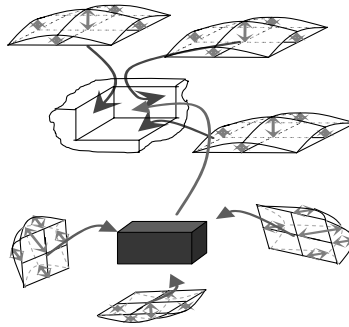
To solve an optimization problem, the definition of this problem must contain a function to minimize, stop criteria, and constraints to enable solver convergence. We have just defined two optimization functions; the stop criterion will be detailed in the next sections. The definition of constraints in this modeling symbolizes the condition of no inter-penetration of assembly parts. Two constraints have been developed, based on the tools explained in previous section, the characterization of volumes and one-on-one distances. The criterion for the constraint based on volumes obliges all signed volumes of each elementary mesh to stay positive. The principle of constraint based on one on one distance is to force all scalars to be positive.

### **13.3. Experimentation**

The topic of this chapter is to realize an assembly method comparison including form defects. The previous section explained the context, presented the assembly method and detailed the different optimization functions and constraints for the assembly. This section introduces the studied case and simulation setup.

#### **13.3.1. Case study**

To compare the assembly methods, a two part model has been realized. An initial assembly without form defect has been designed on CAD CATIA<sup>TM</sup> software in STL format. Polynomial form defects have then been applied on the STL coordinate nodes. Then, the optimization problem has been solved. Finally, the upgraded geometric assembly has been displayed. Figure 13.8 represents the realized initial assembly. It is composed of two half cubes (one part male, one part female), with polynomial form defects applied, remote of definite value. The goal of this experience is to analyze the final contact configuration of the parts in the assembly. Different polynomial defects have been tested to simulate assemblies with different part shapes (convex or concave).



**Figure 13.8.** *Assembly studied case*

Six objective functions have been tested with the two types of constraints previously defined; positive minimum distance or positive minimum volume. This leads to 12 optimization criteria for each of the four simulated cases. The distance gaps between the three one-on-one faces have been summarized, for each criterion, in the tables that follow.

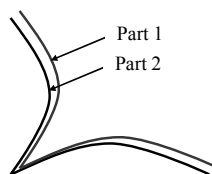
### 13.3.2. *Simulation setup*

The simulation setup contains information on the geometry and the solver parameters of the model. The magnitude of the form defects have been chosen in respect to the usual tolerances of general mechanics.

The initial half cubes have 100 millimeter sides and the absolute values of the polynomial coefficients are 0 for the constant, 0.002 for the first degree parameter and 0.001 for the second one.

## 13.4. Result discussion

### 13.4.1. *Case 1*



**Figure 13.9.** *Contact configuration 1*

This configuration represents an assembly composed of a convex female part (part 2) and a concave male part (part 1). The results obtained after optimization are equivalent for all the 12 criteria. Minimal and maximal gap distances are close and of the order of magnitude of the maximum solver precision ( $10^{-18}$ ). The difference between minimal and maximal distances is due to the solver precision; the contact is reached with an inaccuracy of  $10^{-18}$  mm. This value corresponds to the numerical zero. In this case, all optimization methods can be used to realize the contact between the parts.

n°	Objective function	Constrain	P1maxl	P1minl	P2maxl	P2minl	P3maxl	P3minl	Optimisation method
1	V	Distance >0	6,94E-18	-5,6E-18	6,94E-18	-5,6E-18	6,94E-18	-6,9E-18	Newton (Right tangent)
2	V²		6,94E-18	-5,6E-18	6,94E-18	-5,6E-18	6,94E-18	-6,9E-18	Quadratic gradient
3	MAX V		6,94E-18	-5,6E-18	6,94E-18	-5,6E-18	6,94E-18	-6,9E-18	Newton (Centred tangent)
4	D		6,94E-18	-5,6E-18	6,94E-18	-5,6E-18	6,94E-18	-6,9E-18	Newton (Right tangent)
5	D²		6,94E-18	-5,6E-18	6,94E-18	-5,6E-18	6,94E-18	-6,9E-18	Quadratic gradient
6	MAX D		6,94E-18	-5,6E-18	6,94E-18	-5,6E-18	6,94E-18	-6,9E-18	Newton (Centred tangent)
7	V	Volume >0	6,94E-18	-5,6E-18	6,94E-18	-5,6E-18	6,94E-18	-6,9E-18	Newton (Right tangent)
8	V²		6,94E-18	-5,6E-18	6,94E-18	-5,6E-18	6,94E-18	-6,9E-18	Quadratic gradient
9	MAX V		6,94E-18	-5,6E-18	6,94E-18	-5,6E-18	6,94E-18	-6,9E-18	Newton (Centred tangent)
10	D		6,94E-18	-5,6E-18	6,94E-18	-5,6E-18	6,94E-18	-6,9E-18	Newton (Right tangent)
11	D²		6,94E-18	-5,6E-18	6,94E-18	-5,6E-18	6,94E-18	-6,9E-18	Quadratic gradient
12	MAX D		6,94E-18	-5,6E-18	6,94E-18	-5,6E-18	6,94E-18	-6,9E-18	Newton (Centred tangent)

Table 13.1. Calculation results of case 1

### 13.4.2. Case 2

This configuration represents an assembly composed of a concave female part (part 2) and a convex male part (part 1). The optimization results of this configuration are similar to case 1. The assembly is obtained with the maximum solver precision. Table 13.2 is an abstract of all the results which are identical to Table 13.1. The conclusion in this case is the same as the previous one.

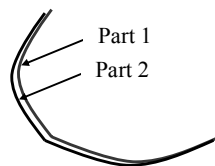


Figure 13.10. Contact configuration 2

P1maxl	P1minl	P2maxl	P2minl	P3maxl	P3minl
6,94E-18	-5,6E-18	6,94E-18	-5,6E-18	6,94E-18	-6,9E-18

Table 13.2. Calculation results of case 2

### 13.4.3. Case 3

The case 3 configuration represents an assembly composed of a convex female part (part 2) and a convex male part (part 1). This configuration is problematic for the solver. Even for real assemblies, it presents geometric instability, since there are multiple configurations which minimize the objective functions. The constraint based on signed volume does not converge as efficiently as the distance constraint. Criteria 1 and 4 need much less calculus time than criteria 2, 3, 5 and 6. Criteria 5 and 6 give a minimal distance smaller than for criteria 1 and 4, subjected to the fact that the results are near the numerical zero.

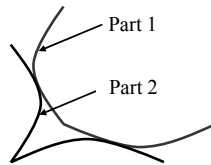


Figure 13.11. Contact configuration 3

n°	Objective function	Constrain	P1maxi	P1mini	P2maxi	P2mini	P3maxi	P3mini	Optimisation method
1	V	Distance >0	0,246377	-1,6E-16	0,246377	-1,6E-16	0,246377	0	Newton (Right tangent)
2	V²		0,266378	2,28E-14	0,256944	1,39E-17	0,287778	0,021474	Quadratic gradient
3	MAX V		0,247263	3,44E-07	0,254813	0,007919	0,246836	3,18E-15	Newton (Centred tangent)
4	D		0,246377	-1,3E-16	0,246377	-1,3E-16	0,246377	2,78E-17	Newton (Right tangent)
5	D²		0,246377	2,08E-17	0,246377	2,08E-17	0,246377	1,39E-17	Quadratic gradient
6	MAX D		0,246377	2,08E-17	0,246377	2,08E-17	0,246377	1,39E-17	Newton (Centred tangent)
7	V	Volume >0	0,221609	-0,02005	0,221609	-0,02005	0,221609	-0,02005	Newton (Right tangent)
8	V²		0,221609	-0,02005	0,221614	-0,02005	0,221608	-0,02005	Quadratic gradient
9	MAX V		0,339935	-0,02166	0,330178	-0,0259	1,264921	1,005352	Newton (Centred tangent)
10	D		0,221609	-0,02005	0,221609	-0,02005	0,221609	-0,02005	Newton (Right tangent)
11	D²		0,221609	-0,02005	0,221609	-0,02005	0,221609	-0,02005	Quadratic gradient
12	MAX D		0,221609	-0,02005	0,221609	-0,02005	0,221609	-0,02005	Newton (Centred tangent)

Table 13.3. Calculation results of case 3

### 13.4.4. Case 4

Case 4 represents an assembly composed of a convex female part (part 2) and a convex male part (part 1). The constraint based on signed volume does not converge as efficiently as the distance constraint. Criteria 1 and 4 need much less calculus time than criteria 2, 3, 5 and 6. Criteria 5 and 6 give a minimal distance smaller than for criteria 1 and 4 subjected to the fact that the results are near the numerical zero.



n°	Objective function	Constrain	P1maxi	P1mini	P2maxi	P2mini	P3maxi	P3mini	Optimisation method
1	V	Distance >0	0,246377	-1,6E-16	0,246377	-1,6E-16	0,246377	-1,6E-16	Newton (Right tangent)
2	V²		0,246379	1,75E-08	0,246379	1,75E-08	0,246379	1,75E-08	Quadratic gradient
3	MAX V		0,247031	5,86E-08	0,247031	5,86E-08	0,247031	5,86E-08	Newton (Centred tangent)
4	D		0,246377	-1,3E-16	0,246377	-1,3E-16	0,246377	-1,3E-16	Newton (Right tangent)
5	D²		0,246377	2,08E-17	0,246377	2,08E-17	0,246377	2,08E-17	Quadratic gradient
6	MAX D		0,246377	2,08E-17	0,246377	2,08E-17	0,246377	2,08E-17	Newton (Centred tangent)
7	V	Volume >0	0,221609	-0,02005	0,221609	-0,02005	0,221609	-0,02005	Newton (Right tangent)
8	V²		0,221609	-0,02005	0,221609	-0,02005	0,221609	-0,02005	Quadratic gradient
9	MAX V		0,221609	-0,02005	0,221609	-0,02005	0,221609	-0,02005	Newton (Centred tangent)
10	D		0,221609	-0,02005	0,221609	-0,02005	0,221609	-0,02005	Newton (Right tangent)
11	D²		0,221609	-0,02005	0,221609	-0,02005	0,221609	-0,02005	Quadratic gradient
12	MAX D		0,221609	-0,02005	0,221609	-0,02005	0,221609	-0,02005	Newton (Centred tangent)

Table 13.4. Calculation results of case 4

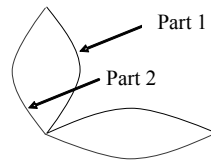


Figure 13.12. Contact configuration 4

### 13.5. Summary

This chapter introduced a method to realize simple assemblies with form defects. This method is based on the optimization under constraints of the part positions, moving the elements from the initial configuration to a final assembly with contacts. For that purpose, the form defects are described by polynomials which are applied to shift the nodes of a STL model which represents each part of the assembly. Different objective function and constraints have then been tested to simulate the assembly.

### 13.6. Bibliography

- [BAL 01a] BALLU A., MATHIEU L., DANTAN J.Y., "Global view of geometrical specification", *Selected Conference Papers from the 7th CIRP International Seminar on Computer-Aided Tolerancing*, Cachan, 24-25 April 2001, Kluwer Academic Publishers, p.13-24.
- [BAL 01b] BALLOT E., BOURDET P., "Determination of relative situations of parts for tolerance computation", *Selected Conference Papers from the 7th CIRP International Seminar on Computer-Aided Tolerancing*, Cachan, 24-25 April 2001, Kluwer Academic Publishers, p.63-72.

- [BOU 88] BOURDET P., CLEMENT A., "A study of optimal-criteria identification based on the small displacement screw model", *Annals of CIRP*, vol.37, 1988, p.503-506.
- [CLE 97] CLÉMENT A., RIVIÈRE A., SERRÉ P., VALADE C., "The TTRS: 13 constraints for dimensioning and tolerance", *Proceedings of the 6th CIRP International Seminar on Computer-Aided Tolerancing*, Toronto, 1997 p.197-206.
- [FOR 05] FORMOSA F., SAMPER S., "Modal Expression of Form Defects", *Selected Conference Papers from the 9th CIRP International Seminar on Computer-Aided Tolerancing*, Tempe, 10-12 April, 2005, Springer, p.13-23.
- [TEI 99] TEISSANDIER D., COUETARD Y., GERARD A., "A computer aided tolerancing model: proportioned assembly clearance volume", *Computer-Aided Design*, vol.31, 1999 p.805–817.
- [VIG 05] VIGNAT F., Contribution à l'élaboration d'un modèle 3D de simulation de fabrication pour l'analyse et la synthèse des tolérances le modèle MMP, PhD thesis, Institut National Polytechnique de Grenoble, 2005.

## Chapter 14

# Influence of Geometric Defects on Service Life

### 14.1. Introduction

#### 14.1.1. *Topic*

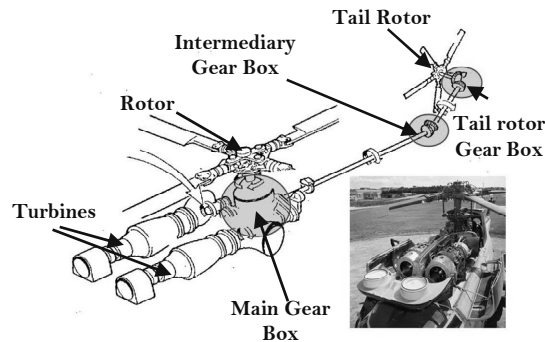
In the aeronautical industry, the mechanical performance of mechanisms is obtained principally by the weight reduction and relevant geometric design of mechanical parts. A light material (housing made of aluminum or magnesium material, transmission part made of titanium material) and a decrease in the number of parts enables us to obtain this performance in helicopter gear boxes (Figure 14.1).

In particular, in the rotational guidance of rolling elements, the weight reduction is obtained by using raceways directly integrated into the shafts or the housings of the gear boxes.

These new mechanical parts make it possible to reduce, considerably, the weight of the helicopter gear boxes, but the manufacturing cost of these parts is very high.

---

Chapter written by Laurent ZAMPONI, Emmanuel MERMOZ, Jean-Marc LINARES and Jean-Michel SPRAUEL.



**Figure 14.1.** *Studied mechanisms*

The origin of this cost is principally the complexity of the geometry and the high geometric quality of such parts (geometric specifications with tight tolerance interval). With mechanical parts having high geometric quality, the assembling requirement is always respected. In opposite, the requirement of operating performance is more critical than the assembling requirement. The choice of values of the functional condition linked with the service life is, generally, based on the industrial background. The modification of functional condition values induces potential risks on the reliability of service, particularly in the aeronautic industry.

#### **14.1.2. Service life functional requirements**

The aim of this chapter is to study the effect of geometric errors on the operation performance of a mechanism. For aeronautical rolling bearings, the first source of failure is pitting of rolling elements or raceways. The second damage is the cracking in the cage. A typical pitting failure is represented in Figure 14.2. It occurs as a result of normal fatigue in current use of rolling bearings.



**Figure 14.2.** *Flaking*

This fatigue is created by successive rolling contacts during the rotation. These contacts induce stress in the raceways and the rolling elements. In our mechanisms, this phenomenon is a functional requirement, since it limits the service life of the helicopter gear box. The second limit for the service life is a breaking of the cage. In our applications, this failure exists only on ball bearings. In such bearings, which are subjected to severe distortion of the raceway, the fatigue strength of the cage is also affected by the spreading of the rotational speed of the rolling elements.

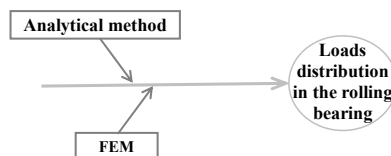


**Figure 14.3.** *Crack in the cage*

Indeed, during one revolution of the bearing, if all the balls do not rotate at the speed of the cage, it may also occur that some balls compensate for the cavity backlash (clearance between the cage and the ball). Such kinematic incompatibility may generate stresses in the cage, or sliding at the contact between the balls at weakest load, and the raceways. This kinematic incompatibility of the orbital speed is chosen as a functional requirement.

#### **14.1.3. State of the art**

In this section, we aim to expose the different methods used to calculate the two previous functional requirements. Their calculations have needed to control the load distribution in the rolling bearing, the evaluation of the contact pressure and the modeling of geometric defects.



**Figure 14.4.** *Load distribution in rolling bearing*

For the first aspect, two methods are used: analytical and FEM tools. The analytical method proposed by Harris [HAR 01] is based on the assumption that displacements in a bearing are caused exclusively by the clearances and local deformation in the contact zones. This assumption is no longer valid if the bearing raceways are of low thickness, and even more so if the raceways are integrated with the shaft or the housing. This is the case for aircraft bearings. In the contribution by Harris and Jones [JON 63], the classical Harris method was modified by introducing flexibility coefficients which account for the deformation of the outer raceway of an idler gear. This raceway is incorporated into the idler gear immediately beneath the gear teeth. Zupan and Prebil [ZUP 01] generalized this approach using the finite element method (FEM) to calculate the flexibility matrix of the structure in order to account for the overall deformation of the structure. The calculation of the flexibility matrix is however limited by the structure size because the inversion of the stiffness matrix requires long computing times. To overcome this problem, Hauswald and Houpert [HAU 00] used a matrix condensation technique (condensation of the stiffness matrix at the link nodes).

For the FEM methods, Bourdon *et al.* [BOU 99] developed a hybrid model to account for the overall deformation, whereby the mechanism is meshed by classical elements and the rollers or balls of each bearing are replaced by non-linear elements attached to the two rings. In the work by Lovell *et al.* [LOV 96], the contact between a ball and two parallel plates was modeled by FEM. The results were found to be close to those obtained by Hertz theory. Zhao [ZHA 98] used 2D contact FEM to calculate the load distribution in a bearing subjected to a radial load. Kang *et al.* [KAN 06] propose a modification to Hertz contact law based on the modeling of the local contact by FEM. A similar approach was also used by Ludwik [LUD 06] to characterize the contact behavior between the roller and the raceways. From these results, Ludwik modeled a slewing bearing by replacing the contacts with elements exhibiting non-linear behavior.

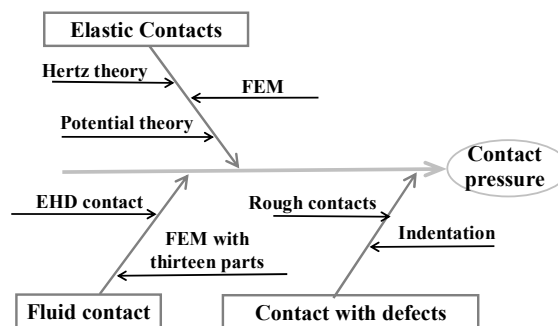


Figure 14.5. Contact pressure methods

The methods described in this section do not enable us to directly calculate the functional requirements (pressure and orbital speed) versus the surface and geometric defects. With the load distribution in the bearing, it is possible to calculate each contact pressure. Figure 14.5 describes the existing methods to calculate the contact pressure for various types of contact. The Hertz theory of elastic contact has been used in our study. The influences of oil, roughness and indentation are not taken into account. Now, the effect of the form and geometry defects can be introduced into our model. The existing methods used for this purpose are shown in Figure 14.6. The small displacement screw approach and Fourier series are used to model the defects.

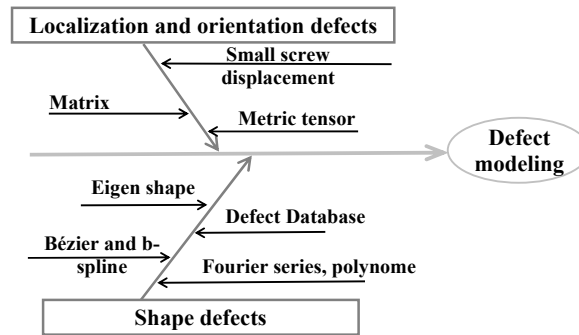


Figure 14.6. Model of geometric defects

In this chapter, the influence of geometric defects on the service life (orbital speed and contact pressure) of the rolling bearing is studied. The first part focuses on the calculation methodology. The method of introducing the geometric defects will be explained. In the second part, the obtained simulation results are then presented and discussed. These results can be used to modify the value of tolerance intervals of the geometric specifications without impacting the service life of this mechanism.

## 14.2. Calculation methodology of contact pressure and orbital speed variation

In this part, we describe the method used to calculate the contact pressure calculation and the orbital speed of bearing balls. This methodology can be applied to helicopter mechanisms. The modeling of the gearbox is achieved by FEM. The various parts of the gearbox are connected together through mechanical links. To simulate the behavior of the mechanism, these links must thus be modeled. In the case of rolling element links, a model that accounts for the non-linear behavior and the load distribution of each rolling element has been established. Contact conditions

between the raceways and the rolling elements are replaced by substitution features (spring oriented element; see Figure 14.8). The bearing is simply represented by its outer ring, these substitution elements and the inner raceway integrated with the shaft. This modeling enables us to calculate the internal equilibrium of a bearing accounting for its internal geometry, the deformability of its contacts, the bearing raceways, the shaft and the housing.

The methodology presented does not account for the dynamic loads and the friction forces. In the context of studied gearboxes, these effects can be neglected. The effects of lubrication are also neglected. In this chapter, the micro-geometric defects (surface roughness, indentation, etc.) are not taken into account. Only the macro-geometric defects (position, misalignment and undulation) are studied. The modeling of the mechanism is performed in the steady-state condition (constant temperature). Thermal expansion is taken into account, in order to deduce the operating clearances of the bearings. The preloads are introduced by the boundary conditions in the FEM, either through the displacement, or through the loads on the bearings. The method presented has been integrated in the CATIA V5 FEM module. This enables us to maintain the link with the geometric model of the mechanism.

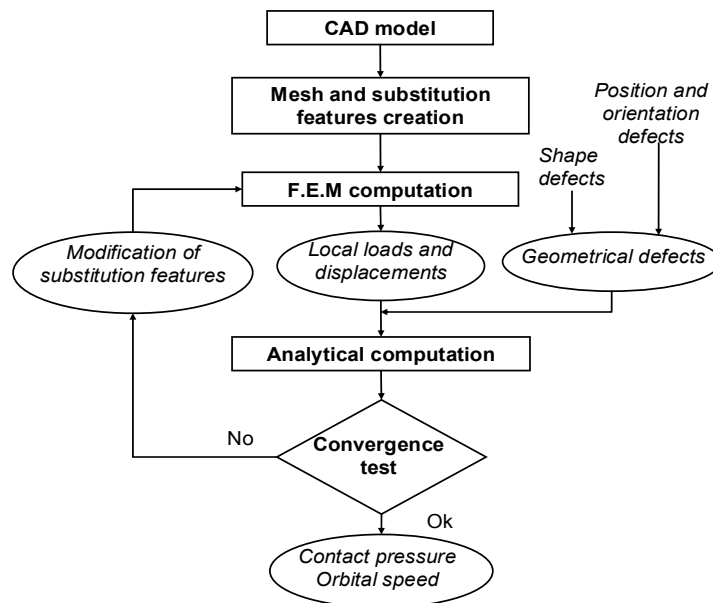


Figure 14.7. Flow-chart of the method



#### 14.2.1. Schedule of the methodology

The global behavior of the mechanism is treated by FEM. The local behavior of the contact is described by analytical approaches. These two procedures are also coupled in this calculation.

The calculation procedure is detailed in the flow chart of Figure 14.8. At each iteration, the FEM calculation with its substitution elements is performed. The variables of the substitution elements (stiffness, orientation) are recalculated at each iteration. Convergence is assumed to be achieved when the variation of the stiffness of the substitution element is less than 0.1% between two successive steps. The analytical method for calculating the substitution elements is based on the Harris equations in [HAR 01]. The characteristics of the elements are controlled by a VB macro in CATIA V5. At each iteration, the input data of the analytical calculations are, for each substitution element, the relative displacements between attachment zones and sustained loads. Moreover, geometric defects (position, orientation, form and undulation) of the bearings may be added. From these data, the local contact displacement and the orientation of the load may be determined. The analytical module and substitution elements are different if the bearing contains balls or rollers. Figure 14.6 shows the feature modeling for a ball bearing.

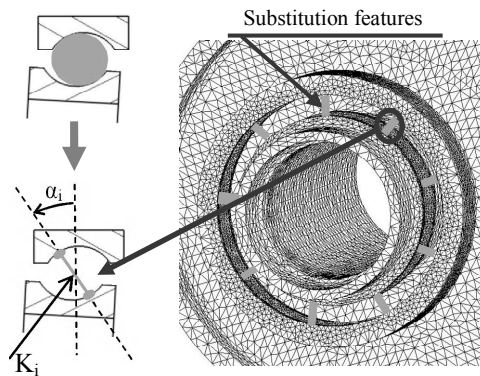
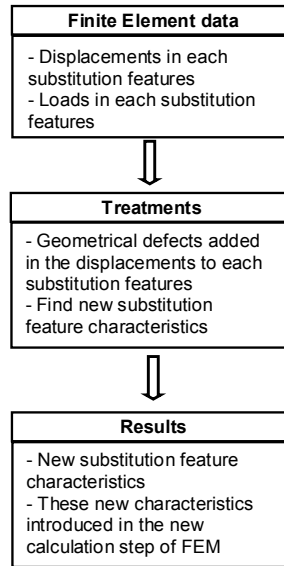


Figure 14.8. Substitution feature modeling

#### 14.2.2. Introduction of geometric defects in FEM

At the first iteration, the substitution elements gain their initial orientation and stiffness. For subsequent iterations, the orientation and stiffness of each substitution element are then recalculated. The relative displacements and the load for each substitution element are obtained using the FEM calculations. At this step, the

geometric defects of the bearing can be added to previous relative displacements. This calculation is detailed in Figure 14.9.



**Figure 14.9.** *Flow-chart of the method*

The iterative process terminates when the variation in stiffness between two consecutive iterations is less than 0.1%.

#### 14.2.3. Model of geometric defect

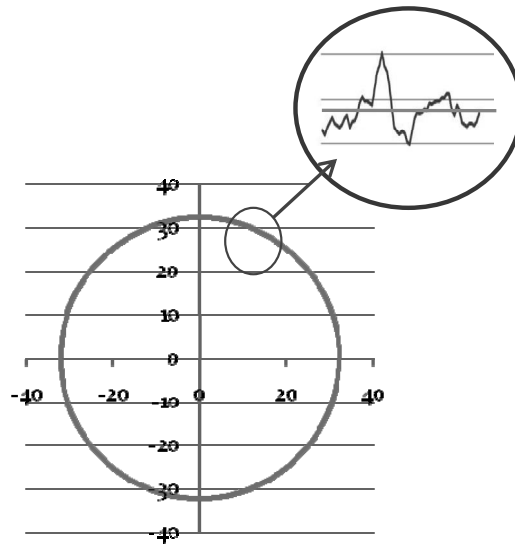
The displacement created by the geometric defects in the ball bearing is decomposed into a radial component named  $U_{ri}$  and an axial component named  $U_{ai}$ . These values include the effects of the position error (coaxiality), the form defect (cylindricity) and undulation. The radial component of each substitution element,  $i$ , is expressed in following equation:

$$U_{ri} = \underbrace{U_{r_{\text{position}}} \cdot \cos(\psi_i + \varphi_{r_{\text{position}}})}_{\text{Position error}} + \underbrace{\sum_{k=1}^n U_{rk} \cdot \cos(k \cdot \psi_i + \varphi_{rk})}_{\text{Form + undulation defects}} \quad [14.1]$$

The axial contribution is written as:

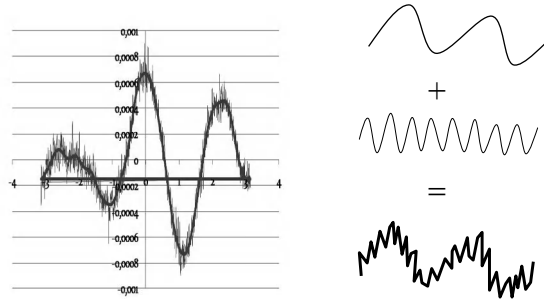
$$U_{ai} = \underbrace{U_{ai_0}}_{\text{Axial deviation}} + \underbrace{U_{a_1} \cos(\psi_i + \phi_{a_1})}_{\text{Orientation error}} \quad [14.2]$$

These equations describe the position and orientation defects between the inner and outer raceways of the bearing. These defects are induced by the geometric variations of the parts of the gear box (housing, shaft, casings, etc.). For the moving parts, the calculation of these geometric defects is very difficult. In fact, it is necessary to calculate the geometric defects between the raceways for any angular position. In our model the constants characterizing the form and undulation defects are based on measurements carried out on real raceways (see Figure 14.10).



**Figure 14.10.** *Measurements of raceways*

For this purpose the point coordinates acquired on manufactured surfaces are fitted by a Fourier series expansion, using a least squares optimization method. This allows us to evaluate the magnitude of the form defects and the undulation amplitude (Figure 14.11).

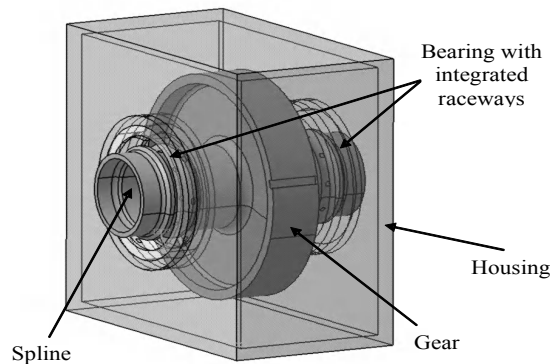


**Figure 14.11.** *Model of form and undulation defects*

### 14.3. Simulation

#### 14.3.1. *Studied case*

In previous section, a hybrid method for modeling bearing guides in a mechanism was presented. This method was validated in [ZAM 07a] and [ZAM 07b]. It is now applied to the simple gearbox design represented in Figure 14.12.



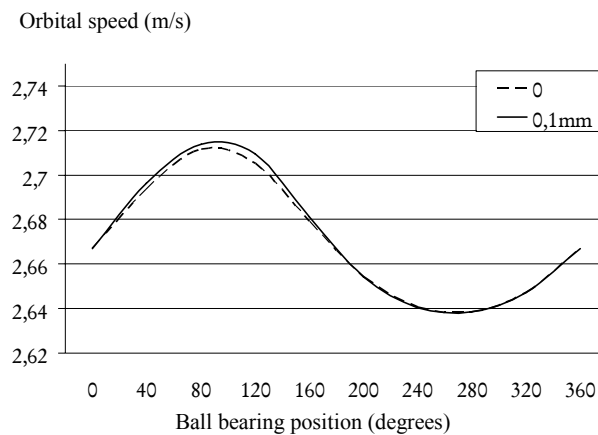
**Figure 14.12.** *Studied mechanism*

The system consists of a housing, containing a gear and two bearings. The wheel is guided to the housing via two integrated ball bearings. The mechanical torque transmitted by the wheel is 200 Nm. The finite element model of the presented gearbox has 80,000 nodes. The various simulations presented in Figures 14.13 to 14.16 highlight different phenomena like the impact of the geometric defects of the mechanism on the pressures and orbital speeds.

### 14.3.2. Effect of the localization defect on orbital speed variation

The studied bearing assembly behaves in a flexible manner which affords it a low sensitivity to positioning defects of the raceways. However, this type of defect modifies the position of the shaft in the housing, which may generate overpressures or slippage at the gear contacts.

Figure 14.13 presents the evolution of the orbital speed of the balls versus the angular position. The calculations were performed either without any defect, or with a misalignment of 0.1 mm. It shows a low influence of such defect, due to the flexibility of the assembly.



**Figure 14.13.** *Orbital speed variation of the ball bearing speed*

### 14.3.3. Effect of the orientation defect on the contact load and orbital speed variation

Figure 14.14 shows a polar plot of the pressure distribution in the ball bearings. It has been calculated for different values of the orientation defect. This ball bearing was subjected to axial and radial loads and a bending moment. According to this simulation, the pressure distribution in the ball bearings is found to be relatively insensitive to orientation defects. The pressure at the most highly loaded contacts does not vary. However, for the least loaded zones, the variations are significant. This phenomenon reduces the bearing service life by a few percent. In our case study, the service life reduction is estimated to be about 6% for the maximum orientation defect.

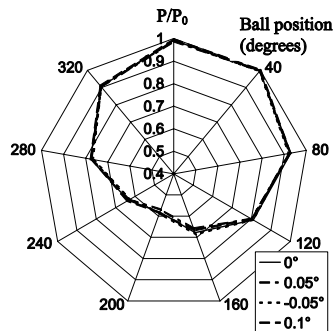


Figure 14.14. Contact pressure distribution

The orbital speed variation in the ball bearings is plotted in Figure 14.15, for different values of the orientation defect. In this simulation, the defect was introduced in the most detrimental position. The variations of the orbital speed are amplified by the orientation defect. For a maximum orientation defect of  $0.1^\circ$ , the increase was evaluated as 50% compared to the nominal fluctuations.

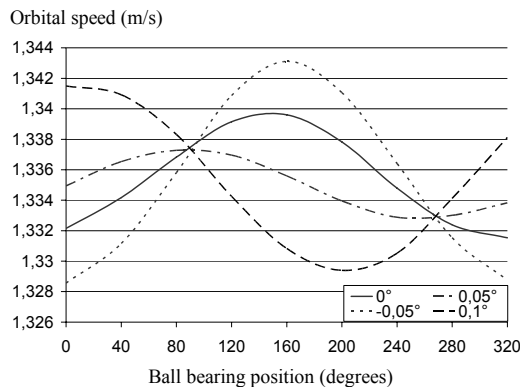
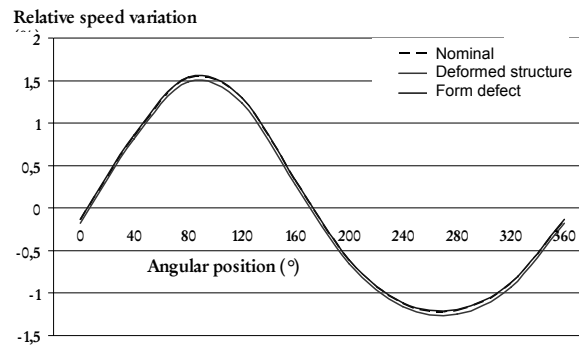


Figure 14.15. Orbital speed variation of the ball bearing speed

14.3.4. Effect of the form defects and undulation on speed variation

Figure 14.16 shows the effect of form defects and undulation on the orbital speed variation. It demonstrates that such imperfection has a low influence on the behavior of the bearing.



**Figure 14.16.** *Orbital speed variation of the ball bearing speed*

These simulations bring to the fore the impact of geometric defects and of the part's flexibility on the behavior of integrated raceway bearings in helicopter gearboxes. In the studied cases, the part's flexibility allows a better pressure distribution and increases the bearing service life. Rolling bearings are sensitive to orientation defects, but the mechanism flexibility reduces its overpressure effects. Ball bearings are better able to withstand orientation defects, but this increases the orbital speed variations. The combination of the mechanism flexibility and an orientation defect may generate fatigue loads on the cage. Cage failure is a serious destruction mode. This failure leads to the crash of the mechanism. This type of simulation allows us to predict the service life of integrated raceway bearings. After experimentation, it may lead to dimensioning optimization or to a change in the value of geometric specifications of integrated raceways.

#### 14.4. Summary

The hybrid model presented in this chapter enabled us, on the one hand, to account for the global behavior of bearings within a complete flexible mechanism, and on the other hand, to determine precisely the local behavior of the rolling elements. Additionally, the deformations of the structure and the geometric defects of all the parts in the mechanism were included in this methodology. This proposal is now, directly, implemented in CATIA V5 environment, used in design. The presented simulations bring to the fore the effects of the flexibility of the structure and the geometric defects of the parts on the behavior of the bearing (deformation, contact pressure, orbital speed variation). The load distribution in the bearing is modified by the flexibility of the parts and the bearing raceways. The bearing service life is increased by this phenomenon. However, for ball bearings, this flexibility increases the ball's orbital speed variation which can lead to failures of

the cage. Positioning defects in our assemblies have proved to give insignificant effects.

## 14.5. Bibliography

- [BOU 99] BOURDON A., RIGAL J., PLAY D., "Static rolling bearing model in a C.A.D. environment for the study of complex mechanisms: part I and II-rolling bearing model", *ASME Trans. J. Tribology*, vol. 121, 1999, p.205-224.
- [HAR 01] HARRIS T., *Rolling Bearing Analysis*, 4th edition, Wiley- Interscience, 2001.
- [HAU 00] HAUSWALD T., HOUPERT L., "Numerical and experimental simulations of performances of bearing system, shaft and housing; Account for global and local deformations", *SIA seminar "Fiabilité expérimentale"*, 2000.
- [JON 63] JONES A. B., HARRIS T., "Analysis of a Rolling Element Idler Gear Bearing Having a Deformable Outer Raceway Structure", *ASME Trans J. Basic Eng*, 1963, p. 273-279.
- [KAN 06] KANG Y., SHEN P.C., HUANG C.C., SHYR S.S., CHANG Y.P., "A Modification of the Jones-Harris Method for Deep-Groove Ball Bearings", *Tribology*, vol.39 no. 11, 2006, p.1413-1420.
- [LOV 96] LOVEL M.R., KHONSARI M.M., MARANGONI R.D., "A finite element analysis of the frictional forces between a cylindrical bearing element and MoS2 coated and uncoated surfaces", *Wear*, vol. 194, 1996, p.60-70.
- [LUD 06] LUDWIK K., "Modelling of rollers in calculation of slewing bearing with the use of finite elements", *Mechanism and Machine Theory*, vol. 41, 2006, p.1359-1376.
- [ZAM 07a] ZAMPONI L., MERMOZ E., LINARES J.M., "Étude des méthodes de calcul des pressions de contact dans les roulements à pistes intégrées des boîtes de transmission aéronautiques", *Mécanique & Industries*, vol.8, no.6, 200, p.567-576.
- [ZAM 07b] ZAMPONI L., MERMOZ E., LINARES J.M., "Contact pressure calculation methodologies in aeronautic gearboxes in the CAD process", *The Future of Product Development: Proceedings of the 17th CIRP Design Conference*, 2007, Berlin, Springer, p.451-462.
- [ZHA 98] ZHAO H., "Analysis of load distribution within solid and hollow roller bearings", *ASME Trans. J. Tribology*, vol.120, 1998, p.134-139.
- [ZUP 01] ZUPAN S., PREBIL I., "Carrying angle and carrying capacity of large single row ball bearing as a function of geometry parameters of the rolling contact and the supporting structure stiffness", *Mechanism and Machine Theory*, vol.36, 2001, p.1087-1103.



## Chapter 15

# GapSpace Multi-dimensional Assembly Analysis

Assembly tolerance analysis is the process of determining the effect that tolerances specified on individually manufactured parts have on an assembly of these parts. Tolerance specifications form an important link between the product design, manufacturing processes and the actual assembly process. Mechanical engineers use tolerances to define allowable/possible manufactured uncertainties to ensure interchangeable assemblies with proper functionalities. This chapter proposes a revised GapSpace assembly (RGSA) analysis model to analyze the ease of assembly of the design through allocating various types of tolerance specifications; for example, worst-case tolerance specifications, statistical tolerance specifications, as well as assembly tolerance specifications. The distinct property of this method is that it uses an inter-element gap (the clearance between different mechanical parts) as the basic functional unit for performing various kinds of assembly analyses.

### 15.1. Introduction

Development of the original GapSpace Analysis (GSA) model for one and two dimensional analysis has been reported by Morse and Zou [ZOU 02], [ZOU 03], [MOR 01]. The prominent characteristic of this method is that the assembly rate of the model is exclusively determined by the intrinsic geometric properties of manufactured parts. The revision of this model – the revised GSA (RGSA) – was developed in order to implement it in a practical CAD system, and poses some

---

Chapter written by Edward MORSE and Xiaobin YOU.

interesting challenges. The RGSA representation has a tree-structure as shown in Figure 15.1. It is composed of four main elements: dimensions and tolerances (including both limit tolerances and geometric tolerances), gaps, constraining simplices, and fitting conditions.

Dimensions and tolerances constrain functional requirements of the design and are the origins of tolerance stack-ups in the assembly. A gap describes the relationship between a pair of features on different parts and is the starting point for constructing the RGSA model. A constraining simplex (CS) is a geometric unit representative of a part and is the basic functional unit in fitting conditions. Each constraining simplex has a value that is determined according to the sine law. According to the equal value property of the sine law, each constraining simplex has two equivalent representations: a gap representation and a geometric representation. The gap representation is a group of gaps on a part that fully constrain its movement. The geometric representation is a combined dimension whose variation is equal to that of the linear sum of the gap representation. In the RGSA model, the nominal dimension of a constraining simplex is represented by a linear or non-linear combination of dimensions and tolerances specified on the part.

A fitting condition is a necessary condition for checking the ease of assembly of the design and is the key element for performing various GSA analyses. Each fitting condition is formed by one or more loops of gaps over the constraining simplices to fully constrain the movement of some parts in the assembly. The set of independent fitting conditions completely represents the geometric ease of assembly of the design, that is the set is sufficient to guarantee assembly. As with the constraining simplices, each fitting condition also has two equivalent representations: a gap representation and a geometric representation. Through analyzing them, four types of assembly analyses are realized by the RGSA model. They are:

- ease of assembly analysis: the ease of assembly of the design is checked with various dimensioning and tolerancing schemes;
- sensitivity analysis: the sensitivity of a specific parameter with respect to a certain dimension or tolerance is checked by differentiating the corresponding fitting condition or parametric representation of the constraining simplex;
- quality check: the quality (clearance) of the assembly is checked using the revised simplex algorithm by pre-assuming some limitations to gaps. This check can also be applied to relative motion between the parts;
- tolerance synthesis: the assembly analysis results obtained above are used to improve the tolerance design.

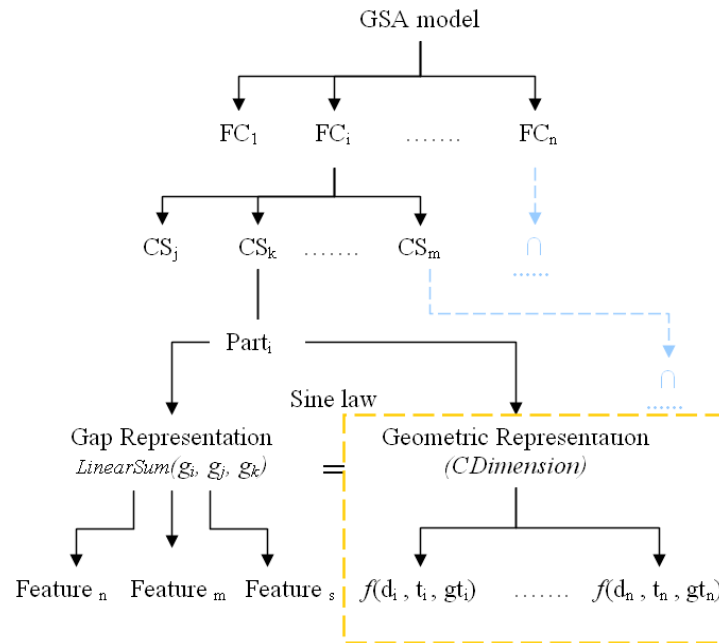


Figure 15.1. Structure of the RGSA model

## 15.2. Representing dimensions and tolerances

In the RGSA model, three types of variations – limit tolerances, geometric tolerances and kinematic variations – are used to represent the allowable variation of the assembly; limit tolerances are handled according to the specified dimensioning schemes on parts using a revised tolerance chart method, and geometric tolerances are dealt with by the tolerance zones they form. If geometric tolerances are defined on a feature which is a component of the objective constraining simplex, translational movements of their tolerance zones will be counted into the nominal dimensions of the corresponding constraining simplices; otherwise, rotation movements of them will be considered if they do influence the locations of some assembly associated features of the objective constraining simplices. Geometric tolerances covered by the RGSA model are form, profile, orientation and location tolerances. Other geometric tolerances, such as the runout and material modifier are not yet represented in the model. In an improvement from the former GSA model, some kinematic variations are represented in the RGSA model. They are employed in some specific assemblies, such as floating assemblies and kinematic assemblies, to properly allocate assembly dimensions and tolerance specifications, or to define limits of gaps or fitting conditions.

### 15.3. Geometric tolerances

Geometric tolerances enable the variation in shape, orientation or location of a part feature as defined in ASME Y14.5M-1994 tolerance standard. When geometric variation occurs in features connected by a dimensioning scheme on the same part, or on mating features between parts, they will affect the variation of the whole assembly. Geometric tolerances accumulate and propagate in a different manner than limit tolerances. In this chapter, geometric tolerances are handled by the tolerance zones they form. Most existing GD&T standards are established through years of engineering practice, not from mathematical models. Therefore, not all GD&T specifications are applicable in the RGSA model. Geometric tolerances supported by the RGSA model are form, profile, orientation, location and others. The processing methods for different geometric tolerances are listed below:

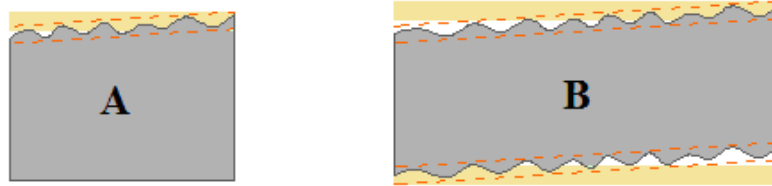
- Profile tolerances are handled according to the method of specification (bilateral or unilateral).
- Location tolerances are counted depending on data to which they refer. They are only allowed to be specified by referring to a coordinate system, typically where two perpendicular pieces of data defined on the part are chosen as the coordinate axes.
- Orientation tolerances are dealt with in two ways: 1) if they are specified on features of a constraining simplex (CS-features), translational movements of their tolerance zones contribute to the CS-dimension; 2) if they are specified on non-CS-features influencing positions of CS-features, angular movements of their tolerance zones will be counted.
- Geometric assembly tolerances are handled by considering only the translational movements of their tolerance zones. Those translational variations between features will be counted into limits of gaps, clearances and fitting conditions.

If a tolerance is a subset of another tolerance, the tolerance with the larger value will be counted. For example, if a flatness tolerance zone is located within a parallelism tolerance, only the impact of the more restrictive parallelism tolerance will be considered.

Runout, which is an integration of form, location and orientation tolerances, is excluded from the RGSA model, due to difficulties with the simultaneous specification of these attributes.

The material condition of a part is neglected if the bonus tolerance has already been considered from the feature of size (i.e. the virtual condition has been established).

Form tolerances are dealt with according to a perfect form tolerance zone (see Figure 15.2), which is formed – in the case of flatness – by two planes that are always parallel with the desired direction of the feature. Available form tolerances are straightness, flatness, circularity, cylindricity and sphericity.

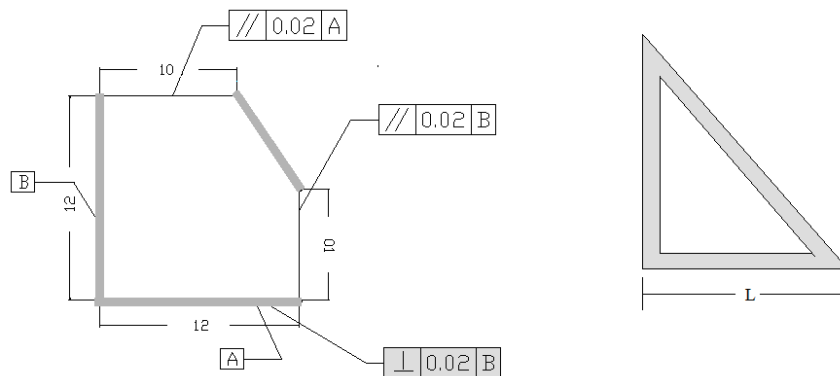


**Figure 15.2.** *The perfect form tolerance zone*

The influence of geometric tolerances on the shape of features varies with the functionality of the features on which they are specified. Geometric tolerances are handled by two methods according to whether the features on which they are specified are member features (CS-feature) of the objective constraining simplex (CS) or not.

*Specified on CS-features of the objective CS*

When a geometric tolerance is defined on the CS-feature (such as the perpendicular tolerance in Figure 15.3) of a CS, variations of its tolerance zone influence the relative location of the CS-feature to the other CS-features. As directions of all the CS-features are assumed to be fixed, therefore, only translational movements of the tolerance zone influence the value of the CS-dimension.

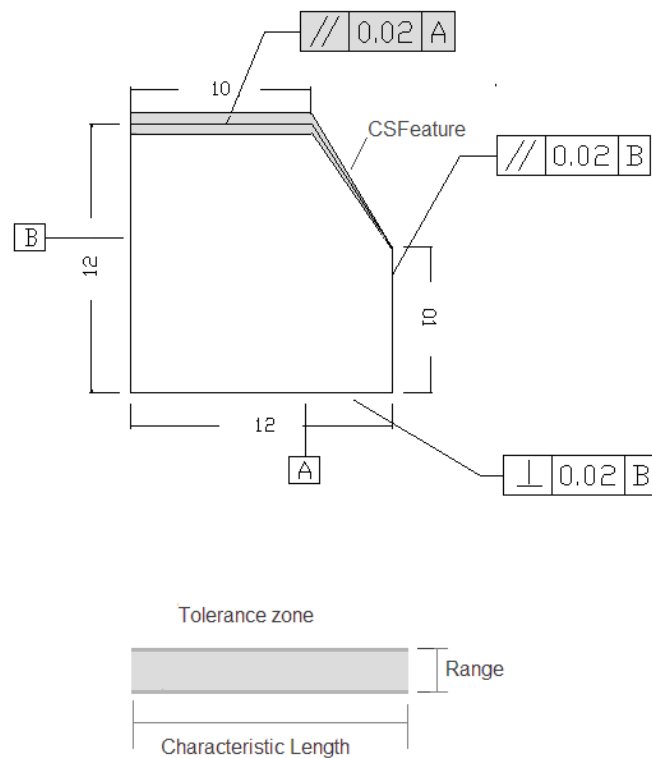


**Figure 15.3.** *Geometric tolerances are specified on CS-features of a constraining simplex (CS)*

*Defined on non-CS-features of the objective CS*

When geometric tolerances are defined on non-CS-features of the objective CS (such as the parallelism tolerance in Figure 15.4), variations of its tolerance zone influence locations of some ends of the CS-features. The influence will be propagated along the specified dimensioning scheme. Therefore, rotation movements of the tolerance zone should be counted into the CS-dimension using the following equation:

$$g\alpha = \Delta\theta = \tan^{-1}\left(\frac{\text{Tolerance Zone}}{\text{Characteristic Length}}\right) \quad [15.1]$$

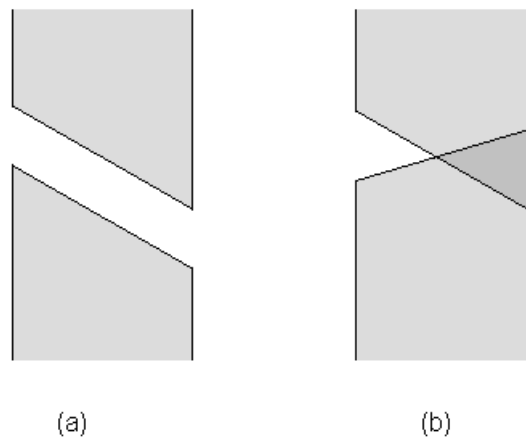


**Figure 15.4.** Geometric tolerances defined on non-CS-features of a constraining simplex (CS)

### 15.4. Perfect form tolerance zones

The perfect form of a tolerance zone means the direction (or normal vector) of the feature is strictly fixed and the tolerance zone is always parallel with the design direction of the feature. Rotation errors of a feature will be contained in the perfect form tolerance zone (PF-tolerance zone).

Most tolerance zones are of perfect form; however, some tolerance zones, such as flatness, are not always parallel with the nominal direction of the feature. In the D&T integrating process, their PF-tolerance zones are created by projecting their standard tolerance zones into some zones that are parallel with design directions of features, which will make them work like parallelism tolerance zones. Sometimes, imperfect shapes of features may increase the ease of assembly between two parts (see Figure 15.5a); sometimes, they will worsen the assembly conditions (see Figure 15.5b). For independently manufactured parts, those two cases should have the same rate of occurrence. However, both of them are treated as unacceptable assembly conditions by the PF-tolerance method. Therefore, the PF-tolerance zone theory is a relatively conservative method.



**Figure 15.5.** *Impact of imperfect shape on two assembled features*

### 15.5. Assembly tolerance specification

Assembly dimension and tolerance (D&T) specifications are used to enhance functional requirements of the design. They are represented by limits of gaps, clearances and overall dimensions of an assembly which are critical to performance. A system of assembly D&T specifications patterned after ASME Y14.5M has been proposed [CAR 93]. The Y14.5 feature controls requiring a piece of data are used as

assembly controls. In the design process, assembly D&T specifications are usually mixed in with component D&T specifications. Therefore, it is necessary to strictly distinguish between them. The main characteristics of assembly D&T specifications are: 1) they are usually specified with some kinematic mechanisms; 2) they are usually defined by referencing to a datum or a feature on a different part; 3) they are defined between parts, therefore, they are independent of the absolute coordinate positions of the parts, but dependent on the relative positions between those parts. Not all the assembly D&T controls are applicable to the RGSA model; assembly length, assembly gap and assembly geometric tolerance are supported.

In the original GSA model, assembly D&T specifications are not addressed. Gaps without range limits are used as the basic analysis unit. Therefore, the model only represents the geometric ease of assembly of the design. However, as described before, assembly D&T specifications do bring limits to some gaps and define some relationships between parts; this is useful in solving some assembly conditions with kinematic mechanisms or floating parts. In this chapter, assembly D&T specifications are employed to calculate limits of fitting conditions, check the quality of the assembly, and resolve a few kinematic problems or floating assemblies.

– Calculating limits of fitting conditions

If adequate D&T specifications are given, each gap of a fitting condition has a range limit, and the fitting condition will be constrained by some assembly limits.

$$FC_{\max} \geq FC(d_1 \cdot t_1 \cdot d_2 \cdot t_2 \cdots) \geq FC_{\min} \quad [15.2]$$

In most cases,  $FC_{\min}$  is equal to zero and not all the fitting conditions have assembly limits.

– Resolving specific assemblies

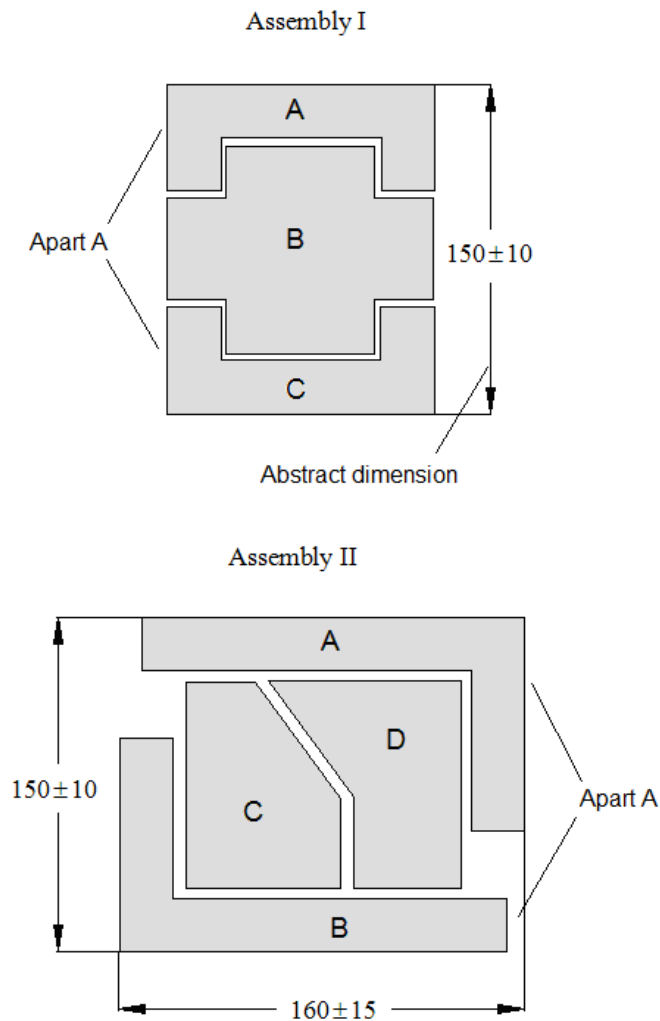
Some well-chosen assembly D&T specifications can be used to solve some kinematic problems or floating assemblies by treating some parts connected by an assembly D&T specification as an abstract part (A-part), and regarding the assembly D&T specification as the size variation of an abstract feature of the A-part.

## 15.6. Floating assembly

As shown in Figure 15.6, the two assemblies are under-constrained in that part A and part B can move freely along some directions if no assembly D&T specifications are made. For example, in Assembly-I, they can move without constraint along the vertical direction; in Assembly-II, they can move along both the



vertical and horizontal directions. These problems can't be resolved by the former GSA model because gaps between part A, part B and part C can be expanded without limits, which means fitting conditions containing them are unbounded. However, if part A and part B are connected by some assembly D&T specification, we can treat them as an abstract part (A-part A). After the A-part is created, gaps between A-part A and part B became constrained, which will make the fitting condition solvable.



**Figure 15.6.** *Floating assemblies with assembly D&T specifications*

### 15.7. Kinematic assembly

Sometimes, kinematic mechanisms are used to enhance the ease of assembly of the design. They permit relatively loose tolerances, which dramatically increases the rate of the assembly. However, the introduction of kinematic mechanisms usually makes it impossible to find effective fitting conditions that fully represent the ease of assembly of the design, as some necessary gaps may be missed. In order to generate a 1D fitting condition for the assembly in Assembly-I (Figure 15.7), there should be a gap between part D and part A in the horizontal direction.

However, part D and part A are actually connected by a spring and also features a and b are not definitely to be parallel with each other. Therefore, there is no guarantee that such a gap exists. Fortunately, since part D and part A are connected by an assembly D&T specification, we can treat them as an abstract part (A-part A) so that there is a gap loop (1D horizontal fitting condition) between A-part A, part B and part C, which makes the assembly solvable. In brief, the idea is to use assembly D&T specifications to represent the kinematic variations and treat the parts connected by kinematic mechanisms as a single abstract part.

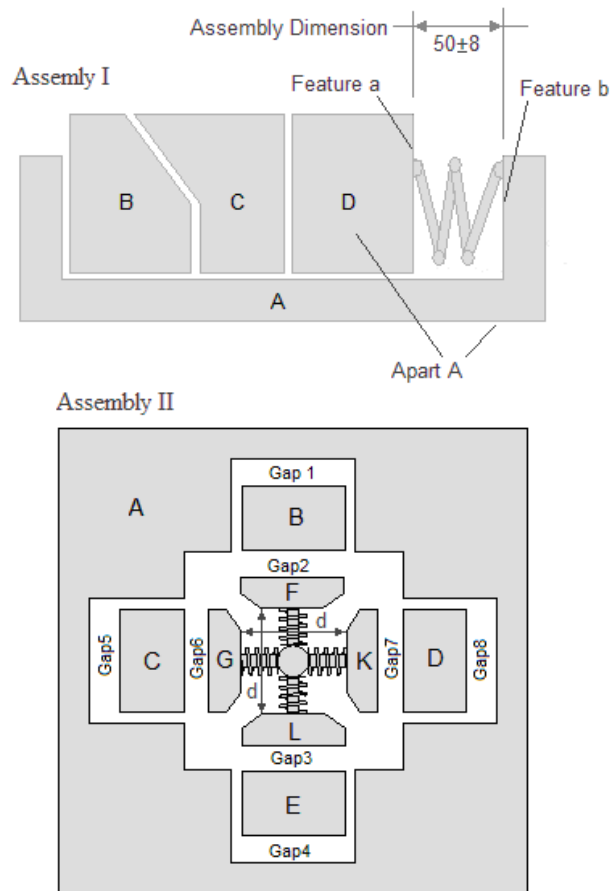
### 15.8. Manufacturing dimensioning schemes

Arbitrary specifications of D&T elements on a part usually result in an assembly model that cannot be solved. Therefore, in the RGSA model, these elements are requested to be specified following some rules similar to 2D mechanical drafting. A manufacturing dimensioning scheme (MD scheme) consistent with engineering dimensioning methods was developed to appropriately specify D&T elements on a part. This is a systematic parametric representation of dimensions and their variations that may be introduced by the manufacturing process. In this scheme, certain dimensions vary as a function of process parameters while other dimensions are dependent on the primary dimension specification.

Because of the diversity of manufacturing processes, the MD scheme is usually not consistent with the parametric dimensioning scheme that is commonly used to express the design. To manufacture a part, many different manufacturing methods might be chosen and each dimension will be the output of a process, which in turn is dependent on its predecessors.

Usually, the range of a dimension that reflects an initial setup by the manufacturing engineer is chosen to represent  $\pm 3\sigma$  of the process used to create it. The MD scheme is widely used in 2D part drawings – often called process sheets – for manufacturing purposes. The advantage of this scheme is relationships between feature variations are explored, which makes the analysis results more reflective of

the actual process. There are two types of MD schemes available in the RGSA model: 1) MD scheme-I, where dimensions and dimensional tolerances are specified and flatness tolerances are employed to express possible shape variations of features; 2) MD scheme-II, where basic dimensions are defined and geometric tolerances, such as parallelism, perpendicularity and profile, are used to illustrate possible form variations of features.



**Figure 15.7.** Assemblies with kinematic mechanisms

In any MD scheme, at least two (usually two) pieces of data should be defined to control the manufacturing process. Two perpendicular pieces of data that are referenced by most dimensions and tolerances are chosen as the standard pieces of

data while generating the revised tolerance chart (RTC) for the MDS (see MDS-RTC in the following section). In engineering practices, there are so many ways to specify manufacturing dimensioning schemes that some of them are difficult or even impossible to be identify and integrate. Therefore, in order to generate an effective and complete RTC, some dimensioning rules of the MD scheme must be established. While these rules will not be listed here, they comprise a method that allows the systematic description of the manufacturing drawing for CAD representation.

### 15.9. The revised 2D tolerance chart

To effectively model the tolerance stack-up within a part, a 2D revised tolerance chart (2D RTC) was developed in this chapter to evaluate the variations of CS-dimensions. Based on the work of [XUE 01] and others, it is built by transforming positions of features on a part from the global coordinate system to a component coordinate system whose origin is determined by the start point of tolerance stacking-up within the part. In engineering practice, there are usually two perpendicular data features locating the assembly analysis plane of the RGSA model. A 2D-RTC is composed of two dimension and tolerance trees (D&T-trees): a horizontal D&T-tree and a vertical D&T-tree. The horizontal D&T-tree starts from the vertical datum (Y-datum), while the vertical D&T-tree starts from the horizontal datum (X-datum). This method is similar to other decomposition methods for tolerance accumulation [CHA 97, CHA 99, XUE 01]. In the 2D-RTC, each D&T-tree is composed of several dimension chains, each of which represents an actual manufacturing path or a tolerance stack-up route.

### 15.10. Parametric representation of the PF-tolerance zone of a CS-feature

The dimension of a CS is totally determined by position and size of the PF-tolerance zones of its CS-features, which are influenced by the dimensioning scheme specified on their parent part. Therefore, there should be a way to integrate different dimensioning schemes into the PF-tolerance zone of a CS-feature. The RTC of a part represents the inter-relationships between different dimensions and tolerances specified on the part. Thus, it should be effective tool to count interactions between various dimensions and tolerances into the PF-tolerance zone of a CS-feature. The PF-tolerance zone of a CS-feature is not only determined by the position of the CS-feature, but also decided by the geometric tolerances specified on it. If a dimension on the path is defined on a single feature (not two parallel features), angular variations of the geometric tolerances specified on the same feature must be counted in the PF-tolerance zone of the corresponding CS-feature.

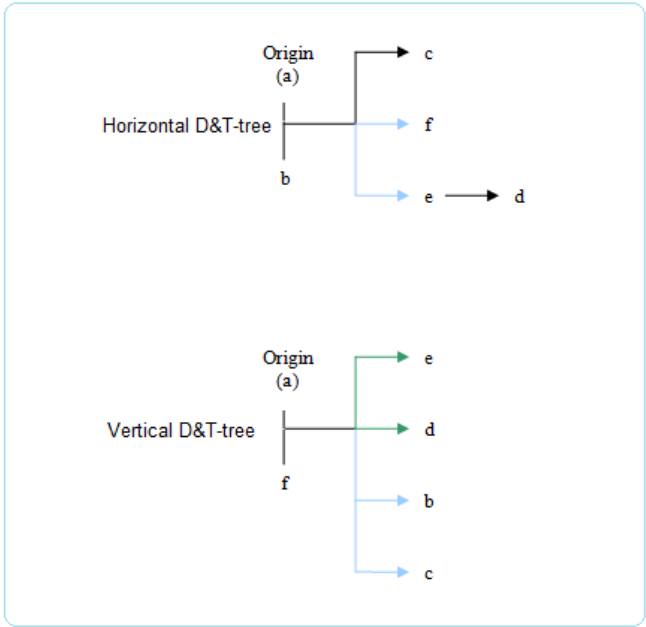
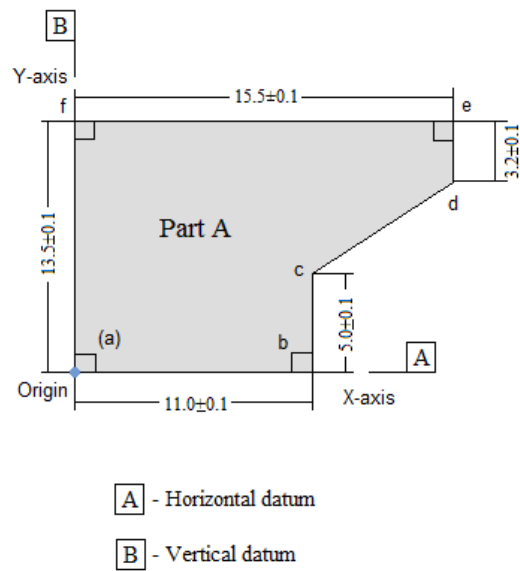


Figure 15.8. The structure of a 2D-RTC based on the MD scheme

When limit tolerances are used in the MD scheme, the X-position and Y-position of the two ends of any feature may be controlled separately, which may result in variation of the direction of a CS-feature. This is in conflict with the assumption that each CS-feature should keep its design direction while modeling. The problem is solved by projecting the position variations of the two ends of a CS-feature into its PF-tolerance zone.

In the 2D-RTC, the tolerance stack-up starts from the intersection point of the two standard pieces of data. While calculating the position of an end of a CS-feature, if a dimension without a dimensional tolerance is directly specified on a feature influencing the position of the CS-feature, its angular tolerances and/or geometric tolerances should be counted in the equation; otherwise, those tolerances items are neglected. The position of an end of a CS-feature is calculated using one of the below equations according to the type of the specified MD scheme.

*Angular tolerances are considered*

$$\begin{cases} p_x = \sum_{i=1}^{n_x} \text{sign}(d_i) \cdot d_i \cdot \cos(\pm \Delta \theta_i \pm \sum \Delta g \theta_k) + \sum_{j=1}^{m_x} \text{sign}(d_j) \cdot d_j \cdot \cos(\theta_j \pm \Delta \theta_j \pm \sum \Delta g \theta_k) \\ p_y = \sum_{i=1}^{n_y} \text{sign}(d_i) \cdot d_i \cdot \sin(\pm \Delta \theta_i \pm \sum \Delta g \theta_k) + \sum_{j=1}^{m_y} \text{sign}(d_j) \cdot d_j \cdot \sin(\theta_j \pm \Delta \theta_j \pm \sum \Delta g \theta_k) \end{cases} \quad [15.3]$$

where  $d$  is a dimension between the origin and the point,  $\text{sign}(d)$  is  $\pm 1$ , based on the dimension,  $\theta$  is the angle of the feature,  $\Delta \theta$  is its angular tolerance and  $\Delta g \theta$  is the angular variation of the geometric tolerance.

*Angular tolerances are neglected*

$$\begin{cases} p_x = \sum_{i=1}^{n_x} \text{sign}(d_i) \cdot d_i \cdot \cos(\pm \sum \Delta g \theta_k) + \sum_{j=1}^{m_x} \text{sign}(d_j) \cdot d_j \cdot \cos(\theta_j \pm \sum \Delta g \theta_k) \\ p_y = \sum_{i=1}^{n_y} \text{sign}(d_i) \cdot d_i \cdot \sin(\pm \sum \Delta g \theta_k) + \sum_{j=1}^{m_y} \text{sign}(d_j) \cdot d_j \cdot \sin(\theta_j \pm \sum \Delta g \theta_k) \end{cases} \quad [15.4]$$

Positions of the two ends of a CS-feature can be obtained using the above equations, and its PF-tolerance zone is calculated by projecting the probability distributions of the two ends to a tolerance zone that is parallel with the design direction of the feature. The projection method is described below:

– Equation of the PF-tolerance zone:

$$\Delta t = -(Ax + By + C) \quad [15.5]$$

– Worst-case tolerance analysis.

If worst-case tolerances are used, the value of the PF-tolerance zone is obtained by calculating the difference between the upper limit and the lower limit of the tolerance zone of the CS-feature.

$$\Delta t = \max(f(p)) - \min(f(p)) \quad [15.6]$$

$$f(p) = \begin{cases} -(A \cdot p_{1,x} + B \cdot p_{1,y} + C) \\ or \\ -(A \cdot p_{2,x} + B \cdot p_{2,y} + C) \end{cases}$$

where  $p_1$  and  $p_2$  are the two ends of the CS-feature.

– Statistical tolerance analysis.

When statistical tolerances are used, the value of the PF-tolerance zone is estimated using Monte Carlo simulation. The Monte Carlo simulation is modified by picking up two random numbers from the probability distributions of the two ends at the same time, and then using statistical methods or histogram to model the sample of calculated using the random numbers.

$$\Delta t = -(A \cdot p_x + B \cdot p_y + C) \quad [15.7]$$

where  $p$  is a random position of the two ends.

– The total value of the PF-tolerance zone should also include the influences of geometric tolerances specified on the CS-feature. If the geometric tolerances are specified between the CS-feature and a datum, a tighter tolerance zone will be chosen. If they are specified between two features and none of them is a datum, the half values of the geometric tolerance zones will be added into the calculated tolerance zone.

$$\Delta t_{total} = \Delta t + \sum \Delta gt_i \quad or \quad \Delta t_{total} = \Delta gt_i \quad [15.8]$$

– The final equation of the PF-tolerance zone of a CS-feature:

$$Ax + by + C \pm \Delta t_{total} = 0 \quad [15.9]$$

### 15.11. Surfaces of revolution

Besides polygons, round parts such as cylinders and spheres are also involved in the RGSA model. The CS-feature of a revolving part is represented by an imaginary tangent plane at the contact point. The PF-tolerance zone of the abstract CS-feature is calculated using the following formulas.

1. Radius tolerance is defined:

$$\begin{cases} Ax + By + \Delta C = 0 \\ (x - x_o)^2 + (y - y_o)^2 = (r + \Delta r)^2 \end{cases} \rightarrow \Delta C = |(r + \Delta r)\sqrt{A^2 + B^2} - Ax_o - By_o| \quad [15.10]$$

2. Cylindricity of the cylinder or sphere is defined:

$$\begin{cases} Ax + By + \Delta C = 0 \\ (x - x_o)^2 + (y - y_o)^2 = (r + \Delta c)^2 \end{cases} \rightarrow \Delta C = |(r + \Delta c)\sqrt{A^2 + B^2} - Ax_o - By_o| \quad [15.11]$$

3. The PF-tolerance zone of the abstract CS-feature:

$$Ax + By + C \pm \Delta t = 0$$

where

$$C = (Max(\Delta C) + Min(\Delta C)) / 2 ,$$

and

$$\Delta t = (Max(\Delta C) - Min(\Delta C)) / 2 \quad [15.12]$$

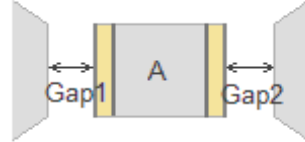
### 15.12. Nominal dimensions of the CS

In the GapSpace “sine law” [ZOU 02], the weighted sum of gaps composing a CS is equal to the variation of a combined dimension of the part. The combined dimension is regarded as a nominal property (CS-dimension) of the CS. Each CS-dimension is a geometric representation of the CS and works as a basic constraint on its parent part in its degrees of freedom during assembly. The sign of the CS-dimension is determined by the material side of the CS, and its value depends on many factors, such as the shape of the part, selection of data, specified D&T scheme, manufacturing process and so on. Mathematical representations of various CS-dimensions are listed below.



### 15.13. 1D constraining simplices

*Type-I: 1D CS of a polygon*



**Figure 15.9.** 1D CS of a polygon

1) Equations of plane features:

$$\begin{cases} \text{Face1: } Ax + By + cZ + d_1 + \Delta t_1 = 0 \\ \text{Face2: } Ax + By + cZ + d_2 + \Delta t_2 = 0 \end{cases} \quad [15.13]$$

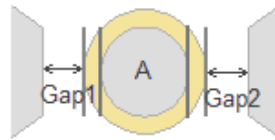
2) Representation of the CS-dimension:

$$\begin{cases} \text{CSDimension} = \frac{|(d_1 - d_2) + (\Delta t_1 - \Delta t_2)|}{\sqrt{A^2 + B^2 + C^2}} \\ \text{CSTolerance} = \frac{|(\Delta t_1 - \Delta t_2)|}{\sqrt{A^2 + B^2 + C^2}} \end{cases} \quad [15.14]$$

where  $\Delta t$  denotes the value of the PF-tolerance zone of the feature.

The CS-dimension is equal to the minimum distance between the two parallel features of the CS, as shown by the highlighted features in Figure 15.9. The two features are located on the same part and are parallel with each other at all times. Out-of-plane errors (rotation variations) of the two features are compensated into their PF-tolerance zones.

*Type-II: 1D CS of a cylinder or sphere*



**Figure 15.10.** 1D CS of a cylinder or sphere

1) Equation of a cylinder:

$$\begin{cases} \text{Cylinder: } (x - x_o)^2 + (y - y_o)^2 = (r + \Delta t)^2 \\ z = (z_1, z_2) \end{cases}$$

or equation of a sphere:

$$\text{Sphere: } (x - x_o)^2 + (y - y_o)^2 + (z - z_o)^2 = (r + \Delta t)^2$$

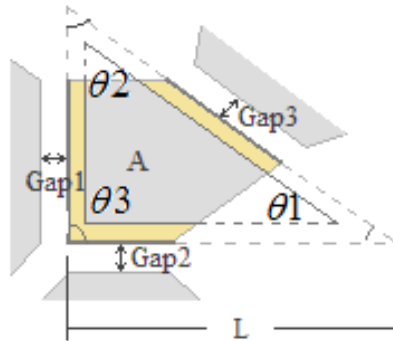
Representation of the CS-dimension:

$$\begin{cases} \text{CSDimension} = R = 2r \\ \text{CSTolerance} = \Delta t \end{cases}$$

The CS-dimension is equal to the diameter of the cylinder or sphere as shown in Figure 15.10. Geometric tolerances of the cylinder or sphere are compensated in the dimensional variation of the diameter (or radius) or the PF-tolerance zones of its imaginary tangent planes.

#### 15.14. 2D constraining simplices

*Type-I: 2D CS of a polygon*



**Figure 15.11.** 2D CS of a polygon

1) Equations of pane features:

$$\begin{cases} Face1 : A_1x + B_1y + C_1Z + d_1 + \Delta t_1 = 0 \\ Face2 : A_2x + B_2y + C_2Z + d_2 + \Delta t_2 = 0 \\ Face3 : A_3x + B_3y + C_3Z + d_3 + \Delta t_3 = 0 \end{cases}$$

For 1D or 2D GSA analyses, the above equations should be changed to the following formats:

2) Equations of edges of the 2D CS:

$$\begin{cases} Edge1 : A_1x + B_1y + d_1 + \Delta t_1 = 0 \\ Edge2 : A_2x + B_2y + d_2 + \Delta t_2 = 0 \\ Edge3 : A_3x + B_3y + d_3 + \Delta t_3 = 0 \end{cases}$$

3) Representation of a 2D CS-dimension:

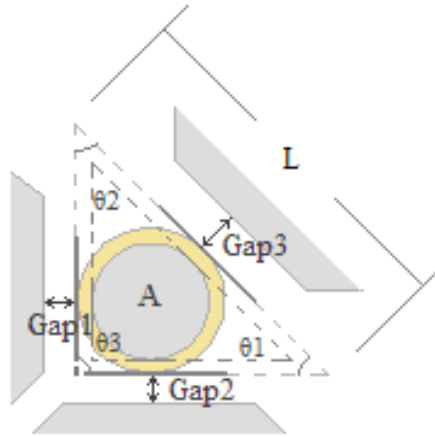
$$\begin{cases} CSDimension = d \sin(\theta_1) \sin(\theta_2) \\ CSTolerance = \Delta d \sin(\theta_1) \sin(\theta_2) \\ d = \sqrt{(p_{1,x} - p_{2,x})^2 + (p_{1,y} - p_{2,y})^2} \\ \Delta d = \sqrt{(\Delta p_{1,x} - \Delta p_{2,x})^2 + (\Delta p_{1,y} - \Delta p_{2,y})^2} \end{cases}$$

where:

- a)  $d$  is the CS-dimension of an edge of the CS,
- b)  $\theta_1, \theta_2$  are the two angles associated with the edge, and
- c) 
$$\begin{cases} Po_{int1} : \begin{cases} p_{1,x} = ((d_3 + \Delta t_3)B_1 - (d_1 + \Delta t_1)B_3) / (A_1B_3 - B_1A_3) \\ p_{1,y} = ((d_3 + \Delta t_3)A_1 - (d_1 + \Delta t_1)A_3) / (A_3B_1 - B_3A_1) \end{cases} \\ Po_{int2} : \begin{cases} p_{2,x} = ((d_3 + \Delta t_3)B_2 - (d_2 + \Delta t_2)B_3) / (A_2B_3 - B_2A_3) \\ p_{2,y} = ((d_3 + \Delta t_3)A_2 - (d_2 + \Delta t_2)A_3) / (A_3B_2 - B_3A_2) \end{cases} \\ \Delta Po_{int1} : \begin{cases} \Delta p_{1,x} = (\Delta t_3B_1 - \Delta t_1B_3) / (A_1B_3 - B_1A_3) \\ \Delta p_{1,y} = (\Delta t_3A_1 - \Delta t_1A_3) / (A_3B_1 - B_3A_1) \end{cases} \\ \Delta Po_{int2} : \begin{cases} \Delta p_{2,x} = (\Delta t_3B_2 - \Delta t_2B_3) / (A_2B_3 - B_2A_3) \\ \Delta p_{2,y} = (\Delta t_3A_2 - \Delta t_2A_3) / (A_3B_2 - B_3A_2) \end{cases} \end{cases}$$

The shape of a 2D CS is represented by a triangle whose sides are composed of CS-features as shown in Figure 15.11. The CS-dimension of a 2D CS is equal to one side of the triangle multiplied by the sine values of the two angles associated with it. Physically speaking, the value of the CS-dimension is equal to the diameter of the circumscribed circle of the triangle times the sine values of its three angles.

*Type-II: 2D CS of a cylinder or sphere*



**Figure 15.12.** 2D CS of a cylinder or sphere

If the equation of the feature interfering with the cylinder or sphere is  $A_1x + B_1y + D_1 = 0$ , the equation of the imaginary tangent plane contacting the cylinder or sphere is:

$$A_1(x - x_o) + B_1(y - y_o) \pm (r + \Delta t)\sqrt{(A_1^2 + B_1^2)} = 0$$

The triangle of the 2D cylinder/sphere CS is formed by three imaginary tangent planes created at the contact points of the cylinder or sphere as shown in Figure 15.12. The tolerance zone of the cylinder or sphere is transformed into the equivalence tolerance zones of the three imaginary tangent planes.

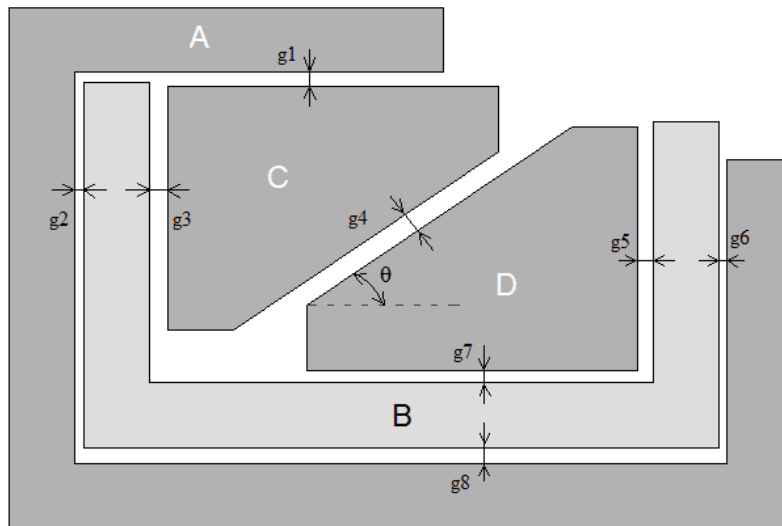
The value  $\Delta t$  of the cylindricity tolerance zone is equal to the value  $\Delta t$  of the parallelism tolerance zone of an imaginary tangent plane. As rotations of parts are forbidden during analyzing, the three contact points on the cylinder or sphere should

remain the same all the time. The CS-dimension of the 2D cylinder/sphere CS is calculated in the same way as the 2D polygon CS.

### 15.15. Case study

The RGSA model has been tested by using it to solve various assembly conditions, such as floating assemblies, kinematic assemblies, static assemblies and so on. In each case, different dimensioning schemes and tolerances were allocated on parts in order to verify the validity of developed tolerance integrating and validating methods, and the analysis results were compared with other tolerance analysis tools, such as CETOL 6Sigma, as well as the GSA model. In most cases, statistic assembly analyses are performed using Monte Carlo simulation and histogram methods, and the contributors' tolerances defined on the assembly are assumed to correspond to 3 or 6 standard deviations ( $\Delta d = 6\sigma$ , for example). By using it to solve these real engineering problems, the applicability of the RGSA model is examined.

As shown in Figure 15.13, the 2D polyhedron assembly is composed of four polyhedrons. Manufacturing dimensioning schemes are defined on all of them to guide manufacturing processes.



**Figure 15.13.** 2D polyhedron assembly

There are two fitting conditions within these polyhedrons. One is a 1D fitting condition, which is composed of ( $g_2, g_6$ ); the other is a 2D fitting condition composed of ( $g_1, g_3, g_4, g_5, g_7, g_8$ ). The 2D polyhedron assembly has been well-analyzed using worst-case tolerance analyses. In this case, real G&T data coming from manufacturing processes are used to represent possible variations of the polyhedrons. The contributors' tolerances defined on them are assumed to correspond to 3 standard deviations ( $\Delta d = 3\sigma$ ).

– Representations of the fitting conditions

Gap representation:

$$FC_1 = g_2 + g_6$$

$$FC_2 = g_1 \cos \theta + g_3 \sin \theta + g_4 + g_5 \sin \theta + g_7 \cos \theta + g_8 \cos \theta$$

Geometric representation:

$$FC_1 = CS(A_2) - CS(B_1)$$

$$FC_2 = CS(A_1) \cos \theta + CS(B_2) \sin \theta - CS(C_1) - CS(D_1) - CS(B_3) \cos \theta$$

– Calculation of part A

In part A (Figure 15.14), as every feature is parallel with one of the two standard pieces of data, dimensions with dimensional constraints are allocated between edges according to requirements of manufacturing. As opposed to part C, all the dimensions are specified between parallel features, and no constraints are defined, such as parallelism or perpendicularity. Relationships between individual dimensions, tolerances and pieces of data of part A are modeled by the 2D-RTC (Figure 15.15).

As shown in Figure 15.15, there are two 1D CSs ( $A_1$  and  $A_2$ ) on part A.  $CS-A_1$  controls the vertical movement of the part A, whereas  $CS-A_2$  controls its horizontal movement. The CS-dimension of  $A_1$  is equal to the distance between feature  $ed$  and feature  $fg$ . As there is a dimension with a dimensional tolerance defined between them, the CS-dimension of  $A_1$  should be equal to the dimension. This is consistent with the analysis result of the 2D-RTC.

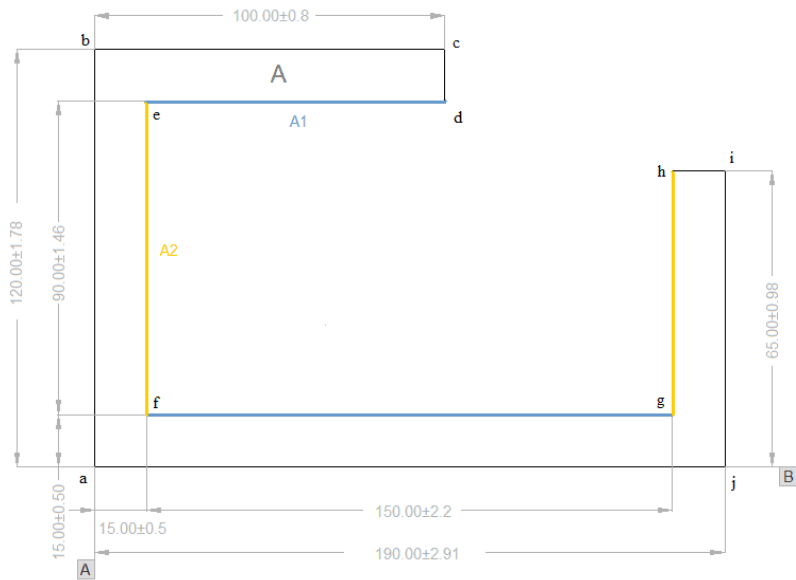


Figure 15.14. The MD dimensioning scheme of part A

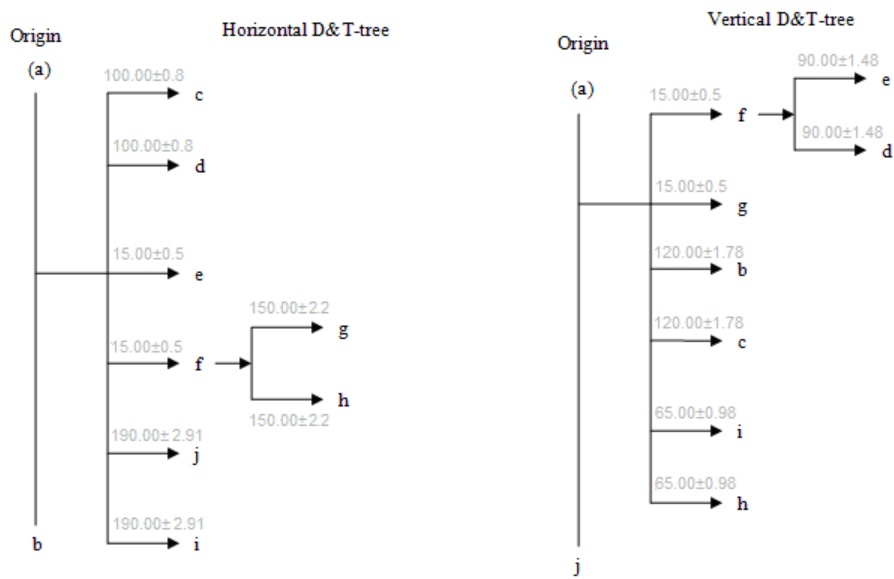


Figure 15.15. The 2D RTC of part A

1) Representation of CS-A<sub>1</sub>

$$A_1 = dis(ed, fg)$$

2) Equation of feature *ed*

$$y - d_1(15.00 \pm 0.50) - d_2(90.00 \pm 1.46) = 0$$

3) Equation of feature *fg*

$$y - d_1(15.00 \pm 0.50) = 0$$

4) The CS-D&T of CS-A<sub>1</sub>

$$CS - D \& T(A_1) = d_2(90.00 \pm 1.46)$$

The CS-D&T of CS-A<sub>2</sub> is calculated in the same way as CS-A<sub>1</sub>. Detailed steps are not given here. The calculation results are listed below:

1) Representation of CS-A<sub>2</sub>

$$A_2 = dis(ef, hg)$$

2) The CS-D&T of CS-A<sub>2</sub>

$$CS - D \& T(A_2) = d_{10}(150.00 \pm 2.20)$$

As shown from the above results, the calculation results of the RGSA model are consistent with our observations.

## – Calculation of the fitting conditions

The probability distributions of the fitting conditions are obtained through Monte Carlo simulation by picking up random CS values according to the calculated probability distributions of their CSs.

$$FC_1 = d_{18}(2.87 \pm 5.34)$$

$$FC_2 = d_{19}(6.02 \pm 6.11)$$



$FC_1 = CS(A_2) - CS(B_1)$	
$CS(A_2)$	$CS - D \& T(A_2) = d_{10}(150.00 \pm 2.20)$
$CS(B_1)$	$CS - D \& T(B_1) = d_{11}(147.10 \pm 3.12)$

**Table 15.1.** Calculation of the fitting condition  $FC_1$ 

$FC_2 = CS(A_1) \cos \theta + CS(B_2) \sin \theta - CS(C_1) - CS(D_1) - CS(B_3) \cos \theta$	
$CS(A_1)$	$CS - D \& T(A_1) = d_2(90.00 \pm 1.46)$
$CS(B_2)$	$CS - D \& T(B_2) = d_{12}(116.00 \pm 1.80)$
$CS(C_1)$	$CS - D \& T(C_1) = d_9(60.52 \pm 1.68)$
$CS(D_1)$	$CS - D \& T(D_1) = d_9(60.52 \pm 1.68)$
$CS(B_3)$	$CS - D \& T(B_3) = d_{13}(15.00 \pm 0.60)$

**Table 15.2.** Calculation of the fitting condition  $FC$ **15.16. Conclusion**

By integrating various D&T elements and dimensioning schemes into the RGSA model and analyzing the linear or non-linear representation of the set of independent fitting conditions using Monte Carlo simulation or optimization methods, the RGSA model was enriched to include two main components of modeling an assembly: a complete tolerance stack-up model and a systematic analysis procedure with established rules for various D&T specifications. The RGSA model is more understandable than before by virtue of using dimensions and tolerances, which are elements common to engineering practices, as the sources of engineering variations.

By applying it to resolving some practical engineering issues, the RGSA model has proved to be a reasonable and effective tolerance analysis method. However, a comprehensive assembly analysis model should cover various capabilities and characteristics of analyzing and improving the design. The RGSA model developed above is still a long way from completely realizing its goals. Future refinements and enhancements of the model are necessary to extend its applications in engineering practices.

### 15.17. Acknowledgments

The authors are pleased to acknowledge the financial support for this work from the National Science Foundation (CMMI-0237501). Any opinions, findings and conclusions or recommendations expressed in this chapter are those of the authors and do not necessarily reflect the views of the National Science Foundation.

### 15.18. Bibliography

- [CAR 93] CARR, C.D., A Comprehensive Method for Specifying Tolerance Requirements for Assemblies, MS thesis, Brigham Young University, 1993
- [CHA 97] CHASE, K.W., and MAGLEBY, S.P., "A comprehensive system for computer-aided tolerance analysis of 2D and 3D mechanical assemblies", *The 5th International Seminar on Computer-Aided Tolerancing*, 1997
- [CHA 99] CHASE, K.W., Tolerance analysis of 2D and 3D assemblies, ACATS Report No. 99-4, 1999.
- [MOR 01] MORSE, E. P., Capturing assembly tolerances and criteria in a common model, DETC2001/DFM-21107, 2001.
- [XUE 01] XUE, J.B., JI, P., "A 2D tolerance chart for machining angular features", *Int. J. Av. Manuf. Technol.*, 2001, 17:523-530
- [ZOU 02] ZOU, Z., MORSE, E. P., *Assembleability analysis using GapSpace model for 2D mechanical assembly*, DETC2002/DFM-34187, 2002.
- [ZOU 03] ZOU, Z., Multi-dimensional tolerance analysis of mechanical assemblies, PhD thesis, UNC Charlotte, 2003.

## PART III

# Measurement

## Chapter 16

# Impact of the Sampling Strategy on Geometrical Checking Uncertainties

### 16.1. Introduction

Coordinate measuring machines (CMM) have brought a significant enhancement of the industrial geometrical verification process. It has enabled greater access to information than is possible with classic metrology. Conversely, results obtained via a CMM do not provide values directly corresponding to the ISO or ANSI geometrical specifications. The real surface to be verified is composed of infinity points which could be considered to be the statistical population to be characterized. This set of points contains both information of localization and intrinsic dimension of the measured surface. Most of the current geometrical verification methods consist of two separated and independent steps. Firstly, an estimation of the real surface is performed. Results are provided under the form of a set of values representing geometrical parameters of a fitted mean surface. Secondly, an estimation of the uncertainties is performed. This calculation enables the construction of conformance zones. However, these conformance zones are, most of the time, 1D, which is not adapted for 3D geometrical verification. As these two steps of the verification are almost independent, this kind of verification process does not enable us to control the uncertainty of the verification result. In particular, the impact of the probing strategy, which can be defined by the number and the repartition of the measured point, cannot be evaluated. In previous series of research work [SPR 01], [BAC 04], [MAI 08], a verification method based on virtual gauges,

---

Chapter written by Jean MAILHE, Jean-Marc LINARES, Jean-Michel SPRAUEL and Jean-Paul RAYNAL.

including measurement uncertainties, was proposed. This method uses a statistical modeling of real surfaces. This model, called the field of probability of presence of the matter (FPPM), enables us to express the probability of any point of the space to be located inside the matter. If this point is taken as a given location of the virtual gauge, the obtained probability represents the risk of interference between the virtual gauge and the real surface. This enables the construction of an interference probability map (IPM) risking, under the form of a graphic plot, non-conformity of the part. By using this method of geometrical verification, this chapter proposes to study, the effect of the sampling strategy on conformity. Research work already shows the impact of probing strategy on measurement uncertainties [WEC 05]. Supported by two simple cases, an envelope specification and a perpendicularity constraint with maximum material requirement modifier will be considered. This paper will thus deal with the effect of the number of points and their repartition on the verification results.

## 16.2. Geometrical verification and virtual gauges

If the concept of a physical and virtual gauge is still the same, i.e. testing if the matter is completely inside/outside a spatial boundary, there are, however, different ways to perform it. The first method is to directly check the real part with a material gauge. The second method is based on a set of digitized points either tested without any kind of best fitting or described by a feature element derived by a best fit method.

### 16.2.1. Verification by virtual gauge without best fit

The aim of this method is to find the optimal position of the virtual gauge which includes the whole set of digitized points (Figure 16.1). Of course, this position shall be in agreement with the degrees of freedom given by the geometrical specifications.

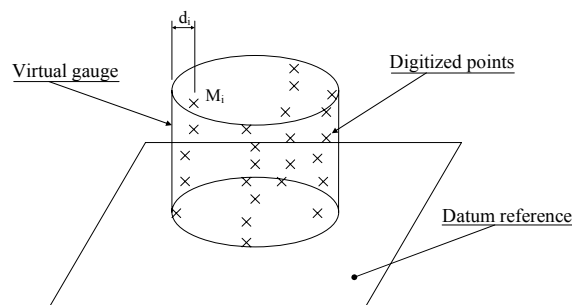
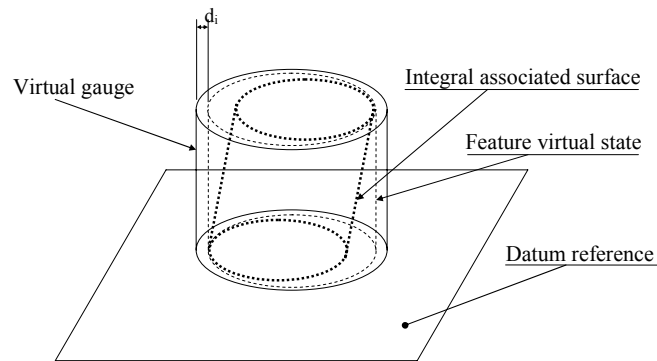


Figure 16.1. Verification of a cloud of points

From a mathematical point of view, an algebraic distance  $d_i$  will be calculated between each digitized point  $M_i$  and the surface of the virtual gauge. The conformance test will be to check if all the distances  $d_i$  are positive or negative, i.e. if the points are inside or outside the virtual gauge, according to the geometrical specifications. The main advantage of this kind of conformance test is to avoid any geometrical construction and hence to keep away from uncertainty propagation. However this does not account for some statistical experimental perturbations.

### 16.2.2. Verification with associated feature

The principle behind this method is to perform an assembly test between an estimated and/or constructed feature and the virtual gauge (Figure 16.2).



**Figure 16.2.** Verification with virtual state of the matter

For that purpose, a surface envelope representing the virtual state of the feature is constructed. Its estimation results from the addition of the perpendicularity error, and the evaluated dimension of extreme fit. Then, to be accepted, the virtual state dimensions must be lower or greater than the virtual gauge dimensions, i.e. it must be inside or outside the matter according to the geometrical specifications.

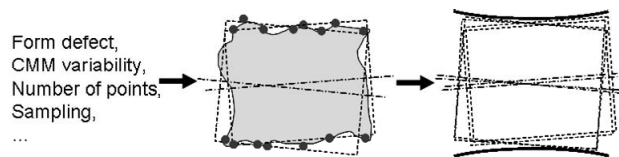
The virtual gauge could also have a fitting behavior [PAI 97]. In that case, an extreme fitting of the whole set of digitized features will be performed in a particular order defined by the geometrical specifications. Then the same test as above will be applied between the fitter gauge and the limiting gauge obtained from the geometrical specifications.

### 16.2.3. Statistical point of view

All previous kinds of verification do not account for measurement uncertainties, but each acquired coordinate is assumed to perfectly describe the real surface. Actually, the real surface to be verified is composed of infinity points which could be described as a statistical population to be characterized. Hence the acquired coordinates are a random sampling of the real points of the tested surfaces, including measurement perturbations. The aim of the geometrical verification is thus to estimate the probability of the real surface conforming the virtual gauge. In the next three sections, a geometrical verification method based on the virtual gauge and including uncertainties will be presented.

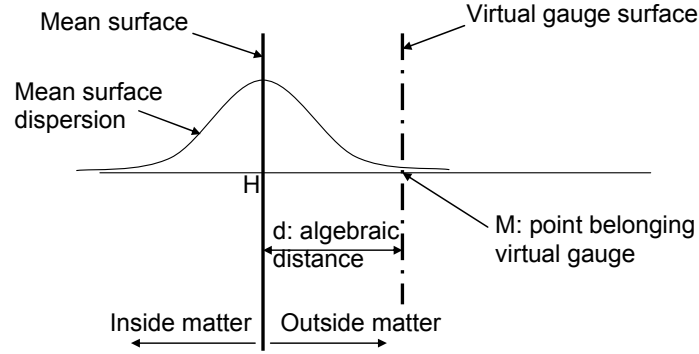
### 16.3. Field of probability of the presence of matter

The first step of the method used in this paper is the statistical modeling of a real surface. There are different sources of uncertainties: geometry and thermal expansion compensation errors, form defects not described by the selected surface model, sampling strategy, etc. These uncertainties will be propagated when estimating the best fitted surface (Figure 16.3). The instrument errors (geometry and thermal expansion deviations, etc.) are nevertheless assumed to be completely corrected and their uncertainties are neglected. This important point will however be treated in future research works.



**Figure 16.3.** Best fit uncertainty effect

Statistical modeling of a surface does not define a finite best fitted surface, but a fuzzy limit of the matter. This model consists of providing a random vector describing a set of stochastic variables representing a point, a vector and, if necessary, a set of intrinsic geometrical parameters. This enables us to define the mean values and uncertainties, of the localization, orientation and dimensions of a measured feature. A best fitting of the acquired points provides a mean vector and a covariance matrix [SPR 01]. At this time, an iterative non-linear least squares optimization method is employed for that purpose. The covariance matrix is obtained by a classic propagation of the best fit residues to the estimated random vector.



**Figure 16.4.** Presence of matter probability

Our goal is then to calculate the probability of any point M to be located inside the matter, i.e. to have a negative algebraic distance. To perform this calculation, all the uncertainties integrated in the random vector are propagated to the estimated integral surface. For that purpose the projection H of point M, to the mean integral surface is first computed. The expression of the algebraic distance between M and the best fitted feature is thus easily derived [16.1]:

$$d_M = \overline{HM} \cdot \vec{n}_S \quad [16.1]$$

where  $\vec{n}_S$  is the normal vector of the integral surface at point H. The classic propagation method is then used to calculate its variance [16.2]:

$$\text{var}(d_M) = J \cdot \text{Cov}(\vec{p}) \cdot J^T \quad [16.2]$$

where J represents the Jacobian vector of scalar  $d_M$ . However, this variance only characterizes the variability of the estimated integral surface. To define the boundaries of the probed feature, the variance of the acquired points, as defined by the mean least squares residues, also has to be added to it [16.3].

$$\sigma_{\text{Global}/n_s}^2 = J \cdot \text{Cov}(\vec{p}) \cdot J^T + \sigma_{\text{Residues}}^2 \quad [16.3]$$

This enables us to calculate the probability  $\text{prob}(M)$  of any point M to be located inside the matter by using a classic integration of a Gaussian law (Figure 16.4). Thus, a 3D scalar function  $\text{prob}(M)$  is built called field of probability of the presence of matter (FPPM).

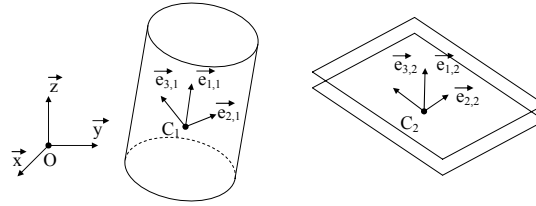


### 16.4. Virtual gauges

The geometrical product specification (GPS) language is based on the notions of tolerance zone and modifiers (maximum material condition (MMC), least material condition (LMC), envelop requirement (E), etc.). This enables us to define a set of acceptable part geometries. The boundaries of any tolerance zone can be represented by elementary virtual gauges. Virtual gauges are the numerical and extended version of physical gauges. Each elementary gauge, of index  $i$ , can be represented by a family of seven vectors, named  $E_i$ , see equation [16.4].

$$E_i = \{\vec{x}_i \quad \vec{y}_i \quad \vec{z}_i \quad \vec{e}_{00i} \quad \vec{e}_{1,i} \quad \vec{e}_{2,i} \quad \vec{e}_{3,i}\}^T \quad [16.4]$$

The first three vectors form the construction basis which will enable us to express the link between all elementary gauges. Fourth vector defines the translation direction of the gauge. The last three vectors form the local basis which characterizes the orientation of the gauge. Figure 16.5 represents two virtual gauge systems connected by their construction basis.



**Figure 16.5.** *Virtual gauge assembly*

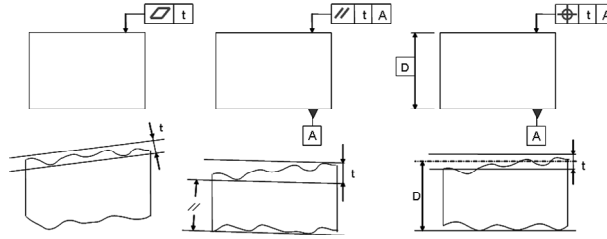
The vector family of an elementary gauge can be efficiently modeled by a Gram matrix  $\overline{\overline{G_i}}$  [CLE 99] defined by the following tensorial product [16.5]:

$$\overline{\overline{G_i}} = E_i \otimes E_i^T \quad [16.5]$$

Gram matrix  $\overline{\overline{G_i}}$  is a second order tensor of rank 3 (3D space) and size 7 x 7. The construction of the global virtual gauge requires a connection between the different elementary entities (Figure 16.5). This condition is realized by imposing the equality of the entire construction basis  $(\vec{x}, \vec{y}, \vec{z})$ . It is performed by a connection operator  $C$  which represents all connection specifications [16.6].

$$\overline{\overline{G}}_f = C \cdot \overline{\overline{G}}_{nc} \cdot C^T \quad \overline{\overline{G}}_{nc} = \begin{bmatrix} \overline{\overline{G}}_1 & 0 & 0 \\ 0 & \ddots & 0 \\ 0 & 0 & \overline{\overline{G}}_n \end{bmatrix} \quad [16.6]$$

Tensor  $\overline{\overline{G}}_{nc}$  represents the disconnected global virtual gauge, constructed with all the (number  $n$ ) elementary entities. The linear operator  $C$  is a matrix of size  $7 \times n$ . The final Gram matrix  $\overline{\overline{G}}_f$  represents the global virtual gauge. It is still rank 3, but has a size of  $(7 \times n) \times (7 \times n)$ . The result of the connection is a global virtual gauge given in a specific position. However tolerance zones can have their own degrees of freedom (DOF) (Figure 16.6). To model these DOFs, a perturbation operator is introduced [SER 05].



**Figure 16.6.** DOF of tolerance zones or gauges

The principle of the perturbation is to express a variation of the vector family and thereafter to derive the resulting Gram matrix [16.7].

$$\begin{aligned} \overline{\overline{G}}'_f &= (I + \Omega) \cdot \overline{\overline{G}}_f \cdot (I + \Omega)^T \\ &= (I + \Omega) \cdot C \cdot \overline{\overline{G}}_{nc} \cdot C^T \cdot (I + \Omega)^T \end{aligned} \quad [16.7]$$

Matrix  $\Omega$  represents the variations  $\Delta E_i$  applied to the different vector families  $E_i$ . Hence the following relation is obtained [16.8]:

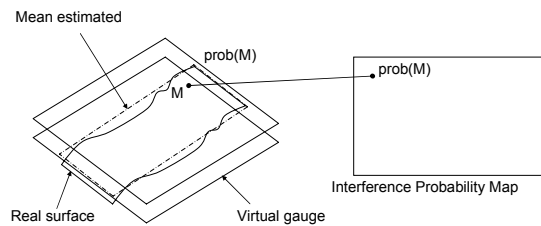
$$\begin{bmatrix} \Delta E_1 \\ \Delta E_2 \\ \vdots \\ \Delta E_n \end{bmatrix} = \Omega \cdot \begin{bmatrix} E_1 \\ E_2 \\ \vdots \\ E_n \end{bmatrix} \Rightarrow \begin{aligned} E' &= E + \Delta E = (I + \Omega) \cdot E \\ \overline{\overline{G}}' &= E'^T \otimes E' \\ \overline{\overline{G}}' &= (I + \Omega) \cdot \overline{\overline{G}} \cdot (I + \Omega)^T \end{aligned} \quad [16.8]$$

where  $E$  represents the global family of vectors and  $E'$  the perturbed result.

The last step of the virtual gauge construction is the expression of its surface boundaries. Such surface will be characterized by a parametric equation based on the local basis of each elementary virtual gauge. Scanning of the virtual gauge surface is possible using curvilinear coordinates of the parametric formulation.

### 16.5. Interference probability map

The virtual gauge has been defined as the boundary of a tolerance zone. It represents a volume of 3D space in which the real surface must be found. A part will be rejected if an intersection between the real surface and the virtual gauge exists. The probability of such an intersection can be represented graphically, at any point on the gauge. This is a 2D scalar field (the virtual gauge being a surface) which can be presented in the form of an interference probability map (IPM). The FPPM is particularly well adapted to virtual gauges. During the checking phase, point M is just taken as a given point of the virtual gauge. Then the FPPM enables us to calculate the corresponding probability  $\text{prob}(M)$  (Figure 16.7). This probability represents the risk of the selected point M of the virtual gauge to enter the matter, i.e. the non-conformance risk at this location.



**Figure 16.7.** *Interference probability map*

This calculation can be done for any point of the virtual gauge elements. A set of probabilities is thus calculated which allows the construction of an IPM.

#### 16.5.1. Geometrical verification process

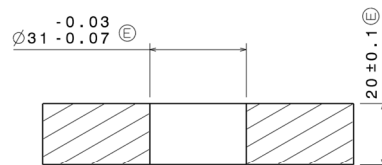
The geometrical verification based on virtual gauge and FPPM consists of verifying if the whole set of probabilities obtained from points of the virtual gauge remains below the risk level fixed by the quality control inspector. To maximize the chance of a part conforming, the position of the global virtual gauge which minimizes the maximum interference probability must be found. This optimization problem corresponds to a Mini Max problem applied to the whole set of interference probabilities.

## 16.6. Experiment

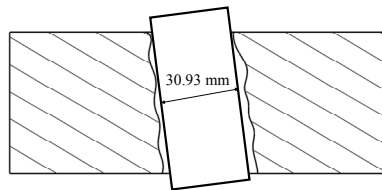
This method has been applied to highlight the impact of two aspects of the sampling strategy: the number of probed points and their repartition. In the next two subsections, the geometrical verification problem of a bore in a parallelepiped will be considered. Firstly the case of an envelope requirement will be studied. The considered bore will be measured in three different ways. Then a perpendicularity condition will be checked using the three same kind of probing strategy.

### 16.6.1. Envelope zone specification

Figure 16.8 presents the case of a bore geometrically specified by an envelope requirement. According to (ISO 8015 - 1985) standards, the principle of envelop requirement implies the nominally cylindrical real surface of the bore remaining outside a perfect cylinder at the state of maximal material (Figure 16.9). In the case under consideration the envelope diameter is 30.93 mm (Figure 16.9). Additionally, every distance between two opposite points must be less than the maximum allowed distance of 30.97 mm, in our case (ISO 14 660-1). However, our study will just focus on the constraint imposed by the envelope zone.



**Figure 16.8.** Nominal design and geometrical tolerance



**Figure 16.9.** Conformance test

Basically, the virtual gauge will be a perfect cylinder with six degrees of freedom. Thus, optimization of the gauge position will be gained on the three rotations and the three translations.

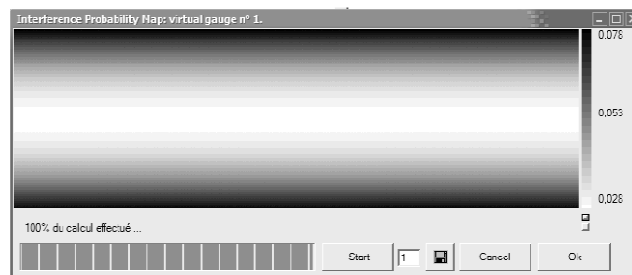
Three different probing strategies have been applied for the measurement of the bore:

- Firstly, 16 points have been probed evenly distributed on the surface of the measured feature.
- Secondly, the 16 points have been concentrated at the edge of the bore.
- Thirdly, a set of 32 points has been acquired with a uniform repartition on the considered bore.

For each case the random vector of the surface has been defined by best fit, using the maximization of the likelihood function. This enabled us to express the FPPM for each estimated surface.

Before seeing the statistical geometrical verification result, a classic verification process based on least square and the shape defect has been made:

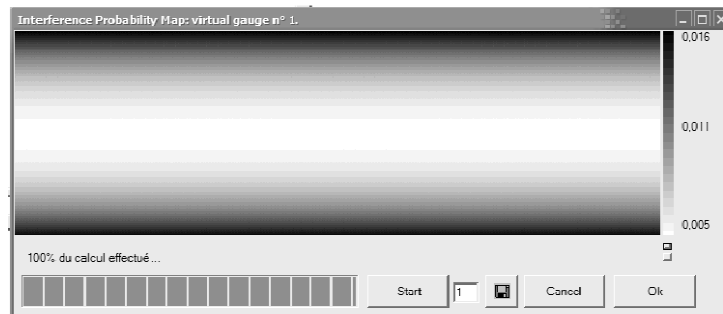
- In the case of 16 points evenly distributed, a diameter of 30.987 mm and a shape defect of 0.021 mm have been found. Hence the diameter of the smallest envelope tangent to the matter is estimated to be about  $30.987 - 0.021 = 30.966$  mm, which is large enough to accept the part.
- In the case of 16 points concentrated at the edge of the bore, a diameter of 30.987 mm and a shape defect of 0.018 mm have been found. Hence the diameter of the smallest envelope tangent to the matter is estimated to be  $30.987 - 0.018 = 30.969$  mm, which is large enough to accept the part.
- In the case of 32 points, a diameter of 30.988 mm and a shape defect of 0.018 mm have been found. Thus the part should be declared as conforming to an estimation of the diameter of the smallest envelope tangent to the matter of 30.970 mm. Note that these results do not account for measurement uncertainties.
- In the case where the part is characterized from the set of 16 points, the following IPM is obtained after optimization (see Figure 16.10).



**Figure 16.10.** *Interference probability map for 16 points*

This IPM shows three different zones. The centered one is the best characterized zone of the part; here the probability of interference between the real surface and the virtual gauge is small (below 5.3%). This zone is located around the barycenter of the digitized points. Next, there are the two extremity zones where the knowledge of the part is the worst (from 5.3% to 7.8% at edges); here the uncertainty on the mean surface increases proportionally with the distance to the barycenter of the acquired coordinates.

An obvious fact is the symmetry around the plane perpendicular to the cylinder axis. This shows that the optimization of the gauge position leads us to put the gauge axis collinear to the mean associated surface axis. This alignment seems foreseeable due to the envelope requirement verification keeping all degrees of freedom on the gauge position.



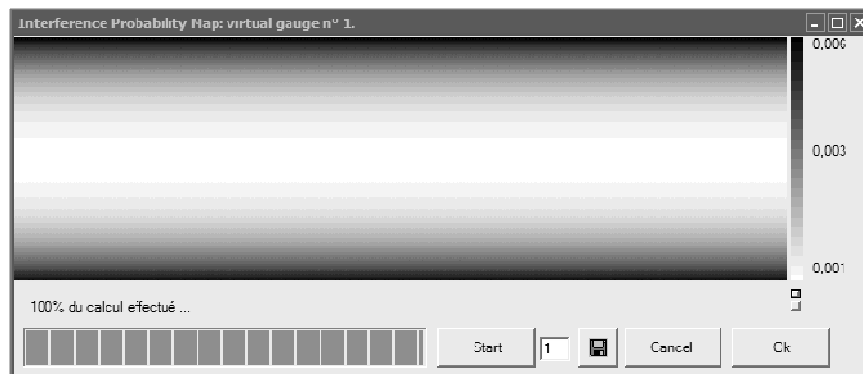
**Figure 16.11.** *Interference probability map for 16 points at the edge of the bore*

Revolution symmetry is notable. This is a particular case. Indeed the covariance matrix is symmetrical and defined positively. With the propagation calculation, using the Jacobian operator, the theoretical shape of a statistical envelop is a hyperboloid with an elliptic base. At the moment only first and second moment orders are used for part characterization. Moreover, for the best fit, the assumption that all points have the same standard deviation is made. Therefore, this symmetry shows that the digitized points were selected symmetrically. In the case where the part is characterized from the set of 16 points located at the edge of the bore, following IPM is obtained after optimization (Figure 16.11).

In this case, the verification uncertainties are five times lower than for previous point repartition. Actually, the difference between these two cases is the orientation uncertainty. The small lever effect of the point repartition in the second case is favorable to the estimation of the orientation. However, this kind of repartition is really dangerous because the form defect of the bore becomes undefined. Hence this

kind of reparation should be applied only for high quality surfaces with low form defect.

In the case where the part is characterized from the set of 32 points, the following IPM is obtained after optimization (Figure 16.12).



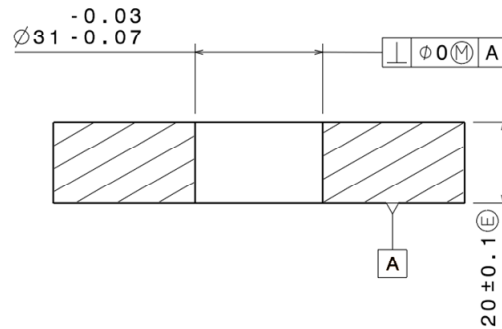
**Figure 16.12.** *Interference probability map for 32 points*

The maximal interference probability is 0.6% at the edge. This great decrease of uncertainties is due to the increase in point numbers. The form defect also decreases from 0.021 mm with 16 points to 0.018 mm.

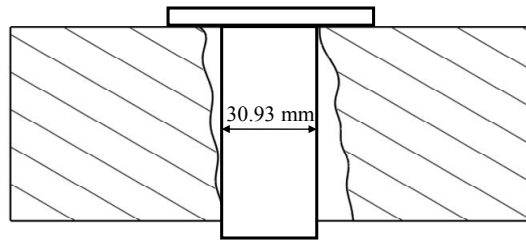
#### **16.6.2. Perpendicularity specification**

In this subsection, the case of a perpendicularity requirement between a bore and a plane is considered (Figure 16.19). Plane A is taken as datum reference surface. In this case, only acquisitions with 16 and 32 points evenly distributed will be studied.

According to geometrical specification standards, the datum reference surface is defined as the perfect plane extreme fitting to the real surface, nominally plane A, and minimizing the highest gap. To be accepted the nominally cylindrical real surface of the bore must be outside a perfect cylinder perpendicular to plane A, with a diameter of 30.93 mm (ISO 2692 - 1988) (Figure 16.14). The difference with the first case study is the constraint put on the virtual gauge. Indeed the degrees of freedom are now restricted to two translations leaving reference plane A globally invariant.



**Figure 16.13.** Nominal design and geometrical tolerance



**Figure 16.14.** Conformance test

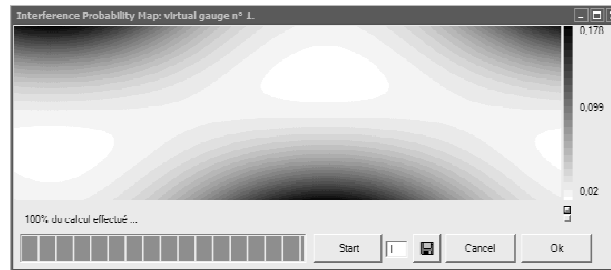
The surface characterization is achieved with the two previous sets of digitized points. The datum reference surface is built on a cloud of 16 points. Although it is just a first approach, the uncertainty of this surface is neglected. Using the classic least squares and shape defect method the following results are obtained:

- For 16 points, the measured diameter is 30.987 mm, the shape defect is 0.021 mm and the perpendicularity defect is 0.029 mm. Hence the diameter of the perfect cylinder representing the state of the maximum of matter is 30.937 mm. Thus, the part should be accepted and has a clearance of 7  $\mu\text{m}$ .

- For 32 points, the measured diameter is 30.988 mm, the shape defect is 0.018 mm and the perpendicularity defect is 0.028 mm. Hence the diameter of the perfect cylinder representing the state of the maximum of matter is 30.942 mm. Thus, the part should be accepted and has a clearance of 12  $\mu\text{m}$ .

In the case where the part is characterized from the set of 16 points, the following IPM is obtained after optimization (Figure 16.15).





**Figure 16.15.** *Interference probability map for 16 points*

With this IPM, two critical zones of the verified cylinder can be highlighted. In these two zones, the maximal probability of the part being non-conforming is 17.8%. This high risk is mainly due to the uncertainties about the cylinder direction and shape error, on the one hand, and to the mean high orientation error, on the other hand.



**Figure 16.16.** *Interference probability map for 32 points*

In the case where the part is characterized from the set of 32 points, the following IPM is obtained after optimization (Figure 16.16): with such a high number of digitized points, the uncertainties on the direction are greatly decreased. Here the probability of interference falls to 7.4% at the critical zone.

## 16.7. Conclusion

In this chapter, a method of geometrical checking based on virtual gauges using a statistical criterion has been presented. The FPPM model combined with a virtual gauge design enabled an efficient estimation of verification risks. The use of IPMs then allowed a fast and clear interpretation of the verification result. In addition, a fast estimation of the efficiency of the measurement process planning was possible.

This enabled us to adjust the measurement process for critical cases. This method has been applied to discussions on the impact of the probing strategy on verification uncertainties. A case study of a bore with an envelope requirement and a perpendicularity specification with maximum material requirements has been considered for that purpose. Two aspects of the probing strategy have been studied. Firstly, the repartition of the probed points has been tested when checking the envelope requirement. It has shown that a repartition at the edge of the measured surface decreases the orientation uncertainty of the best fitted surface. However, this kind of strategy should be used carefully. Actually, probing only the edge of a surface hides the impact of the form defect. It has also been shown that increasing the number of points highly improves the accuracy of measurements.

## 16.8. Bibliography

- [BAC 04] BACHMANN J., LINARES J.M. SPRAUEL, J.M., BOURDET P., “Aid in decision-making: contribution to uncertainties in three-dimensional measurement”, *Precision Engineering*, Vol. 28, p.78-88, 2004.
- [CLE 99] CLÉMENT A., RIVIÈRE A., SERRÉ P., “Global Consistency of Dimensioning and Tolerancing”, *Proceeding of the 6th CIRP International Seminar on Computer-Aided Tolerancing*, Twente, Kluwer Academic Publishers, p.1-26, 1999.
- [MAI 08] MAILHE J., LINARES J.M., SPRAUEL J.M. , “Geometrical checking by virtual gauge, including measurement uncertainties”, *CIRP Annals-Manufacturing Technology*, Vol. 57, p.513-516, 2008.
- [PAI 97] PAIREL E., “The Gauge model: a new approach for coordinate measurement”, *Proceeding of the XIV IMEKO World Congress*, Tampere, p. 278-283, June 1997.
- [SER 05] SERRÉ P., RIVIÈRE A., CLÉMENT A., “Dependence and Independence of Variations of Geometric Object”, *Selected Conference Papers from the 9th CIRP Computer-Aided Tolerancing Seminar*, Tempe, Springer, p.23-34, 2005.
- [SPR 01] SPRAUEL J.M., LINARES J.M., BOURDET P. “Contribution of nonlinear optimization to the determination of measurement uncertainties”, *Selected Conference Papers of the 7th CIRP Seminar on Computer-Aided Tolerancing*, Cachan, Kluwer Academic Publishers, p. 235-44, 2001.
- [WEC 05] WECKENMANN A., LORZ J., BEETZ S., “Monitoring coordinate measuring machines by user-defined calibrated parts”, *Selected Conference Papers from the 9th CIRP Computer-Aided Tolerancing Seminar*, Tempe, Springer, p.125-135, 2005.

## Chapter 17

# Predetermination of Measurement Uncertainty in the Application of Computed Tomography

X-ray computed tomography (CT) is the latest innovation in manufacturing metrology as it offers several opportunities which are not possible with conventional tactile or optical measurement devices. Due to this fact current research work is concerned with the determination of the task-specific measurement uncertainty for CT measurements as it is an important parameter describing the quality and the reliability of measurement results. In this chapter we present research work focused on the determination of influences which can be controlled by the machine operator when preparing the measurement data acquisition and evaluation, like the magnification of the workpiece, the number of projections taken, the resolution of the projections (detector pixel binning) or the used analysis software. After the quantification of these influences a task-specific measurement uncertainty budget according to GUM has been calculated. These results can either be used to compare the user-controllable influence to the influence of the machine components on measurement uncertainty or as guidance for the operator to reduce uncertainty in preparation for measurements.

### 17.1. Introduction

X-ray CT is a rather new technology in manufacturing metrology, as the first devices designed specifically for metrological purposes came to the market after the year 2000. Before that time CT scanners for medical purposes had been adopted,

---

Chapter written by Albert WECKENMANN and Philipp KRÄMER.

especially for non-destructive testing of safety critical components in aviation, i.e. rotor or turbine blades. With developments that increased the accuracy of CT systems, i.e. developments in X-ray components like X-ray tubes or detectors, the use of CT in manufacturing metrology made sense. The incorporation of manufacturers known from CMM metrology ensured the traceability of CT systems and made the use of CT as a measurement device possible.

Research work in the field of computed tomography in manufacturing metrology is focused on the estimation of the task-specific measurement uncertainty as it is an important parameter describing the quality and the reliability of the measurement results. Others deal with the qualification of this novel technique in industrial applications, like the estimation of the capability of the measurement process or device and dealing with mixed material, e.g. for the inspection of multi-material workpieces like electronic components [WEC 07].

## 17.2. Prior investigations

As the CT measurement process is quite complex and therefore difficult to model for example, Monte Carlo simulations or analytic calculations, today it is only possible to analyze the CT measurement uncertainty with the help of calibrated reference workpieces according to GUM. In industrial application this approach is best-suited for the determination of the device's capability which is especially important in the approval of testing processes [BAR 08].

Past and current research work dealing with the estimation and quantification of influences was focused mainly on the modeling of CT components like X-ray sources, detectors or the configuration of the measurement device itself. Other publications were focused on the influence of the measurement object, e.g. its surface roughness and geometry [BAR 04a], [BAR 04b].

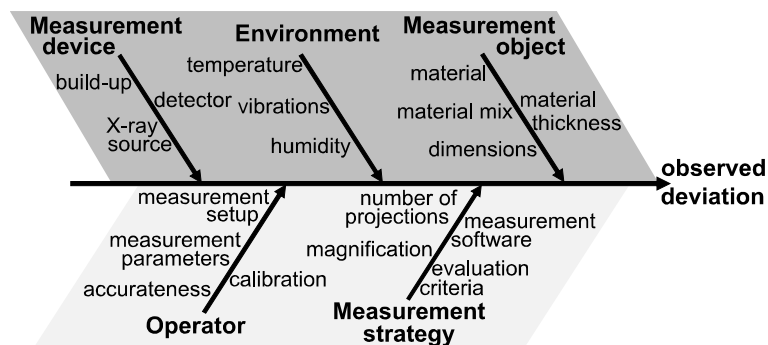


Figure 17.1. Influences on CT measurements

When it comes to measurements with today's modern CT measurement devices the user is typically not able to choose the different machine components himself as these choices have been made by the manufacturer.

As a result of this, analysis and understanding of the CT components is vital for setting up measurement devices as it has great influences on the possible accuracy and measurement uncertainty of the device. So typically the manufacturer tries to increase the potential accuracy as much as possible always regarding the desired choice of measurement objects, e.g. deciding whether the system is suited for engine blocks or small plastic connectors.

However the operator of the measurement device has no influence on the used components like the X-ray tube or detector but nevertheless he has influence on the measurement uncertainty of CT measurements. The control software of the CT offers several parameters for data acquisition: such as radiation energy, detector integration time, magnification, orientation of the measurement object, etc.

As the choice of these parameters is mainly influenced by the experience of the operator, it is important to determine how much he influences the observed deviations and as such the measurement uncertainty. This information may even be used in the preparation of CT measurements to predetermine the measurement uncertainty and the possible accuracy.

### **17.3. Measurements of user-controllable influences**

The investigations for this work were focused on the four main influences by the user when setting up a CT measurement. These parameters are typically accessible in every common user interface of a CT measurement device:

- number of projections (angle steps);
- magnification (resulting voxel size);
- orientation of the workpiece in relation to the X-ray beam and the axis of the rotary table;
- method for threshold estimation (used analysis software tool).

The number of projections directly influences the necessary measurement time and as a result of this industry users try to reduce the amount of projections as much as possible to speed up their measurements to generate results quickly and to reduce the costs associated with the measurement. Preparatory work showed that the size of

the image stack influences the observed deviations, but with more than 800 projections, the results could only be increased by less than 10%.

The size of a workpiece influences the maximum possible magnification, especially if the operator tries to avoid raster tomography where several image stacks representing only parts of the workpiece are combined to a large data set. When short measurement times are needed or desired, lower magnifications are chosen to image the workpiece entirely on the detector during a single measurement.

In contrast, raster tomography could increase the accuracy by reducing the voxel size but the influence of the accuracy of the machine guidance gets more important. The orientation of the measurement object to the rotation axis has influence on the length of the way the rays have to pass through the workpiece and the variation of this length during the rotation while the object is measured.

If the length changes significantly, it is possible that in projections with shorter lengths the object is outshone, while in projections with greater lengths the X-rays parts of the image are too dense and the remaining intensity is too weak for proper reconstruction.

Both situations have to be avoided as the back projection algorithms require well exposed projections in all angle positions to prevent artifacts during the reconstruction of the volumetric model. As a result of this the operator normally tries to position the measurement object so that the length the rays travel through the workpiece is equally distributed along the angle positions. Depending on the geometry and especially the aspect ratio of the measurement object, this problem could cause significant trouble, e.g. for the measurement of PCBs or sheet metal parts with their typical high aspect ratios.

The method for surface extraction, which is often called the “threshold algorithm”, is known to have significant influence on the observed measurement results. If the user has the opportunity to choose between different analysis software, the threshold algorithm is typically chosen.

To represent the extrema of using a simple but less accurate software tool and a more complex and more accurate tool, two different threshold strategies have been investigated using a global and a local adaptive threshold strategy. The software VG Studio MAX 2.0 offers the possibility of using the two different threshold methods and was used for these evaluations.

For these measurements a Werth TomoCheck CT has been used, its parameters are listed in Table 17.1. The settings for the parameters orientation of the workpiece

and magnification had to be chosen prior to the data acquisition. To compare these influences the image stacks have been acquired using parallel and perpendicular orientation to the rotation axis with magnification set to single and twice.

Parameter	Value
Measurement range	h=200 mm, d=90 mm
X-ray source	microfocus source V <sub>max</sub> = 130 kV I <sub>max</sub> = 300 $\mu$ A
Detector	1024 $\times$ 1024 pixels pixel size 50 $\mu$ m
Magnification	pre-calibrated, 1 $\times$ -10 $\times$
Manipulator axes	air beared scale resolution 0.1 $\mu$ m
Additional sensors for multisensor measurements	Image processing, fiber probe, low-force probe, Foucault laser

**Table 17.1.** *Specification of Werth TomoCheck 200 3D*

The measurement parameters X-ray energy, integration time and number of projections for averaging (noise reduction) had to be fixed before the data acquisition to ensure good contrast in the projections and thus enable the reconstruction of the volumetric model. The resulting parameters used for the PVC cylinder are shown in Table 17.2.

Parameter	Value
Acceleration voltage	90 kV
Current	200 $\mu$ A
Detector integration time	250 ms
Averaging of projections	2
Number of projections	1600

**Table 17.2.** *Measurement parameters for PVC workpiece*

These parameter settings represent typical values for the industrial use of CT, especially regarding the measurement time. The observed deviations could be reduced, e.g. by raising the number of projections taken for averaging, but this would also increase the necessary measurement time and thus the trade-off has to be made. For all measurements the maximum possible amount of projections (angle positions) was chosen, the image stack was thinned out after the acquisition and the resulting image stacks consisting of 1,600 or 400 projections were reconstructed to estimate the influence of the size of the image stack.

The next step was the reconstruction of the image stacks using the reconstruction software of the measurement device which is based on the implementation of the filtered backprojection algorithm by the Fraunhofer EZRT. The evaluation of the volumetric data sets was done using VG Studio MAX 2.0 as it allows the comparison of surface extraction with global and local threshold algorithms.

Simple hollow cylinders made of different materials were used as measurement objects. To represent a variety of materials, typical for the application of the used CT, cylinders made of aluminum, PMMA and PVC have been measured. With a height of 10 mm and a diameter of about 15 mm, it is possible to measure them with different magnifications without using raster tomography. These objects can be measured without using the maximum possible X-ray tube power. This limits the size of the focal spot and limits the measurement uncertainty caused by the X-ray source to a few microns.

In order to compare the CT measurement results to the real diameter of the cylinders, reference measurements of the workpieces have been carried out using a tactile CMM Zeiss UPMC 1200 Carat. These results were used to calculate the deviations of the CT measurements without taking care of the deviations of the manufacturing process. For the tactile measurements three sections at both the inner and outer cylinder have been scanned using a tip of 1.000 mm radius. The diameters of the resulting cylinders fitted in the tactile points cloud consisting of 10,000 points, are shown in Table 17.3.

Material of workpiece	Diameter in mm	
	outer	inner
Aluminum	14.9630	10.2516
PMMA	15.0169	10.0860
PVC	14.9879	10.0170

**Table 17.3.** Reference values of cylinder diameters



An experimental design has been setup to facilitate the evaluation of the measured deviations of the cylinders' diameters. The following factors and their corresponding two settings (-/+) for each parameter are listed in Table 17.4.

factor	Chosen settings	
	-	+
magnification	1×	2×
orientation	parallel to rotation axis	perpendicular to rotation axis
number of projections	400	1,600
threshold method	global	local adaptive

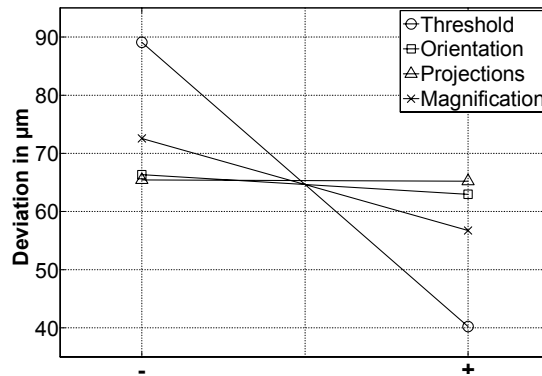
**Table 17.4.** *Factor settings for evaluation of measurements*

#### 17.4. Estimation of influences

With the help of VG Studio MAX 2.0 the inner and outer diameters of the cylinders in the different volumetric models has been evaluated. Based on eight manually chosen points on the surface, a curvature-based algorithm extracted 1,000 points from the CT points cloud and fitted a cylinder into these points using a Gaussian best-fit algorithm. The resulting diameters have been compared to the reference values to determine the deviation of the CT measurement process.

The result of the evaluation process is shown in Figure 17.2 which illustrates the calculated effects of the different factor settings for the estimation of the outer cylinder. It is obvious that the threshold algorithm is the most important influence on the operator controls.

Although a global threshold extraction is quick and simple, it is far less accurate than the local adaptive method. In order to reduce the measurement uncertainty and increase the accuracy of the measurements, software using local surface extraction should always be preferred.



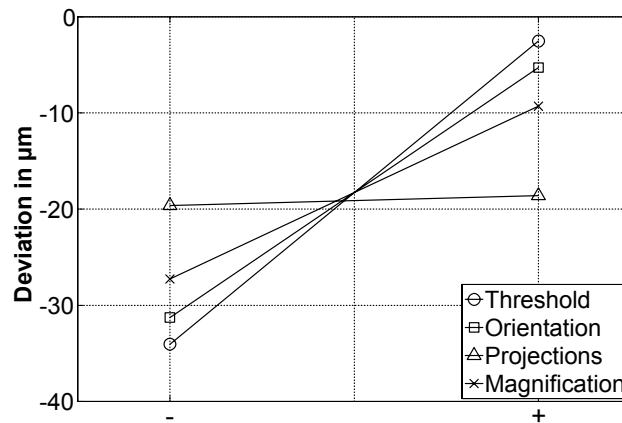
**Figure 17.2.** Effect diagram of the outer diameter of the hollow PVC cylinder

Further investigations could compare different software tools with different local threshold algorithms (edge finder) to analyze their influence in detail. The next important factor is the magnification of the measurement object. It has only about 1/10 the effect of the threshold, but as it influences the resulting voxel size (which is related to the resolution of the measurement), it influences the accuracy as well. Further examinations should point out, how far the deviations could be reduced by using even higher magnifications and how raster tomography influences the gain in accuracy. In practice the operator should at least try to choose as high a magnification as possible, although the size of the measurement object sets the limit.

The influence of the orientation of the workpiece is much less than expected. It seems that for simple geometries, like the hollow cylinder, the influence is not as important as for real complex shaped workpieces. Further studies have to be done using real workpieces like plastic connectors towards a more accurate estimation of this influence.

The number of projections is the least important influence factor in this examination. The assumption based on practical experience and preparatory work was proofed, it is sufficient to use 400-800 projections for accurate reconstruction of the measurement object. Measurement time can be saved here which reduces the costs involved, the time could better be used for the extraction of the surface using local threshold algorithms.

Figure 17.3 shows the effect diagram for the measurement of the diameter of the inner cylinder which is quite the opposite to Figure 17.2. The measurement strategy was the same as for the outer diameter.



**Figure 17.3.** *Effect diagram of inner diameter of the hollow cylinder made of PVC*

This symmetrical behavior can be explained with threshold caused deviations. If the outer diameters are measured as large, the threshold is chosen as low and such the workpiece seems to consist of more material. In contrast a thicker workpiece due to too low a threshold leads to smaller inner diameters which can be seen in Figure 17.3. Comparing the two figures we can guess that there are some systematic deviations in the process chain which cause the described effect.

Figure 17.3 also shows that the measurement deviations can be reduced to a few microns only by using local threshold, a proper orientation of the workpiece in the X-ray beam and as high a magnification as possible. The number of projections here again has much less influence and should be chosen to reduce the necessary measurement time.

### 17.5. Calculation of the task-specific measurement uncertainty according to GUM

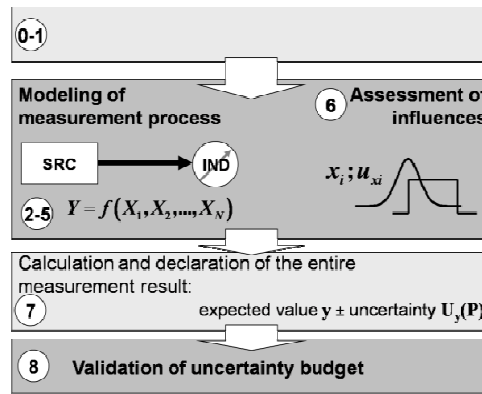
Using the measurement results described above, the user-influenced uncertainty budget for the measurement of the inner and outer cylinder was calculated. The procedure for the determination of the measurement uncertainty according to GUM is shown in Figure 17.4.

The formulation of the measurement process, the examined input quantities and the measurement task has already been described above. The next step is the modeling of the measurement process. As the CT measurement process is quite

complex, a closed formulation cannot be given. A general approach is shown in equation [17.1]:

$$Y_{IND} = Y_{object} + Y_{components} + Y_{indication} \quad [17.1]$$

The input quantities can be divided into three groups: measurement object, measurement device and evaluation or indication. The measurement object is influenced by its geometry (thickness, aspect ratio), material or its surface (roughness, waviness), etc. The influences of the measurement device itself are more numerous, the main contributions derive from the X-ray source (spectrum, focal spot size, stability), the detector (pixel size, amount of pixels, linearity) and the position system (accuracy of scales and guidance, calibration of the scales, accuracy of rotation axis). The indication mainly consists of the algorithms of the measurement software (surface extraction, fitting algorithms) and the reconstruction software.



**Figure 17.4.** Determination of the measurement uncertainty according to GUM

As this chapter focuses on the influences the measurement device operator controls, only four input quantities are taken into account and expressed using equation [17.2]:

$$X_{IND} = h(Y, \delta Y, X_1, \dots, X_i, \Delta X_{IND}, \delta X_{IND}) \quad [17.2]$$

with:

$X_{IND}$ : indicated value;

$Y$ : measurand;

$\delta Y$ : deviation of measurand embodiment.

For the four influences regarded here the model equation of the measurement process after inversion of the cause-and-effect-chain results in equation [17.3]. This formula was used to calculate the task-specific measurement uncertainty budget here.

$$Y = Y_{IND} - X_{Mag} - X_{Thres} - X_{Proj} - X_{Orient} \quad [17.3]$$

with

$X_{Mag}$ : influence of magnification;

$X_{Thres}$ : influence of threshold algorithm;

$X_{Proj}$ : influence of number of projections;

$X_{Orient}$ : influence of orientation of the workpiece.

The four input quantities have been modeled using the parameters in Table 17.5. As all values have been gained by measurements the PDF is always Gaussian.

Quantity	Expected value $x_i$ in mm	Uncertainty $u_{xi}$ in mm	PDF
Magnification of workpiece	-0.017	$8.73 \times 10^{-3}$	Gaussian
Threshold algorithm	-0.050	0,026	Gaussian
Number of Projections	$200 \times 10^{-6}$	$103 \times 10^{-6}$	Gaussian
Orientation of workpiece	$4.90 \times 10^{-3}$	$2.53 \times 10^{-3}$	Gaussian

**Table 17.5.** *Propagation of observed input quantities*

A software tool (GUM Workbench) was afterwards used to calculate the measurement uncertainty budget and to indicate the entire measurement result. The resulting budget consists of the following quantities and their proportions are shown in Table 17.6.

Quantity	Uncertainty contribution in mm	Index
Magnification of workpiece	$-8,7 \times 10^{-3}$	10.2%
Threshold algorithm	-0,026	89.0%
Number of Projections	$-100 \times 10^{-6}$	> 0.1%
Orientation of workpiece	$-2.5 \times 10^{-3}$	0.9%

**Table 17.6.** Contributions to the uncertainty budget for the measurement of the outer cylinder

With an average measured diameter for the outer cylinder of 14.988 mm the entire measurement result can be expressed by equation [17.4]:

$$Y = 15.050 \text{ mm} \pm 0.055 \text{ mm} \quad (k_p = 2) \quad [17.4]$$

As all influences have been estimated using measurements, the coverage factor has been set to two. From this result it can be seen that the uncertainty is about twice the voxel size and mainly influenced by the threshold algorithm of the measurement software.

The uncertainty budget was also calculated for the estimation of the inner cylinder of the workpiece. The following table lists the four quantities and their contribution to uncertainty.

Quantity	Uncertainty contribution in mm	Index
Magnification of workpiece	$9.2 \times 10^{-3}$	15.2%
Threshold algorithm	-0,017	51.7%
Number of Projections	$-540 \times 10^{-6}$	0.0%
Orientation of workpiece	-0.014	33.1%

**Table 17.7.** Contributions to uncertainty budget for the measurement of the inner cylinder

With an average measurement value of 10.017 mm for the diameter of the inner cylinder the entire measurement result can be expressed by equation [17.5]:

$$Y = 9.992 \text{ mm} \pm 0.05 \text{ mm} \quad (k_p = 2) \quad [17.5]$$

It can be seen that the measurement uncertainty is – as expected – in the same range as for the estimation of the outer cylinder. To sum up the assessment of the measurement uncertainty of simple measurement tasks, it can be seen that the user has great influence in the observed measurement deviations. The most important choice the user influences is the evaluation software as its surface extraction algorithms are very important for the accuracy and thus the uncertainty of the measurement task.

The next two important influences are the magnification and the number of projections taken. The magnification should be as high as possible such that the measurement object fits to the detector size and preferably a large area of it is used. The number of projections can be limited to 400-800 as greater values have no significant influence on the accuracy of the measurements but do influence the measurement time needed. The orientation of the workpiece was not as important as expected probably due to the simple geometry of the hollow cylinder. In practice this factor should have more influence, especially with complex shaped workpieces like plastic connectors used in automobiles. Further investigations with real workpieces are needed for the clarification of the amount of this influence.

## 17.6. Summary

Past and current research work focused on the estimation and quantification of influences was focused on the modeling of CT components like X-ray sources, detectors, the configuration of the measurement device itself or the estimation of the influence of the workpiece properties like roughness or geometry.

In this chapter the estimation of user- and pre-controllable influences was demonstrated by the assessment of four quantities: magnification, orientation of the workpiece, threshold algorithm and the number of projections taken. These results will now be used during the preparation of measurements to increase the accuracy by reducing the measurement uncertainty prior to the data acquisition. Together with the results from future investigations an assistance system will support the operator with the CT measurements.

In order to get a better knowledge of the CT measurement process and to be able to indicate the measurement uncertainty in detail, the published results should be combined and used to model the CT process chain. As the estimation of some

influences is still complicated, modern simulation tools could help with the determination of the input quantities and the calculation of the resulting measurement uncertainty.

### 17.7. Acknowledgments

The underlying research is gratefully founded by the German Research Foundation (DFG) as part of the collaborative research center 694 “Integration of Electronic Components into Mobile Systems”.

### 17.8. Bibliography

- [BAR 04a] BARTSCHER, M., FIEDLER, D., SAEWERT, H.-C., “Dimensional measurement deviation of an industrial 2D CT scanner: Influence of work piece roughness”, *DACH Tagung*, Vol. 17, 19 May 2004, Salzburg, Austria, 2004.
- [BAR 04b] BARTSCHER, M., FIEDLER, D., SAEWERT, H.-C., WÄLDELE, F., “Dimensional measurement deviation of an industrial 2D CT scanner: Influence of work piece geometry”, *Conference “Sensoren und Messsysteme”, VDI-Berichte 1829*, Ludwigsburg, Germany, p. 583-593, 2004.
- [BAR 08] BARTSCHER, M., HILPERT, U., FIEDLER, D., “Determination of the Measurement Uncertainty of Computed Tomography Measurements using a Cylinder Head as an example”, *tm – Technisches Messen*, Vol. 75, No. 3, p. 178-186, 2008.
- [WEC 07] WECKENMANN, A., KRÄMER, P., HOFFMANN, J., “Manufacturing metrology – state of the art and prospects”, *Proceedings of the 9th International Symposium on Measurement and Quality Control (ISMQC)*, Chennai, India, p. 1-8, 2007.



## Chapter 18

# Application of Function Oriented Parameters for Areal Measurements in Surface Engineering

### 18.1. Introduction

Many engineering surfaces are manufactured to have functional properties such as bearing, sealing or to have high fluid retention capabilities. According to the requirements of the engineering application, a functional surface has to have some specific topographic features that are beneficial to the application [STO 93]. Furthermore in some applications of micro and nanotechnologies, surfaces are not manufactured to have a specific task but it is seen that, they play important roles in the development of new products. For example, high power density CPU (central power unit) chips of new computers need greater cooling capacity, which can be realized by micro-channel cooling techniques. Advances come from the increased convection heat transfer coefficients in the small flow channels as well as a higher surface to volume ratio [ROS 02]. Additionally, the important role of wall roughness in affecting the heat transfer in the micro-channel has been reported in many studies [ROS 02, GUO 03, KO 07]. Examples can be extended but it is clear that information from surface analysis is important to improve the functional surface behavior under any engineering application.

If understanding the importance of surface is the first step, then characterizing it should be the second step. Thanks to the latest developments in measurement techniques, there are now many tools to characterize these surfaces. Information

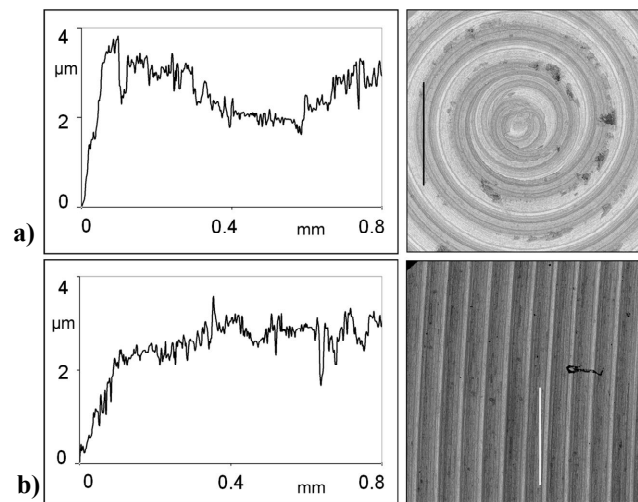
---

Chapter written by Albert WECKENMANN and Özgür TAN.

from these measurements could only lead to desired characterization if the technical function of the product surface is clearly understood. Only in this way, could applied parameters be task related and be able to characterize the functional task. Otherwise there would be many parameters which are unhelpful in describing the way a product would perform against a given functional task. This problem is summarized very well by Whitehouse and is called “parameter rash” [WHI 82]. The core aim of surface characterization should be finding a relationship between parameters to be measured and the task of the product surface.

## 18.2. Surface measurements

A basic task for surface measurements is to characterize an unknown object to obtain information about its shape and texture. Characterization of technical surfaces is mostly done by 2D and also 3D measurement techniques and the information from measurements is used to make different decisions. In order to make correct decisions, it is helpful to get more information about the surface. From this point of view, it is clear that the more data present, the better the evaluation. Due to the fact that 3D measurement results provide more information than 2D measurement results, they are more reliable and more representative. Another advantage of 3D measurements is their ability to better visualize the surface. Both of these advantages are shown in Figure 18.1.



**Figure 18.1.** a) Profile and a photo simulation of a ground surface; b) profile and a photo simulation of a turned surface

2D data and photo simulations from 3D data of a ground and turned surface are shown in Figure 18.1. Although the profiles of surfaces seem very similar to each other, their photo simulations look different. It is impossible to predict the real surface just by looking at a 2D profile. Additionally, volumetric information of the surface is also available in 3D measurement data. As an example, specifications of material volume or void volume could be used to predict functional properties like fluid retention or running-in. In many cases a full understanding of the connection between surface topography and functional performance can only be realized if a 3D approach to surface characterization is utilized. Because of this a significant effort has been made by a European consortium in order to lay down a basis for a unified approach to 3D surface finish assessment. The result of this work was reported in [STO 93]. Although there are many 3D parameters, only some of the functional parameters are mentioned in the following sections.

### 18.3. Functional parameters

For many applications (friction, lubrication, coating, spreading etc.), in which mechanical parts are in contact with another material, the functional characterization of the surface is very important. Depending on the specific functional application, surfaces have to fulfill some functional requirements and these requirements can be characterized with some functional parameters. An overview of some important 2D and 3D functional parameters which depend on the Abbott-Firestone curve is shown in the following.

#### 18.3.1. 2D functional parameters from ISO 13565-2 [ISO 96]

Parameters from the Abbott-Firestone curve, which are defined in DIN EN ISO 13565-2, are used to characterize different functional properties in relation to their mechanical resistance. An overview of these  $R_k$  parameters ( $R_k$ ,  $R_{pk}$ ,  $R_{vk}$ ,  $M_{r1}$  and  $M_{r2}$ ) can be seen in Figure 18.2.

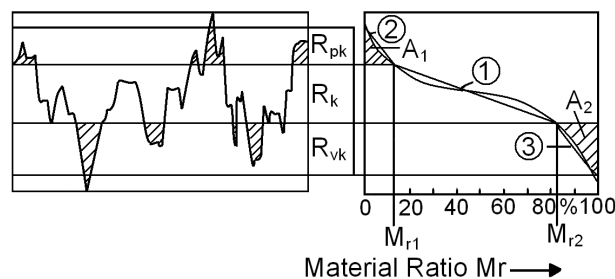


Figure 18.2. Characteristics of Abbott curve [ISO 96]

The material ratio curve can be divided into three main regions. The *core roughness depth* (1),  $R_k$  is the height of the core material. In this region, the change of the slope of the tangencies is slow and the increase in material is large. Mechanical load capacity and the mechanical resistance of the materials can be characterized by this region. Smaller  $R_k$  values indicate higher mechanical load capacities.

- The *parameters*  $M_{r1}$  and  $M_{r2}$  (in percentage) limit the area where the highest increase of material of the surface topography is found. In other words, core roughness depth is defined with  $M_{r1}$  and  $M_{r2}$  values.

- The *reduced peak height* (2),  $R_{pk}$  shows the height of the profile peak which stays above the core region. Running-in characteristics of the surfaces can be characterized with this parameter. In order to get a bearing process, a short running-in time is advantageous and good running-in properties are denoted by small  $R_{pk}$  values.

- The *reduced valley depth* (3),  $R_{vk}$  is the depth of the profile valley which is extended into the core region. For the acceptance of lubricant in a surface, which has the structure of a “plateau”, a high  $R_{vk}$  value is desired.

### 18.3.2. 3D functional parameters

The results of 2D measurements give enough information if the surface structures have a defined direction or an isotropic stochastic character [WIL 03]. Since in most cases technical surfaces do not have an isotropic characteristic, application of the “areal material ratio curve” is more useful for many cases. As described in [STO 93], functional characterization of the Abbott curve can be extended to the characterization of 3D surfaces.

Similar to a 2D curve, the areal material ratio curve is constructed from the highest peak of the topography to the deepest valley. The additional letter “S” given at parameters indicates that it is a surface parameter. The most important difference from the 2D parameters is that, the areal material ratio curve is calculated for a complete topography measurement. It should also be noted that  $SM_{r1}$  and  $SM_{r2}$  are not determined automatically, but they can be set by the user. The determination of these values results either from constructional design or they are identified by analysis. This free selection of  $SM_{r1}$  and  $SM_{r2}$  makes it possible to choose independent tolerances for the peak height, the core roughness depth and the valley depth so that changes in the peak and core areas (e.g. mechanical wear) do not have any effects on the valley areas. It should also be noted that the choice of these values is very important to obtain a function related to results from different surfaces. These parameters are also specified in [ISO 10].

#### 18.4. Characterization of the whole application

Although there are many functional parameters, it is not easy to predict the surface behavior in real engineering applications. The easiest way to investigate how a surface behaves under certain conditions is to create a setup for an engineering application and to observe the surface. As an example from [WHI 94], if any part has to have some frictional properties at a certain condition, then the test to be applied should be a friction test at a given load and speed. Because of the fact that, this test should have to be repeated for different cases, applications of functional tests are not only possible for every condition but also non-economical. Indirect tests could be seen as an alternative to direct tests.

The main idea in indirect tests is to build up a relationship between technical function and the surface. By means of this relationship, functional behavior of the surface can be predicted from surface information. In order to find out or to choose the most suitable surface parameters to describe the functional behavior, the whole application has to be investigated and the interactions between system parameters have to be well understood. In order to achieve this, a concept with six steps is proposed to give an overview for characterizing technical surfaces with functional parameters.

In the first step, all available information about the technical function has to be systematically collected. The goal of this step is gathering factors which have an influence on the system performance. System behavior under different operating conditions with specified influencing factors should be modeled in the second step. In this step, it is crucial to perform a literature survey to find out possible relations. In the third step, information about the behavior of the system has to be collected. This can either be achieved by functional tests or with some simulations. Identification of requirements on the surface is the aim of the next step.

For some applications, the surface needs to have rough characteristics (like friction enhancement) and for other applications, smooth surfaces are preferred (like gliding). Information from the literature and observations from the investigations could be used during this stage. Instruments which are applied to get surface data must be chosen properly, in the fourth step. In particular, resolution capacities of the instruments should be well understood.

Finally, in the last step, based on the information from previous stages, functional parameters have to be defined or chosen from available parameters. Task-related performance of functional surfaces can only be evaluated with correctly chosen or precisely applied functional topographical parameters.

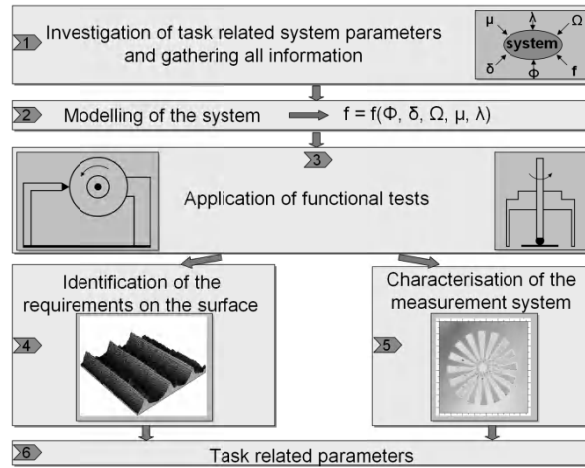


Figure 18.3. Concept for defining task related parameters

## 18.5. Case study: spreading liquid on metal surfaces

In order to give an application of this concept, the influence of surface topography on spreading of liquids on steel surfaces has been investigated. In this case study, three steel surfaces have been manufactured by different roughness values and the spreading of liquid on these surfaces has been experimentally studied.

### 18.5.1. Step 1: gathering information

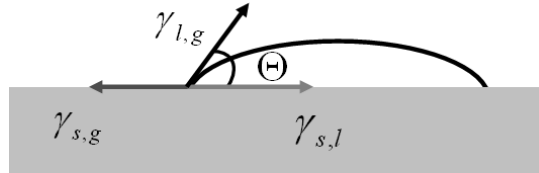
In this step, physico-chemical principles underlying the wetting process are investigated and it is seen that when a solid is wet by a liquid, three different interfacial boundary surfaces (solid-liquid, solid-gas and liquid-gas) are elementary. Among environmental conditions, the type of fluid and characteristics of solid surface have to be taken into account.

### 18.5.2. Step 2: modeling the system

A typical wetting system is shown in Figure 18.4. The well known Young's equation [YOU 05], which was developed for perfectly smooth, chemically homogeneous and non-reactive surfaces, characterizes wetting processes.

$$\gamma_{s,g} = \gamma_{s,l} + \gamma_{l,g} \cdot \cos \Theta \quad [18.1]$$

where  $\gamma_{s,g}$ ,  $\gamma_{s,l}$  and  $\gamma_{l,g}$  are interfacial tensions of solid-gas, solid-liquid and liquid-gas, respectively. The contact angle is denoted by  $\Theta$ .



**Figure 18.4.** *A wetting system*

Due to the fact that Young's equation is valid for perfectly smooth surfaces, it cannot be directly applied to rough surfaces. In wetting phenomena, Wenzel [WEN 36] related the effect of topography of a rough but chemically homogeneous surface to the contact angle of an ideally smooth surface, using equation [18.2].

$$\cos \Theta_{app} = r \cdot \cos \Theta \quad [18.2]$$

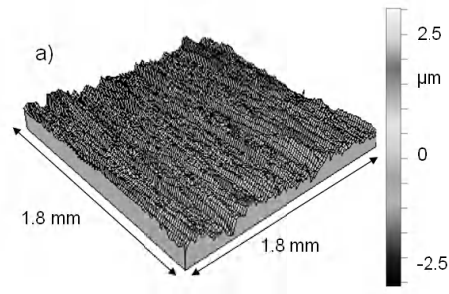
where  $\Theta_{app}$  is the apparent contact angle (experimentally accessible angle) and  $\Theta$  is the Young's contact angle (the angle related to the solid surface energy observed on a smooth surface) and  $r$  is called a roughness factor and represents the ratio of the average area of the interface actually attached to its projected part. Another factor which can be important for this specific case study is the lateral capillary forces acting on the liquid. These forces provide the driving force for the transport of liquids through the valleys on the surface.

From the model of the wetting process, it is clear that surface topography has an important role and in the following steps we try to characterize it with functional parameters.

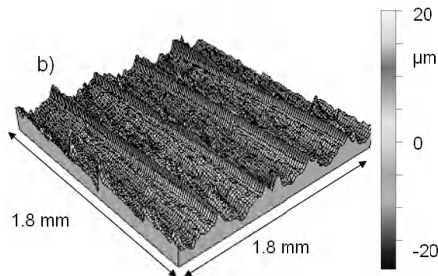
### 18.5.3. Step 3: application of a functional test

#### *Manufacturing of technical surfaces*

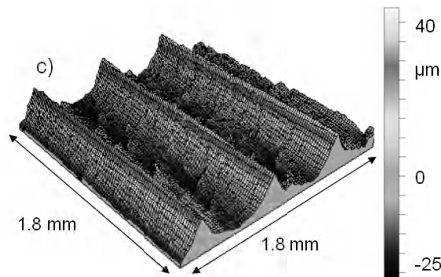
In order to investigate the significance of proposed parameters, an experimental investigation has been performed. Three steel surfaces with different roughness values have been manufactured as seen in Figure 18.5a-c.



**Figure 18.5a.** *Topography of shaped surface 1 with  $Sa\ 0.47\ \mu\text{m}$*



**Figure 18.5b.** *Topography of shaped surface 2 with  $Sa\ 4.75\ \mu\text{m}$*



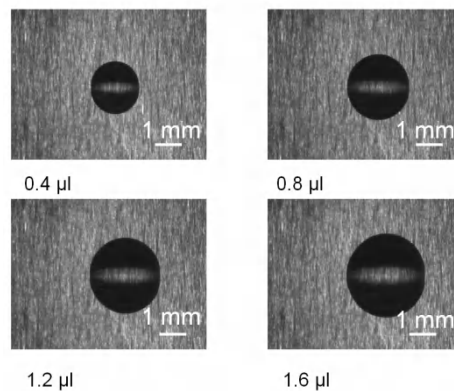
**Figure 18.5c.** *Topography of shaped surface 3 with  $Sa\ 12.55\ \mu\text{m}$*

It should be emphasized that these surfaces are prepared under “practical” conditions, i.e. without rigorous chemical purification, and have oxidized surfaces which are under the risk of possible contamination, e.g. adsorption of organic substances present in air.



### Experiments with spreading behavior

Spreading behavior of a liquid (in this case pure water), with the help of a micro-syringe, has been analyzed. Controlled volume water droplets are given at well defined positions and later the same regions are evaluated by the measurement instrument. Improvement of the wetted area of water droplets is used to compare different cases. Images of these wetted areas, which are acquired by the coordinate measuring machine Werth Video-check IP 250, are seen in Figure 18.6.



**Figure 18.6.** Droplet images acquired by camera system

Areas of images for each surface have been evaluated and the improvement of the wetted areas can be seen in Table 18.1.

	Calculated wetted areas in mm <sup>2</sup> on		
	Surface 1	Surface 2	Surface 3
at 0.4 µl	5.58	5.82	6.65
at 0.8 µl	8.91	9.06	10.12
at 1.2 µl	11.68	11.84	14.58
at 1.6 µl	14.30	14.63	16.18

**Table 18.1.** Improvement of wetted areas for each surface

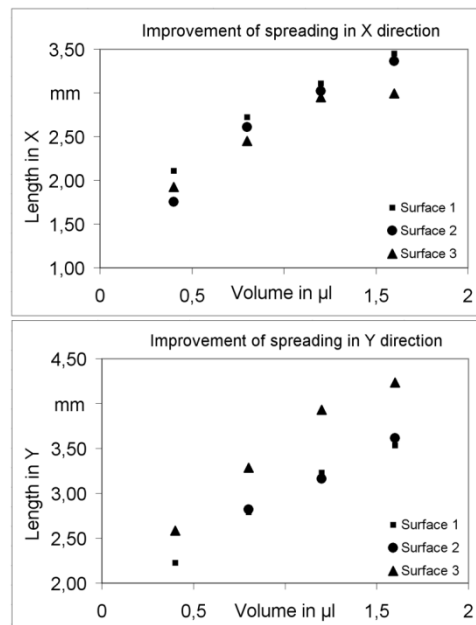
As seen in Table 18.1, the largest wetted area for a certain liquid volume is always observed on surface 3. This may be explained not only by the roughness character of the surface but also by the lateral capillary forces which act in the direction of manufactured grooves.

In order to compare the spreading of liquid on the different surfaces, an additional parameter  $A_v$  is defined as, wetted area per unit liquid volume. Calculated values are seen in Table 18.2. High  $A_v$  values of surface 3 show the high spreading ability of liquid on this surface.

Surfaces	$A_v$ in $\text{mm}^2/\mu\text{l}$
1	7.23
2	7.31
3	8.26

**Table 18.2.** *Wetted area per unit volume ( $A_v$ ) for each surface*

Another important observation during the experiments is the directional dependence of spreading. Additional to the total area, improvement of each droplet has also been evaluated in X and Y directions. As seen in Figure 18.7, spreading behavior in X and Y directions are different from each other. Although there is not a great difference in the X direction, spreading of liquid on surface 3 in the Y direction is much more than the other ones. These results show the need to characterize the anisotropic structure of the surfaces.



**Figure 18.7.** *Improvement of spreading in a) X and b) in Y directions*

The experiments showed that the spreading behavior of liquid strongly depends on the roughness and texture of metal surfaces. Capillary channeling along manufactured grooves affected the spreading and wetting behavior of liquid on metal surfaces.

#### **18.5.4. Step 4: surface requirements**

In this case study, due to the anisotropic structures of the shaped surfaces, 2D measurements of the surfaces would give different results according to the measurement direction. Because of this, the degree of anisotropy should also be characterized. It is also obvious that, the spreading of the liquid takes place on the whole surface of the metal, so it is not enough to evaluate only the projected area. Peaks and valleys of the surfaces have to be considered. As seen in experiments, void volumes of the manufactured grooves maintain the required space for the liquid to spread on the surface. On the other hand, asperities of these grooves can be seen as resistance to spreading out. Additionally, valleys where the retention of liquid takes place have to be characterized.

#### **18.5.5. Step 5: measurement system**

Areal investigations of the surfaces have been performed by a white light interferometer (Taylor Hobson Talysurf CCI 1000) with the following specifications.

Measurement Range (X x Y x Z)	1,800 x 1,800 x 400 ( $\mu\text{m}$ x $\mu\text{m}$ x $\mu\text{m}$ )
Number of data points	1,024 x 1,024
Vertical resolution	0.01 nm
Lateral resolution	1.76 $\mu\text{m}$
Working distance	7.4 mm
Numerical aperture	0.3

**Table 18.3.** *Specifications of white light interferometer*

Note that, independent from manufacturer specifications, with additional measurements the actual resolution capacities of the instrument have to be investigated.

### 18.5.6. Step 6: functional parameters

In most cases more than one parameter is needed to describe the surface so that throughout the characterization of the spreading behavior of liquids on metal surfaces, not only two important parameters from “surface material curve”, namely  $S_{pk}$  and  $S_{vk}$ , but also the valley fluid retention index  $S_{vi}$  are used to describe the topography. The parameter  $S_{pk}$  indicates the material which stays above the core area. It can be used to describe the running-in and wear characteristics of the surface [ISO 96]. The parameter  $S_{vk}$  indicates the volume which is extended into the material and describes characteristics of surfaces like fluid retention properties. Another important surface parameter is the valley fluid retention index  $S_{vi}$ . This is the ratio of the void volume of the unit sampling area at the valley zone over the RMS deviation and a larger  $S_{vi}$  indicates good fluid retention in the valley zone. In order to indicate the surface isotropy, texture aspect ratio  $S_{tr}$  is used. By definition it has a value between 0 and 1. If the value is close to 1, the surface is said to be isotropic, i.e. has the same characteristics in all directions. If the value is close to 0, the surface is anisotropic, i.e. has an oriented and/or periodical structure.

#### Calculation of the surface parameters

Surface data of regions where the spreading takes place are acquired using the measurement instrument WLI. After having filled the non-measured points, the indexes mentioned have been calculated. As seen from the calculated parameters in Table 18.4,  $S_{vi}$  shows that the fluid retention ability of the surface in valley regions is largest for surface 1.

	$S_{vi}$	$S_{pk}$ , $\mu\text{m}$	$S_{vk}$ , $\mu\text{m}$	$S_{tr}$
Surface 1	0.12	0.39	0.50	0.09
Surface 2	0.09	6.36	3.23	0.11
Surface 3	0.05	16.5	5.76	0.12

**Table 18.4.** Calculated surface parameters

This could be used to explain the smaller  $A_v$  values measured for surface 1. Calculated  $S_{pk}$  values explain the largest resistance of surface 3 against the spreading of liquid in directions perpendicular to manufactured grooves. Parameter  $S_{vk}$  indicates that the volume extended into the material has the larger values at surface 3. Smaller  $S_{tr}$  values of the surfaces indicate the anisotropic structure of the surface. Although it is not the aim of this case study, based on experimental results with different surfaces a correlation study can be performed.

## 18.6. Conclusions

Developments in manufacturing techniques make it possible to produce technical surfaces with defined micro-structured properties. Only when the information from the surface topography measurement is related to the engineering application, is it possible to make a statement about the task-related performance of the surface. This can be achieved by the functional characterization of the surfaces. In this chapter, firstly the importance of areal information in the analysis of functional performance is discussed with a comparison to information from a 2D profile. Some of the problems encountered during the evaluation of 2D profiles are shown. Additionally 2D parameters from the Abbott curve, which are defined in ISO 13565-2, are compared to their 3D counterparts. Finally a concept is proposed to choose or to define functional parameters for a specific task. The aim of this concept is to set up a relationship between these parameters and the other system factors for a certain task in order to improve the long term functional properties during the whole product life cycle. Applicability of this concept has been shown with the example, spreading of liquids on metal surfaces. The calculated functional surface parameters showed good description abilities for the experimental observations and it is necessary to perform a correlation study with additional experiments.

## 18.7. Acknowledgments

The research and development project was kindly funded by the German Research Foundation (DFG) and has been carried out by priority program 1159 “New strategies for measurement and test techniques for production of microsystems and nanostructures”.

## 18.8. Bibliography

- [GUO 03] GUO Z.Y., LI Z.X., “Size effect on microscale single phase flow and heat transfer”, *Int. J. Heat and Mass Transfer*, Vol. 46, p. 149-159, 2003.
- [ISO 96] “Surfaces having stratified functional properties – Part 2: Height characterization using the linear material ratio curve”, *Geometrical Product Specifications (GPS) – Surface Texture: Profile Method*, ISO 13565-2, ISO, 1996.
- [ISO 10] “Geometrical Product Specification (GPS) – Surface Texture: Areal – Part 2. Terms, Definitions and Surface Texture Parameters”, ISO/DIS 25178-2, ISO, 2010.
- [KO 07] KO H.S., LIU C.W., GAU C., YANG C.S., “Fabrication and design of a heat transfer micro-channel system by a low temperature MEMS technique”, *J. Micromech. Microeng.*, Vol. 17, p. 983-993, 2007.

- [ROS 02] ROSTANI, A.A., MUJUMDAR, A.S., SANIEL, N., "Flow and heat transfer for gas flowing in microchannels: a review", *Heat and Mass Transfer*, Vol. 38, p. 359-367, 2002.
- [STO 93] STOUT K.J., SULLIVAN P.J., DONG W.P., MAINSAH E., LUO N., MATHIA T., ZAHOUANI H., The development of methods for the characterization of roughness in three dimensions, EUR 15178 EN, 1993
- [WEN 36] WENZEL, R. N., "Resistance of solid surfaces to wetting by water", *Ind. Eng. Chem.*, Vol. 28, p. 988-994, 1936.
- [WHI 82] WHITEHOUSE, D.J., "The parameter rash", *Wear*, Vol.83, p. 75-78, 1982.
- [WHI 94] WHITEHOUSE, D.J., *Handbook of Surface Metrology*, London, IOP Publishing, 1994.
- [WIL 03] WILHELM, H., SEEWIG, J., BODSCHWINNA, H., BRINKMANN, S., "Kenngrößen der Abbott-Kurve", *MTZ*, Vol. 5, p. 438-444, 2003.
- [YOU 05] YOUNG, T., "An essay on the cohesion of fluids", *Philos. Trans. R. Soc.*, London, vol. 95, pp. 65-87, 1805.

## Chapter 19

# Validation of a Reception or Production Control Process by the Inertial Indicator $I_G$

### 19.1. Introduction

Ensuring adequate gauge capability is an important aspect of quality. The measurement variability is a component of the observed variability of a characteristic. The gauge precision has an impact on the good knowledge of the process capability and on the conformity decision for a part [POU 07]. The automotive industry [AIA 02, CNO 91] proposes standards for the determination of gauge capability and the acceptance of a measurement process. The first standard [AIA 02] separates the notion of reproducibility and repeatability (R&R), from the measurement accuracy (bias, linearity, stability). However, the second standard [CNO 91] takes into account the repeatability and the accuracy, but not the reproducibility. Erner [ERN 06] shows the limitations of the R&R analysis and Wheeler [WHE 89] introduces the  $ndc$  ratio in order to compare the production variance and the gauge variance.

The reproducibility and the accuracy of a gauge are traditionally studied separately. However both these notions are not really independent! It is obvious that a good accuracy allows us to accept a precision of the instrument which is worse than in the case of limit accuracy. The originality of the gauge capability index presented in this paper is to integrate the same calculation into the repeatability, reproducibility and the accuracy.

---

Chapter written by Daniel DURET, Maurice PILLET, Alain SERGENT and Dimitri DENIMAL.

## 19.2. Comparison of the “production controls” and “reception controls” approaches

The process of control is generally validated using an indicator comparing its “performance” to the tolerance given by the customer [19.1]:

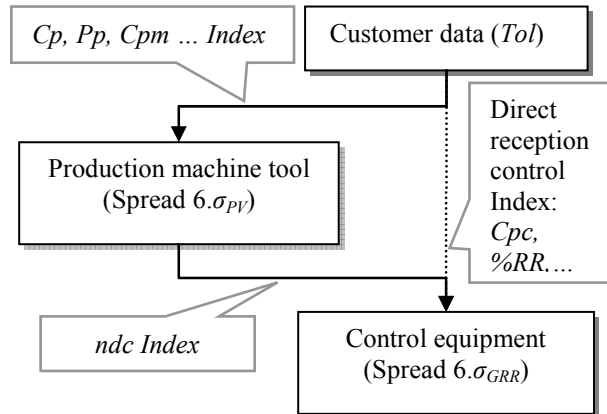
$$\text{Indicator} = \frac{\text{Performance}}{\text{Tolerance}} \quad [19.1]$$

In the case of a single reception control, this approach is justified. On the other hand, if the aim of the control process is to allow the piloting of a production process (able, without excess), it is necessary to compare the respective performances of these two processes. MSA [AIA 02, WHE 89] developed this concept by reusing an *ndc* (*Number of Distinct Categories*) indicator defined by:

$$\text{ndc} = \sqrt{2} \cdot \frac{\sigma_{PV}}{\sigma_{GRR}} \quad [19.2]$$

- $\sigma_{PV}$  is an indicator of the variability of the production process (*part variation*);
- $\sigma_{GRR}$  is an indicator of the reproducibility of the gauge process, highlighting the influence of the equipment and the operators [SWE 07].

These different processes are respectively validated by a set of indicators (*Cp* then *ndc*):



**Figure 19.1.** To integrate a reception or production control process



If, for the choice of the production means, we retain, for example, an indicator  $C_p$  which must be higher than or equal to  $4/3$ , that gives:

$$C_p = \frac{Tol_{Customer}}{6 \cdot \sigma_{PV}} \geq \frac{4}{3} \quad [19.3]$$

which gives:

$$\sigma_{PV} \leq \frac{Tol_{Customer}}{8} \quad [19.4]$$

If we retain an indicator “ $ndc$ ”, equal to or higher than 5 [AIA 02], [19.2] gives:

$$\sigma_{GRR} \leq \frac{\sqrt{2}}{5} \cdot \sigma_{PV} \quad [19.5]$$

While combining [19.4] and [19.5], we obtain a threshold value which can be used directly [MAJ 06]:

$$\sigma_{GRR} \leq \frac{\sqrt{2}}{40} \cdot Tol_{Customer} \approx \frac{Tol_{Customer}}{28} \quad [19.6]$$

This inequality is to be compared with the rule of thumb of 1/10:

$$\%RR = \frac{6 \cdot \sigma_{GRR}}{Tol_{Customer}} \leq 10\% \quad [19.7]$$

That is:

$$\sigma_{GRR} \leq \frac{Tol_{Customer}}{60} \quad [19.8]$$

We prefer to observe the less restrictive rule [19.6], by adding the concept of accuracy simultaneously.

Some companies use the capability index  $C_{pc}$

$$C_{pc} \leq \frac{Tol_{Customer}}{6\sigma_{GRR}} \quad [19.9]$$

### 19.3. Production bias and measure bias

The batch of parts provided to the customer is characterized by its standard deviation (indicator  $\sigma_{PV}$ ) and by a bias compared to the target, noted  $\delta_P$ . In fact, the estimate of these two indicators is disturbed by the control process involving a parasitic variation and bias. This total identification of quality is quantified by:

$$\begin{aligned}\sigma_{TV} &= \sqrt{\sigma_{PV}^2 + \sigma_{GRR}^2} \\ \delta_T &= \delta_P + \delta_G\end{aligned}\quad [19.10]$$

Industrially, the “measurement process spread” aspect is well integrated. On the other hand, the estimate of bias, requiring the use of standards, is often ignored. The concept of inertial tolerance, will allow us to use a systematic analysis treating these two components simultaneously. Relative compensations will be allowed.

### 19.4. Inertial capability

Inertial tolerancing [PIL 04] checks that a  $Y$  characteristic (for a batch of  $k$  products) presents an acceptable spread and an acceptable bias. Residual spread and bias compared to the target can be represented as the components of a pseudo vector [BOY 91] [CHA 96] [KHO 05]:

$$\mathbf{I_P} \begin{vmatrix} \sigma_{PV} \\ \delta_P \end{vmatrix} \quad [19.11]$$

Compensations between spread and bias are authorized on the  $Y$  characteristic. For example a weak spread  $\sigma_{GRR}$  makes it possible to accept a residual bias  $\delta_P$  compared to the target  $Y_0$ .

The magnitude  $\| \cdot \|_2$  applied to  $\mathbf{I_P}$ , gives the compensation formula.

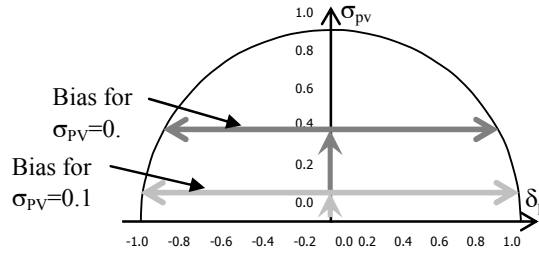
This magnitude will be noted  $I_P$ . Conformity for the  $Y$  characteristic will be validated if:

$$I_P = \sqrt{\sigma_{PV}^2 + \delta_P^2} \leq I_{Max} \quad [19.12]$$

Maximum inertia will be deduced from the traditional tolerance by:

$$I_{Max} = \frac{Tol_{Customer}}{6} \quad [19.13]$$

The customer can decide to allot a specific inertia which the manufacturer will have to respect [ADR 07].



**Figure 19.2.** Example of link between  $\sigma_{PV}$  and  $\delta_P$

By analogy with the indicator  $Cp$ , it is possible to define a new capability index [PIL 04]:

$$Cpi = \frac{I_{Max}}{\sqrt{\sigma_{PV}^2 + \delta_P^2}} = \frac{I_{Max}}{I_P} \geq Cpi_{mini} \quad [19.14]$$

This calculation remains theoretical. Actually, uncertainties and bias of measurement come and disturb this calculation:

$$Cpi_{Obs} = \frac{I_{Max}}{\sqrt{\sigma_{TV}^2 + \delta_T^2}} \quad [19.15]$$

### 19.5. Inertia of the control process and inertia of the production process

Total vector inertia  $\mathbf{I}_T$  is the combination of the vector inertia of production  $\mathbf{I}_P$  and the vector inertia of control  $\mathbf{I}_G$ .

$$\mathbf{I}_P \begin{vmatrix} \sigma_{PV} \\ \delta_P \end{vmatrix} \quad \text{and} \quad \mathbf{I}_G \begin{vmatrix} \sigma_{GRR} \\ \delta_G \end{vmatrix} \quad [19.16]$$

#### 19.5.1. Law of composition

The total of vector inertias is provided using an internal law of composition:

$$\mathbf{I}_T = \mathbf{I}_P \oplus \mathbf{I}_G \quad [19.17]$$

This gives the following formulae for the components:

$$\mathbf{I_T} \left| \begin{array}{l} \sigma_T = \sqrt{\sigma_{PV}^2 + \sigma_{GRR}^2} \\ \delta_T = \delta_P + \delta_G \end{array} \right. \quad [19.18]$$

Resulting inertia (magnitude) is equal to:

$$\begin{aligned} I_T &= \sqrt{(\sigma_{PV}^2 + \sigma_{GRR}^2) + (\delta_P + \delta_G)^2} \\ I_T &= \sqrt{(I_P^2 + I_G^2) + 2 \cdot \delta_P \cdot \delta_G} \end{aligned} \quad [19.19]$$

### 19.5.2. Disturbances due to bias

Equation [19.19] cannot be reduced to a quadratic sum:

$$I_T^2 = \sum_i I_i^2 \quad [19.20]$$

We will write [19.18], in the form:

$$I_T^2 = I_P^2 + I_G^2 + 2 \cdot (\delta_T - \delta_G) \cdot \delta_G \quad [19.21]$$

–  $\delta_G$ , bias of the control process will be estimated using a sample of comparisons with a standard value close to the dimensions of the parts in production.

–  $\delta_P$ , bias of production, is not directly estimated. A log book of the production (standard “Statistical Process Control”) gives us total bias  $\delta_T$ .

– We replace  $\delta_P$  by  $\delta_T - \delta_G$ .

### 19.5.3. Definition of the inertial “ndc”

*Origin of the “ndc”*

On the basis of the idea that variation of the control process intervenes in total variability, we define a factor of discrimination  $DR$  [WHE 89] as:

$$\begin{aligned}
DR &= \sqrt{\frac{1 + \frac{\sigma_{PV}^2}{\sigma_T^2}}{1 - \frac{\sigma_{PV}^2}{\sigma_T^2}}} = \sqrt{\frac{\sigma_T^2 + \sigma_{PV}^2}{\sigma_T^2 - \sigma_{PV}^2}} = \sqrt{\frac{2 \cdot \sigma_{PV}^2 + \sigma_{GRR}^2}{\sigma_{GRR}^2}} \\
DR &= \sqrt{\frac{2 \cdot \sigma_{PV}^2}{\sigma_{GRR}^2} + 1} = \sqrt{ndc^2 + 1} \\
ndc &= \sqrt{2} \cdot \frac{\sigma_{PV}}{\sigma_{GRR}}
\end{aligned} \tag{19.22}$$

According to the importance of the percentage of variability due to the control process, the ratio  $DR$  can vary from one to infinity.

*Proposal of an “inertial  $ndc$ :  $ndc_I$ ”*

$$\begin{aligned}
DR_I &= \sqrt{\frac{1 + \frac{I_P^2}{I_T^2}}{1 - \frac{I_P^2}{I_T^2}}} = \sqrt{\frac{I_T^2 + I_P^2}{I_T^2 - I_P^2}} = \sqrt{\frac{2 \cdot I_P^2 + I_G^2 + 2 \cdot \delta_P \cdot \delta_G}{I_G^2 + 2 \cdot \delta_P \cdot \delta_G}} \\
DR_I &= \sqrt{\frac{2 \cdot I_P^2}{I_G^2 + 2 \cdot \delta_P \cdot \delta_G} + 1} = \sqrt{ndc_I^2 + 1} \\
ndc_I &= \sqrt{2} \cdot \frac{I_P}{\sqrt{I_G^2 + 2 \cdot \delta_P \cdot \delta_G}}
\end{aligned} \tag{19.23}$$

As  $\delta_P$  is measured indirectly, we will retain the following practical formula:

$$ndc_I = \sqrt{2} \cdot \frac{I_P}{\sqrt{I_G^2 + 2 \cdot (\delta_T - \delta_G) \cdot \delta_G}} \tag{19.24}$$

By piloting the production, we can make the bias  $\delta_P$  tend towards 0. The indicator  $ndc_I$  has the following limit:

$$ndc_I \xrightarrow{\delta_P \rightarrow 0} \sqrt{2} \cdot \frac{I_P}{I_G} \tag{19.25}$$

$$ndc_I \text{ limit} = \sqrt{2} \cdot \frac{I_P}{I_G} \tag{19.26}$$

It is necessary to choose a control process whose value  $I_G$ , relative to the production inertia  $I_P$ , complies with the following rule:

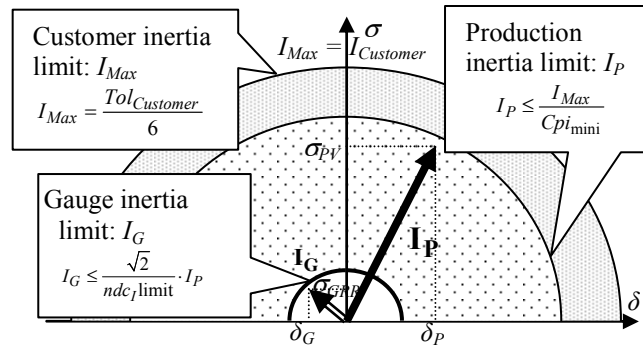
$$I_G \leq \frac{\sqrt{2}}{ndc_I \text{ limit}} \cdot I_P \quad [19.27]$$

–  $I_G$  is determined by:

- a study of “repeatability – reproducibility” giving  $\sigma_{GRR}$  [AIA 02],
- a study of the measurement bias giving the estimate  $\delta_G$ .

–  $I_P$  is obtained indirectly by comparison with the total inertia  $I_T$ , which is determined starting from an SPC analysis and using the control inertia  $I_G$ . If  $I_P$  is not known and we make the assumption of ( $\delta_G = 0$ ), then  $I_G$  can be compared directly with  $I_T$  [19.28]:

$$I_G \leq \frac{\sqrt{2}}{\sqrt{(ndc_I \text{ limit})^2 + 2}} \cdot I_T \quad [19.28]$$



**Figure 19.3.** Case of production control (inertias  $I_P$  and  $I_G$ )

### 19.6. Inertia of the control process and total customer inertia (control of reception)

If we want to directly compare  $I_G$  with  $I_T$  (case of acceptance sampling for the suppliers) starting from the preceding inequalities [19.27] and [19.14], we obtain:

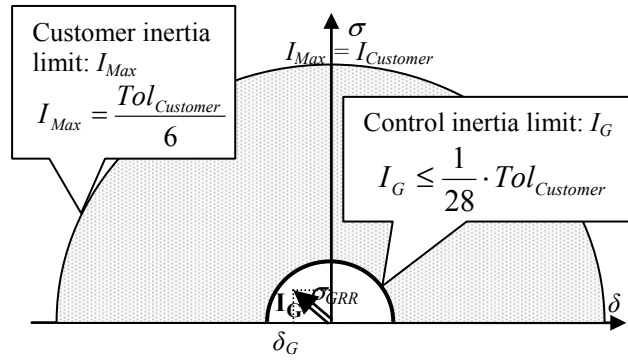
$$I_G \leq \frac{\sqrt{2}}{ndc_I \text{ limit}} \cdot I_P \leq \frac{\sqrt{2}}{ndc_I \text{ limit}} \cdot \frac{I_{Max}}{Cpi_{mini}} \quad [19.29]$$

For example, for an  $ndc_I$  limit of 5 and one  $Cpi_{mini}$  of 1.33, which either gives the approximate ratio:

$$I_G \leq \frac{1}{5} \cdot I_{Max} \quad [19.30]$$

or, approximately:

$$I_G \leq \frac{1}{28} \cdot Tol_{Customer} \quad [19.31]$$



**Figure 19.4.** Case of reception control (inertias  $I_{max}$  and  $I_G$ )

## 19.7. Conclusions

In the validation of the processes of control, the traditional approach consists of either validating the accuracy and reproducibility separately, or simply adding the variances of these two elements. The proposal of the inertial indicator  $I_G$  is an original approach making it possible to give more coherence to the two studies of fidelity and accuracy by fixing a limit which depends on the combination of these two elements.

This new indicator,  $I_G$ , appears more demanding, but it has the advantage of simultaneously treating the reproducibility and the error in accuracy by authorizing compensations. We understand well that if the accuracy is perfect, it is possible to accept more defects in the area of reproducibility. The error of accuracy often remains the weak point of industrial studies. The definition of the inertia of the control process  $I_G$  formalizes this intuitive approach. In particular, that makes it possible to make a decision using graphs as a starting point, since they are easier to interpret than a list of numbers.

Indicator  $I_G$  can also be used in the management of the means of measurement to monitor the drifts. That allows us to:

- establish a certificate of conformity immediately;
- analyze the drifts;
- observe the intervention rules of the statistical control of the processes applied to the inertial tolerance case and to make the right decision (validation, downgrading, rejection or final improvements according to the case and the context of the control process).

## 19.8. Bibliography

- [ADR 07] ADRAGNA P.A., Tolérancement des Systèmes assemblés, une approche par le tolérancement Inertiel et Modal, PhD Thesis, University of Savoy, 2007.
- [AIA 02] AUTOMOTIVE INDUSTRY ACTION GROUP (AIAG), Measurement Systems Analysis Reference Manual, 2002, 3rd edition. Chrysler, Ford, General Motors Supplier Quality Requirements Task Force.
- [BOY 91] BOYLES R.A., “The Taguchi capability index”, *Journal of Quality Technology*, Vol. 23, No. 1, January 1991.
- [CHA 96] CHAO M.T., CHENG S.W., “Semicircle control chart for variables data”, *Quality Engineering*, Vol. 8, No. 3, pp. 441-446, 1996.
- [CNO 91] CNOMO, Moyens de production (Agrément Capabilité) des moyens de mesure - Moyens de contrôle spécifique, CNOMO E.41.36.110.N, 1991.
- [ERN 06] ERNER, “Improved gage R&R measurement studies”, *Quality Progress*, March 2006.
- [KHO 05] KHOO M.B.C., “Two modified semicircle control charts for detecting process improvement”, *Quality Engineering*, Vol. 17, No. 3, pp. 453-458, July, 2005.
- [MAJ 06] MAJESKE K.D., GEARHART C., “Approving measurement systems when using derived values”, *Quality Engineering*, Vol. 18, No. 4, pp. 523-532, October, 2006.
- [PIL 04] PILLET M., “Inertial tolerancing”, *The Total Quality Management Magazine*, Vol. 16, No. 3, pp. 202-209, May 2004.
- [POU 07] POU J.M., VAISSIERE D., Limite de la norme ISO 14253-1 et de la notion de capabilité dans le cadre de la déclaration de conformité, Congrès de métrologie de Lille, 2007.
- [SWE 07] SWEENEY S., “Analysis of two-dimensional gage repeatability and reproducibility”, *Quality Engineering*, Vol. 19:21-37, No. 1, January, 2007
- [WHE 89] WHEELER D.J., LYDAY R.W., *Evaluating the Measurement Process*, Second Edition, SPC Press Inc., 1989.



## Chapter 20

# Detection of Areas with Critically Reduced Thickness of Formed Sheet Metal Parts Using Two Oppositely Positioned Fringe Projection Systems

In order to identify unallowable thinning places of formed sheet metal parts, two oppositely positioned fringe projection systems are used. They enable us to scan the sheet metal part from two sides. Using mathematical parameters, obtained point clouds are transformed into one coordinate system. This chapter presents the algorithm for calculation of minimal wall thicknesses using point clouds and surface polygonal models. This enables us to find the shortest distance from each measuring point on one side of the sheet metal to the opposite side, regardless of the direction of this distance, and proved that some of those distances exceed the lower tolerance limit.

### 20.1. Introduction

Formed sheet metal parts such as pressed parts of the car body, different housings and enclosures etc. are generally susceptible to reduction (too thinned) in some areas. Therefore, a fast, accurate, reliable, measuring method for area-wise measurement and detection of such thinning places in zones of high deformation grade is required [ERN 03, WEC 04].

---

Chapter written by Albert WECKENMANN and Natasa PETROVIC.

Determination of thickness (distances between two sides) of sheet metal using common measurement procedures such as ultrasonic measurement, laser thickness measurement, radiographic measurement, measurement by tactile coordinate measuring machines etc., offer results that are associated with one, or sometimes more, predefined directions. Those direction-related results are caused by the functional principle of the equipment used (laser thickness measurement) or by dependence on coordinate systems (e.g. measurement on tactile CMM using single point mode).

Measurement direction is thereby usually oriented orthogonally to one, or approximately to both sides of the measured part. Such solutions are not easily applied on the curved formed sheet metal parts for various reasons. The measuring direction should be direction orthogonal to the measured surface and that is difficult here, or even not possible to ensure.

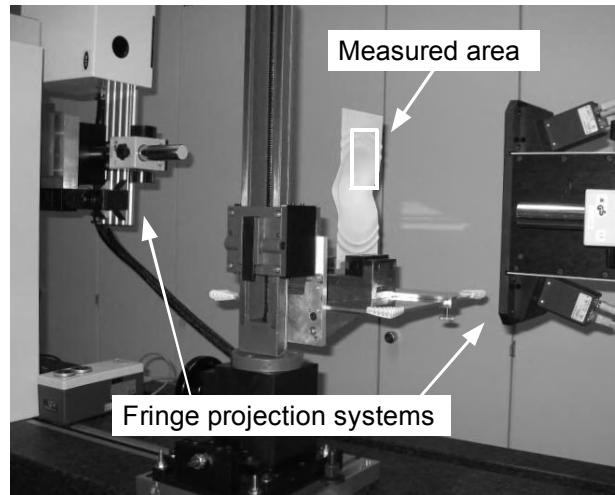
Furthermore we must decide which side of the workpiece to select as the referent side – two actual sides of the formed sheet metal part are not always parallel to each other. The problem is particularly emphasized if the minimal thickness of the sheet metal is to be determined. Through measurement in predefined directions the minimal thicknesses can be overlooked as it is in a different direction to the selected direction for the measurement.

To go beyond this problem scanning measuring systems that enable probing of workpieces with high point density can be used. Those systems are for example tactile CMMs used in scanning mode, 3D laser scanners or fringe projection systems [SAV 07]. Point clouds that are the result of such scanning can be further processed and the possibility to create adequate evaluation solutions for described measurement tasks appears.

## **20.2. Methods**

### **20.2.1. *Measuring system and data fusion***

In order to provide data suitable for further processing – calculation of the shortest distances between two sheet metal sides and identification of unallowable thinning places (areas with critically reduced sheet metal thickness), measuring system must enable rapid and accurate probing of sheet metal surfaces with high point density and have a sufficiently large measuring range [MUR 03]. The specified accuracy of the measuring system must be better than 0.05 mm, lateral resolution less than 0.5 mm and measuring range for typical measuring tasks larger than several cm<sup>2</sup>. Fringe projection systems satisfy those requirements.



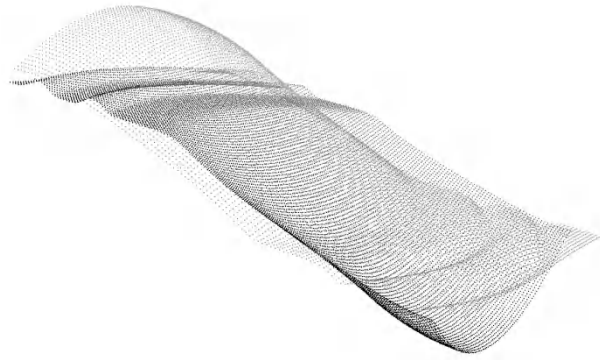
**Figure 20.1.** *Measuring system and measured sheet metal part*

The experimental setup made for probing measuring points consists of two oppositely positioned fringe projection systems MikroCAD and TopoCAM both from GF Messtechnik GmbH. The vertical resolution of MikroCAD is given by the manufacturer as  $1\text{ }\mu\text{m}$  and by TopoCAM as  $2\text{ }\mu\text{m}$ . Two systems are placed and oriented relative to each other so that their measuring ranges overlap with a common range of  $90\text{ mm} \times 70\text{ mm} \times 40\text{ mm}$ . Thus, the selected area of sheet metal can be scanned from two sides without moving either measuring equipment or a workpiece. Figure 20.1 shows the measuring system used and the selected area of the sheet metal scanned as an example for explanations in the chapter.

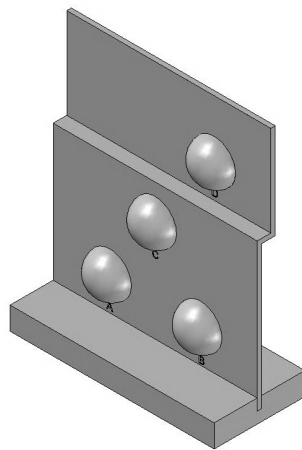
Since scanning is done using two independent fringe projection sensors, obtained point clouds are located in two independent coordinate systems and coordinates of the measured points have mutually independent values – two point clouds are oriented unintentionally to each other. Using the software PolyWorks® from InnovMetric Software Inc. two point clouds before their fusion are visualized in Figure 20.2.

To reliably represent the selected area of the sheet metal, one of two point clouds must be mathematically transformed and brought into position relative to another one, as if they were scanned originally in one coordinate system. In order to enable mathematical correction by translation and rotation parameters the mentioned deviations of one coordinate system relative to another must be determined in previous calibration of sensors to each other. The calibration procedure has been created within the research activities of the project presented here.

This is made using the artifact presented schematically in Figure 20.3.



**Figure 20.2.** *Point clouds before the data fusion*



**Figure 20.3.** *Artifact for calibration of the fringe projection systems to each other*

The artifact consists of four calibration spheres made of titanium with a diameter 19.05 mm, with diffuse reflecting surfaces and a very small sphericity deviation (less than 0.635  $\mu\text{m}$ ). The spheres are not in one plane, but all of them must be within the measuring range during the measurement.

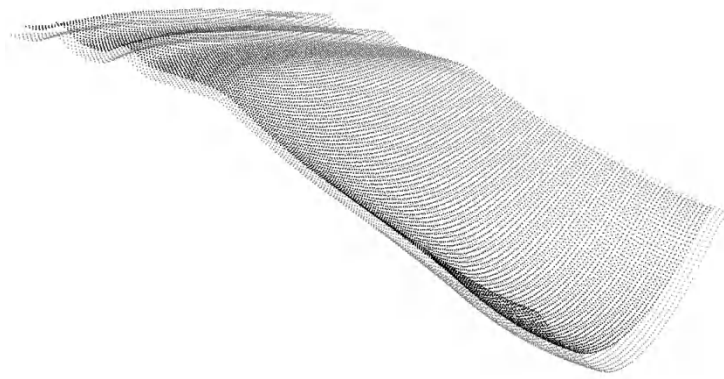
The calibration procedure consists of:

- scanning the spheres from both sides;

- generating center points of associated Gauss-spheres;
- determining center points starting coordinates on the side that will be transformed during the fusion process;
- determining the new coordinates of the same points after transformation (convergence) to the fixed set of center points (this can be conducted by any commercial data processing and visualization software, here PolyWorks® is used);
- calculating rotation and translation parameters using starting and end center point coordinates. Thus, position and orientation deviations of two sensor coordinate systems which will be corrected later in the merging/fusion process are quantified (the calculation program for this purpose is implemented in MATLAB® from The MathWorks GmbH).

Once calibrated, measuring systems can be used for measurements until mutual position and orientation of the sensors is not changed, otherwise the calibration must be repeated.

Using mathematical parameters obtained by calibration, data from two sensors are merged, reliably representing a selected area of the formed sheet metal (Figure 20.4). The merging/fusion is actually a calculation of new data coordinates of one point cloud using rotation and translation parameters, which is for this purpose implemented in MATLAB®. Visualization is again made in PolyWorks®.



**Figure 20.4.** *Point clouds after the data fusion*

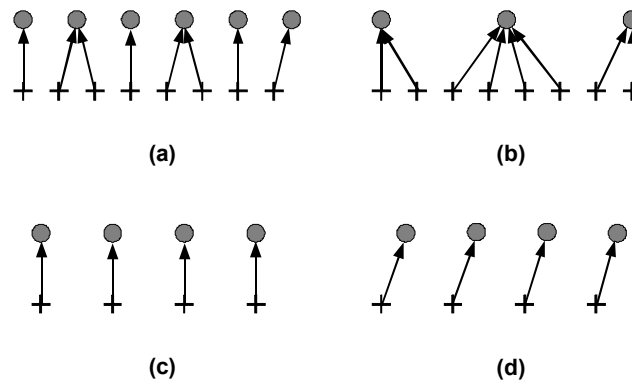
Such obtained point clouds are further processed for calculation of minimal distances between two sheet metal surface sides.

### 20.2.2. Methods of data analysis

To identify areas with critically reduced sheet metal thickness, the shortest distances between two surface approximations in different selected evaluation points must be determined. For that purpose the following can be used: two opposite point clouds directly, two polygonal models of measured surfaces obtained through triangulation of those points, or a combination of point clouds on the one side and a polygonal surface on the other.

The first option would be the simplest one for the implementation. But, such calculation would probably yield incorrect results if the lateral raster of the measured points is not the same for both point clouds. This is the case in the measuring system used: MikroCAD has a lateral resolution of  $56\text{ }\mu\text{m}$  and TopoCAM  $60\text{ }\mu\text{m}$ .

Even if lateral rasters have the same dimension, incorrect results would appear if rasters are mutually shifted in the lateral direction, which is actually always the case.



**Figure 20.5.** *Dependence of shortest distances on lateral resolution and relative displacement of the two point clouds*

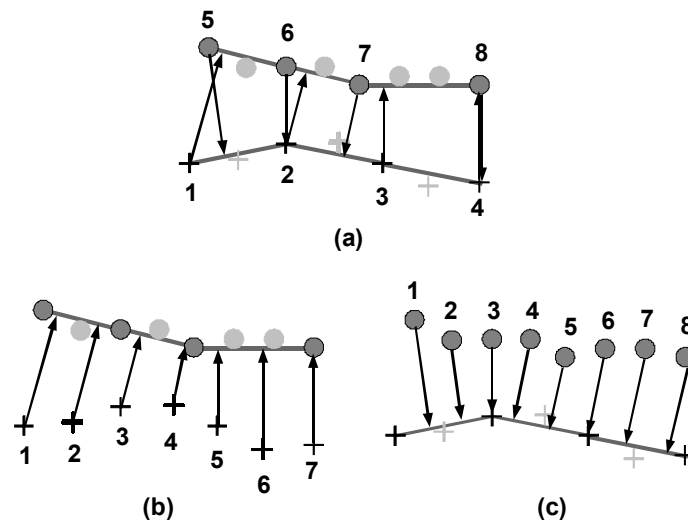
The problems are illustrated in Figure 20.5 for 2D cases. Figures 20.5a and b represent how the shortest distances measured from the lower point set change for different point densities of the upper point set. Figures 20.5c and d illustrate the dependence of the measured results on lateral displacement between two data sets. Having these problems in mind, such a solution is not considered further and its implementation is rejected.

The solution to the problem of finding the shortest distances using two polygonal models of measured surfaces is also rejected due to the following reasons:

- all the shortest distances between two triangles of the polygonal models correspond to some of the vertices of one or the other polygonal data set;
- if the information carriers are unavoidably the vertices, then it is better to replace one of the triangulated surfaces with originally measured points from the point cloud: the information density would be greater, results would be distributed in a regular raster grid and calculation would be simpler.

A schematical 2D illustration of this analysis is presented in Figure 20.6.

Triangles are replaced with line segments but principally it is the same case.



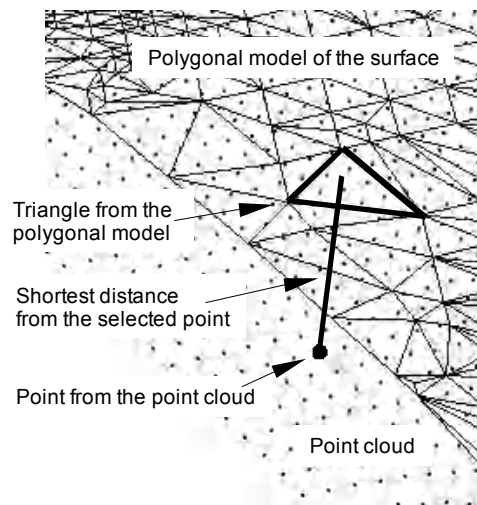
**Figure 20.6.** Solutions for determination of the shortest distances using polygonal surface models

Not all points from the point cloud became vertices of the triangulated surface, and the shortest distances between such surfaces go unavoidably through their vertices (Figure 20.6a). Thus, information density will be significantly greater if, instead of vertices, measured points are used as outgoing points for calculations (Figure 20.6b and c).

Therefore, the method for calculation of minimal distances using measuring points from one sheet metal side and polygonal triangulated approximation of the surface on the opposite side has been implemented. Schematically this is shown in Figure 20.7. Such a solution for determining distances conforms to the distance definition in [ISO 08].

In order to get polygonal approximations of the surfaces, triangulation can be made in e.g. MATLAB® or in any commercial software for data visualization and analysis (here PolyWorks® is used).

The calculations of shortest distances must be made twice, thereby changing two sides – “outgoing” (points side) and “target” side (polygon surface side).



**Figure 20.7.** *The shortest distance between the measuring point on one sheet metal side and the polygonal surface on the opposite side*

### 20.2.3. Algorithm for the calculation of minimal wall thicknesses

The algorithm applied for calculation of minimal distances presents the iterative search for the minimal distance from each measuring point of one sheet metal side, to triangles of the opposite polygonal surface. The calculation result is a sequence of the minimal distances corresponding to appropriate measuring points of the parent point cloud.

The algorithm for calculation consists of the following steps:

- division of input data in subareas (calculation blocks): dividing the whole area to small blocks in order to reduce the number of unnecessary calculations;
- calculation of the shortest distance from each measuring point from “starting” side, to each triangle of the opposite polygonal surface, respectively to its vertices, edges and face [LIN 91], belonging to the corresponding selected area;



- extraction of the minimum of calculated values for certain measuring points and its final assignment to that point;
- creation of output variables and termination of the algorithm.

#### 20.2.3.1. *Input variables*

Input data for the calculation are measuring points from one point cloud and triangulated surface of the opposite side.

Measuring points are represented in the form of a matrix variable with three rows for x, y and z coordinates of each point.

Triangles of the polygonal surface are imported into the calculation program as the matrix of triangle vertices and the matrix of triangle normal vectors. Both are matrices with three rows for x, y and z components of points and vectors.

#### 20.2.3.2. *Calculation algorithm – extraction of a minimal thickness value for certain measuring points*

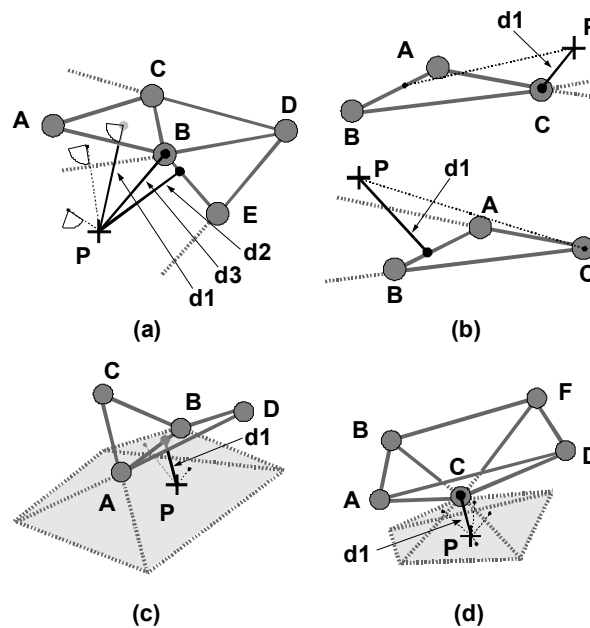
The iterative calculations of the shortest distances between one point and each triangle on the opposite side present the main core of the calculation section.

Figure 20.8 schematically represents different possible cases of the position and orientation of one point and one triangle that are considered during the creation of the calculation procedure.

The first step of the shortest distance calculation is to distinguish if the intersection point of the orthogonal distance line which goes through the measuring point (designated as P in Figure 20.8) with the triangle plane, is inside or outside of the face. If it is inside, the shortest distance from the point to triangle is the distance from this intersection point to the measuring point. Such distance is for example the distance d1 shown in Figure 20.8 a. If the intersection point lies outside of the face then the shortest distance is the distance from the point to some of the triangle's edges or vertices (distances d2 to the triangle BDE and d3 to the triangle BCD in Figure 20.8a).

The second step is analogous to the first one. It will be determined if the necessary condition is fulfilled: for any orthogonal distance from point P to the given face edge to be the shortest distance to the triangle. If this condition is not fulfilled, then it is definitively the distance to some of the vertices. The example is the triangle BDE, shown in Figure 20.8a. The first step is to determine the point on a certain edge line that lies on the corresponding orthogonal distance line from the measuring point P. If the distance between the determined point and the point P is possibly the shortest one, the previously determined point must lie on the line

segment limited by two vertices of the associated edge line (distance  $d_2$  to the triangle BDE in Figure 20.8a). If the condition is not satisfied for any of three edge lines, then the distances from point P to the triangle vertices must be calculated and the shortest must be found (e.g. distance  $d_3$  to the triangle BCD in Figure 20.8a). Furthermore, if the previous condition is satisfied for only one or several edge lines, the shortest of them will be selected and compared with the distance from point P to the triangle vertex which does not lie on the corresponding edge. The shortest of those two distances is then the resulting distance (see Figure 20.8b).



**Figure 20.8.** *Different cases of the shortest distance from the point to the triangles*

Two typical cases when the triangles lie in the vicinity of the measuring points and the shortest distance is nevertheless to be found from that point to the edge or vertex – rather than to the triangle face – are shown in Figures 20.8c and d. The triangles ABC and ABD in Figure 20.8c make a convex surface to the point P. In this case, there is a whole area where the measuring points can be placed and its orthogonal distances to the planes in which triangles lie will not be the shortest to the triangles. In this example, the shortest distance is the distance from point P to the common edge for both triangles. If the convex surface to the measuring point is made from more than two triangles, then the shortest distance is the distance to its common vertex (see Figure 20.8d).

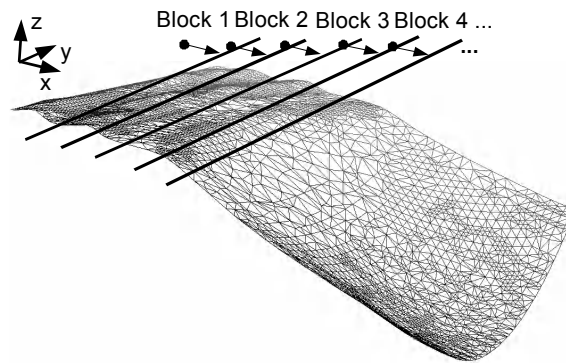
Repeating the described calculations for one point and one triangle at a time from the same calculation block as the point, the shortest of all distances for the point can be determined. Thereby, each new calculated value will be compared with the previous one, and only the smaller one will be retained for comparison in the next iteration. The value retained in the last iteration will be assigned to the matrix of output values. This matrix consists of a sequence of values – one value corresponds to each measuring point.

#### 20.2.3.3. Calculation blocks

To reduce the calculation time the input data are divided into blocks. For each outgoing point only the shortest distance to triangles which belong to the same block will be calculated. Thus all unnecessary calculation of distances to triangles that certainly lie far away from the point are avoided.

The input data are firstly classified in ascending order regarding the x coordinate. This is the simple procedure for point data. The vertex matrix is classified in the same way, but only one of the vertices is considered relevant – the other two and the corresponding triangle normal are dedicated to the first vertex.

The data classified in such a way can be easily divided into areas using some minimal and maximal x values as area limits (Figure 20.9).

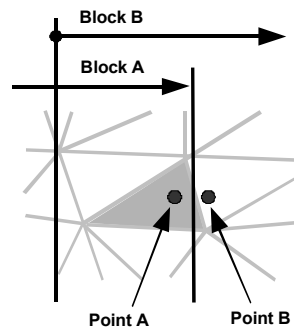


**Figure 20.9.** Calculation blocks

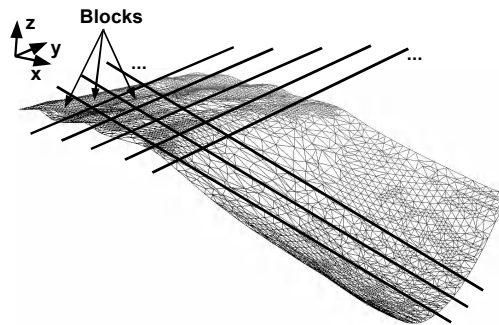
In this procedure overlapping areas of neighbor areas have to be allowed. Two typical cases that can occur in the border zone between blocks A and B are presented in Figure 20.10. If it is assumed that the marked triangle is classified to belong to area A, according to the x value of one of two left vertices, then, this triangle will be taken into the calculation as the possible target triangle for calculation of distances from point A. A problem will appear if the mentioned triangle is the closest one for

point B too, and overlapping of the areas is not enabled. In this case, a wrong distance would be calculated. Therefore the border beginning area B must be shifted back some values.

The minimal length of the overlapping area is determined using the value of the “maximal edge length” which is the parameter defined during the triangulation procedure. There is no triangle in the surface model that has an edge longer than this value. Using this value as the relevant value for the proper selection of the number of blocks, the wrong results caused through classification of the data according to the x value of only one of the vertices of each triangle are prevented.



**Figure 20.10.** *Overlapping calculation blocks*



**Figure 20.11.** *Calculation blocks made by divisions in both directions x and y*

In order to reduce calculation time even more, additional division of previously determined blocks has been made. Blocks resulting from division in the x direction are in the same way further divided into sub-blocks in y direction (Figure 20.11).

The calculation time decreases principally with the number of blocks or, in other words, with decreasing block size. The maximal number of blocks for a certain data set depends on the polygonal surface, particularly from the “maximal edge length” parameter determined during triangulation. The minimal size of blocks, in combination with appropriate length of overlapping areas, must be selected thus to decrease the number of unnecessary calculations for each outgoing point from the point cloud to minimum, but also to ensure repeated calculations for outgoing points are avoided where possible. The selected number of outgoing points from the point cloud (point density) affects the calculation time, but for algorithm optimization regarding its speed-up it is irrelevant.

Division into calculation blocks also enables the parallelization of this algorithm. The nature of the problem is such that processing the data from one block can be done independently, and will not affect calculations in other blocks. Since nowadays typical PCs contain multiple CPUs, remarkable speed-ups can be achieved through parallelization.

#### 20.2.3.4. *Creation of output variable*

By allowing overlapping of the calculation areas the calculation of the shortest distances for some points will be made twice or even four times. The output matrix will therefore be unnecessarily large if such repeated values are not eliminated. The elimination is made in the following way. Each point has already been uniquely enumerated in the process of disassembling the original input matrix. Finally, all results with repetitive numeration values are compared and the smallest one selected as the output value for a distance.

The algorithm and visualization has been implemented in MATLAB®.

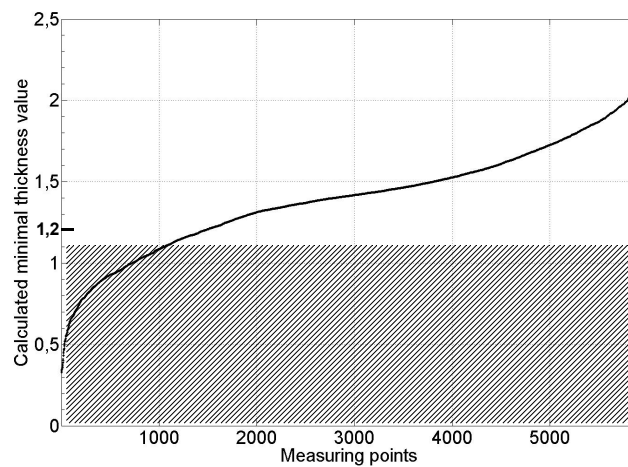
### 20.3. Visualization and discussion of results

Calculated data can be further processed to determine if there are local areas of critically short distances. This can be made through simple analysis of obtained numerical values. In Figure 20.12 results for the sheet metal part area (marked in Figure 20.1) are represented. Calculation for the example has been made using 6,000 outgoing measurement points (selected point density approximately 1 point per mm, calculations on 150 blocks). The nominal value of the workpiece thickness is 1.2 mm. If the thickness tolerance in a negative direction is 0.1 mm, the lower tolerance limit is 1.1 mm. From the diagram shown we can see for how many measuring points the calculated thickness lies out of the tolerance.

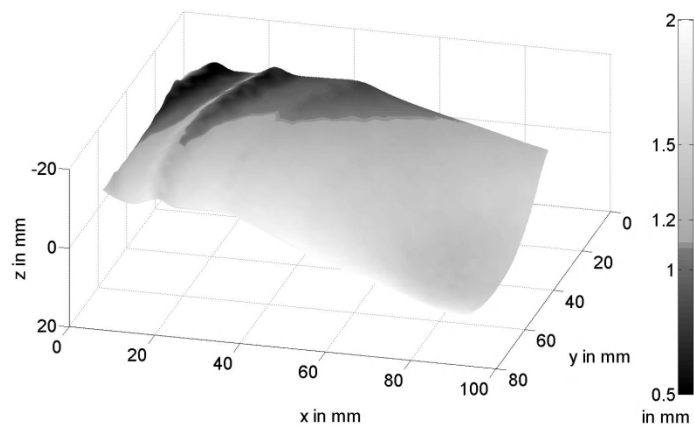
For localization of thinned areas, data can be visualized in 3D. The visualization has been made, in a similar manner to the calculation, for both sides of the sheet

metal. In Figure 20.13 the distribution of thicknesses for the selected area of the measured sheet metal part is shown. Areas which are out of tolerances are marked with dark-gray.

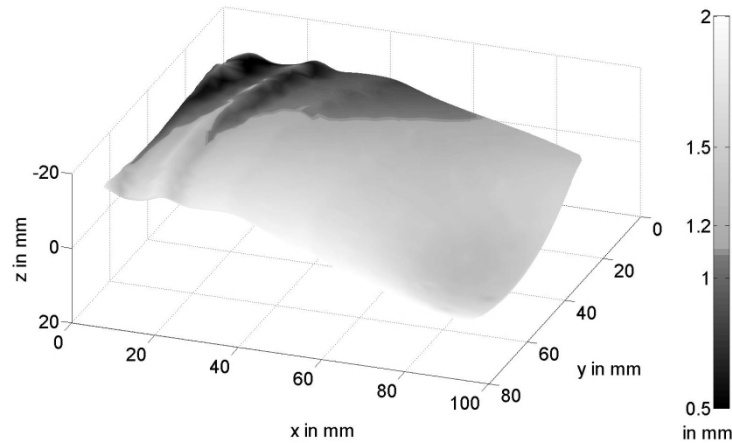
Results of measurements for the opposite side are shown in Figure 20.14.



**Figure 20.12.** *Calculated thickness values for selected measuring points*



**Figure 20.13.** *Color-coded thickness distribution on the lower surface (grayscale used here) with marked areas which are out of tolerance*



**Figure 20.14.** Color-coded thickness distribution on the upper surface (grayscale used here) with marked areas which are out of tolerance

The results are similar but not the same. For example, thinning places are distributed on the same corner of the measured area but they are different in size and form. This is an expected problem of non-commutativity, a difference in the results for two directions [ERN 03, WEC 04, MUR 03]. This is not a calculation procedure problem, but is an unavoidable effect caused by non-parallelism of actual sheet metal sides.

If more detailed analysis of the detected critical areas is required, the calculation can be repeated using even maximal point density allowed by the lateral resolution of the measuring systems. In that case it is recommended to reduce the calculation area.

#### 20.4. Summary

For measurement of sheet metal parts and detection of areas with critical reduced thickness, a measuring system consisting of two oppositely placed fringe projection systems has been designed. The system allows fast, accurate and high point density scanning of high deformed sheet metal areas. It can be easily integrated in automated manufacturing processes. The solution for the fusion of two independent measuring data sets (point clouds) has been found and implemented. Results of fusion are two point clouds which represent a reliably scanned sheet metal area. A new algorithm for the calculation of the shortest distances between two sheet metal

sides has been implemented. It enables the accurate calculation of such distances assigned to each measuring point. The visualization of obtained calculation results enables the localization of areas with critical reduced thickness.

## 20.5. Acknowledgments

This work was supported by the German Research Foundation DFG (Deutsche Forschungsgemeinschaft) within the second phase of project No. WE 918/19-2 “Optical Three-Dimensional Wall Thickness Measurement and Detection of Defects”.

## 20.6. Bibliography

- [ERN 03] ERNST R., WECKENMANN A., VELGAN, R., “Local wall thickness measurement of formed sheet metal using fringe projection”, *Proceedings of XVII IMEKO World Congress*, Dubrovnik, Croatia, p. 1802-1805, June 22-27, 2003.
- [ISO 08] ISO/DIS 25378.2, Geometrical product specifications (GPS) - Characteristics and conditions - Definitions, International Organisation for Standardisation, Geneva, Switzerland, 2008.
- [LIN 91] LIN M. C., CANNY J. F., “A Fast Algorithm for Incremental Distance Calculation”, *Proceedings of the 1991 IEEE International Conference on Robotics and Automation*, p. 1008-1014, Sacramento, California, USA, April, 1991.
- [MUR 03] MURMU N. C., VELGAN R., “Detection of defects in formed sheet metal using medial axis transformation”, *Proceedings of SPIE*, Vol. 5144, p. 651-658, 2003.
- [SAV 07] SAVIO E., DE CHIFFRE L., SCHMITT R., “Metrology of freeform shaped parts”, *Annals of the CIRP*, Vol. 56/2/2007, p. 810-835, 2007.
- [WEC 04] WECKENMANN A., ERNST R., VELGAN R., NALBANTIC K., “Detection of defects in sheet metal by using fringe projection system”, *Proceedings of 8th International Symposium on Measurement and Quality Control in Production*, p. 231-236, Erlangen, Germany, VDI Berichte 1860, October 12-15, 2004.



## Chapter 21

# Variability of the Manufacturing Process in the GPS Framework: A Case Study

During the product lifecycle several types of uncertainty contribute to making it increasingly difficult to control product quality.

The geometrical product specifications and verification approach (GPS) provides a methodology to match the ideal product with the manufactured workpiece by considering three sources of variability and their related uncertainties: correlation, specification and measurement uncertainty.

In this chapter we analyze the uncertainties adopted in GPS, and use independent component analysis (ICA) and time series analysis to discriminate the various sources of process variability. This will be done with particular focus on roughness measurements.

### 21.1. Introduction

When a product has been designed, the designer images it as an ideal and perfect object. However, during the product lifecycle, errors arise and the real workpiece is far from perfect. Moreover, it is not possible to fully know what the real workpiece is, owing to the measurement uncertainty. Taking into account the overall variability of the workpiece, the intent is to discriminate sources that contribute to such variability. The GPS approach provides a methodology to match the ideal product

---

Chapter written by Manuela DE MADDIS and Martina GANDINI.

with the manufactured workpiece by considering three sources of variability and their related uncertainties: correlation, specification and measurement uncertainty.

First of all, components to be included in uncertainty are listed and evaluated, according to the *Guide to the Expression of Uncertainty in Measurement* (GUM) [GUM 93], its development with the Procedure for Uncertainty of Measurement Management (PUMA) [ISO/TS 14253-2:1999]. Then the extended uncertainty proposed by GPS is calculated.

Correlation and specification uncertainties are considered in order to assess the reliability of geometrical control. Without loss of generality it is possible to minimize the contribution of correlation and specification uncertainties. Correlation uncertainty originates when geometrical specifications do not completely fulfill workpiece functionality. There are examples, part matching, where such uncertainty contribution can be minimized. Specification uncertainty arises when geometrical control is not completely specified on the drawing. When a designer does not indicate the computation method for a workpiece characteristic (and a default condition is not available), he introduces specification uncertainty. There are many examples where such uncertainty contribution can be minimized. With an accurate choice of experimental tests, correlation and specification uncertainties can be neglected. The measurement uncertainty could be evaluated according to the GUM, and its development with the PUMA method.

What remains are measures that indicate processes which could or could not be in statistical control. If measurements of a workpiece are in the non-conformity zone, it could be interesting to investigate and discriminate sources of variability to assess which of the contributors lead to the main variability in the process. However, a great variability in the results, bring higher costs even if the processes are in control.

In order to discriminate sources of variability, multivariate statistical analysis is adopted to handle the problem. However, most of the statistical methods use a Gaussian distribution to model errors but this is not suitable to model most of the manufacturing processes and non-Gaussian approaches are investigated.

A set of simulated turned workpieces manufactured with different parameters, and under different process condition, is analyzed with time series analysis (TSA) and independent component analysis (ICA). The TSA is widely adopted in the search of periodical pattern in economical researches, and we apply the technique to detect and describe the periodical behavior of manufacturing processes. The ICA is a common tool in signal process analysis allowing the separation of contributions deriving from different unknown sources. This method is efficient when all sources present non-Gaussian distributions; at most one Gaussian source is permitted.

According to the literature, a fingerprint coming from turning processes follows a beta distribution, so ICA could be applied to discover and classify the main contributions to manufacturing errors.

In this paper preliminary results demonstrate that large work has to be developed to assure reliability and robustness of such analyses, but they also represent an interesting challenge in the facilitation of GPS implementation.

### 21.2. Variability sources

A perfect verification “operator” could be defined for the verification of the specification of a certain value of  $Ra$  (e.g.  $Ra = 1.5 \mu\text{m}$ ).

The first step is the partition (choice) of the required surface from the actual workpiece. The second step is the partition of non-ideal profiles by the physical positioning of the measuring instrument in multiple places. So the data are extracted from the surface with an instrument in accordance with the requirement indicated in [ISO 3274:1996], using the evaluation length given in [ISO 4288:1996]. Then data are filtered using a Gaussian filter with a cut-off wavelength determined by the rules in [ISO 4288:1996] and the corresponding stylus tip radius and sample spacing. Once the points are sampled, the last step is to evaluate  $Ra$  and the other parameters associated with roughness, keeping the 16% rule.

For requirements specified by the upper limit of a parameter, the surface is considered acceptable if not more than 16% of all the measured values of the selected parameter, based upon an evaluation length, exceed the value specified on the drawings or in the technical product documentation. For requirements specified by the lower limit of the surface parameter, the surface is considered acceptable if no more than 16% of all the measured values of the selected parameter, based upon an evaluation length, are less than the value specified on the drawings or in the technical product documentation.

For proving conformance or non-conformance with specification, measured values of parameters shall be compared with the specified limiting values taking into account the uncertainty of measurement according to the rules given in [EN ISO 14253-1:1998]. In the case of comparing results of measurements with upper and lower limits, the uncertainty of measurements shall be estimated without taking into account the inhomogeneity in the surface which is already accounted for in the 16% allowance.

Since each of these operations is a perfect verification operation [ISO/TS 17450-2:2002] and they are performed in the order prescribed in the specification, this

verification operator is a perfect verification operator. Therefore it is possible to neglect the “method uncertainty” due to the understanding of the measurements specification and define only a part of the measurement uncertainty which is the “implementation uncertainty”, so the divergence between the metrological characteristics of the actual operator and the ideal metrological characteristics defined by a perfect verification operator.

### 21.2.1. Measurement uncertainty

First of all, the components of measurement uncertainty are considered. As previously mentioned, we focus our attention on simulations of profiles extracted with a roughness tester. This obviously brings a sum of uncertainty terms, which is different from those arising from other measuring devices such as coordinate measuring machines. The way to handle measurement uncertainty is defined in the PUMA method [ISO/TS 14253-2:1999], which consists of an iterative procedure, based on GUM method [GUM 93] for measurement uncertainty estimation.

According to [GUM 93], “The objective of a measurement is to determine the value of the measurand, that is, the value of the particular quantity to be measured”, so, first of all, we need to define the measurand.

The measurand considered for quantifying measurement uncertainty is the roughness parameter  $Ra$ , defined as:

$$Ra = \frac{1}{lr} \int_0^{lr} |Z(x)| dx$$

where  $lr$  is the base length and  $Z(x)$  is the profile, which obviously is not a continuous function, but consists of points sampled with a rugosimeter. So  $Ra$  is defined as:

$$Ra \approx \frac{1}{n} \sum_{i=1}^n |Z_i|$$

where  $n$  is the number of discrete displacements of the profile.

The calculation of components of measurement uncertainty could be reported, with appropriate modifications, also for the other roughness parameters, such as the root mean square deviation of the assessed profile  $Rq$ , the skewness  $Rsk$ , or the kurtosis  $Rku$  [ISO 4287: 1997].

The measurand cannot be completely described without an infinite amount of information; it is not possible to measure all the infinite profiles on a cylindrical surface along the axis. Thus, to the extent that it leaves room for interpretation, incomplete definition of the measurand introduces into the uncertainty of the result of a measurement a component of uncertainty that may or may not be significant relative to the accuracy required of the measurement. We simulate to have taken various profiles for each of the produced workpiece, and calculate the combined standard uncertainty  $u_c(y)$ ; if its value is greater than the objective uncertainty, the highest components should be reconsidered (according to [ISO/TS 14253-2: 1999]) in order to check if the estimate of measurement uncertainty was too conservative. Even if it is only a simulation, the objective uncertainty could be imagined to be settled at a value of  $0.10 \mu\text{m}$ . The measurements are simulated to be made with a rugosimeter, taking 10 profiles on the same surface. The thermal variations of the temperature of laboratory during measurements could be controlled. The starting condition for laboratory temperature is  $20^\circ\text{C} \pm 1^\circ\text{C}$ . The thermal variation of the rugosimeter within the measurement is registered at  $0.25^\circ\text{C}$ . The workpiece is made of steel. The operator has familiarity with the measuring equipment.

For a correct measurement with the rugosimeter, it is necessary to correctly position the workpiece, transversal to the direction of the cutting tool used for manufacturing, and then to choose the profiles to be extracted. Therefore the symmetry axis of the workpiece should be parallel to the scanning direction.

If the uncertainty on a measure of  $Ra$  is considered, first of all it is necessary to do some replicate measurements on the reference sample for  $Ra$ , having a value close to the value of the specification. Then the mean of the measures is calculated and the error  $E_j$ , that is a systematic component that takes into account the difference between the mean of the measures and the value certified on the standard. Then, at least 10 measures should be done on the surface to be controlled, so that the coefficient  $h$  could be settled to the value 1. Finally, the expanded uncertainty  $U_{Ra}$  has to be calculated as [ZAH 03]:

$$U_{Ra} = |E_j| + k \times u_c$$

where  $u_c = \sqrt{(h\sigma_m)^2 + \left(\frac{U_{reference}}{2}\right)^2}$  and  $\sigma_m$  is the standard deviation of the measures. Then the  $U_{reference}$  could be determined as a multiplication of  $u_{reference}$  by a coverage factor 2, therefore having a confidence level of about 95%.

The procedure of evaluating the associated uncertainty conforms to the law of propagation of uncertainty as given in the GUM. The combined standard uncertainty for  $Ra$  is:

$$u_{reference}^2(Ra) = \sum_{i=1}^N [c_i \cdot u(x_i)]^2 \quad [21.1]$$

where the  $c_i$  are the sensitivity coefficients and  $u(x_i)$  is the uncertainty value for the  $i$ -esim contributor. The main sources contributing to the uncertainty in roughness measurement by stylus method are considered to be due to [ZAH 03]:

- uncertainty in Z-axis calibration:  $c_{zc} \cdot u_{zc}$  ;
- uncertainty in X-axis calibration:  $c_{xc} \cdot u_{xc}$  ;
- uncertainty in straightness in the external guide:  $c_{sg} \cdot u_{sg}$  ;
- noise:  $c_{no} \cdot u_{no}$  ;
- uncertainty in stylus geometry:  $c_{st} \cdot u_{st}$  ;
- uncertainty in measuring force:  $c_{mf} \cdot u_{mf}$  ;
- uncertainty in filter characteristic:  $c_{f\lambda} \cdot u_{f\lambda}$  (considering uncertainties in short cut-off and long cut-off);
- uncertainty in sampling interval:  $c_{si} \cdot u_{si}$  ;
- repeatability:  $c_{rpt} \cdot u_{rpt}$  ;
- homogeneity:  $c_{hg} \cdot u_{hg}$  .

Equation [21.1] could be written as:

$$u_{reference}^2(Ra) = [c_{zc} \cdot u_{zc}]^2 + [c_{xc} \cdot u_{xc}]^2 + [c_{sg} \cdot u_{sg}]^2 + [c_{no} \cdot u_{no}]^2 + [c_{st} \cdot u_{st}]^2 + [c_{mf} \cdot u_{mf}]^2 + [c_{f\lambda} \cdot u_{f\lambda}]^2 + [c_{si} \cdot u_{si}]^2 + [c_{rpt} \cdot u_{rpt}]^2 + [c_{hg} \cdot u_{hg}]^2$$

A disadvantage of this approach is that the  $c_i$  coefficients could not be easily determined, owing to the non-linear nature of the  $f$  functions between the roughness and the other coefficients.

In the example  $u_{reference}$  is 0.005  $\mu\text{m}$  and  $\sigma_m^2$  is 0.06  $\mu\text{m}$ ; so  $u_c$  is 0.0602  $\mu\text{m}$ . Since  $u_c$  is less than objective uncertainty, further iterations to reduce uncertainty (as indicated in [ISO/TS 14253-2: 1999]) are no longer necessary and the uncertainty evaluation could be stopped at this stage.

In this computation, other contributions, such as the thermal variation, are not reported because under controlled conditions are of the order of 1/10 of a nanometer.

Another approach, equivalent to the one presented here is to determine  $u_{reference}$  with ANOVA analysis [ISO/TS 14253-2: 1999]. In this case the random effects contributing to the observed variability are:

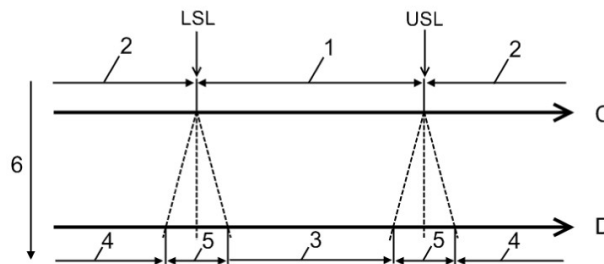
- variation of the  $Ra$  value across the roughness measurement standard;
- variation of the  $Ra$  value between evaluations;
- repeatability of the contact (stylus) instrument.

Each of these random effects is assumed to have associated with it an unknown variance, denoted by  $\sigma_R^2$ ,  $\sigma_E^2$  and  $\sigma_M^2$ , respectively, where index R stands for roughness measurement standard (variation across roughness measurement standard); index E stands for evaluation (between evaluation effects); and index M stands for contact (stylus) instrument (repeatability of the contact (stylus) instrument). The ANOVA provides estimates of the above variances. The combined standard uncertainty is thus

$$u_{reference} = \sqrt{s_E^2 + s_M^2 + u_{cal}^2}$$

where the last term is the standard uncertainty estimate, derived from the calibration certificate.

The conformity and non-conformity zones are reduced by the ambiguity zone [EN ISO 14253-1:1998]. In Figure 21.1 it could be seen how they change from the specification phase (C) to the verification phases (D). The zone under specification (1) reduces to the conformity zone (3), owing to the ambiguity zone (5) that depends on the increment in measurement uncertainty  $U$  (6). Also the non-conformity zones (4) reduce themselves owing to the ambiguity zone (5).



**Figure 21.1.** Change of conformity zone due to measurement uncertainty

The measurement uncertainty introduces an ambiguity zone. A determined value for the specification is not variable; it is defined through the indications in the drawings and through the detailed description of the characteristic of measurement equipment and the indication of the maximum permissible error. The extended uncertainty measurement is a variable that depends on the uncertainty components. So, the width of the conformity and the non-conformity zones are variables, because they depend on the estimated value of measurement uncertainty  $U$ .

### **21.2.2. Process variability**

Having considered measurement uncertainties and specification uncertainty, we still need to analyze what affects various processes to be different from each other and to reach different performances.

The value of a measurand can be calculated after a filtering process with a Gaussian filter as indicated in [ISO 11562: 1996] with appropriate cut-off length, according to the theoretical roughness of the simulated profiles. This kind of filtering, however, could remove contributions to the workpiece error that arise from the process and not from the measure. Within our point of view, we keep the whole profile and try to discriminate contributions to the errors, in order to analyze how the manufacture has been performed.

The reference profile is considered a profile only with the fingerprint, due to the cutting tool. In this way, all departures from the reference profile indicate other kind of errors in turning workpieces and are indications of errors in the manufacturing process. These errors could be not so large, so that the workpiece remains in tolerance, but separating the various components of errors could be useful to indicate which of the processes could give a lower cost, keeping the values of the parameter in a more narrow range. Otherwise, if the workpiece is not in tolerance, it could set an alert for the operator, because something in the process is out of control.

### **21.3. Simulations**

Roughness parameters are usually calculated after filtration techniques described in the normative. However, the aim of this chapter is to propose techniques to investigate and separate components of process variability, in order to gain all the available information about the manufacturing of the workpieces.

It was decided to take the original profiles to do simulations; this in order to avoid the elimination through filtering of anomalies (e.g. cracks) maybe due to anomalies in the manufacturing and not in the verification phase.



In the simulations, three profiles have been compared; one with the usual surface roughness, which can be considered the usual fingerprint left from the manufacturing tool, another one with an ondulation, and the last with an ondulation plus a drift. This was done in order to simulate different anomalies in the functioning of machine tools, leading to different sources of variability in the resulting profiles. Moreover, a Gaussian noise with variance equal to  $10^{-2} \mu\text{m}$  was added on the last two profiles.

Separation of variability sources has been done using two different statistical techniques: independent component analysis (ICA) and seasonal trend decomposition (STL). In Table 21.1 the nominal values for the roughness parameters are reported.

Roughness parameter	Nominal value
$Ra$	$0.3978 \mu\text{m}$
$Rq$	$0.0020 \mu\text{m}$
$Rsk$	$-0.6094 \mu\text{m}$
$Rku$	$2.1438 \mu\text{m}$

**Table 21.1.** *Nominal values of roughness parameters*

### 21.3.1. Simulations with independent component analysis (ICA)

As seen in the literature, the manufacturing process leaves a fingerprint on the workpiece that is often non-Gaussian, but that follows a beta distribution. This leads to the need for the research of techniques to handle non-Gaussian distributions. With this point of view, the technique of independent component analysis could be used to separate non-Gaussian components.

Independent component analysis (ICA) is a statistical technique whose main applications are blind source separation, blind deconvolution, and feature extraction. In the simplest form of ICA, we observe  $m$  random variables  $\mathbf{x}_1, \mathbf{x}_2, \dots, \mathbf{x}_m$  which are assumed to be linear combinations of  $n$  unknown independent components, denoted by  $\mathbf{s}_1, \mathbf{s}_2, \dots, \mathbf{s}_n$ . The independent components  $\mathbf{s}_i$  are assumed to be mutually statistically independent, and zero-mean. Arranging the observed variables

$\mathbf{x}_j$  into a matrix  $\mathbf{x} = (\mathbf{x}_1, \mathbf{x}_2, \dots, \mathbf{x}_m)^T$  and the component variables  $\mathbf{s}_i$  into a matrix  $\mathbf{s} = (\mathbf{s}_1, \mathbf{s}_2, \dots, \mathbf{s}_n)^T$ , the linear relationship can be expressed as:

$$\mathbf{x} = \mathbf{A}\mathbf{s}$$

Here,  $\mathbf{A}$  is an unknown  $m \times n$  matrix of full column rank, called the mixing matrix. The basic problem of ICA is then to estimate both the mixing matrix  $\mathbf{A}$  and the realizations of the independent components  $\mathbf{s}_i$ , using only observations of the mixtures  $\mathbf{x}_j$ . In a practical situation, the matrix equation is different, because of the unavoidable addition of environmental noise. So the equation should be rewritten as follows:

$$\mathbf{x} = \mathbf{A}\mathbf{s} + \mathbf{n}$$

where  $\mathbf{n}$  is the Gaussian noise.

The idea of signals separation could be transported in the manufacturing field, where the signals could be thought of as the roughness deriving from the turning process, and the other due to imperfections in the machine functioning. Starting from the profiles registered, we propose a method to discriminate the sources of workpiece errors, with the aim of understanding why the process is out of control.

Synthetically, the idea behind the ICA algorithm is the maximization of non-gaussianity. This is done through the maximization of a certain negentropy function.

Let  $\mathbf{W}$  be the inverse of the estimate of matrix  $\mathbf{A}$ . Moreover, the negentropy  $J$  is given by:

$$J(\mathbf{y}) = H(\mathbf{y}_{gauss}) - H(\mathbf{y})$$

where  $\mathbf{y}_{gauss}$  is a Gaussian random vector of the same covariance matrix as  $\mathbf{y}$ , and  $H$  is the differential entropy. Negentropy is a measure of nongaussianity. Using the concept of differential entropy, we can define mutual information  $I$  between the  $n$  scalar random variable  $y_i$ ,  $i=1, \dots, n$  as a measure of the dependence between random variables. It is particularly interesting to express mutual information using negentropy, constraining the variables to be uncorrelated. In this case, we have:

$$I(y_1, y_2, \dots, y_n) = J(\mathbf{y}) - \sum_i J(y_i)$$

The fastICA consists of maximizing the function  $J_G$ , given by:

$$J_G(\mathbf{w}) = \left[ E\{G(\mathbf{w}^T \mathbf{x})\} - E\{G(v)\} \right]^2$$

where  $\mathbf{w}$  is an  $m$ -dimensional vector constrained so that  $E\{(\mathbf{w}^T \mathbf{x})^2\} = 1$  and  $G$  is a function defined in [HYV 99]. More details could be found in [HYV 99].

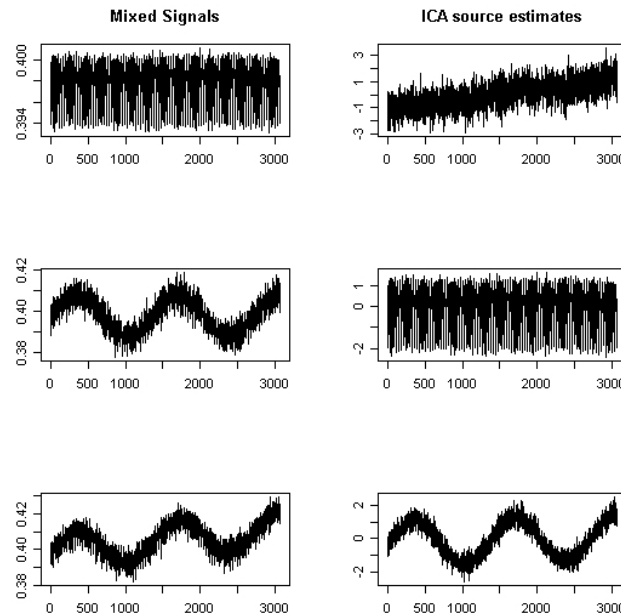
Synthetically, the algorithm is the following:

- Center the data to make its mean zero.
- Whiten the data to give  $\mathbf{z}$ , instead of the vector  $\mathbf{x}$ .
- Choose  $m$ , the number of independent components to estimate. Set counter  $p=1$ .
- Choose an initial value of unit norm for  $\mathbf{w}_p$ , e.g. randomly;  $\mathbf{w}_p$  is the initial estimate for each row of  $\mathbf{W}$ .
- Let  $\mathbf{w}_p = E\{zg(\mathbf{w}_p^T \mathbf{z})\} - E\{g'(\mathbf{w}_p^T \mathbf{z})\}\mathbf{w}_p$ , where  $g$  is defined in [HYV 99].
- Do the following orthogonalization:  $\mathbf{w}_p = \mathbf{w}_p - \sum_{j=1}^{p-1} (\mathbf{w}_p^T \mathbf{w}_j) \mathbf{w}_j$
- Let  $\mathbf{w}_p = \mathbf{w}_p / \|\mathbf{w}_p\|$
- If  $\mathbf{w}_p$  has not converged, go back to step 5.
- Set  $p = p + 1$ . If  $p \leq m$  go back to step 4.

As can be seen in Figure 21.2, with the ICA method the three sources of variability are discriminated. On the left, the original profiles are reported, while on the right, can be seen the three independent components extracted with fastICA.

This analysis has also been performed with another ICA algorithm (JADE), which uses a different objective function to maximize non-gaussianity. However, this leads to analogous results.

ICA is a promising technique, but improvements should be made and implemented in order to reduce the influence of the Gaussian noise on extracted data. Moreover, owing to the nature of the algorithm, there is an ambiguity of sign in the extracted components that should already be removed.



**Figure 21.2.** *Original signals and ICA source estimates*

The application of a modified version of the algorithm for noise reduction has lead to an improvement in signal extraction, but Gaussian noise has not been fully cancelled.

#### 21.4. Simulation with seasonal trend decomposition (STL)

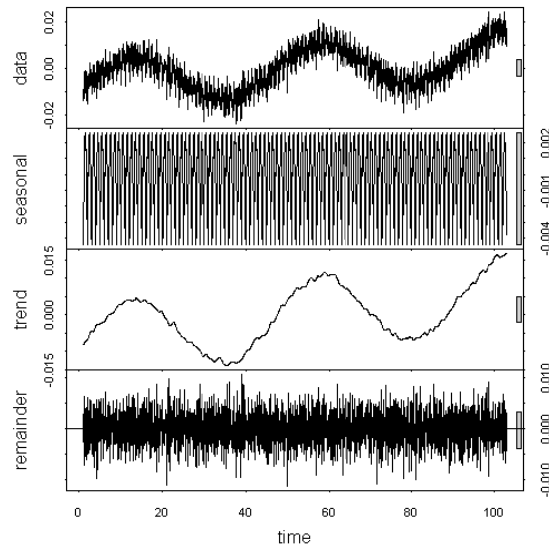
Other analyses have been performed with standard time series analysis techniques, imaging the extracted profile as a time series. This has a physical significance, because the order of points sampled corresponds to subsequent parts worked.

STL is a technique that separates, in time series, the seasonal component from the trend. In formulae, starting from a time series  $Y$ , the series can be broken down into the following components:

$$Y = T + S + R$$

where  $Y$  is the time series,  $T$  is the trend component,  $S$  is the seasonal component, and  $R$  is the remainder. Details about the algorithm and its performances can be

found in [CLE 90]. Figure 21.3 shows the profile simulated with ondulation and drift.



**Figure 21.3.** *Discrimination of roughness and other sources of variability using STL*

It can be noted that the roughness profile could be distinctly recognized in the seasonal component, but the trend component could not discriminate ondulation from the drift. However, an advantage is that it can consider a unique profile, avoiding the necessity to compare it with a reference profile. This technique should be improved, in order to discover multiple periodical patterns. However, one limit is that it recognizes only periodical patterns and one trend, not including incidental errors in workpiece machining or more sources of variability.

## 21.5. Summary

This chapter is a preliminary study of process variability. Since measurement uncertainty and specification uncertainties are identified and quantified, what remains to fully define the manufacturing process is to identify the process itself, with all the causes of distortion. In order to do this, ICA was implemented for a rather simple situation; the promising results encourage its application in more complicated situations, where subsequent processes bring a different component of variability that adds together to give the total variability.

## 21.6. Bibliography

- [CLE 90] CLEVELAND R., CLEVELAND W., MCRAE J., TERPENNING I., “STL: A seasonal-trend decomposition procedure based on loess”, *Journal of Official Statistics*, Vol. 6, No 1., p. 3-73, 1990.
- [GUM 93] *Guide to the Expression of Uncertainty in Measurement (GUM)*, ISO, 1993.
- [EN ISO 14253-1: 1998] Geometrical Product Specifications (GPS) – Inspection by measurement of workpieces and measuring equipment – Decision rules for providing conformance or non-conformance with specifications, EN ISO 14253-1, 1998.
- [HYV 99] HYVARINEN A., “Fast and robust fixed-point algorithms for independent component analysis”, *IEEE Transaction on Neural Networks*, Vol. 10, No. 3, p.626-634, 1999.
- [ISO 3274: 1996] Geometrical Product Specifications (GPS) – Surface texture: Profile method – Nominal characteristics of contact (stylus) instruments, ISO 3274, 1996.
- [ISO 4288: 1996] Geometrical Product Specifications (GPS) – Surface texture: Profile method – Rules and procedures for the assessment of surface texture, ISO 4288, 1996.
- [ISO 11562: 1996] Geometrical Product Specifications (GPS) – Surface texture: Profile method – Metrological characteristics of phase correct filters, ISO 11562, 1996.
- [ISO 4287: 1997] Geometrical Product Specifications (GPS) – Surface texture: Profile method – Terms, definitions and surface texture parameters, ISO 4287, 1997.
- [ISO 12179: 2001] Geometrical Product Specifications (GPS) – Surface texture: Profile method – Calibration of contact (stylus) instruments, ISO 12179, 2001.
- [ISO/TS 14253-2: 1999] Geometrical Product Specifications (GPS) – Inspection by measurement of workpieces and measuring equipment – Part 2: Guide to the estimation of uncertainty in GPS measurement, in calibration of measuring equipment and in product verification, ISO/TS 14253-2, 1999.
- [ISO/TS 17450-2:2002] Geometrical Product Specifications (GPS) – General concepts – Part 2: Basic tenets, specifications, operators and uncertainties, ISO/TS 17450-2, 2002.
- [ZAH 03] ZAHWI S., KOURA M., MEKAWI A., “Factors influencing uncertainty evaluation for surface roughness measurements”, *Proceedings of XVII IMEKO World Congress*, Dubrovnik, Croatia, June 22-27, 2003.

## Chapter 22

# Virtual CMM-based Sampling Strategy Optimization

Several sources of uncertainty contribute to the Coordinate Measuring Machines (CMM) overall uncertainty, including hardware characteristics, measurement environment, fixturing, and the measurement strategy (i.e. the number of sampling points taken and the sampling pattern). The measurement strategy is the key factor in CMM flexibility and is a very important source of uncertainty. Additionally, because the measurement strategy can be easily modified, it is also significant for measurement optimization.

In this work, measurement strategy optimization will be discussed. A methodology will be proposed that considers the presence of a “manufacturing signature” left by the manufacturing process. The methodology aims to be a trade off between inspection costs and measurement uncertainty, with the addition of a simultaneous sampling pattern optimization.

### 22.1. Introduction

Measurement and product/process quality are strictly related. In fact, any quality control system is based on the measurements performed on quality characteristics. Perhaps the most apparent aspect of this relationship is conformance testing; a characteristic of a product is measured, and from the measurement result it is

---

Chapter written by Giovanni MORONI and Stefano PETRÒ.

decided whether the product fits the use or not. Usually, a part that is non-conforming is discarded or scheduled for reworking.

Measurement error can substantially reduce the effectiveness of quality control. Of course, any measurement may incur some amount of error. Consider a generic functional check: a characteristic of the product is measured, and the measurement result is compared to some “specification limit” *SL* (a statement on the maximum deviation permissible for a given characteristic). An inspection error occurs if, because of some measurement error, the measurement result for a conforming part does not comply with *SL* (type I error), or the measurement result for a non-conforming part complies with *SL* (type II error). Type I error costs are usually easy to define: a part that could be sold is not sold or has to be reworked, such that loss equals the value of the part or the cost of reworking. Costs related to type II error are not directly assessable. The part may need to be assembled so that the finished product that it will need to fit will have to be discarded/reworked, or the part will be sold, and this will usually degrade the relationship with the customer.

Measurement error is strictly related to uncertainty [ISO 07], which characterizes the typical dispersion of values for a specific measurement method/device. This uncertainty can be attributed to a measurand, and therefore, the typical measurement error can be quantified. A low value for the measurement uncertainty will reduce the probability that an inspection error occurs. However, low uncertainty measurement systems are usually more expensive than high uncertainty measurement systems. Therefore, “inspection error costs” and “measurement costs” should be balanced.

#### **22.1.1. Conformance to geometric tolerances**

Geometric tolerances [ISO 04a] are becoming more prevalent in the field of mechanics. A geometric tolerance states how much a real part can differ from its ideal, designed geometry. Therefore, a geometric tolerance usually only defines an upper specification limit for the geometric error (i.e. a “perfect” part is always considered to be a confirming part).

Typically, the check of a geometric tolerance involves the estimate of the geometric error, and an uncertainty evaluation should be associated with this estimate. However, even providing this data may not be sufficient for stating conformance. Bachmann *et al.* [BAC 04] observed that the dispersion of measurement error influences the possibility of committing a type II error and suggested the consideration of this possibility in the conformance statement. However, a universal criterion for the integration of this information is not proposed.



Therefore, clear rules for stating conformance or non-conformance are required [WEC 00]. This problem is addressed by the ISO 14253 [ISO 98, ISO 99, ISO 02] standards series. In particular, ISO 14253-1 [ISO 98] proposes “guidelines for decision rules” for “considering uncertainty in determining conformance to specifications”. A decision rule should essentially identify three regions for the measurement result:

- *Acceptance region*. If the measurement result falls in this area, then the measured part is accepted.

- *Rejection region*. If the measurement result falls in this area, then the measured part is rejected.

- *Transition region*. If the measurement result falls in this area, it is not possible to state whether the measured part conforms or does not conform to the tolerance.

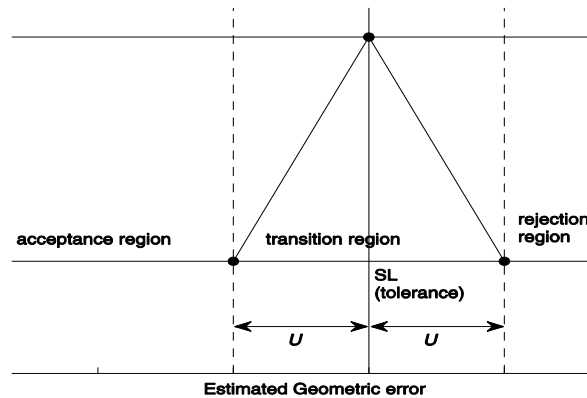
The ISO 14253-1 standard clearly defines these three regions. In particular, a part should be accepted if its geometric error estimate is lower than the geometric tolerance reduced by the extended uncertainty  $U$  [ISO 07] and rejected if its geometric error estimate is greater than the geometric tolerance augmented by  $U$ . The region  $(SL - U, LS + U)$  is considered to be the transition region. In particular, the standard states that if a supplier has to prove conformance, a part falling in the transition region cannot be considered to be a conforming part. Additionally, if a customer wishes to prove non-conformance, a part falling in the transition region cannot be considered non-conforming (see Figure 22.1). In the following sections, we will consider a supplier’s point-of-view.

### 22.1.2. Evaluating geometric error

A commonly used device for evaluating geometric error is a “coordinate measuring machine” (CMM), which is a system that can sample numerous points on any surface. A “substitute geometry” is fitted at these points, and the geometric error is evaluated as the maximum distance from this geometry, i.e. the actual limiting amplitude of the tolerance zone is evaluated (see e.g. Anthony *et al.* [ANT 96]). Because only a few points usually define the amplitude of the tolerance zone, only these points are relevant when evaluating the geometric error.

It is interesting to note that “anomalous” zones (those zones which define the geometric error) of the profile/surface will tend to be the same throughout the entire production. This is because every part produced by the same production process will be similar to the others, even for defects that it presents (e.g. in a face work a turned cylindrical shaft will usually be slightly conical, but if the part is mounted between centers, the result could be an hourglass shape). It can therefore be stated that the

part presents a “manufacturing signature”, i.e. the form deviations are constituted by the sum of a random part and a systematic part, which creates the signature.



**Figure 22.1.** Regions as described by the ISO 14253-1 standard

Edgeworth and Wilhelm [EDG 99] and Sprauel *et al.* [SPR 03] observed that the actual geometric error might interact with the measuring strategy, thus increasing or decreasing the measurement error and therefore increasing or decreasing the uncertainty. Killmaier and Babu [KIL 03] suggested taking advantage of this interaction based on the knowledge of the geometric error provided by the signature identification. Only those areas that are systematically anomalous should be densely sampled, which results in only a few points remaining in the other areas. A similar point distribution should reduce any uncorrected measurement bias, and because of the increased knowledge of critical areas, the point distribution should reduce the amount of uncertainty.

### 22.1.3. Goals

In this chapter, a methodology will be proposed for finding an optimal sampling strategy when estimating geometric error by means of a CMM device. The method will be based on a cost function that depends on the sampling strategy (i.e. the number and location of the sampling points). The sampling strategy will be optimal if the best trade-off between measurement costs and inspection error costs is found. A heuristic algorithm will be adopted to minimize the function. To make the methodology applicable when a generic task specific uncertainty has to be evaluated, uncertainty evaluation will be performed by means of a virtual CMM [WIL 01]. The virtual CMM model will be validated according to the ISO/TS

15530-4 [ISO 08] technical specification. A case study will be presented that involves the roundness of C20 steel turned shafts.

## 22.2. State of the art

Several studies have been performed regarding the interaction between the sample size and measurement error. Lee *et al.* [LEE 97] analyzed the different behavior of uniform, random and Hammersley sequence based sampling strategies for cylindrical, conical and dome shaped surfaces and suggested the Hammersley sequence as the best strategy. Kim and Raman [KIM 00] also obtained a similar result. Chan *et al.* [CHA 96] studied the influence of point location when measuring the diameter of a circular part; they primarily focused on the performance of different probing heads. Namboothiri and Shunmugam [NAM 99] proposed an index based on the probability of the measurement result lower than a chosen value that would lead to the right choice of the sample size for a random sampling strategy.

However, these papers did not consider the interaction between the actual form error when suggesting an optimal sampling strategy, i.e. they disregarded the presence of a signature. Signature based sampling strategies are proposed by Henke *et al.* [HEN 99, SUM 02], who suggested a method to model the signature and an algorithm to choose the best sampling point locations. However, the problem of choosing the right sample size was not addressed. Colosimo *et al.* [COL 08a] proposed a different solution than the one proposed by Henke *et al.* that did not require an explicit model for the signature to be applied.

Capello and Semeraro [CAP 01a, CAP 01b] considered the typical harmonic content of a profile/surface and proposed an economic function based on this content to choose the right sample size. This method is limited to the evaluation of size and location tolerances, and because of the harmonic model that they adopted, it was determined that the sampling strategy should be uniform.

Finally, Badar *et al.* [BAD 05] suggested an adaptive approach such that sampling points are added until the measurement error is assumed to be sufficiently low. However, the termination condition is not clear and the continuous change of the sampling strategy required by an adaptive strategy is difficult to implement on standard CMMs.

The problem of choosing the right sampling locations and sample size when the inspected phenomenon has a spatial evolution has been addressed in the field of meteorology and hydrology [DIX 96]. Because a “sampling point” in that field consists of a meteorological station or a drilled well, which are expensive and cannot

be moved after being built, a great effort has been undertaken to propose methods to choose the correct “sampling strategy”, i.e. the location of stations. The only limitation to the direct application of these methods to industrial metrology is the lack of systematic behavior in meteorological and hydrological phenomena (i.e. no signature is considered, nor does a signature necessarily exist). A similar methodology for planning the CMM measurement strategy has been proposed by Moroni and Petrò [MOR 08]. An uncertainty evaluation is implicit in the methodology, which is based on the ISO 15530-3 standard [ISO 04b].

### 22.3. Proposed methodology

The proposed methodology is based on the integration of a virtual CMM and a manufacturing signature model, which will serve as an input for the virtual CMM. This integration will ensure that the virtual CMM will take into account the interaction between the actual geometric error and the sampling strategy during the uncertainty evaluation. Consideration of this interaction will enable signature-based sampling strategy optimization, as suggested in section 1.1.2.

Before introducing the adopted virtual CMM, the optimality function for choosing the sampling strategy is introduced. Because the inspection process (due to measurement costs and inspection error costs) may significantly affect overall production costs, an economic approach will be proposed.

The basic structure of the function, which will evaluate inspection costs  $C_I$  for a single workpiece, will be:

$$C_I = C_M + C_E \quad [22.1]$$

where  $C_M$  is the “measurement cost”, the cost of performing a single measurement task, and  $C_E$  is the “error cost”, the cost generated by measurement error that assumes that the uncertainty is large enough to significantly affect the possibility of type I and type II errors.

#### 22.3.1. Evaluation of $C_M$

For a CMM, the cost related to the sampling strategy primarily depends on the measuring time. As the measuring time increases, the cost also increases. The measuring time also depends on the sample size, so  $C_M$  can be expressed as:

$$C_M = c_M t = c_M t_p n = c_p n \quad [22.2]$$

where  $c_M$  is the CMM hourly cost,  $t$  is the time required to perform the measurement task,  $t_p$  is the time for sampling a single point and  $n$  is the sample size.

In equation [22.2], the cost related to each sampling point is assumed to be constant, i.e. each point requires the same amount of time to be sampled. This is not always true because point-to-point distances may vary, and the travel time varies depending on the location of the points. However, because the contact time for a CMM is usually predominant, we will consider this difference to be negligible. Furthermore, the time required to set-up the machine, align the parts, etc. is not considered because it does not depend on the sampling strategy.

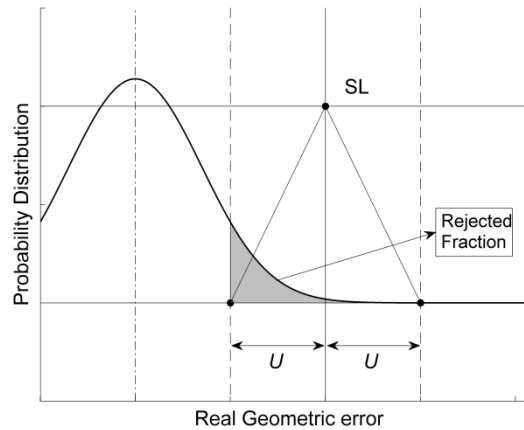
### 22.3.2. Evaluation of $C_E$

Depending on the approach chosen by the manufacturer to deal with non-conforming parts, the evaluation of  $C_E$  is often a subjective procedure. In fact, labeling a conforming part as defective, even if it is conforming, can lead to discarding the part, reworking the part, or other expensive and unnecessary actions. Defining the cost of mislabeling a defective part as conforming is even more difficult, because it can cause a finished product to be defective or a customer to reject a batch of products. In this chapter, a simple approach will be proposed.

Assume that the conformance to a tolerance has to be proven, and the ISO 14253-1 [ISO 98] approach for stating conformance is followed. Furthermore, assume that  $x$ , the real geometric error of the part, behaves according to some statistical distribution (e.g. Gaussian distribution). Therefore, if uncertainty increases, a higher number of parts will be rejected even if they should be accepted (see Figure 22.2). The proposed expression for evaluating  $C_E$  is given as:

$$C_E = c_w P(SL - U < x < SL) \quad [22.3]$$

where  $c_w$  is the cost of a part or reworking it, or any action which is performed on the part itself when declared non-conforming. The term  $P(SL - U < x < SL)$  can be regarded as the probability that the real geometric error will fall in the portion of the transition region that is part of the conformance zone when uncertainty is zero (we cannot state conformance for the part, but the part is conforming). This probability represents the average fraction of conforming parts that are declared to be non-conforming. In equation [22.3], it has been assumed that only an upper bound exists for  $x$ , which is typical for geometric tolerances. However, if both upper and lower bounds exist, equation [22.3] can be easily modified.



**Figure 22.2.** *Rejected fraction of conforming parts*

We might indicate that this formulation of error cost does not take into account the cost of type II errors. However, the ISO 14253-1 criterion for stating conformance has been designed to avoid these types of errors. It is assumed that when the probability of a non-conforming part (characterized by  $x > SL$ ) is measured, the estimated geometric error  $y < SL - U$  is very small.

Another issue to consider is that the geometric error evaluation is often biased due to under-sampling. If the sampling strategy is not sufficient enough to guarantee complete coverage of the profile/surface to inspect, it is possible that the maximum deviation will not be identified. Therefore, equation [22.3] may not be adequate to estimate  $C_E$  if the bias is not considered. However, the bias must be considered in uncertainty evaluation as indicated in the ISO/TS 15530-3 [ISO 04b] international standard, thereby reducing its influence. Furthermore, a correct signature based sampling strategy should reduce bias [SUM 02], even if the sample size is small.

### 22.3.3. Evaluating the uncertainty: the virtual CMM

Wilhelm *et al.* [WIL 01] identified six ways for evaluating the CMM measurement uncertainty: sensitivity analysis, expert judgment, the use of calibrated objects, computer simulation, statistical estimation from measurement history, and hybrid methods. Among these methodologies, only the computer simulation method is truly suitable for evaluating a reliable “task specific uncertainty” for CMM measurement because it has the required flexibility and is not considered to be a subjective method such as expert judgment. Software that simulates the behavior of

a CMM, thus allowing uncertainty evaluation, is commonly known as “virtual CMM”.

A classic virtual CMM [WIL 01, BAL 99] is based on the simulation of ideal (but not necessarily perfect, e.g. they can contain some undulations) geometric features for which the geometric error is known. A measurement error is simulated according to a model of the real behavior of the CMM for which the uncertainty is being evaluated and added to the ideal feature. The measurement uncertainty is evaluated by comparing geometric errors evaluated on the “perturbed” features and the known geometric errors of ideal features. The overall methodology can be regarded as a Monte Carlo simulation of ideal profiles and sampling errors from which a Monte Carlo simulation of geometric tolerance evaluation error  $x - y$  is derived.

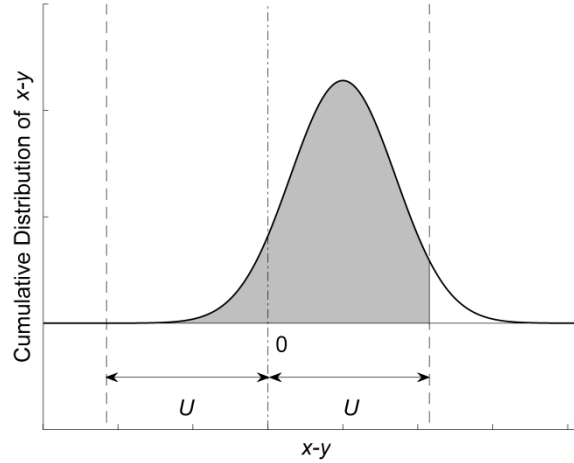
Various sources of error should be considered in the error simulations, including measurement strategy, environmental conditions, CMM volumetric errors, and so on. A complete list of these sources can be found in the ISO/TS 15530-4 standard [ISO 08]. This standard deals with the problem of validating virtual CMM models by proposing four methodologies for the validation, one of which has been adopted in this work to validate the virtual CMM that is developed.

Several methodologies have been proposed to extrapolate the uncertainty from the simulation results. In this chapter, the approach proposed by Schwenke *et al.* [SCH 00] has been adopted. This approach does not allow for the explicit calculation of the standard uncertainty  $u$ . Instead, an expanded uncertainty  $U$  characterized by some coverage probability  $p$  [ISO 07] is used. Assume that a Monte Carlo simulation of several (thousand) geometric tolerance evaluation errors  $x - y$  is available. From this data, a Monte Carlo evaluation of the statistical distribution of  $x - y$  is derived.  $G(x - y)$  is then defined as the empirical cumulative distribution of  $x - y$ . An evaluation of the expanded uncertainty  $U$  characterized by the coverage probability  $p$  can then be obtained as:

$$G(U) - G(-U) = p \quad [22.4]$$

Note that the resulting evaluation of  $U$  is consistent with the definition of coverage probability and any uncorrected bias is considered [SCH 00].

To simulate geometric errors, an approach based on the results from Van Dorp *et al.* [VAN 01] has been implemented. The developed model is based on the frequency content of the error signal and can be applied to a “Zeiss Prismo” CMM. At this time, the virtual CMM model only takes into account the geometric error of the CMM and the adopted sampling strategy as sources of uncertainty.



**Figure 22.3.** *Uncertainty evaluation according to equation [22.4]*

To validate the virtual CMM, the approach proposed in Appendix C.2 of the ISO/TS 15530-4 standard has been chosen. The virtual CMM generated an uncertainty evaluation for the roundness measurement of a calibrated plug gauge, ensured a 95% coverage probability and simulated one thousand measurement repetitions. The uncertainty statement is assumed to be valid for the “Zeiss Prismo” CMM, which is available at Politecnico di Milano (where this work was developed). The calibrated plug gauge has been measured one hundred times. The formula [ISO 08]:

$$|y_{cal} - y| \leq \sqrt{U_{cal}^2 + U^2} \quad [22.5]$$

has been applied to prove the usability of the uncertainty evaluation, where  $y_{cal}$  is the calibrated roundness of the plug gauge and  $U_{cal}$  is the calibration expanded uncertainty with a coverage probability of about 95%. Because 97 of 100 measurement repetitions satisfied equation [22.5], the virtual CMM uncertainty evaluation is proven to be reasonable.

Finally, the entirety of this work is based on the idea of a virtual CMM accounting for the interaction between the actual form error and the sampling strategy when evaluating the measurement uncertainty. This is not difficult to obtain with a Monte Carlo simulation based virtual CMM; it is sufficient to simulate nominal profiles according to a signature model. If the simulated ideal profiles are generated according to a real signature model instead of being perfect features, or characterized by “standard” errors such as undulations, then the uncertainty



evaluation will implicitly consider the signature. It will suffice to simulate, according to the manufacturing signature model, a sufficient number of profiles on a dense set of sampling points; the geometric error evaluated on these profiles is denoted as  $x$ . Simulation of the geometric error evaluation can be performed by extracting a subset of the generated points. This subset corresponds to the strategy for which the uncertainty is evaluated. Then, a random measurement error will be added to each point; the error evaluated on this “perturbed” profile is denoted as  $y$ . Measurement error  $x - y$  can finally be evaluated.

#### 22.3.4. Cost function minimization

If the exact strategy of minimizing equation [22.1] is required, the only possible method is to evaluate equation [22.1] for any possible subset of the dense cloud that constitutes simulated nominal features. However, the number of possible subsets is usually very large, and because the optimal solution is affected by a certain degree of “uncertainty”, a nearly optimal solution should be regarded as sufficient.

Several algorithms have been proposed to handle the problem of subset choice. A “simulated annealing” (SA) [KIR 83] algorithm has been chosen from the available literature on the design of groundwater monitoring networks [NUN 04], which proposes similar problems to those considered in this chapter.

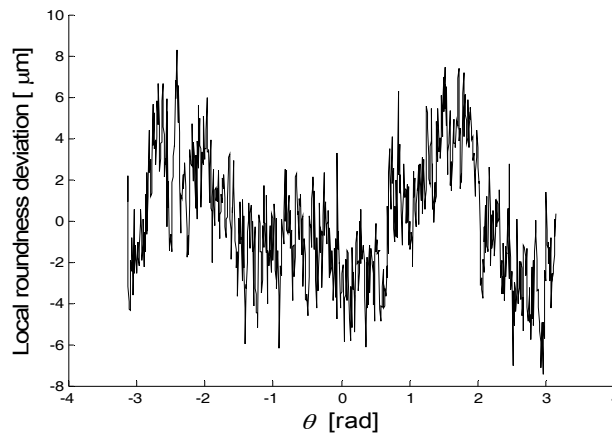
For a given set of points, the SA algorithm seeks an optimal subset that can act as a surrogate for the entire set with respect to  $C_I$ . A subset of initial points is selected and passed to the SA algorithm. The algorithm then selects a random subset in the “neighborhood” of the current subset (the new subset will be similar to the original subset, differing only for a few points, and will contain a number of sampling points which is only slightly different from the original) and determines if it should replace the current subset or not according to the simulated annealing rule, i.e. always replace if the alternative subset value of  $C_I$  is lower; or replace using the probability  $\exp((C_{I,i} - C_{I,i-1})/T)$ , where  $T$  decreases throughout the iterations of the algorithm.

The SA algorithm has shown the ability to quickly converge to a solution, which should be near the true optimal solution.

#### 22.4. Case study

To prove the effectiveness of the proposed methodology, the manufacturing signature model by Colosimo *et al.* [COL 08b] is considered. This model describes the signature of roundness profiles obtained by turning C20 steel bars. The nominal

diameter of the specimens was 26 mm (using a cutting speed equal to 163 m/min, a feed equal to 0.2 mm/rev and two cutting steps of 1 mm depth each). An instance of the geometric error simulated for this manufacturing signature is depicted in Figure 22.4, which shows the local form deviation as a function of the angle  $\theta$  at which the point has been simulated.

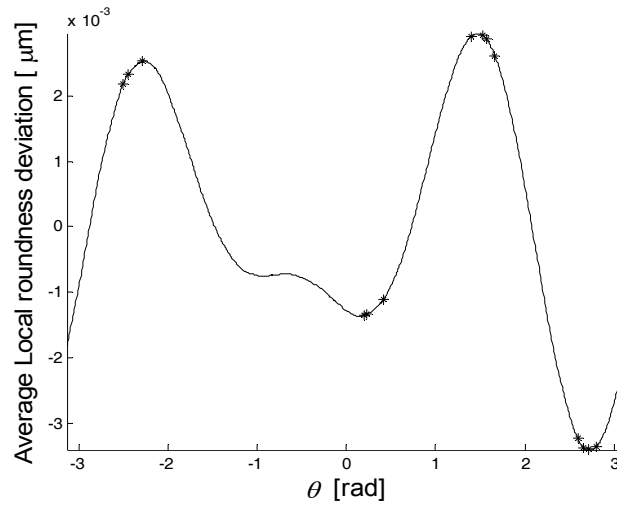


**Figure 22.4.** *An example of a simulated profile*

By using the signature model, one thousand “ideal” profiles have been simulated and the roundness error has been chosen as the reference value. Roundness reference values have shown a normal distribution of geometric error, therefore it is assumed that  $x \sim N(14.6, 1.4)$ , where the mean and standard deviation are expressed in units of  $[\mu\text{m}]$ . Furthermore, a roundness tolerance of  $25 \mu\text{m}$  is considered for the profiles, and for the evaluation of costs,  $c_p = 0.027 \text{ €/point}$  and  $c_w = 10 \text{ €/part}$  have been considered.

A simulated sampling error has been added to the simulated profiles, thereby generating one thousand “perturbed” profiles as described in section 22.3.2. Finally, the SA algorithm has been applied to this data to optimize the sampling strategy. An optimal sampling strategy consisting of 14 points has been identified (see Figure 22.5). As expected, the sampling points are concentrated where the roundness deviation is greatest so that the bias in the measurement of the geometric error is minimized. In particular, the inspection cost for the optimal sampling strategy is  $0.44 \text{ €/part}$ . This cost is compared to a uniform sampling strategy with 14 points where the inspection cost is  $2.62 \text{ €/part}$ ; the inspection cost has been reduced by one fifth. Furthermore, we can compare the expanded uncertainty related to the optimized strategy, which is equal to  $7 \mu\text{m}$  and to the uncertainty of the uniform

strategy, which is equal to  $9.3 \mu\text{m}$  (a coverage probability of 95% for both of the expanded uncertainty evaluations). The performance of the optimized strategy can also be compared to the performance of a uniform strategy by only optimizing the sample size. The optimal uniform strategy consists of 31 points and results in a cost of 0.93 €/part. Therefore, the optimized strategy is able to reduce both the inspection cost and the time by a factor of one half because the sample size is also reduced by a factor of one half.



**Figure 22.5.** Optimal sampling strategy

To better understand the effectiveness of the proposed methodology, consider Figure 22.6, which shows the decreasing expanded uncertainty as the sample size increases. Even if the uncertainty decreases for both the uniform and signature optimized sampling strategies, it is apparent that the uncertainty is always lower for the optimized strategy. Similarly, Figure 22.7 shows the relationship between the sample size and the cost of inspection. As in the previous case, the optimized sampling strategy outperforms the uniform sampling strategy. It should be noted that if the sample size is large enough, then the inspection cost does not depend on the optimized or uniform sampling strategy that is adopted. It then depends on the uncertainty reduction, which is sufficient to minimize the term  $C_E$  in equation [22.3] (even if Figure 22.6 shows a significant difference for  $U$ ).

Regarding the sensitivity of the solution, we first consider a variation in  $c_w$ . Figure 22.8 shows the variation of the optimal sample size  $n$  as the inspection error cost for a single part  $c_w$  changes, and as expected, the results are directly

proportional. Similarly, we can expect it to be inversely proportional to  $c_p$ . Perhaps the sensitivity of the solution to  $SL$  (Figure 22.9) is more interesting. It is observed that if  $SL$  is close to or less than the average value of  $x$ , then the optimal sample size is small. This is because, regardless of the measurement strategy, a large portion of the products are defective – the algorithm is simply suggesting a change in the manufacturing process, which is not sufficiently capable. On the other hand, when  $LS$  is large with respect to the average value of  $x$ , again the sample size is small. This is because, although the manufacturing process is very capable, it is not necessary to check every part – most of the production is conforming, so we must ensure that the process is stable.

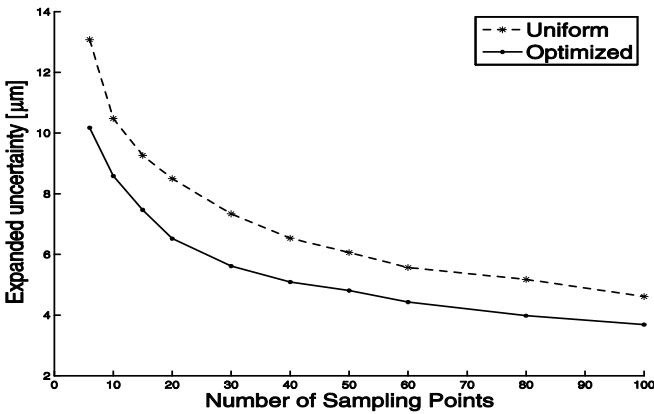


Figure 22.6. Relationship between sample size and uncertainty

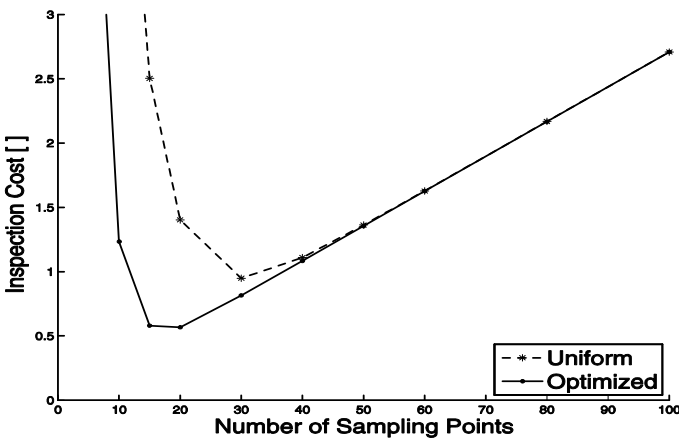


Figure 22.7. Relationship between sample size and costs

Finally, assume that because the same set of 1,000 simulated profiles and 1,000 perturbed profiles has been adopted to optimize the sampling strategy and to evaluate sampling strategy performance, the sampling strategy may only be effective for these specific simulated profiles. To prove the general effectiveness of the strategy, 1,000 simulations have been performed and an independent uncertainty evaluation has been performed based on these new profiles.

The results are not distinguishable from those proposed in Figures 22.6 and 22.7, thus proving the generalized nature of the result. This may be due to the large number of simulations performed compared to the number of sampling points taken – if more sampling points were chosen, the strategy could then “adapt” itself to the actual simulated profiles.

## 22.5. Conclusions

In this chapter, a methodology has been proposed to plan sampling strategies (sampling points number and positions) for inspecting geometric tolerances. The developed strategy optimizes the inspection cost that arises from measuring workpieces, plus costs linked to both type I and type II measurement errors. This inspection cost is primarily related to the number of sampling points taken (which is proportional to the measurement cost) and the probability of errors (which is proportional to the errors cost). Therefore, even if the methodology simultaneously optimizes the number and the location of sampling points, it can be considered to be a two step methodology: in the first step, the uncertainty is minimized from the given sample size; in the second step, the optimal sample size is chosen.

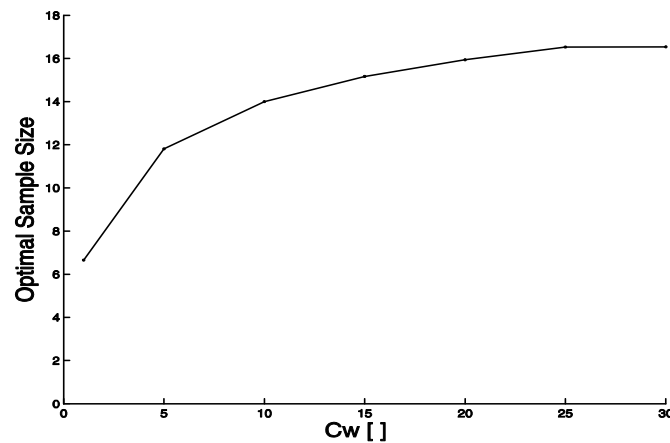
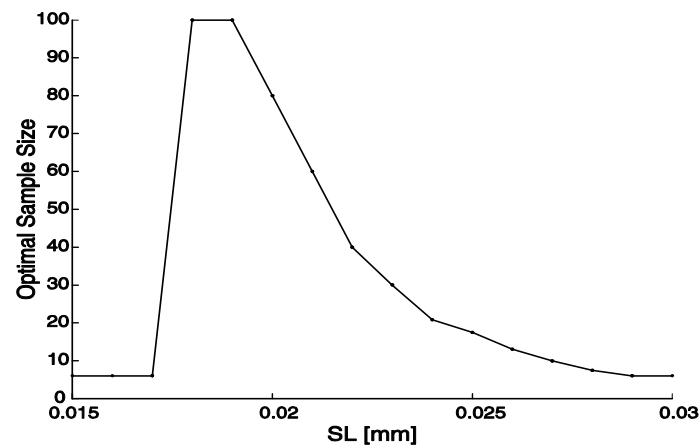


Figure 22.8. Solution sensitivity to variations in the product cost

The optimization of the sampling point locations is based on the presence of a “manufacturing signature”, which is a systematic behavior of the real geometric feature. The proposed methodology adopts a Virtual CMM model that takes into account the signature and its interaction with the sampling strategy when evaluating the measurement uncertainty. Therefore, when comparing several possible sampling strategies, the strategy characterized by the minimum uncertainty should be selected.



**Figure 22.9.** Solution sensitivity to variations in  $SL$

The methodology can be applied even if no signature is present or if no signature is assumed to be present; however, the resulting strategies should not differ significantly from the uniform or random strategies, and the optimization will only account for the sample size.

The primary drawback of a signature-based sampling strategy is if the signature changes, the measurement uncertainty will probably increase. However, if a model for the manufacturing signature is known, then it would be possible to adopt efficient “statistical process control” techniques to identify the signature modifications, and a signature model is implicit in the proposed methodology. Similar methodologies have been proposed by Colosimo *et al.* [COL 08b, COL 07], and the application of these techniques is useful because a modification to the signature usually causes a degradation of the product quality and is related to undetected failures in the manufacturing process.

Future goals include a refinement in the evaluation of  $C_E$ , the possibility of linking a strategy plan to more efficient sampling plans [MON 04], and the analysis of redundant inspection if considered from the signature point-of-view.

## 22.6. Acknowledgments

Financial support for this work has been provided by the Italian Ministry of Education, University and Research.

## 22.7. Bibliography

- [ANT 96] ANTHONY G.T., ANTHONY H.M., BITTNER B., BUTLER B.P., COX M.G., DRIESCHNER R., ELLIGSEN R., FORBES A.B., GROSS H., HANNABY S.A., HARRIS P.M., KOK J., "Reference software for finding Chebyshev best-fit geometric elements", *Precision Engineering*, Vol. 19, No. 1, 1996, p. 28–36.
- [BAC 04] BACHMANN J., LINARES J.M., SPRAUDEL J.M., BOURDET P., "Aide in decision-making: contribution to uncertainties in three-dimensional measurement", *Precision Engineering*, Vol. 28, No. 1, 2004, p. 78–88.
- [BAD 05] BADAR M.A., RAMAN S., PULAT P.S., "Experimental verification of manufacturing error pattern and its utilization in form tolerance sampling", *International Journal of Machine Tools and Manufacture*, Vol. 45, No. 1, 2005, p. 63–73.
- [BAL 99] BALSAMO A., DI CIOMMO M., MUGNO R., REBAGLIA B.I., RICCI E., GRELLA R., "Evaluation of cmm uncertainty through Monte Carlo simulations", *CIRP Annals-Manufacturing Technology*, Vol. 48, No. 1, 1999, p. 425–428.
- [CAP 01a] CAPELLO E., SEMERARO Q., "The harmonic fitting method for the assessment of the substitute geometry estimate error. Part I: 2D and 3D theory", *International Journal of Machine Tools and Manufacture*, Vol. 41, No. 8, 2001, p. 1071–1102.
- [CAP 01b] CAPELLO E., SEMERARO Q., "The harmonic fitting method for the assessment of the substitute geometry estimate error. Part II: statistical approach, machining process analysis and inspection plan optimization", *International Journal of Machine Tools and Manufacture*, Vol. 41 No. 8, 2001, p. 1103–1129.
- [CHA 96] CHAN F.M.M., KING T.G., STOUT K.J., "The influence of sampling strategy on a circular feature in coordinate measurements", *Measurement*, Vol. 19, No. 2, 1996, p. 73–81.
- [COL 07] COLOSIMO B.M., MAMMARELLA F., PETRÒ S., "Quality control of manufactured surfaces", *Proceedings of the IX Intl. Workshop on Intelligent Statistical Quality Control*, Beijing, China, September 2007.
- [COL 08a] COLOSIMO B.M., GUTIERREZ MOYA E., MORONI G., PETRÒ S., "Statistical sampling strategies for geometric tolerance inspection by cmm", *Economic Quality Control*, Vol. 23, No. 1, 2008, p. 109–121.
- [COL 08b] COLOSIMO B.M., SEMERARO Q., PACELLA M., "Statistical process control for geometric specifications: On the monitoring of roundness profiles", *Journal of Quality Technology*, Vol. 40, No. 1, 2008, p. 1–18.

- [DIX 96] DIXON W., CHISWELL B., “Review of aquatic monitoring program design”, *Water Research*, Vol. 30, No. 9, 1996, p. 1935–1948.
- [EDG 99] EDGEWORTH R., WILHELM R.G., “Measurement uncertainty due to work-piece error interaction with sampling period”, *SSM '98: Proceedings of the IFIP TC5 WG5.3 International Conference on Sculptured Surface Machining*, Kluwer, Deventer, The Netherlands, 1999, p. 196–200.
- [HEN 99] HENKE R.P., SUMMERHAYS K.D., BALDWIN J.M., CASSOU R.M., BROWN C.W., “Methods for evaluation of systematic geometric deviations in machined parts and their relationships to process variables”, *Precision Engineering*, Vol. 23, No. 4, 1999, p. 273–292.
- [ISO 98] ISO, ISO 14253-1: Geometrical Product Specifications (GPS) – Inspection by measurement of workpieces and measuring equipment - Part 1: Decision rules for proving conformance or nonconformance with specifications, International Organization for Standardization, Geneva, Switzerland, 1st edn., 1998.
- [ISO 99] ISO, ISO/TS 14253-2: Geometrical Product Specifications (GPS) – Inspection by measurement of workpieces and measuring equipment - Part 2: Guide to the estimation of uncertainty in GPS measurement, in calibration of measuring equipment and in product verification, International Organization for Standardization, Geneva, Switzerland, 1st edn., 1999.
- [ISO 02] ISO, ISO/TS 14253-3: Geometrical Product Specifications (GPS) – Inspection by measurement of workpieces and measuring equipment - Part 3: Guidelines for achieving agreements on measurement uncertainty statements, International Organization for Standardization, Geneva, Switzerland, 1st edn., 2002.
- [ISO 04a] ISO, ISO 1101: Geometrical Product Specifications (GPS) - Tolerances of form, orientation, location and run out, International Organization for Standardization, Geneva, Switzerland, 2nd edn., 2004.
- [ISO 04b] ISO, ISO/TS 15530-3: Geometrical Product Specifications (GPS) – Coordinate measuring machines (CMM): Technique for determining the uncertainty of measurement – Part 3: Use of calibrated workpieces or standards, International Organization for Standardization, Geneva, Switzerland, 1st edn., 2004.
- [ISO 07] ISO/IEC, *ISO/IEC GUIDE 99:2007(E/F): International Vocabulary of basic and general terms in Metrology (VIM)*, International Organization for Standardization, Geneva, Switzerland, 1st edn., 2007.
- [ISO 08] ISO, ISO/TS 15530-4: Geometrical Product Specifications (GPS) – Coordinate measuring machines (CMM): Technique for determining the uncertainty of measurement - Part 4: Evaluating task-specific measurement uncertainty using simulation, International Organization for Standardization, Geneva, Switzerland, 1st edn., Jun. 2008.
- [KIL 03] KILLMAIER T., BABU A.R., “Genetic approach for automatic detection of form deviations of geometrical features for effective measurement strategy”, *Precision Engineering*, Vol. 27, No. 4, 2003, p. 370–381.



- [KIM 00] KIM W.S., RAMAN S., "On the selection of flatness measurement points in coordinate measuring machine inspection", *International Journal of Machine Tools and Manufacture*, Vol. 40, No. 3, 2000, p. 427–443.
- [KIR 83] KIRKPATRICK S., GELATT C.D., VECCHI M.P., "Optimization by simulated annealing", *Science*, Vol. 220, No. 4598, 1983, p. 671–680.
- [LEE 97] LEE G., MOU J., SHEN Y., "Sampling strategy design for dimensional measurement of geometric features using coordinate measuring machine", *International Journal of Machine Tools and Manufacture*, Vol. 37, No. 7, 1997, p. 917–934.
- [MON 04] MONTGOMERY D.C., *Design and Analysis of Experiments*. New York, Wiley, 6th edn., 2004.
- [MOR 08] MORONI G., PETRÒ S., "CMM measurement uncertainty reduction via sampling strategy optimization", *Proceedings of the 9th Biennial ASME Conference on Engineering Systems Design and Analysis*, Haifa, Israel, July 2008, CD-ROM.
- [NAM 99] NAMBOOTHIRI V.N.N., SHUNMUGAM M.S., "On determination of sample size in form error evaluation using coordinate metrology", *International Journal of Production Research*, Vol. 37, No. 4, 1999, p. 793–804.
- [NUN 04] NUNES L., CUNHA M., RIBEIRO L., "Optimal space-time coverage and exploration costs in groundwater monitoring networks", *Environmental Monitoring and Assessment*, Vol. 93, No. 1, 2004, p. 103–124.
- [SCH 00] SCHWENKE H., SIEBERT B.R.L., WÄLDELE F., KUNZMANN H. "Assessment of uncertainties in dimensional metrology by Monte Carlo simulation: Proposal of a modular and visual software", *CIRP Annals-Manufacturing Technology*, Vol. 49, No. 1, 2000, p. 395–398.
- [SPR 03] SPRAUER J.M., LINARES J.M., BACHMANN J., BOURDET P., "Uncertainties in CMM measurements, control of ISO specifications", *CIRP Annals-Manufacturing Technology*, Vol. 52, No. 1, 2003, p. 423–426.
- [SUM 02] SUMMERHAYS K.D., HENKE R.P., BALDWIN J.M., CASSOU R.M., BROWN C.W., "Optimizing discrete point sample patterns and measurement data analysis on internal cylindrical surfaces with systematic form deviations", *Precision Engineering*, Vol. 26, 2002, p. 105–121.
- [VAN 01] VAN DORP B.W., HAITJEMA H., DELBRESSINE F., BERGMANS R.H., SCHELLEKENS P.H.J., "Virtual CMM using Monte Carlo methods based on frequency content of the error signal", J.E. DECKER, N. BROWN, eds, *Proceedings of SPIE 4401 - Recent Developments in Traceable Dimensional Measurements*, SPIE, Vol. 4401, 2001, p. 158–167.
- [WEC 00] WECKENMANN A., RINNAGL M., "Acceptance of processes: do we need decision rules?", *Precision Engineering*, Vol. 24, No. 3, 2000, p. 264–269.
- [WIL 01] WILHELM R.G., HOCKEN R., SCHWENKE H., "Task specific uncertainty in coordinate measurement", *CIRP Annals-Manufacturing Technology*, Vol. 50, No. 2, 2001, p. 553–563.

## Chapter 23

# Impact of Workpiece Shape Deviations in Coordinate Metrology

In coordinate metrology results are based on a set of probed points from the workpiece surface, which are evaluated with the use of ideal substitute geometries. Shape deviations of the workpiece lead to non-uniform influence of single points on the result. In this chapter, a method for analyzing the influence of single measurement points on the result and for computing the uncertainty of the evaluation is proposed. The statistical resampling technique “the Jackknife” is adapted for use with CMM point clouds. This technique enables the bias and standard error of the measurand to be estimated. The outcome is analyzed with computer simulations, whose results are presented in this chapter.

### 23.1. Introduction

Coordinate measurement machines (CMM) are widely used for the measurement of geometric features, due to their large application scope and flexibility in the measurement of different workpieces and inspection features. The precision of the measurement results is an important aspect, especially when small tolerances are required as is the case for precision and micro-structured workpieces, i.e. workpieces with structures between 1  $\mu\text{m}$  and 1 mm [HES 02]. In these cases reliable results are necessary to enable an interpretation and thus to identify reject parts. The common way to describe the reliability of measurement results is to specify the measurement uncertainty. On this basis, it is possible to construct a

---

Chapter written by Gisela LANZA and Jochen PETERS.

confidence interval around the result, in which the true measurand lies with a given probability. This information has to be considered when interpreting measurement results. For this reason detailed information about measurement uncertainty and its composition is necessary, especially when the uncertainty in relation to the tolerance limits is large.

In coordinate metrology shape deviations of the workpiece lead to an increasing influence of the sampling strategy, i.e. the number and position of probing points on the workpiece surface. Furthermore, shape deviations lead to a non-uniform influence of the points on the result. Information about shape deviations is lost during evaluation of the measurement results since the information in the point cloud is reduced to only a few parameters of an ideal substitute geometry. The existence of exceptionally influential points is problematic, because they bias the geometric parameters, which are the basis for the results. Additionally, the informational value of the geometry, and thus the measurement result, depend on how closely the structure resembles the ideal geometry. In other words, shape deviations of the measured structure, the use of a certain sampling strategy and ideal geometries for the evaluation lead to uncertainty in the result.

This effect increases with the measurement of small structures. An illustrative example with two 2D circles is shown in Figure 23.1. Both circles show the same roundness, i.e. the same goodness of shape, but the larger circle resembles an ideal circle much more than the smaller one.

In this chapter, a method of analyzing the influence of single measurement points on the result and computing the uncertainty of the evaluation with ideal substitute geometries is proposed. The proposed method adapts the statistical resampling technique “the Jackknife” [QUE 49], [TUK 58] for use with CMM data. To show the applicability of the method, the following section gives a statistical point-of-view of the evaluation process in coordinate metrology. In section 23.3 the Jackknife is explained in detail. The application of the Jackknife on CMM point clouds and the proposed method for examining the influence of single points and the evaluation uncertainty is then explained thoroughly in section 23.4 and is followed by an example of use. The behavior of the Jackknife results is explored in computer simulations. The simulation procedure and the results are discussed in section 23.5.

In the following explanations, errors in the probing process are neglected. The text focuses on the evaluation process of workpieces with large shape deviations and assumes that these are observed correctly.

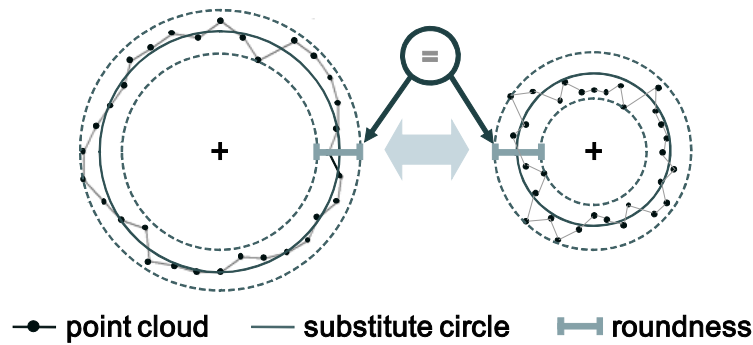


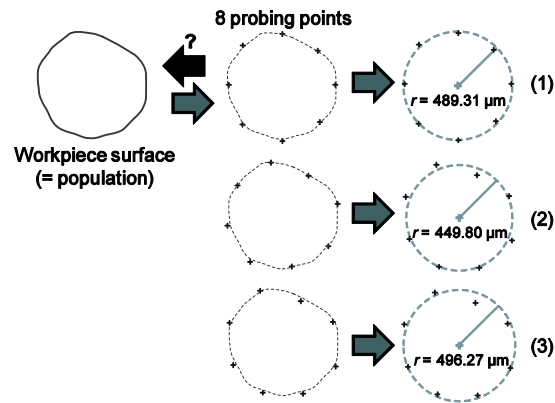
Figure 23.1. Influence of size on the perceived

### 23.2. Evaluation in coordinate metrology

In coordinate metrology results are based on a set of probed points from the workpiece surface and, as such, on a sample of the total surface. This point cloud is evaluated with ideal substitute elements. These are ideal geometries (i.e. lines, planes, circles, spheres, cylinders, cones, etc.) which can be described mathematically with few parameters. The substitute elements are fitted into the point cloud by finding a parameter combination which is optimal under a specified criterion like the Gauss or minimum-zone (MZ) criterion for example. In this process the information in the point cloud is reduced to geometric parameters.

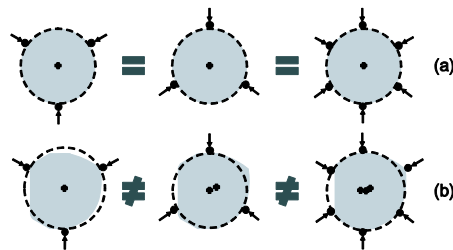
From a more general point-of-view, the workpiece surface represents the *population* of all possible measurement points. Every measurement with a CMM can only take a *sample* from this population, since the number of probing points is limited even with scanning sensors. In the evaluation process, information about the measured element is deduced from the observed sample, i.e. the point cloud. We can say that a measurement result is estimated from the observed sample or that the measurement result (the geometric parameter of the substitute element) is an *estimate* of the true value.

Estimators are always subject to uncertainty, based on the sample and the way they are calculated. Figure 23.2 illustrates this fact with the evaluation of the radius of a 2-dimensional circle. Eight probing points are taken from a workpiece surface with obvious shape deviations. The radius is evaluated with a Gaussian circle. As can be seen, the resulting radius varies highly depending on the sample taken, i.e. the distribution of the probing points. This shows that a measurement result can only be an estimate.



**Figure 23.2.** Example for the variance of results introduced by shape deviations

It should be noted, that this variance in the results is only introduced by the shape deviations of the measured element. In the case of a perfectly round structure it does not matter how many points are used and how they are distributed, the result is always the same (Figure 23.3).



**Figure 23.3.** Influence of the sampling strategy without (a) and with (b) shape deviations

When considering measurement uncertainty, the precision of the estimate is very important. The precision can be quantified by the standard error of the estimate, which describes the standard deviation of the error in the estimation. In other words, it describes the evaluation uncertainty.

There are several ways to calculate the standard error of an estimate. Usually these methods depend on certain and often restricting assumptions, like a certain distribution and independence of the observations. Resampling techniques provide a way to do this without restricting prerequisites, which makes their application on the evaluation process in coordinate metrology favorable.

### 23.3. The Jackknife

Statistical resampling is a universal and computer-based tool to calculate properties of statistical estimates. The basic idea is to create additional samples by drawing observations from the original sample of the population, which is usually done by computer (see Figure 23.4). The estimate of interest is then calculated based on every created subsample. Variance in the population propagates to the observations in the original sample and from there to the calculated estimates for the subsamples. The subsample estimates are the basis for the computation of standard errors of the estimate and introduced bias. With this information confidence intervals around the estimate can be constructed.

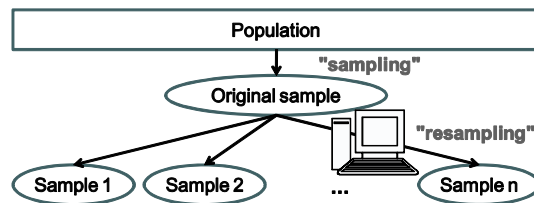


Figure 23.4. Statistical resampling

The advantage of resampling methods is their application to a wide range of different estimates and the fact that they are not based on the assumption of a certain distribution or other properties of the population. A disadvantage is their computational complexity compared to other methods. The way subsamples are created and how the information in the subsamples is evaluated depends on the specific resampling technique. This research utilizes the Jackknife technique. It was originally developed to identify and correct the bias of statistics, but it is also able to estimate the variance of statistics [QUE 49], [TUK 58]

The method is based on the repeated evaluation of the estimate with subsets of the original sample. The  $n$  available datasets (observations) are resampled by leaving out one observation at a time, leading to  $n$  new samples with  $n-1$  observations each. The examined estimate  $\hat{\theta}$  is then calculated for each sample, leading to the subset estimates  $\hat{\theta}_1, \dots, \hat{\theta}_n$ . With this information the bias and the standard error (SE) of the estimate can be calculated from the subset estimates of equations [23.1] and [23.2].

$$\text{Bias}(\hat{\theta}) = (n-1) \left( \frac{1}{n} \sum_{i=1}^n \hat{\theta}_i - \hat{\theta} \right) \quad [23.1]$$

$$SE(\hat{\theta}) = \sqrt{\frac{n-1}{n} \sum_{i=1}^n \left( \hat{\theta}_i - \frac{1}{n} \sum_{i=1}^n \hat{\theta}_i \right)^2} \quad [23.2]$$

The equations are derived from the examination of the arithmetic mean  $\bar{x}$ . The context is generalized to arbitrary estimators by the use of so called pseudo-values. These are the basis for the calculation of the bias and the standard error. The exact derivation can be found in [EFR 98].

## 23.4. Application to CMM data

### 23.4.1. Resampling point clouds

The Jackknife as explained in the preceding section is applied to CMM point clouds, with the goal of quantifying the influence of shape deviations of the measured element on the measurement result. The subsamples are used to analyze the influence of single measurement points on the result and to estimate the contribution to measurement uncertainty, which is introduced by the evaluation process.

Figure 23.5 shows the application of the Jackknife on CMM point clouds. In the example eight measurement points are used to probe the workpiece surface. The radius of the 2D circle is evaluated by the Gaussian criterion. The result with all eight points is 489.31  $\mu\text{m}$ . Then the point cloud is resampled using the Jackknife technique by leaving out one point at a time and evaluating the radius on the subset. The variation of the resulting radii  $r_1, \dots, r_n$ , which is introduced by the shape deviations of the measured element, can easily be seen.

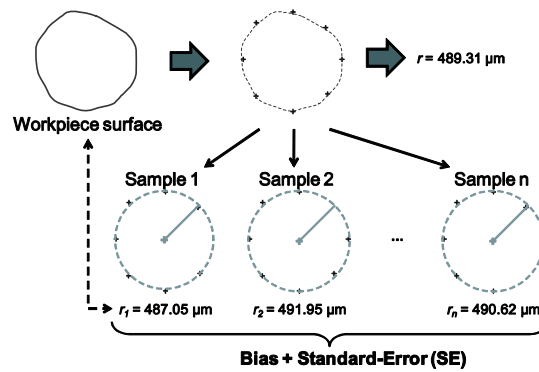


Figure 23.5. Jackknife resampling with CMM point clouds

### 23.4.2. Influence of single measurement points

To analyze the influence of single measurement points on the result, the difference  $d_i$  between the result with all points and the result when point  $i$  is omitted is examined for all geometric parameters of the substitute element. Intuitively, this value represents the influence the omitted point has on the resulting geometry parameter. In this way it is possible to assign the influence to a certain feature of the measured element.

In the case of an evaluation with the Gaussian criterion every point has an influence on the result, even though a prerequisite of the Gaussian criterion is that all points should have a uniform influence. By checking if there are points with exceptional influence, it is possible to review if the use of a Gaussian substitute element is justified. There are generally two possible ways of identifying exceptionally influential points. One is the assumption of a statistical distribution for the differences of the results. Based on the assumed distribution limits for exceptional differences can be calculated with a given statistical probability.

Since a general assumption for a distribution cannot be made, the use of non-parametric methods, i.e. methods that are not based on the assumption of a distribution, have a more practical use. An easy and intuitive way is to use the outlier limits from statistical boxplots [CHA 83]. In boxplots outliers are marked based on the distance of the 25% and 75% quantile ( $q_{0.25}$  and  $q_{0.75}$ ) of the observed values. The lower ( $LB$ ) and upper bounds ( $UB$ ) for outliers are calculated with equations 23.3 and 23.4. Their use is shown in Figure 23.6.

$$LB = q_{0.25} - 1.5 \cdot (q_{0.75} - q_{0.25}) \quad [23.3]$$

$$UB = q_{0.75} + 1.5 \cdot (q_{0.75} - q_{0.25}) \quad [23.4]$$

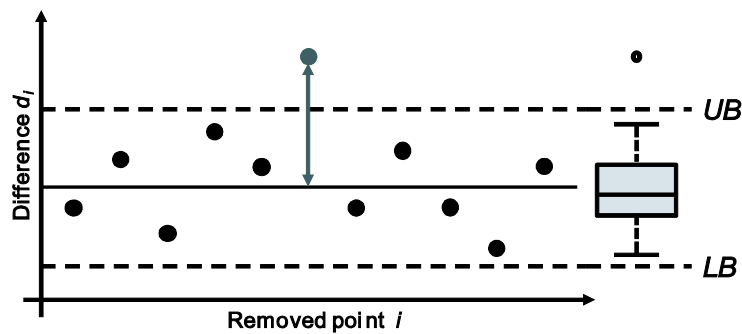


Figure 23.6. Analysis of measurement point influence



The proposed method of determining exceptional influence can only be applied with the Gaussian criterion. In case of criteria that are based only on extreme points, like the minimum-zone criterion for example, a removal of non-supporting points has no influence on the result. The problem that arises here is that there is not enough data to provide a basis to compare the influence of the support points and thus to calculate reliable outlier limits.

For criteria that rely on only a few supporting points, the proposed method has to be extended by an iterative approach. To obtain a data basis for the calculation of outlier limits, the point that shows the highest difference, i.e. that has the highest influence, is removed, the difference is stored and the procedure is repeated until the minimum number of points for the criterion and the geometry at hand is reached. Naturally, this leads to a decrease of the observed shape parameter. This way the shape of the measured element and the position of the non-supporting points with regard to the evaluation criterion can be taken into account for the calculation of outlier limits.

#### **23.4.3. Evaluation uncertainty**

After analyzing the influence of single points and assigning the influence to geometric parameters, the Jackknife results are used to calculate the standard error of the evaluation process. The standard error can be regarded as a contribution to measurement uncertainty, caused by the perceived shape deviation of the measured element and the evaluation with ideal geometries. As explained above, the perceived shape depends on the sampling strategy, which is why the sampling strategy influences the standard error.

Additionally, with the Jackknife analysis the bias of the estimator, i.e. the measurement result, can be calculated. The bias describes the difference between the expected value of the estimate and the true value. It can be regarded as a systematical error of the evaluation process. An estimator is biased, for example, when it is based on extreme points, as when evaluating shape or minimum circumscribed or maximum inscribed elements.

The proposed method allows us to quantify the influence of shape deviations of the measured element on measurement uncertainty. The standard ISO/TS 15530-3 [ISO 04], explains the composition of measurement uncertainty in coordinate metrology as derived by experimentation. The standard introduces a term for workpiece influence  $u_w$ . Even though the workpiece shape has definite influence (not only in evaluation) there is no viable method available to quantify this influence. The standard error as calculated by the proposed method in this chapter

allows the influence of shape deviations in the evaluation with regard to uncertainty to be described. In the following it is referred to as the evaluation uncertainty  $u_{eval}$ .

#### 23.4.4. Example of use

The use and results of the Jackknife are shown in the following example. For illustrative reasons, a 2D circle with the coordinates of the center point  $x_0$  and  $y_0$  and the radius  $r$  as result parameters was chosen again. However, the method is not restricted to simple geometries, but can be applied to any standard geometry (2D and 3D) used in coordinate metrology. The dataset was computer generated by adding a normal distributed error with a standard deviation of 0.02 mm to  $n = 32$  equally distributed points on an ideal circle with center coordinates (0.0, 0.0) and radius 0.5 mm. This resulted in the center coordinates  $(x_0, y_0) = (-4.46, -0.69) \mu\text{m}$  and the radius  $r = 0.50427$  mm as evaluated with the Gaussian criterion. The shape of the circle is heavily disturbed with a roundness of  $82.3 \mu\text{m}$ . A plot of the point cloud can be found in Figure 23.7.

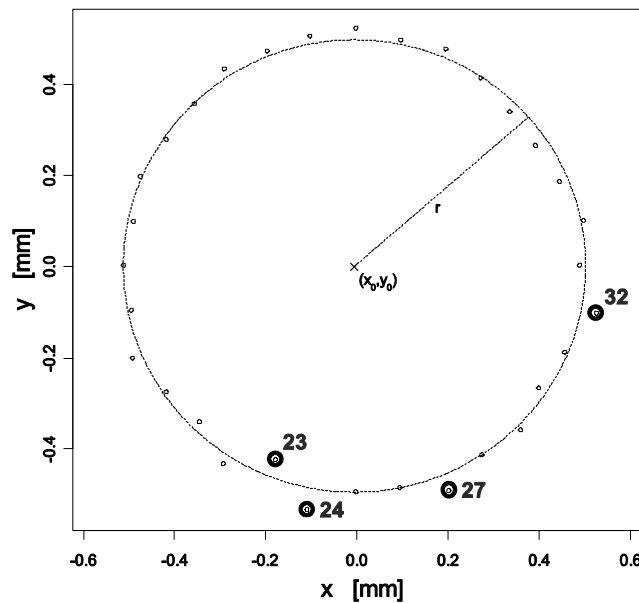
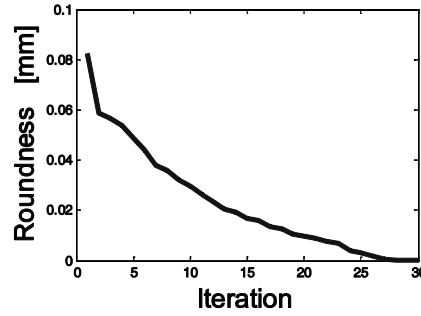


Figure 23.7. Example point cloud with marked influential points

Even though the distances of the points to the substitution circle did not show any special characteristics and fulfilled the demands of the Shapiro-Wilk [ROY 82]

and the Anderson-Darling [THO 02] tests for normality, exceptionally influential points on  $x_0$ ,  $y_0$ , the radius  $r$  and the evaluated roundness could be identified with the proposed method. These points are marked in Figure 23.7.

Point 23 and 24 show distinct influence on  $x_0$ ,  $y_0$ , and  $r$ . Point 27 has impact on  $y_0$  and point 32 on  $x_0$ . These results are intuitively understandable, since point 23 and 24 have the largest distance to the fitted circle and have a great effect on the circle as a whole. The positions of point 27 and 32 at the bottom and right hand side of the plot explain the exceptional influence on y- and x-position. For the analysis of the roundness the proposed iterative method was applied. Figure 23.8 shows the decrease of the perceived shape with the removal of points. Point 24 was identified in the first iteration.



**Figure 23.8.** Decrease of perceived roundness in the iterative analysis of point influence

With the results the non-uniform influence of the single points in the point cloud was shown and assigned to the different geometry parameters. This non-uniform influence is the consequence of observed shape deviations in the point cloud. In the next step, the effect of these shape deviations on measurement uncertainty is quantified with bias and the standard error of the result, as estimated with the Jackknife method. With the standard error a 95% confidence interval ( $\alpha = 0.05$ ) around the bias-corrected result was constructed using equation [23.5] by assuming a t-distribution [HIN 77]. Results are shown in Table 23.1.

$$\hat{\theta} - \text{Bias}(\hat{\theta}) \pm t_{(n-1)}^{(1-\alpha/2)} \cdot SE(\hat{\theta}) \quad [23.5]$$

The bias of  $x_0$ ,  $y_0$ , and  $r$  is only a small fraction of the estimated standard error, and thus can be neglected. In contrast, the estimated roundness  $f_a$  is clearly negatively biased, with values in the range of the standard error. As explained above, this result was to be expected because the evaluation of roundness is based on single, extreme points. So the resulting roundness tends to be larger with a larger

sample size, since the chance of observing extreme points increases. For this reason the result is naturally biased.

For  $x_0$ ,  $y_0$  and  $r$  the standard errors and the width of the confidence intervals are in the range of 3-4  $\mu\text{m}$  and 7-11  $\mu\text{m}$ , respectively. The standard error of the roundness  $f_a$  is much higher and, accordingly, the confidence interval is wider. These quite large values for a contribution of measurement uncertainty are explained by the large discrepancy between the point cloud and the ideal substitute circle. It is intuitively understandable that more precise statements of the circle parameters cannot be expected with a shape deviation of 82.3  $\mu\text{m}$ . This correlation was further investigated by computer simulations, as described in the next section.

	Jackknife estimate [ $\mu\text{m}$ ] with 95%-CI	Bias [ $\mu\text{m}$ ]	SE [ $\mu\text{m}$ ]
$x_0$	-13.53 < <b>-4.46</b> < 4.60	0.00	4.44
$y_0$	-11.75 < <b>-0.66</b> < 10.43	-0.02	5.44
$r$	497.09 < <b>504.25</b> < 511.41	0.03	3.51
$f_a$	66.16 < <b>118.17</b> < 170.18	-35.87	25.50

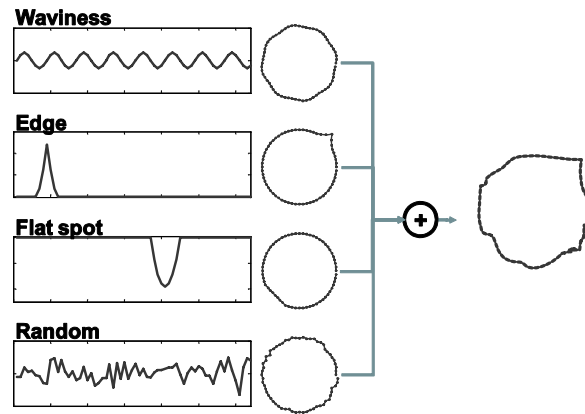
**Table 23.1.** Jackknife results for the example point cloud

### 23.5. Simulation

The behavior of the proposed method in the presence of different shape deviations is analyzed with computer simulations, which are performed for different geometries and result parameters. The simulation results are presented in this chapter along with the created regression models.

#### 23.5.1. Simulation procedure

The target of the simulations is to achieve a data basis for further analysis. The necessary data are the number of measurement points, the shape of the measured element and the resulting Jackknife results. In these simulations point clouds are generated according to an ideal geometry. These point clouds are overlaid with systematic and stochastic deviations (Figure 23.9). Afterwards the shape of the point cloud is evaluated and bias and standard error of the measurement result of interest are calculated with the Jackknife approach.



**Figure 23.9.** Generation of different shape deviations

The simulation is performed for different geometries and geometry parameters. During the simulation the number of probing points and the shape deviations in type and dimension are varied.

### 23.5.2. Simulation results

In the following section, simulation results for the radius of a 2D circle with random shape deviations are presented. The simulation was performed with 16, 32 and 64 probing points and standard deviations of the random deviation at levels of 0.50, 0.75, 1.00 and 1.25  $\mu\text{m}$ . This led to roundness values between 1 and 6  $\mu\text{m}$ . Each factor combination was repeated 25 times, which means overall 300 simulation runs were performed. In each run a new point cloud was generated, the radius was evaluated by the Gaussian criterion, and the Jackknife calculations were performed. As expected the bias did not differ significantly from 0 in any of the runs. The calculated standard error of the measurand, however, showed interesting results (Figure 23.10).

The plot and the regression lines show an increase of the standard error with increasing roundness, i.e. increasing deviation from an ideal circle. The evaluation uncertainty is lower with a higher number of measurement points than with fewer points, which also conforms to intuition. Of particular interest is the fact that the standard error difference between the different number of measurement points decreases with decreasing shape deviation. This can be explained, with the theoretical observation that with a perfectly measured element (and in the absence of measurement errors), the number and position of probing points does not matter. In this case the minimum number of points (three in the case of a 2D circle) is

sufficient. Any additional points do not change the result. This theoretical aspect is very well represented by the Jackknife results of the simulation.

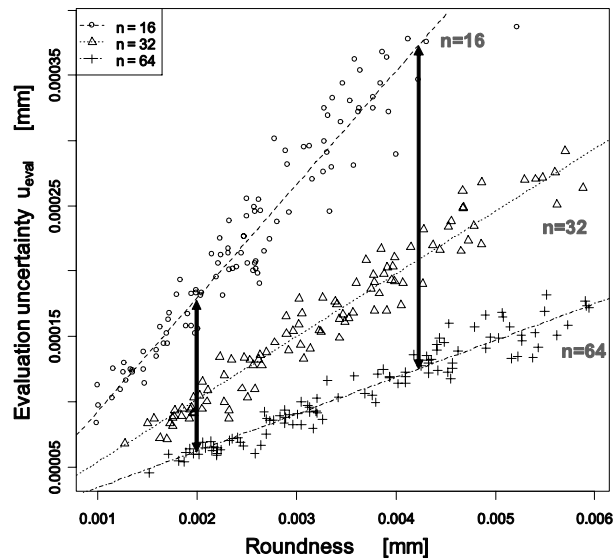


Figure 23.10. Simulation results with regression lines

### 23.6. Summary and outlook

In this chapter an approach to quantifying the impact of shape deviations on the measurement result in the evaluation process of coordinate metrology was presented. It is based on the application of the statistical resampling method “the Jackknife” on CMM point clouds. The Jackknife was used to calculate the influence of single measurement points on the result, as well as, the bias and the standard error of the measurand introduced by the evaluation process. To show the applicability of the method the evaluation process in coordinate metrology was examined from a statistical point-of-view. The approach was explained in detail with an example of use, and the results of computer simulations with the radius of a 2D circle were presented. The results represent theoretical and practical observations.

The proposed approach allows the investigation of the influence of the workpiece shape in the evaluation process with regard to measurement uncertainty. The results are assigned directly to the geometric parameter of interest and the applied evaluation criterion. In contrast to many other approaches no assumptions of normality or independence for the deviation of the measured elements are needed. Additionally the method can be applied automatically for every measured

workpiece, without the need for repeated measurements or other expenditure, except for additional evaluations of the point cloud.

The results also support the user of a CMM. First, measurement results that rely heavily on only one or a few measurement points can be identified to warn the user without the time consuming work of checking the point cloud manually. Highly influential points are the result of critical shape deviations which bias the result and which make the use of ideal substitute geometries unsafe. Second, the created regression models of the behavior of evaluation uncertainty can support the user in defining the sampling strategy. A minimum number of probing points can be deduced easily, if an expected shape deviation and the tolerance limits are given.

In further research the analysis of the Jackknife results will be extended to other 2D and 3D substitute geometries and their parameters, as well as to a wider range of different types of shape deviations.

### 23.7. Bibliography

- [CHA 83] CHAMBERS, J. M., CLEVELAND, W.S., KLEINER, B., TUKEY, P.A., *Graphical Methods for Data Analysis*, Wadsworth & Brooks/Cole, 1983.
- [EFR 98] EFRON B., TIBSHIRANI R.J., *An Introduction to the Bootstrap*, Chapman & Hall, pp. 141-152, 1998.
- [HES 02] HESSELBACH J., *mikroPRO - Untersuchung zum internationalen Stand der Mikroproduktions-technik*, Technische Universität Braunschweig, Universität Karlsruhe (TH), Fraunhofer IPT Aachen, 2002.
- [HIN 77] HINKLEY D.V., "Jackknife confidence limits using Student t approximations", *Biometrika*, Vol. 64, No.1, pp. 22-28, 1977.
- [ISO 04] ISO/TS 15530-3, Geometrical product specifications (GPS) - Coordinate measuring machines (CMM): Technique for determining the uncertainty of measurement - Part 3: Use of calibrated workpieces or standards, 2004.
- [QUE 49] QUENOUILLE M.H., "Approximate tests of correlation in time series", *J. R. Statist. Soc. B 11*, pp. 18-84, 1949.
- [ROY 82] ROYSTON P., "Algorithm AS 181: The W Test for Normality", *Applied Statistics*, Vol. 31, pp. 176-180, 1982.
- [THO 02] THODE Jr. H. C., *Testing for Normality*. Marcel Dekker, New York, 2002.
- [TUK 58] TUKEY J. W., "Bias and confidence in not quite large samples (abstract)", *Ann. Math. Statist.*, Vol. 29, p. 614, 1958.

## Chapter 24

# Quality Assurance of Micro-gears via 3D Surface Characterization

A challenging task for systematic quality assurance is the characterization of micro-gears via metrology. Additional factors in micrometer dimensions such as significant shape deviations of the produced micro-gears increase the complexity.

This chapter describes an approach for 3D surface characterization of the tooth flanks of micro-gears. A 3D point of view defines the functionally relevant tooth flanks as a surface in contrast to the common definition via 2D characteristics. Additionally, this chapter describes how these flank characterizations can be used for matching micro-gears afflicted with shape deviations for functioning gearings.

### 24.1. Introduction

Micro-gears are continuously gaining importance in multiple industries such as the automotive, medical technology and consumer electronics industries [WEC 06]. Micro-gears are primarily used together in micro-gear drives. One reason for the rising importance of the micro-gear drives is the demand to simultaneously increase the functionality of devices while decreasing their size and weight. To meet these requirements micro-gear drives must continue to become smaller and more accurate.

There are diverse challenges when trying to determine the quality of the micro-gears. Firstly, micro-gears are characterized by significant shape deviations in comparison to their part-size. The pattern and size of these shape deviations differ

---

Chapter written by Gisela LANZA and Benjamin VIERING.

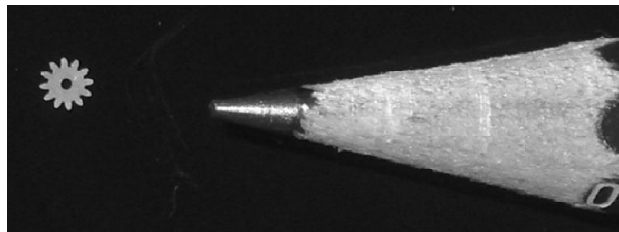


depending on the manufacturing process. Secondly, the number of probing points especially for tactile sensors is limited since the probe and the structure to be measured are practically the same size. Thirdly, there is currently no measurement standard available for the 3D characterization of involute micro-gears [ALB 08].

To develop quality assurance strategies for micro-gears approaching these challenges, the Institute of Production Science (wbk) is working on a joint research project with the Institute of Product Development (IPEK) at the Karlsruhe Institute of Technology (KIT). The approach of this research project is to combine dimensional metrology and functional testing for micro-gears. The goal is to combine the two methods in the most intelligent way to benefit from the advantages of both methods.

#### 24.2. Test specimen and experimental equipment

The object of study is an involute micro spur gear with a modulus of 0.169 mm and a tip diameter of about 2.3 mm. Figure 24.1 shows a test specimen next to the tip of a pencil to give a sense of its dimensions. Such a gear can be used for instance in planetary transmissions.



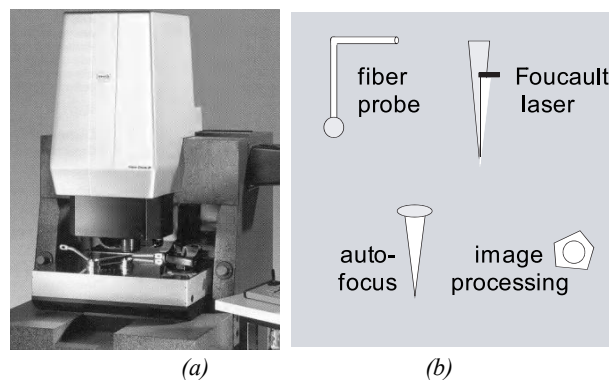
**Figure 24.1.** *Test specimen in comparison to pencil tip*

Because of its large field of application and its flexibility in the measurement of geometrical features a multi-sensor coordinate measuring machine (CMM) is used to characterize the geometry of the micro-gears.

The CMM, a Werth Video Check HA 400, has a measuring range of 400 x 400 x 200 mm<sup>3</sup> and an incremental measuring system resolution of 0.01 μm. The 3D linear measuring tolerance according to the manufacturer is  $(1.5 + L/500)$  μm where L is indicated in mm. Figure 24.2 shows the utilized CMM and its sensors. The CMM is equipped with a Foucault laser and an optical autofocus sensor for characterizing the top surface of the test specimen. An integrated image processing unit is available for

example for edge detection. Additionally, the CMM is equipped with the opto-tactile Werth fiber probe (WFP).

The opto-tactile WFP was chosen because of its wide applicability for several cases of operation. The stylus tip of the WFP is small enough for the dimensional quality characteristics of the micro parts at hand. The stylus tips are available with a diameter as small as 10  $\mu\text{m}$ . However, a disadvantage of the WFP is its inability to probe vertically.



**Figure 24.2.** CMM Werth Video Check HA 400 (a) [WER 08] and applied sensors (b)

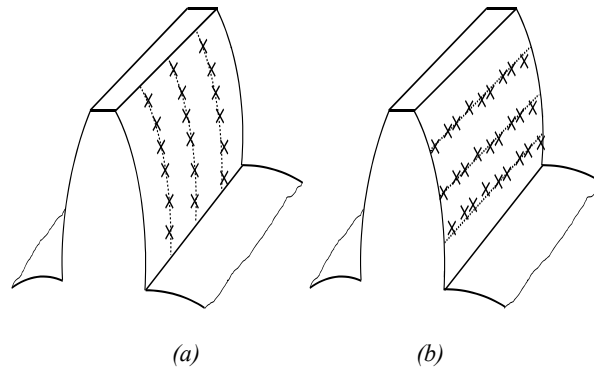
### 24.3. 3D characterization

#### 24.3.1. Benefits of a 3D characterization

The shape deviations that can be observed in micro-dimensions, as mentioned in the introduction, constitute a big challenge to achieving a functioning micro-gear drive. Therefore, a way needs to be found to match micro-gears afflicted with shape deviations in such a way that the needed function can still be fulfilled.

For the matching of two micro-gears the tooth flanks are especially relevant because they define the contact area for the transmission of motion. Up to now the flanks have been typically characterized by 2D parameters like the profile deviations ( $F\alpha$ ,  $fH\alpha$ ,  $ff\alpha$ ) or the helix deviations ( $F\beta$ ,  $fH\beta$ ,  $ff\beta$ ). The disadvantage of this procedure is that the tooth flank is only characterized in those areas of the surface where the lines that determine the profile deviations or the helix deviations are located. Shape deviations apart from these lines are not considered. Figure 24.3 shows a tooth flank with probing points for determining the profile (Figure 24.3a) and helix (Figure 24.3b) of the tooth flank. Furthermore, standards like the DIN 3960 ff or the DIN 58400 ff only cover tolerances for the profile and helix

deviations of gears with moduli greater than 1 mm and 0.1 mm respectively. However, micro-gears are defined as gears with a modulus smaller than 0.2 mm, according to the German guideline VDI 2731. This means that today's standards do not cover most micro-gears.



**Figure 24.3.** Exemplary probing points for determining profile (a) and helix (b) of the tooth flank

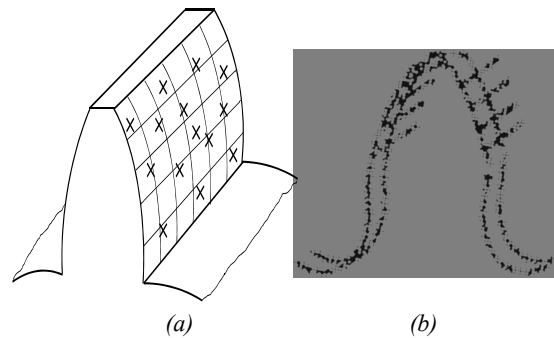
Due to the explicit shape deviations in micrometer dimensions, the tolerances cannot just be scaled down from larger dimensions to smaller dimensions. This would lead to quality classes that could not be achieved with the existing manufacturing processes.

Instead of exclusively using the 2D parameters like the profile and the helix deviations the whole tooth flank should be considered. A function-oriented evaluation is necessary to connect the measured points [GOC 03, WEC 99]. According to [IMM 03] it is necessary to switch to analytical modeling of the tooth geometry. On this model, software to measure and evaluate gears as a part of the quality assurance in production could be built.

One advantage of a 3D description of the tooth flank is that the positioning of the gear on the CMM does not affect the results. To determine deviations like the profile or helix deviation, the pitch, tooth thickness, flank topography and the flank modifications using the conventional methods require measurements at predefined points.

Since the size, shape and position deviations can be determined with the defined flank surface, no exactly defined measurement positions for the profile, the helix or the pitch of a gear are necessary when using a 3D description [LOT 03]. This is shown in Figure 24.4a, where a tooth flank, randomly placed probing points and the

resulting 3D description are pictured. Actual measuring results are shown in Figure 24.4b for a single tooth. These probing points were gathered via the conventional method along the profile and helix of the micro-gear.



**Figure 24.4.** Randomly placed probing points for a 3D tooth flank description (a) and conventional flank characterization via the profile and helix (b)

[LOT 05] developed a surface model to characterize the tooth flanks as 3D surfaces. The challenge is to adapt the existing surface model developed by [LOT 05] to micro-gears. The model of [LOT 05] was also further extended to use the obtained results of the surface model as inputs for the matching of micro-gears in such a way that the required function of the micro-gearing can be fulfilled.

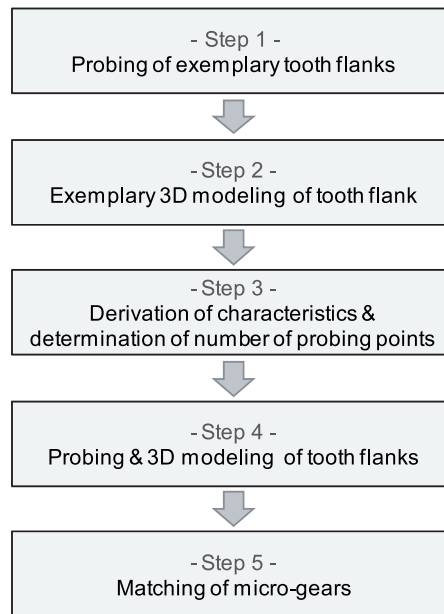
#### 24.3.2. Approach

To ensure an efficient measurement it is necessary to determine the required number of probing points for sufficiently characterizing the tooth flanks. This is part of the probing strategy. An approach for the determination of the probing strategy and the matching of micro-gears is shown in Figure 24.5. The steps of the approach are explained in the following.

##### 24.3.2.1. Step 1 – probing of exemplary tooth flanks

To develop a probing strategy a methodology for experimentally deducing probing strategies was developed by [BUC 08]. The input parameters needed are the measuring task, the evaluation strategy, the choice of a sensor and the fixation of the workpiece on the measuring table. The first step consists of probing a high number of probing points to ensure the efficiency of the approach [BUC 08]. The coordinates of the probing points can be determined by a random generator for instance.

A few measuring objects, in this case different tooth flanks, are probed to deduce the probing strategy, regarding subsets of the probing points. Along with these subsets, diagrams will be drawn in step 3 to show the interrelation between the number of probing points and the shape deviation. The approach is to analyze the development of the quantified shape deviation with an increasing number of probing points. For this purpose, the tooth flank needs to be modeled beforehand. This is carried out in step 2.



**Figure 24.5.** Approach for 3D probing and matching micro-gears

#### 24.3.2.2. Step 2 – exemplary 3D modeling of tooth flank

The second step is the evaluation of the probing points via a best fit method to obtain an involute equation as a substitute element for the tooth flank.

The most important parts of digital workpiece models are the measuring elements [LOT 05]. The workpiece surface can be represented by these measuring elements. [LOT 05] describes geometrical and analytical models for the coordinate measuring of involute gears. He introduces the 2D involute and the 3D involute helicoid as a measuring element.

One important difference between the 3D modeling and the conventional 2D approach is that even when probing points are placed randomly on the tooth flank,

the tooth flank can be evaluated accurately [LOT 05]. The innovation of step 2 in this approach compared to [LOT 05] is the adaption of the 2D involute and the 3D involute helicoid to involute micro-spur gears to evaluate the tooth flank.

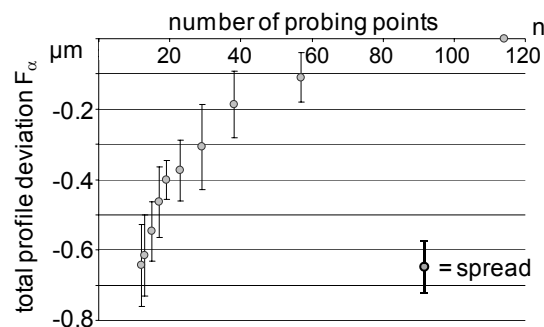
Although [LOT 05] proposes using a 2D model for micro-gears, we regard a 3D model as an indispensable step to ensure the increasing demands of accuracy for micro-gears are met. The reason is that the shape of the whole tooth flank is functionally relevant.

As a result of step 2 a flank model of the entire number of measuring points, probed in step 1 is created.

#### 24.3.2.3. Step 3 – derivation of characteristics and determination of the number of probing points

In the third step, conventional characteristics like profile or helix deviations will be calculated from the 3D flank description. This is essential to ensure comparability of the received results with conventional characteristics. One goal of this research project is to describe the micro-gears with as many conventional characteristics as possible.

The course of the respective shape deviation can be portrayed in a diagram. One resulting diagram is shown in Figure 24.6 [BUC 08]. The abscissa represents the number of probing points  $n$  and the ordinate represents the difference from the maximum observable total profile deviation  $F_\alpha$  obtained by the maximum number of probing points, e.g. 115 in Figure 24.6, probed in step 1.



**Figure 24.6.** Interrelation between the number of probing points and the detected shape deviation [BUC 08]

Figure 24.6 clearly shows the interrelation between the number of probing points and the total profile deviation including the spread. With an increasing number of probing points, a higher shape deviation is detected.

When the maximum allotted time for measurements is considered, a recommendation for the number of probing points can be derived and the probing strategy is determined.

This observation is certainly transferable to parameters other than the total profile deviation.

#### 24.3.2.4. *Step 4 – probing and 3D modeling of tooth flanks*

By the developed probing strategy all the flanks of the micro-gears can be measured with the number of probing points needed, and every tooth flank can be modeled analogous to the procedure in step 2.

#### 24.3.2.5. *Step 5 – matching micro-gears*

The fifth step proposes a way to simulate the matching of micro-gears with the modeled 3D involute tooth flanks.

In micro manufacturing processes in general and particularly in manufacturing processes for micro-gears the achievable tolerances are limited and cannot be simply scaled down from larger dimensions. Due to size effects in the production of micro parts [FLE 07], shape deviations occur that affect the function of the micro-gear drive.

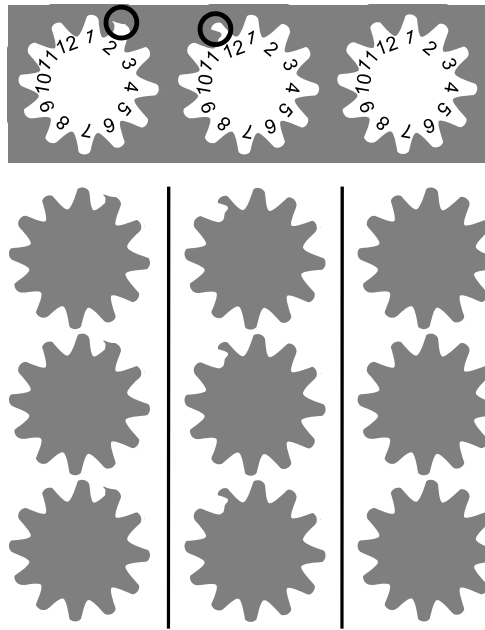
To ensure the function of a micro-gear drive, one possible strategy is to match micro-gears afflicted with shape deviations in a systematic way. Thereby, the function of the micro-gear drive could be assured despite shape deviations. Unlike larger dimensions where gears are matched to ensure an exact transmission of motion, in micro-dimensions even the primary function, for example the torque transmission, needs to be ensured by matching the micro-gears. Even today the quality assurance of micro-gears is often performed by listening to the gears in operation.

A cost-effective mass production with high quantities excludes single part measurements. However, the quality of the micro-gears must be quantified despite the inability to measure every gear.

The following example illustrates a possible approach for the quality assurance of micro-gears which are produced by micro powder injection mouldings. In this process multiple mould cavities are used at the same time. Each mould cavity is

afflicted with different shape deviations. All the parts produced by the same cavity are afflicted with the shape deviations of the cavity.

Figure 24.7 is an exaggerated example to illustrate this idea. At the top of Figure 24.7 three mould cavities are shown. The first cavity is characterized by a shape deviation at tooth No. 2, the second cavity is at tooth No. 12, both deviations are deliberately shown in an exaggerated way. The third cavity shows no significant shape deviations. Below each cavity three gears produced from the mould cavity above are shown. These gears are afflicted with the same shape deviations as the mould cavity above.



**Figure 24.7.** *Mould cavities and the produced micro-gears*

The approach now is to characterize only the mould cavities and deduce the shape of the produced micro-gear. The most important part of the characterization should be the 3D surface characterization of the functionally relevant tooth flank as described in step 2. With this information the micro-gears can be divided into groups depending on the mould cavity with which they were produced.

Additional shape deviations can certainly occur during processes fulfilled afterwards, for example during handling of the parts. But this would lead to a single



part consideration because the shape deviations would differ from each part within a group and will therefore not be considered for this approach.

At last, a simulation matches the groups of micro-gears to functioning gearings via best fit.

The five steps described in the approach above are currently being developed for involute micro-spur gears. The difference compared to other approaches is the consideration of challenges specifically for micro-gears mentioned in the introduction above. For example [BAU 08] applies a functional point-of-view of the tooth flanks but considers bevel gears in macro-dimensions as an object of observation. The separation of the tooth flank topography into three global form deviations, carried out by [PFE 01], is also made for part dimensions above the micrometer range because a separated look at shape, waviness and surface roughness is hard to make in micro-dimensions [BUC 08]. Other approaches like [BOU 07] propose algorithms for automated control of complex structures in general, whereas the described approach is designed to suit involute profiles

#### **24.4. Summary**

This article described an approach for a quality assurance of involute micro-spur gears via 3D surface characterization. It was shown that with increasing accuracy requirements of micro-gearings, despite significant shape deviations of the micro-gears, a 3D characterization of the tooth flanks is necessary.

The steps of the developed approach were partly based on an approach by [LOT 05] for gears in larger dimensions, and were also adapted to work for micro dimensions. A concept to match micro-gears afflicted with shape deviations was also presented as part of the approach.

Using the completely elaborated approach it is possible to use imperfect micro-gears to obtain micro-gear drives capable of fulfilling higher accuracy requirements than currently possible.

#### **24.5. Acknowledgments**

The research work at the Institute of Production Science at the Karlsruhe Institute of Technology (KIT), Germany was funded by the German Research Foundation (DFG). We gratefully acknowledge the support of the DFG within the Priority Program SPP 1159.

## 24.6. Bibliography

- [ALB 08] ALBERS A., FLEISCHER J., ELLMER C., HAUSER S., VIERING B., BUCHHOLZ I. and SCHLIPF M., “Development of quality assurance for micro-gear wheels by dimensional metrology and functional testing”, *Proceedings of 10th International Conference of the European Society for Precision Engineering and Nanotechnology (EUSPEN)*, Zürich, Switzerland, p. 261-265, 2008.
- [BAU 08] BAUDOUIN C., BIGOT R., LELEU S. and MARTIN P., “Gear geometric control software: approach by entities”, *The International Journal of Advanced Manufacturing Technology*, Vol. 38, p. 120-129, 2008.
- [BOU 07] BOUKEBBAB S., BOUCHENITFA H., BOUGHOUAS H. and LINARES J.M., “Applied iterative closest point algorithm to automated inspection of gear box tooth”, *Computers & Industrial Engineering*, Vol. 52, p. 162-173, 2007.
- [BUC 08] BUCHHOLZ I., *Strategien zur Qualitätssicherung mikromechanischer Bauteile mittels multi-sensorieller Koordinatenmesstechnik*, Karlsruhe University (TH), Institute of Production Science, Diss, 2008.
- [FLE 07] FLEISCHER J., SCHLIPF M., BEHRENS I. and PETERS J., “Aspects of estimating CMM measurement uncertainty for micro parts with respect to similarity requirements and influences of manufacturing processes”, *Proceedings of 7th International Conference of the European Society for Precision Engineering and Nanotechnology (EUSPEN)*, Bremen, Germany, p. 349-352, 2007.
- [GOC 03] GOCH G., “Gear Metrology”, *CIRP Annals*, Vol. 52, No. 2, p. 659-695, 2003.
- [IMM 03] IMMAMK D., WERNER K., OHNHEISER R., HENNINGER B. and PISMIOK P., “Messsoftware für echte 3D-Messung von Verzahnungen auf Koordinatenmessgeräten”, *Karlsruher Kolloquium - Verzahnen*, p. 33-43, 2003.
- [LOT 03] LOTZE W., “Flächenhafte Auswertung von Zahnflanken und Stirnrädern mit Evolventenverzahnung”, *Karlsruher Kolloquium - Verzahnen*, p. 45-59, 2003.
- [LOT 05] LOTZE W., *Zahnradmessung mit Koordinatenmessgeräten*, self-published, Dresden, Germany, 2005.
- [PFE 01] PFEIFER T., KUROKAWA S. and MEYER S., “Derivation of parameters of global form deviations for 3-dimensional surfaces in actual manufacturing processes”, *Measurement*, Vol. 29, p. 179-200, 2001.
- [WEC 99] WECKENMANN A. and GAWANDE B., *Koordinatenmesstechnik - Flexible Meßstrategien für Maß, Form und Lage*, Carl Hanser Verlag, München, Germany, 1999.
- [WEC 06] WECKENMANN A., Preamble VDI-Berichte 1950 – Messtechnik für Mikro- und Nano-Engineering, VDI-Verlag, Düsseldorf, Germany, 2006.
- [WER 08] WERTH MESSTECHNIK GMBH, product information, Giessen, Germany, 2008.

## PART IV

# Tolerancing in the PLM

## Chapter 25

# Geometric Specification at the Beginning of the Product Lifecycle

### 25.1. Introduction

Producibility improvement is a major challenge for design and manufacturing factories. In the aircraft industry, assemblies have thousands of parts, so a functional design method that helps the designer early has to be defined. In these types of new technologies, a way to improve this point is to ensure better assemblability of the products. To achieve this goal, geometric variations in manufacturing have to be carefully specified and controlled.

Indeed, currently, the specification is based on expert methods. The designers, have to use their knowledge to generate specifications from an analysis of the system. Indeed, it is easy to forget data and that cannot be allowed because it results in the manufacturing of assemblies that are non-mountable or non-compliant with the consumer's requirements. Parts need to come back to be reworked, which leads to additional cost for the product and to a waste of time. To reduce these problems, the tolerances of parts are tightened to limit the risks. The disadvantage of this technique is that it is expensive for a non-guaranteed result.

There is an increasing industrial need, it is a “semi-automatic” assistance to generation of tolerance specification.

There are several 3D tolerance analysis simulation tools:

- Anatole [MAR 03]

---

Chapter written by Renaud COSTADOAT, Luc MATHIEU, Hugo FALGARONE and Benoît FRICERO.

- Mecamaster [CLO 01]
- Söderberg's software [WIC 01]

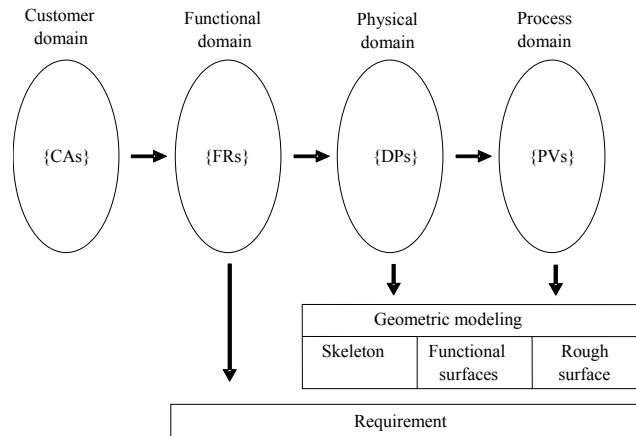
However, none go as far as tolerance specification.

The CLIC method [ANS 06], which allows us to generate ISO specifications, proceeds expertly from an analysis of the system and not from simulation models.

The idea of this work is to develop a method that leads to the tolerance specification from the simulation model.

The advantage of this method is the ability to specify at the earliest, in the lifecycle of the product. This involves different stages of model design:

- Skeleton: model of the mechanism including only joints, requirements and their relative position.
- Functional surfaces: model of the parts including key surfaces and some dimensions of the mechanism.
- Rough surfaces: model of the parts including the rest of the surfaces of the mechanism.



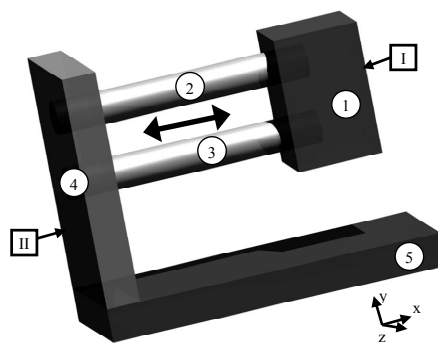
**Figure 25.1.** *Domains of the lifecycle*

The model chosen for the simulation of geometric variations is the small displacements torsor [BOU 96]. This helps to maintain coherence with the design, the manufacture and the metrology. Some studies use the same model in other steps of the product's lifecycle: manufacture [VIL 01] and metrology [BOU 96].

As previously mentioned, the method occurs at the beginning of the lifecycle of the product, during the design stage of the mechanism. Roughness and form deviations are not taken into account. The positions and deviations of the parts and the surfaces are modeled by small displacements torsors. Taking into account the tolerancing management during the design process, it is possible to optimize the mechanism to assist tolerance specification.

The method includes two steps. The first step consists of determining the limits of variations of each key surface. The skeleton is strictly created from the functional requirements. It is represented by a graph which is the support of the study and the way to implement requirements. Additional information and hypothesis are added later and allow to go through the different stages of design. Section 25.2 presents the skeleton of the mechanism via the graph of joints. Then, as presented in section 25.3 the designer generates new equations taking into account key surfaces via the graph of contacts. Once the representation of the functional model of the product is terminated, the designer has to solve the system of equations governing the specification of the assembly. The limits of geometric variations of the mechanism come from the result of this computation. At this step of the study, the inequations generated constrain the mechanism. The second step aims to translate these variations into a language of specification such as in section 25.4. Previous specifications have to be useful for manufacturing. The distribution of tolerances is achieved through the skills of designers who make choices with their experience or through industrial in-house methods. The method must help the designer to choose the specifications from the simulation model. The aim of the method is to try to minimize and evaluate these uncertainties of specification due to these choices. Finally section 25.5 summarizes the major issues and points out further investigations.

This method can be applied to a simple example of the prismatic joint, shown in Figure 25.2.



**Figure 25.2.** Mechanism model [BAL 08]

## 25.2. Study of the skeleton

The graph will be presented and its use to conduct an analysis of tolerances and obtain a specification of the mechanism will be described. The models used will be presented first to show the hypothesis made.

### 25.2.1. Presentation of the models used

The method presented uses models to simulate and model the mechanism. To find out the consequences of their uses, the assumptions they imply must be specified.

How to describe the variations?

#### 25.2.1.1. The torsor of small displacements

The first model is the small displacements torsor. It is used to model joints.

Each component of the small displacements torsor corresponds to deviations of position and orientation between the two joined parts. They take into account the deviations of the surfaces in contact as well as the gap in the interface. It is used as a model for the representation of degrees of freedom of the parts.

To use it, it must be assumed that small displacements of a part are much smaller than the dimensions of that part. This applies to all mechanisms studied. The following torsor represents a prismatic joint.

$$\{T_{III}\}_O = \left\{ \begin{matrix} \mathbf{R}_{III} \\ \mathbf{D}_{III_O} \end{matrix} \right\}_O = \left\{ \begin{matrix} \alpha_{III} & U_{III} \\ \beta_{III} & v_{III} \\ \gamma_{III} & w_{III} \end{matrix} \right\}_O \quad [25.1]$$

The formalism chosen is:

- capital letter = big displacement
- lowercase letter = small displacement

As mentioned earlier, this model allows the link between design, manufacturing and metrology.

How to describe the structure of the mechanism?

### 25.2.1.2. *The graph of joints*

This is a representation of the mechanism, it is valid during the entire lifecycle of the product, from design to metrology. It represents the product structure (parts, joints, requirements, etc.). It is a great way to collect and structure data. And it is also a way to analyze the system.

The graph model has been validated to be used in our context [BAL 99], [MAN 98]. To create and edit graphs in this study, the GAIA software, developed by EADS has been used [FAL 04].

### 25.2.2. *Description of the mechanism and first simulations*

The mechanism requirement's that have to be designed specify that it is a prismatic joint between two elements. A requirement is imposed between the two parts. Surface deviations of each part are not taken into account in this part of the study, since the work is on the skeleton. The result is the graph shown in Figure 25.3. It is built by modeling the parts or assembly as a circle and the joints as segments. The requirements are displayed by dotted lines.

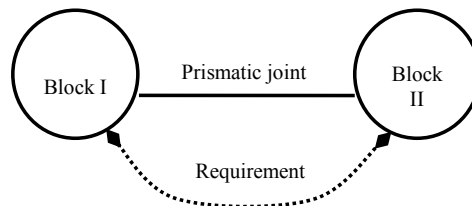


Figure 25.3. *Graph of joints*

The kinematic sketch of Figure 25.4 shows the kinematic modeling of the prismatic joint. By establishing kinematic requirements at this stage of the study, it is possible to build an initial specification. This will enable the subcontract of the design of the mechanism. This data includes some intrinsic dimensions of the skeleton, these are influential for kinematics or for the points of application of requirements.

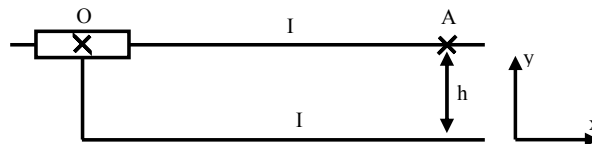


Figure 25.4. *Kinematic sketch of the mechanism*



With a measure of the sensitivity of the joints, the designer will be able to specify the mechanism at this step. To do so, the torsor of the kinematic pair must be moved to the point of applying of the requirement (equations [25.2] and [25.3]). The requirement must be modeled by a small displacement torsor. For this example, the condition is:  $h \in [h - t_h; h + t_h]$

$$\mathbf{D}_{I/III_A} = \mathbf{D}_{I/III_O} + \mathbf{AO} \times \mathbf{R}_{I/III} \quad [25.2]$$

$$\{D_{I/III}\}_A = \begin{Bmatrix} \alpha_{I/III} & U_{I/III} \\ \beta_{I/III} & v_{I/III} - \mathbf{AO} \cdot \mathbf{x} \times \gamma_{I/III} \\ \gamma_{I/III} & w_{I/III} + \mathbf{AO} \cdot \mathbf{x} \times \beta_{I/III} \end{Bmatrix} \quad [25.3]$$

By translating the requirement using the following equation a specification can be deduced.

$$-t_h \leq \mathbf{D}_{I/III_A} \cdot \mathbf{y} \leq t_h \quad [25.4]$$

$$-t_h \leq v_{I/III} - \mathbf{AO} \cdot \mathbf{x} \times \gamma_{I/III} \leq t_h \quad [25.5]$$

The designer can already take into account the specification (inequation [25.5]) to help him determine the dimension  $\mathbf{AO} \cdot \mathbf{x}$ , and specify the quality of the joint.

The next step of the skeleton modeling is the enrichment of the mechanism. The designer can, with his own choices, detail the mechanism by splitting the kinematic joints or splitting assemblies into parts.

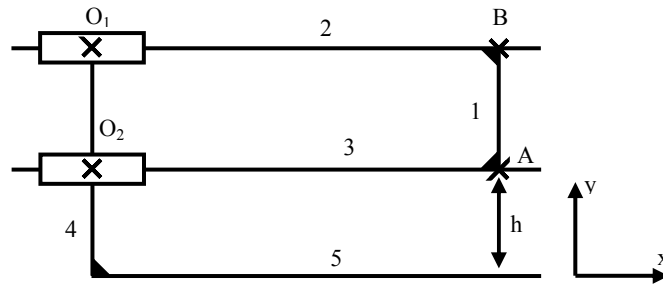


Figure 25.5. Kinematic model enriched

In this case, like in Figure 25.5, the prismatic joint has been turned into two parallel cylindrical joints and blocks of parts have been cut, as follows:

- Block I: Parts 1, 2 and 3
- Block II: Parts 4, 5

The small displacement torsors of the joints obtained are: joints  $\{D_{12}\}$ ,  $\{D_{13}\}$  and  $\{D_{45}\}$  which are complete joints and joints  $\{D_{24}\}$  and  $\{D_{34}\}$  which are cylindrical joints.

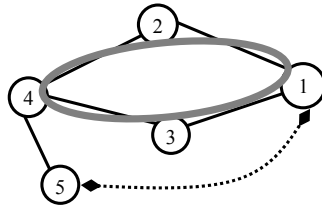
$$\{D_{12}\}_B = \begin{Bmatrix} \alpha_{12} & u_{12} \\ \beta_{12} & v_{12} \\ \gamma_{12} & w_{12} \end{Bmatrix}_B \quad [25.6]$$

$$\{D_{24}\}_{O_1} = \begin{Bmatrix} A_{24} & U_{24} \\ \beta_{24} & v_{24} \\ \gamma_{24} & w_{24} \end{Bmatrix}_{O_1} \quad [25.7]$$

By modifying the kinematic structure of the mechanism, the designer generates over-constraints which can be detected via the graph of joints.

#### 25.2.2.1. Generating inequations from cycles of mountability

Indeed, a cycle in the graph of joints identifies a risk of over-constraint. The idea is to find all cycles in the graph and check if there is any over-constraint using the small displacements torsor.



**Figure 25.6.** Over-constraint cycle

By calculating the equation corresponding to the cycle of Figure 25.6, it is possible to determine if there is an over-constraint and what the key components are.

$$\{D_{12}\}_A + \{D_{24}\}_A + \{D_{43}\}_A + \{D_{31}\}_A = \{0\}_A \quad [25.8]$$

$$\begin{aligned} \alpha_{12} + A_{24} + A_{43} + \alpha_{31} &= 0 \\ \beta_{12} + \beta_{24} + \beta_{43} + \beta_{31} &= 0 \\ \gamma_{12} + \gamma_{24} + \gamma_{43} + \gamma_{31} &= 0 \\ u_{12} + \text{AB.y} \times \gamma_{12} + U_{24} \\ \text{AO}_1.\text{y} \times \gamma_{24} + U_{43} + u_{31} &= 0 \\ v_{12} + v_{24} - \text{AO}_1.\text{x} \times \gamma_{24} + v_{24} - \text{AO}_2.\text{x} \times \gamma_{43} + v_{31} &= 0 \\ w_{12} - \text{AB.y} \times \alpha_{12} + w_{24} + \text{AO}_1.\text{x} \times \beta_{24} - \text{AO}_1.\text{y} \times \gamma_{24} \\ + w_{43} + \text{AO}_2.\text{x} \times \beta_{43} + w_{31} &= 0 \end{aligned} \quad [25.9]$$

For each equation, we will test whether the components are only components of small displacements, (equations [25.9]), each cycle corresponds to an over-constraint degree.

To ensure assemblability, the design must impose a gap in the joints. As previously mentioned, the gap is included in each component of the torsor of small displacements. The idea now is to split each component into two values, one for the gap  $g$ , the other for deviations  $d$ , like in equation [25.10].

$$D_{ij} = Dg_{ij} + Dd_{ij} \quad [25.10]$$

The gap of each component for each equation corresponding to an over-constraint must be limited by a lower bound. This will impose a gap and thanks to this the joint will guarantee the assemblability of the mechanism. A technical choice of the designer for this example is to share the deviations in the two joints represented by the torsors  $\{D_{24}\}$  and  $\{D_{43}\}$ . Equation [25.10] is included in equations [25.9].

$$\begin{aligned} \beta g_{24} + \beta g_{43} &\geq \beta_{12} + \beta d_{24} + \beta d_{43} + \beta_{31} \\ \gamma g_{24} + \gamma g_{43} &\geq \gamma_{12} + \gamma d_{24} + \gamma d_{43} + \gamma_{31} \\ v g_{24} + v g_{43} &\geq v_{12} + v d_{24} - \text{AO}_1.\text{x} \times \gamma_{24} + v d_{43} - \text{AO}_2.\text{x} \times \gamma_{43} + v_{31} \end{aligned} \quad [25.11]$$

At the end of this stage, taking into account the inequations generated guarantees the assemblability of the mechanism.

### 25.2.2.2. Generating inequations from cycles of requirement

There are two cycles through this requirement to which two inequations are related.

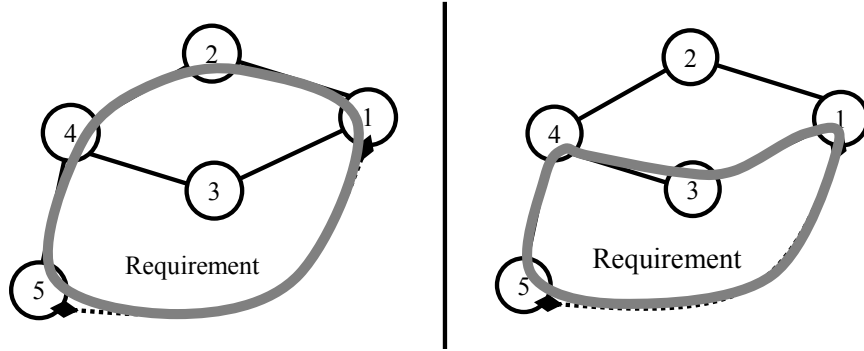


Figure 25.7. Requirement cycles

An inequation corresponds to each cycle of Figure 25.7, which must be generated in order to limit variations of the parts and gaps in the interfaces, from inequation [25.5] comes:

$$\begin{aligned} -t_k &\leq v_{12} + vd_{24} + vg_{24} - AO_1.x \times (\gamma d_{24} + \gamma g_{24}) + v_{45} \\ -AC.x \times \gamma_{45} &\leq t_k \end{aligned} \quad [25.12]$$

$$\begin{aligned} -t_k &\leq v_{13} + vd_{34} + vg_{34} - AO_2.x \times (\gamma d_{34} + \gamma g_{34}) + v_{45} \\ -AC.x \times \gamma_{45} &\leq t_k \end{aligned} \quad [25.13]$$

### 25.2.3. Conclusion of the first step

At the end of this first step, the innovation is the specification by the inequations of the mechanism's skeleton. This first study allowed us to detect the presence of over-constraints, which leads us to generate specifications for mountability (inequations [25.11]). Requirement *th* is also respected thanks to inequations [25.12] and [25.13]. All those elements have been detected automatically, avoiding oversights by the designer.

Modeling the surfaces is hardly taken into account. In addition, as deviations are global on the joints, it is impossible to specify the parts individually. The next step consists of adding the surfaces to take into account their deviations for each part.

### 25.3. Study of the functional surfaces

Now surfaces are going to be integrated to the simulation model. This requires us to define new models and their consequences.

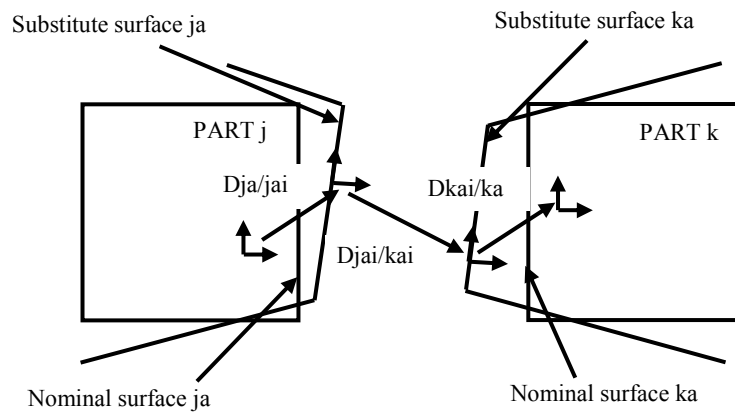
#### 25.3.1. Presentation of the models used

The next three models will be used into integrate some surface deviations in the model. The aim of this step is first to verify that the addition of surfaces to the model does not compromise the mountability of the mechanism. The study also allows us to take into account the deviations of the surfaces and spread over each part deviations on the joints calculated in the previous chapter.

How to identify the surfaces of each part?

##### 25.3.1.1. Substitute surfaces

The model developed first by Wirtz [WIR 91] then by Ballot [BAL 03], allows us to integrate a deviation position of the surfaces without integrating the form deviation. It uses vectorial tolerancing to distinguish substitute surfaces from nominal surfaces of the mechanism, like in Figure 25.8.



**Figure 25.8.** *Substitute surfaces*

This new model is adapted to the small displacement torsors as explained in the following section.

How do we differentiate the deviations of the surfaces from the gaps?

### 25.3.1.2. Deviation and Gap torsors

Each joint between two parts can be broken down thanks to the substitute surfaces model. Each part involved in the joint is represented by a surface (surfaces  $a$  in this example), which corresponds to the element of the situation of the link. A substitute surface (surfaces  $ai$ ) is associated with the nominal surface as explained in the previous paragraph and a torsor of deviations represents the displacements between the two surfaces.

The interface between the substitute surfaces is modeled by a gap torsor. The study which leads to equation [25.15] allows us to give a lower limit to the gap to guarantee the assemblability of the mechanism. For a joint between two parts  $j$  and  $k$ , the result is:

$$D_{jk} = D_{ja/jai} + D_{jai/kai} + D_{kai/ka} \quad [25.14]$$

$$Dd_{jk} = D_{ja/jai} + D_{kai/ka} \quad [25.15]$$

$$Dg_{jk} = D_{jai/kai} \quad [25.16]$$

How can we describe the surfaces on the graph?

### 25.3.1.3. Graph of contacts

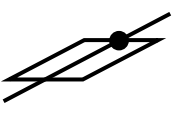


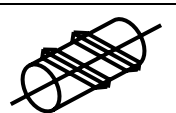
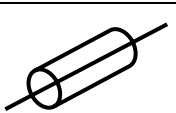
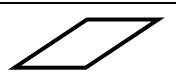

To take into account the functional surfaces, the graph of joints must evolve into the graph of contacts.

This new representation is a more complete version of the graph of joints introducing the key surfaces. They will be represented by a grey oval around the circle which represents parts, like in Figure 25.10. This will be the connector between the parts, joints and requirements. Each surface of the mechanism belongs to a class of geometrical features presented in Table 25.1.

## 25.3.2. Details of the mechanism and second step of simulation

In this section, the detail of the mechanism is to add a “skin” to the skeleton [BAL 06]. To do so, the designer can choose the surfaces within seven classes [CLE 98] [ISO 05], like in Table 25.1. These surfaces are ideal features classified by type, such as plane, cylinder, cone, sphere, torus, etc. They are defined by characteristics

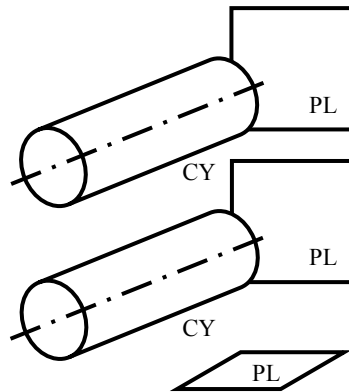
which are for example, the diameter of a cylinder, the distance between a plane and the center of a sphere or the angle between the axis of a cylinder and a plane.

	D	Corresponding displacement	Situation features
	0	$E$ identity displacement	Plan of $E3$ , line of $E3$ , point of $E3$
	1	$T_D$ Unidirectional translation	Plan parallel to $D$ , line parallel to $D$
	1	$R_D$ Rotation around a line with a point	Line $D$ , point of $D$
	1	$H_{D,P}$ Screw displacement	Line $D$ axis of the screw
	2	$C_D$ Actuator displacement	Line $D$ axis of the cylinder
	3	$G_D$ Planar displacement	Plan parallel to $P$
	3	$S_D$ Spherical displacement	Point $O$ center of the sphere

**Table 25.1.** *The 7 classes of geometrical features*

The ideal surfaces used to define the nominal model are called nominal surfaces. They are independent from the model of the non-ideal surface (“skin model”). The ideal features, whose characteristics depend on the model of the non-ideal surface are called associated features. The substitute surfaces previously presented are associated features.

For example, the example presented in Figure 25.9 consists of several ideal features whose types are planes and cylinders. All ideal features belong to one of the seven classes defined in Table 25.1.



**Figure 25.9.** *Ideal features forming the nominal model*

The idea here is that each surface of the mechanism will be listed in a class of surface and then type of surface. This will be useful for two related reasons. First it allows us to identify the influences of the deviations of the surface on the behavior of the mechanism. Second it allows us to determine the specification corresponding to that surface as well as its situation features. Indeed, even if the language of specification has not yet been chosen at this step of the study, the classes and types of surfaces are common to all languages.

To do so, some characteristics have been defined in GeoSpelling [MAT 03]. At this step of the study, they determine the geometry of the mechanism. They are defined:

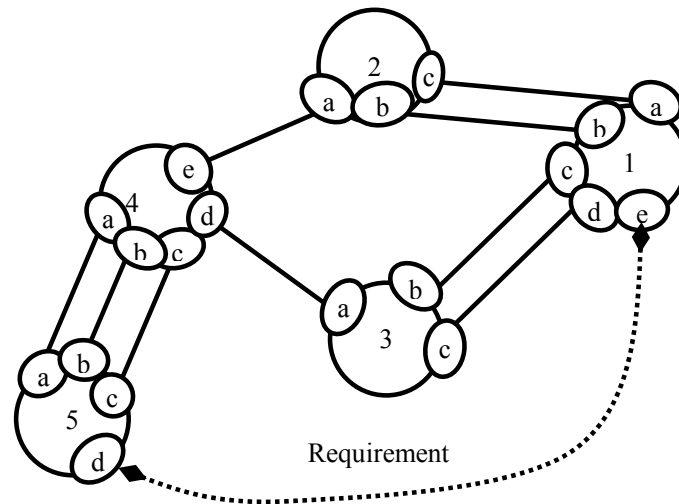
- on ideal features, and they are called intrinsic characteristics
- between ideal features, and they are called situation characteristics
- between ideal and non-ideal features, and they are also called situation characteristics.

The intrinsic characteristics of an ideal element are specific to the ideal element itself. They can be diameters, lengths, etc.

The situation characteristics define the relative situation between two features and they can be divided into position and orientation characteristics. These characteristics are lengths or angles. Non-ideal features do not appear in the study because the form deviations are not taken into account, so the third characteristic is not defined.

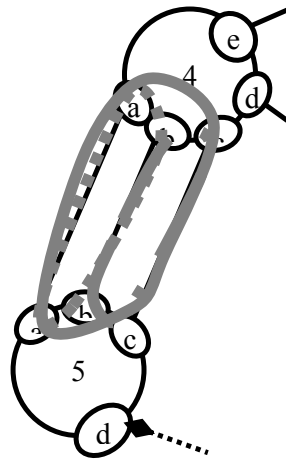


Now that these features forming the skin of the mechanism have been defined, it is possible to represent them on the graph of contacts defined in Figure 25.10.



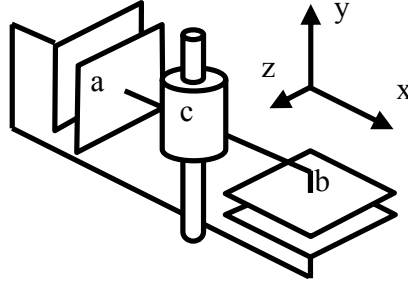
**Figure 25.10.** *Graph of contacts*

Based on the new data, new simulations are made because at this stage of the study, the decomposition of joints creates new over-constraints. Each cycle which is a risk must be verified.



**Figure 25.11.** *Over-constraint in a parallel joint*

In Figure 25.11, the joint between parts 4 and 5 is modeled by three interfaces. Figure 25.12 shows the models chosen for this complete joint. A screw in the cylinder locks and the tightens the two parts.



**Figure 25.1.** Kinematic sketch of this assembly

The interfaces are:

- $\{D_{4a/5a}\}$ , planar joint, axis  $x$
- $\{D_{4b/5b}\}$ , planar joint, axis  $y$
- $\{D_{4c/5c}\}$ , cylindrical joint, axis  $y$

In this system there are over-constraints. The designer has to modify the interface and determine the relative positioning of the two parts.

Each cycle corresponds to one of the three systems of equations presented below according to the model of the substitute surfaces.

$$D_{55} = D_{5a/5ai} + D_{5ai/4ai} + D_{4ai/4a} + D_{4b/4bi} + D_{4bi/5bi} + D_{5bi/5b} = 0 \quad [25.17]$$

$$D_{55} = D_{5b/5bi} + D_{5bi/4bi} + D_{4bi/4b} + D_{4c/4ci} + D_{4ci/5ci} + D_{5ci/5c} = 0 \quad [25.18]$$

$$D_{55} = D_{5a/5ai} + D_{5ai/4ai} + D_{4ai/4a} + D_{4c/4ci} + D_{4ci/5ci} + D_{5ci/5c} = 0 \quad [25.19]$$

Note that the components of gap torsors  $i$  compensate the deviations of the parts. The equations corresponding to over-constraints have been extracted from the system of equations and are presented in the following.

$$\begin{cases} \gamma_{4a/5a} + \gamma_{5b/4b} = 0 \\ \gamma_{4a/5a} + \gamma_{5c/4c} = 0 \\ u_{4a/5a} + u_{5c/4c} + AC.y \times \gamma_{5c/4c} = 0 \\ \alpha_{4b/5b} + \alpha_{5c/4c} = 0 \\ \gamma_{4b/5b} + \gamma_{5c/4c} = 0 \\ v_{4b/5b} - AB.x \times \gamma_{4b/5b} + V_{5c/4c} - AC.x \times \gamma_{5c/4c} = 0 \end{cases} \quad [25.20]$$

For example, one choice of positioning is to make the plan parallel to the axis of the predominant cylinder by tightening the screw. This is supplemented by the second plan and then by the cylinder.

1. Plan b
2. Plan a
3. Cylinder c

The modification depending on the designer's choice requires the specification of the gap in the joint by changing the components of the torsors of the interface.

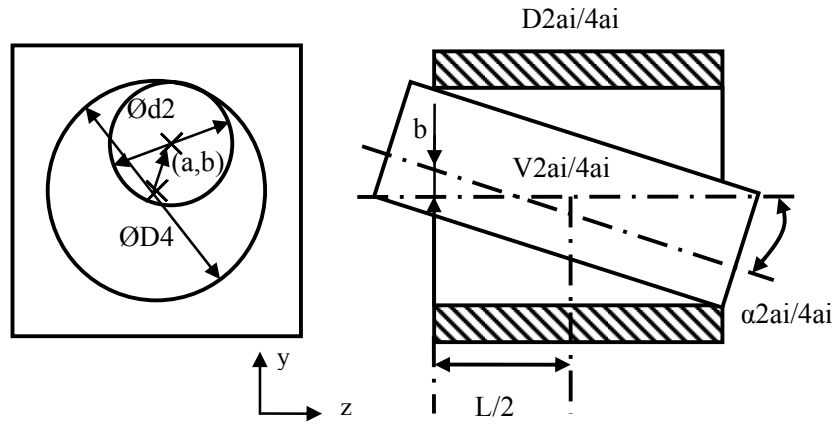
One solution here is to set a minimum for the following gaps:

$$\gamma_{4ai/5ai}, \alpha_{4ci/5ci}, \gamma_{4ci/5ci}, u_{4ci/5ci} \quad [25.21]$$

Another point that has to be tested to guarantee the assemblability at this stage of the study is the management of contacts. For example, the joint between parts 2 and 4 is modeled by a cylinder-cylinder interface, like in Figure 25.13.

In the previous study, on the skeleton, it was decided to impose a gap between the two parts. This gap must now be translated on the model with the skin of the mechanism. To do so, a study has been made of the cylinder-cylinder interface in order to translate the components of the small displacement torsor into the intrinsic dimensions of the parts.

In this case the modeling was done using a continuous mathematical model. However, it is clear that it is not possible with all types of interface. For example, if the interface is a plan-plan type, surfaces have to be discretized (on the boundary of the surface for example).



**Figure 25.13.** *Interface cylinder-cylinder*

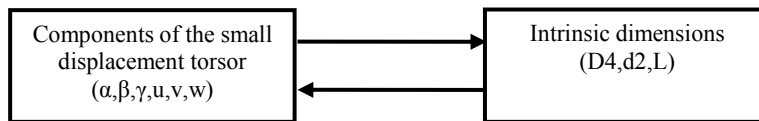
Nevertheless, this model was chosen to present the method. Results of the trigonometry study are presented below.

$$\sqrt{a^2 + b^2} \leq D_4 - d_2, \text{ with :} \quad [25.22]$$

$$a = w_{2ai/4ai} + \beta_{2ai/4ai} \times \frac{L}{2} \quad [25.23]$$

$$b = v_{2ai/4ai} + \gamma_{2ai/4ai} \times \frac{L}{2} \quad [25.24]$$

The previous step allows us to specify the components of the small displacements torsor. Now, thanks to this inequation, the specifications can be applied to the intrinsic dimensions of the mechanism.



**Figure 25.14.** *Translation via the contacts*

The last inequations to be generated during this study on the skin are those concerning requirements. Indeed, it is now possible to differentiate the parts in these

inequations and thus it will be possible to specify the parts individually from equations [25.25] and [26.26].

$$\begin{aligned}
 -t_h \leq & v_{1b/1bi} + v_{1bi/2bi} + v_{2bi/2b} + v_{2a/2ai} + v_{4ai/4a} \\
 & -AO_1.x \times (\gamma_{2a/2ai} + \gamma_{4ei/4e} + \gamma_{2ai/4ei}) + v_{2ai/4ai} + v_{4b/4bi} \\
 & + v_{4bi/5bi} + v_{5bi/5b} - AC.x \times (\gamma_{4b/4bi} + \gamma_{4bi/5bi} + \gamma_{5bi/5b}) \leq t_h
 \end{aligned} \tag{25.25}$$

$$\begin{aligned}
 -t_h \leq & v_{1d/1di} + v_{1di/3ci} + v_{3ci/3c} + v_{3a/3ai} + v_{4di/4d} \\
 & -AO_1.x \times (\gamma_{3a/3ai} + \gamma_{4di/4d} + \gamma_{3ai/4di}) + v_{3ai/4di} + v_{4b/4bi} \\
 & + v_{4bi/5bi} + v_{5bi/5b} - AC.x \times (\gamma_{4b/4bi} + \gamma_{4bi/5bi} + \gamma_{5bi/5b}) \leq t_h
 \end{aligned} \tag{25.26}$$

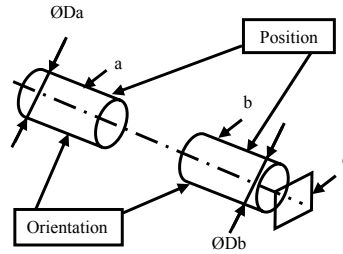
### 25.3.3. Conclusion of the second step

At the end of this second step, the specification of the mechanism has been completed. The previous specifications on the skeleton are now shared out among the parts. This will be the beginning for the expression of the specification of the parts individually. Inequations [25.25] and [25.26], allow us to control the variations of the key surfaces of the parts. The enrichment of the mechanism adds over-constraints, so the study on the skin detects new cycles and new equations related to this. To guarantee the assemblability of the mechanism, two kinds of inequations have been generated, one from the graph of contacts (inequations [25.22]), the other from isolated joints (equations [25.20]), which have been solved by giving minimal gaps to some components of the small displacements torsor [25.21]. The distribution of variations in all the components of the small displacements torsors is not part of the study. The continuation of the study will be the impact of these results on the mechanism's geometry. Indeed, at the end of this section, the mechanism is fully constrained, but, with the view of enabling the manufacture of the parts, these results must be summarized (see section 25.4).

## 25.4. Specification

The idea of this section is to specify each part individually. To do so, part 2 will be taken as an example.

The first step is to extract the key surfaces of this part and determine which class and type they depend on. Here, surfaces *a* and *b* are cylinders and surface *c* is a plane. These surfaces have intrinsic characteristics (diameter for cylinders) and extent parameters (e.g. length for cylinders) [ISO 05].

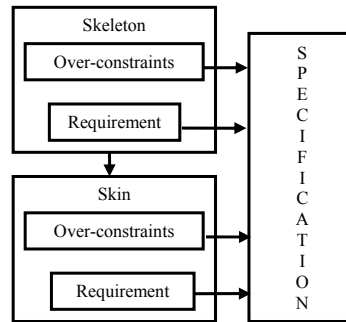


**Figure 25.15.** *Specification of a part*

All the components of the small displacement torsor related to this part have to be extracted from the previous systems of inequations. In the case of the example, the domain allowed for part 2  $[h - t_{h2}; h + t_{h2}]$  is part of the whole domain of variation  $[h - t_h; h + t_h]$ . So, the specification for this part is:

$$-t_{h2} \leq v_{2bi/2b} + v_{2a/2ai} - AO_1.x \times (\gamma_{2a/2ai}) \leq t_{h2} \quad [25.27]$$

The result of the study shows that the part should take into account two requirements, one of position ( $v_{2bi/2b}$  and  $v_{2a/2ai}$ ) and one of orientation ( $\gamma_{2a/2ai}$ ), which are related. This specification allows all the other parameters to vary, because they are not involved in the requirement.



**Figure 25.16.** *Structure of the study*

## 25.5. Conclusion

This paper outlines a new approach to tolerancing: early tolerancing. The idea is to start to specify the problem as soon as possible so that the specifications evolve in parallel with the design. The idea is to ensure the correspondence between the

specifications and the model of the mechanism at any time. Tolerancing is not treated at the end of the design process but earlier and at different stages, on the skeleton, on the interfaces and on the final volumes once the processes have been chosen.

The result at the end of the study is a specification of the parts of the mechanism according to the requirements. Variations are forced to a minimum to ensure assemblability as well to ensure the requirements are taken into account. These specifications are hard to use directly. A way to make it easier for users is to translate it into a defined language of specifications, like ISO or GeoSpelling; however this process of translation implies specification uncertainties.

This method makes the work of the designer easier because constraints of assembly are detected automatically. The same goes for geometric requirements because the cycles of influence directly generate inequations giving the sensitivities of the components of the small displacements torsor. The parametric modeling used at each step simplifies the design by variants. The use of tools, like graphs, to capture data and knowledge all along the functional and structural breakdown enables the traceability of information and allows choices to be carried out. It also authorizes impact analysis when requirements or specifications change, and is totally adapted to a knowledge-based engineering level.

There are several ways to improve the method. The first is to determine how to distribute variations once the specification of the global system is set and once it constrains the mechanism. The second is to study how to manage the contacts discretizing parts. A way to determine the number and the position of those points discretization should result from a trade-off between an accurate discretization and a reasonable computation duration.

## 25.6. Bibliography

- [ANS 06] ANSELMETTI B., "Generation of functional tolerancing based on positioning features", *Computer-Aided Design*, Vol. 38, p. 902-919, 2006.
- [BAL 03] BALLOT E., BOURDET P. and THIEBAUT F., "Determination of relative situation of parts for tolerance computation", *7th CIRP International Seminar on Computer Aided Tolerancing*, ENS de Cachan, Kluwer Academic Publishers, p. 63-72, 2003.
- [BAL 99] BALLU A. and MATHIEU L., "Choice of functional specifications using graphs within the framework of education", *6th CIRP Seminar on Computer Aided Tolerancing*, Enschede (The Netherlands), Kluwer Academic Publishers, p. 197-206, 1999.
- [BAL 06] BALLU A., FALGARONE H., CHEVASSUS N. and MATHIEU L., "A new design method based on functions and tolerance specifications for product modelling", *CIRP Annals - Manufacturing Technology*, p. 139-142, 2006.

- [BAL 08] BALLU A., PLANTEC J.Y. and MATHIEU L., "Geometrical reliability of overconstrained mechanisms with gaps", *CIRP Annals - Manufacturing Technology*, Vol. 57, Issue 1, p. 159-162, 2008.
- [BOU 96] BOURDET P., MATHIEU L., LARTIGUE C. and BALLU A., "The concept of small displacement taylor in metrology", *Advances in mathematics for applied sciences*, Vol. 40. World Scientific, 1996.
- [CLE 98] CLÉMENT A., VALADE C., SERRÉ P. and RIVIÈRE A., "The TTRS: 13 oriented constraints for dimensioning, tolerancing and inspection", *Geometric Design Tolerancing: Theories, Standards and Applications*, pp. 122-131, Chapman and Hall, 1998.
- [CLO 01] CLOZEL P., "3D tolerances analysis, from preliminary study", *7th CIRP Seminar on Computer Aided Tolerancing*, Kluwer Academic Publisher, p. 93-104, 2001.
- [FAL 04] FALGARONE H. and CHEVASSUS N., "An innovative Design Method and Tool for Structural and Functional Analysis". *Proceedings of CIRP Design Seminar*, Cairo, Egypt, 2004.
- [ISO 05] ISO TS 17450-1, Geometrical product specifications (GPS), General concepts Part 1: Model for geometrical specification and verification, 2005.
- [MAN 98] MANTIPRAGADA R. and WHITNEY D.E., "The datum flow chain: a systematic approach to assembly design and modelling", *Research in Engineering Design*, p. 150-165, 1998.
- [MAR 03] MARGUET B., CHEVASSUS N., FALGARONE H. and BOURDET P., "Geometrical behaviour laws for computer-aided tolerancing: AnaTole a tool for structural assembly tolerance analysis", *Proceedings of the 8th CIRP Seminar on Computer Aided Tolerancing*, Charlotte, USA, p. 301-310, 2003.
- [MAT 03] MATHIEU L., BALLU A., "Geospeeling: a common language for geometrical product specification and verification to express method uncertainty", *Proceedings of the 8th CIRP Seminar on Computer Aided Tolerancing*, Charlotte, USA, p. 70-79, 2003.
- [VIL 01] VILLENEUVE F., LEGOFF O. and LANDON Y., "Tolerancing for manufacturing: a three dimensional model", *International Journal of Production Research*, Vol. 39, No. 8, p. 1625-1648, 2001.
- [WIC 01] WICKMAN C., SODERBERG R. and LINDKVIST L., "Toward non-nominal virtual geometric verification by combining VR and CAT technologies", *Geometric Product Specification and Verification: Integration of Functionality*, Kluwer Academic Publishers, Dordrecht, p. 301-310, 2001.
- [WIR 91] WIRTZ A., "Vectorial tolerancing for production quality control and functional analysis in design", *Proceedings of the CIRP International Working Seminar on Computer-Aided Tolerancing*, CIRP, p. 77-84, 1991.



## Chapter 26

# Ontological Model of Tolerances for Interoperability in Product Lifecycle

### 26.1. Introduction

The effects of dimensional and geometric variations of a part in a product/assembly span the whole lifecycle of that product from manufacturing to inspection, assembly, testing, use and maintenance and to the ultimate disposal of that product. In a design specification, tolerances specify the limits to the dimensional and geometric variation of a product.

There are two techniques for tolerance specification – conventional and geometric. In conventional tolerance specification the variation of a specific dimension is controlled only in the direction of that dimension. Tolerances are specified with upper and lower limits and are associated with a dimension. Since perfect parts cannot be manufactured, additional control of the manufacturing process is needed to control various functional aspects of parts or assemblies, i.e. form, size, orientation, profile etc. This combination of different types of tolerances was not possible with conventional tolerancing. Thus, geometric tolerances were introduced. In this way multiple tolerances can be placed on a feature (such as a tab or hole), to control distinct characteristic, such as the form or orientation, of that feature. Tolerances such as orientation and position control various degrees of freedom (rotation and translation) of the toleranced feature. Standards, such as ASME Y14.5-1994 and ISO 1101, govern the method (and a language) of specifying tolerances.

---

Chapter written by Gaurav AMETA and Patrick HOFFMANN.

Identification of the causes of the dimensional and geometric variations is the major concern in manufacturing research while the effects of the dimensional and geometric variations have to be analyzed in the design stage. Due to the utilization/impact of tolerances in/on all the stages of a product life cycle, tolerance research spans the whole product lifecycle. Research related to different aspects of tolerances has been surveyed in the literature [CHA 91], [EVA 75], [GER 96], [HON 02], [NIG 95], [PAS 03], [SHA 07] and [SHE 05]. Based on these surveys, in this paper, tolerance research is classified into tolerancing, tolerance transfer, tolerance evaluation, tolerance modeling and representation. Tolerancing includes tolerance specification, tolerance analysis and assemblability and tolerance allocation. Out of the different aspects of tolerance research, tolerance modeling and representation is the most pervasive research area and influences all aspects of information exchange during the product life cycle, especially design, manufacturing and inspection.

Product design, manufacturing and inspection in the current global market are collaborative in nature. Collaborative product development entails the use of various software tools and techniques. Moreover, these software tools and techniques utilize various data standards for representing tolerance information such as STEP [STE 94] and DMIS [ANS 01]. Therefore, there is a need for unambiguous interpretation of tolerance specification by various computer softwares being utilized in the collaborative product development. Furthermore the exchanged tolerance information should be robust, consistent and valid. The exchange and use of the exchanged information among different software is called interoperability [IEE 90].

Towards creating a tolerance information exchange that is robust, consistent, valid and unambiguous, this chapter takes a first step by creating an ontological model of tolerances. Since, most of the tolerances control degrees of freedom of a feature, the proposed tolerance information model is based on degrees of freedom.

This chapter is organized as follows. Section 26.2 presents background on ontology followed by a literature survey of various information models of tolerances (section 26.3). Section 26.4 presents the proposed ontological model of tolerances. Then, section 26.5 presents an example of the instantiation of the ontology followed by future directions of the proposed approach (section 26.6).

## **26.2. Ontology**

This section will be discussed in two parts: first introduction to ontology as a means for modeling information and second discussing a particular ontology language choice.

### 26.2.1. *Information modeling as an ontology*

Ontologies are artefacts that aim at representing knowledge about a domain, tasks and so forth, by relating classes that represent concepts in a directed graph [SOW 09].

“An ontology is an explicit, formal specification of a shared conceptualization of a domain of interest” [GRU 91]. Ontology represents a shared understanding of concepts in a domain of interest to support interoperability and have strict definitions of the relation between the concepts.

One main advantage of ontology modeling is the ability to formally represent knowledge. Ontology can be mathematically defined as  $O := \{I, C, R, A\}$ , where  $O$  is an ontology for a domain of interest;  $I$  is a set of individuals or objects in a domain;  $C$  is a set of concepts in a domain;  $R$  is a set of relations among concepts, relations and objects;  $A$  is a set of axioms holding among concepts, relations and objects.

There are two types of relations  $R$  (or properties) that can be used in an ontology – object and datatype properties. The object properties in ontology specify or restrict relations between an instance and another instance. The datatype properties in ontology specify or restrict relations between instances and data values.

### 26.2.2. *Choice of ontology language*

To represent knowledge/information in a formal manner, the language utilized to encode the knowledge is as expressive as the knowledge. For a comparison of several different description logic (DL) languages for modeling product information please refer to [FIO 08, 1]. This chapter uses ontology Web language (OWL) for creating the proposed ontological model of tolerances, as OWL is based on a subset of first order logic called description logic. Therefore, OWL supports the four reasoning mechanisms found in description logic: consistency checking, subsumption, realization and retrieval [BAA 02]. The use of XML-based format of OWL is intended to facilitate sharing and reuse of knowledge [PAT 04].

OWL is an ontology language for the semantic Web, developed by the World Wide Web Consortium (W3C) Web Ontology Working Group [MCG 03, SMI 04]. Examples of some of the OWL constructs are given in Table 26.1. For more information regarding other OWL constructs, please refer to [MCG 03]. In this chapter the Protégé ontology editor is used to create the ontological mode of tolerances.

OWL (Ontology Web Language)	Intuition
<b>RDF Schema Features</b>	
<code>rdfs:subClassOf(A,B)</code>	Class A is a particular type of class B, in other words class B is more general than class A.
<code>rdfs:subPropertyOf(A,B)</code>	Property A is a particular type of property B, in other words property B is more general than property A.
<b>Property Restrictions</b>	
<code>P OWL:allValueFrom(C)</code>	All values of property P belongs to class C
<code>P OWL:someValueFrom(C)</code>	Some value of property P belongs to class C
<b>Restricted Cardinality</b>	
<code>P OWL:miniCardinality(n)</code>	The number of values that property P can take must be greater than or equal to n
<code>P OWL:maxCardinality(n)</code>	The number of values that property P can take must not exceed n
<code>P OWL:Cardinality (n)</code>	The number of values that property P takes is exactly n

Table 26.1. Example of OWL constructs

### 26.3. Literature survey

Many authors have identified the need for an information model in product life cycle [YAN 08, THI 06 and FEN 03]. Yang *et al.*, [YAN 08] presented a product information model for mass customization based on OWL. Thimm *et al.* [THI 06] proposed modeling product information with unified markup language (UML) [ISO 05]. The author focused on interoperability between different product lifecycle, such as the lifecycle of a manufacturing machine and the lifecycle of the product that the machine is manufacturing. Feng and Yong [FEN 03], presented a model for exchange of product information for interoperability in design and manufacturing.

Only a few authors have attempted to create an information model solely of tolerances for supporting interoperability [DAN 07, DES 07, ZHA 06 and RAC 06a]. Dantan *et al.*, [DAN 07] proposed a UML based product information model for tolerance management in car and aircraft industries. They used graphs to

represent product and process information and extend the key characteristics approach described by Thornton [THO 99]. Desrochers [DES 07] only provide a classification of product information and do not create an information model of the classification. Zhao *et al.* [ZHA 06] proposed an XML based information model for integrated measurement processes. The model relies on three layers to support interoperability between tolerance representation in STEP, DMIS and a representation based on ASME Y14.5 classes of tolerances. The model only supports interoperability at the inspection stage.

Rachuri *et al.* at the National Institute of Standards and Technology (NIST), proposed a generalized information model in UML, called a Core Product Model (CPM), for representing electro-mechanical products. An extension of the CPM, called the object assembly model (OAM), has also been developed for representing product information at assembly level [RAC 06b]. Fiorentini *et al.* [FIO 07, 08] have worked towards representing the OAM model in OWL. OAM represents tolerances only as attributes of the parts and features.

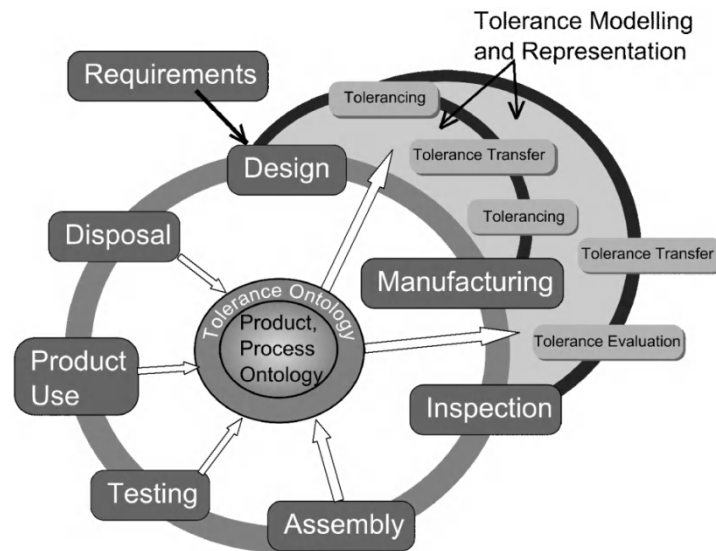
#### 26.4. Ontology of tolerances

Figure 26.1 shows the proposed tolerance ontology as a building block for creating tolerance modeling and representation, which in turn support all the activities in design, manufacturing and inspection related to tolerances. These activities include: tolerancing (tolerance specification, analysis and allocation) at the design stage, tolerance transfer and process level tolerancing at the manufacturing stage, tolerance transfer and tolerance evaluation at the inspection stage.

The main idea for developing the proposed ontological model of tolerances is to support a larger product and process ontology. The proposed tolerance ontology will also support capture of knowledge/information from assembly, testing, product use and disposal phases of a product lifecycle.

The degree of freedom (DOF) concept utilized in [WU 03] for classifying tolerances has been adopted to build the ontological model of tolerances. The DOF concept presented in [WU 03] introduces new DOF; size and shape DOF, in addition to rotational and translation DOF. The size and shape DOF account for the allowable variations of shape and size of a feature.

The ontological mode of tolerances consists of three main classes (DOF, GeometricEntity and Tolerance) derived from a parent/default OWL class Thing. These three classes are declared disjoint from one another, as a DOF cannot be a GeometricEntity or a Tolerance. There are four child classes of DOF called, TranslationalDOF, RotationalDOF, SizeDOF and ShapeDOF.



**Figure 26.1.** Role of tolerance ontology in the product's life cycle and related tolerance activities

The class *GeometricEntity* is specialized by two classes, *Group* and *Individual* for representing groups of geometric entities and individual geometric entities. *Group* is further specialized by *Cluster* (of features) and *Pattern* (of features). Individual geometric entities are specialized by *Point*, *Vector*, *Line*, *Plane*, *FeatureofSize* and *FreeForm* geometric entities.

*DimensionalTolerance* and *GeometricTolerance* classes specialize the *Tolerance* class. There are two types of Dimensional tolerance called, *Linear* and *Size*. *GeometricTolerance* class is specialized by *Location*, *Orientation* and *Form* classes.

The sub-classes of the concept profile tolerance, as classified in the ASME Y14.5M standard, have been reclassified to the concepts of form, orientation and location tolerances depending on the DOF that the profile tolerance controls. If the profile tolerance controls only the shape of the feature (i.e. no datum is required with the profile tolerance), it is considered a part of form tolerance. This sub-classification (described in [WU 03]) is embedded into the tolerance ontology developed in this paper. According to the DOF re-classification of profile tolerance, the *Form* class is specialized by *FormProfile*, *Flatness*, *Circularity*, *Cylindricity* and *Straightness* child-classes.

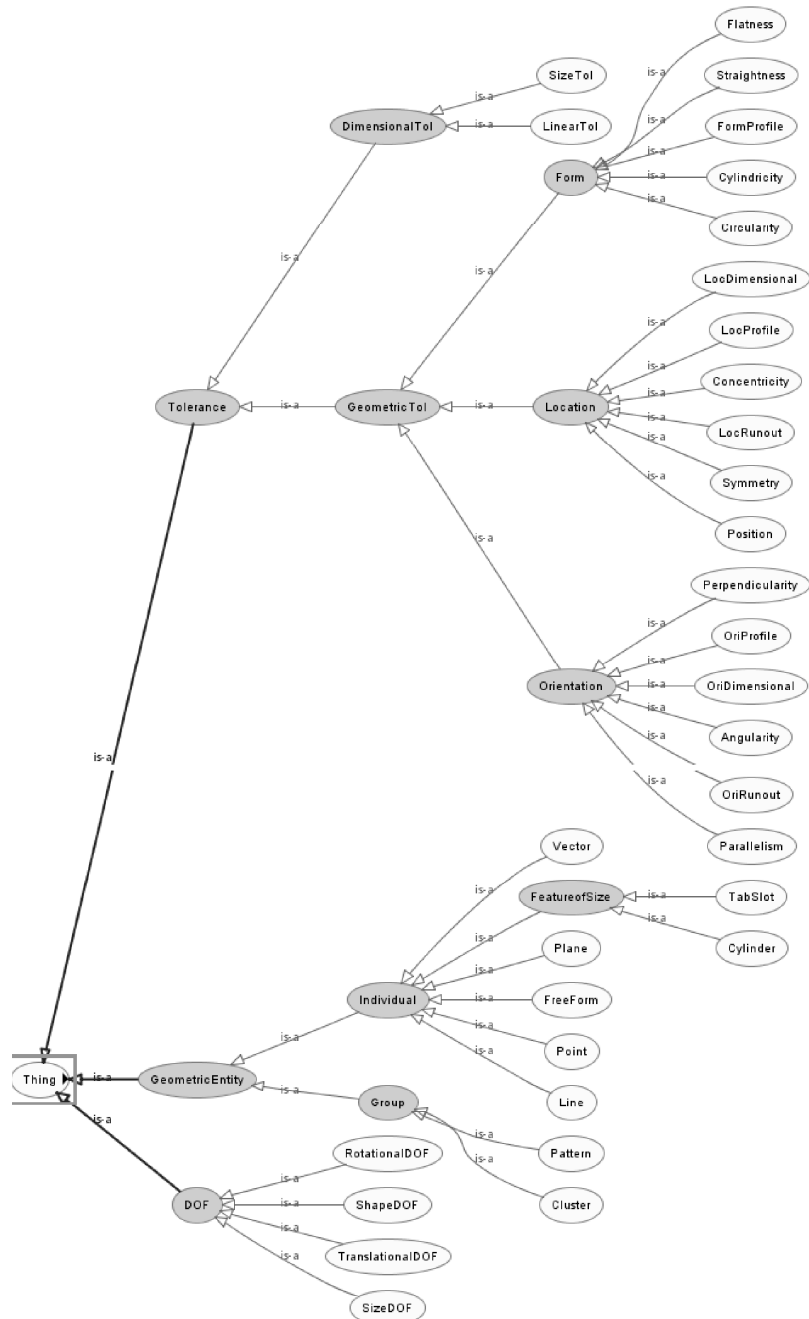


Figure 26.2. Tolerance ontology in Protégé ontology editor

Similarly, the specialization of runout tolerances described in the ASME Y14.5M standard, has been re-classified into orientation and location tolerances. According to the DOF re-classification of runout and profile tolerances, Orientation class is specialized by Angularity, Perpendicularity, Parallelism, OriRunout and OriProfile classes. Similarly, the Location class is specialized by LocProfile, LocDimensional, LocRunout, Concentricity, Symmetry and Position classes. Figure 26.2 presents the classification used in the proposed ontological model of tolerances.

Similar to the concept of child classes, child properties have been defined in the ontology for modeling generally to specific relations between the concepts in the ontology. Table 26.2 displays various object properties declared in the ontology. The properties shown in Table 26.2 are only the parent properties. The property `has_a_datum` is specialized by `has_a_primary_datum`, `has_a_secondary_datum` and `has_a_tertiary_datum`. Each property in ontology may have an associated inverse property. In the proposed ontology the `is_a_datum_of` property is the inverse of the `has_a_datum` property. For example, if the tolerated feature is a pin has a position tolerance P and the primary datum is Plane A, then the relation between P and A is P `has_a_primary_datum` A. For the inverse property, A `is_a_primary_datum_of` P. Each property has an associated domain and range. Domain refers to the concepts to which the property belongs, while range refers to the concepts to which the property can be applied. For example `has_a_datum` property can only be a part of location and orientation tolerances in the proposed ontology. So location and orientation tolerances are the domain of the property. Similarly, only a geometric entity can be a datum of a tolerance, therefore geometric entity is the range of the property `has_a_datum`. Other properties, inverse properties, and the concepts that are the domain and range of these properties are listed in Table 26.2.

Figure 26.3 shows the class description of concept `LocDimensional`, which is a specialization of the concept `Position`. The class description shows super classes and super properties, inherited classes and inherited properties, disjoint classes and individuals (instantiations) of the class.

Relation/ Property	InverseProperty	Domain	Range
<code>has_a_datum</code>	<code>is_a_datum_of</code>	Location / Orientation	GeometricEntity
<code>has_a_normal</code>	<code>is_a_normal_of</code>	GeometricEntity	Vector
<code>has_a_plane</code>	<code>is_a_plane_of</code>	FeatureofSize	Plane
<code>has_a_point</code>	<code>is_a_point_of</code>	GeometricEntity	Point
<code>has_a_DOF</code>	<code>is_a_DOF_of</code>	GeometricEntity / Tolerance	DOF
<code>has_a_tolerance</code>	<code>is_Applied_to</code>	GeometricEntity	Tolerance

**Table 26.2.** Object properties, their inverse, domain and range for the ontology





**Figure 26.3.** Class description of an ontology in Protégé for *LocDimensional* class

After the creation of the ontology various reasoners (such as Racer, Fact++, Pellet, etc.) can be utilized to validate the ontology. The reasoners verify that the axioms stated about the concepts, instances and relations of concepts and instances do not contradict one another, in the ontology. The output is an inferred classification of the concept in the ontology. If the initial (asserted) classification and the inferred classification are not the same, the ontology is found to be logically

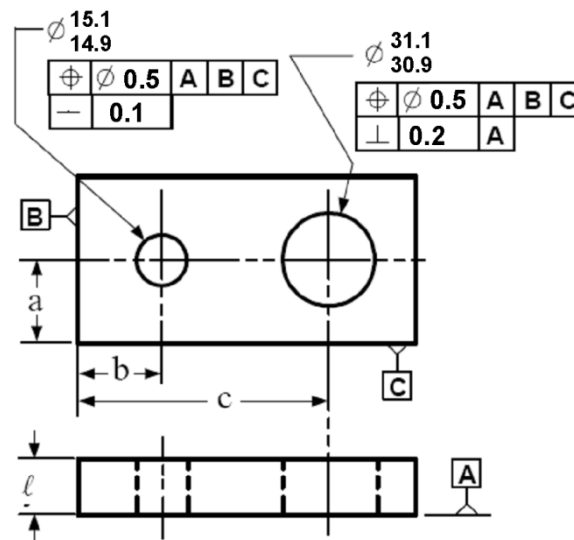
inconsistent. The inferred ontology may reveal new axioms regarding the described ontology. The reasoner also includes a summary of various metrics related to the ontology.

Fact++ and Pellet reasoners were utilized to verify the ontology. In the current ontological model, there are a total of 44 classes, 23 object properties and 13 data properties. Total class axioms generated in the ontological model are 98 for subclasses, 11 for equivalent classes assertion axioms and 70 for disjoint classes. The object property axioms are nine for subobject properties, three for equivalent object properties and two for inverse object properties.

This section presented an initial ontology of tolerances. Section 26.5 will demonstrate the instantiation of the concepts in the ontology.

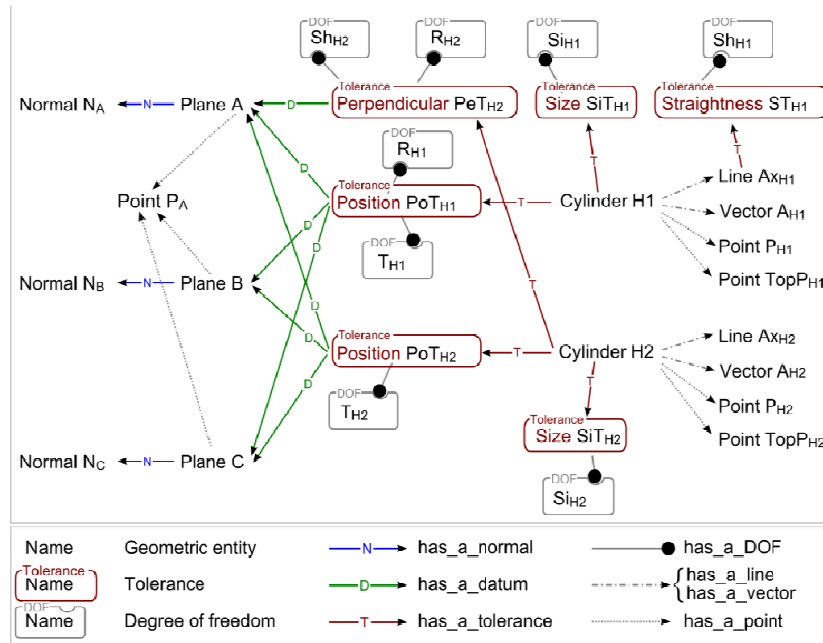
### 26.5. Example of tolerance ontology instantiation

A tolerated part as shown in Figure 26.4 is instantiated. The part consists of three datum planes (A, B, and C) and two cylindrical holes. One of the cylindrical holes has size, position and straightness tolerances while the other has size, position and perpendicularity tolerances.



**Figure 26.4.** An example part with tolerance specification used as a demo for ontology instantiation (adapted from [BHI 07])

The part shown in Figure 26.4 is instantiated. The datum planes, their normal and a point for each plane were instantiated. Then, two size tolerances (15.1-14.9 mm and 31.1 - 30.9 mm), two position tolerances (0.5 mm each), a straightness tolerance (0.1mm) and a perpendicularity (0.2 mm) tolerance with the respective DOF were instantiated. Geometrical features such as two cylinders and an axis are instantiated. Other objects and properties related to the cylinder and axis were also instantiated, such as axis direction, diameters (15.0mm and 31.0mm), height and the nominal location of cylinders. After all the relation for each of the instantiated objects was created, reasoners such as FACT++ and Pellet are applied on the ontology. Figure 26.5 shows a graph of the instances geometry, tolerances, DOF and object properties relating each of them. There were a total of 31 class assertion axioms, 41 object property axioms and forty-two data property axioms that were checked by the reasoners.



**Figure 26.5.** Graph showing the instances of geometric entities and the object properties relating these instances for the example part shown in Figure 26.4

## 26.6. Summary

An ontological model of tolerances was proposed and validated using FACT++ and Pellet ontology reasoners in this chapter. An example of instantiation of this

model was also presented. The proposed ontological tolerance model is not yet complete (symmetry tolerances not incorporated), but it is a step forward in building ontology for product modeling so as to serve interoperability in the product lifecycle. In the future the ontological model of tolerances can be incorporated as a portion of the multi-level feature based ontology model proposed in [HOF 08]. The model needs further improvement with respect to the following aspects:

- Extending the ontological model to include assembly constraints and support for various aspects of tolerance activities, such as tolerance analysis, allocation, evaluation and transfer.
- Integrating the ontological model of tolerances with product and process ontology.
- Adding concepts in the model to support multi-environment integration, such as for electro-mechanical product development.
- Incorporating rules in the ontological model that cannot be checked at the concept level but can only be checked at the instance level. For example, Rule#1 of the ASME Y14.5M standard, requires checking the tolerance values that are only available when the concepts of size tolerance and form tolerances are instantiated.

## 26.7. Bibliography

- [ANS 01] ANSI/CAM-I 104.0-2001, Part 1, Revision 04.0. Dimensional Measuring Interface Standard. Computer Aided Manufacturing, International Inc., Arlington, USA.
- [ASM 94] American National Standard ASME Y14.5M, Dimensioning and Tolerancing, The American Society of Mechanical Engineers, New York, 1994.
- [BAA 02] BAADER F., CALVANESE D., MCGUINNESS D., NARDI D. and PATEL-SCHNEIDER P., *The Description Logic Handbook: Theory, Implementation and Applications*, Cambridge University Press, 2002.
- [BHI 07] BHI S., AMETA G., DAVIDSON J.K. and SHAH J., 2007, "Tolerance-maps applied to the straightness and orientation of an axis, in models for computer-aided tolerancing in design and manufacturing", *Proc., 9th CIRP Int'l Seminar on CAT*, April 10-12, 2005, Tempe, AZ, USA), p. 45-54, Springer, Dordrecht, Netherlands, 2007.
- [CHA 91] CHASE K. W., "A survey of research in the application of tolerance analysis to the design of mechanical assemblies", *Research in Engineering Design*, Vol. 3, p. 23-37, 1991.
- [DAN 07] DANTAN J.Y., LANDMANN T., SIADAT A. and MARTIN P., "Information modeling to manage tolerances during product and process design", *Models for Computer Aided Tolerancing in Design and Manufacturing*, Springer, Netherlands, p. 55-64, 2007.

- [DES 07] DESROCHERS A., “Geometrical variations management in multi-disciplinary environment with the Jacobian-torsor model”, *Models for Computer Aided Tolerancing in Design and Manufacturing*, Springer Netherlands, 75-84, 2007.
- [EVA 75] EVANS D.H., “Statistical tolerancing: The state of the art. Part II: methods for estimating moments”, *Journal of Quality Technology*, Vol. 7, No. 1, p. 1-12, 1975.
- [FEN 03] FENG S. and SONG Y., “An information model of manufacturing processes for design and process planning integration”, *Journal of Manufacturing Systems*, Vol. 22(1), p. 1 – 28, 2003.
- [FIO 07] FIORENTINI X., GAMBINO I., LIANG V.C., FOUFOU S., RACHURI S., MANI M., and BOCK C.E., *An Ontology For Assembly Representation*, National Institute of Standards and Technology, NISTIR 822740, 2007.
- [FIO 08] FIORENTINI X., RACHURI S., MANI M., FENVES S.J. and SRIRAM R.D., *An Evaluation of Description Logic for the Development of Product Models*, NISTIR 7481, 2008.
- [GER 96] GERTH R.J., “Engineering tolerancing: A review of tolerance analysis and allocation methods”, *Engineering Design and Automation*, Vol. 2, No. 1, p. 3-22, 1996.
- [GRU 91] GRUBER T.R., *Ontolingua: A mechanism to support portable ontologies*, Technical report KSL, p. 91-66. Stanford University, Knowledge Systems Laboratory, 1991.
- [HOF 08] HOFFMANN P., FENG S C., AMETA G, GHODOUS P, QIAO L and SRIRAM RD., *Towards an Approach for multi-view semantic model for product development, Collaborative Product and Service Life Cycle Management for a Sustainable World*, In Springer book series, Advanced Concurrent Engineering, Part 5, p. 205-213, 2008.
- [HON 02] HONG Y.S. and CHANG T.C., “A comprehensive review of tolerancing research”, *International Journal of Production Research*, Vol. 40, No. 11, p. 2425-2459, 2002.
- [IEE 90] Institute of Electrical and Electronics Engineers, *IEEE Standard Computer Dictionary: A Compilation of IEEE Standard Computer Glossaries*, IEEE, New York, USA, 1990.
- [ISO 05] ISO/IEC 19501, *Information technology — Open Distributed Processing — Unified Modeling Language (UML) Version 1.4.2*, 2005.
- [ISO 83] Organization for Standardization ISO 1101: *Geometrical tolerancing – Tolerancing of form, orientation, location and run-out – Generalities, definitions, symbols, indications on drawings*, ISO, 1983.
- [ISO 94] *Industrial Automation Systems and Integration — Product Data Representation and Exchange, Part 1: Overview and Fundamental Principles*. ISO 10303-1, ISO, Switzerland, 1994.
- [MCG 03] MCGUINNESS D.L. and VAN HARMELEN F., *OWL web ontology language overview*, <http://www.w3.org/TR/owl-features/>, 2003.
- [NIG 95] NIGAM, S.D. and TURNER J.U., “Review of statistical approaches to tolerance analysis”, *Computer-Aided Design*, Vol. 27, p. 6-15, 1995.

- [PAS 03] PASUPATHY T.M.K., MORSE E.P. and WILHELM R.G., "A survey of mathematical methods for the construction of geometric tolerance zones", *J. of Computing and Information Science in Engineering*, Vol. 3, p. 64-75, 2003.
- [PAT 04] PATEL-SCHNEIDER P.F., HAYES P. and HORROCKS I., OWL web ontology language semantics and abstract syntax. W3C recommendation, <http://www.w3.org/TR/owl-semantics/>, 2004.
- [PRO 08] <http://protege.stanford.edu/>
- [RAC 06a] RACHURI S., HAN Y., FOUFFOU S., FENG S., ROY U., WANG F., SRIRAM R. and LYONS K.W., Assembly Model Representation from Conceptual to the Detailed Design, National Institute of Standards and Technology, NISTIR 822267, 2006.
- [RAC 06b] RACHURI S., HAN Y., FOUFFOU S., FENG S., ROY U., WANG F., SRIRAM R. and LYONS K.W., "A model for capturing product assembly information", *Journal of Computing and Information Science in Engineering*, Vol. 6, No. 1, p. 11 – 21, 2006.
- [SHA 07] SHAH J.J., AMETA G., SHEN Z. and DAVIDSON J. K., "Navigating the tolerance analysis maze", *Computer Aided Design and Applications*, Vol. 4, No. 5, p. 705-718, 2007.
- [SHE 05] SHEN Z., AMETA G., SHAH J.J. and DAVIDSON J. K., "Comparative study of tolerance analysis methods", *J. of Computing and Information Science in Engineering*, Vol. 5, No. 3, p. 247-256, 2005.
- [SMI 04] SMITH M.K., WELTY C. and MCGUINNESS D.L., OWL web ontology language guide. W3C recommendation. <http://www.w3.org/TR/2004/REC-owl-guide-20040210/>, 2004.
- [SOW 09] SOWA J.F., Building Sharing and Merging Ontologies, retrieved from <http://www.jfsowa.com/ontology/ontoschar.htm>, 2009.
- [STE 94] STANDARD FOR EXCHANGE OF PRODUCT DATA (STEP) – ISO 10303-1994, Industrial automation systems and intergration – Product data representation and change, ISO, 1994.
- [THI 06] THIMM G., LEE S. G. and MA Y.S., "Towards unified modelling of product life-cycles", *Computers in Industry*, Vol. 57, p. 331-341, 2006.
- [THO 99] THORNTON A.C., "Variation risk management using modeling and simulation", *Journal of Mechanical Design*, Vol. 121, p. 297-304, 1999.
- [WU 03] WU Y., SHAH J.J. and DAVIDSON J. K., "Computer modelling of geometric variations in mechanical parts and assemblies", *Journal of Computing and Information Science in Engineering*, Vol. 3, No. 1, p. 54-63, 2003.
- [YAN 08] YANG D., DONG M. and MIAO R., "Development of a product configuration system with an Ontology-Based Approach", *Computer Aided Design*, Vol. 40, p. 863-878, 2008.
- [ZHA 06] ZHAO X., PASUPATHY T.M.K. and WILHELM R.G., "Modeling and representation of geometric tolerances information in integrated measurement process", *Computers in Industry*, Vol. 57, p. 319-330, 2006.

## Chapter 27

# A PLM-Based Multi-Sensor Integration Measurement System for Geometry Processing

The multi-sensor integration measurement system is given increasing consideration for quality control, reverse engineering and other engineering applications. However, there are still some difficulties when we implement it in practice, such as sensor fusion, multiple data merging, etc. We developed a multi-sensor integration system based on the view of PLM context. The system integrates a laser scanner, a touch probe and a chromatic confocal sensor onto a CMM platform. It can be divided into data acquisition sub-system and geometry processing sub-system. In the data acquisition sub-system, a physical integration method is demonstrated to achieve the sensor fusion. A laser guide planning metrology is achieved for optimizing the measuring strategy. And a standardize data model was established for integration with other activities in the PLM context. In the geometry processing sub-system, the discrete curvatures on each vertex are estimated based on the polyhedral surfaces approximated from the point data. Then two surface indicators, shape index and curvedness, are introduced for the segmentation. For each segmented region, the tolerance model is established for quality analysis.

### 27.1. Introduction

3D coordinate metrology plays a critical role in tolerance evaluation and quality control [HOC 05]. In modern design and production, the complicated shapes and tighter tolerancing are widely implemented. Therefore, more and more rigorous

---

Chapter written by Zhao HAIBIN, Nabil ANWER and Pierre BOURDET.

requirements are being exercised on the coordinate metrology. Many attempts have already been made to improve the existing metrological techniques or to develop new ones [GAL 05, HOC 05, ZHA 06]. Generally, the widely-used sensing techniques in the market for coordinate metrology can be classified into three categories: contact metrology such as trigger probing, contact scan probing, etc., optical methods, also known as non-contact which contain the technologies such as triangulation, photogrammetry, interferometric, etc., and others, which are not been considered in the first two categories such as CT, supersonic, etc. Only the first two categories are considered in our work scope.

Both of the contact and optical metrologies have their own characteristics and applications. Generally, contact metrology is maximum accuracy, simple for operation and more adaptable to surface condition and environment but with very slow capturing speed (only 1~2 points/second). It can be used to measure the surface with less sampling density, such as prismatic workpiece, objects with known shapes and surfaces without large variation.

Optical metrology, on contrast, can acquire considerable high density of point data from the surface with rapid speed (for example, the Kreon laser scanner can reach 30,000 points/second). Its non-contact nature also makes it suitable to digitize the surface with flexible or soft materials. However, the optical metrology has its own limits too, such as lower accuracy, occlusion and limited viewpoint, is sensitive to the surface optical conditions like specular surface which is not suitable for optical measurement. The data acquired by the optical sensor is always noisy and imperfect, due to redundancy in some areas and missed data in others. Therefore optical metrology is suitable for the surface digitalization and topography measurement.

The two kinds of sensing techniques have their own extinct merits and deficiencies. In modern coordinate metrology, it would be difficult to fulfill all the requirements with only one sensor even in a single inspection task. Multi-sensor integration measurement should be a perfect solution to utilize the advantages of individual sensors and overcome their disadvantages simultaneously.

Some advanced CMM systems have already offered multi-sensor integration solutions, like Mahr, Werth Messtechnik, Zeiss, etc. Many researchers have also given their considerations on that domain. The system integrated with a contact probe and an optical sensor whether a vision camera or a laser scanner is discussed in some articles [CHE 03, SHE 01, HUA 07, CHA 01, CAR 01]. Cooperative sensor integration has been proposed to automate the coordinate acquisition in which the global shape information was acquired by an optical sensor to guide the tactile probing or other sensors [HUA 07, CHA 01].



The result processing for point data from measurement systems for GD&T evaluation or shape analysis have already been given great attention by [WEB 02]. However, some others focus their research on the merging of multiple data obtained from the sensors with different accuracy and resolution [NAS 97] or shape digitization from unknown geometries in the context of reverse engineering [IP 07].

From a system integration point-of-view, some institutes have done their own contributions to integrate the measurement system with CAD/CAM system and inspection execution activity and the standards employed to these kinds of integration are developed, e.g. STEP AP213, AP219 and DMIS used for CAD/CAIP integration and I++DME, DML used for integration with inspection planning system and execution system are developed by the standardization organizations.

However, there are still some difficulties in multiple sensor integration because of the differences in physical structures, work principles, data representations and analysis. Therefore, the main contribution of this chapter is to propose an approach for PLM-based measurement system with multi-sensors integration in which the integration methodology and an unambiguous data representation model are described, the result analysis for geometry processing such as shape analysis and tolerance evaluation is expatiated.

The remainder of the chapter is organized as follows: section 27.2 describes the setup of the multiple sensors integration system for data acquisition; section 27.3 presents a sharable data representation model in PLM context for data integration with other activities; section 27.4 and section 27.5 expatiate the result analysis for geometry processing in details; some example for validation are proposed in section 27.6, finally the conclusion is in section 27.7.

## **27.2. Sensor integration methodology**

### **27.2.1. System framework**

The multi-sensors integration measurement system can be divided into two basic sub-systems: data acquisition sub-system and geometry processing sub-system. The main purpose of the data acquisition system is to digitize the surfaces of an object into 3D point sets with an appreciable accuracy and rapid speed.

The core of the data acquisition system is the multiple sensors and their integration. Various kinds of sensors exist in the market. Obviously, it is impossible and unnecessary to integrate all of them into one measurement system. It is enough for the participants to select only the minimum sensors that can satisfy their

measurement tasks. But for general research purposes, three very different kinds of sensors are selected for the system setup, which are the Kreon Zephyr KZ25 laser scanner from Kreon Technologies (<http://www.kreon3d.com>), Renishaw TP2 touch probe from Renishaw (<http://www.renishaw.com>) and STIL CL2 chromatic confocal lens (<http://www.stila.com>).

The Kreon laser scanner which is based on triangulation observes the point data in 2D space using its CCD camera. Therefore, a special calibration procedure is required to map the 2D point data into 3D coordinates space. For more calibration details refer to [LAR 03].

The Renishaw touch trigger probe can acquire the 3D coordinates of points directly from the surface with the accuracy of about 0.5  $\mu\text{m}$ . However, because of the limit of its slow capturing rate, the density of the points is usually sparse and cannot include enough information of the digitized surfaces.

The STIL chromatic confocal sensor works on the chromatic confocal imaging principle [HOC 05, COS 07], and is only a 1D data capture. The STIL sensor can only sense the depth information (Z axis) of a point. Coordinates in another two axes (X axis and Y axis) depend on the observation values in the corresponding axes of CMM. Because of the limited measurement range, only 400  $\mu\text{m}$ , the STIL sensor is only implemented in micro-metrology.

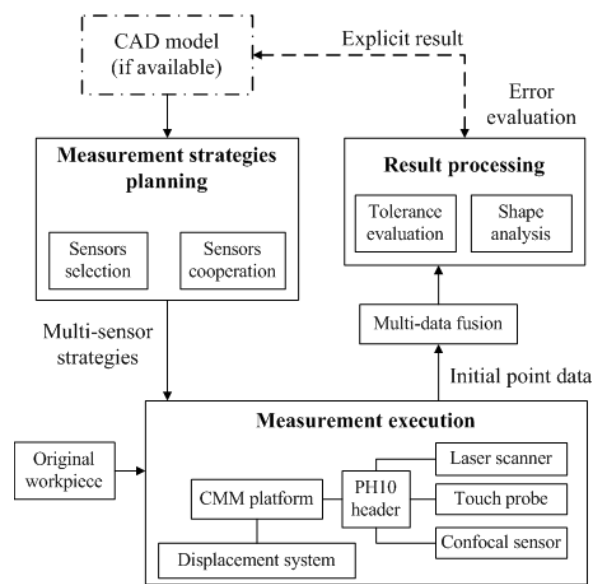
With the three sensors, the measurement system could cover the metrologies both in macro and micro levels with 1D, 2D and 3D data acquisition by contact and optical capturing techniques. Therefore, it could cover the general applications of metrology.

In order to integrate the three sensors together on the CMM platform, we designed the system framework as shown in Figure 27.1. The framework contains three parts: measurement strategies planning, measurement execution and result processing. The first two procedures belong to the data acquisition sub-system.

Measurement strategy planning is used to plan the measurement strategies for multi-sensor cooperation, such as sensor selection, seamless connection of the measurement paths, etc. While measurement execution includes two parts: CMM platform integrated with three sensors, which is known as measurement devices, and the displacement system which is known as electronic units used for displacement control.

The measurement strategies are different and should be planned respectively considering the conditions with or without the input CAD model of the workpiece. If the CAD model is available, the detailed measurement features can be extracted

from the CAD model based on the design specifications. Therefore, measurement strategies can be planned based on the CAD model [ZHA 06]. On the other hand, if the CAD model is not available, the measurement features need to be acquired from the workpiece directly, by manual experiences or optical measurement. The optical measurement is addressed further here. In our system, laser guide metrology is developed. The laser scanner is first implemented to acquire the global information of the workpiece. And then the global information is used to guide other sensors for more detailed measurements (see section 27.2.3).



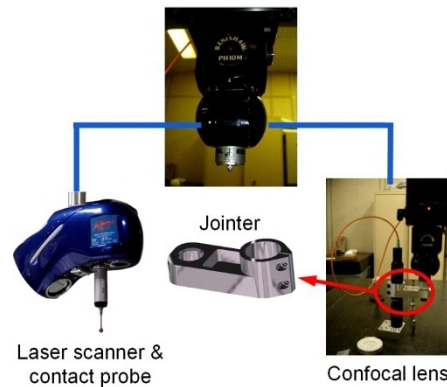
**Figure 27.1.** Framework of multi-sensor integration measurement system

### 27.2.2. Physical integration of multiple sensors

The multi-sensor fusion is one of the critical issues for the function achievement. There are several problems that should be considered for the sensor fusion, e.g. the sensors must not intervene with each other during the system setup and must not collide with each other or other components of the system during measuring. In order to facilitate the sensor fusion, the PH10M header from Renishaw is used to assemble the three sensors onto the CMM platform, shown in Figure 27.2.

Due to the limitation of the STIL sensor in work distance (the maximum is only 11 mm between the lens and the digitized surface), It is too difficult to avoid the collision during measuring if we integrate the three sensors at the same time.

Fortunately, owing to the only implementation in micro-metrology, the STIL sensor is not as commonly used as the other two sensors in tolerance evaluation and shape analysis. It is only necessary to integrate the STIL lens on the PH10M header when it is required.



**Figure 27.2.** *Physical integration of multiple sensors*

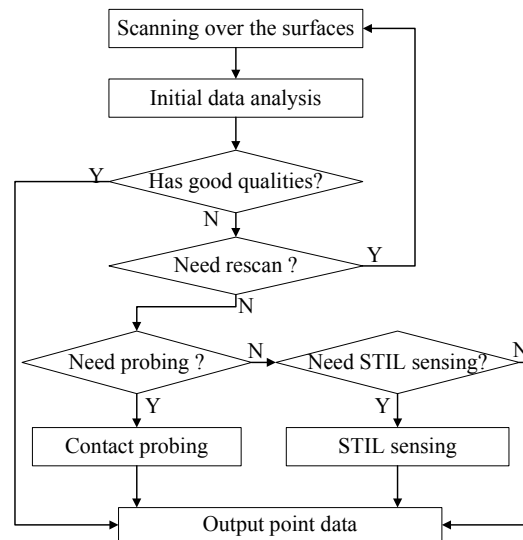
According to the above analysis, the physical fusion of sensors should consist of two procedures. One is the integration of the laser scanner and the contact probe. The Kreon laser scanner provides the interface with the Renishaw contact probe and the PH10M header. Hence, the integration step is achieved simply. The other procedure is to integrate the STIL lens into the system. In this procedure, a precise workpiece called jointer is designed and manufactured in order to mount the STIL lens on the PH10M header with accurate location and orientation, more details can be referred to [COS 07]. The STIL lens should be hung up in the measurement with the first integration procedure for collision-avoid purpose, and vice versa.

In practice, in order to harmonize the consistency of the whole measurement, the three sensors are arranged by different priorities. The primary is the laser scanner, followed by the contact probe and the lowest is the STIL sensor.

### **27.2.3. Laser guide metrology**

Laser guide metrology is an important application to show the advantages of multiple sensor integration, especially when the CAD model of the workpiece is unavailable. An initial laser scanning is implemented first to acquire the global information of the digitizing surfaces. The global information is then used to guide other sensors (laser scanner again, touch probe or STIL lens) to perform optimized measurements with higher quality.

Figure 27.3 gives an overall description of the algorithm of laser guide metrology. The object is scanned first by a laser scanner. The key features of the object are identified from the point data and the quality of the point data is estimated by initial data analysis, described by a set of indicators. The commonly used indicators are noise which are used for a noise degree evaluation, and completion which is to evaluate whether the point data is overlapped or missing points in some areas, etc. [LAR 02]. Then, whether a more detailed inspection procedure is needed or not is determined accordingly. If yes, the areas requiring more digitizing are first distinguished and their feature attributes are analyzed to determine which kinds of sensors are suitable. And then, three Boolean indicators corresponding to the three sensors are set to represent the sensors selection results (if the rescan is needed, for example, the indicator for laser scanner is set as TRUE, otherwise it should be set as FALSE). According to the status of the three indicators, the measurement strategies are planned based on the attributes both of the sensors and features needed to be re-digitized. Finally, the point data with pretty quality can be outputted from the data acquisition sub-system.



**Figure 27.3.** Overall algorithms of laser guide metrology

### 27.3. Ontology modeling in a PLM-context

The multi-sensor integration measurement system needs to access some resources or data from other activities for its function achievement. And it should also provide the interfaces for other activities to share its own data and knowledge.

Therefore, the measurement system should be integrated with other activities in a PLM context. For the purposes of integration and also for the facility of system development, the various data and knowledge in the measurement system should be represented in a standardized and unambiguous way. The knowledge is modeled here based on ontology modeling methodology.

### **27.3.1. Description of ontology modeling**

Ontology is an explicit specification of a conceptualization and representational vocabulary for a shared domain of discourse including definitions of classes, relationships, functions or other objects [OWL]. The main purpose of ontology modeling is to capture the underlying conceptualization where all concepts and relationships can be clearly and unambiguously defined with structured knowledge. Ontology can make the sharing and reusing of a given domain knowledge much simpler.

Applications of ontology modeling can be widely found in AI (Artificial Intelligence), computer science, etc. [AND 07]. Many languages and tools are specifically used for ontology modeling: EXPRESS which is an object-oriented data specification language endorsed by ISO, UML (unified modeling language), RDF (resources description framework) and OWL (ontology Web language).

However, only a few articles discuss the methodology of ontology modeling in a dimension metrology domain [AND 07, BAR 03]. Here, the knowledge model in dimension metrology with multiple sensor integration is developed in Protégé [PRO] and EXPRESS is selected as the modeling language.

### **27.3.2. Ontology modeling in Protégé**

According to STEP AP213 and AP219, all the resources and knowledge in coordinate metrology can be catalogued into four basic groups: specifications of measurement geometries; measurement strategy planning, execution resources and result data analysis.

Considering the measurement requirements, in the group of Specifications of measurement geometries, the geometries of the object are reclassified into three basic classes: Geometry schema, Topology schema and Geometric property schema which define the detailed properties for the geometries, such as position, tolerances, size, shape specifications, etc. The three schemas refer to each other and construct the complete data model according to the measurement requirements.

Measurement strategy planning specifies the related knowledge required for measurement strategy planning and generation. The data in this group is considered as algorithms, such as sensor selection algorithms, collision-avoid algorithms, position and orientation of sensors determining and path generation algorithms, etc. which are referred to the data group of specifications of measurement geometries and supported by the specifications of measurement devices.

The group of execution resources defines the information of the devices such as multiple sensors, CMM and others, the specifications of device setup and calibration, the environment conditions required for the measurement, and so on.

The last group describes the data appearing in result analysis, such as initial data, quality estimation model of point data, polyhedral surface model, tolerance evaluation model and shape analysis model, etc.

The four groups of data models could contain much more complicated knowledge and data, all of which are organized by multi-hierarchies structures in Protégé. Figure 27.4 shows the four main basic classes and their top hierarchies in the ontology model of dimension metrology, visualized in Protégé. The gray triangles in the left of classes indicate that the classes have additional sub-classes.

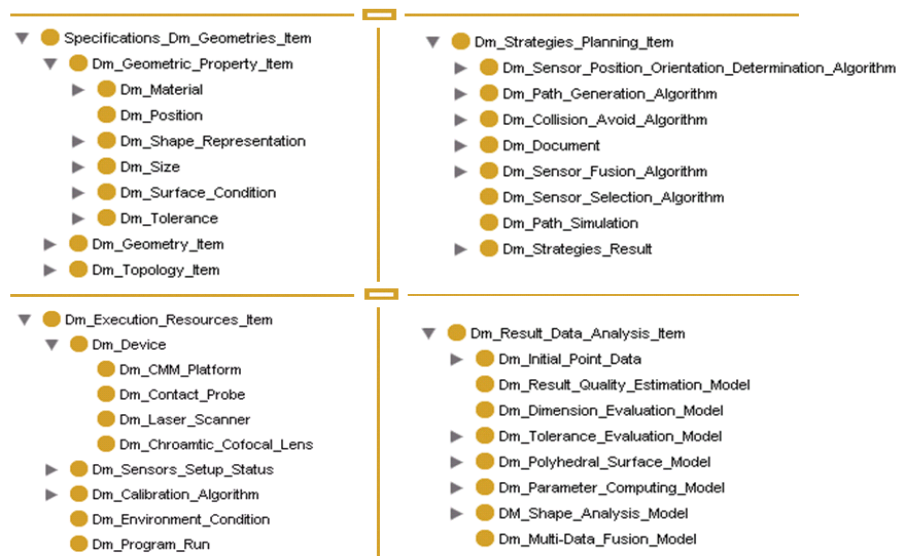


Figure 27.4. Main basic classes and their top hierarchy structures visualized in Protégé

The ontology model of dimension metrology is built close to the industrial standards (especially the STEP), so it is unambiguous. It provides a strong ability for data exchange and shares in the PLM context.

#### 27.4. Geometry processing

For recovering the geometry information from the point data acquired by the data acquisition system, the local neighbor relationships should first be constructed. The Delaunay triangulation based polyhedral surfaces approximation is used here. The algorithm is developed by Cohen-Steiner *et al.* [COH 03]. Based on the polyhedral model, the differential parameters (e.g. the principal curvatures) can be properly estimated. The principal curvatures are critical important for the later procedures, such as identification, segmentation, etc.

##### 27.4.1. Shape analysis based on the shape index and curvedness

The shape index introduced by Koenderink and van Doorn [KOE 92] is a single value to measure the intuitive notion of local shape type. The shape index is defined in terms of the two principal curvatures, as in the following expression:

$$s = \begin{cases} \frac{2}{\pi} \arctan\left(\frac{\kappa_1 + \kappa_2}{\kappa_1 - \kappa_2}\right) & (\kappa_1 > \kappa_2) \\ \text{sign}(\kappa_1) & (\kappa_1 = \kappa_2 \neq 0) \end{cases} \quad [27.1]$$

The shape index is a number within the range  $[-1, 1]$  from formula [27.1] Except the planar shape which has an indeterminate value of the shape index, all other shape types can be mapped into  $[-1, 1]$  according to the shape index.

Curvedness [KOE 92], also known as bending energy, is used to measure the intensity of the degree a surface is curved. Curvedness is a positive value and can be defined as formula [27.2]:

$$c = \sqrt{(\kappa_1^2 + \kappa_2^2) / 2} \quad [27.2]$$

Both the shape index and curvedness are transition and rotation invariants. They are the surface descriptors specifying the second order geometry. The pair of shape index and curvedness describes the surface information completely. Because of the two surface indicators independence from each other, they are more convenient for further shape analysis.



Based on the shape index map, the shape categories can be predefined based on the shape index to judge the local shape type. In our implementation, the predefined shape categories are defined as 10 basic shapes: spherical (concave and convex) ellipsoidal (concave and convex), parabolic (concave and convex), saddle-parabolic (concave and convex) saddle and planar. For more details refer to [KOE 92].

Because of the indeterminate shape index value of the planar shape, the planar shape can be identified according to the curvedness. Theoretically, the curvedness of a planar vertex is equal to 0. In practice, if the curvedness of a vertex is smaller than a given threshold ( $1.0 \times 10^{-5}$  for example), the vertex can be determined as a planar vertex.

The curvedness of each vertex can also be obtained due to formula [27.2]. With the pair of shape index and curvedness, the boundary recognition and point partition can be made.

Generally, points in the same shape category and with similar curvedness values should be classified into the same region, except for the replicated features. However, considering the influence of measuring errors and the computing errors in the previous procedures, the overall algorithms for point partition can be described as follows:

- (1) The point data is first classified into 10 shape clusters according to the shape index values. However, because of the noise points and the computing errors, the clusters are not appropriated, shown in Figure 27.6 (2).
- (2) In order to improve the qualities of the clustering, the sharp edge and high curvature points are identified based on curvedness, shown in Figure 27.6 (3).
- (3) According to the sharp edge and high curvature points, the shape clusters are rectified as the most appropriated as possible, see Figure 27.6 (4).
- (4) The region growing algorithms are implemented to partition the point data into several simplex regions, each of which can be represented as a single surface as shown in Figure 27.6 (5).

Finally, each of the segmented regions can be associated and the actual dimension and tolerance parameters can be computed to evaluate the quality of the workpiece.

#### **27.4.2. *Quality evaluation***

The ultimate purpose of a multi-sensor measurement system is to obtain the explicit geometrical parameters model of the measured workpiece. In order to

construct the mathematical model of the local surface patch, the local coordinate framework is established in which, the original point is the centroid of the segmented subset of the points. This can be calculated as:

$$P_c(x_c, y_c, z_c) = \frac{1}{n} \sum_{p \in N_p} P_i(x, y, z) \quad [27.3]$$

where  $P_c$  is the centroid of  $p$  in  $N_p$ .  $N_p$  represents the points belong to the local region,  $n$  is the point number in the local region.

The classic PCA (principal component analysis) [LIU 08] is implemented to determine the directions of coordinate axes. In the PCA method, the coordinate axes are calculated first as the three principal components of the local sub-point set, and then, the z-axis is determined. The x-axis and y-axis can be determined based on the right-hand rule.

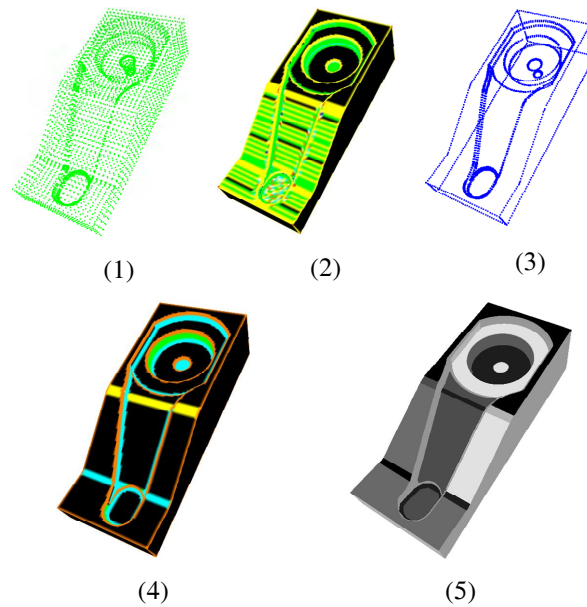
After the estimation of the local coordinate framework, the coordinates of all the point sets in the same region can be transformed into the local coordinate framework; within the same coordinate framework, the shape mathematic model can be associated by the least-square method, and the comparison with the theoretical shape can be done. There are already many articles with this focus.

### 27.5. Experiments validation

A multi-sensor integration measurement system is constructed to validate the proposed methods. The framework of the data acquisition system is discussed in section 27.2.1, so the geometry processing is addressed further in this section.

In order to demonstrate the effectiveness of the proposed algorithms, a mechanical workpiece has digitized from multiple views of the laser scanner. Some regions (like the interior of the cylinder surfaces) are probed by touch probe. The small patch of the bottom of the lacuna on the top of the lower end is detected by STIL lens. After coordinates transformation, the point data acquired from multiple views and sensors can be fused together. After some pre-processing procedures of Denoising and filtering, the inputted point data in the geometry processing sub system is like the point data shown in Figure 27.6 (1).

After the estimation of shape index and curvedness, the point data of the measured workpiece can basically be clustered as shown in (2). The sharp edges and high curvature points are extracted as shown in (3). The rectified clusters are shown in (4) and the final segmentation of the point data is shown in (5) with gray scales.



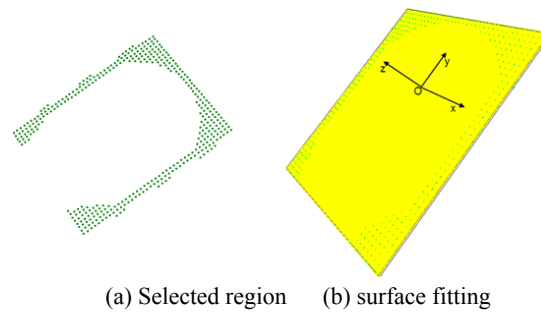
**Figure 27.6.** Shape analysis for the workpiece

The point set of the workpiece could be partitioned into 41 sub-regions represented with different colors. And from the shape index map, we can recognize that the local surface types contain plane, cylinder cone and other transition surfaces.

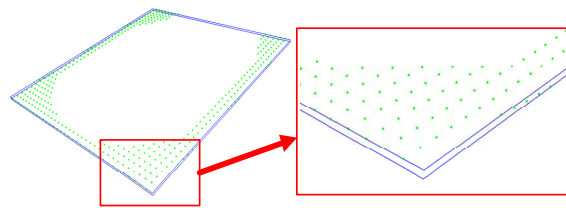
As an example for the quality evaluation, the top region is selected to estimate the quality of the planar region synthetically, as shown in Figure 27.7a. In order to establish the local coordinate framework, the coordinates of the local original point are calculated using formula [27.3]. The direction of the z-axis is evaluated by the expectation of the normal directions of the overall selected points and the x-axis and y-axis are selected with the same set of the points. The planar region can be associated with the local framework, as shown in Figure 27.7b.

Based on the associate surface, the deviation of each point from the associated surface can be computed and the tolerance zone can then be computed based on the associated plane, as shown in Figure 27.8. With the help of the theoretical CAD model, the maximum and average deviation values can be calculated to evaluate the quality of the actual surface conditions. The important factor that must be considered is the uncertainty of the measurement system. Therefore, the calculated values can give the optimum evaluation when the uncertainty values of the measurement system are added.

Other tolerances and dimension values could also be analyzed with a similar approach.



**Figure 27.7.** *Surface fitting of the selected regions points*



**Figure 27.8.** *Tolerance zone for the selected region points*

## 27.6. Conclusion

A PLM-based measurement system with multi-sensor integration for geometry processing in 3D coordinate metrology is presented. With the implementation of the system, the contributions of this chapter are as follows: (1) with the unique sensor fusion approach, a laser-guide metrology is addressed to improve the robustness and effectiveness of the existing measurement system; (2) a PLM based ontology model is constructed for knowledge and data management which is shown as unambiguous and clear; (3) the introduced surface descriptors: shape index and curvedness, show their convenience for representating the geometries; (4) the quality evaluation of the measured workpiece is facility based on the segmentation of the point data; (5) the geometry processing system is less sensitive to the noise because the segmentation algorithms use the curvedness map to reduce the influences of the noisy points. For future work that focuses on tolerance evaluation algorithms should be extended to all the tolerances in mechanical engineering.

## 27.7. Acknowledgments

We would like to thank Prof. Jean-Claude Paul (Tsinghua University and LIAMA/INRIA) for his support of this work and to acknowledge the Sino-French PLM Innovation Center at Tsinghua University for funding this project.

## 27.8. Bibliography

- [AND 07] ANDERSEN O., VASILAKIS G., “Building an ontology of CAD model information”, *Geometric Modeling, Numerical Simulation, and Optimization Applied Mathematics at SINTEF*, p. 11-40, 2007.
- [BAR 03] BARREIRO J., LABARGA J., VIZÁN A. *et al.*, “Information model for the integration of inspective activity in a concurrent engineering framework”, *Journal of Machine Tools and Manufacture*, Vol. 43, p. 797-809, 2003.
- [CAR 01] CARBONE V., CAROCCI M., SAVIO E. *et al.*, “Combination of a vision system and a coordinate measuring machine for the reverse engineering of freeform surfaces”, *International Journal of Advanced Manufacturing Technology*, Vol. 17, No. 4, p. 263-271, 2001.
- [CHA 01] CHAN V., BRADLEY C., VICKERS G., “A multi-sensor approach to automating coordinate measuring machine-based reverse engineering”, *Journal of Computers in Industry*, Vol. 44, p. 105-115, 2001.
- [CHE 03] CHEN H., WANG B. *et al.*, “Multi-sensor integrated automated inspection system”, *Proceedings of SPIE*, Vol. 5253, p. 528-531, 2003.
- [COH 03] COHEN-STEINER D., MORVAN J.M., “Restricted Delaunay triangulations and normal cycle”, *In Proceedings of 19th Annual ACM Symposium on Computational Geometry*, p. 237-246, 2003.
- [COS 07] COSTADOAT R., Implantation d’un capteur Stil dans une cellule de mesure multi-capteurs, Master thesis, ENS de Cachan, 2007.
- [GAL 05] GALANTUCCI L. and PERCOCO G., “A multilevel approach to edge detection in tessellated point cloud”, *CIRP Annals – Manufacturing Technology*, Vol. 54, No. 1, p. 127-130, 2005.
- [HOC 05] HOCKEN R., CHAKRABORTY N. and BROWN C., “Optical metrology of surfaces”, *CIRP Annals – Manufacturing Technology*, Vol. 54, No. 1, p 41-46, 2005.
- [HUA 07] HUANG Y. and QIAN X., “A dynamic sensing-and-modeling approach to three-dimensional point-and-area-sensor integration”, *Journal of Manufacturing Science and Engineering*, Vol. 129, p. 623-635, 2007.
- [INR] <http://cgal.inria.fr/Reconstruction/submit.html>
- [IP 07] IP C., GUPTA S., “Retrieving matching CAD models by using partial 3D point clouds”, *Journal of Computer-Aided Design & Applications*, Vol. 4, No. 5, p. 629-638, 2007.

- [KOE 92] KOENDERINK J.J., VAN DOORN A.J., "Surface shape and curvature scales", *Image and Vision Computing*, Vol. 10, No. 8, p. 557-565, 1992.
- [LAR 02] LARTIGUE C., CONTRI A., BOURDET P., "Digitised point quality in relation with point exploitation", *Journal of Measurement*, Vol. 32, p. 193-203, 2002.
- [LAR 03] LARTIGUE C., BOURDET P., MATHIEU L. *et al.*, "Algorithms for the calibration of laser-plane sensors on CMM", *Advanced Mathematical & Computational Tools in Metrology*, Vol. I, p. 82-97, 2003.
- [LIU 08] LIU Y., RAMANI K., "Robust principal axes determination for point-based shapes using least median of squares", *Computer-Aided Design*, 2008.
- [NAS 97] NASHMAN M., TOSHIMI B., *et al.*, "A unique sensor fusion system for coordinate measuring machine tasks", *Proceeding of SPIE*, Vol. 3209, p. 145-156, 1997.
- [OWL] <http://www.w3.org/TR/owl-feature>
- [PRO] <http://protege.stanford.edu/>
- [SHE 01] SHEN T., HUANG J. and MENQ C., "Multiple-sensor planning and information integration for automatic coordinate metrology", *Journal of Computing and Information Science in Engineering*, Vol. 1, p. 167-179, 2001.
- [WEB 02] WEBER T., MOTAVALLI S., FALLAHI B. *et al.*, "A unified approach for form error evaluation", *Precision Engineering*, Vol. 26, p. 269-278, 2002.
- [ZHA 06] ZHAO H., WANG J., WANG B. *et al.*, "A PLM-based automated inspection planning system for coordinate measuring machine", *Proceedings of SPIE*, Vol. 6358, p. 6358291-6358296, 2006.

## Chapter 28

# Comparison of Gear Geometric Specification Models Regarding the Functional Aspect

### 28.1. Introduction

As technology increases and performance requirements continually tighten, the cost and required precision of assemblies increase as well. There is a strong need for increased attention to tolerance design to enable high-precision assemblies to be manufactured at lower costs. Indeed, geometric variation management is a key element in industry for improving product quality, in particular for gears (complex geometry, complex behavior, etc.).

The tolerancing process is defined through all the activities involved by geometric product variation management: tolerance design, manufacturing tolerance analysis, and tolerance verification. Tolerance verification enables us to close the process loop, to check the product conformity, to verify assumptions made by the designer, and to control the process. Production metrology always aims at providing reliable information as a basis for decisions. Measurement results are afflicted with measurement uncertainty, which leads to technical and economical risks in industrial companies. By assessing the risks and the connected consequences of the decisions (conformity verification), the value of the measurement result can be evaluated. Modeling the functional chain for conformity assessments enables us to follow simulations, which generate an estimation of the economical benefit and value of measurements independent of measurement uncertainty and the performance of the underlying production process.

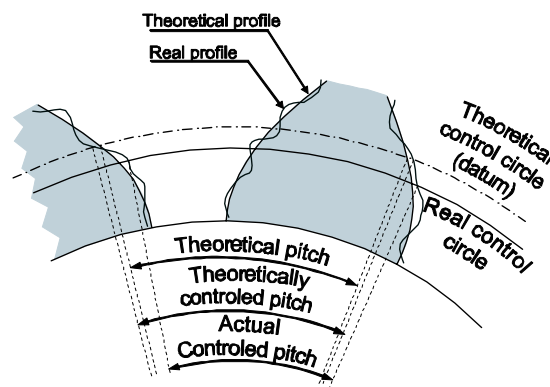
---

Chapter written by Jean-Paul VINCENT, Jean-Yves DANTAN, Gerth GOCH and Régis BIGOT.

The notion of uncertainty is by now well entrenched in metrology. In the ISO TS17450-2, the notion of uncertainty is generalized to specification and verification. In fact, the uncertainties throughout the product lifecycle begin from the design intent to the inspection activity. The uncertainty is divided into correlation uncertainty, specification uncertainty and measurement uncertainty:

- Correlation uncertainty characterizes the fact that the intended functionality and the controlled characteristics may not be perfectly correlated.
- The specification uncertainty characterizes the ambiguity in the specification expression.
- And the measurement uncertainty is considered by metrologists and is well described in GUM. The measurement uncertainty includes all the causes of variation from the geometric specification to the result of inspection.

In industry, engineers try to lower these uncertainties to ensure the product is as functional as possible. This study focuses on the pitch error which is defined in the AGMA 2009-B01 [ANS 05].



**Figure 28.1.** Influence of the control circle deviations on the pitch error estimation

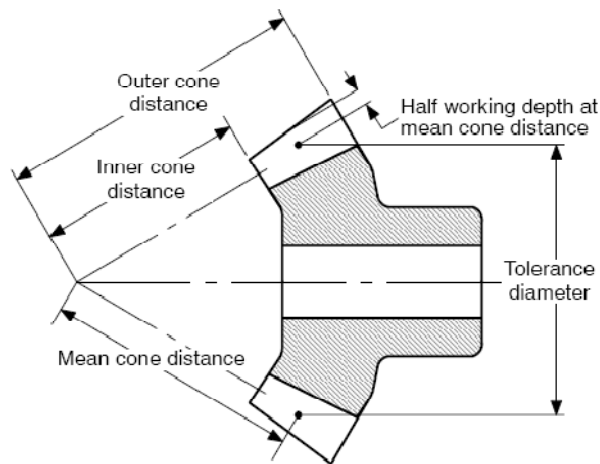
To illustrate the measurement uncertainty, the example of the definition of the pitch error can be taken: the pitch of a bevel gear is defined as the arc length between all consecutive left or right flanks of one gear, measured at the pitch diameter  $d$  at a distance  $R$  from the apex of the reference cone. To estimate these deviations, it proposes some metrology strategies than consist of probing one point of the flanks, either by using one probe device or two probe devices. These strategies provide short quality inspection times but are very sensitive to the measurement uncertainties (Figure 28.1). Indeed, if there is a gap between the real



control circle and the theoretical control circle, the pitch that has to be measured at the datum circle will differ from the controlled pitch.

To evaluate the pitch error, some mathematical models and calculation steps are needed, based on the set of points of the metrology. To decrease these uncertainties, Guenther [GUE06] proposes a new metrology strategy.

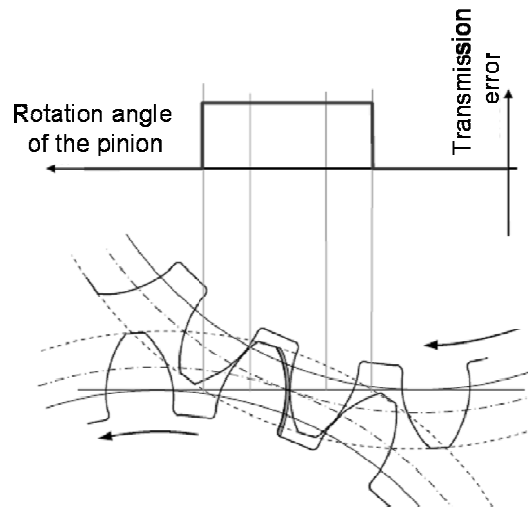
To illustrate the specification uncertainties, the following example can be used: the AGMA 2009-B01 notes that “Measurements for determining single pitch variation, cumulative pitch variation, and index variation are made at the tolerance diameter, relative to the gear datum axis of rotation, tangent to the tolerance diameter in the plane of rotation”. The tolerance diameter,  $d_t$ , is “the diameter where the mean cone distance  $R_m$  and the midpoint of the working depth intersect”. Furthermore, “ $R_m$  is the distance from the apex of the pitch cone to the middle of the face width”. But how to obtain the middle point of the face width is not explained: is it taken from a randomly chosen tooth? Is it a mean of all teeth? How is the middle of the face width calculated? And what is the metrology strategy to obtain it? In this case, the specification is ambiguous. It characterizes the specification uncertainties. Figure 28.2 represents the tolerance diameter according to [ANS 05].



**Figure 28.2.** *Tolerance diameter*

Correlation uncertainties characterize the fact that the intended functionality and the controlled characteristics may not be perfectly correlated. In the case of gears, the deviations of the geometry impact the transmission error (difference between the

theoretical and real instantaneous angle of rotation of the wheel). For example, a pitch error will lead to a step on the transmission error (Figure 28.3)



**Figure 28.3.** Influence of pitch error on the transmission error [BAU08]

In practice, the designer limits the pitch error in order to limit the transmission error. Indeed, even if the relative variations of real gear ratio are minor, induced accelerations are not negligible and an angular velocity jump must be avoided in order to reduce noise level and vibrations [DRI 01]. Unfortunately there is no explicit relation between the transmission error, and the geometric deviations (like pitch errors, runouts, form deviations, etc.). In this case there exist correlation uncertainties between the deviations and the transmission error or the kinematic characteristics.

Different specification models can be defined to express the pitch error (between two points as defined in the AGMA 2009-B01, or between two fitted features, using association criteria for example). The pitch error estimated using the two points strategy is based on the angle made by points taken on two flanks, around the axis of rotation of the measured gear. In the case of pitch error estimation between two fitted features, ideal features are associated with measured flanks [BOU 07] using a fitting criterion, and only the angle of rotation around the hole axis is free of movement. This is a simple decomposition [PFE 01].

This chapter focuses on the comparison of specification models and inspection strategies regarding functional conformity assessment in order to quantify and qualify the correlation between kinematic characteristics based on mathematical

models established with virtual metrology, and the kinematic characteristics from “real” geometry.

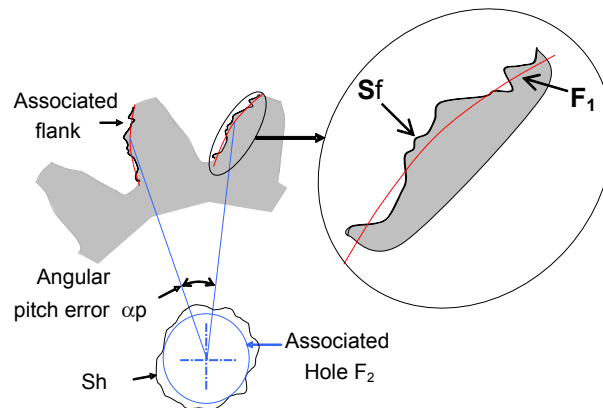
First, the different specification models used to perform the comparison will be detailed, then the method followed to perform this comparison will be detailed and finally the results will be discussed.

## 28.2. Specification models

The objective of this section is to present the specification model used to perform the comparison between different association criteria and metrology strategies. In our case, the specification model focuses on the deviation between flanks: the pitch errors.

Based on Geospelling [MAT 03], a specification is a condition on a characteristic defined from geometric features created from a skin model. Therefore, the pitch errors can be defined between two features, using different fitting criteria and metrology strategies.

Figure 28.4 expresses the pitch error when its specification is based on two fitted features:



**Figure 28.4.** *Features and characteristics*

Table 28.1 shows the geospelling expression [DAN 07] for specification of the pitch error. To associate the ideal feature  $F_1$  with  $S_f$ , the non-ideal feature, which is nominally a spherical involute (obtained by an operation of Partition), the following association criterion are used:

- The most common is the least squares criterion (or L2 norm). This criterion minimizes the sum of the square distance of the measured points to the surface. The great advantage of this criterion is its robustness and its stability to the presence of an aberrant point.
- The minimax criterion (or  $L^\infty$  Norm) minimizes the maximum distance of the measured points to the fitted feature.
- The Chebychev criterion minimizes the maximum distance of the measured points to the fitted feature that is tangent and outside the matter.

Definition of the non-ideal surface $Sh$
<b>Partition</b> $Sh$ , non-ideal feature, nominally type cylinder
Definition of the associated hole $F_2$
<b>Association</b> $F_2$ , ideal feature, type Cylinder. <u>Constraints</u> : Minimum signed distance ( $Sh, F_2$ ) $\geq 0$ <u>Objective to maximize</u> : diameter of $F_2$
Definition of the non ideal surface $Sf$
<b>Partition</b> $Sf$ , non-ideal feature, nominally type spherical involute
Definition of the associated spherical involute $F_1$
<b>Association</b> $F_1$ , ideal feature, type spherical involute <u>Constraints</u> : Coaxiality between $F_2$ and the axis of $F_1$ <u>Objective to minimize</u> : depends on the association criterion
Definition of the toleranced characteristic $\alpha_p$ :
<b>Evaluation</b> $\alpha_p$ : angle between two flanks, around $F_2$ axis.
Definition of the condition:
$\alpha_{inf} \leq \alpha_p \leq \alpha_{sup}$

Table 28.1. Geospeiling expression of a pitch error based on two features

### 28.3. Comparison method

Each specification model provides different geometric features therefore they are compared to evaluate which one is the most relevant regarding the functional aspect. The following section details the approach followed for comparison.

#### 28.3.1. Global approach

The objective of this part is to present the proposed approach used to estimate the comparison between the different association criteria, regarding to the functional aspect. The functional characteristics are the maximum range of the transmission error and the tooth-to-tooth composite deviation (this approach could be applied to

the backlash). To do so, an estimated transmission error based on a substitution model that tries to reflect the real geometry is compared to an estimated transmission error based on the virtual metrology, using association criteria for functional surfaces. Figure 28.5 shows the global approach.

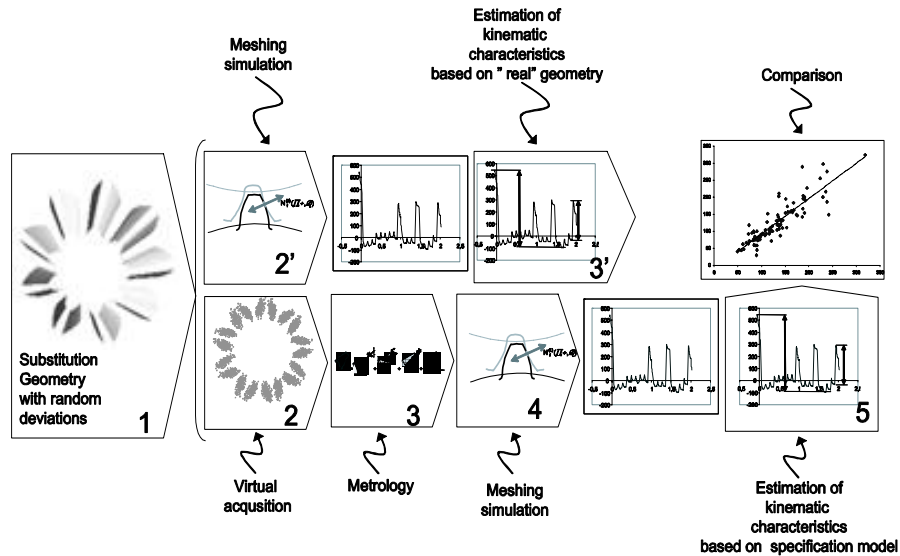


Figure 28.5. Proposed approach for the comparison of fitting criteria

1. In the first step, substitution geometry with random deviations is generated. The substitution model is an image of a real gear. This geometry is a set of analytic polynomial surfaces: smooth Bezier surfaces. Analytic surfaces are required to apply the tooth contact analysis to simulate the meshing.

2. A virtual acquisition of the substitution model is performed. Each Bezier surface is discretized into a set of equidistant points.

3. The virtual metrology of the set of points obtained in step 2 is performed. Deviations between the hole and the teeth are calculated. The pitch errors are estimated for each fitting criterion. A mathematical model based on the metrology is created.

2' & 4. The meshing is simulated using the Tooth Contact Analysis (TCA) program and leads to an estimation of the transmission error.

3' & 5. Kinematic characteristics are evaluated. These characteristics are the maximum transmission range error, and the tooth-to-tooth composite deviation. The maximum transmission range error is the amplitude of the transmission error during

more than one revolution of the studied gear. The tooth-to-tooth composite deviation is the greatest amplitude of the transmission occurring within the duration of a one-tooth meshing.

To finish, a Monte Carlo simulation reiterates all the steps from one to six, and for each studied criterion, a set of characteristics is obtained.

### 28.3.2. Geometric modeling

To simulate the meshing, TCA is used. TCA requires a mathematical expression of the tooth surfaces. These surfaces include geometric deviations and parameters such as the rotational angle of the pinion and the wheel. The geometric deviations can be introduced using vectorial dimensioning and tolerancing (VD&T) strategy. The principle of VD&T is based on the concept of substitute surfaces. A substitute feature is an imaginary geometric ideal surface which is represented by a parametric vector.

#### 28.3.2.1. Substitution model (step 1)

The substitute tooth surface  $\Sigma_i$  is described by its parametric model in the local coordinate system as a function of two parameters ( $u_1, v_1$ ) or ( $u_2, v_2$ ) in a certain closed interval. The position vectors of tooth surface  $\Sigma_i$  of pinion 1 and wheel 2 are denoted as  $R_k^{(i)}$  for part (i) in the coordinate system “k”. Rotation parameters are introduced by changing the orientation of the coordinate system in the global system Sf. In this system, the surfaces depend on their description parameters  $u_i, v_i$  and the rotational angle  $\Phi_i$ .

#### 28.3.2.2. Geometric model based on metrology (step 3)

The geometric model based on metrology is only built for the pinion. The metrology performed in step 3 provides an estimation of the pitch error. The deviations between the hole and the teeth are introduced by changing the local coordinate system of the teeth ( $S_t$ ) to the coordinate system of the hole ( $S_h$ ). Mht is the homogenous coordinate transform matrix from  $S_t$  to  $S_h$ . Pitch errors are introduced for each tooth by performing a rotation of the tooth around the axe of the hole. The surface in the global coordinate system for the pinion, for this model, is denoted by:

$$Rm_f^{(i)}(u_1, v_1, \Phi_1) = M_{fh} \cdot M_m \cdot Rn^{(i)}(u_1, v_1)$$

$Rn^{(i)}(u_1, v_1)$  is the nominal rigid surface of the pinion tooth.

### 28.3.3. Virtual meshing simulation

The aim of TCA (step 2' and 4) is to obtain the real gear ratio at the mean contact point during the meshing, contact path, orientation and size of contact ellipse [LIT 06]. Only real gear ratio is evaluated in this study. If the teeth surfaces and the relative positions are perfect, the instantaneous gear ratio would be constant. Due to misalignment and parts deviations, this instantaneous kinematic relationship is changing [BRU 07].

The most difficult in TCA is to solve a system of non-linear equations that translate the contact between the two surfaces. When the position of contact points are known, it is easy to determine the real gear ratio and transmission error, the contact paths on the gear tooth surfaces.

During the meshing, the two surfaces in contact are tangential and the necessary and sufficient conditions for this situation are well known:

$$\left\{ \begin{array}{l} R_f^{(1)}(u_1, v_1, \Phi_1) = R_f^{(2)}(u_2, v_2, \Phi_2) \\ n_f^{(1)}(u_1, v_1, \Phi_1) = c \cdot n_f^{(2)}(u_2, v_2, \Phi_2) \\ (u_1, v_1) \in [0, 1]^2 \\ (u_2, v_2) \in [0, 1]^2 \\ (\Phi_1, \Phi_2) \in R^2 \\ c \in R \end{array} \right. \quad [28.1]$$

with  $n_f^{(1)}$  and  $n_f^{(2)}$ , the surface normal vector. This system has 6 equations with 6 unknowns.

In some cases, the contact point can reach the boundary of one surface. The meshing goes on with the contact point staying on a surface boundary. In this case, the surface normal is not defined and system [28.1] is not valid. It is necessary to replace the normal equation with another. Assume the contact point is on line  $L_{ulf}^{(1)}$  defined in  $S_f$ :

$$\begin{aligned} L_{ulf}^{(1)}(v_1, \Phi_1) &= R_f^{(1)}(u_1^*, v_1, \Phi_1) \\ v_1 &\in [0, 1]; u_1^* \text{ fixed} \end{aligned}$$

So, when the contact occurs on  $L_{ulf}^{(1)}$ , the tangent of  $L_{ulf}^{(1)}$  at this point is perpendicular to  $n_f^{(2)}$ . Then, the new equation is:

$$\frac{\partial R_f^{(1),j}(u_1^*, v_1, \phi_1)}{\partial u_1^*} \cdot n_f^{(2),k}(u_2, v_2, \phi_2) = 0$$

The new equations of meshing are in this case:

$$\left\{ \begin{array}{l} R_f^{(1)}(u_1^*, v_1, \phi_1) = R_f^{(2)}(u_2, v_2, \phi_2) \\ \frac{\partial R_f^{(1)}(u_1^*, v_1, \phi_1)}{\partial u_1^*} \cdot n_f^{(2)}(u_2, v_2, \phi_2) = 0 \\ v_1 \in [0, 1] \\ (u_2, v_2) \in [0, 1]^2 \\ (\phi_1, \phi_2) \in R \\ u_1^* \text{ fixed} \end{array} \right. \quad [28.2]$$

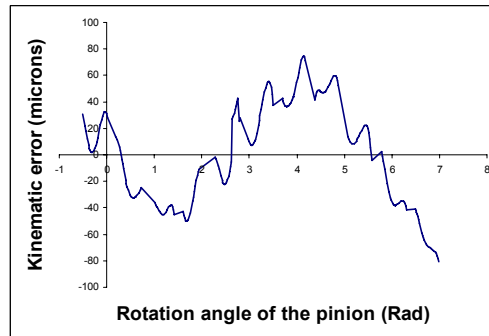
The system of equations for meshing is known [28.2] and the tooth contact analysis is undertaken to determine  $\Phi_2$ ,  $u_1$ ,  $v_1$ ,  $u_2$  and  $v_2$  as a function of  $\Phi_1$ . This mathematical problem does not have an explicit solution in the general case. We may only have an approximate numerical solution. With this aim, the following method is used:

- Choose a series of values for  $\Phi_1$ .
- For each value of  $\Phi_1$ , solve the system of equations [28.1]: 6 scalar equations and 6 unknowns,  $j$  and  $k$  are known.
- If one of the parameters  $\{u_1, v_1, u_2, v_2\}$  is not in its validity domain, a new equations system like [28.2] (4 scalar equations and 4 unknowns) must be solved.
- Analyze the instantaneous kinematics error, paths of contact, etc.

To find the zeroes of non-linear system, several numerical methods exist. The most famous of them is the Newton Raphson algorithm. This method consists of linearizing the system at the value approached to the zero of the system. This method gives a recurrent relation that requires the calculation of the Jacobian matrix of the system. This method generally offers a good convergence, but is not the fastest. Indeed the Jacobian is more time-consuming because the system is complex. Levenberg-Marquardt Optimization is a virtual standard in nonlinear optimization which significantly outperforms gradient descent and conjugate gradient methods for medium sized problems. It is a pseudo-second order method which means that it works with only function evaluations and gradient information but it estimates the Hessian matrix using the sum of outer products of the gradients. Thereby the square of the system norm is minimized.



In this study, Levenberg-Marquardt algorithm offers an average residual of  $8 \times 10^{-27}$ . Figure 28.6 shows a simulated kinematic of an ISO class 10 bevel gear with random deviations.



**Figure 28.6.** *A simulated kinematic error*

#### **28.3.4. Virtual metrology**

In this section, the methods used to build the geometric model at step 3 are described.

##### *28.3.4.1. Geometric model of metrology*

The result of gear metrology is the estimation of values of characteristics identified in AGMA 2009-B01. In our study only the pitch errors are taken into account.

The metrology strategy is similar to the Geospeeling expression of pitch error (Table 28.2).

##### *28.3.4.2. Estimation of deviations between the flanks*

The deviation between nominal flank and measured flank can be characterized by the angle made between the measured flank, and the nominal flank, around the axis of rotation of the hole. To estimate this angle, the nominal set of points of the considered flank is fitted to the virtually measured corresponding flank, considering one degree of freedom: the angle around the hole rotation axe.

The association criteria cited in section 8.2 are used to fit the nominal set of points of active tooth surface to a measured set of points. The metrology strategy proposed by the AGMA 2009-B1 Standard (evaluation of the pitch error with point taken on the flanks) is implemented too.

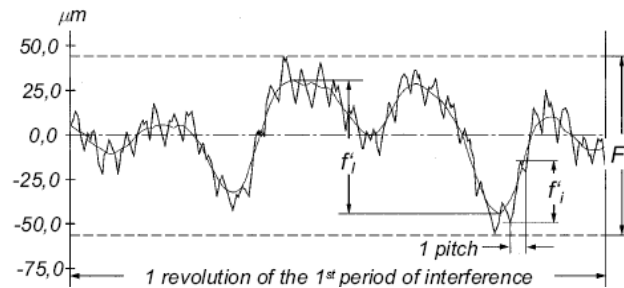
Definition of a set of points {Sh}
<b>Extraction</b> {Sh}, set of points, nominally cylinder type
Definition of the associated hole $F_2$
<b>Association</b> $F_2$ , ideal feature, type Cylinder. <u>Constraints</u> : Minimum signed distance ( $\{Sh\}, F_2 \geq 0$ ) <u>Objective to maximize</u> : diameter of $F_2$
Definition of a set of points {Sf}
<b>Extraction</b> {Sf}, set of points, nominally spherical involute type
Definition of the associated spherical involute $F_1$
<b>Association</b> $F_1$ , ideal feature, spherical involute type <u>Constraints</u> : Coaxiality between $F_2$ and the axis of $F_1$ <u>Objective to minimize</u> : depends on the association criterion
Definition of the tolerated characteristic $\alpha_p$ :
<b>Evaluation</b> $\alpha_p$ : angle between two flanks, around $F_2$ axis.
Definition of the condition:
$\alpha_{inf} \leq \alpha_p \leq \alpha_{sup}$

**Table 28.2.** Measurement process of a pitch error base on two features

### 28.3.5. Evaluation of the kinematic characteristics

Kinematic metrology includes two inspection methods: tangential composite and radial composite inspection [GOC 03]. Tangential composite inspection allows determining transmission error of the product, gear are mounted in the roll testing machine with backlash, under desired condition, and only right or lefts flank are engaged during the meshing. Radial composite inspection shows the changes in the center distance or the rotating gears. Gears are mounted in the roll testing machine without backlash at a variable center distance. Flanks, left and right of the gears are in contact by dint of force acting in the radial direction. The tangential composite inspection (also called single flank gear roll testing) closely simulates the behavior of the product in their application, whereas the radial composite inspection (also called double flank gear roll testing) only reflects the changes in the centre distance of the rotating gear, that is why, if the function of the product must be tested, the tangential composite inspection will be performed. Figure 28.7 shows an example of a transmission error from a single flank roll testing.

In order to compare fitting criteria regarding the functional aspect, the maximum transmission range error and the tooth-to-tooth composite deviations are evaluated for each model and compared to those obtained with the substitution model.



**Figure 28.7.** Kinematic error from a tangential composite inspection [GOC 03]

## 28.4. Criteria comparison

### 28.4.1. Objective

The objective of this section is to compare the three used criteria and the one point approach regarding the functional aspect, i.e. the kinematic characteristics: the maximum transmission range error and the tooth-to-tooth composite deviation.

In the study presented three quality class gears have been tested: ISO quality 10, 7 and 4 [ISO 95]. For each class, 100 geometries have been generated and simulated: a Monte Carlo simulation reiterates steps 1, 2, 3, 4, 5, 2', 3'. A set of values for the maximum transmission range error and the tooth-to-tooth composite deviation is thus obtained. Furthermore, information is provided to perform the comparison. For each criterion, each class and each studied kinematic characteristic is calculated:

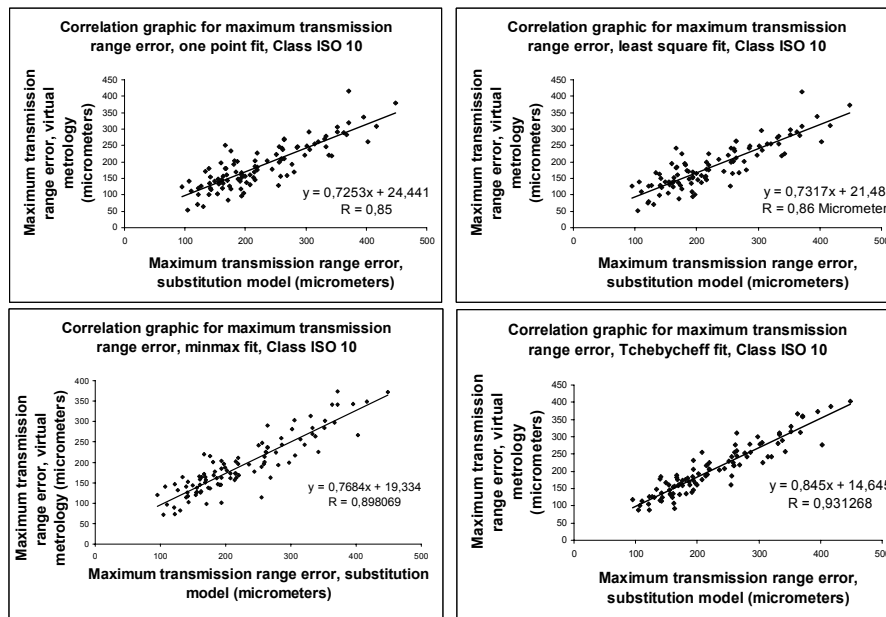
- The linear regression: the equation of the linear regression shows the trend of the correlation.
- The confidence intervals of the estimated slope and Y-intercept of the linear regression: enables us to affirm that the exposed values are contained into an interval by taking a risk of 5% in our case. This allows us to validate the results.
- The linear correlation coefficient  $r$  provides information about the quality of the correlation.

### 28.4.2. Example

The following example shows the result of 100 simulations performed on an ISO class 10 gears for each association criterion. The studied kinematic characteristic is

the maximum range of the transmission error. Figure 28.8 shows the correlation graphics.

The linear regression is obtained by fitting the data points using the least square method. The correlation coefficient shows a good correlation between the maximum transmission range error based on the substitution model and the one based on the virtual metrology for each case.



**Figure 28.8.** Class 10 gears correlation graphics for maximum transmission range error

#### 28.4.3. Comparing the results

This section shows the results obtained for each criterion performed on ISO class 10, 7 and 4 gears. For each criterion and for each characteristic, 100 simulations have been performed, that is, 2,400 simulations. The obtained results are regrouped in Table 28.3.

The table shows that:

- for both studied characteristics, and for all class qualities, the same trend is observed: the Chebychev criterion offers the best correlation between a virtual metrology model and a substitution model regarding the functional aspect. The

worst correlation is given by the one point fit. The least square criterion is close to the one point criterion regarding to the correlation, and the minmax criterion offers the second best correlation after Chebyshev criterion;

– the better the quality is, the less the correlation is because the ratio “pitch error tolerance/form deviation tolerance” increases when the quality is better.

Kinematic characteristic	ISO class	Estimated parameter	Fitting criterion			
			One point	Least Square	Minmax	Chebyshev
Maximum transmission range error	10	Linear regression	0.72x+24.44	0.73x+21.49	0.77x+19.33	0.84x+16.64
		Correlation coefficient	0.85	0.86	0.9	0.93
		Confidence interval of the slope	0.01	0.01	0.01	0.01
		Confidence interval of the Y-intercept	25.8	25.75	22.18	14.62
	7	Linear regression	0.56x+28.19	0.57x+26.73	0.60x+24.65	1.03x-11.53
		Correlation coefficient	0.75	0.77	0.85	0.88
		Confidence interval of the slope	0.01	0.01	0.01	0.02
		Confidence interval of the Y-intercept	17.71	17.62	15.38	9.69
	4	Linear regression	0.39x+32.11	0.39x+30.9	0.53x+22.9	0.76x+12.9
		Correlation coefficient	0.5	0.51	0.69	0.77
		Confidence interval of the slope	0.01	0.01	0.02	0.02
		Confidence interval of the Y-intercept	16.83	17.24	14.11	11.57
	All	Linear regression	0.77x+3.80	0.77x+2.51	0.80x+2.43	0.89x+3.60
		Correlation coefficient	0.89	0.9	0.93	0.94
		Confidence interval of the slope	0.01	0.01	0.01	0.01
		Confidence interval of the Y-intercept	8.77	8.78	7.49	5.82
Tooth-to-tooth composite deviation	10	Linear regression	0.40x+23	0.38x+23.79	0.38x+25.26	0.57x+17.21
		Correlation coefficient	0.45	0.43	0.43	0.57
		Confidence interval of the slope	0.09	0.08	0.08	0.08
		Confidence interval of the Y-intercept	3	2.97	2.94	2.79
	7	Linear regression	0.52x+9.83	0.51x+10.04	0.53x+10.36	0.81x+2.33
		Correlation coefficient	0.55	0.54	0.55	0.66
		Confidence interval of the slope	0.19	0.19	0.18	0.18
		Confidence interval of the Y-intercept	2.09	2.08	2.07	2.12
	4	Linear regression	0.44x+8.46	0.44x+8.36	0.44x+9.53	0.64x+4.81
		Correlation coefficient	0.41	0.41	0.4	0.53
		Confidence interval of the slope	0.28	0.28	0.29	0.3
		Confidence interval of the Y-intercept	2.2	2.21	2.15	2.05
	All	Linear regression	0.45x+9.47	0.53x+9.90	0.54x+10.80	0.72x+5.89
		Correlation coefficient	0.59	0.58	0.58	0.67
		Confidence interval of the slope	0.31	0.21	0.21	0.21
		Confidence interval of the Y-intercept	1.26	1.26	1.23	1.2

**Table 28.3.** Results of the criteria comparison

## 28.5. Conclusion

A comparison of different fitting criteria was performed, regarding the functional aspect of gears.

Two kinematic characteristics were evaluated by simulating the meshing with two different models: the substitution model built with smooth Bezier surfaces and the virtual metrology model built with a nominal surface fitted to the set of points from the metrology, using the one point fit, the least squares fit, the minmax fit and the Chebychev fit.

After having performed the simulation it appears that:

- the Chebychev fit offers the best correlation with the substitution model, contrary to the one point fit;
- the estimated characteristics are all under evaluated and the better the quality class, the more the estimated characteristics are under-evaluated;
- if a classification is done, regarding the functional aspects, for the best to the worst fitting criteria, we obtain: the Chebychev fitting, the Minmax fitting, the LSQ fitting and the one point fitting.

This proposition is a natural consequence of taking an integrated view of functionality, specification and verification. Srinivasan said: “Correlation uncertainty, in particular, is an uncharted territory. Standards don’t tell us how to find this. They provide a language to describe it. This should be an area for some intense research” [SRI 01]. In fact, this opens up a wide area for research.

## 28.6. Bibliography

- [ANS 05] ANSI/AGMA 2009-B01, Bevel Gear Classification, Tolerances, and Measuring Methods, 2005.
- [BAU 08] BAUDOUIN C., BIGOT R., LELEU S. and MARTIN P., “Gear geometric control software: approach by entities”, *International Journal of Advanced Manufacturing Technology*, Vol 38, p. 120-129, 2008.
- [BOU 07] BOUKEBBAB S., BOUCHENITFA H., BOUGHOUAS H. and LINARES J.M., “Applied iterative closest point algorithm to automated inspection of gear box tooth”, *Computers & Industrial Engineering*, Vol. 52, p. 162-173, 2007.
- [BRU 07] BRUYERE J., DANTAN J.Y., BIGOT R. and MARTIN P., “Statistical tolerance analysis of bevel gear by Tooth Contact Analysis and Monte Carlo Simulation”, *Mechanism and Machine Theory*, Vol. 42, No. 10, p. 1326-1351, 2007.
- [DAN 07] DANTAN J.Y., BRUYERE J., BAUDOUIN C. and MATHIEU L., “Geometric specification for gear-Expression, metrology and analysis”, *CIRP Annals, Manufacturing Technology*, Vol. 56, No. 1, p. 517-520, 2007.
- [DRI 01] DRIOT N., RIGAUD E., SABOT J. and LIAUDET-PIERRET J., “Allocation of gear tolerances to minimize gearbox noise variability”, *Acta-acustica*, Vol. 87, p. 67-76, 2001.

- [GUE 06] GUENTHER A., "Evaluation of runout deviation at bevel gears based on pitch measurements", *CIRP Annals*, Vol. 55, No. 1, p. 539-542, 2006.
- [GOC 03] GOCH G., "Gear metrology, keynote papers", *CIRP Annals*, Vol.52, p. 1–37, 2003.
- [ISO 95] ISO 1328-1, Engrenages cylindriques-Système ISO de précision, Partie 1: Définitions et valeurs admissibles des écarts pour les flancs homologues de la denture, 1995.
- [LIT 06] LITVIN F.L., FUENTES A. and HAYASAKA K., "Design, manufacture, stress analysis, and experimental tests of low-noise high endurance spiral bevel gears", *Mechanism and Machine Theory*, Vol. 41, p. 83-118, 2006.
- [MAT 03] MATHIEU L. and BALLU A., "GeoSpelling: a common language for specification and verification to express method uncertainty", *Proc. of 8th CIRP Seminar on Computer Aided Tolerancing*, North Carolina, USA, 2003.
- [PFE 01] PFEIFER T., KUROKAWA S. and MEYER S., "Derivation of parameters of global form deviations for 3-dimensional surfaces in actual manufacturing processes", *Measurement*, Vol. 29/3/01, p. 179-200, 2001.
- [SRI 01] SRINIVASSAN V., "An integrated view of geometric product specification and verification", *CIRP Seminar on Computer Aided Tolerancing*, France, 2001.

## Chapter 29

# Effects of Geometric Variation on Perceived Quality

### 29.1. Introduction

One purpose of striving for high geometric quality in consumer products is to ensure that the relationships between visible parts will not impact negatively on the consumer's quality perception. The consequences of visible deviations on perceived quality depend on the product's visual robustness to geometric variation. In this paper, visual robustness is defined in relation to research on consumer response to product appearance. A framework for visual robustness is presented, and a method for evaluating the fit complexity of design concepts is suggested.

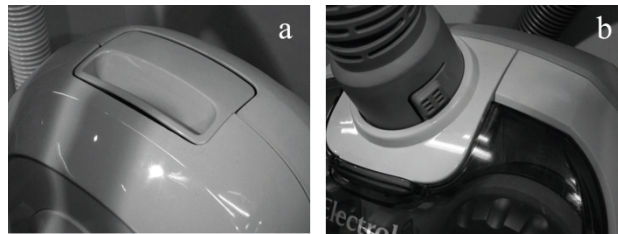
When analyzing certain assemblies, it becomes clear that product appearance have set a high level of difficulty for achieving visually acceptable relationships between parts. This visual robustness to geometric variation (Figure 29.1) is regarded here as product behavior that does not depend on the risks for large assembly variation in terms of tolerances or geometric robustness; rather it depends on something intrinsic in the structure, form, colors and materials of visible parts. Virtual non-nominal visualization tools [WIC 03, JUS 01] have enabled the early detection of visually sensitive design solutions. However, these tools do not help in the analysis of what makes a specific product appearance visually sensitive to variation. If tolerances and geometric robustness are set, the appearance may need adjustment in order for the end result to be acceptable. In the development of consumer products, product appearance is normally the responsibility of industrial

---

Chapter written by Karin FORSLUND and Rikard SÖDERBERG.



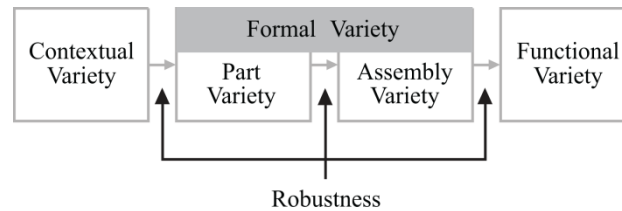
designers and is developed in an early design phase. Within industrial design research, little attention has been given to the effects of variation, and it is not a central concern in industrial design activities. Here we take a close look at the concept of visual robustness in order to promote the creation of robust appearance solutions in industrial design. As visual robustness here is defined as independent of the detailed risks for deviations, it is suggested that product appearance can be evaluated before locating schemes are determined or tolerances defined. Apart from in industrial design activities, visual robustness is relevant during various tasks throughout the product lifecycle. A satisfactory assessment is needed when determining critical product dimensions (i.e. key characteristics), establishing their requirements level and defining priorities between these requirements, which serves as relevant input for assembly robustness optimization.



**Figure 29.1.** *Visually sensitive (a) and robust (b) solution*

#### **29.1.1. Types of robustness**

From a general perspective, robustness [TAG 89] aims at “improving the quality of a product by minimizing the effect of the causes of variation without eliminating the causes” [PHA 89]. This implies that a product’s functions and properties should not be sensitive to variation caused by noise factors. However, as implied in [SMI 05] robustness efforts can have different foci depending on what are regarded as control factors and noise factors in a specific design task. In Figure 29.2, the link between contextual variety, formal variety and functional variety is illustrated. The relationship between contextual and part variety is exemplified in [PHA 89], where the dimensional variation of tiles, burnt in a kiln with uneven temperature distribution, is reduced by increasing the lime content in the tile clay. The assembly robustness to part variation is improved in CAT tools when optimizing locating schemes and decreasing assembly coupledness [SÖD 99]. Any efforts to improve robustness by reducing the amount of critical dimensions or making functions and properties less dependent on any precise dimensions concern the relationship between formal and functional variety.



**Figure 29.2.** *Different foci of robustness, based on [SMI 05]*

### 29.1.2. *The product experience*

Set in a context of human-product interaction, the product communicative functions and perceived properties depend on the subjective product experience. The product experience has been defined as “the entire set of effects that is elicited by the interaction between a user and a product”, and is often classified as aesthetic pleasure, attribution of meaning and emotional response [HEK 06]. Visual robustness can be regarded as the ability of a product’s visual appearance to stimulate the same visual product experiences despite small variety in its visual design properties. Though the product experience is a subjective phenomenon and visual appearance does not in a strict mathematical sense cause a consumer response, designers still have intent with the product appearance and aim for it to be experienced in a certain way [CRI 08]. It is in relation to this intent that the effects of variation need to be investigated.

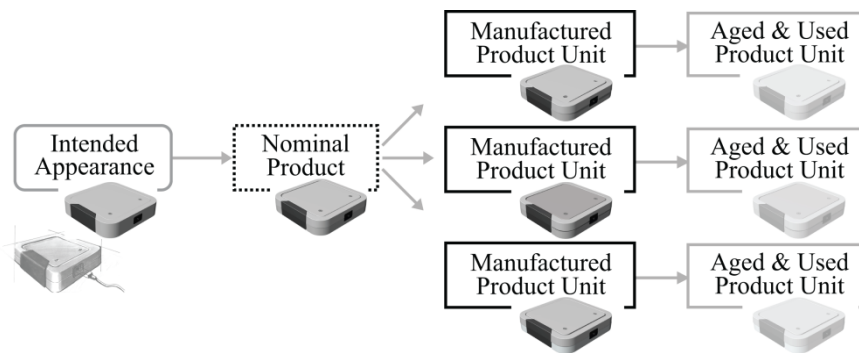
Generally, visual robustness refers to a functional insensitivity to variation in any of the visual design properties (“structure”, “form”, “color”, “gloss” and “texture” [FOR 07]), stemming from any type of noise factors. In the following section, the focus is on visual robustness to geometric manufacturing variation. In this, the visual aspects affected by variation are studied separately from any functional or assembly aspects influenced by variation.

### 29.1.3. *Perceived quality of non-nominal products*

In order to study visual robustness, the way in which the product experience is affected by non-nominality is of interest. In this, an assumption is made that the nominal concept is always more attractive than any non-nominal manufactured unit. This suggests that all visible dimensions follow the nominal-the-best criterion. To perceive a geometric deviation from the nominal form, a consumer (defined here as a person without insight into the product specification, design intent or design history) needs to interpret the geometric intent as well as the deviation from it. As

consumer products are very seldom accompanied by a detailed geometric specification, consumers infer their own specifications.

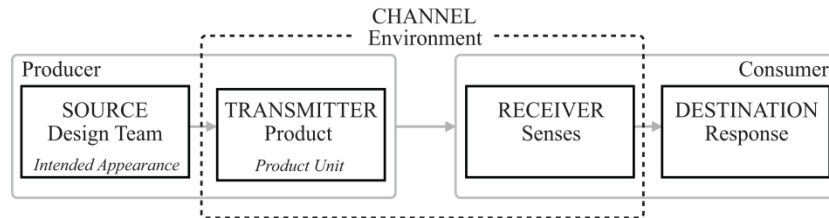
In this context, it is important to separate the intended design message (function) from the detailed intended geometry (form), which is the carrier of the design message. Inferences on deviations from intent (Figure 29.3) can occur when it is clear that the nominal product was not the initially intended appearance (for instance when unsightly elements such as screws or fasteners are visible) or when it is clear that a manufactured unit deviates from the nominal product (i.e. product specification). Here, the concept of visual robustness is relevant. The suggestion is that the details often associated with poor “quality appearance” or “craftsmanship” (see for instance [WAN 00, HOS 04, MCL 05]), could be made acceptable if they were emphasized or well-integrated in the overall design, as for instance when putting Allen screws on a fuel cap. It is the “lack of intent” that causes a poor quality impression.



**Figure 29.3.** *Intent distortion throughout the product lifecycle*

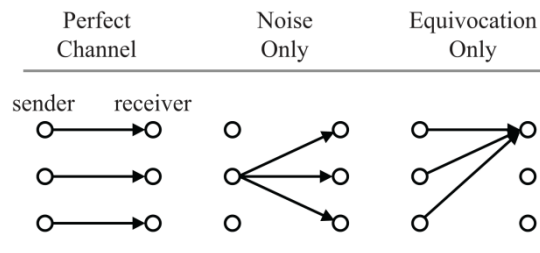
#### **29.1.4. Design as a process of communication**

The relationship between design intent and consumer response can be seen as a process of communication (Figure 29.4) [CRI 08, MON 97, CRI 04]. The idea is based on Shannon’s basic communication model from 1948 [SHA 48]. Within information theory, noise occurs when a sender cannot be certain about how a message will be received [KRI 86] and each step in the communication process is a possible noise source. When the model was applied to product design (a form of mass-communication [CRI 04]), the original purpose was to point out that an intended visual product message should be created to support varying circumstances during the communication process. When connecting this model to visual robustness, its significance is somewhat altered.



**Figure 29.4.** *Design as a process of communication*

If manufacturing noise occurs between the intended appearance and a transmitting product, the noise from the later steps of communication is beneficial in hiding these distortions. This communication noise should ideally result in equivocation (Figure 29.5). Equivocation occurs when a receiver is unable to differentiate between two or more messages sent [KRI 86]. The model of design as a process of communication is used here as an underlying structure for describing visual robustness.



**Figure 29.5.** *Noise and equivocation*

## 29.2. A framework for describing visual robustness to geometric variation

The experience of a geometric deviation is a complicated process of sensation, perception, cognition and emotion. It depends on product properties, the consumers' personal characteristics and environmental parameters. This situation has been divided into four levels:

- *The visual reference level* is sense-independent and product-focused and describes the type and amount of recognizable shapes and relations between shapes. Given that there are visual references to be recognized, the provided information can be intensified or suppressed at the subsequent levels.

– *The optical level* is sense-dependent and relates to the interplay between the product's optical properties, light and eye receptors. It describes the risk for an observer receiving sensory information on deviations from geometric intent.

– *The perceptual level* refers to the tendency of the human perceptual senses to amplify, i.e. perceive clearly, or suppress sensory information on deviations from geometric intent.

– *The response level* assumes that the human clearly perceives the deviation and makes a judgment thereafter. At the response level, the concept of perceived quality is most relevant, addressing issues such as the consumer's perceived values in relation to expectations and other product attributes.

### 29.2.1. Visual reference level

At this stage, we will look at all shapes of a product and their ability to visually communicate geometric design intent. This occurs if shapes and relationships are present that can be recognized without prior knowledge of the design specification. The visible cues that reveal intent are referred to as *visual references*. The term is chosen for the following reason: in order to recognize something, it is often necessary to have some guidance, either from known concepts or from related information on the product. For separate shapes, some basic regular geometries can be recognized by themselves as being intended. For relationships between shapes or relationships between parts, one form is often required as a reference to recognize the intended, form, size, shape or orientation of the other shape. This implies that the shape structure of a form has numerous relative cross references, but no absolute reference. Robust shapes and relationships are achieved if small deviations in form, size, orientation or translation are unrecognizable. Ultimately, this would be achieved either by avoiding having regularities built into the product or by assuring that the conditions indicated by visual references remain unchanged if subject to deviations.

There are four types of visual references on a product (Figure 29.6). They function differently and reveal different types of geometric deviations. Separate shapes are regarded here as curves undivided by vertices and surfaces undivided by edges. Given this, the following conditions apply for the types of visual references:

– For *separate shapes*, a straight line and a plane are examples of recognizable shapes, while a curve in R3 space (that is neither straight nor circular) or a sculptured surface have no visual references. One difficulty is that the irregular separate shapes insensitive to form variation often result in many visual references to other parts.

- When shapes have *intrapart references* (i.e. recognizable relationships with other elements on the same part), part distortions such as warping, for which the separate form elements are still intact, are revealed.
- Assembly deviations as well as part deviations are revealed through *interpart* references, for which there are no visual references on the parts.
- Finally, deviations can be recognized at the *whole product level* where, for instance, the size of the intended regular distance between two parts (i.e. gap) can be compared to the gap between two other parts.

Parts		Assemblies	
Shapes		Split-line segments	
Separate shapes	Intrapart relationships	Interpart relationships	Whole product level
Straightness Circularity Flatness Cylindricity Conicity Sphericity Profile  Horizontal Vertical	Parallelism Perpendicularity Distance Regularity Symmetry	Parallelism Perpendicularity Distance Regularity Surface Continuity Curvature Continuity	Symmetry Consistency

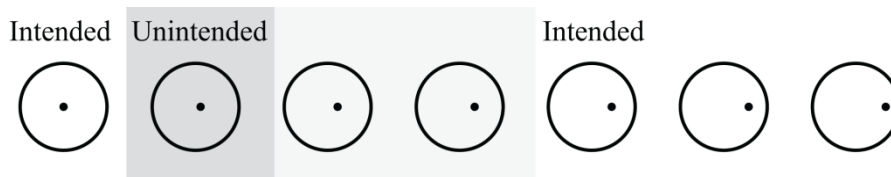
  

Figure 29.6. Types of visual references [FOR 06]

The classification refers to curves or surfaces with an overall level of smoothness and continuity. Local and discrete blemishes, depressions or waviness can be spotted on any of these curves and surfaces. If a mass-produced part nominally had an extremely rough surface corresponding to the magnitude of the blemish, it would be visually robust to the blemish. The detailed risks for different types of deviations, in terms of manufacturing and assembly variation, are regarded as unknown at this stage. Instead, focus is set on the general behavior that shapes could exhibit as a result of variation. If returning to Figure 29.6, there is clearly a greater risk for deviations affecting the inter-part relationships, as they require at least two different manufactured parts with different locating schemes and ingoing part tolerances. In

product design, the prospects of removing visual references between parts are also greater than designing irregularity into the separate shapes. Therefore, the assembly relations will be in focus.

Recognizing visual references is a cognitive process in which the onlooker perceives an object and relates the stimuli to previous knowledge. The extent to which a person will perceive the design intent will vary. When perceiving a relationship between elements, there is a zone in which the relationship is interpreted as unintended. If the relationship between the point and the circle in Figure 29.7 is one of those in the grey zone, it may be interpreted as unintended, even if this is the nominal design. To achieve a good result, the departure from regularity should, in the nominal design, be large enough to look intended, as in the right examples in the figure. Regardless of whether it is nominal, the second circle looks unintended.

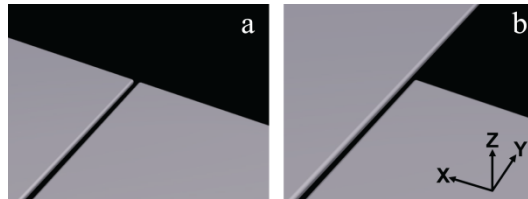


**Figure 29.7.** *Zones for when shapes appear intended*

Why humans tend to see shapes in certain ways has been treated within perception psychology. One branch is the gestalt theory, which treats the inferences people make when perceiving shapes. Human interpretation of artifacts may have both innate and culturally affected components. Here, no attempts will be made to explain *why* people interpret intent through visual references, as this is an extensive question by itself. Although all consumers may not interpret the same visual references, one important purpose of identifying possible visual references is that if there are no visual references, it is not possible to interpret intent. This also implies that visual references are not in fact exclusively visual, but rather comprehensible conditions in geometry. Three examples are provided:

- For the angular relationship between two lines, perpendicularity and parallelism are recognizable states. However, if the nominal angle is  $37^\circ$ , this is impossible to recognize without prior knowledge.
- Figure 29.8a implies that alignment is intended between the two parts in the y-direction. Meanwhile, there is no indication of the intended position for the part in picture a.

– Although large gap sizes for some products are associated with low quality, there is no information on the intended gap if the distance between parts is regular (Figure 29.9), given that there are no secondary effects such as see-through and no references on the whole product level.



**Figure 29.8.** *With (a) and without (b) visual reference*



**Figure 29.9.** *Large intended gap*

Apart from studying visual references with the purpose of removal, the conditions indicated by the visual references constitute the visual information fragments that are to be studied on the optical and perceptual levels of visual robustness.

### 29.2.2. *Optical level*

Some deviations are more visually prominent than others. As described above, optical and perceptual levels address how prominent deviations are when perceived through visual senses. The difference between the optical and perceptual level requires some further explanation. Optical level covers how light beams hit the product, are reflected and meet the eye. Parameters such as illumination, reflections,



shadows, colors, textures and viewing angles are relevant. Perceptual factors have a stronger connection to the perceptual senses, and require a holistic view of the total impression gained when looking at a form. Examples of optical phenomena are that dark parts often hide the distance between parts and that glossy dark parts reveal surface discontinuity (implied continuity between separated parts) better than light matte parts.

One reason to separate optical and perceptual factors is that optical factors are more effectively evaluated in virtual environments, given realism in shaders, rendering type and illumination. Perceptual factors may however not be as adequately evaluated. It has been shown that differences remain between perception in physical and virtual environments [WIC 07]. Although designers use their perceptual senses to form an impression when looking at visualizations, they may not capture the effects that emerge in reality. Further motivations for the separation are that different approaches are needed when conducting research on visual robustness on the optical or the perceptual level or both. If the perceptual sensitivity of deviations on different geometries is studied, the deviations must be equally visible and vice versa.

### **29.2.3. Perception level**

Visual references are recognized through the perceptual organization of visual stimuli, yet that only addresses what could be seen, not what is prominent. On the perceptual level, this prominence is in focus. The perceptual intensity of the cues that reveal deviations could be compared to the probability of someone interpreting something as intended. Perception psychology, including the rules of gestalt interpretation, affects how objects are perceived. In Figure 29.10, the gestalt rule of good continuation is illustrated. The rules of gestalt interpretation can hide deviations as the human perceptual senses do not function like a camera [GRE 07]. Scanning a visual scene is selective. This means that the scene is examined for the information that is required to perform the simulation necessary to form a mental representation of a scene. What is not actively seen is reconstructed to fill in the gap between the scanned areas. Here it is important that geometric deviations do not capture attention. More relevant, however, is the fact that perception of geometric deviations may not reach the conscious level. A product may lead to a feeling of poorness without the user being able to specify why. How to tackle this within research and industry is a concern. By asking potential consumers how they experience a deviation, they become informed of it and may consider things that would otherwise have been left unnoticed. An example of perceptual phenomena is that non-parallelism in geometry with little other visual information may be more prominent than one with more visual references and increased complexity.



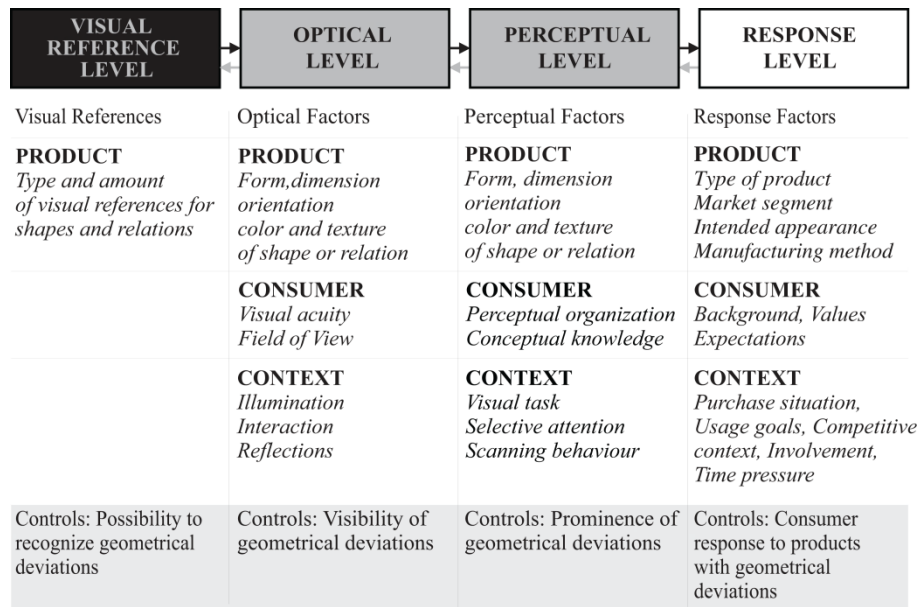
**Figure 29.10.** *Rule of good continuation*

#### **29.2.4. Response level**

Here, a different perspective is embraced. It is not so much about the visibility of a deviation as the aesthetic impression, the meaning conveyed and emotions elicited. For instance, misalignment between two chrome strips on a car is considered as severe, as chrome is supposed to signal exclusivity. Had the parts been made of plastic from start, the intended expression would have been less distorted. Studying visual robustness on the response level (Figure 29.11) has a more strategic ingredient. Questions addressed are, for instance: (1) What overall level of geometric quality is required for a specific industrial design concept or theme? (2) Do product models aimed at different market segments require different levels of geometric quality? (3) How does geometric quality relate to other perceived quality aspects? (4) How does product category affect the required geometric quality? Within the automotive industry, fit and finish aspects have gone from being called “craftsmanship” issues [WAN 00, HOS 04] to “perceived quality” issues. However, perceived quality refers to the consumer’s product judgment from a holistic perspective.

According to Benedict [BEN 90], quality perceptions are formed by intrinsic quality cues that are part of the product itself and extrinsic quality cues in terms of product related information, such as brand, country of origin, price and retailer reputation. The cues are valued because of their perceived connection to quality attributes. The quality attributes are in turn divided into experience attributes, such as comfort, for which feedback is given during consumption and credence attributes, such as durability, which can never really be experienced but remain dependant on the quality cues. No doubt the geometric deviations can serve as intrinsic quality cues. However, intrinsic visual quality cues are not specifically manufacturing issues; rather they are anything visible on the product. Therefore, when as in industry connecting geometric quality issues to perceived quality, there is no exclusive connection between the two. Other issues, such as industrial design in general or visual brand identity might, also affect the perceived quality. From that

perspective, it would be interesting to look at all issues connected to poor product realization to see if they connect to any specific types of consumer responses.



**Figure 29.11.** Levels of visual robustness

### 29.3. Visual fit complexity assessment method

To analyze the visual robustness at the visual reference level, we propose the fit complexity assessment method. This method has been developed in order to support comparisons between form division concepts and the identification of sensitive relationships between adjacent parts. The main principle of the method is to identify the translations, rotations and dimensional scaling for which there are no visual references.

When using the method, each interface between two different adjacent parts is analyzed separately, and a total score is obtained by summarizing the complexity of the interfaces. Additional visible interfaces will always increase complexity substantially. Any geometric assembly connections between parts are at this stage regarded as unknown. Parts are considered to be rigid, and part deviations are simplified as dimensional scaling in three dimensions. Every coordinate system is local and should be placed along the most regular directions of each interface. It is also assumed that the assembly requirements will be met by the current design,

implying that the nominal gaps are interpreted as assigned taking collisions into account.

The complexity of an interface is estimated following the table in Figure 29.12a. For the relationship between two parts, one point is assigned (indicated as “x”) for degrees of freedom or dimensional deviations for which there are visual references.

– For *translations* (T), the positive and negative directions in each interface each result in one point, and three degrees of freedom (DOF) are studied, leading to a total score of six points.

– For *rotations* (R), there are many possible centre points. Instead of assigning a point for each opposite direction of a rotation, which has little relevance regarding visual references, a best case (bc) and a worst case (wc) rotation is studied. For rotations the *best case* means that there exists a centre of rotation through which the relationship with visual references would remain unaffected. In one DOF, the score is therefore one point if the interface supports only a best case rotation and two if all possible rotations are revealed.

– For *dimensional scaling* (D), the best case and worst case deviation modes are also studied. If a part has many visual references to another part in one dimension (for instance through alignment or curvature continuity), it is not possible to later adjust the locating schemes to fix the part with the visual reference and take up the variation in the other end. Therefore, the worst case means that there is no way to fit in dimensionally deviating parts and results in two points, while one point is assigned if it is possible to fit in a deviating part without revealing it. The maximum total score per interface is therefore 18.

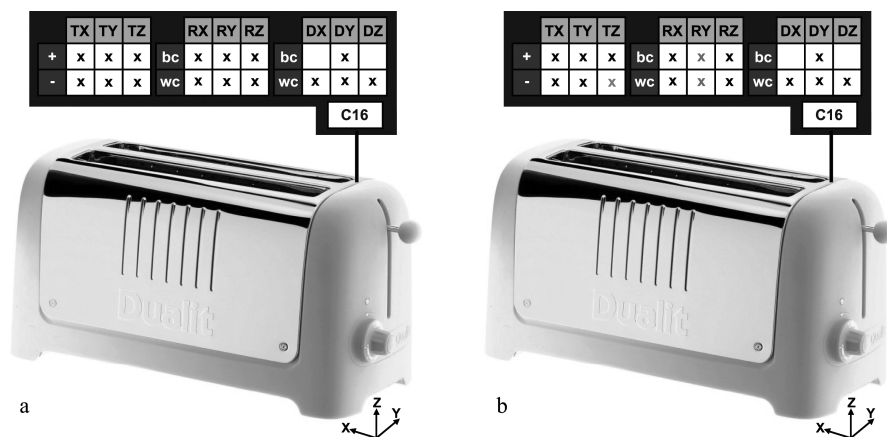














Figure 29.12. Fit complexity assessment for the relationship between parts

When using the method, the main structure of a product is studied, and minor parts not part of the overall form division [DAG 07] concept are ignored, as they could be added or removed independently of the rest of the structure. For the example in Figure 29.12, the inter-part visual references are equal distance between the two parts and surface continuity. There are two allowable deviations in this example: (1) scaling in the x dimension, given the best case, which means that all vertical parts of the interface are equally affected. As the lower horizontal relationship is of a different size, it does not function as a reference for the intended vertical distances, and (2) scaling in the z-direction, given the best case. This means that the surface continuity on the top face is not affected, while the lower horizontal distance can support variation.

*Optical and perceptual factors in relation to fit complexity*

The presented fit complexity tick-box can also be used as a basis to indicate the subjectively assessed most sensitive deviations and more robust deviations, according to conditions given on the other levels of visual robustness. As an example, the lower horizontal parallelism (Figure 29.12.b) is considered to be more sensitive than other deviations. This is due to a combination of being clearly in the field of view (visual level) and belonging to an area with graphics and details that capture attention (perceptual level). As the toaster is clearly targeted at design-conscious consumers, has a styled industrial design, and efforts have been made to ensure a sensory pleasing experience through the selected materials, it can be assumed that conformance to geometric specification is important for the consumer's product experience (response level). A frame of reference is provided in Figure 29.13 in order to compare different structural solutions.

Nº parts	Type	Complexity	Nº parts	Type	Complexity
2		 C2	4		 C53
<hr/>					
		 C16			 C96
3		 C28	6		 C105

**Figure 29.13.** Fit complexity assessment of different toasters

## 29.4. Discussion and conclusions

The framework for visual robustness, including the four levels of analysis, is useful for understanding how to approach perceived quality as connected to geometric deviations. To summarize the relevance of the framework:

- It provides a terminology for and increased understanding of the mechanisms that make products visually robust to variation.
- It serves as a theoretical basis for the design of experiments when conducting research on the visual perception of deviations.

In order to look at visual robustness, some simplifications of the way in which products are influenced by part and assembly variation are necessary. However, this facilitates the evaluation of concepts at a very early stage in product development. Even from a rough industrial design sketch, it is possible to draw some conclusions on its visual robustness.

Still little is known of the mechanisms controlling visibility on the perceptual level. However, the aim here is to clarify that research on the subject should have a clear focus in terms of what levels are studied when doing different types of experiments. What product representations are used, how questions are asked, and how respondents are allowed to interact with the product representation should be studied according to the proposed levels of visual robustness.

The core messages of this chapter are that:

- Communicative product aspects are functions for which robustness can be ensured by looking at the formal-functional relationship. Therefore the visual consequences of variation can be studied separately from detailed risks for variation.
- The concept of intent has a central role in the connection between geometric quality and consumer perceived quality. Intent, and deviations from it, can be recognized both for the intended design message and for the intended geometry.

Finally, the proposed fit complexity assessment method supports robustness evaluation on the visual reference level. One concern is that systematic analyses of this type are time-consuming and slightly complicated. The aim is therefore to continue the research in order to find guidelines for visual product design that are graspable within industrial design practice. In the end, the fit complexity assessment could be computerized. Yet as is the case for many design methods, it is the cognitive process of setting the scores and not the final result that is the core value.

## 29.5. Bibliography

- [BEN 90] BENEDICT J. and STEENKAMPF E.M., "Conceptual model of the quality perception process", *Journal of Business Research*, Vol. 21, p. 309-333, 1990.
- [CRI 04] CRILLY N., MOULTRIE J. and CLARKSON J., "Seeing things: consumer response to the visual domain in product design", *Design Studies*, Vol. 25, No. 6, p.547-577, 2004.
- [CRI 08] CRILLY N., GOOD D., MATRAVERS D. and CLARKSON J., "Design as communication: exploring the validity of relating intention to interpretation", *Design Studies*, Vol. 29, No. 5, p. 425-457, 2008.
- [DAG 07] DAGMAN A. and SÖDERBERG R., "Geometrically Robust Form Division", *Proceedings of the ASME 2007 International Design Engineering Technical Conferences & Computers and Information in Engineering Conference*, Las Vegas, September 4-7, 2007.
- [FOR 06] FORSLUND K., DAGMAN A. and SÖDERBERG R., "Visual Sensitivity: Communicating Poor Quality", *Proceedings of the Design 2006 9th International Design Conference*, Dubrovnik, May 15-18, p. 713-720, 2006.
- [FOR 07] FORSLUND K. and SÖDERBERG R., "Categories of Visual Quality Cues", *Proceedings of the ASME 2007 International Design Engineering Technical Conferences & Computers and Information in Engineering Conference*, Las Vegas, September 4-7 2007.
- [GRE 07] GREGORY R.L., *Eye and Brain - The Psychology of Seeing*, Oxford, Oxford University Press, 2007.
- [HEK 06] HEKKERT P., "Design aesthetics: principles of pleasure in design", *Psychology Science*, Vol. 48, No. 2, p. 157-172, 2006.
- [HOS 04] HOSROY I., PAPALAMBROS P., GONZALES R. and AITKEN T.J., "Modeling Customer Perceptions of Craftsmanship in Vehicle Interior Design", *Proceedings of the 5<sup>th</sup> International Symposium on Tools and Methods of Competitive Engineering*, Lausanne, April 12-16, 2004.
- [JUS 01] JUSTER N.P., FITCHIE M., TAYLOR S., DEW P., MAXFIELD J. and ZHAO J., "Visualizing the impact of tolerances on cosmetic product quality", *Proceedings of the 13<sup>th</sup> International Conference on Engineering Design*, Glasgow, August 21-23, 2001.
- [KRI 86] KRIPPENDORFF K., *Information Theory - Structural Models for Qualitative Data*, Newbury Park, Sage Publications, 1986.
- [MCL 05] MCLOUGHLIN J., "Beauty - Not Just Skin Deep", *Proceedings of The Art of Plastics Design*, Berlin, October 18-19, 2005.
- [MON 97] MONÖ R., *Design for Product Understanding*, Stockholm, Liber, 1997.
- [PHA 89] PHADKE M.S., *Quality Engineering using Robust Design*, Englewood Cliffs, New Jersey, P T R Prentice-Hall Inc., 1989.

- [SHA 48] SHANNON C. E., "A mathematical theory of communication", *The Bell Systems Technical Journal*, Vol. 27, p. 379-423, 1948.
- [SMI 05] SMITH J. and CLARKSON P.J., "A method for assessing the robustness of mechanical designs", *Journal of Engineering Design*, Vol. 19, No. 5, p. 493-509, 2005.
- [SÖD 99] SÖDERBERG R. and LINDKVIST L., "Computer aided assembly robustness evaluation", *Journal of Engineering Design*, Vol. 10, No. 2, p. 168-181, 1999.
- [TAG 89] TAGUCHI G., ELSAYED E.A. and HSIANG T., *Quality engineering in production systems*, Singapore, McGraw-Hill Book Company, 1989.
- [WAN 00] WANG J.H. and HOLDEN J., "Craftsmanship evaluation in automotive products", *International Journal of Industrial Engineering*, Vol. 7, No. 4, p. 286-290, 2000.
- [WIC 03] WICKMAN C. and SÖDERBERG R., "Increased concurrency between styling and design using CAT technology combined with virtual reality", *Journal of Concurrent Engineering: Research and Applications*, Vol. 11, No. 1, p. 7-15, 2003.
- [WIC 07] WICKMAN C. and SÖDERBERG R., "Perception of gap and flush in virtual environments", *Journal of Engineering Design*, Vol. 18, No. 2, p. 175-193, 2007.



## Chapter 30

# Geometric Requirement Variations Throughout the Product Lifecycle

### 30.1. Introduction

Today, design is increasingly widening in scope as additional views of a given product are being taken into account early in the product development process in order to lead to a better integration of marketing, engineering and costs requirements. This has translated as Design for X or DFX where X may be manufacturing (DFM) or assembly (DFA), etc. In a more comprehensive scope, Design should be embraced across the full lifecycle spectrum.

This would translate as additional product requirements reflecting the changing environment to which a product is being subjected throughout its life. In a more comprehensive way, a given functional requirement could have a different value in the lifecycle stage when it is useful compared to the stage when its value is being verified or measured. It then appears necessary to create a link between the different values of a given functional requirement to ensure these values are compatible.

As each stage of the lifecycle occurs in a different set of environmental and utilization conditions the mechanism is subject to thermo-mechanical load variations while stepping from one stage of the product lifecycle to another. As a consequence, an integrated design would take into account these load variations, hence helping the assembly meet a broader range of product requirements.

---

Chapter written by Guillaume MANDIL, Alain DESROCHERS and Alain RIVIÈRE.

A typical application that best illustrates the above idea would be a jet engine for which the functional requirements vary during its lifecycle. Indeed, the clearance between the rotor blades and engine housing (or stator) of the turbine will be quite different at assembly and in operation due to the high temperature and rotation velocity to which the rotor is subjected in service

The main purpose of this research is to create, through computations and simulations, links between the values of the loads, dimensions and functional requirements during the successive phases of the life cycle of some given product.

### **30.2. Literature review**

As stated in the introduction, this work includes topics from three different fields. The current section mainly presents prior work in the field of functional requirements.

In this area a large amount of research has been done on issues such as tolerance and dimension specification, tolerance analysis, tolerance synthesis, part geometry optimization or geometry variations.

#### **30.2.1. *Related standards***

In the GD&T there are some standards. There are ANSI standards edited by the ASME [ASM 94a][ASM 94b][ASM 03]. These are specifying the semantic used to define geometric features and their associated tolerances on 2D and 3D mechanical drawings. In addition the majority of the concepts related in these standards have also been reproduced by the ISO, which has released a set of international standards. The organization of this set [MAR 04] is synthetically presented by Marchèse [MAR 04]. These standards aspire to improve the consistence of geometric specifications with actual measuring techniques (3D measuring machine, etc.) and to avoid ambiguity or any kind of user interpretation while using GD&T techniques. The benefits of using these techniques have been pointed out by Chiabert [CHI 98].

#### **30.2.2. *Related research***

Here prior research, which has retained our attention, is presented.

Firstly, Samper [SAM 98] presents an approach which allows us to consider the influence of both deformation of part and fit of joint into the analysis or synthesis of tolerances zones. The authors assumed that deformation of part and fit of joint have independent effects. A similar hypothesis which will be discussed in section 30.4.1

is considered in this chapter. In order to evaluate the influence of the two parameters named upper, Samper uses four models to represent a mechanical assembly:

- rigid parts and perfect mechanism;
- rigid parts and imperfect mechanism;
- flexible parts and perfect mechanism;
- flexible parts and imperfect mechanism.

In this chapter, calculations are made sequentially on the three firsts models and the obtained results are compiled on the fourth which is the most complex. In a subsequent paper, the same authors [SAM 03] proposed an extension of their approach in order to make simultaneous calculations.

Secondly, Cid [CID 07] presented research which enables the evaluation of clearances under loads thanks to a clearance torsor introduced in [CID 04]. This study investigates the case of the clearance between a vehicle door and its frame. The representation of parts uses the simplification of considering 3D surfaces instead of 3D volumes.

Thirdly, Pierre [PIE 08] addressed the particular case of the jet engine mentioned in the introduction, using detailed geometries and finite elements technique for the calculation of parts deformation.

### 30.3. Definitions and concepts

Here are defined some terms used in the following sections of this paper. The example presented in Figure 30.1 will be used to illustrate the following definitions.

#### 30.3.1. Dimensions

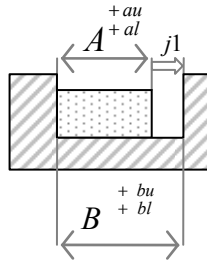
*Nominal dimension*: effective dimension of the part used in the CAD model. This is noted  $d_n$  in this section. In Figure 30.1 there are two nominal dimensions graphically represented by  $A$  and  $B$ .

*Tolerance*: interval which define the acceptable variation of a measured dimension around its nominal value. This is noted  $[tl;tu]$  in this section. The boundaries of the tolerance interval ( $tl$  and  $tu$ ) can be positive or negative. In Figure 30.1, the tolerance associated with the dimension  $A$  is  $[al;au]$ .

*Minimal dimension:* minimal acceptable value for a measured dimension. This is noted  $d_{min}$  in this section and  $d_{min} = d_n + tl$ . In Figure 30.1, the tolerance minimal dimension of  $A$  is  $A_{min} = A + al$

*Maximal dimension:* maximal acceptable value for a measured dimension. This is noted  $d_{max}$  in this section.  $d_{max} = d_n + tu$ . In Figure 30.1, the tolerance maximal dimension of  $A$  is  $A_{max} = A + au$

*Mean dimension:* this is noted  $\bar{d}$  in this section.  $\bar{d} = d_n + (tl + tu)/2$ . In Figure 30.1 the mean dimension of  $A$  is  $\bar{A} = A + (al + au)/2$ .



**Figure 30.1.** Example for definitions

For each dimension defined above in this section  $d_{(SI)}$  represents the dimension  $d$  at the S1 stage of the lifecycle of the product.

### 30.3.2. Functional requirements

*Dimension chain:* mathematical relation which links the value of a functional requirement with the dimensions of individual parts. In Figure 30.1 the dimension chain associated with the  $j1$  functional requirement can be expressed thanks to equation [30.1] below, where  $i$  stand for whichever subscript. Two individual dimensions ( $B$  and  $A$ ) are involved in this chain.

$$j1_i = B_i - A_i \quad [30.1]$$

*Nominal or real value of functional requirement:* value of a given functional requirement calculated with nominal or real dimensions. In Figure 30.1 this could be expressed with  $j1 = B - A$  for a nominal functional requirement and with  $j1_r = B_r - A_r$  for a real functional requirement.

*Mean functional requirement:* value of a given functional requirement calculated with mean dimensions. In Figure 30.1 this can be expressed using expression [30.2] below.

$$\overline{j_1} = (B + (b_l + b_u)/2) - (A + (a_l + a_u)/2) \quad [30.2]$$

*Minimal and maximal functional requirement:* these values are calculated using techniques of analysis of tolerance zones. These techniques stack-up tolerance zones specified for individual dimensions for a given functional requirement through the corresponding dimension chain. The result of this calculation is an interval which represents the possible range of variation for the functional requirement. This interval is centered on the mean value of the functional requirement. In Figure 30.1 the following values are obtained:  $j_1 \min = B \min - A \max$  and  $j_1 \max = B \max - A \min$ .

### 30.4. Functional requirements throughout lifecycle stages

This section discusses how the evolution of the product along its life-cycle leads to changes of functional requirement values.

#### 30.4.1. General principles

Considering an assembly, there are two ways that the possible values of a given functional requirement vary.

There is first the stack-up of all the uncertainties due to machining and measuring techniques. This problem has been largely studied, and there exists some techniques of tolerances analysis to predict the possible variations of a given functional requirement. If the width of the possible range for a functional requirement  $j_i$  is noted  $\Delta j_i$  then it is expressed using:  $\Delta j_i = j_i \max - j_i \min$ . These variations are not directly linked to the whole product lifecycle. They are specifically related to the manufacturing and assembly stages. The manufacturing stage determines the accuracy of individual dimensions: the measured dimensions associated with their corresponding uncertainties have to meet the specified tolerances. Then, if required, a part could be matched at the assembly stage [BJO 89] in order to meet the functional requirement specifications. In a more comprehensive way, the narrower the tolerances are, the smaller the range of possible variation for the functional requirement ( $\Delta j_i$ ) will be.

Secondly, the study must take into account the changing environment from an initial stage “Si” to a final stage “Sf” of the product lifecycle. Note that the terms initial and final are just relative to calculations steps. In a more comprehensive way the initial stage could be considered in operation and the final stage could be at the assembly situation. This allows us to express, in the same formalism, the shift from the S1 to S2 stage and the shift from S2 to S1. Then, as mentioned in the introduction, the loads received by the assembly are subject to changes during this shift. This causes some deformation on the mechanism parts. These deformations can be viewed as a variation of individual dimensions. Let us be precise about which of the dimensions defined in section 30.3.1 are affected by part deformation.

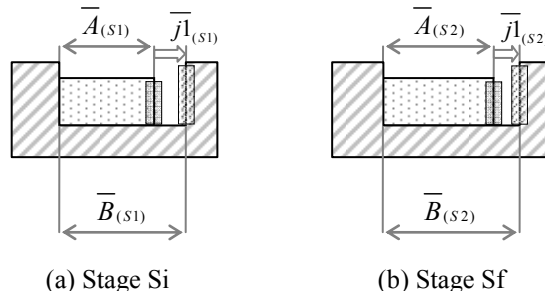
If the parts of Figure 30.1 are considered precise enough then it is possible to write down relation [30.3].

$$au - al \ll \bar{A} \quad [30.3]$$

Additionally, if the deformations are assumed to be small (i.e.  $\Delta \bar{A} \ll \bar{A}$ ) then with [30.3] we obtain relation [30.4]. This hypothesis is always verified if deformations are considered as elastic and linear which is the case in this research.

$$\Delta(au - al) \ll \Delta \bar{A} \ll \bar{A} \quad [30.4]$$

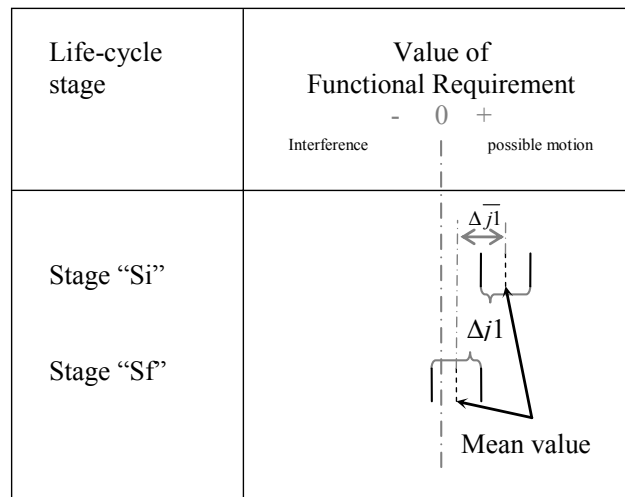
Equation [30.4] above means that the variation of the width of the tolerance zone is not, at a first order approximation, a significant source of variation compared to the variation of the mean value of the dimension. Consequently the width of the tolerance zone associated with the part at stage “Si” is approximately the same as the width of the tolerance zone associated with the part at the stage “Sf”.



**Figure 30.2.** Variation of individual dimensions due to loads

This explain that while stepping from the “Si” to “Sf” lifecycle stage in Figure 30.2 the width of the tolerance zone is unchanged and only the mean dimension is subject to some variations. This means that parts deformations due to

loads can be viewed as a variation of mean values of individual dimensions. As tolerance stack-up techniques do not consider the dimensions but their possible variations we can infer that the value of  $\Delta j_i$  do not vary across these two lifecycle stages. Finally, variations of functional requirements across two lifecycle stages can be represented in Figure 30.3 below.

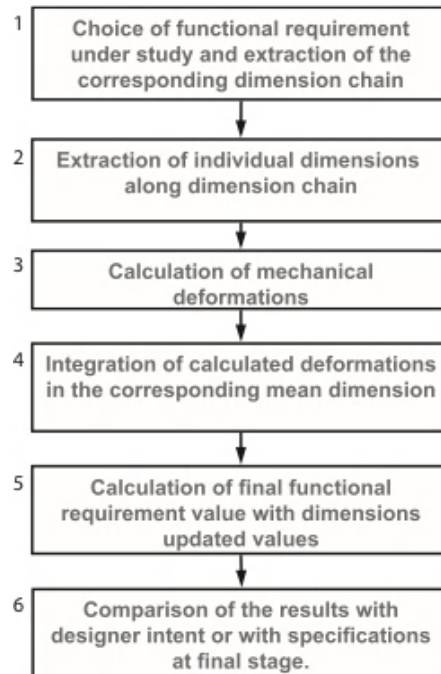


**Figure 30.3.** Functional requirement variations due to loads

#### 30.4.2. Computational rules

As shown in the previous section, functional requirements are subject to some variations along the product lifecycle. In order to calculate the variation of the mean value of a given functional requirement several steps have to be followed. First, we have to calculate (using any existing technique) the deformation due to loads for each part. Then, for these deformations, corresponding mean values of the dimensions involved in the dimension chain of the studied functional requirement have to be extracted. From there, it becomes possible to obtain the relation between the values of this functional requirement at two different stages of the product lifecycle. In accordance with the previous section, from here, all values used in the following are mean values.

These results have to be compared to the specifications for the functional requirements at the appropriate stage of the lifecycle in order to ensure their continued compatibility while stepping along the lifecycle. Depending on the hypothesis and known variables three kinds of calculations can be made.



**Figure 30.4.** *Dimension driven calculation*

#### 30.4.2.1. *From dimensions to functional requirement*

This computational approach (Figure 30.4) is dimension driven meaning that changes on individual dimensions prompted by lifecycle evolution are translated into corresponding functional requirement values. This approach is used to check that dimensions chosen for the stage  $S_i$  of the product lifecycle are compatible with the required functional requirement value at the stage  $S_f$ .

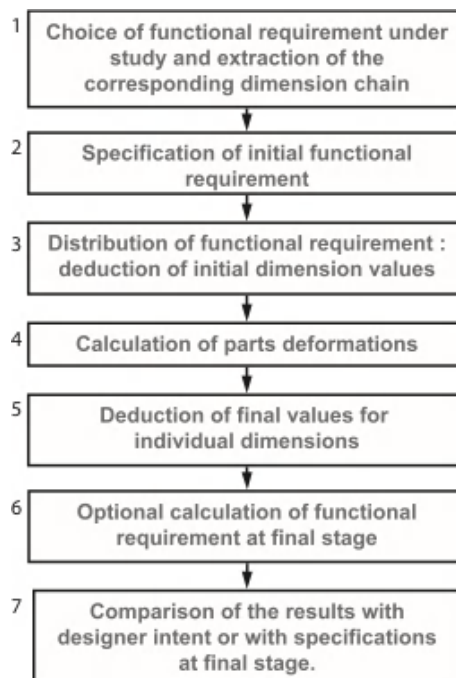
In Figure 30.4, steps 1 and 2 are not dependent on the product lifecycle. They are used to point out which functional requirement and dimension chain are under study. The dimension chain indicates the relation between the individual dimensions and the value of the functional requirement (section 30.3.2). This relation is unchanged across the product lifecycle. Then, step 3 allows the shift from  $S_i$  to  $S_f$  through calculations of the deformations due to loads variations. Finally steps 4 and 5 are required to express the results obtained at step 3 in terms of dimensions and functional requirement at the stage  $S_f$  of the product lifecycle. At step 6, this result is compared to specifications or to designer intent in order to validate the design of the product.



### 30.4.2.2. From functional requirement to dimensions

Unlike the previous section, here the functional requirements are used as input to find compatible dimension values in the initial and final lifecycle stage. This calculation (Figure 30.5) allows the designer to assign values to the individual dimensions of the product at stage  $S_i$  of the lifecycle in order to ensure the assembly meets a given value for the studied functional requirement under the  $S_f$  stage of the product lifecycle. As several dimensions are involved in the dimension chains, the result of this calculation is a range of acceptable values. In order to assign only one value to each dimension other criteria have to be considered.

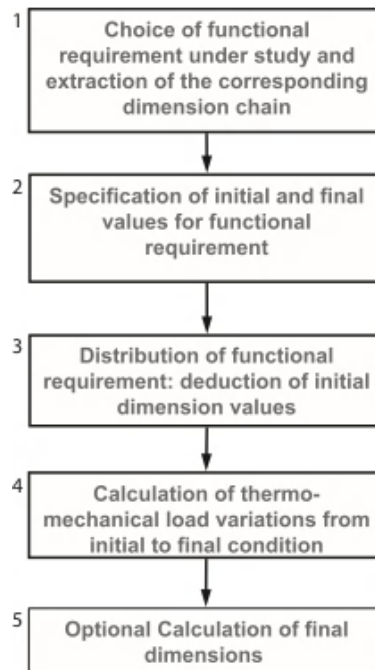
In Figure 30.5 the first step is lifecycle independent while it consists of choosing the functional requirement under study. Steps 2 and 3 occur in the initial stage of the product lifecycle. The result of these steps is the determination of initial individual dimension values. Then, the calculations made during step 4 authorize the shift from  $S_i$  to  $S_f$ . The results are expressed in the final stage in step 5. If necessary, the final value of the functional requirement could be calculated in step 6 thanks to individual dimensions obtained in step 5. Finally these results are compared to specifications or to designer intent in order to validate the current design of the product.



**Figure 30.5.** Functional requirement driven calculation

### 30.4.2.3. Determination of acceptable operating conditions

Here it is assumed that the geometry of the product is completely defined. In a more comprehensive way, this means that the values of the functional requirements are specified both at the initial and final stage of the product lifecycle. The aim of this calculation (Figure 30.6) is to provide the designer with the acceptable variation of the environmental conditions and loads in relation to the specified values of a functional requirement along the product lifecycle.



**Figure 30.6.** *Geometry driven calculation*

The first three steps described in Figure 30.6 establish the required input data for the problem at hand. Step 1 consists of choosing a functional requirement. Step 2 specifies its values at the initial and final stage of the lifecycle. Afterwards, step 3 of the methodology assigns an initial value to individual dimensions involved in the chain. From there the dimensions at the initial phase of the product lifecycle are obtained. Then the acceptable thermo-mechanical load variation is calculated during step 3. If several thermo-mechanical loads are subject to variations then the result of this step should be expressed as a range of possible variation for each thermo-mechanical load. Ultimately and if necessary, final dimensions can be calculated using the dimension driven technique previously described.

### 30.5. Case study: a simple 1D crosshead guide

In this section a simple application case is presented. The studied guide presented in Figure 30.7 is constituted of a one-piece wheel shaft positioned in a one-piece frame.

We have deliberately chosen a simple example in order to present in a simple way the benefits and the perspectives of our approach. This case is considered as 1D and the thermo-mechanical loads are limited to temperature variation. Admittedly the chosen case is not realistic, but it is simple enough to be calculated and verified with existing theoretical formulations.

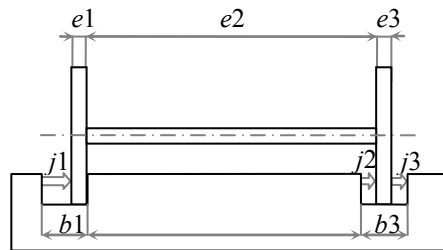
#### 30.5.1. Hypothesis

##### 30.5.1.1. Lifecycle

This case will be studied while stepping from the initial stage  $S_i$  to the final stage  $S_f$  of this product lifecycle. It should be noted however that those generic initial and final lifecycle stages do not necessarily have to follow a temporal sequence. In other words, depending on the problem perspective, the initial stage could be the product use in operation whereas the final stage would be the product at the assembly phase.

##### 30.5.1.2. Geometry

The geometry chosen for this study is presented in Figure 30.7 below. It is described using six dimensions.



**Figure 30.7.** 1D case study

For all the following calculations the dimensions  $e1$ ,  $e2$  and  $e3$  are considered as hard constraints and their imposed values at 20°C are exposed in Table 30.1. The example case study consists of designing the frame.

Dimension	Value at 20°C
$e1_{(20^{\circ}C)}$	$60^{\pm 0,1} mm$
$e2_{(20^{\circ}C)}$	$1440^{\pm 0,1} mm$
$e3_{(20^{\circ}C)}$	$60^{\pm 0,1} mm$

**Table 30.1.** *Dimension of the shaft at 20°C***30.5.1.3. Materials**

The wheel shaft is built from aluminum and the frame is made of steel.

**30.5.1.4. Loads and behavior law**

It is assumed that during its lifecycle this mechanism is subject to a temperature variation which will result in linear deformations such as presented in equation [30.5] below.

$$l_{(sf)} - l_{(si)} = \alpha \cdot l_{(si)} \cdot (t_{(sf)} - t_{(si)}) \quad [30.5]$$

In equation [30.5]  $l$  represents the length of a given dimension and  $t$  stands for the temperature. Finally,  $\alpha$  designates the coefficient of thermal dilatation. Typical values of  $\alpha$  are presented in Table 30.2 below.

Material	Notation	Coefficient of thermal dilatation
Steel	$\alpha_s$	$1.20 E-05 K^{-1}$
Aluminum	$\alpha_a$	$2.38 E-05 K^{-1}$

**Table 30.2.** *Typical coefficient values of thermal dilatation***30.5.1.5. Functional requirements**

This case also defines three functional requirements  $j1$ ,  $j2$  and  $j3$  which will be studied. It is also assumed that each functional requirement can have a minimum and/or a maximum required value for each stage of the product lifecycle.

**30.5.1.6. Dimension chains**

For each requirement it is possible to define a dimension chain from which the following equations [30.6], [30.7] and [30.8] are derived to calculate the values of the functional requirements.

$$\begin{cases} j1 = b1 - e1 \\ j1 \min = b1 \min - e1 \max \\ j1 \max = b1 \max - e1 \min \end{cases} \quad [30.6]$$

$$\begin{cases} j2 = e2 - b2 \\ j2 \min = e2 \min - b2 \max \\ j2 \max = e2 \max - b2 \min \end{cases} \quad [30.7]$$

$$\begin{cases} j3 = b2 + b3 - e2 - e3 \\ j3 \min = b3 \min - e3 \max - e2 \max + b2 \min \\ j3 \max = b3 \max - e3 \min - e2 \min + b2 \max \end{cases} \quad [30.8]$$

#### 30.5.1.7. Implementation

All the above exposed hypothesis have been introduced into an Excel spreadsheet for each kind of calculation presented in section 30.4.2. For these calculations two lifecycle stages Si and Sf are considered.

#### 30.5.2. Dimension driven calculation

This first calculation aims at answering the question: “What will be the value of a given functional requirement after thermal dilatation of the parts?”

##### 30.5.2.1. Hypothesis

The studied functional requirements are  $j1$   $j2$  and  $j3$  which can be calculated using the dimension chains [30.6][30.7][30.8].

Variable	Value
$t_{(Si)}$	$20^{\circ}\text{C}$
$t_{(Sf)}$	$50^{\circ}\text{C}$
$b1_{(Si)} \text{ at } 20^{\circ}\text{C}$	$60.3^{+0.1} \text{ mm}$
$b2_{(Si)} \text{ at } 20^{\circ}\text{C}$	$1439.7^{+0.1} \text{ mm}$
$b3_{(Si)} \text{ at } 20^{\circ}\text{C}$	$60.8^{+0.1} \text{ mm}$

**Table 30.3.** First calculation hypothesis

This represents the steps 1 and 2 of Figure 30.4 methodology. As the initial temperature is 20°C the values of  $e1$   $e2$  and  $e3$  are those presented in Table 30.1. The initial values presented in table 1 and table 3 will be introduced in the Excel spreadsheet in order to map the value of functional requirements along with the temperature variations.

### 30.5.2.2. Calculations

This is the 3<sup>rd</sup> and 4<sup>th</sup> step of the methodology in Figure 30.4. The previously described hypotheses are then used as input for calculating the deformations thanks to equation [30.5]. The results obtained are presented in Table 30.4.

Initial dimension at stage Si (at 20°C)	Deformation	Final dimension at stage Sf (50°C)
$\overline{e1}_{(Si)} = 60mm$	$\Delta e1 = 0.043mm$	$\overline{e1}_{(Sf)} = 60.043mm$
$\overline{e2}_{(Si)} = 1440mm$	$\Delta e2 = 1.028mm$	$\overline{e2}_{(Sf)} = 1441.028mm$
$\overline{e3}_{(Si)} = 60mm$	$\Delta e3 = 0.043mm$	$\overline{e3}_{(Sf)} = 60.043mm$
$\overline{b1}_{(Si)} = 60.3mm$	$\Delta b1 = 0.022mm$	$\overline{b1}_{(Sf)} = 60.322mm$
$\overline{b2}_{(Si)} = 1439.7mm$	$\Delta b2 = 0.518mm$	$\overline{b2}_{(Sf)} = 1440.218mm$
$\overline{b3}_{(Si)} = 60.8mm$	$\Delta b3 = 0.022mm$	$\overline{b3}_{(Sf)} = 60.822mm$

**Table 30.4.** Deformation and final dimensions for dimension driven calculation

### 30.5.2.3. Results

For the 5<sup>th</sup> step of Figure 30.4 methodology the values presented in Table 30.4 are introduced in dimensions chains [30.6], [30.7] and [30.8]. The results for the functional requirements are presented in Table 30.5.

Functional requirement	Mean values	Range of possible values
$j1_{(Si)}$ at 20°C	0.3 mm	[0.1 ; 0.5] mm
$j2_{(Si)}$ at 20°C	0.3 mm	[0.1 ; 0.5] mm
$j3_{(Si)}$ at 20°C	0.5 mm	[0.1 ; 0.9] mm
$j1_{(Sf)}$ at 50°C	0.279 mm	[0.079 ; 0.479] mm
$j2_{(Sf)}$ at 50°C	0.810 mm	[0.610 ; 1.010] mm
$j3_{(Sf)}$ at 50°C	-0.031 mm	[-0.431 ; 0.369] mm

**Table 30.5.** Results of dimension driven calculation

First, the tolerances along dimension chains [30.6], [30.7] and [30.8] have been analyzed in order to calculate the range of possible values for the functional requirements at stage Si. Then, mean values of functional requirement are calculated at stage Sf and they are associated with the range of possible variations resulting from the tolerance analysis and which do not vary along the lifecycle (see section 30.4.1.).

### 30.5.2.4. Conclusion

The results of Table 30.5 show that at stage Sf (under 50°C) some interference on the functional requirement  $j3$  might appear. If this interference is not compatible with the product functionality (step 6 in Figure 30.4) then the dimensions of the mechanism must be reviewed.

### 30.5.3. Functional requirement driven calculation

Which dimension has to be chosen in order to obtain a given value of a functional requirement after thermal dilatation?

In this section the studied problem is the calculation of the dimensions of the frame at 20°C which ensure given values for functional requirements  $j1$   $j2$  and  $j3$  at 50°C (step 1 of the methodology in Figure 30.5).

## 30.5.3.1. Hypothesis

Considering the objectives discussed above, the initial conditions are considered at 50°C and the final stage is at 20°C (see Table 30.7). The targeted values for functional requirement are shown in Table 30.6 (steps 1 and 2 in Figure 30.5).

Functional requirement	Mean values	Acceptable values
$j1_{(Si)}$ at 50°C	0.25 mm	[0.05 ; 0.45] mm
$j2_{(Si)}$ at 50°C	0.4 mm	[0.2 ; 0.6] mm
$j3_{(Si)}$ at 50°C	0.45 mm	[0.05 ; 0.85] mm

**Table 30.6.** Values for functional requirement at 50°C

Moreover, the dimensions of the shaft at 50°C can be found in Table 30.4. Therefore, the values of the dimensions and tolerance zones of the frame at 50°C can be deduced using dimension chains [6][7][8] (step 3 in Figure 30.5). These values are displayed in Table 30.7.

Variable	Value
$t_{(Si)}$	50°C
$t_{(Sf)}$	20°C
$e1_{(Si)}$ at 50°C	$60.043^{+0.1}_{-0.1}$ mm
$e2_{(Si)}$ at 50°C	$1441.028^{+0.1}_{-0.1}$ mm
$e3_{(Si)}$ at 50°C	$60.043^{+0.1}_{-0.1}$ mm
$b1_{(Si)}$ at 50°C	$60.293^{+0.1}_{-0.1}$ mm
$b2_{(Si)}$ at 50°C	$1440.628^{+0.1}_{-0.1}$ mm
$b3_{(Si)}$ at 50°C	$60.893^{+0.1}_{-0.1}$ mm

**Table 30.7.** Functional requirement driven calculation inputs

## 30.5.3.2. Calculations

The calculations of thermal deformation (step 4 in Figure 30.5) are performed in the same way as in section 30.5.2.



### 30.5.3.3. Results

Final dimensions after step 5 in Figure 30.5 are presented in Table 30.8.

Final dimension at stage Sf (20°C)
$\overline{e1_{(Sf)}} = 60mm$
$\overline{e2_{(Sf)}} = 1440mm$
$\overline{e3_{(Sf)}} = 60mm$
$\overline{b1_{(Sf)}} = 60.271mm$
$\overline{b2_{(Sf)}} = 1440.109mm$
$\overline{b3_{(Sf)}} = 60.871mm$

**Table 30.8.** Final dimensions at 20°C for functional requirement driven calculation

The optional 6<sup>th</sup> step of Figure 30.5 is used there as a validation process for individual dimensions. The calculations are made in the same way as in section 30.5.2. Final values of functional requirements are presented in Table 30.9.

Functional requirement	Mean values	Acceptable values
$j1_{(Sf)}$ at 20°C	0.271 mm	[0.071 ; 0.471] mm
$j2_{(Sf)}$ at 20°C	-0.110 mm	[-0.310 ; 0.09] mm
$j3_{(Sf)}$ at 20°C	0.981 mm	[0.581 ; 1.381] mm

**Table 30.9.** Functional requirement values at 20°C

### 30.5.3.4. Conclusion

The results in Table 30.9 show that at stage Sf (under 20°C) some interference on functional requirement  $j2$  might appear. If this interference is not compatible with the product functionality (step 7 in Figure 30.5) then the dimensions of the mechanism must be reviewed. A greater initial mean value for the functional requirement or a narrower range for the corresponding tolerance zone must be used as an updated input for this calculation.

### 30.5.4. Geometry driven calculation

Which loads are acceptable in order to ensure the respect of a functional requirement at two stages Si and Sf of the lifecycle?

## 30.5.4.1. Hypothesis

First, the designer must impose a mean value on functional requirements at stages Si and Sf of the product lifecycle. The initial temperature is set to 20°C. Due to Table 30.1 dimensions, dimension chain expressions [30.6][30.7][30.8] and functional requirement values at Si, we can deduce values of  $\overline{b1_{(Si)}}$ ,  $\overline{b2_{(Si)}}$  and  $\overline{b3_{(Si)}}$ . These values can be found in Table 30.10.

This represents steps 1 and 2 of the methodology in Figure 30.6.

Variable	Value
$\overline{t_{(Si)}}$	20 °C
$\overline{j1_{(Si)}}$ at 20°C	0.3 mm
$\overline{j2_{(Si)}}$ at 20°C	0.3 mm
$\overline{j3_{(Si)}}$ at 20°C	0.5 mm
$\overline{j1_{(Sf)}}$	0.25 mm
$\overline{j2_{(Sf)}}$	0.4 mm
$\overline{j3_{(Sf)}}$	0.45 mm
$\overline{e1_{(Si)}}$ at 20°C	60 <sup>±0,1</sup> mm
$\overline{e2_{(Si)}}$ at 20°C	1440 <sup>±0,1</sup> mm
$\overline{e3_{(Si)}}$ at 20°C	60 <sup>±0,1</sup> mm
$\overline{b1_{(Si)}}$ at 20°C	60.3 <sup>±0,1</sup> mm
$\overline{b2_{(Si)}}$ at 20°C	1439.7 <sup>±0,1</sup> mm
$\overline{b3_{(Si)}}$ at 20°C	60.8 <sup>±0,1</sup> mm

**Table 30.10.** Geometry driven calculation inputs

## 30.5.4.2. Calculations

This part of the method represents the 3<sup>rd</sup> step of the methodology in Figure 30.6. The use of dimension chains and the deformation law will be detailed here for the calculation relative to the j3 functional requirement. A similar approach is used for j1 and j2. First, the expression of the dimension chain [30.8] is used to calculate the mean value of the functional requirement j3 given at the initial stage [30.9] and at the final stage [30.10].

$$\overline{j3_{(Si)}} = \overline{b2_{(Si)}} + \overline{b3_{(Si)}} - \overline{e2_{(Si)}} - \overline{e3_{(Si)}} \quad [30.9]$$

$$\overline{j3_{(Sf)}} = \overline{b2_{(Sf)}} + \overline{b3_{(Sf)}} - \overline{e2_{(Sf)}} - \overline{e3_{(Sf)}} \quad [30.10]$$

From these expressions the variations of these mean values are deduced with [30.11].

$$\Delta \bar{j3} = \overline{b2_{(Sf)}} - \overline{b2_{(Si)}} + \overline{b3_{(Sf)}} - \overline{b3_{(Si)}} - \overline{e2_{(Sf)}} + \overline{e2_{(Si)}} - \overline{e3_{(Sf)}} + \overline{e3_{(Si)}}$$

with  $\Delta \bar{j3} = \overline{j3_{(Sf)}} - \overline{j3_{(Si)}}$  [30.11]

Additionally, with behavior law [30.5], the following set [30.12] of the lifecycle dependence relation is obtained.

$$\begin{cases} e3_{(Sf)} = \alpha_a \cdot e3_{(Si)} \cdot (t_{(Sf)} - t_{(Si)}) + e3_{(Si)} \\ e2_{(Sf)} = \alpha_a \cdot e2_{(Si)} \cdot (t_{(Sf)} - t_{(Si)}) + e2_{(Si)} \\ b3_{(Sf)} = \alpha_s \cdot b3_{(Si)} \cdot (t_{(Sf)} - t_{(Si)}) + b3_{(Si)} \\ b2_{(Sf)} = \alpha_s \cdot b2_{(Si)} \cdot (t_{(Sf)} - t_{(Si)}) + b2_{(Si)} \end{cases} \quad [30.12]$$

Finally, with the substitution of final values [30.12] in equation [30.11] the equation [30.13] gives the expression of the admissible final temperature for  $j3$ .

$$t_{(Sf)} = t_{(Si)} + \frac{\Delta \bar{j3}}{\alpha_s \cdot (\overline{b3_{(Si)}} + \overline{b2_{(Si)}}) - \alpha_a \cdot (\overline{e3_{(Si)}} + \overline{e2_{(Si)}})} \quad [30.13]$$

#### 30.5.4.3. Results

The calculations presented in the previous paragraph give the results presented in Table 30.11.

Functional requirement to be respected	Admissible temperature at final stage
$j1$	91.0 °C
$j2$	25.9 °C
$j3$	22.8 °C

**Table 30.11.** Admissible temperature for geometry driven calculation

These results are those obtained after the 4<sup>th</sup> step of the methodology in Figure 30.6. A 5<sup>th</sup> step consists of choosing the most restrictive value for the final temperature which is 22.8°C in this case. Under this condition, final dimensions can be deduced using a dimension driven calculation (section 30.5.2).

#### 30.5.4.4. *Conclusion*

This resulting limited range of temperature variation means that if solutions presented in the conclusion of section 30.5.3 are not applicable, then, the only way to ensure mechanism functionality is to reduce the possible range of load variation.

### 30.6. Conclusion and perspectives

#### 30.6.1. *High level management of functional requirements*

This simple study has shown the interest of considering functional requirement variations along the various phases of the product lifecycle. As the proposed approach does not affect the width of the tolerance zones, it consequently does not impact machining costs either. This aspect is very interesting because it enables possible improvements of the mechanism functionality at a given stage of the product lifecycle without increasing its cost. Moreover, the previous section (section 30.5) has been organized as a high-level design methodology. This methodology consists of three successive steps. First, the current design of the product is checked with a dimension driven calculation (section 30.5.2). If the resulting functional requirement is not meeting products specifications at the target of final phase of the product lifecycle, then a second step of redesign is undertaken using a functional requirement driven calculation (section 30.5.3). The initial stage of the product lifecycle for the functional requirement driven calculation should correspond to the final stage of the dimension driven calculation. For example, if the dimension driven calculation is made from the assembly stage to the operation stage of the product lifecycle, then the functional driven calculation will be made from operation to assembly in order to assign individual dimensions at the assembly stage of the product lifecycle (which are then considered to be the design variables). Finally, if this fails and acceptable values for individual dimensions cannot be found, an ultimate geometry driven calculation (section 30.5.4) can be used to compute the range of acceptable thermo-mechanical load variation between the two stages considered in the product lifecycle.

#### 30.6.2. *Further work*

This study has been illustrated on a very restrictive case and must be extended to a more general case. First this model should be able to tackle 2D and 3D geometries. This must include an appropriate way for the mathematical representation of 2D and 3D dimension chains and an appropriate tool for the calculation of parts deformations under thermo-mechanical loads. The preliminary studies done in this

way suggest the use of TTRS<sup>1</sup> and MGRE<sup>2</sup> [DES 91] for the representation of dimension chains. Additionally, finite element analysis (FEA) appears as the most suitable tool for the calculation of parts deformation as it is commonly used in the mechanical industry. It is worth noting that 2D and 3D dimension chains contain both linear and angular dimensions which must be accounted for by the proposed approach.

Concerning the lifecycle aspects of the methodology, some improvements are planned. There is first the combination of several thermo-mechanical loads as a source of geometric variations. Secondly, the possibility of further constraining the design, by specifying values for the functional requirements at various stages of the product lifecycle, will be investigated.

### 30.7. Acknowledgments

We wish to acknowledge the financial support of the Natural Science and Engineering Council of Canada for funding this research through its Discovery grant program.

### 30.8. Bibliography

- [ASM 94a] ASME, “Y14.5M - 1994 Dimensioning and Tolerancing”, Y 14.5M, American Society for Mechanical Engineers, 1994.
- [ASM 94b] ASME, “Y14.5.1M - 1994 Mathematical Definition of Dimensioning and Tolerancing Principles”, Y14.5.1M, American Society for Mechanical Engineers, 1994.
- [ASM 03] ASME, “Y14.41 - 2003 Digital Product Definition Data Practices”, Y14.41, American Society for Mechanical Engineers, 2003.
- [BJO 89] BJORKE O., “Manufacturing principles”, in *Computer-Aided Tolerancing*, 2nd Ed. ASME Press, New York, USA, Chap. 6, pp. 77-84, 1989.
- [CHI 98] CHIABERT P., LOMBARDI F. and ORLANDO M., “Benefits of geometric dimensioning and tolerancing”, *Journal of Materials Processing Technology*, Vol. 78, No. 1-3, pp. 29-35, 1998.
- [CID 04] CID G., THIEBAUT F. and BOURDET P., “Taking the deformation into account for components’ tolerancing”, *5th International Conference on Integrated Design and Manufacturing in Mechanical Engineering (IDMME 2004)*, University of Bath, UK, pp. 40, 2004.

---

<sup>1</sup> Technologically and topologically related surfaces

<sup>2</sup> Minimum geometric reference element

- [CID 07] CID G., THIEBAUT F. and BOURDET P., “Geometric study of assembly behaviour, taking into accounts rigid components deviations, actual geometric variations and deformations”, *Models for Computer Aided Tolerancing in Design and Manufacturing*, pp. 301-310, 2007.
- [DES 91] DESROCHERS A., “Modèle conceptuel du dimensionnement et du tolérancement des mécanismes. Représentation dans les systèmes CFAO”, PhD thesis, Ecole Centrale de Paris, 1991.
- [ISO 95] ISO, “Spécification Géométrique Des Produits (GPS) - Schéma Directeur”, ISO/TR 14638, International Organization for Standardization, 1995.
- [MAR 04] MARCHÈSE J., “Spécification Géométrique Des Produits (GPS)”, Techniques De l’Ingénieur, [www.techniques-ingenieur.fr/book/r1210/specification-geometrique-des-produits-gps.html](http://www.techniques-ingenieur.fr/book/r1210/specification-geometrique-des-produits-gps.html), 1999, updated in 2004.
- [PIE 08] PIERRE L., TEISSANDIER D. and NADEAU J.P., “Tolerancing analysis taking into account thermomechanical strains”, *Proceedings of IDMME - Virtual Concept 2008*, Beijing, China, October 8 – 10, 2008.
- [SAM 03] SAMPER S. and GIORDANO M., “Simultaneous analysis method for tolerancing flexible mechanisms”, in *Geometric Product Specification and Verification: Integration of Functionality*, Pierre BOURDET and Luc MATHIEU (eds.), pp. 127-134, Kluwer Academic Publishers, 2003.
- [SAM 98] SAMPER S. and GIORDANO M., “Taking into account elastic displacements in 3D tolerancing: models and application”, *Journal of Materials Processing Technology*, Vol. 78, No. 1-3, pp. 156-162, 1998.

## List of Authors

Pierre-Antoine ADRAGNA  
LASMIS  
University of Technology of Troyes  
France

Gaurav AMETA  
Washington State University  
USA

Bernard ANSELMETTI  
LURPA  
ENS Cachan  
France

Nabil ANWER  
LURPA  
ENS Cachan  
France

Régis BIGOT  
LCFC  
Arts et Métiers ParisTech  
Metz  
France

Robert BOHLIN  
Geometry and Motion Planning  
Group  
Fraunhofer-Chalmers Research  
Centre  
Gothenberg  
Sweden

Pierre BOURDET  
LURPA  
ENS Cachan  
France

Jérôme BRUYÈRE  
LaMCoS  
University of Lyon  
France

Johan S. CARLSON  
Geometry and Motion Planning  
Group  
Fraunhofer-Chalmers Research  
Centre  
Gothenberg  
Sweden

Anders CARLSSON  
Department of Manufacturing  
Methods and Tools  
Volvo Car Corporation  
Gothenberg  
Sweden

Robin CHAVANNE  
LURPA  
ENS Cachan  
France

André CLÉMENT  
LISMMA  
Sup-Meca  
Saint-Ouen  
France

Renaud COSTADOAT  
LURPA  
ENS Cachan  
France

Jean-Yves DANTAN  
LCFC  
Arts et Métiers ParisTech  
Metz  
France

Manuela DE MADDIS  
Polytechnic of Turin  
Italy

Dimitri DENIMAL  
SYMME  
University of Savoy  
France

Alain DESROCHERS  
Department of Mechanical  
Engineering  
University of Sherbrooke  
Quebec  
Canada

Daniel DURET  
IUT  
University of Savoy  
France

Hugo FALGARONE  
EADS  
Suresnes  
France

Karin FORSLUND  
Department of Product and  
Production Development  
Chalmers University of Technology  
Gothenberg  
Sweden

Pasquale FRANCIOSA  
University of Naples Federico II  
Italy

Benoît FRICERO  
EADS  
Suresnes  
France

Martina GANDINI  
Polytechnic of Turin  
Italy

Salvatore GERBINO  
University of Molise  
Campobasso  
Italy

Max GIORDANO  
SYMME  
University of Savoy  
France

Gerth GOCH  
BIMAQ  
Bremen  
Germany



Zhao HAIBIN  
LURPA  
ENS Cachan  
France

Pascal HERNANDEZ  
SYMME  
University of Savoy  
France

Patrick HOFFMANN  
LIRIS  
University Claude Bernard  
Lyon  
France

Mojtaba KAMALI NEJAD  
G-SCOP  
University of Grenoble  
France

Philipp KRÄMER  
Chair Quality Management and  
Manufacturing Metrology  
University of Erlangen-Nuremberg  
Germany

Gisela LANZA  
wbk - Institute of Production Science  
Karlsruhe Institute of Technology  
(KIT)  
Germany

Yann LEDOUX  
TREFLE  
University of Bordeaux  
France

Jean-Marc LINARES  
IMS/GIBO  
Aix Marseille University  
Aix-en-Provence  
France

Lars LINDKVIST  
Wingquist Laboratory  
Chalmers University of Technology  
Gothenberg  
Sweden

Jean MAILHÉ  
EAMS2  
Aix Marseille University  
Aix-en-Provence  
France

Guillaume MANDIL  
Department of Mechanical  
Engineering  
University of Sherbrooke  
Quebec  
Canada

Luc MATHIEU  
LURPA  
ENS Cachan  
France

Harald MEERKAMM  
Department of Mechanical  
Engineering  
Chair of Engineering Design  
Erlangen  
Germany

Emmanuel MERMOZ  
Eurocopter  
Marignane  
France

Faïda M'HENNI  
LISMMA  
Sup-Meca  
Saint-Ouen  
France

Stéphane MORIÈRE  
IMS/GIBO  
Aix Marseille University  
Aix-en-Provence  
France

Giovanni MORONI  
Department of Mechanics  
Polytechnic of Milan  
Italy

Edward MORSE  
UNC Charlotte  
USA

Stanislao PATALANO  
University of Naples Federico II  
Italy

Jochen PETERS  
wbk - Institute of Production Science  
Karlsruhe Institute of Technology  
(KIT)  
Germany

Stefano PETRÒ  
Department of Mechanic  
Polytechnic of Milan  
Italy

Natasa PETROVIC  
Chair Quality Management and  
Manufacturing Metrology  
University of Erlangen-Nuremberg  
Germany

Maurice PILLET  
SYMME  
University of Savoy  
France

Ahmed Jawad QURESHI  
LGIPM  
University of Metz  
France

Jean-Paul RAYNAL  
EAMS2  
Aix Marseille University  
Aix-en-Provence  
France

Alain RIVIÈRE  
LISMMA  
Sup-Meca  
Saint-Ouen  
France

Johan SEGEBORN  
Department of Manufacturing  
Methods and Tools  
Volvo Car Corporation  
Gothenberg  
Sweden

Alain SERGENT  
SYMME  
University of Savoy  
France

Philippe SERRÉ  
LISMMA  
Sup-Meca  
Saint-Ouen  
France

Samir SID-AHMED  
TREFLE  
University of Bordeaux  
France

Rikard SÖDERBERG  
Wingquist Laboratory  
Chalmers University of Technology  
Gothenberg  
Sweden

Domenico SPENSIERI  
Geometry and Motion Planning  
Group  
Fraunhofer-Chalmers Research  
Centre  
Gothenberg  
Sweden

Jean-Michel SPRAUEL  
IMS/GIBO  
Aix Marseille University  
Aix-en-Provence  
France

Tobias STOLL  
Department of Mechanical  
Engineering  
Chair of Engineering Design  
Erlangen  
Germany

Özgür TAN  
Chair Quality Management and  
Manufacturing Metrology  
University of Erlangen-Nuremberg  
Germany

Denis TEISSANDIER  
LMP  
University of Bordeaux  
France

Benjamin VIERING  
wbk - Institute of Production Science  
Karlsruhe Institute of Technology  
(KIT)  
Germany

Frédéric VIGNAT  
G-SCOP Laboratory  
University of Grenoble  
France

François VILLENEUVE  
G-SCOP Laboratory  
University of Grenoble  
France

Jean-Paul VINCENT  
LCFC  
Arts et Métiers ParisTech  
Metz  
France

Albert WECKENMANN  
Chair Quality Management and  
Manufacturing Metrology  
University of Erlangen-Nuremberg  
Germany

Stefan WITTMANN  
Department of Mechanical  
Engineering  
Chair of Engineering Design  
University of Erlangen-Nuremberg  
Germany

Xiaobin YOU  
UNC Charlotte  
USA

Laurent ZAMPONI  
Eurocopter  
Marignane  
France

## Index

3D  
  characterization, 420-421  
  inertial tolerancing, 99, 112  
  tolerance chains, 210

### A, B, C

accuracy, 345-347, 353  
AND/OR, 193  
assembly, 521-531, 542  
  constraints, 209-213, 227  
  planner, 201-206  
  robustness, 504  
  sequence, 178-188, 191-193, 201-203  
  simulation, 213  
  tolerance, 273  
body-in-white, 177-185  
capability, 345-349  
CAT system, 38  
chronological framework, 176-180, 188  
clearance effect, 19  
clearances, 523  
collision detection, 232-236, 241-242  
computed tomography, 317-319  
contact, 245-254

coordinate measuring machine (CMM), 301, 385-394, 400  
coordinate metrology, 405-417  
correlation uncertainty, 486, 500  
*Cp*, 346-347, 349

### D, E, F, G

datum flow chain, 192-195  
design for assembly, 192  
deviation domains, 62-63  
dimensions, 522-540  
equipment utilization, 175-180, 186-188  
feature modeling, 211  
fingerprint, 373, 378-379  
fixtures, 197  
fringe projection systems, 355-358, 369  
function oriented parameters, 331  
functional  
  condition, 260  
  requirement, 1-17, 261, 522, 527-540  
GapSpace, 273, 288  
gears, 485-487, 496-501

geometric  
 product specification, 371, 372, 373  
 variations, 433, 434, 435  
 product specification, 98, 371  
 quality, 177, 191-194, 202-207  
 specifications, 301, 302, 303  
 verification, 301-310  
 GPS, 97-99, 114, 121

## **H, I, L, M**

helicopter engine, 75, 94  
 independent component analysis, 371-373, 379-383  
 industrial design, 504, 513-517  
 inertial tolerance, 348, 354  
 interoperability, 456-458, 466  
 ISO standards, 54  
 lifecycle, 521-540  
 locating scheme, 178, 184-186, 195-206  
 loss function, 6-10  
 manufacturing  
 errors, 373  
 metrology, 317, 318  
 measurement uncertainty, 371-378, 383, 405-417  
 mechanism, 19-35  
 metrology, 419-420, 469-477, 482  
 strategy, 487, 495  
 micro-gears, 419, 427  
 model of manufactured part, 145-146  
 Monte Carlo simulation, 123-124, 132-141, 393-394  
 multiple sensors, 471-477

## **N, O, P, Q**

*ndc*, 345-351  
 non-nominal visualization, 503  
 non-quality cost, 1  
 ontological model, 456-466

optimization, 203-206, 245-256, 385, 390, 400  
 overconstraint, 20  
 parametric tolerancing, 28  
 path planning, 193, 202-207  
 perceived quality, 503, 508, 513-517  
 PLM, 469-477, 482-483  
 point clouds, 355-360, 369  
 positioning part table, 39, 50, 55  
 process plan, 146-151, 161-165, 170  
 product, 521-540  
 architecture, 178-183  
 lifecycle, 456-459, 466  
 realization, 192  
 quality assurance, 419-428  
 quantified constraint satisfaction problems, 130

## **R, S**

relative positioning, 232-240  
 repeatability, 345, 352  
 reproducibility, 345-346, 352-353  
 robot path planning, 188  
 roughness, 371-383  
 sampling strategy, 388-400  
 seasonal trend decomposition, 379-382  
 segmentation, 469, 478-482  
 semantic, 457  
 service life, 260-263, 269-271  
 shape deviation, 406-428  
 sheet metal assembly, 176-183, 188-189  
 specification  
 models, 488, 489  
 synthesis, 38  
 spot welds, 177  
 stability analysis, 198, 205-206  
 stamping, 177  
 statistical  
 analysis, 140  
 approaches for the tolerance, 58

- resampling, 405-406, 417
- tolerance, 2-11, 16, 106, 287
- surface
  - engineering, 331
  - parameters, 335, 342, 343

## **T, U, V, W**

- takt time, 178
- task-specific measurement
  - uncertainty, 317-318, 325-327
- time series analysis, 371-372, 382
- tolerance, 346, 348, 522, 525, 535
  - allocation, 3, 12, 17
  - analysis, 58-62, 69, 123-141, 145-149, 155-161, 170, 209-210, 231-242, 273, 287, 293-297
  - evaluation, 469-477, 482
  - representation, 459
  - synthesis, 58-59, 99-102, 117-119
- tolerancing, 435, 442, 452
  - analysis, 86
  - rules, 38, 50
- tooth contact analysis, 491-494
- TTRS, 540
- uncertainties of specification, 435
- uncertainty, 301-304, 311-315, 385-400
  - variability, 371-372, 377-383
- variation analysis, 199
- visualization, 234, 240-241
- weld load balancing, 188
- welding sequences, 188
- worst case analysis, 140